THE INFLUENCE OF ARABIAN GULF ENVIRONMENT ON MECHANISMS OF REINFORCEMENT CORROSION

MOHAMMED MASLEHUDDIN

Doctor of Philosophy

THE UNIVERSITY OF ASTON IN BIRMINGHAM

September 1994

THE UNIVERSITY OF ASTON IN BIRMINGHAM

The Influence of Arabian Gulf Environment On Mechanisms of Reinforcement Corrosion

Mohammed Maslehuddin

Doctor of Philosophy

October 1994

SUMMARY

The reduction in the useful-service life of reinforced concrete construction in the Arabian Gulf is attributed to reinforcement corrosion. While this phenomenon is primarily related to chloride ions, the concomitant presence of sulfate salts may accelerate the deterioration process. Another factor which might influence reinforcement corrosion is the elevated ambient temperature. While few studies have been conducted to evaluate the individual effect of sulfate contamination and temperature on chloride binding and reinforcement corrosion, the synergistic effect of these factors on concrete durability, viz.- a- viz., reinforcement corrosion, needs to be evaluated. Further, the environmental conditions of the Arabian Gulf are also conducive for accelerated carbonation. However, no data are available on the concomitant effect of chloride-sulfate contamination and elevated temperature on the carbonation behaviour of plain and blended cements.

This study was conducted to evaluate the conjoint effect of chloride-sulfate contamination and temperature on the pore solution chemistry and reinforcement corrosion. The effect of chloride-sulfate contamination and elevated temperature on carbonation in plain and blended cements was also investigated. Pore solution extraction and analysis, X-ray diffraction, differential thermal analysis, scanning electron microscopy, DC linear polarization resistance and AC impedance spectroscopy techniques were utilized to study the effect of experimental parameters on chloride binding, reinforcement corrosion and carbonation.

The results indicated that the concomitant presence of chloride and sulfate salts and temperature significantly influences the durability performance of concrete by: (i) decreasing the chloride binding, (ii) increasing reinforcement corrosion, and (iii) accelerating the carbonation process. To avoid such deterioration, it is advisable to minimize both chloride and sulfate contamination contributed by the mixture ingredients. Due to the known harmful role of sulfate ions in decreasing the chloride binding and increasing reinforcement corrosion, limits on allowable sulfate contamination in concrete should also be established.

Key Words: Alkalinity, Chloride-Sulfate contamination, Carbonation, Humidity, Temperature

IN MEMORY

OF

MY FATHER

AND

PROFESSOR RASHEEDUZZAFAR

ACKNOWLEDGMENTS

I sincerely appreciate the help and guidance provided by late Professor Rasheeduzzafar in the conduct of this work. I am grateful to Professor C. L. Page for his helpful suggestions and comments.

The kind assistance provided by the Research Institute and the department of Civil Engineering, King Fahd University of Petroleum and Minerals is highly appreciated. Many thanks are also due to Dr. Abdulaziz I. Al-Mana for his support.

I am indebted to Dr. O. S. B. Al-Amoudi for his untiring efforts in reviewing this report at various stages of its preparation. A word of appreciation is also due to many of my friends and colleagues whose moral support provided an impetus for the completion of this work.

Lastly, but not the least, I would like to thank my family for providing me the much needed support and encouragement; without their patience this work would not have been completed.

TABLE OF CONTENTS

LIST OF TABLES

LIST OF FIGURES

CHAPTER 1

INTRODUCTION

1.1 DETERIORATION OF CONCRETE STRUCTURES IN THE ARABIAN GULF

Portland cement concrete has been extensively used to build the infrastructure needed for the modern development. The potential of using this material has been fully exploited by the construction industry and research was carried out to make concrete stronger and more economical. Researchers have been successful in this pursuit, in that the production of very high strength concrete, of the order of 100 MPa (14,500 psi), is now possible.

While cement industry's research and development efforts were totally diverted towards the production of energy-efficient and high-strength cements, the durability performance of such cements due to the resulting changes in the chemical composition was not studied. It was assumed that concrete produced by mixing of cement, aggregate and water can withstand all the weather and exposure conditions. Concrete was thought to be a maintenance-free material, until durability problems were reported from various parts of the world.

Notable among the case histories, where concrete was blamed for poor durability performance are the bridge decks in USA and Europe, and the deterioration of reinforced concrete structures in the coastal areas of the Arabian Gulf. It is estimated that more than $ 20 billions are needed for the repair and rehabilitation of highway structures in USA [1], and more than £ 600 millions for repairing road bridges in the UK [2]. The cost of repair and rehabilitation of reinforced concrete structures in the

Arabian Gulf is not very well documented, but undoubtedly, considerable resources have to be allocated towards restoring the useful service-life of concrete structures serving in this environment. While the deterioration of highway structures in North America and Europe is attributable to the use of deicer salts, the deterioration of concrete structures in the Arabian Gulf is caused by: (i) severe climatic and geomorphic conditions and (ii) incorrect material specifications and defective construction practices. In this respect, it is not out of place to mention that to meet the growing demand for infrastructure, specifications borrowed from other parts of the world were injudiciously used by the construction industry in this part of the world. The adequacy of the imported specifications was not questioned until after failures were observed within a short span of about 10 to 15 years [3].

The climate, which is characterized by high temperature and humidity conditions and large fluctuations in the diurnal and seasonal temperature and humidity, adversely affects concrete durability in the Arabian Gulf. The temperature can vary by as much as 20 °C during a typical summer day and the relative humidity ranges from 40 to 100% over 24 hours. These sudden and continuous variations in temperature and humidity initiate ever present cycles of expansion/contraction and hydration/dehydration which cause damage due to thermal and mechanical stresses. The damage to concrete due to these stresses is reflected by microcracking and enhanced permeability, which results in a tremendous increase in the diffusion of aggressive species, such as chloride, oxygen, carbon dioxide and moisture, towards the steel-concrete interface.

The other factor which contributes to the poor durability performance of concrete is the quality of local aggregates. Most of the aggregates available in the region is crushed limestone which is marginal, porous, absorptive, relatively soft and excessively dusty on crushing. These drawbacks are attributable to the source material, which comprises poor quality sedimentary outcrops of younger tertiary dolomitic limestone. The aeolin

dune and coastal sands form the main source of fine aggregate. These sands are essentially fine grained and have narrow grading. Nearly all the material passes No. 30 sieve and an appreciable portion, 10 to 20% passes No. 100 sieve. The fineness modulus is less than 1.3, (ASTM C 33 minimum is 2.3), and lies well outside the ASTM C 33 grading limits and is finer than zone 4 of BS 882 [4]. The excessive fineness of sand and its narrow grading lead to a gap-graded particle size distribution in the combined aggregate grading for nearly all the mixes made using local materials. The coastal sands are mainly of carbonate origin. These sands are usually absorptive, fine, poorly graded and are contaminated with chloride and sulfate salts. The grading characteristics of these sands are more or less similar to those of the dune sands [5].

Furthermore, the fine and the coarse aggregates are characterized by excessive dust content. Dust and excessive fines cause high water demand resulting in lower strength and greater shrinkage of concrete. Dust also forms a fine interstitial coating between the aggregate and the cement paste thereby weakening the bond at the aggregate-paste interface. This transition zone, being the weakest link of the concrete composite, may further lower concrete strength and quality [5].

Sometimes the climatic and geomorphic factors may combine to accelerate the deterioration processes. In the coastal flats, the groundwater table is relatively high and close to the ground surface. The capillary rise of moisture and frequent flooding in conjunction with high evaporation rate leaves a heavy crust of salt in the upper few feet of the soil. This leaves the soil, groundwater and atmosphere heavily contaminated with chloride and sulfate salts [3]. The concrete structures situated in coastal areas are also continuously exposed to the blowing winds which are charged with sea water and sea salts that can attack concrete chemically and physically.

In the aggressive environmental conditions of the Arabian Gulf, the predominant modes of concrete deterioration are: (1) corrosion of reinforcement, (2) sulfate attack, (3) salt weathering, and (4) cracking due to thermal gradients and plastic and drying shrinkage. However, the wide occurrence of deterioration due to reinforcement corrosion overshadows all other forms of concrete failure [6].

Since the aim of this study is to evaluate the influence of the Arabian Gulf environment on reinforcement corrosion further discussion in this chapter, will be concentrated on the factors influencing reinforcement corrosion.

1.2 CORROSION OF REINFORCEMENT IN THE ARABIAN GULF

Concrete provides both physical and chemical protection to the steel. The chemical protection is provided by the highly alkaline pore solution (pH > 13). At this high pH, a sub microscopically thin protective film of γ-ferric oxide is formed on the steel which protects it from corrosion. The physical protection is provided by the dense structure of the concrete which retards the diffusion of the aggressive species, such as oxygen, carbon dioxide, moisture and chloride, to the steel-concrete interface. The break down of the passive layer is brought about mainly by two factors. **Firstly,** it is due to the ingress of atmospheric carbon dioxide to the steel-concrete interface, and **secondly** due to the diffusion of the chloride ions. Field studies conducted at King Fahd University of Petroleum and Minerals (KFUPM) [3] attributed the presence of excessive chloride concentrations in the concrete to be the main cause of reinforcement corrosion.

Concrete construction in the coastal areas of the Arabian Gulf is continually exposed to ground and atmosphere contaminated with salts. Aided by capillary action and high humidity conditions, the salt-contaminated groundwater and the salt-laden airborne moisture and dew find an easy ingress into the concrete matrix. Further, the

salts also pollute the mix water and the aggregates thereby increasing the total salt content of the concrete. In the Arabian Peninsula, sulfates and chlorides occur at several horizons in the geological formations. Numerous salt domes in the Gulf constitute "built-in" sources of salt contamination especially when they are located in the zones of groundwater circulations [7]. Other sources of salt are the numerous sabkhas which constitute natural evaporating pans saturated with brines and which generate chloride, sulfate and carbonate minerals on their surface crusts. These salts are wind blown and have been found to heavily contaminate dune sands up to a distance of 40 kms from the shore.

Table 1.1 [8] compares chloride and sulfate content in the atmospheric air in Dhahran region (July-August) with that in Long Beach, California and Moorhead city along the Atlantic coast. Table 1.2 [8] compares the chloride content in the Arabian Gulf sea water with that in the Mediterranean sea and the Atlantic Ocean, respectively. It is seen that the chloride pollution in the ambient environment in Dhahran is about 490 times that in the air in a typical marine atmosphere in the USA. The chloride content in the Arabian Gulf is about 1.6 to 2 times as high as the sea water from the Mediterranean or the Atlantic.

Table 1.1 Chloride and sulfate content in atmospheric air of Arabian Gulf coast (Dhahran) and Atlantic Coast (Long Beach, Moorehead City), (July-August) [8]

Salt	Dhahran	Long Beach	Moorehead City
Cl^-*	63.2	0.13	0.13
SO_4^{--}*	33.8	0.32	0.54

* micro milligram per cubic meter of air

Table 1.2 Chloride content of various sea waters in parts per million [8]

Mediterranean	Atlantic	Arabian Gulf	Mean Sea Water
21,380	17,840	33,660	19,800

The ingress of chlorides, moisture and oxygen into the concrete matrix, in the Arabian Gulf, is further accentuated by the environmental conditions. Cracking of concrete due to plastic drying shrinkage, early thermal movements and subsidence stresses aid the diffusion of the aggressive species into concrete. These deterioration processes are further aided by the sharp temperature gradients on surfaces and the inner portions of the concrete. The changes in the diurnal and seasonal temperatures cause continuous thermal expansion and contraction cycles which may lead to the cracking of concrete. These expansion-contraction cycles become all the more damaging due to the thermal incompatibility of concrete components. The differential expansion and contraction movements of the aggregate material and hardened cement paste may set up tensile stresses far beyond the tensile capacity of concrete resulting in microcracking. Limestone, the predominantly used aggregate in this region, has a coefficient of thermal expansion of 1 $x10^{-6}$/°C. The coefficient of expansion for hardened cement paste is much higher (usually between 10 x 10^{-6} and 20 x 10^{-6}/°C). With the fall in temperature, tensile and compressive stresses are set up in the cement paste and the aggregates, respectively. With the rise in temperature, the stresses are not exactly reversed but tensile stresses are set up at the aggregate-paste interface tending to cause interface bond failure and significant microcracking around the transition zone. It has been shown by Hsu [9] that a volume change of 0.3% is enough to generate tensile stresses of the order of 800 psi at the aggregate-paste interface. Slate and Matheus [10] have determined volume changes of cement paste and concrete from the time of casting

to an age of 7 days. This work shows that volume changes even larger than 0.3% occur during setting and hardening of concrete. The authors [10], on the basis of a simple mathematical model, have inferred that tensile stresses of more than 250 psi for every 10 °C fall in temperature are set up in the concrete.

In summary, the environmental conditions in the coastal areas of the Arabian Gulf region are conducive for the initiation and propagation of reinforcement corrosion. Further, corrosion of reinforcing steel is mainly attributable to the excessive amounts of chlorides in the concrete which are contributed by the mix constituents or those entering the concrete from the external environment. However, a variety of other factors, such as temperature, sulfate contamination and carbonation may be expected to influence the mechanisms of corrosion of steel reinforcement.

1.3 EFFECT OF TEMPERATURE AND HUMIDITY ON REINFORCEMENT CORROSION

The extreme climatic conditions of the Arabian Gulf are particularly helpful to the chemical reactions involved in the reinforcement corrosion and other disintegration processes. The mean annual temperature is generally 8 °C above the value of 18 °C usually taken to define a hot desert. The summer air temperature frequently reaches 45 to 50 °C. The concrete surface temperature may increase due to solar radiation up to 70 °C [11]. The hot weather conditions in the Arabian Gulf may also cause increased water demand, slump loss and premature setting, resulting in cold joints and insufficient compaction and enhanced tendency for plastic shrinkage and pre-setting cracking in fresh concrete. Concrete cast and cured under hot weather conditions and not cured sufficiently thereafter may show as much as 30 to 40% reduction in strength. Any deficiency in curing, which may have negligible effect in mild climatic conditions, may permanently impair the quality of the cover concrete in hot weather conditions,

thereby weakening the protective shield against the ingress of aggressive species to the steel-concrete interface. High rates of evaporation of mixing and curing water cause significant sulfate and chloride salt concentrations near the surface when concrete is mixed and/or cured with brackish water which may result in sulfate attack and early initiation of reinforcement corrosion, particularly if steel is located near the surface. Thermal and drying shrinkage cracking are a common feature of concrete damage in this region.

The high temperature and humidity conditions in the Arabian Gulf accelerate the chemical reactions. The penetration of aggressive substances such as chlorides and carbon dioxide proceeds more rapidly. Studies [12] carried out on the effect of temperature and humidity on corrosion processes show that when circumstances are such that corrosion can occur, its rate is increased by high temperature and high humidity. The rate of corrosion appears to be sharply increased by an increase in temperature in the range of 20 to 40 °C, especially at high humidity. While this is so, data are lacking on the role of temperature on the mechanisms of reinforcement corrosion in concrete.

Atmospheric humidity also significantly influences carbonation-induced reinforcement corrosion. Low corrosion rates have been associated with dry conditions. It has been suggested that a critical relative humidity for corrosion exists above which extensive condensation occurs in the concrete pores and that corrosion is insignificant at lower humidity. Parrott [13] indicated that the corrosion rates are minimal for RH below 75%.

1.4 EFFECT OF SULFATE ON REINFORCEMENT CORROSION

Deterioration of concrete by sulfates can occur in either or both of the two ways: (a) by expansion and cracking due to the formation of ettringite; (b) by surface softening

due to the formation of gypsum [14]. The deterioration of the first type is due to the reaction of sulfate ions with tricalcium aluminate present in the cement. The second type is due to the formation of gypsum which is produced by the reaction of sulfates with calcium hydroxide. The reaction products have a greater volume than the compounds they replace. The increase in the volume due to formation of gypsum can be more than double the original volume, and that due to the formation of ettringite can be more than three times the original volume. While the effect of sulfate ions on deterioration of concrete has been considerably investigated their influence on corrosion of reinforcing steel has not been adequately researched. Studies conducted by Holden et al. [15] on the pore solution composition of pastes made with fixed quantities of chlorides and sulfates indicated an increase in the OH^- concentration due to inclusion of sulfates compared to the alkalinity of pore solution of cement pastes contaminated with only chloride salts. Their results also showed a substantial decrease in the chloride binding capacity of cements in which sodium chloride and sodium sulfate were mixed. These results reflect the tendency of sulfate ions to react preferentially with the C_3A of cement, thus inhibiting the formation of calcium chloroaluminate (Friedel's salt). Therefore, the corrosion risk is likely to be significantly increased in circumstances where concrete is contaminated with both chloride and sulfate salts. Al-Tayyib et al. [16] reported seven fold increase in corrosion activity in mild steel exposed to sulfate containing calcium hydroxide solutions over those containing chloride salts, particularly at high temperatures. Recent studies [17-19] conducted at KFUPM have indicated that sulfate ions significantly influence the mechanisms of chloride-induced reinforcement corrosion. While the sulfate concentration does not significantly influence the time to corrosion initiation, its presence significantly enhances the rate of reinforcement corrosion [20]. The results of the studies cited above have an important bearing on the durability performance of concrete structures in this region, as groundwater, aggregates and environment are heavily contaminated with both chloride and sulfate salts. These salts may be introduced into the concrete either through the mix constituents or they

may penetrate the hardened concrete from the service environment. Further, the groundwater table being shallow, the concrete components inadvertently get contaminated with chloride and sulfate salts.

1.5 EFFECT OF CARBONATION ON REINFORCEMENT CORROSION

Carbonation involves a reaction of atmospheric carbon dioxide with the $Ca(OH)_2$ and other cement hydration products to form insoluble $CaCO_3$ and water. This reaction results in a significant reduction in the pH of the electrolyte due to removal of hydroxyl ions from the pore water. At low pH, the protective γ-ferric oxide film is not formed and corrosion can occur. Factors influencing carbonation of concrete and the subsequent corrosion of embedded steel include: concrete mix design, improper curing, moisture condition, temperature and the presence of chlorides. For high quality, dry, or water saturated concrete, carbonation is normally not a problem.

Carbonation of concrete may be more rapid in hot dry environments compared to temperate climates [21-22]. The rate of carbonation is reported to be maximum at temperatures of 40 to 50 °C and relative humidity of 50 - 70%, which are typical of the environmental conditions in the countries along the Arabian Gulf [23]. In the presence of chlorides, accelerated reinforcement corrosion may occur in carbonated concrete, especially when it is subjected to wetting or drying or high humidity [24].

The importance of carbonation, which is a slow process under natural conditions, however, has grown in recent years owing to the increased atmospheric pollution and the aging of the structures. Also, no data are available on the interactive effect of chloride-sulfate contamination and hot-weather conditions on concrete carbonation and carbonation-induced reinforcement corrosion.

1.6 RESEARCH OBJECTIVES

While the effect of chlorides on reinforcement corrosion has been investigated by several researchers [25-34], sparse data related to the effect of carbonation, temperature and sulfate salts [16-17, 35-38] on mechanism of chloride-induced reinforcement corrosion are available. The meagre data developed on these aspects deal with the individual effects of these factors on corrosion of reinforcement. This may be due to the fact that in the temperate climatic conditions all these factors rarely act together to accelerate the reinforcement corrosion process. However, in the coastal areas of the Arabian Gulf, the daily and seasonal variations in the temperature and humidity regimes and the salt contamination in concrete contributed by aggregates and mix water combine together to accelerate reinforcement corrosion.

While the presence of sulfate salts may result in the liberation of chloride ions, owing to the preferential formation of calcium sulphoaluminate hydrates [24], the rate of corrosion may increase rapidly when the ambient temperature is increased from 20 to 40 °C. It has been suggested that an increase in temperature of 10 °C can lead to a doubling of the corrosion rate [39]. If this is the case, the corrosion rate in the Arabian Gulf climate may be expected to be up to four times that in Europe [25]. Also, higher rates of carbonation were observed in structures exposed to hot weather conditions [21,40].

Carbon dioxide and chlorides can act synergistically, in that carbonation can lower the pH of the pore water allowing chloride attack to occur at chloride concentrations lower than that required for corrosion in uncarbonated concretes [13]. Furthermore, carbon dioxide may release chlorides for corrosion initiation by decomposing calcium chloroaluminate hydrates formed due to the complexing of chlorides by tricalcium aluminate.

This research was conducted to investigate the synergistic effect of chloride and sulfate contamination, temperature, and carbonation on the mechanism of reinforcement corrosion. The specific objectives of this study were:

(i) to evaluate the effect of temperature on the pore solution composition in plain and blended cements, contaminated with chloride and sulfate salts,

(ii) to investigate the effect of temperature and chloride-sulfate contamination on reinforcement corrosion,

(iii) to study the synergistic effect of temperature and chloride-sulfate contamination on carbonation in plain and blended cements, and

(iv) to assess the conjoint effect of temperature, chloride-sulfate contamination and carbonation on reinforcement corrosion.

1.7 REPORT OUTLINE

This report presents the results of the experimental work carried out to achieve the research objectives as outlined above. ***Chapter 2*** describes the results of field and laboratory work carried out to evaluate the causal factors for deterioration of reinforced concrete structures in the Arabian Gulf. In ***Chapter 3***, the influence of chloride and sulfate contamination and temperature on the pore solution composition in plain and blended cements is discussed. The concomitant effect of chloride and sulfate contamination and temperature on reinforcement corrosion is evaluated in ***Chapter 4.*** In ***Chapters 5 and 6***, the influence of hot weather conditions and chloride and sulfate contamination on carbonation and reinforcement corrosion, respectively, are discussed. Finally, ***Chapter 7*** summarizes the findings of this study and provides recommendations for further research.

CHAPTER 2

DURABILITY PERFORMANCE OF CONCRETE IN THE ARABIAN GULF

2.1 DESCRIPTION OF THE PROBLEM

The poor durability performance of reinforced concrete structures in the coastal areas of the Arabian Gulf is now a well recognized fact. As pointed out in the earlier Chapter, the service conditions for concrete construction in this area are considered to be amongst the most aggressive in the world. The deterioration of concrete structures, and the consequent reduction in the useful service-life, is mainly attributed to reinforcement corrosion. Other forms of deterioration, due to sulfate attack, salt weathering and plastic shrinkage cracking, are not uncommon. However, the overwhelming number of cases of concrete failure due to reinforcement corrosion overshadow deterioration due to other causes. The environmental and geomorphical conditions of this region act together to form a very aggressive service environment for concrete. In such an environment, structures built with concrete, which can be rated as good in the temperate climatic conditions, can hardly serve for a decade or two [41].

The concrete durability problems in the Arabian Gulf region were first reported by Fookes and Collis [42,43] in 1975. They concluded that deterioration of concrete in this hot-humid environment is attributable to the environmental and geomorphical conditions. At the same time, Rasheeduzzafar et al. [3,44] and Al-Gahtani [45] conducted comprehensive condition surveys of 42 reinforced concrete buildings located on habitations along the coastal areas in the eastern Saudi Arabia. Serious deterioration was observed in buildings constructed within 10 to 15 years. These surveys indicated that only 26% of the 168 study areas exhibited slight or no deterioration. The main

causes of deterioration were attributed, in decreasing order of importance, to corrosion of reinforcement, sulfate attack, salt weathering, and cracking due to shrinkage and thermal gradients [46]. The laboratory investigation of the cores obtained from structures 22 to 27 years old indicated that chloride content, cover over reinforcing steel and concrete quality significantly controlled the life of the structure. In buildings more than 20 years old, severe cracking/spalling was observed in structures with 12.7 mm cover. The degree of deterioration was observed to decrease with increasing cover thickness. Rebar corrosion in concrete with 5% water absorption, determined according to BS 1881, was observed to be three times that in concrete with 3% water absorption. The loss of metal due to rebar corrosion in concrete of 13,000 Ω.cm electrical resistivity was 12% after 20 years, whereas it was 80% in concrete with electrical resistivity of 600 Ω.cm [3,45].

Pollock et al. [47], Fookes et al. [40] and Kay et al. [48] inspected several reinforced concrete structures, mainly in the United Arab Emirates. They classified the cracking of concrete into two major categories in terms of their severity: (1) progressive; those caused by diurnal temperature cycles, drying shrinkage, structural distress, alkali-silica reaction and corrosion of reinforcing steel, and (2) non-progressive; those caused by plastic settlement, plastic shrinkage, thermal hydration, shrinkage and crazing.

In the subsequent sections, some of the cases of deterioration of reinforced concrete structures are reported with a view to exploring the possible mechanisms of deterioration. A summary of the possible causes of concrete failure and their implication to this study is also presented.

2.2 CASE STUDIES

This section details the field and laboratory investigations conducted to examine the performance of in-service concrete structures. The test programme included visual examination of the structures, field and laboratory tests to assess the quality of concrete used and evaluation of the severity of the environment. Field observations included visual inspection of the structures to determine the form and nature of deterioration. Wherever possible, concrete core specimens were retrieved from the structures. In some cases, concrete powder was collected using a percussion type drill machine for chemical analyses.

2.2.1 Pier Foundations (Case study 1)

These structures are circular reinforced concrete pier foundations which are about 2 metre in diameter and 10 m deep [49]. The piers are overlaid by a cap which is about 1.2 metre in diameter and 45 cm high. These foundation structures, which support high tension power cables, are buried in a very corrosive sabkha environment. The water table in this region is less than 1 m below grade for most of the year. After about 5 years of service, profuse cracking was observed on the cap surface in most of the structures inspected. These cracks originated from the edges of the stub angle and extended radially to the other edges of the foundation cap. The average width of cracks on the cap surface varied from 0.17 to 0.33 mm (Figure 2.1). About 12 of these concrete structures were examined in detail. More than 150, 75 mm Ø concrete specimens were cored from the structures for testing.

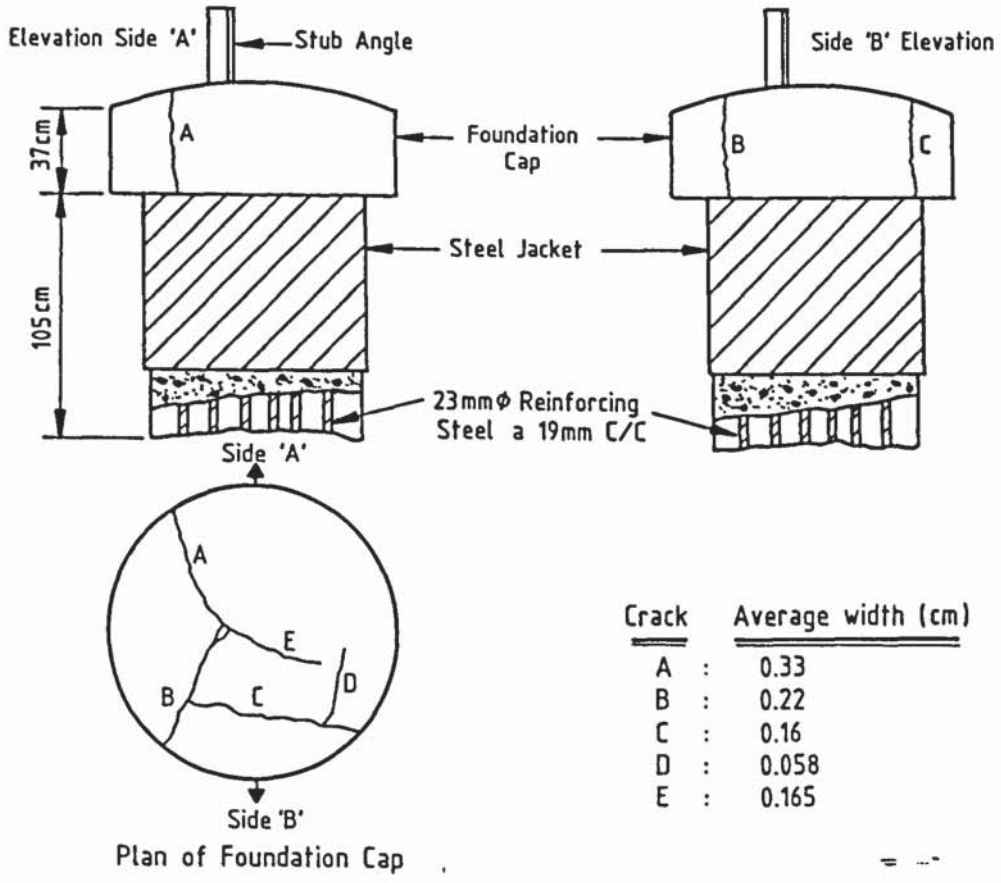

Figure 2.1 Details of the pier foundations inspected (Case Study 1)

The range of physical properties of concrete from these structures is shown in Table 2.1. The compressive strength, pulse velocity, electrical resistivity, absorption, and permeability results indicated that the concrete used in the foundation elements was of medium to good quality [50]. Figure 2.2 shows a typical chloride concentration profile in a pier. The acid-soluble chloride concentration was in the range of 0.27 to 3.3% by weight of concrete. The extremely high concentrations of chlorides in the concrete were attributed to the cumulative effect of the following factors: (a) brackish groundwater was added to the concrete mix during construction, (b) the chloride content of the constituent materials was very high, (c) curing was carried out with brackish water, and (d) infiltration of chloride-bearing groundwater into the hardened concrete had occurred. The groundwater which had diffused through the pier structure evaporated at the grade level leaving the salt in the concrete. The significant build up of the salt concentration at the grade level caused severe corrosion at these locations.

Table 2.1 Results of laboratory tests on concrete from pier foundations (Case Study 1)

Parameter	Range of Values
Water-cement Ratio	0.5 - 0.55
Cement Content (kg/m^3)	314 - 340
Compressive Strength (MPa)	25 - 38
Pulse Velocity (m/s)	3300 - 3800
Concrete density (kg/m^3)	2000 - 2100
Electrical Resistivity (Ω.cm)	670 - 2120
Chloride Concentration (% concrete)	0.22 - 3.30
Sulfate concentration (% concrete)	0.19 - 1.40

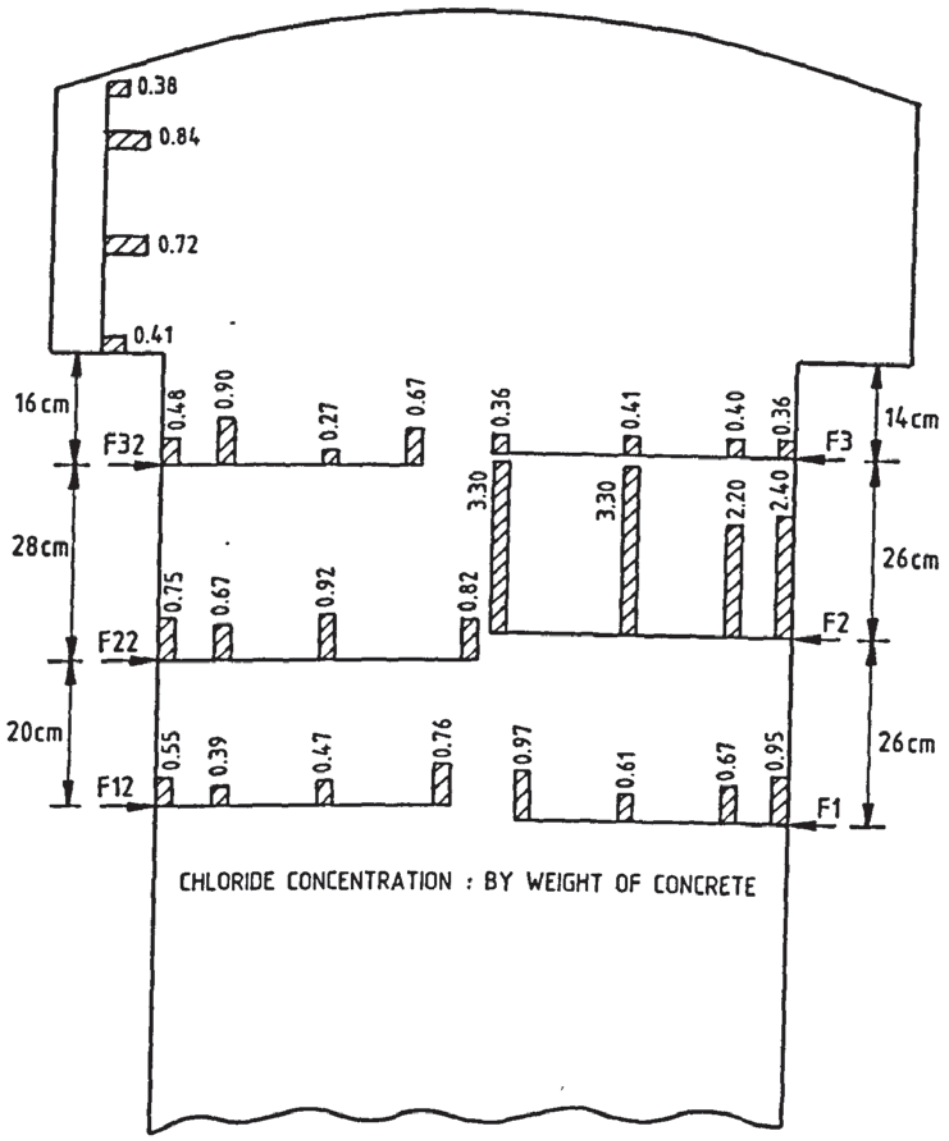

Figure 2.2 Chloride concentration profile in a pier (Case Study 1; Chloride concentration: % wt. of concrete)

2.2.2 *Underground Utility Structures (Case Study 2)*

Severe damage due to chloride-induced reinforcement corrosion was observed in some of the 2500 underground reinforced concrete utility structures [49, 51-52]. These utility structures carry 34.5 to 115 kV power cables and are part of an electrical distribution network. These structures have an internal dimension of up to 8 m and are as much as 6 m below the ground surface (Figure 2.3). The groundwater table in most of the areas is less than 1.5 m below grade. These structures, which are generally octagonal in shape, are spaced on a grid of approximately 200 to 300 m apart.

More than 24 of these utility structures, placed in a highly corrosive sabkha soil, were examined. These structures were in service for about 5 years when deterioration of concrete, mainly on the roof slab, beams and walls, was observed. Cracking of concrete due to corrosion of reinforcing steel on the walls and beams was evident on the severely deteriorated structures. Microcracking, leakage of water from the joints and cable conduits, and salt staining on the walls, floor and roof slab were observed in all the deteriorated structures.

Table 2.2 shows the results of the tests carried out on some of these structures. The data on physical properties indicated that the quality of concrete used in most of the structures was good, except in a few cases it was of medium to good quality [50]. The electrical resistivity of concrete in as-retrieved condition was low in most of the cases, indicating a risk of high corrosion rates.

The chloride and sulfate analysis (Figure 2.4 and 2.5) indicated that the salt concentration was usually high on the surface of the components and decreased with depth. The salt concentration was also high in the lower parts of the walls and in the

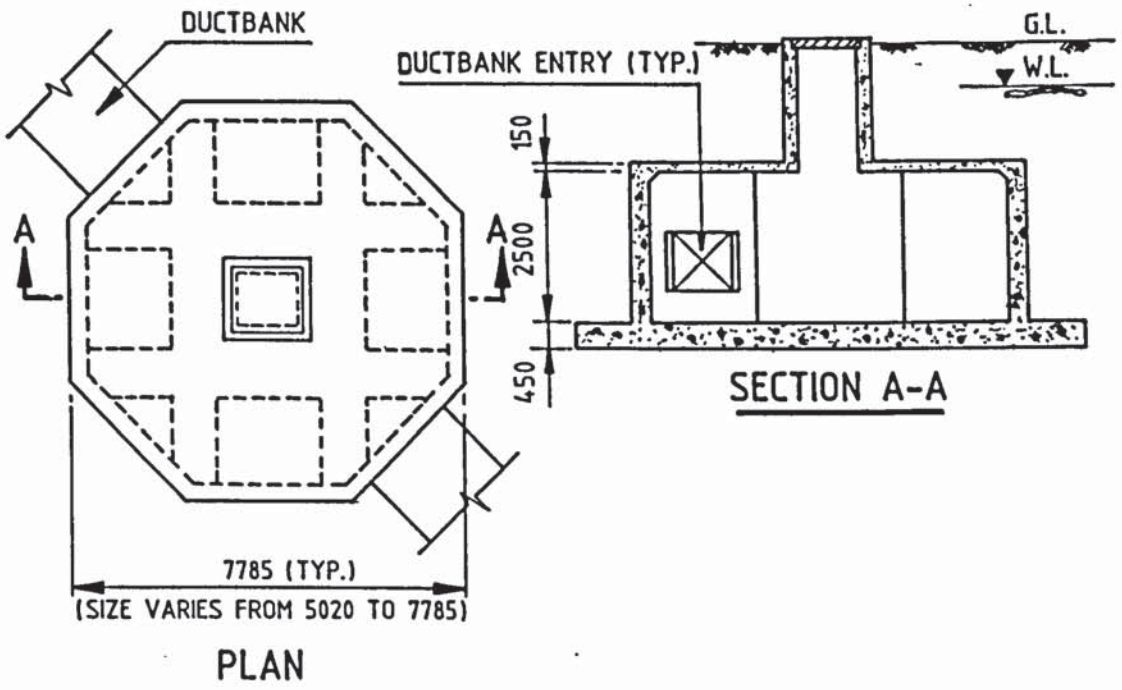

Figure 2.3 Dimensions of a typical underground utility structure (Case Study 2)

Table 2.2: Results of tests carried out on concrete from a typical underground utility structure (Case Study 2)

Parameter	Typical Value
Dry density (kg/m^3)	2235
Pulse velocity (km/sec)	4.0
48-hour Absorption (%)	5.53
Volume of permeable voids (%)	13.22
Chloride concentration (% concrete)	0.01 - 0.24
Sulfate concentration (% concrete)	0.5 - 1.2

base slabs. At 75 mm depth, the chloride concentration was several times the threshold value in most of the structures investigated. The high concentration of salts in the components was contributed by the saline groundwater seeping into the structural components which evaporated through the atmosphere leaving them deposited in the concrete. Deterioration due to sulfate attack was not indicated in any of the structures, apparently due to the use of sulfate resisting cement.

2.2.3 Columns (Case Study 3)

In this case study, the causal factors for deterioration of columns of a three storey building were evaluated [49]. The footings of these columns are founded in a highly corrosive sabkha soil. After four to five years of construction, cracking and spalling of concrete on the columns due to reinforcement corrosion was evident.

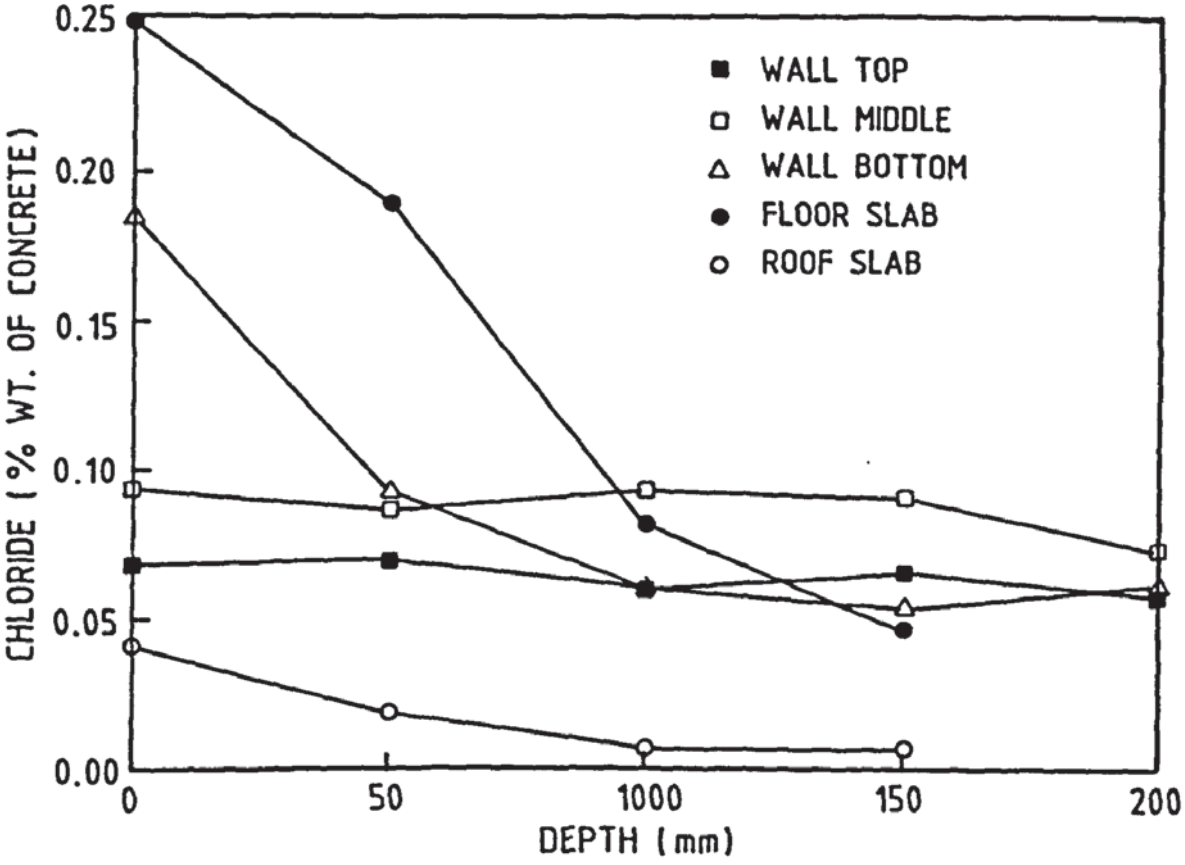

Figure 2.4: Chloride concentration profile in concrete from an underground utility structure (Case Study 2)

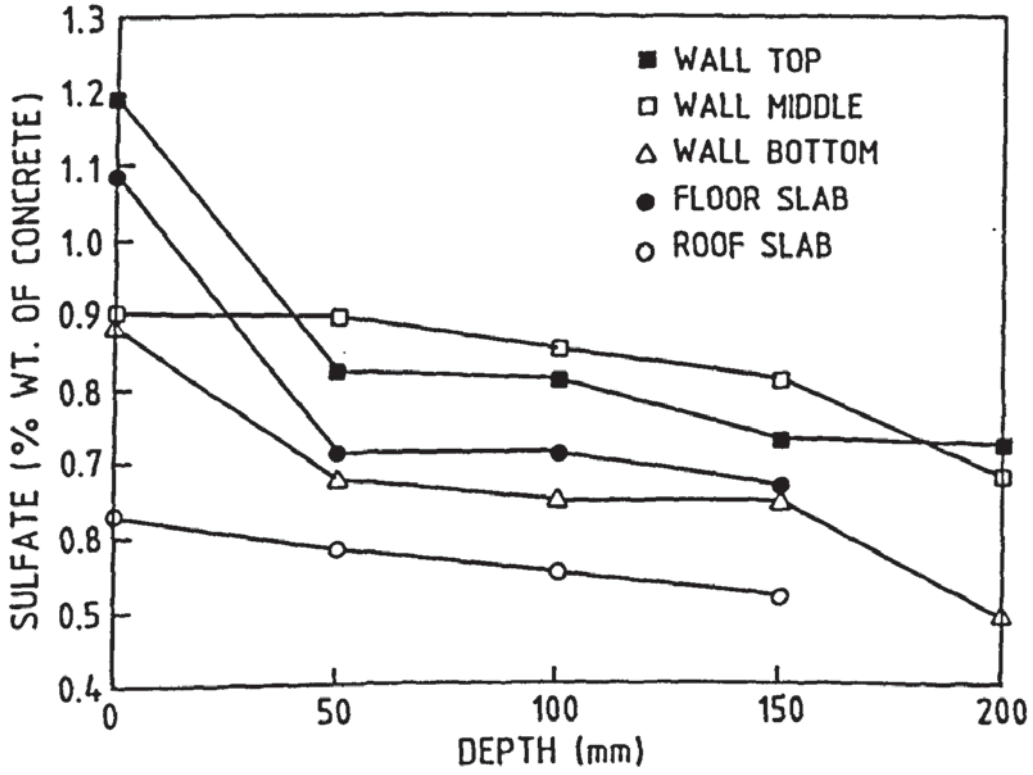

Figure 2.5: Sulfate concentration profile in concrete from an underground utility structure (Case Study 2)

While all the columns exhibited signs of deterioration of varying degree, the footings were in good condition. Four columns, which indicated moderate to severe deterioration, were selected for detailed examination. Cracks along the longitudinal axis were observed on one of these columns. In another column, localized reinforcement corrosion, at about 1 m below the top of the footing, was evident. The concrete in the spalled portions of this column appeared to be very weak and the reduction in the diameter of one of the corroded bars was about 20%. The compressive strength data (Table 2.3) indicated that the concrete used in the columns and footings was of good quality [50].

Table 2.3 Physical properties of concrete (Case Study 3)

Parameter	Range of Values
Compressive strength (MPa)	25 - 40
Electrical resistivity (k.Ω.cm)	3.6 - 11
Volume of permeable voids (%)	5.9 - 12.6
Rebound hammer number	22 - 50
Pulse velocity (km/sec)	3.5 - 4.6
Chloride (% concrete)	0.01 - 0.42
Sulfate (% concrete)	0.32 - 1.60

2.2.4 Shore Line Protection Structures (Case Study 4)

This is a reinforced concrete wall used for shoreline protection [49]. Minor cracks were observed in the wall after about two years of service.

A summary of the field and laboratory tests is shown in Table 2.4. The average compressive strength of concrete in all the members, as indicated by the Schmidt

hammer readings was in the range of 50 - 60 MPa, indicating that very good quality concrete was used in these structures [50]. The concrete cover over the reinforcing steel was more than that usually required for marine structures (> 75 mm). The chloride concentration was high at the surface and decreased with depth as shown in Figure 2.6. In most cases, the chloride concentration was lower than the threshold value of 0.03% by weight of concrete at depths of over 50 mm. The sulfate concentration indicated a similar trend. The sulfate concentration was higher than the threshold value of 0.6% by weight of concrete. Since sulfate resisting cement blended with fly ash was used, there was no noticeable damage due to sulfate attack. The corrosion potentials were in the range of -95 to -606 mV against copper-copper sulfate (CSE) reference electrode. The corrosion potentials on rebars in the splash and tidal zones were more negative than those in the atmospheric zone. The chloride concentration in concrete at a depth of 75 mm (approximate depth over reinforcing steel) is compared with the corrosion status based on ASTM C 876 in Table 2.5. Probability of reinforcement corrosion (values more negative than -350 mV CSE) is indicated in the components where the chloride concentration was more than 0.04% by weight of concrete.

Table 2.4 Test results on concrete from shore line protection structures (Case Study 4)

Parameter	Range of Values
Rebound hammer number	44 - 67
Average cover thickness (mm)	74 - 103
Chloride concentration (% concrete)	0.001 - 0.43
Sulfate concentration (% concrete)	0.1 - 4.7
Corrosion potentials (CSE)	-95 - -606

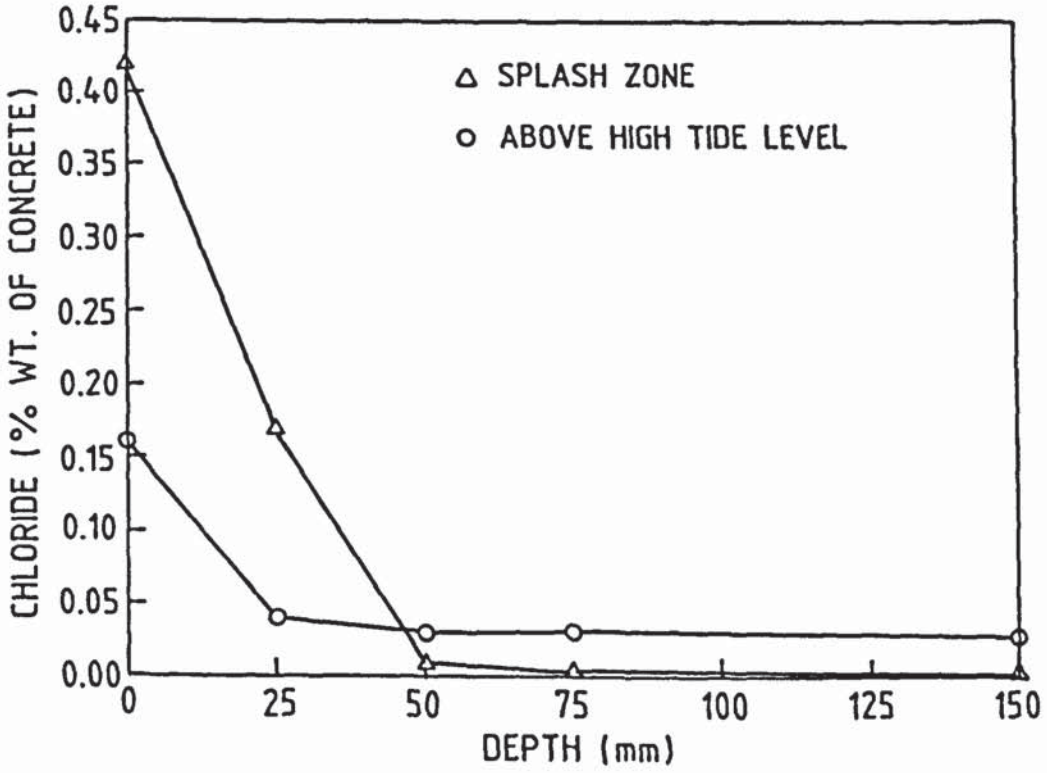

Figure 2.6 Chloride concentration profile in the shoreline structure (Case Study 4)

Table 2.5 Relationship between chloride content and corrosion status (Case Study 4)

Structural Component/Visual Condition	Chloride Concentration at 75 mm Depth (% wt. Concrete)	Corrosion Status*
Beam/Sound	0.001	Uncertain
Beam/Stained	0.008	Active/uncertain
Beam/Cracked	0.003	Uncertain/no corrosion
Panel/Sound	0.020	Uncertain
Panel/Stained	0.050	Active
Panel/Cracked	0.040	Active

* Based on ASTM C 876 criterion

2.2.5 Foundations of a Reinforced Concrete Building (Case Study 5)

This case study pertains the concrete deterioration in the foundations of a reinforced concrete building [53]. This building is a five storey reinforced concrete structure and measures 90 x 90 m and is supported by 256 columns located at a grid of 6 m in each direction. The construction is mainly of cast-in-place concrete columns and slabs and was completed in 1982. The foundations were constructed on compacted sub-grade. The concrete contained 380 kg/m^3 of sulfate resisting cement. The concrete was designed for a 28-day compressive strength of 25 MPa (3600 psi). The reinforcing bars were uncoated deformed with a yield stress of 420 MPa (61,000 psi). The water table was below the footing at the time of the construction. A layer of crushed aggregate and polyethylene sheeting was placed below the footings as a preventive measure. The concrete deterioration in the form of cracking, along the reinforcement, at the grade level on the columns was first observed in 1988. It was noted from

piezometers, installed at the site during this investigation, that the groundwater level had risen after the construction due to irrigation of the heavily landscaped areas around the building.

Selected columns, twelve in number, were exposed for detailed investigation. The average concrete compressive strength was in excess of the specified strength of 25 MPa. Resistivity values of concrete were as low as 500 Ω.cm. Concrete cover over reinforcement was either equal to or more than the specified cover of 50 mm. The average acid-soluble chloride content in the columns below grade at the depth of reinforcement was more than 0.4% by weight of cement. The high chloride concentration in the concrete components, particularly at the grade level indicated that the groundwater seeped from the sides of the footings and columns, where no protection was provided, and diffused through the below-grade portions and evaporated at the grade level, leaving the salts deposited in concrete. Abundant supply of moisture, due to capillary action and oxygen at the grade level contributed to the localized reinforcement corrosion.

2.2.6 Sea Water Cooling Canals (Case Study 6)

This structure is used to supply cooling water to industrial plants in a growing industrial complex. This is a dual canal system, one branch supplying the fresh water, while the other removing the used water, and is 10.6 km in length. Stains were observed on the walls of the canal after about 7 years of service [52,54]. Extensive concrete delamination due to reinforcement corrosion was also observed on the walls. Protective measures, such as cathodic protection, using sacrificial anodes and impressed current systems, were employed to prolong the service life of this structure [54].

2.3 CONCLUSIONS FROM THE CASE STUDIES

The case studies cited above indicate poor performance of concrete in the Arabian Gulf environment, the predominant cause for the concrete deterioration being reinforcement corrosion, initiated by salt inclusion either at the initial stages of mixing or due to ingress from the service environment. While this phenomenon is mainly related to presence of chloride ions, the high sulfate concentration in the environment might have accelerated the deterioration process. The mechanisms of such an acceleration, due to the simultaneous presence of chloride and sulfate, on reinforcement corrosion is not yet fully elucidated. Another factor of interest in the environmental conditions of the Arabian Gulf, which significantly influences the deterioration related to reinforcement corrosion, is the high ambient temperature. The effect of high temperature as well as its variation on the deterioration processes have been discussed in Chapter 1. The high ambient temperature may also influence the rate of diffusion of groundwater into the underground structural components, namely footings and submerged portions of the columns. At the grade level, the moisture evaporates leaving the salts behind. The saline groundwater is then wicked into the concrete maintaining a dynamic water profile/equilibrium [24]. The chlorides tend to concentrate at or about the ground level, leading to excessive corrosion at this location. The evaporation/wicking process, described above, occurs due to the loss of moisture from dry concrete exposed to the high ambient temperatures above the grade. The presence of sulfate ions in the groundwater also significantly influences the mechanisms of reinforcement corrosion in such situations. Thus, it will be worthwhile to investigate the simultaneous effect of sulfate and temperature on chloride-induced reinforcement corrosion. Also, blended cements are increasingly used in the Arabian Gulf to produce dense and impermeable concrete. The effect of chloride-sulfate contamination and temperature on the pore solution chemistry of these cements needs also to be investigated.

Further, the elevated temperature in the Arabian Gulf may also significantly influence the carbonation of concrete. Meagre data are available on the effect of chloride-sulfate contamination and temperature on carbonation. Such a study is also particularly important to evaluate the performance of blended cements in terms of their resistance to carbonation, since pozzolanic action is liable to reduce the alkalinity of the pore solution in these cements.

CHAPTER 3

EFFECT OF TEMPERATURE AND CHLORIDE-SULFATE CONTAMINATION ON THE PORE SOLUTION CHEMISTRY

As pointed out in the preceding Chapter, the deterioration of concrete structures in the Arabian Gulf is primarily attributed to chloride-induced reinforcement corrosion. The chlorides may be introduced by the mix ingredients, namely aggregates, mixing and curing water, and admixtures. Alternatively, they may penetrate the hardened concrete from the service environment. While chloride ions are known for depassivating the steel, the concomitant presence of sulfate ions can alter the kinetics of reinforcement corrosion. Substructural concrete components in the Arabian Gulf are normally in contact with groundwater contaminated with chloride and sulfate salts and are prone to the concomitant effect of these two aggressive species. The conjoint presence of high temperature, chloride, and sulfate salts provides an unique environment for concrete structures in the Arabian Gulf. Another factor, which is predominant in the Arabian Gulf environment, is the high ambient temperature. As such, research to study the concomitant effect of these factors on reinforcement corrosion is highly desirable.

In this Chapter, the effect of temperature and chloride-sulfate contamination on the pore solution composition in the ordinary and blended portland cements was investigated. Research to evaluate the synergistic effect of sulfate and chloride ions and temperature on the pore solution composition in blended cements, such as fly ash, silica fume and blast furnace slag, is all the more important for this area as these materials have to be imported and work out to be costlier than ordinary portland cement (OPC).

The cement mortar specimens were contaminated with chloride and chloride plus sulfate salts. For comparison, specimens contaminated with only sulfate salts were also evaluated. Since sodium chloride and sodium sulfate are the major source of contamination contributed by the mixture constituents, mainly the aggregates and mixing/curing water, these salts were used to provide the chloride and sulfate anions.

3.1 EXPERIMENTAL WORK

3.1.1 Experimental Variables

The experimental work reported in this Chapter was divided into two series.

In *Series I*, the effect of temperature and chloride as well as chloride plus sulfate contamination on the pore solution composition in two ordinary portland cements and one sulfate resisting portland cement (SRPC) was investigated. The experimental variables are detailed in Table 3.1.

Table 3.1: Experimental variables to evaluate the pore solution composition in ordinary and sulfate resisting Portland cements

Variable	Details
Specimens	Mortar specimens made with SRPC, OPC-A, and OPC-B; (C_3A: 3.5, 8.5, and 14.5%)
Contamination Levels	0% 0.8% Cl^- 1.5% SO_3^{--} 0.8% Cl^- + 1.5% SO_3^{--}
Exposure Temperatures	25, 40, 55 and 70 °C
Pore Solution Extrusion	7, 14, 28, 56, and 84 days
Pore Solution Analyses	OH^-, Cl^-, and SO_4^{--}

Selected mortar specimens were analyzed using X-ray Diffraction (XRD) and Differential Thermal Analysis (DTA) techniques.

The chemical composition of the cements used is presented in Table 3.2.

Table 3.2: Chemical composition of cements

Constituent (weight percent)	SRPC	OPC-A	OPC-B
SiO_2	22.00	20.52	19.92
Al_2O_3	4.08	5.64	6.81
Fe_2O_3	4.24	3 .80	2.09
CaO	64.07	64.35	64.70
MgO	2.21	2.11	1.30
SO_3	1.96	2.10	2.61
Loss on Ignition	0.80	0.70	0.90
K_2O	0.31	0.36	0.56
Na_2O	0.21	0.19	0.28
Na_2O equivalent	0.41	0.43	0.65
C_3S	54.57	56.70	57.57
C_2S	21.75	16.05	13.68
C_3A	3.50	8.52	14.50
C_4AF	12.90	11.56	6.36

In *Series II*, the effect of temperature and chloride as well as chloride plus sulfate contamination on the pore solution composition of blended cements was investigated. The experimental variables for this series are detailed in Table 3.3, while Table 3.4 shows the chemical composition of the pozzolanic materials.

As can be seen from Table 3.4, the SO_3 content of the blast furnace slag is higher than that in the other pozzolanic materials. In order to take account of this difference, the total SO_3 content in all the cements was adjusted to 6%. Further, mortar specimens

made using OPC-A, contaminated with 6% SO_3, were also cast to compare the results of blended cements with ordinary portland cement.

Table 3.3: Experimental variables to evaluate the pore solution chemistry in contaminated blended cement mortar specimens

Variable	Details
Cements Investigated	OPC (C_3A: 8.5%)
	ASTM C 618 Type F fly ash cement (20% cement replacement)
	ASTM C 618 Type C fly ash cement (20% cement replacement)
	Silica fume blended cement (10% cement replacement)
	Blast furnace slag cement (70% BFS)
Contamination levels	0%
	0.8% Cl^-
	0.8% Cl^- + 6.0% SO_3^{--}
Exposure Temperature	25, 40, 55 and 70 °C
Pore solution extrusion	After 90 days
Pore solution Analysis	OH^-, Cl^-, SO_4^{--}

3.1.2 Specimen Preparation

Dune sand of specific gravity 2.62, absorption 0.57% and fineness modulus 1.3 was used in the cement mortar specimens. A sand to cementitious material ratio of 2.0, (cement content of 1000 kg/m^3 of mortar) and effective water to cementitious materials ratio of 0.50 was used in all the mortar mixes. In the blended cements, the pozzolanic

materials were used as a replacement of cement. In the fly ash cement mortar specimens, 20% fly ash was used as a replacement of cement. In the silica fume cement mortar specimens, 10% cement was replaced with silica fume, while blast furnace slag cement contained 70% BFS and 30% OPC. 50 mm Ø and 75 mm height cylindrical mortar specimens, cast in plastic vials, were used for extracting the pore fluid and measuring the chloride, sulfate and hydroxyl ion concentration. The sample containers were sealed from all sides to eliminate evaporation of water.

Table 3.4: Chemical composition of the pozzolanic materials

Constituent (weight %)	FAC*	FAF*	BFS*	SF*
SiO_2	51.3	52.3	27.7	92.5
Al_2O_3	24.1	25.2	12.8	0.4
Fe_2O_3	2.0	4.6	1.2	0.4
CaO	14.6	10.0	44.0	0.5
MgO	2.0	2.2	8.8	0.9
SO_3	0.8	0.6	3.1	0.5
Loss on Ignition	0.6	0.4	0.9	2.6
K_2O	3.1	0.1	0.1	0.4
Na_2O	0.3	0 .1	0.4	1.1
Na_2O equivalent	2.3	0.1	0.5	1.4

* FAC: Class C fly ash; FAF: Class F fly ash; BFS: Blast furnace slag; SF: Silica fume

Chloride additions were made by dissolving the required quantities of analar grade sodium chloride, while sodium sulfate was used to obtain the required sulfate concentration. The cementitious materials and sand were mixed in a mortar mixer till a uniform mix was obtained and then placed in the plastic vials. The plastic vials were then tamped lightly to eliminate entrapped air and consolidation of the mixture. After 24 hours of laboratory conditioning, the plastic vials were placed in ovens maintained at 25, 40, 55, and 70 °C till the time of test.

3.1.3 Pore Solution Expression and Analysis

After the designated exposure periods, mortar specimens were retrieved from the oven and directly placed on the base of a high pressure pore solution extrusion devise, similar to that described by Barneyback and Diamond [55], and loading was started immediately. The pressure applied through the piston was gradually increased and sustained till sufficient pore solution was collected. The expressed pore electrolyte, which issued from the fluid drain at the base of the apparatus, was collected in a plastic syringe. Care was taken to avoid undue exposure of the solution to air, and the specimens obtained were stored in sealed plastic tubes till the time of analysis.

The pore solution was analyzed for the following:

1. OH^- concentration by titrating the pore solution against 0.01 M nitric acid. Phenolphthalein was used as an indicator. A burette with a least division of 0.02 ml was used for titration. The titration of the pore solution was carried out after suitable dilution with deionized water. The actual molarity of the nitric acid was determined by titrating against 0.01 M NaOH.

2. Chloride ion concentration using the spectrophotometric method [56]. 0.1 ml of the pore solution was diluted to 10 ml using deionized water. To this solution, 2 ml ferric sulfate indicator and 2 ml ammonium thiocyanate was added. The mixture was mixed slowly and cautiously by swirling the beaker and then kept undisturbed for about 30 minutes before the absorption reading was taken on a Spectronic Model UV 21 spectrophotometer at a wave length of 460 nm against deionized water. The chloride concentration was computed using a computer program which corresponded to a calibration curve prepared earlier using a standard chloride solution. The pore solution extracted from

mortar specimens contaminated with sodium chloride and sodium chloride plus sodium sulfate was serially diluted so that the chloride concentration was less than 10 µg/l.

3. Sulfate concentration using spectrophotometric method outlined in Standard Methods for Analysis of Water and Waste Water, published by the American Water Works Association (AWWA) [57]. The pore solution was diluted and then a buffer solution was added and absorption measured using a spectrophotometer at a wave length of 420 nm. Barium chloride was then added to the solution and mixed for a period of one minute and then the solution was placed in the spectrophotometer and the absorption measured after 5 minutes. The net absorption was used to calculate the sulfate concentration from the calibration curve prepared using a standard sulfate solution. The pore solution extruded from mortar specimens contaminated with sodium sulfate and sodium sulfate plus sodium chloride was serially diluted to maintain the sulfate concentration within the measuring range.

Pore solution was expressed from two specimens for each exposure period and temperature. The average values of OH^-, Cl^- and SO_4^{--} are reported.

3.1.4 X-Ray Diffraction

X-ray diffraction technique was used to monitor the effect of temperature and chloride-sulfate contamination on the phase composition in cements. This is a quantitative analysis method primarily used for determining the weight fractions of crystalline phases down to about 1%.

X-ray diffraction (XRD) analysis was performed on a Phillips PW 1700 automated diffractrometer with a monochromator and spinner. Diffraction patterns

were generated on a vertical goniometer attached to a broad focus X-ray tube with a copper target operating at 45 kV and 30 mA. The analysis is computer assisted so that the interplanar spacing values can be corrected for the instrument error function by analyzing a silicon standard and subsequent quantitative analysis. The mortar specimens were powdered with an agate pestle and mortar and sieved over a #100 (150 μm) sieve to collect the cement. A homogenous sample of this powder was packed into a sample holder and scanned from 4 - 80° 2θ at a speed of 0.01 2θ/sec. In powdered form, many grains come into orientation and the quality of the diffraction pattern is greatly improved. The phase identification process involves calculating the most likely match score for a given phase based on peak intensity and peak position when compared to a database of standard phases, while the weight fraction is calculated by comparing the intensity of the most intense peaks of that phase with standards.

3.1.5 Differential Thermal Analysis

The differential thermal analysis (DTA) technique is a means of measuring the amount of heat evolved or absorbed and the temperature at which these changes take place within a material. The temperature difference between a test substance and reference material is measured as a function of temperature while the substance and the reference material are subjected to a controlled temperature heating. A number of phenomena, such as decomposition, and phase change may take place in a material when heated at a constant rate. Thermogravimetry (TG) is a technique in which the change in mass of a substance is measured as a function of temperature while it is subjected to controlled heating.

Characteristic of decomposition phenomena is the appearance of an endothermic peak in a DTA curve with a corresponding weight loss. Phase change from crystalline

to amorphous is indicated by the presence of an exothermic peak without any weight loss.

The equipment used for thermal analysis was a simultaneous thermal analyzer (STA-429) manufactured by Netzch, Germany. It performs thermogravimetry and differential thermal analysis simultaneously. About 100 milligrams of powdered specimen was tested with alumina as a reference material. The temperature was raised at a uniform rate of 10 °C/min, from room temperature to 1000 °C. In the thermograms, the weight loss and temperature are plotted simultaneously.

3.2 RESULTS AND DISCUSSION

3.2.1 Pore Solution Analysis

3.2.1.1 OH^- Concentration

The OH^- concentration in the SRPC mortar specimens exposed to 25 °C are shown in Figure 3.1. The OH^- concentration in the contaminated specimens was more than that in the uncontaminated specimens. The OH^- concentration in the specimens contaminated with sodium sulfate was more than that in the specimens contaminated with sodium chloride plus sodium sulfate. The OH^- concentration in the latter specimens was, however, more than that in the specimens contaminated with only sodium chloride. Figures 3.2 through 3.4 show the OH^- concentration in the specimens exposed to 40, 55 and 70 °C. These data also indicated a trend similar to that observed in the specimens exposed to 25 °C.

The high OH^- concentration in the pore solution in the contaminated specimens is attributed to the cation type associated with the sulfate and chloride ions. When sodium chloride and/or sodium sulfate are added to cement, Cl^- and/or SO_4^{--} ions react with the cement hydration products, while Na^+ cations are released in the pore solution.

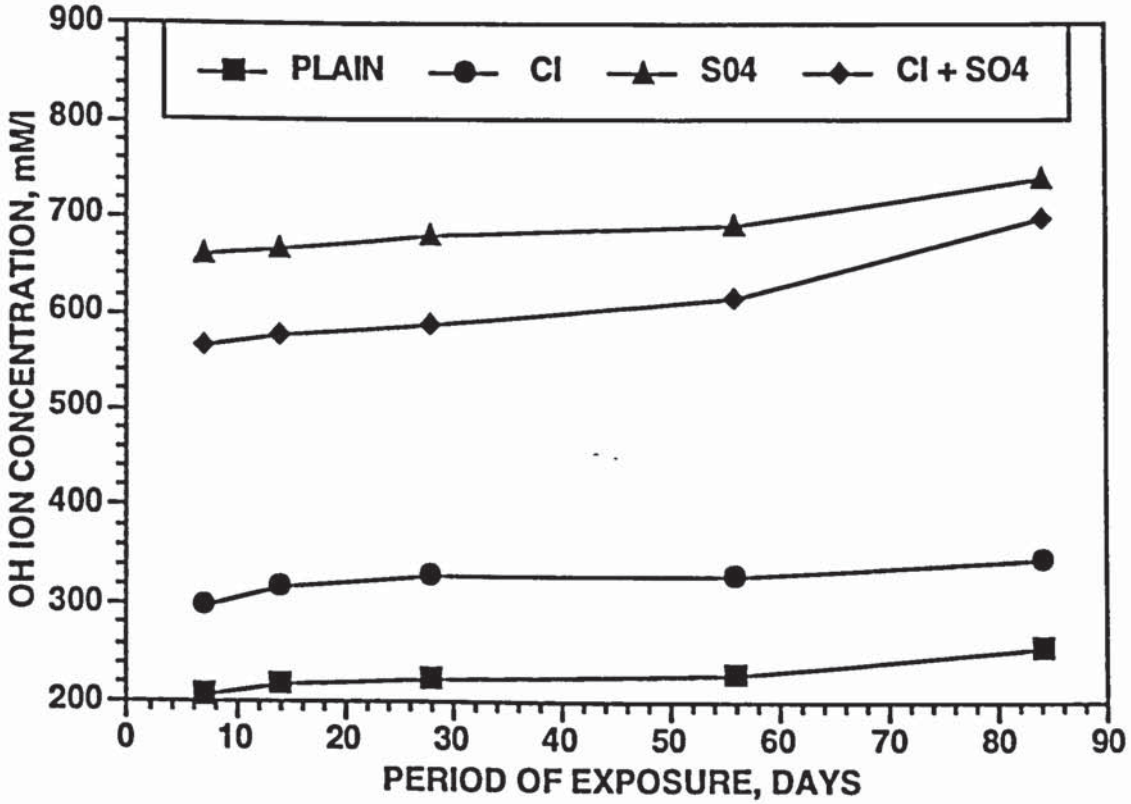

Figure 3.1: Variation of OH^- with age in SRPC mortar specimens exposed to 25 °C

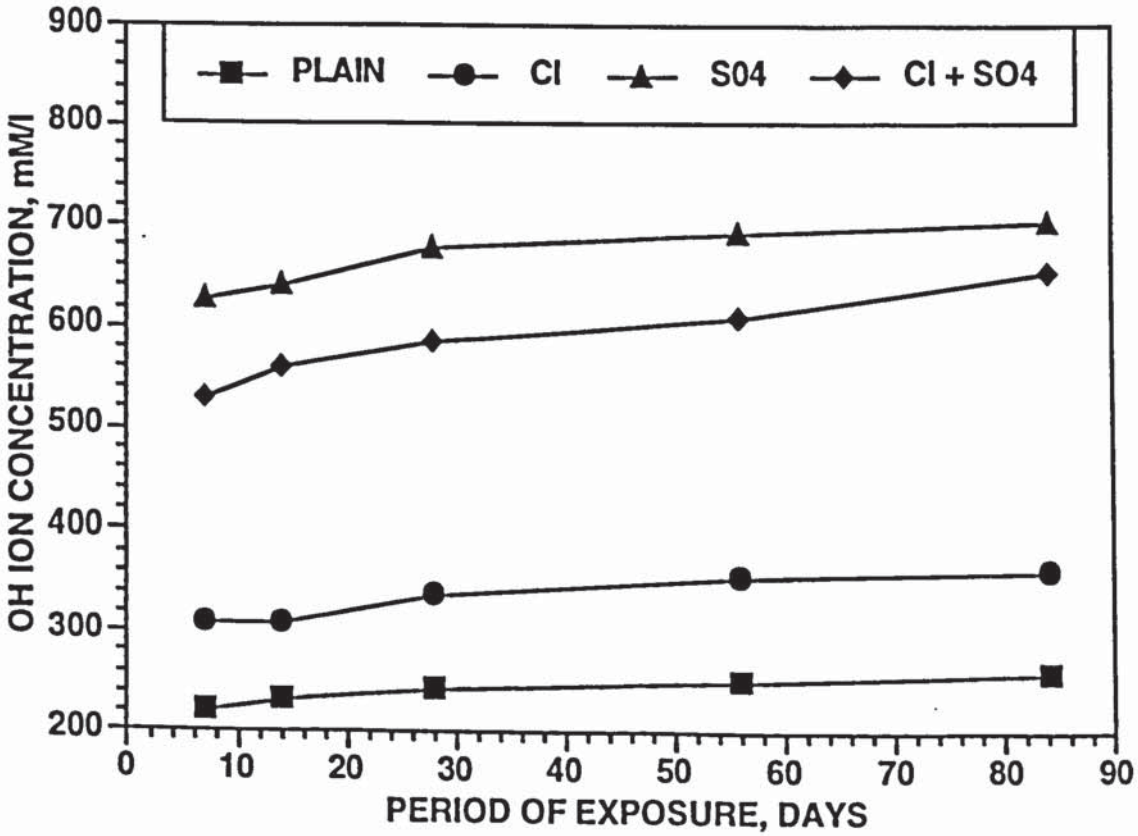

Figure 3.2: Variation of OH^- with age in SRPC mortar specimens exposed to 40 °C

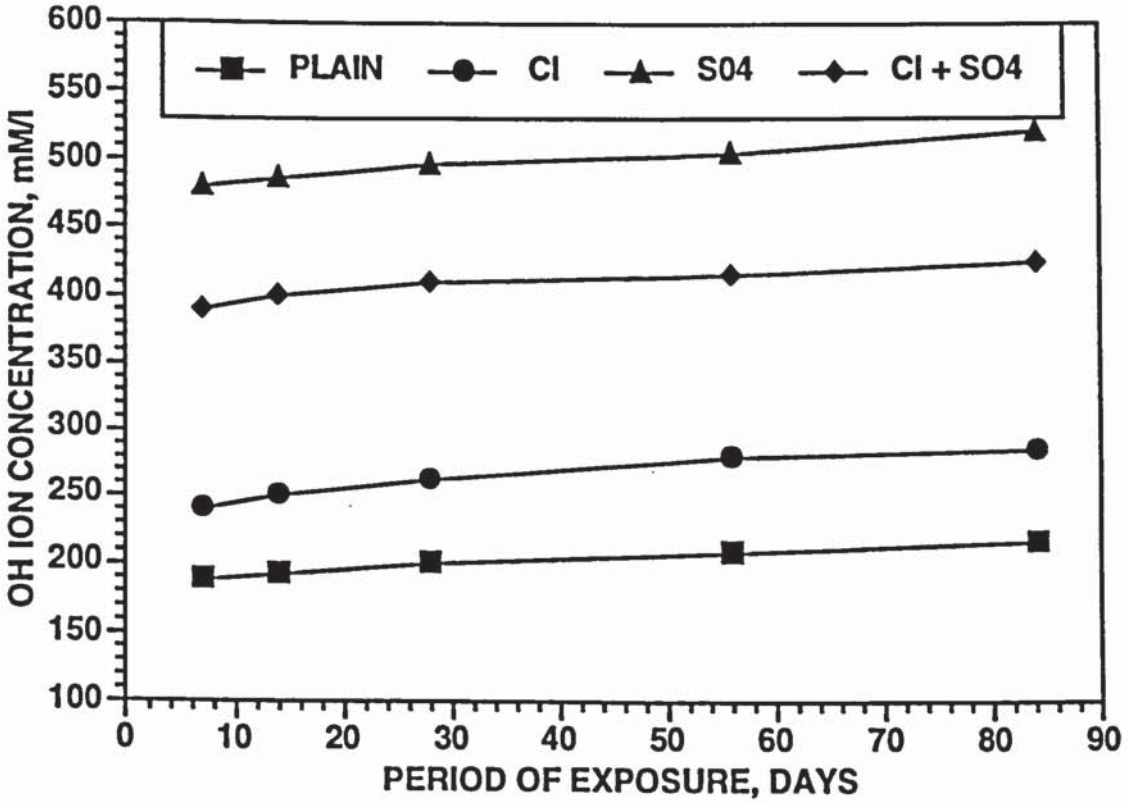

Figure 3.3: Variation of OH^- with age in SRPC mortar specimens exposed to 55 °C

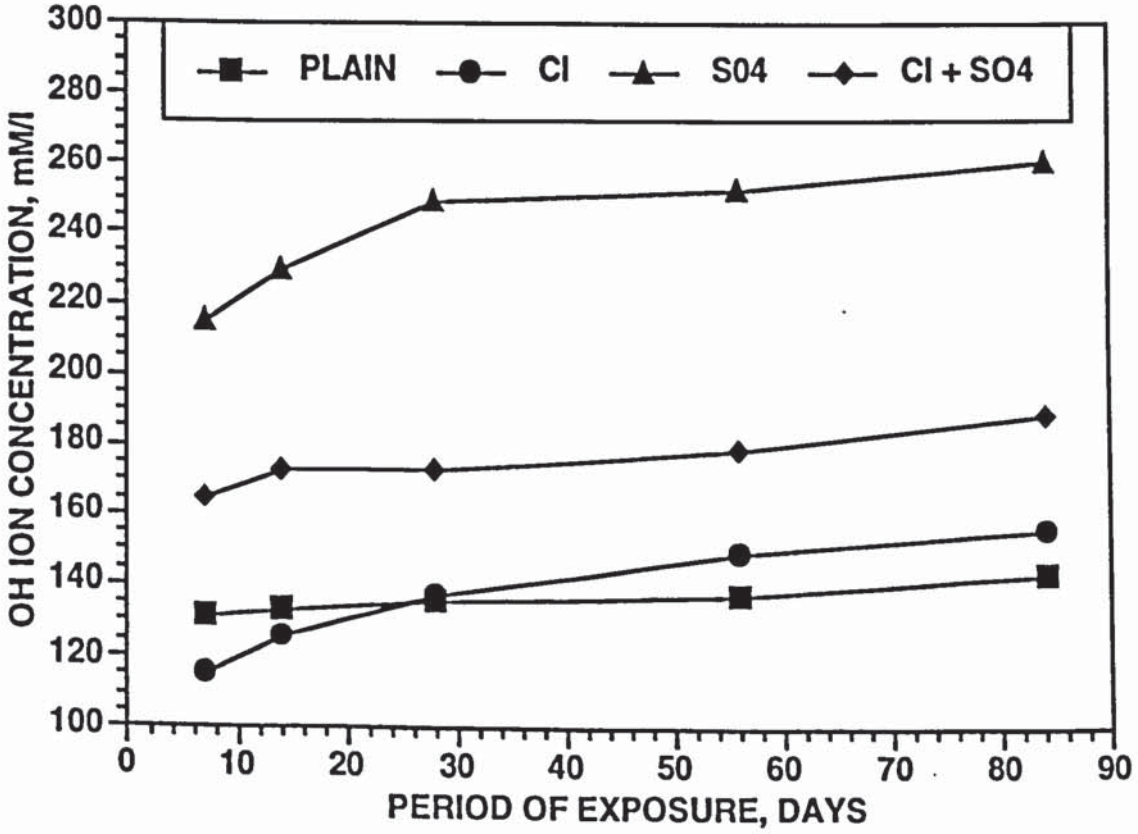

Figure 3.4: Variation of OH^- with age in SRPC mortar specimens exposed to 70 °C

Yonezawa et al. [58] indicated that the increase in the OH^- concentration in the chloride-contaminated cements is attributable to the formation of calcium-chloro aluminate (Friedel's salt) as shown below:

$$2NaCl + Ca(OH)_2 \rightarrow CaCl_2 + 2Na^+ + 2OH^- \quad (3.1)$$

$$3CaO.Al_2O_3.10H_2O + CaCl_2 \rightarrow 3CaO.Al_2O_3.CaCl_2.10H_2O \quad (3.2)$$

They attributed the increase in the OH^- concentration in the pore solution of the specimens contaminated with sodium chloride to the affinity between negative ion-exchangers and Cl^-, OH^- and SO_4^{--} ions as proposed by Kakihana and Mori [59]. The affinity increases in the following order:

$$SO_4^{--} > Cl^- >> OH^- \quad (3.3)$$

According to Equation 3.3, Cl^- ions easily replace the OH^- in negative ion-exchangers. The negative ion-exchange between Cl^- and OH^- can be expressed by the following equation [7]:

$$R\text{-}OH^- + Na^+ + Cl^- \dashrightarrow R\text{-}Cl^- + Na^+ + OH^- \quad (3.4)$$

Where R is an ion-exchanger.

According to Equation 3.4, NaCl added to concrete or mortar transforms to NaOH while Cl^- ions are fixed with the ion exchanger.

Kayyali et al. [60] supported the increase in the OH^- concentration in the pore solution of cement paste specimens contaminated with sodium chloride using Debye-Huckel theory [61] and indicated that when the NaCl concentration was increased, the OH^- concentration also increased.

The OH^- concentration in the uncontaminated and contaminated SRPC mortar specimens are plotted against exposure temperature in Figure 3.5. The OH^- values plotted in this figure represent the average of the concentrations measured at various periods of exposure. The OH^- concentration in both the contaminated and uncontaminated specimens indicated no significant change as the exposure temperature was increased from 25 to 40 °C. However, when the exposure temperature was raised to 55 °C, the alkalinity was significantly reduced. At 70 °C, the difference in the OH^- concentrations in the contaminated and uncontaminated specimens narrows down. The reduction in alkalinity of the pore solution with increasing temperature, particularly above 40 °C, indicates that the reaction of NaCl and/or Na_2SO_4 with the cement hydration products is inhibited at elevated temperatures (55 °C and above).

The decrease in the OH^- concentration in the uncontaminated specimens may be attributed to the instability of calcium sulpho-aluminate hydrate formed due to the reaction of gypsum, normally added to regulate the setting time of cement with C_3A, leading to an increase in the sulfate concentration in the pore solution. When sulfate ions are released into the aqueous phase, electrical neutrality necessitates either the removal of an equivalent quantity of cations or fixation of other anions, amongst which hydroxyl ions constitute the main available species. This effect has been shown by Herr and Wieker [62], who observed that when the temperature was increased from 20 to 60 °C, the OH^- concentration decreased from 600 mM/l to about 400 mM/l, after 180 days of hydration. The difference of 200 mM/l OH^- was balanced by an increase in the sulfate ion concentration of 100 mM/l . Similar results indicating the reduction in the OH^- concentration in the pore solution of cement paste specimens, exposed to temperature of 55 °C and above, have been indicated by Luke and Glasser [63].

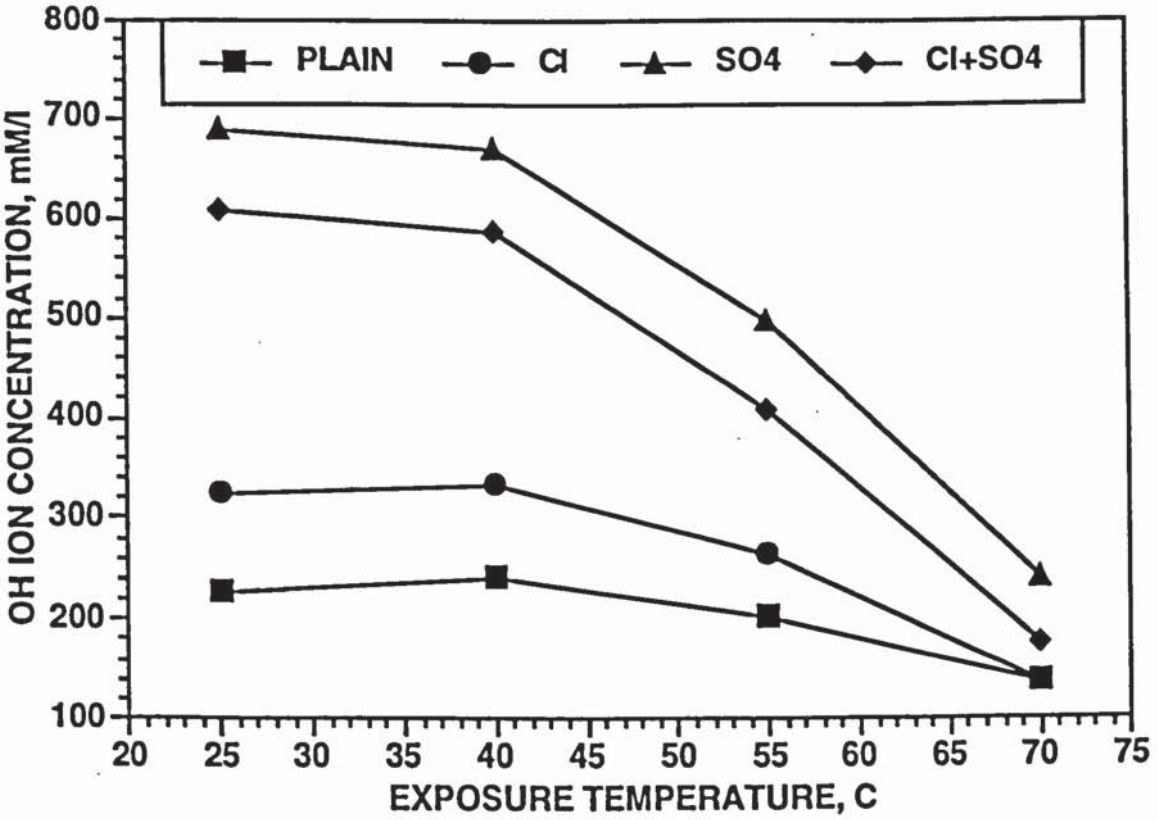

Figure 3.5: Variation of OH^- with exposure temperature in SRPC mortar specimens

The OH^- concentration in the pore solution extruded from OPC-A (C_3A: 8.5%) mortar specimens are shown in Figures 3.6 through 3.9 and the variation in the OH^- concentration with exposure temperature is plotted in Figure 3.10. These data indicated a trend similar to that indicated by SRPC mortar specimens (Figures 3.1 to 3.5).

Figures 3.11 through 3.14 show the OH^- concentration in OPC-B (C_3A: 14.5%) mortar specimens. Figure 3.15 shows the effect of temperature on the OH^- concentration in these specimens. These data also indicated a decrease in the alkalinity of the pore solution with increasing temperature.

The OH^- concentration in the blended cement mortar specimens is plotted against exposure temperature in Figures 3.16 through 3.20. The OH^- concentration in the specimens contaminated with sodium chloride plus sodium sulfate was more than that in the uncontaminated specimens and those contaminated with only sodium chloride. Further, a reduction in the OH^- concentration with increasing temperature was observed in these cements also.

The data in Figures 3.16 through 3.20 indicated that the OH^- concentration in all the blended cement mortar specimens was less than that in the ordinary portland cement mortar specimens. This reduction in the OH^- concentration may be attributed to the reaction between the $Ca(OH)_2$ and the pozzolanic materials. The occurrence of such a phenomenon in blended cements has been reported by several investigators [15,60,64-67]. Studies conducted by Diamond [68] and Holden et al. [15] indicated that the addition of fly ash to portland cement paste causes a small reduction in the pH of the pore solution. Diamond [68] noted that the alkalies included in the fly ash do not cause a significant increase in the pore solution alkalinity and, thus, of the pH value. Nixon et al. [69] indicated a reduction in the OH^- concentration of cement blended with PFA; the OH^- decreasing with the cement replacement level. Their investigation, however,

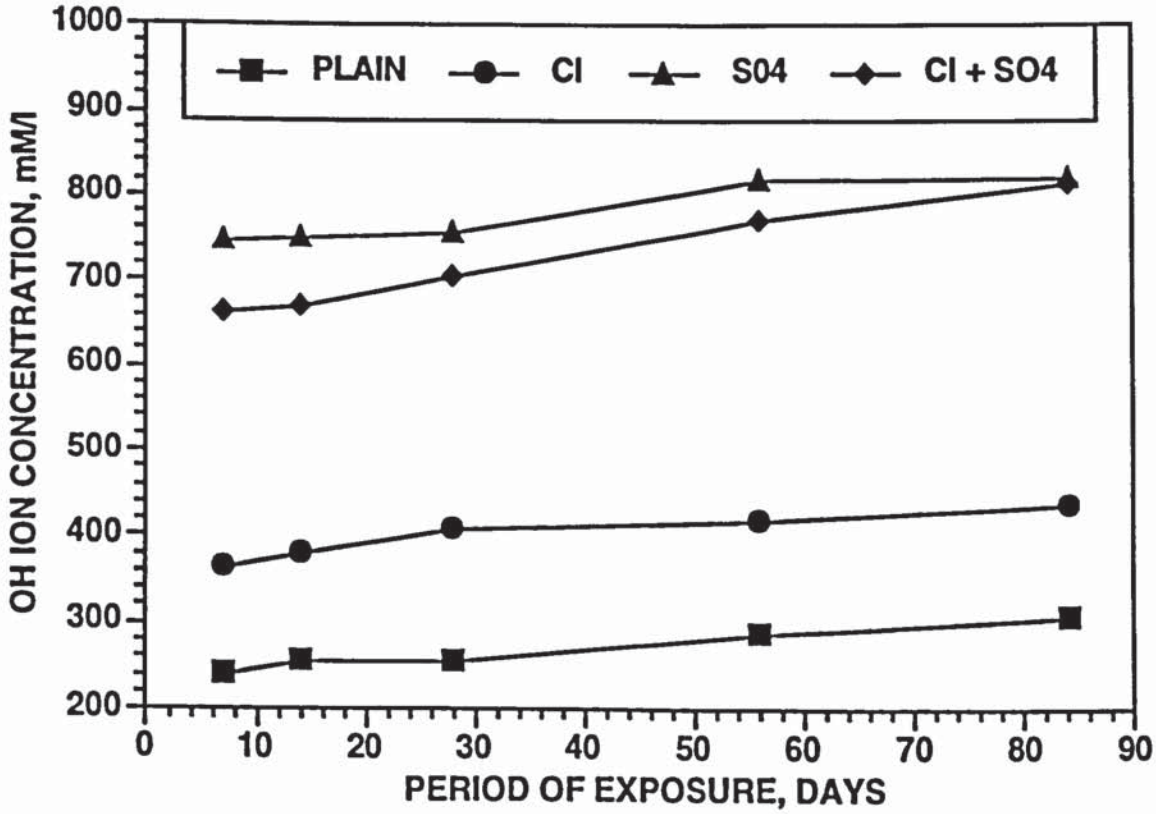

Figure 3.6: Variation of OH^- with age in OPC-A mortar specimens exposed to 25 °C

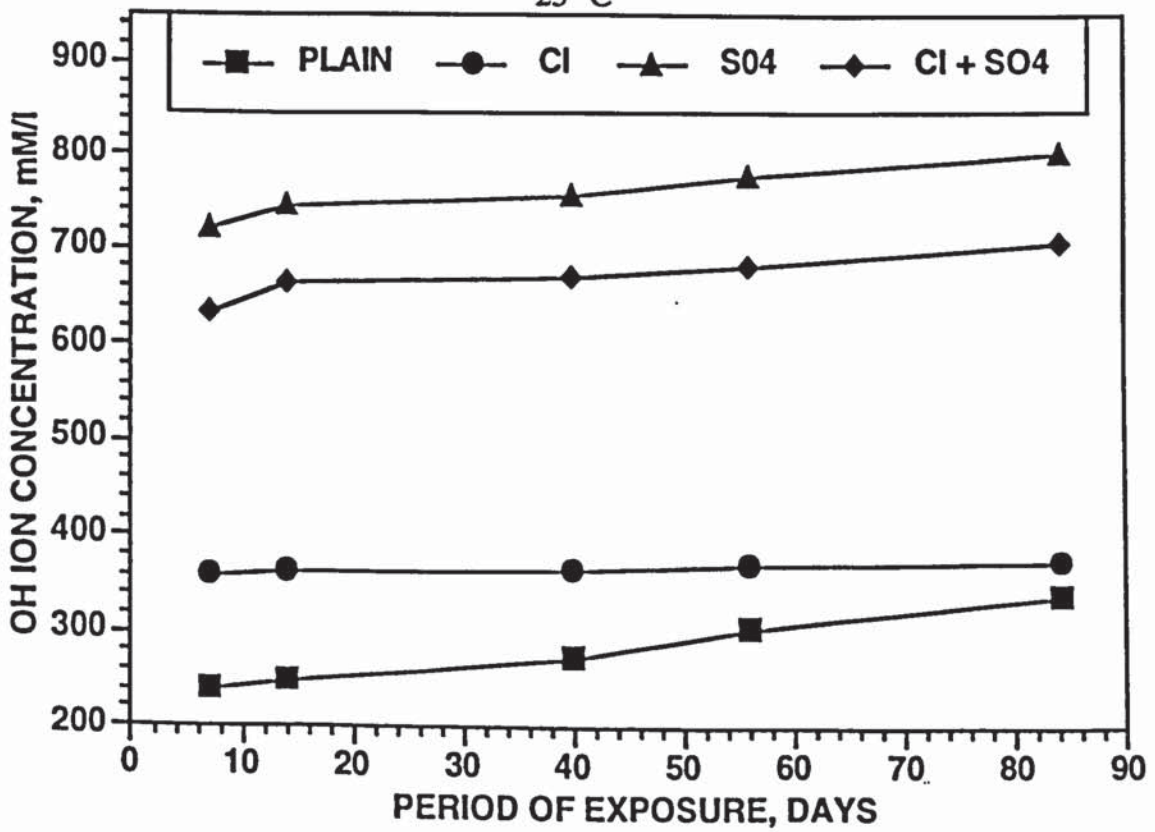

Figure 3.7: Variation of OH^- with age in OPC-A mortar specimens exposed to 40 °C

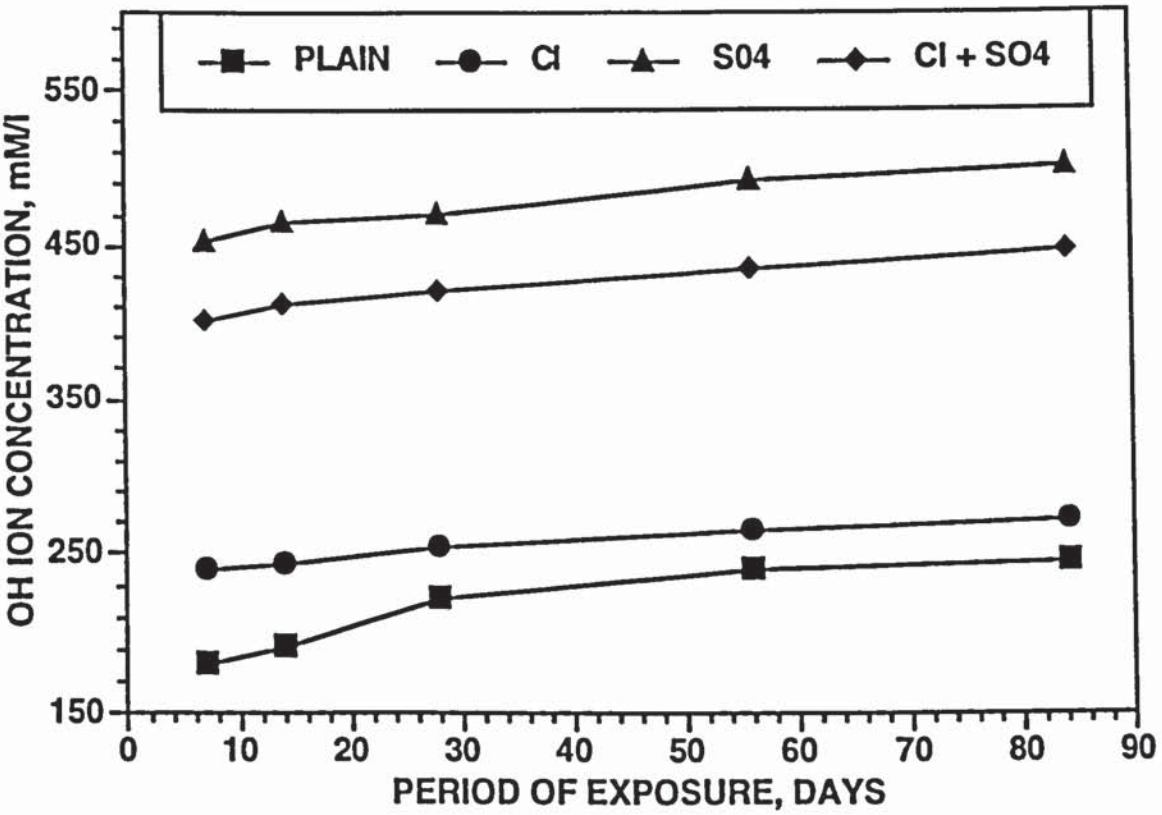

Figure 3.8: Variation of OH^- with age in OPC-A mortar specimens exposed to 55 °C

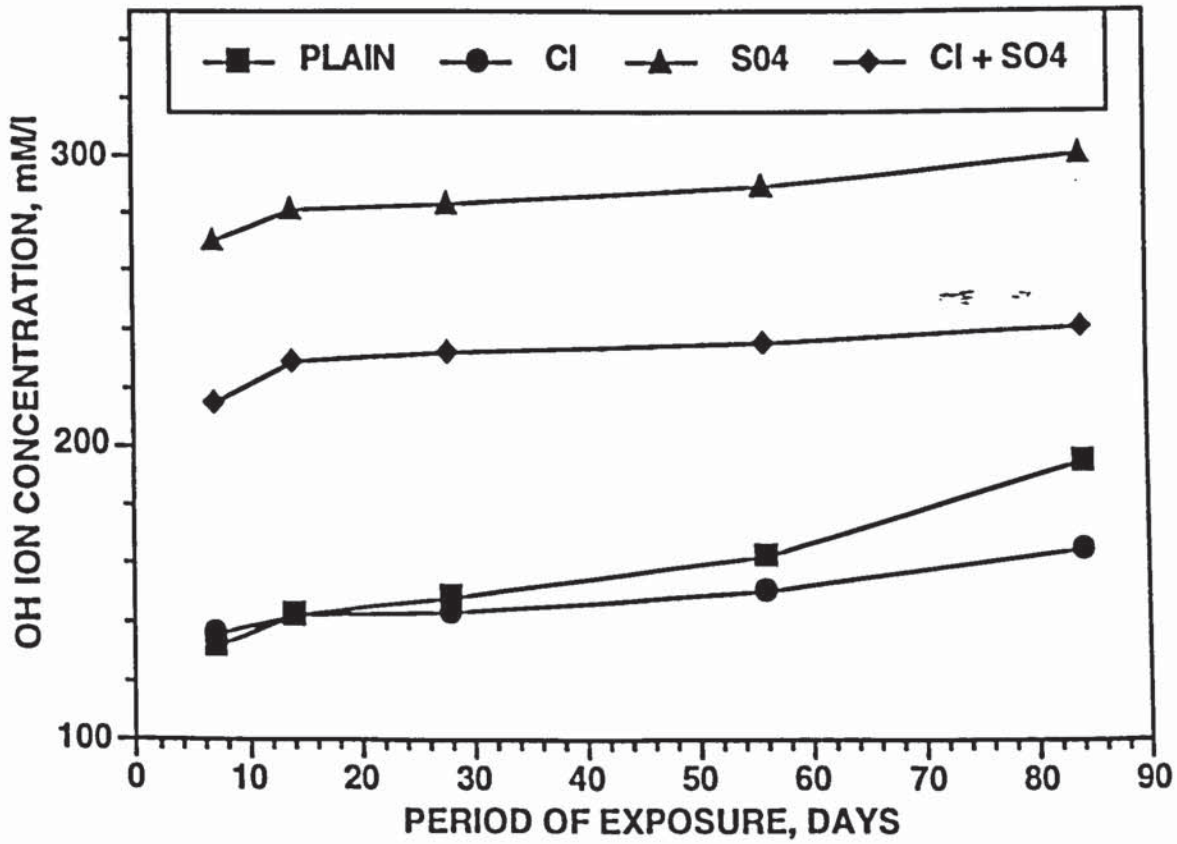

Figure 3.9: Variation of OH^- with age in OPC-A mortar specimens exposed to 70 °C

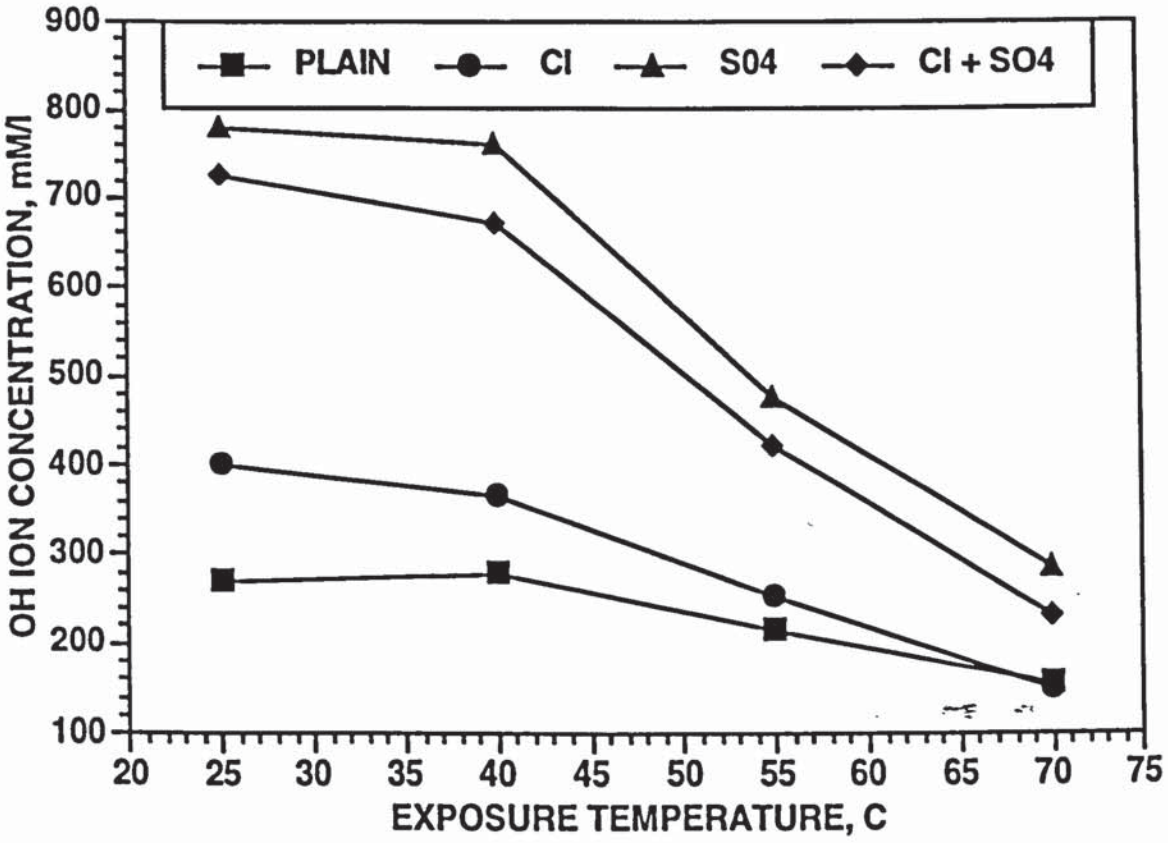

Figure 3.10: Variation of OH^- with exposure temperature in OPC-A cement mortar specimens (SO_3: 1.5%)

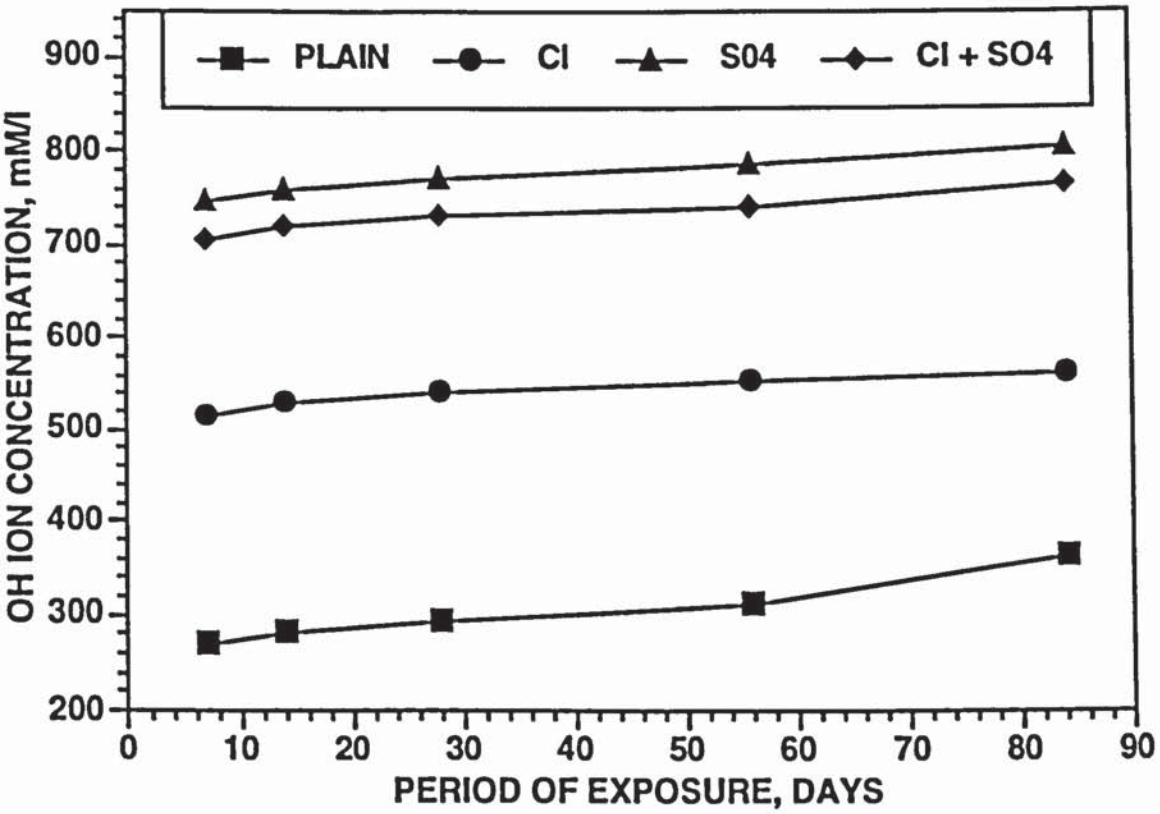

Figure 3.11: Variation of OH^- with age in OPC-B mortar specimens exposed to 25 °C

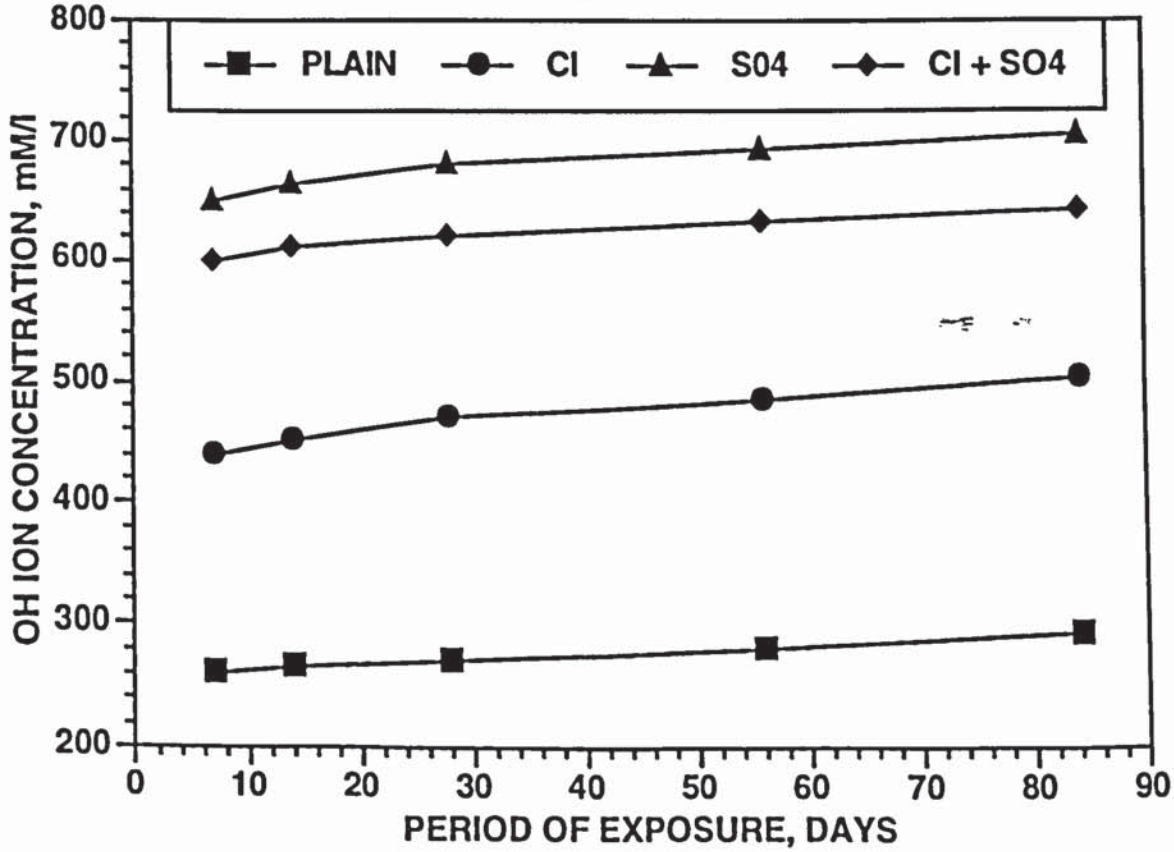

Figure 3.12: Variation of OH^- with age in OPC-B mortar specimens exposed to 40 °C

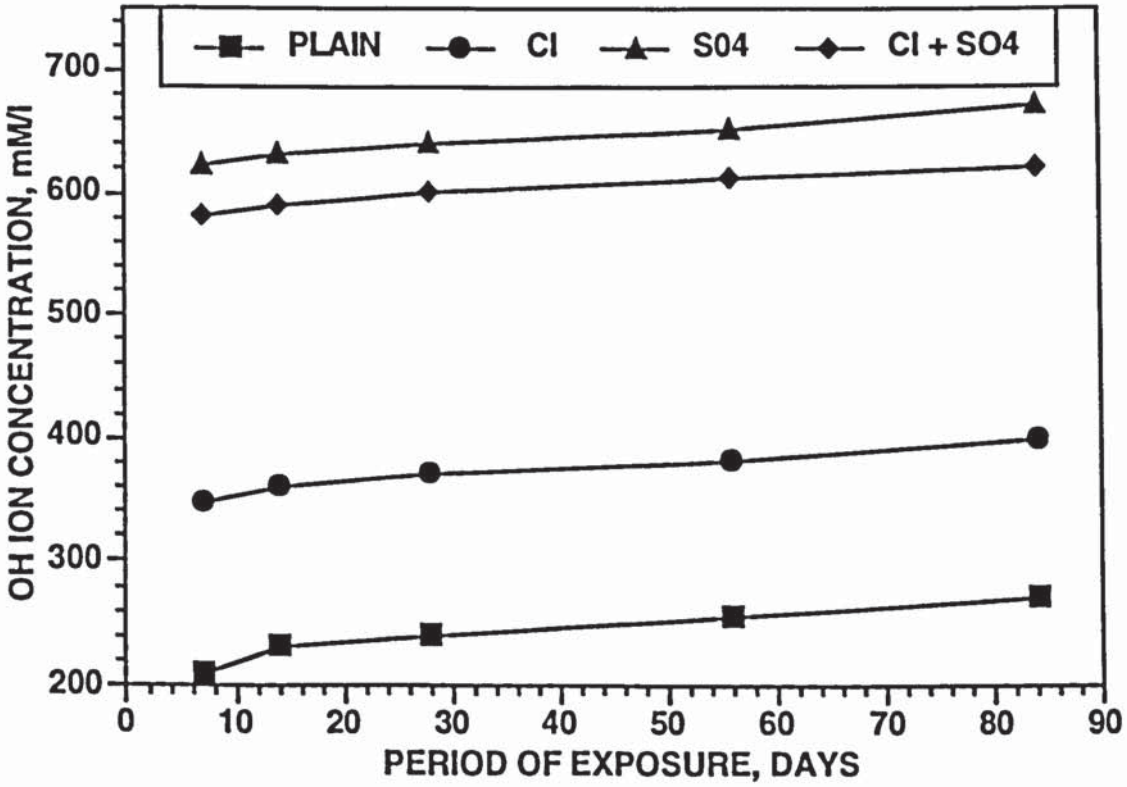

Figure 3.13: Variation of OH^- with age in OPC-B mortar specimens exposed to 55 °C

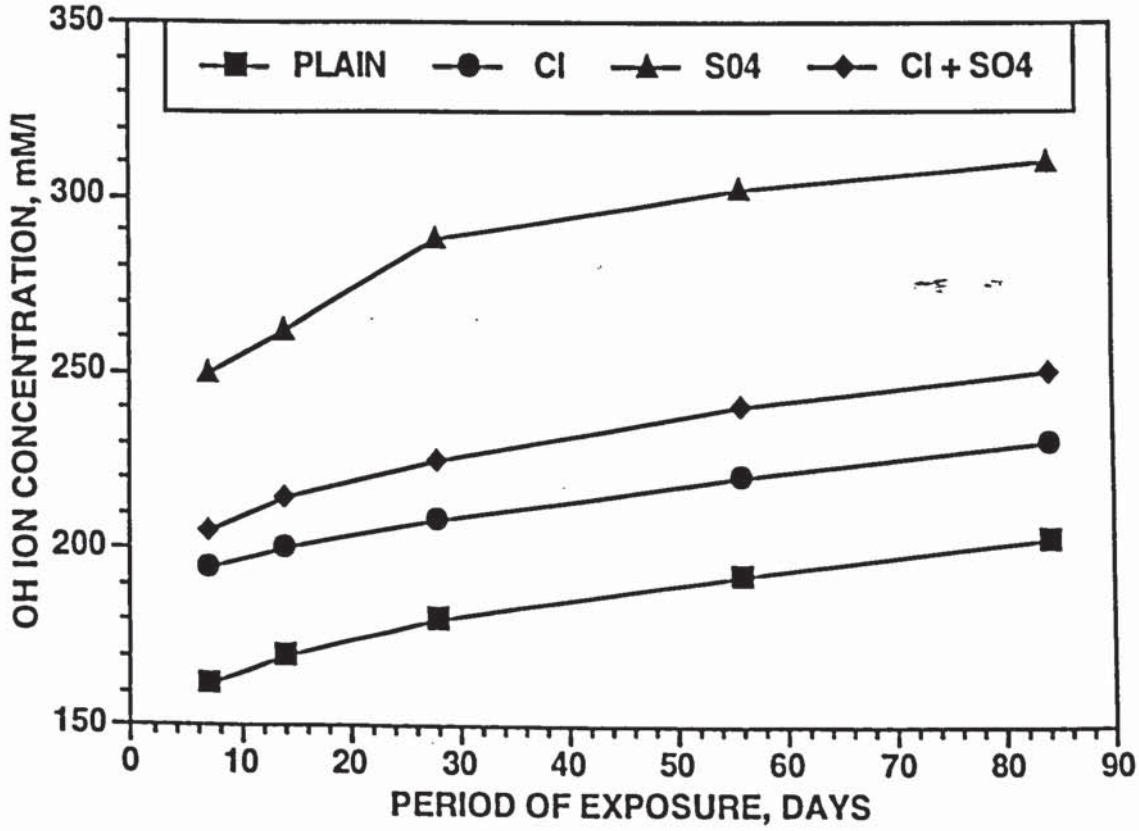

Figure 3.14: Variation of OH^- with age in OPC-B mortar specimens exposed to 70 °C

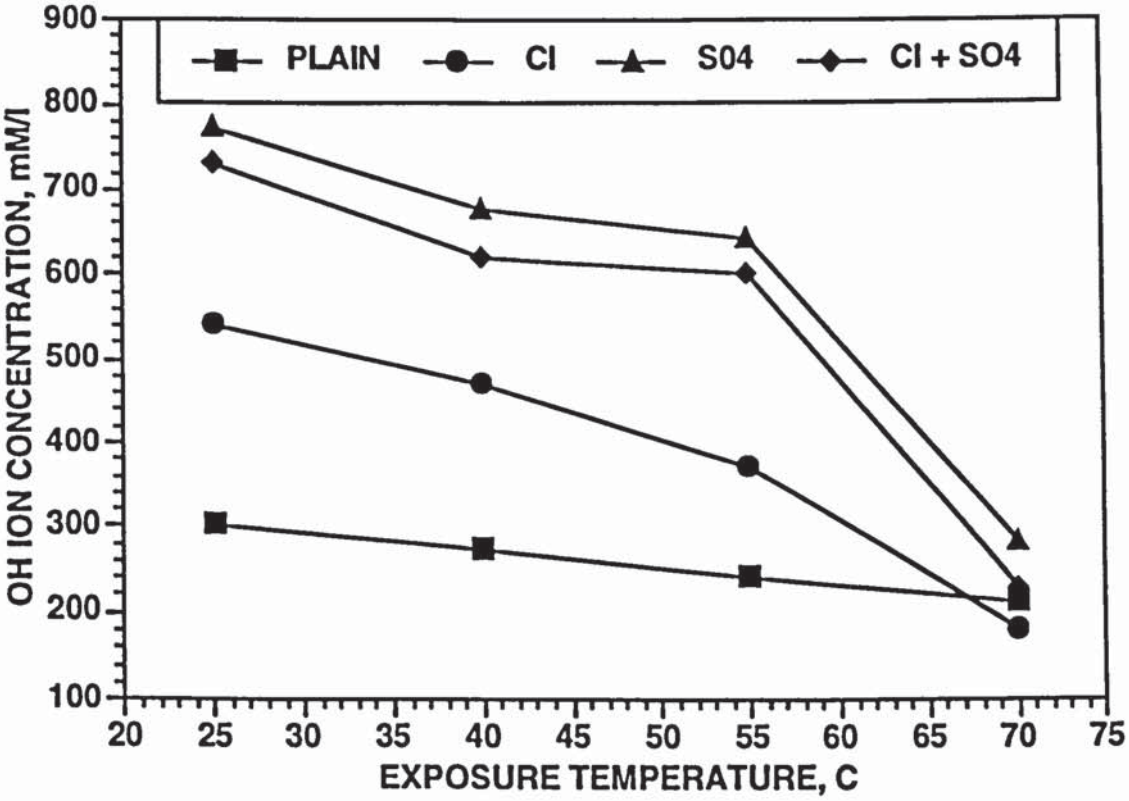

Figure 3.15: Variation of OH^- with exposure temperature in OPC-B cement mortar specimens

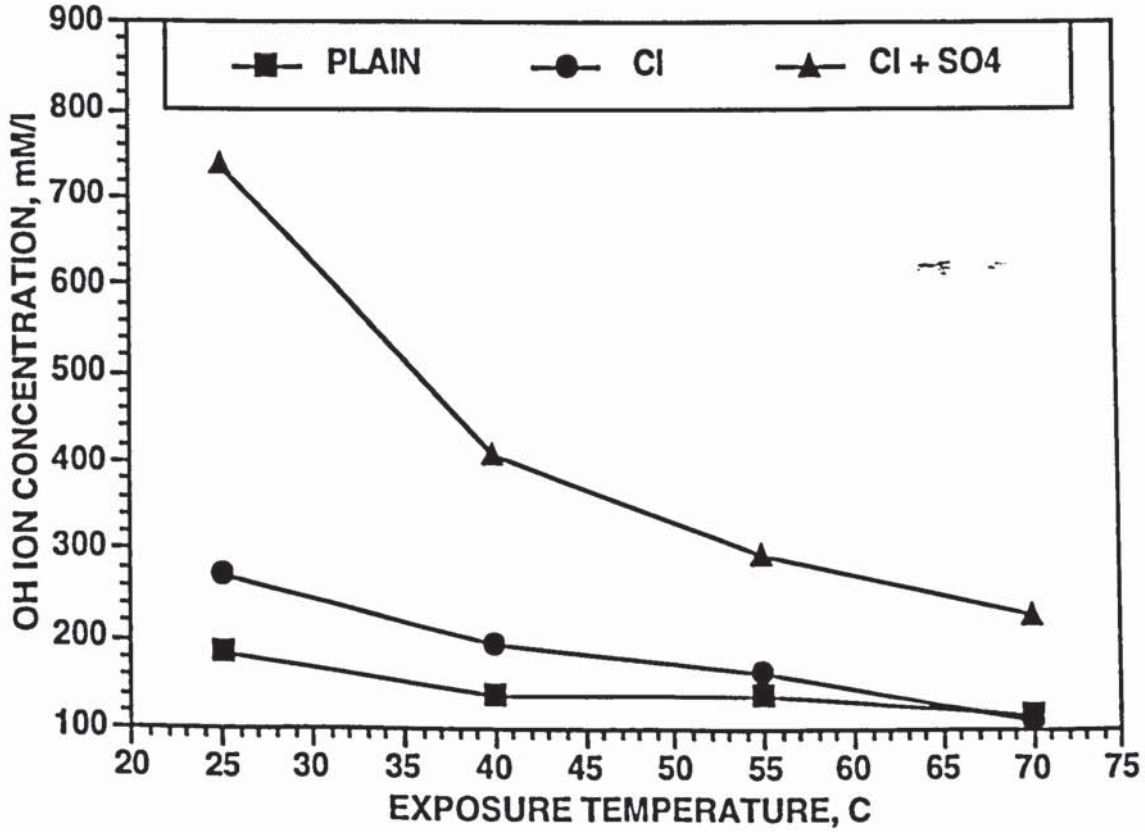

Figure 3.16: OH^- concentration in Class C fly ash cement mortar

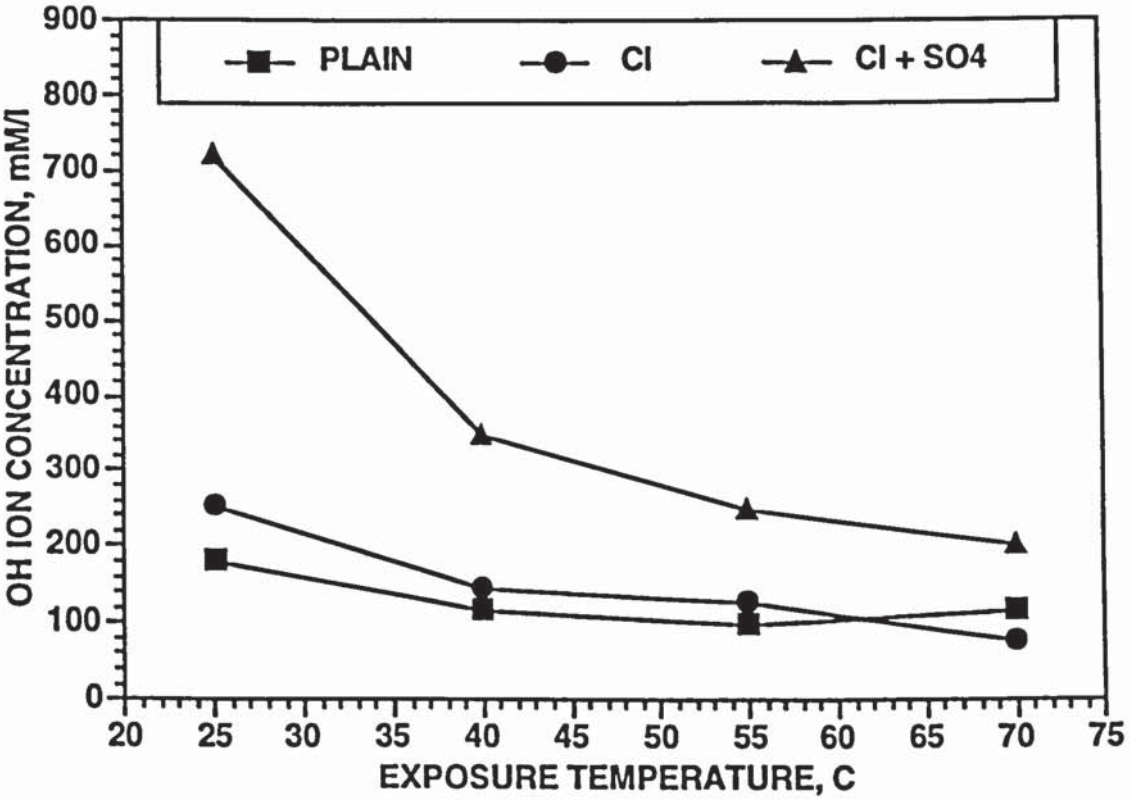

Figure 3.17: OH^- concentration in Class F fly ash cement mortar

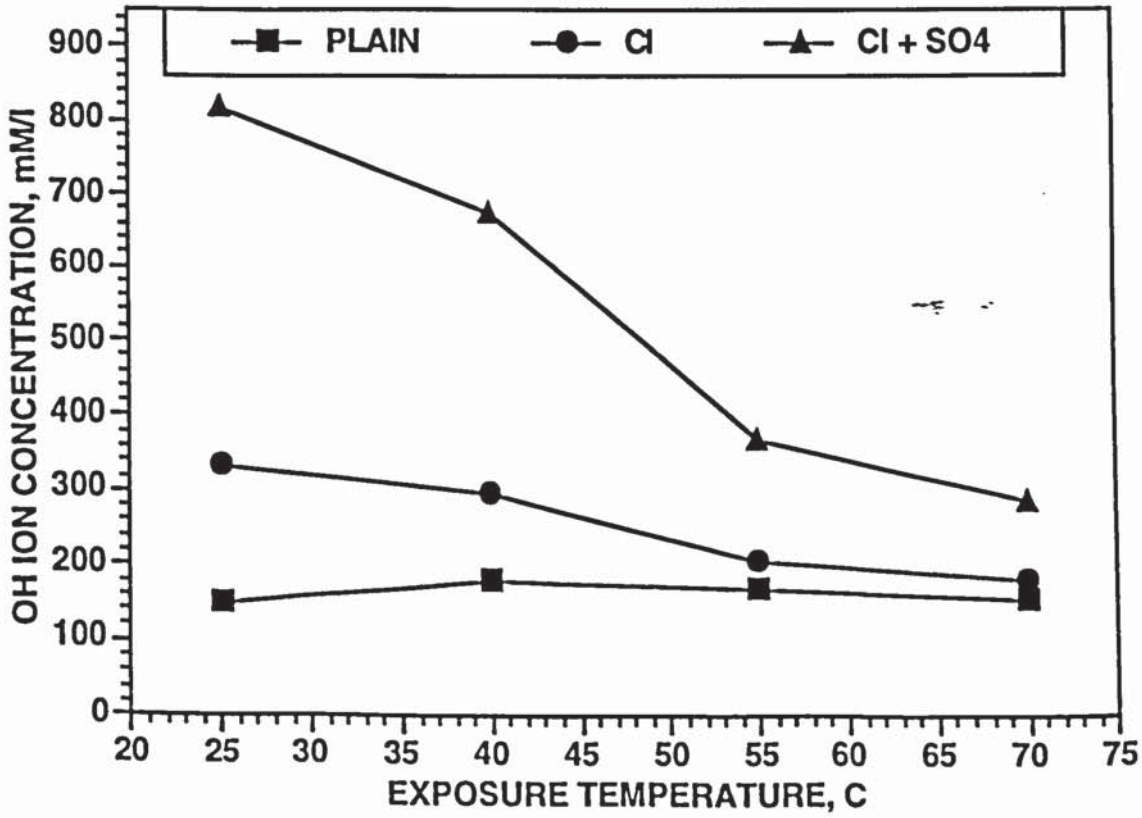

Figure 3.18: OH^- concentration in blast furnace slag cement mortar

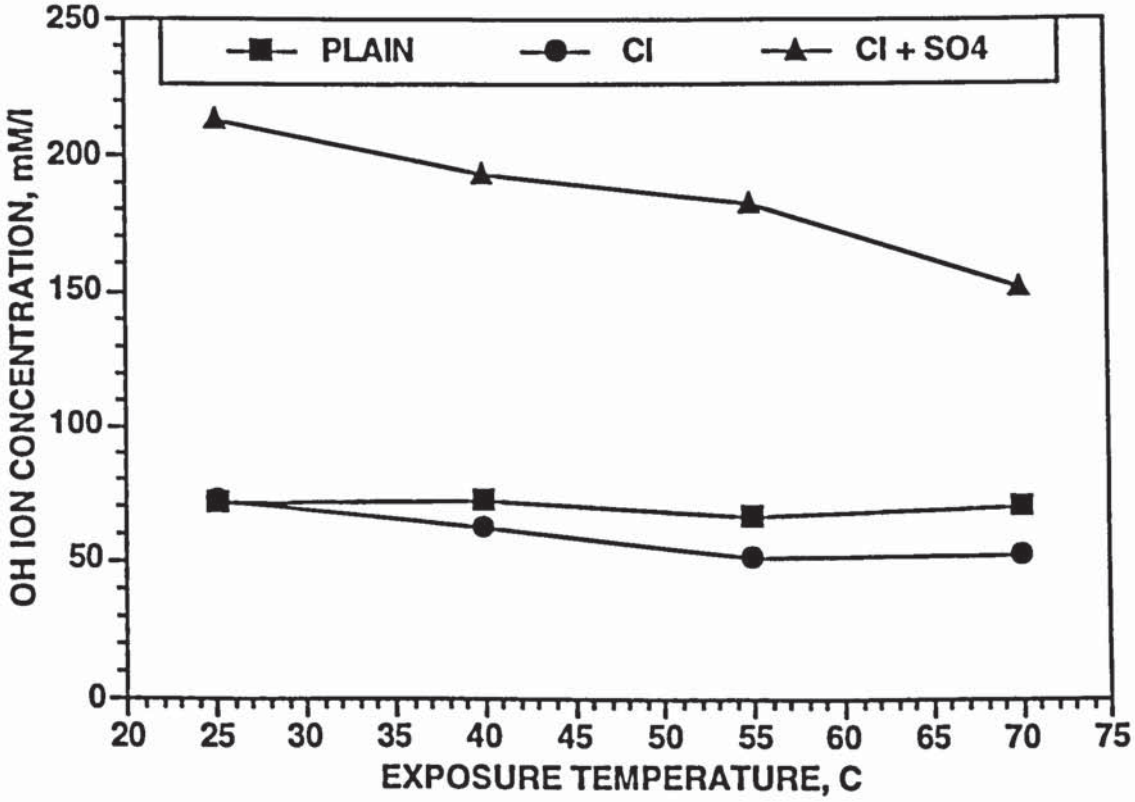

Figure 3.19: OH^- concentration in silica fume blended cement mortar

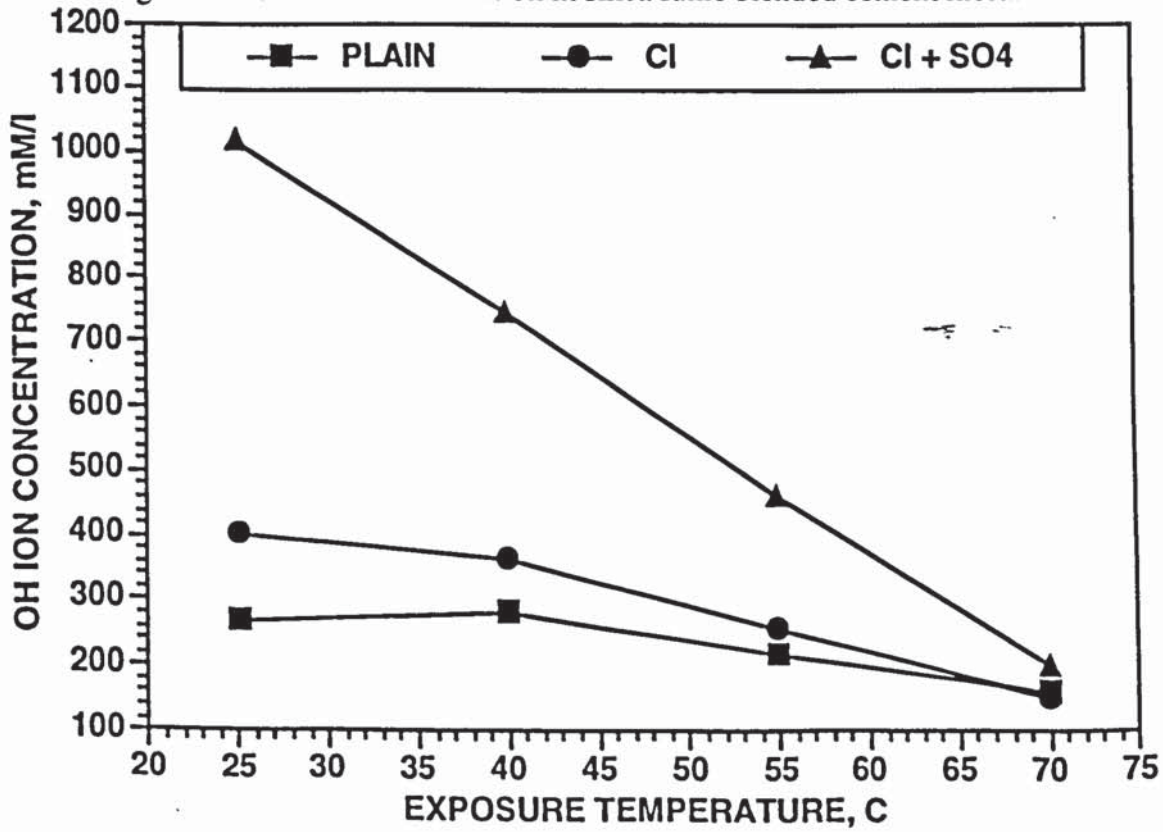

Figure 3.20: OH^- concentration in OPC-A cement mortar (SO_3: 6%)

indicated that the pore solution composition is significantly affected by the alkalinity of the cement and the fly ash. Marsh et al. [70] studied the influence of temperature on the strength gain and calcium hydroxide depletion in hardened cement pastes containing fly ash, cured at various temperatures. The results of that study indicated a reduction in the calcium hydroxide content due to an increase in the curing temperature. Further, the acceleration of the pozzolanic reaction was greater than the acceleration of the hydration of portland cement for a given curing temperature.

Investigations conducted by Page and Vennesland [64] indicated a reduction in the pH of the pore solution with increasing addition of silica fume to the cement paste. The fact that the silica fume reacts with the calcium hydroxide formed during the hydration process has been reported by Sellevold [71]. Byfors [66] attributed the reduction in the pH value of the pore solution in silica fume blended cements to the diluting effect when cement is replaced by silica fume. The reduction in alkalinity of the pore solution of cement paste specimens incorporating silica fume has also been reported by Byfors et al. [67], Rasheeduzzafar et al. [65] and Al-Amoudi et al. [72]. Almost all the researchers attributed the lower alkalinity of the pore solution in the silica fume blended cements to the highly reactive nature of the silica fume which is able to bind considerably more $Ca(OH)_2$ than fly ash and other pozzolanic materials.

The increase in the OH^- concentration in the blended cements due to incorporation of chloride and sulfate contamination may be attributed to the fixation of these anions with the hydration products in these cements, as was hypothesized for plain cements. Similarly, the effect of temperature on the reduction in the OH^- concentration in the contaminated and uncontaminated blended cements may be attributed to the instability of the chloride and sulfate complexing compounds, as was presumed for plain cements.

Another subject of concern pertinent to blended cements relates to their ability to protect the steel due to the apparent reduction in the alkalinity of the pore solution. This apprehension is particularly related to silica fume blended cement which exhibited the lowest OH^- concentration, specially in the specimens exposed to high temperature. The lowest OH^- concentration, 51 mM/l and the corresponding pH of 12.71, was recorded in the chloride-contaminated silica fume cement mortar exposed to 55 °C. This level of alkalinity is unlikely to cause steel depassivation as passive condition is normally observed when mild steel is immersed in aqueous solutions of pure alkali at pH values in excess of 11.5 [73,74]. Page and Havdahl [75] have indicated that depassivation does not occur even when 30% silica fume is used as a replacement of cement. However, concern has been raised as to the effect of this low pH, associated with silica fume blended cement, on steel depassivation in the presence of sulfate ions [76]. Concentrations of Na_2SO_4 as low as 0.2% have been shown to depassivate steel in saturated $Ca(OH)_2$ solution [74] and, in 10 mM/l NaOH, corrosion has been observed at sulfate concentrations of less than 0.3 mM/l [77].

3.2.1.2 Chloride Concentration

The chloride ion concentration in the SRPC mortar specimens exposed to temperatures in the range of 25 to 70 °C are shown in Figures 3.21 through 3.24. These data indicated an insignificant change in the chloride concentration with the period of exposure, the average standard deviation in the measurements at all the ages tested being less than 25 mM/l.

Figure 3.25 shows the effect of temperature on the chloride concentration in the contaminated and uncontaminated SRPC (C_3A: 3.5%) mortar specimens. The chloride ion concentration in the mortar specimens contaminated with sodium chloride was 350 and 363 mM/l at exposure temperatures of 25 and 40 °C, respectively. However,

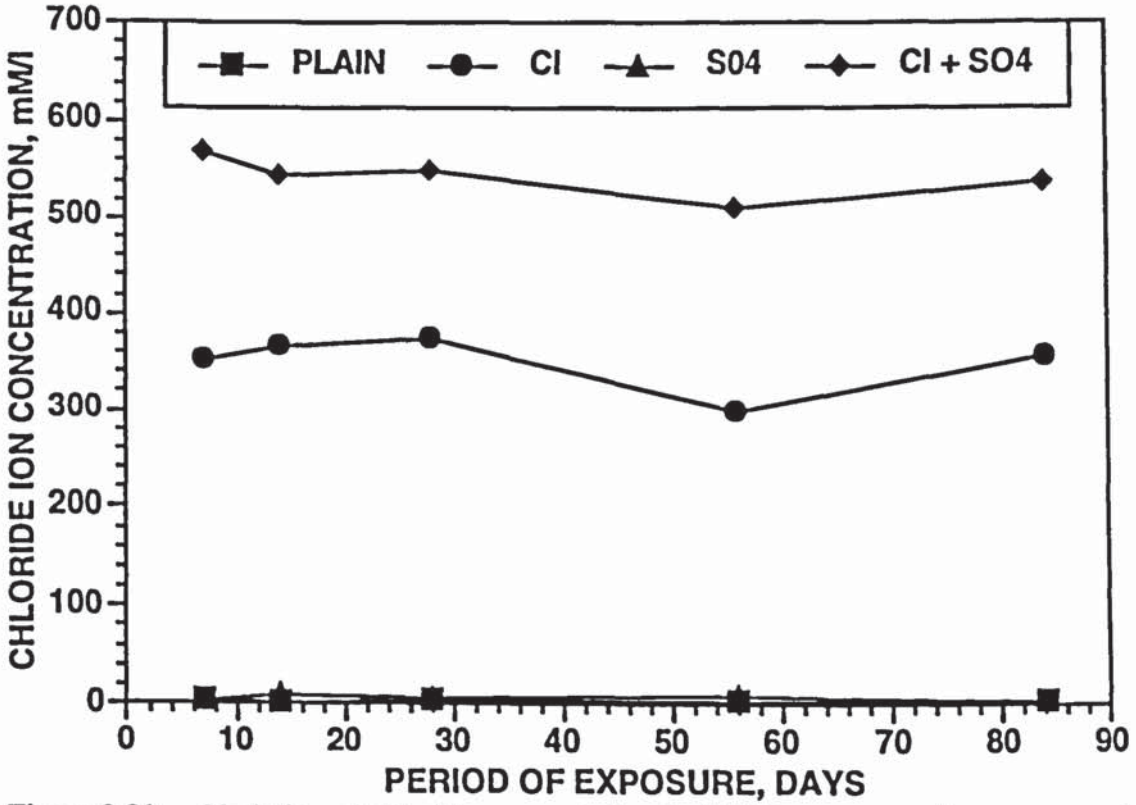

Figure 3.21: Variation of chloride concentration in SRPC mortar specimens exposed to 25 °C

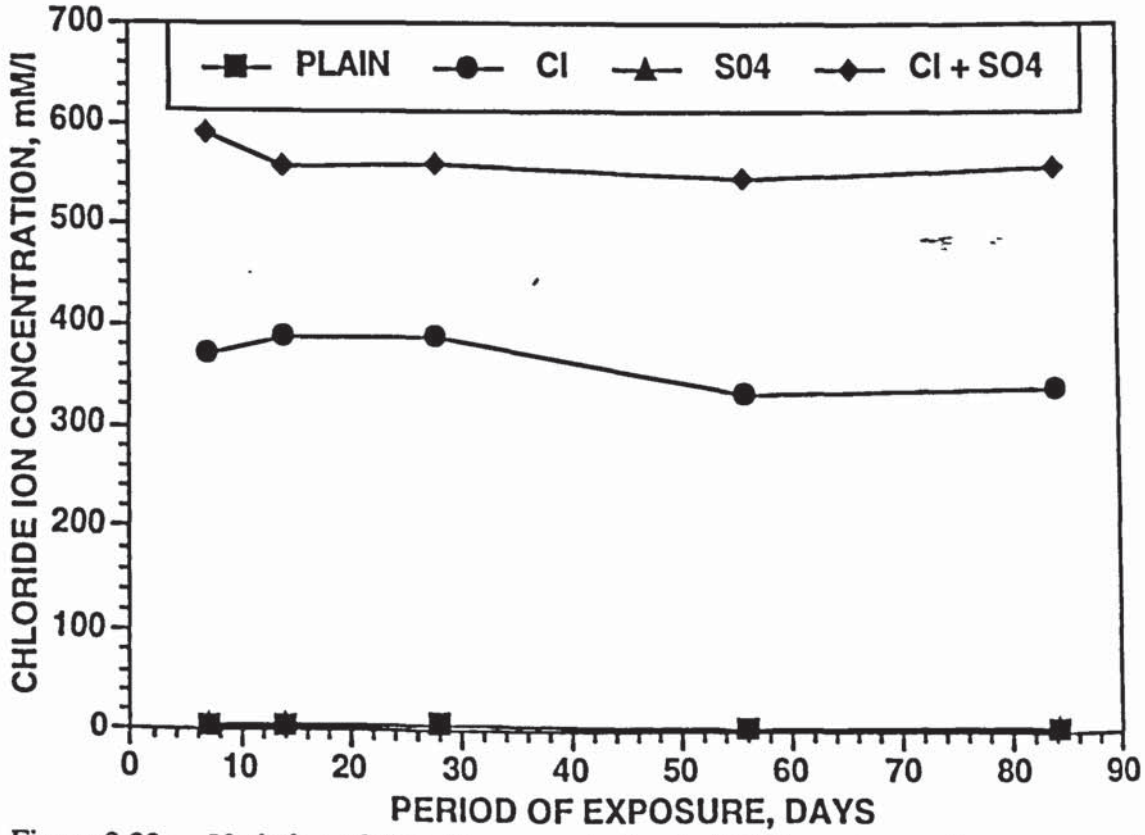

Figure 3.22: Variation of chloride concentration in SRPC mortar specimens exposed to 40 °C

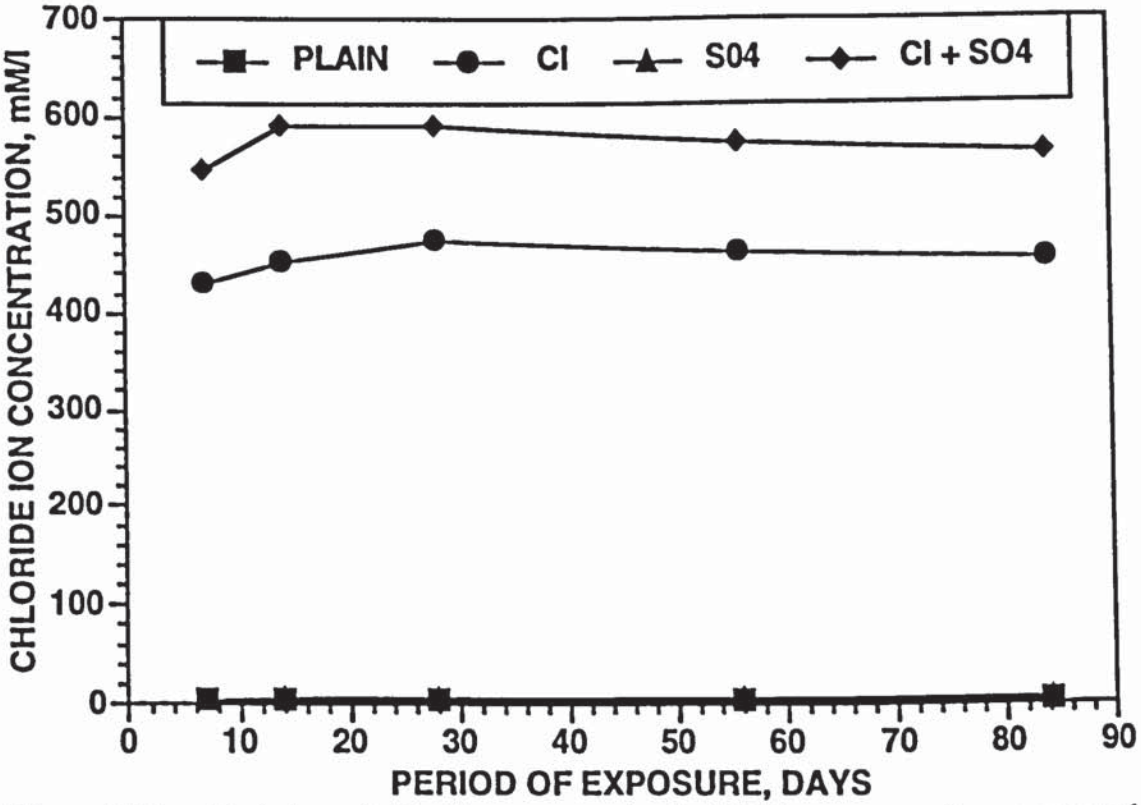

Figure 3.23: Variation of chloride concentration in SRPC mortar specimens exposed to 55 °C

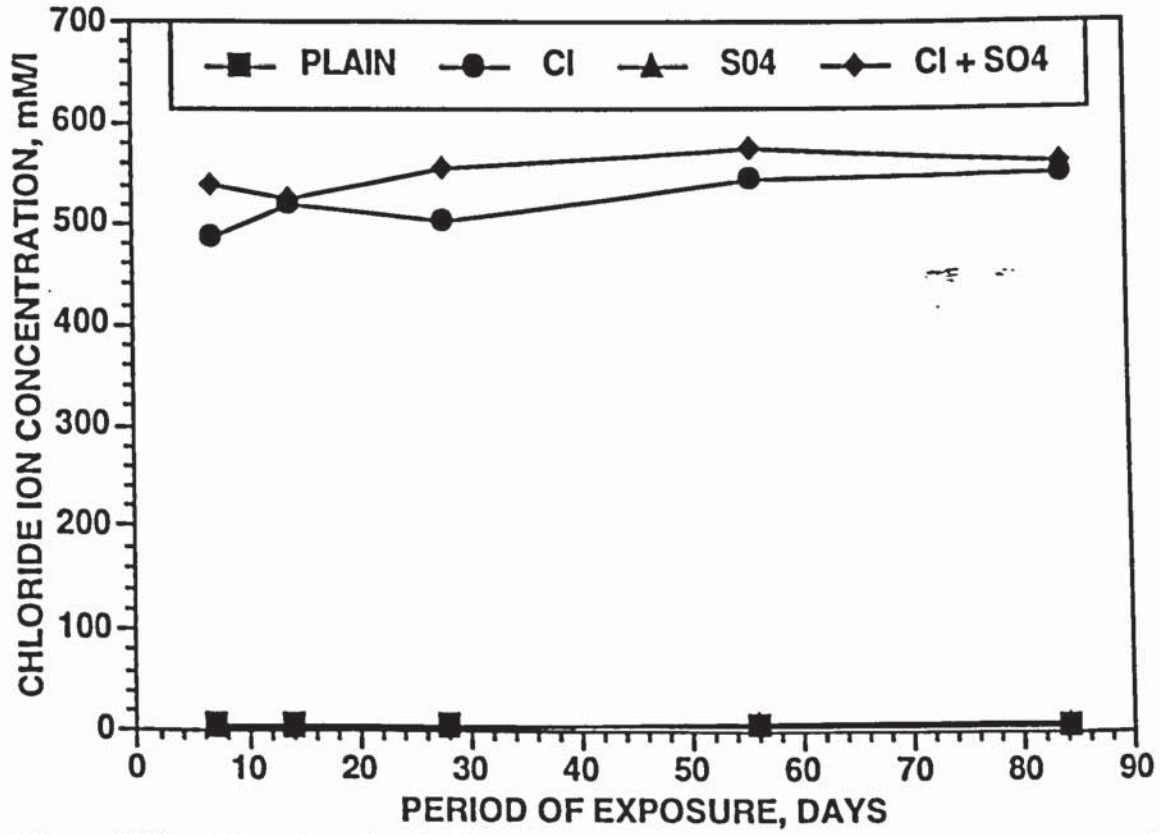

Figure 3.24: Variation of chloride concentration in SRPC mortar specimens exposed to 70 °C

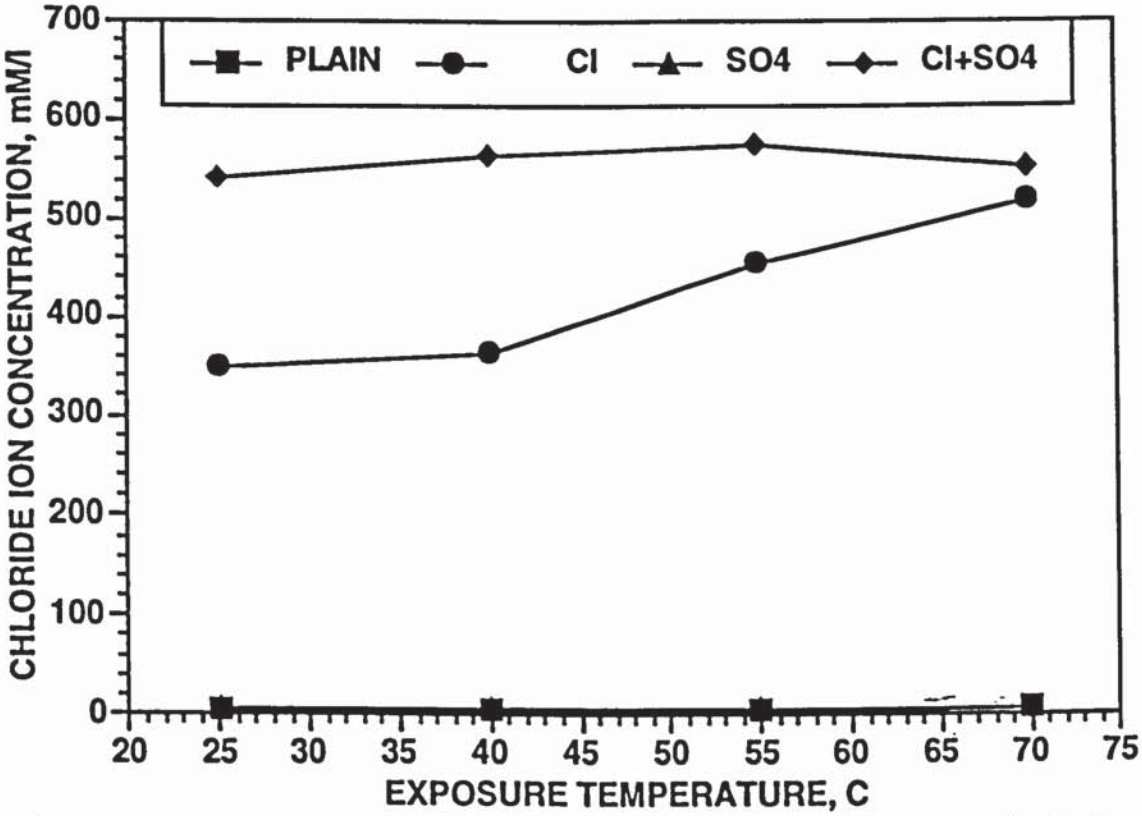

Figure 3.25: Influence of exposure temperature on the chloride concentration in the pore solution of SRPC mortar specimens

when the exposure temperature was raised from 40 to 70 °C, the chloride concentration increased almost linearly to 520 mM/l. The chloride ion concentration in the specimens contaminated with sodium chloride plus sodium sulfate was approximately 550 mM/l at all the exposure temperatures, indicating that the effect of temperature on the chloride concentration in these specimens was insignificant.

The chloride concentration in the contaminated SRPC mortar specimens, expressed as a proportion of its original concentration (735 mM/l), are shown in Table 3.5. The chloride concentration in the specimens contaminated with sodium chloride ranged from 48 to 71 percent for an exposure temperature ranging from 25 to 70 °C. The proportion of chlorides remaining in the pore solution in the specimens exposed to 25 and 40 °C was more or less similar in the range of 48 to 49%. However, the proportion of free chlorides increased with a further increase in the temperature. The chloride concentration in the specimens exposed to 55 and 70 °C was 62 and 71% of the original composition, respectively. The chloride concentration in the pore solution of mortar specimens contaminated with sodium chloride plus sodium sulfate was in the range of 74 to 78% of the original concentration, for exposure temperatures of 25 to 70 °C.

Table 3.5: Chloride concentration in SRPC mortar specimens

Temperature (°C)	Chloride concentration (% of original concentration in the mix water)	
	Chloride	Chloride + Sulfate
25	47.5	73.8
40	49.3	76.6
55	61.9	78.1
70	70.8	75.0

The chloride concentration in the contaminated and uncontaminated OPC-A (C_3A: 8.5%) cement mortar specimens exposed to temperatures in the range of 25 to 70 °C are plotted in Figures 3.26 through 3.29. These data indicate a trend similar to that shown in Figs 3.21 through 3.24. The data in Figures 3.26 through 3.29 are summarized in Figure 3.30, which shows the effect of temperature on the chloride concentration in the OPC-A mortar specimens. These data indicated a trend more or less similar to that shown in Figure 3.25. The chloride concentration in the specimens contaminated with only sodium chloride increased with the exposure temperature, while the chloride concentration in the specimens contaminated with sodium chloride plus sodium sulfate was almost unaffected by the exposure temperature.

Table 3.6 shows the chloride concentration, expressed as a proportion of the original concentration, in the OPC-A mortar specimens. The chloride concentration in the specimens contaminated with sodium chloride and exposed to 25 and 40 °C was 41 and 55% of the original concentration. These values were 63 and 65%, respectively, in the specimens exposed to 55 and 70 °C. The chloride concentration in the specimens contaminated with sodium chloride plus sodium sulfate was in the range of 75 to 78% of the original concentration for exposure temperature varying in the range of 25 to 70 °C.

The variation in the chloride concentration with period of exposure in the contaminated and uncontaminated OPC-B (C_3A: 14.5%) mortar specimens is shown in Figures 3.31 through 3.34. These data indicated a trend similar to that exhibited by SRPC and OPC-A cement mortar specimens. The effect of temperature on the chloride concentration in these cement mortar specimens is plotted in Figure 3.35. The chloride concentration in the specimens contaminated with sodium chloride plus sodium sulfate increased from about 498 mM/l to about 642 mM/l for exposure temperatures in the range of 25 to 70 °C. In the specimens contaminated with only

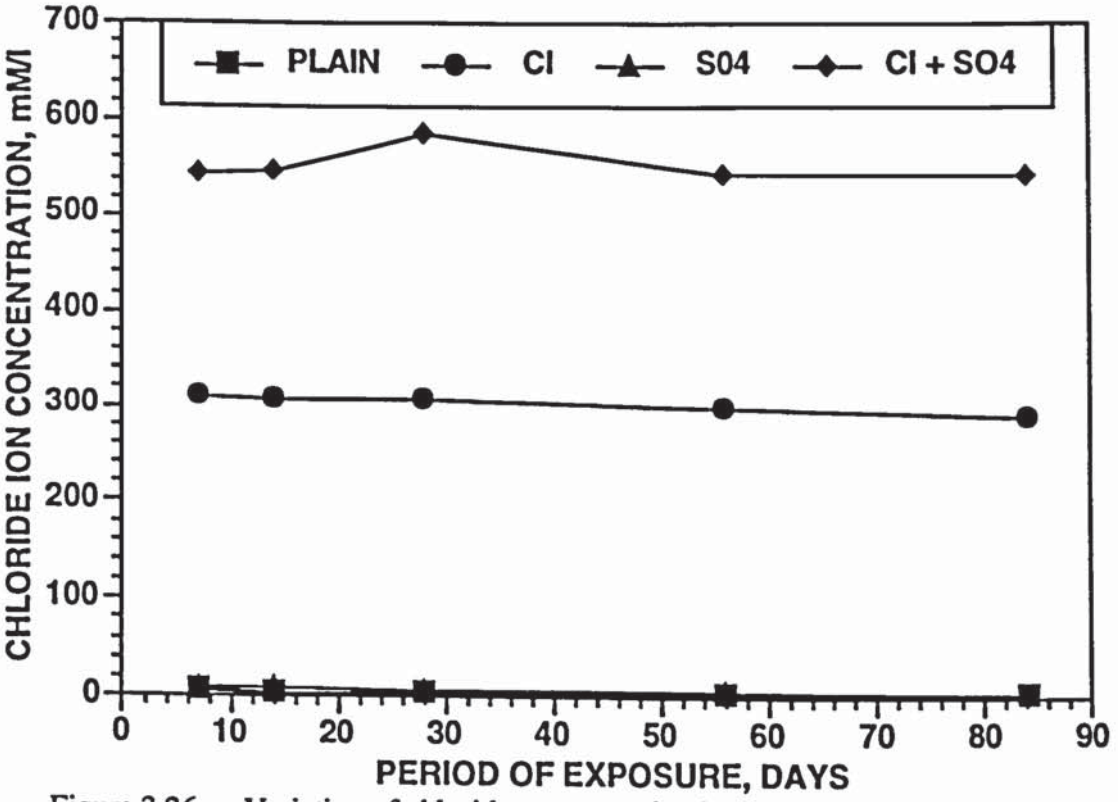

Figure 3.26: Variation of chloride concentration in OPC-A mortar specimens exposed to 25 °C

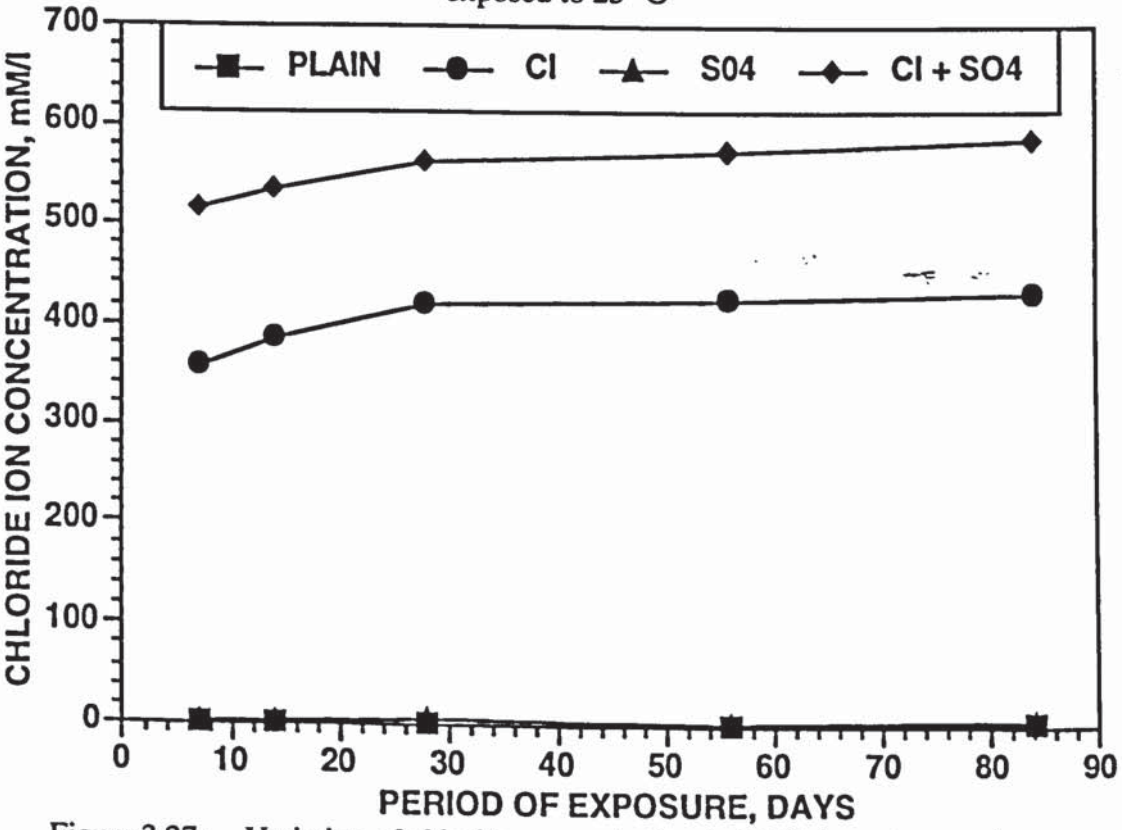

Figure 3.27: Variation of chloride concentration in OPC-A mortar specimens exposed to 40 °C

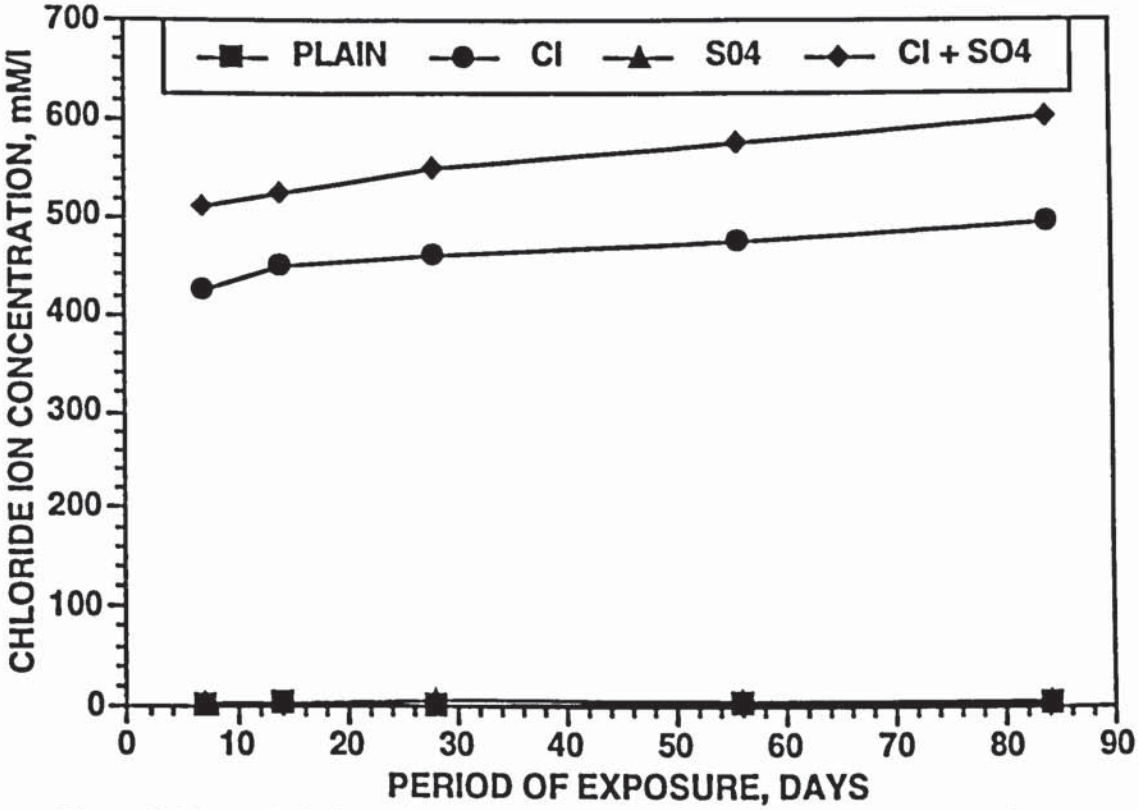

Figure 3.28: Variation of chloride concentration in OPC-A mortar specimens exposed to 55 °C

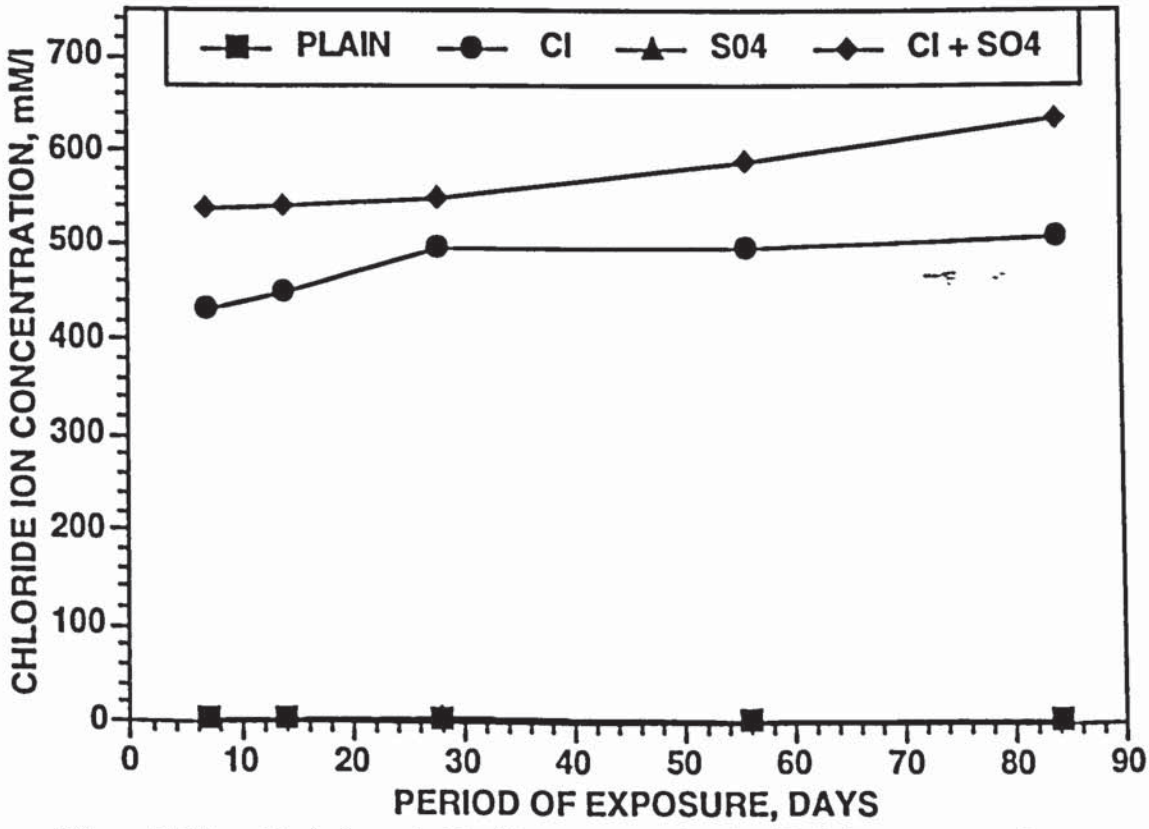

Figure 3.29: Variation of chloride concentration in OPC-A mortar specimens exposed to 70 °C

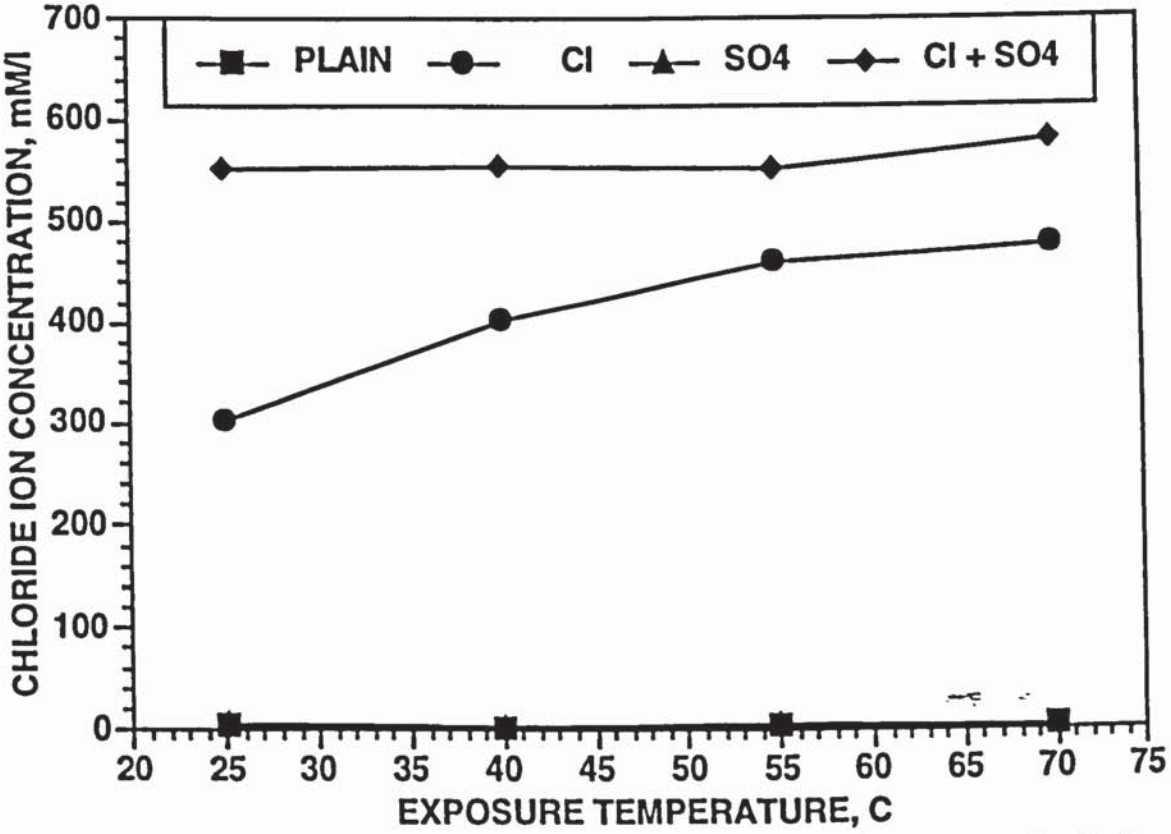

Figure 3.30: Influence of exposure temperature on the chloride concentration in the pore solution of OPC-A mortar specimens

Table 3.6: Chloride concentration in OPC-A mortar specimens

Temperature (°C)	Chloride Concentration (% of original concentration in the mix water)	
	Chloride	Chloride + Sulfate
25	41.0	75.2
40	54.8	75.65
55	62.7	75.1
70	64.8	78.8

sodium chloride, the chloride concentration increased from about 173 mM/l to 457 mM/l due to a similar rise in the temperature. The chloride concentration in OPC-B (C_3A: 14.5%) specimens, expressed as percentage of the original mix water, is shown in Table 3.7. The chloride concentration in the specimens contaminated with sodium chloride and exposed to 25 and 40 °C was 23 and 34% of the original concentration, respectively. In the specimens exposed to 55 and 70 °C, the free chloride concentration was 48 and 62% of the original concentration in the mix water. The chloride concentration in the specimens contaminated with sodium chloride plus sodium sulfate varied from 68 to 87%, of the original concentration for exposure temperatures in the range of 25 to 70 °C.

In summary, the chloride concentration in the three cements investigated was observed to increase with increasing exposure temperature. An exposure temperature of more than 40 °C was observed to be detrimental from the chloride binding standpoint. Data in Tables 3.5 through 3.7 indicated 130 to 270% increase in the chloride concentration in the chloride-contaminated specimens as the temperature was

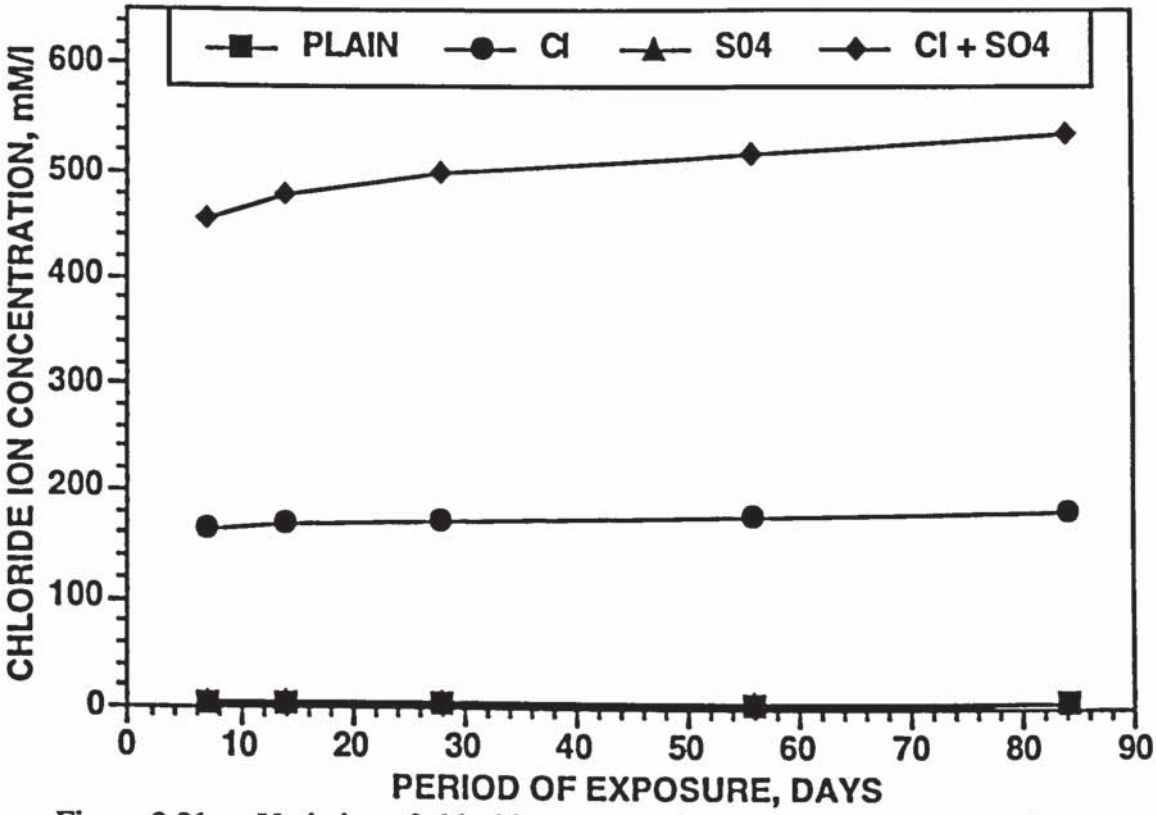

Figure 3.31: Variation of chloride concentration in OPC-B mortar specimens exposed to 25 °C

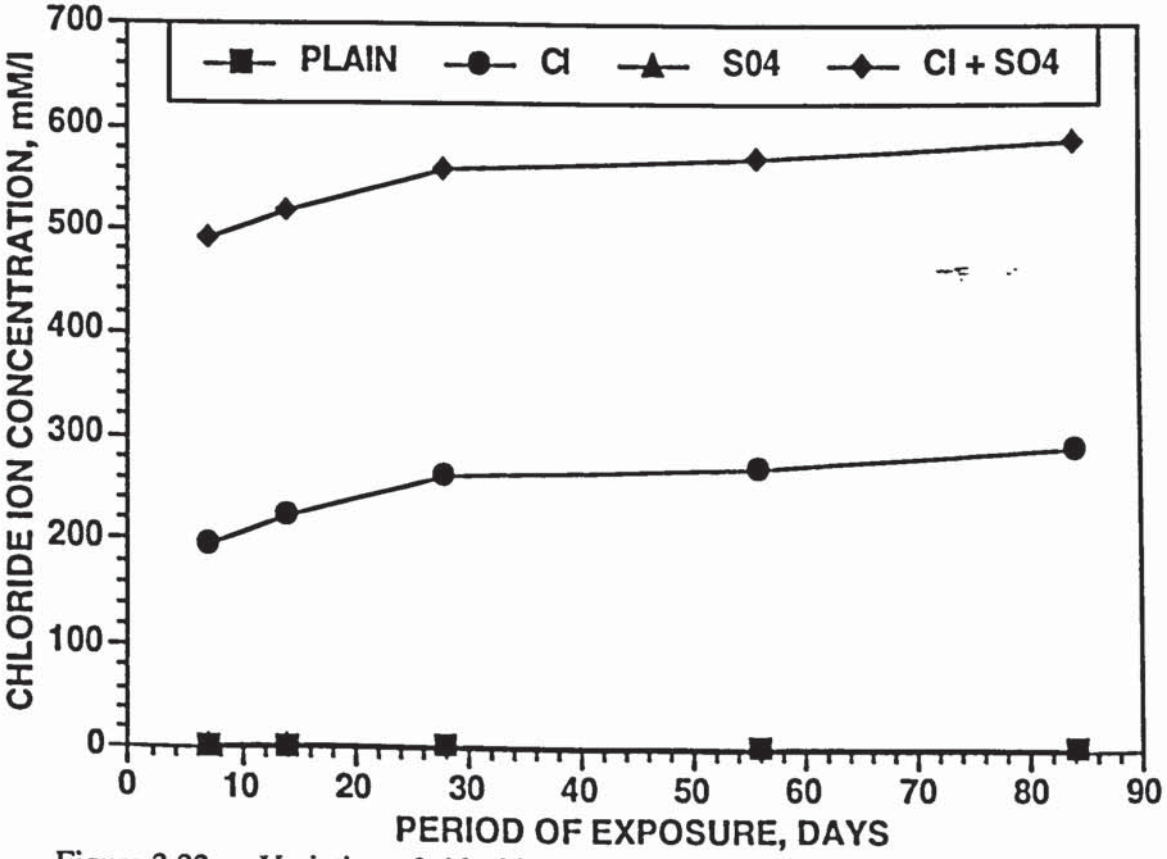

Figure 3.32: Variation of chloride concentration in OPC-B mortar specimens exposed to 40 °C

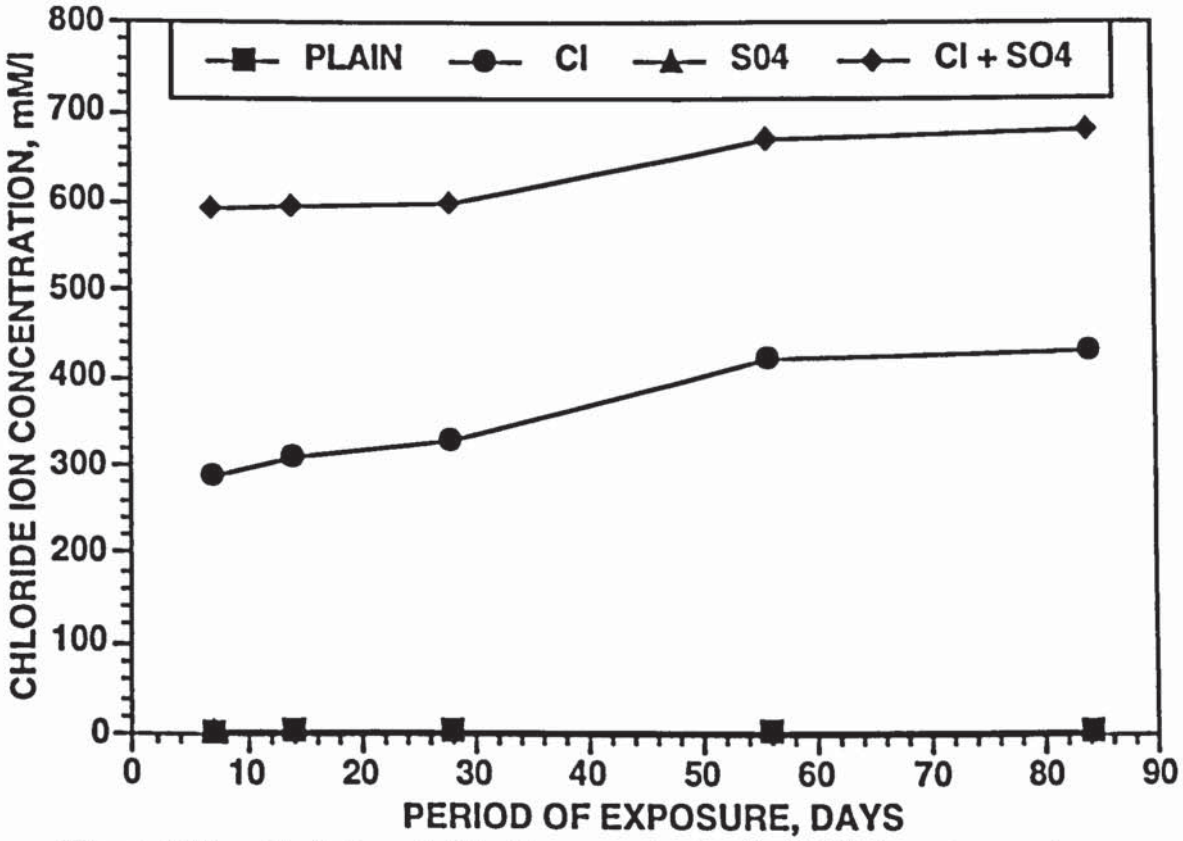

Figure 3.33: Variation of chloride concentration in OPC-B mortar specimens exposed to 55 °C

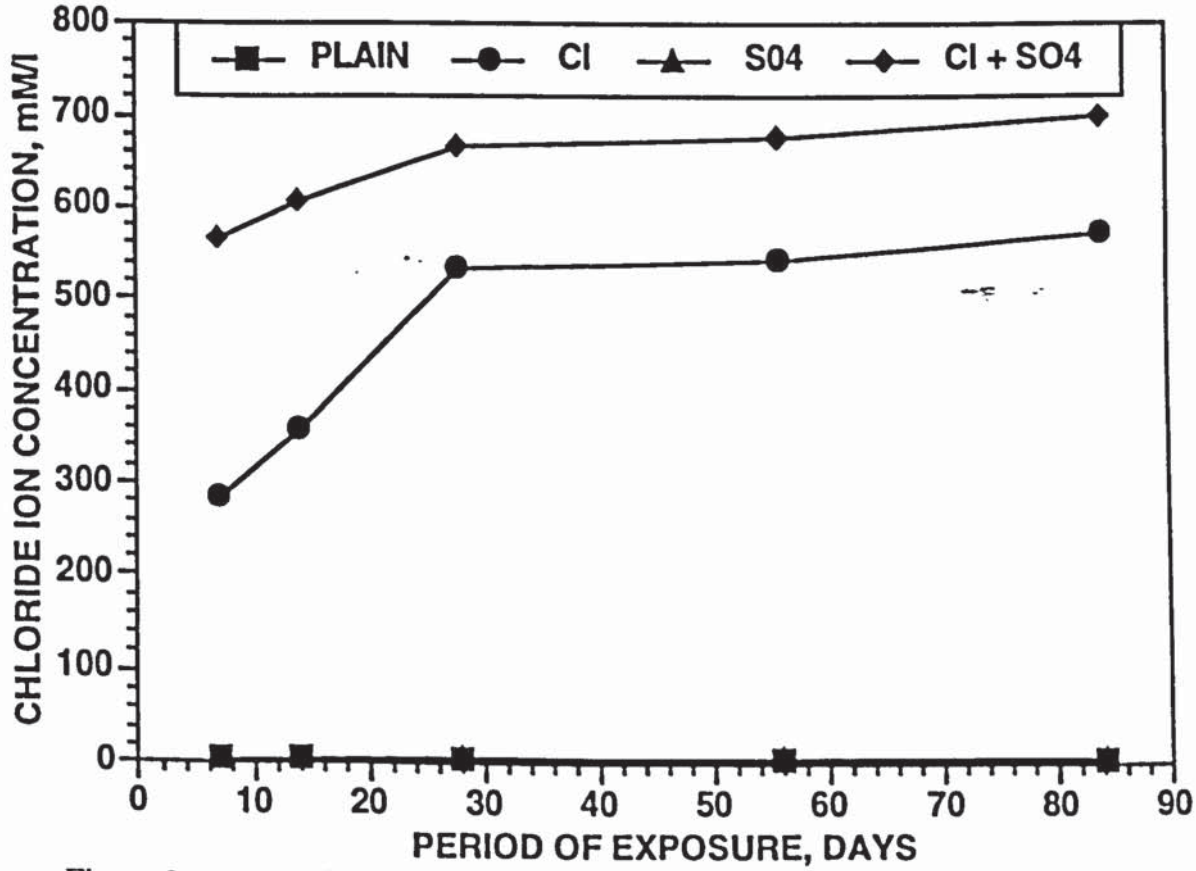

Figure 3.34: Variation of chloride concentration in OPC-B mortar specimens exposed to 70 °C

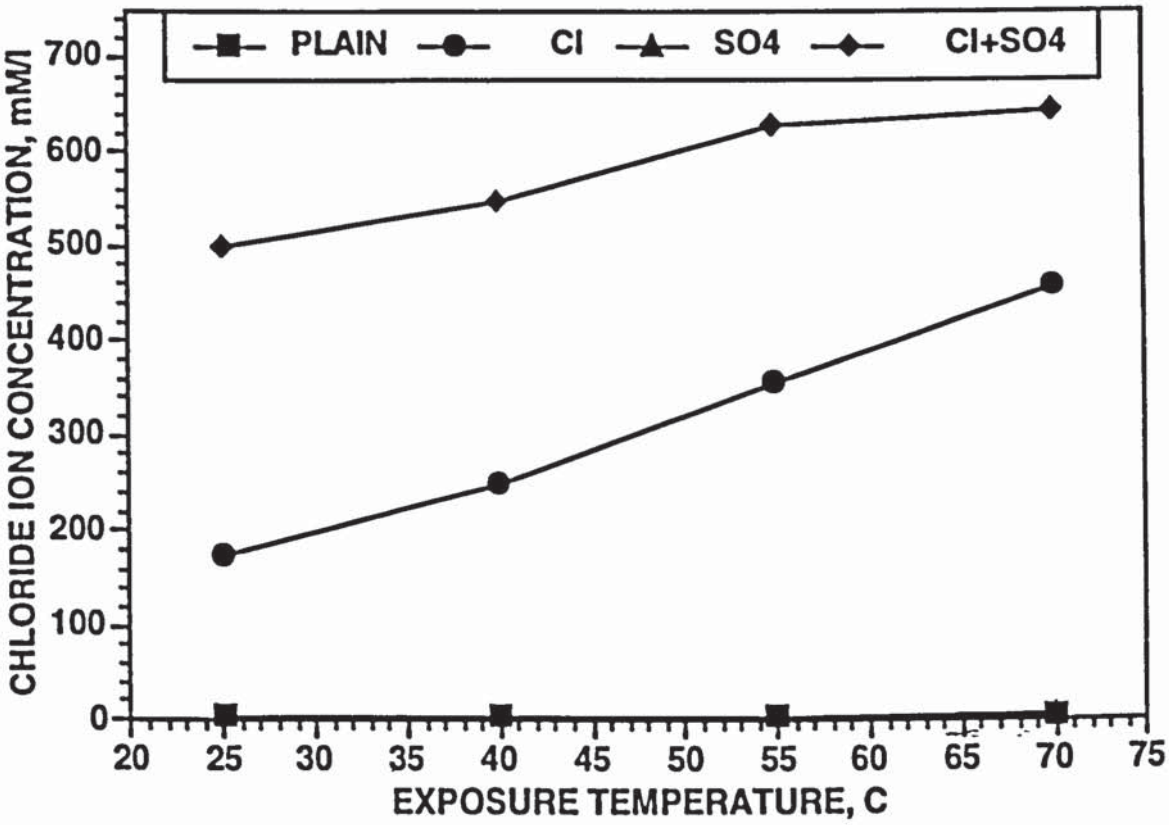

Figure 3.35: Effect of Temperature on the chloride concentration (OPC-B)

Table 3.7: Chloride concentration in OPC-B mortar specimens

Temperature (°C)	Chloride Concentration (% of original concentration in the mix water)	
	Chloride	Chloride + Sulfate
25	23.5	67.8
40	33.8	74.3
55	48.3	85.4
70	62.2	87.4

raised from 25 to 70 °C. These results indicating an increase in the chloride concentration due to rise in the exposure temperature, are in agreement with those reported by Roberts [78]. He evaluated the effect of temperature on the solubility of pure calcium chloro-aluminate compound and found that its solubility in water and in solutions of calcium sulfate and calcium hydroxide increased with increasing temperature. Results of studies conducted by Arya et al. [79], on the factors influencing chloride binding in portland cements, however, contradict Roberts's findings. The increase in the exposure temperature was reported to have an insignificant influence on the chloride concentration in the pore solution. Hussain and Rasheeduzzafar [80], however, reported higher chloride concentration in the specimens exposed to 70 °C compared to those exposed to 25 °C. The contradiction between the results of the present study, those reported by Roberts [78] and Hussain and Rasheeduzzafar [80] on one hand, and by Arya et al. [79] on the other may be attributed to the fact that Arya et al. [79] exposed the specimens to 38 °C. As is manifested in the results of this study, the decrease in chloride binding was only appreciable for exposure temperatures of more than 40 °C. In a later study, however, Arya et al. [81] while working on the methods of determining the free chlorides in chloride-contaminated OPC mortars also studied the effect of temperature of the solvent. They observed that an increase in temperature beyond 45 °C increased the total chlorides passing into solution. They indicated that bound chlorides are released at temperatures higher than

45 °C. These results [81] are in agreement with the data presented in this section, which indicated that considerable chlorides are released into the pore solution for exposure temperatures of more than 40 °C. The increase in the chloride concentration of pore solution due to elevated temperature exposure may be also due to a reduction in its volume. This aspect was not evaluated in this study. However, results of this study are in agreement with those reported by Hussain and Rasheeduzzafar [80], who based their calculations on the pore volume, thereby conforming the negative effect of elevated temperature on chloride-binding.

The decrease in the chloride binding capacity of cements due to the concomitant presence of chloride and sulfate salts, at room temperature, has been reported by Holden et al. [15], Hussain [82] and Al-Amoudi et al. [72,83]. Holden et al. [15] investigated the effect of sulfate ions on the chloride binding in portland and blended cements. Their results [15] indicated a substantial decrease in the chloride binding due to the concomitant presence of chloride and sulfate ions. They attributed the reduction in the chloride binding capacity of the cements, in the presence of sulfates, to the preferential reaction of the latter with the C_3A phase of cement forming calcium sulpho-aluminate hydrates [84]. Tests conducted by Hussain et al. [82] also indicated a similar trend. Al-Amoudi et al. [72] investigated the effect of adding differing quantities of chlorides and sulfates to plain and blended cements on their chloride binding capacity. These investigations indicated a progressive diminution of the chloride binding capacity of the cements with increasing quantum of the sulfate salts.

In addition to the preferential reaction with C_3A, the sulfate ions may also influence the chloride binding by altering the alkalinity of the pore solution. Sulfate ions inducted as sodium sulfate increase the alkalinity of the pore solution. Several investigators [67, 85-86] have reported a significant inhibiting effect of a strong alkaline pore solution environment on the chloride binding capacity of cement. Gunkel [85] has shown that

the alkali effect on weakening of the chloride binding may be even greater than the sulfate effect. In a 0.5 w/c ratio hardened cement paste with 0-0.4% chloride, added as NaCl, the chloride concentration in the pore solution increased from 2900 ppm to 4100 ppm when 0.62% Na_2O was added to the cement through mix water. Chloride concentrations increased to only 3200 ppm when alkali-free 1.36% Ca_2SO_4 was added. However, the free chloride concentration increased to 5700 ppm when both alkalis and sulfates were conjointly inducted through 1.42% Na_2SO_4. Tests conducted by Tritthart [86] also indicated that the uptake of chlorides is reduced to half when the storage of specimens was changed from a 12.5 pH environment (saturated calcium hydroxide solution) to a pH environment of 13.7 (0.5M NaOH solution). Diamond [87] also indicated that when the C_3A content of the cement is similar, the chloride binding is higher for chlorides derived from calcium chloride than that derived from sodium chloride. Several other investigators [79,86,88] have shown that the cation type associated with the added chloride significantly influences the free chloride concentration. Tests conducted by Arya et al. [79] show that for 0.5, 1.0, and 2.0% chloride treatment levels, the chlorides bound when introduced as $CaCl_2$ were 1.3, 1.8, and 3.5 times higher than when inducted as NaCl. Similar results have been reported by Andrade and Page [88], and Theising et al. [89]. The cation effect is ascribable to several factors [86]. **Firstly**, to an enhanced OH^- concentration and alkalinity attributable to NaCl addition thereby inhibiting chloride binding as compared with $CaCl_2$ addition; **secondly**, to an increased hydration promoted by $CaCl_2$ thereby facilitating an enhanced chemical combination and adsorption of chlorides by the solid hydration products; **thirdly**, to the formation of greater quantities of Friedel's salt ($3CaO.Al_2O_3CaCl_2.10H_2O$) and its ferrite analogue ($3CaO.Fe_2O_3.CaCl_2.10H_2O$) in the presence of $CaCl_2$. Further, it has been suggested on the basis of published evidence [90,91] that noticeable amount of calcium chloride is bound by the calcium silicate hydrate (C-S-H) gel, possibly as an inter-layer chemisorbed complex, while there is negligible binding of NaCl by calcium silicate hydrates. Another view point

[92] is to the effect that NaCl must react with $Ca(OH)_2$ to form calcium chloride in order to combine with aluminate phases to form Friedel's salt and calcium chloroferrite.

The variation in the chloride ion concentration with C_3A for the four temperatures investigated and for the specimens contaminated with sodium chloride is shown in Figure 3.36. These curves indicated a decrease in the chloride concentration with increasing C_3A content. The chloride concentration in OPC-B (C_3A: 14.5%) at 25 °C was about 173 mM/l compared to 350 mM/l in SRPC (C_3A: 3.62%), indicating a greater chloride binding in OPC-B due to the higher quantum of C_3A. This behaviour was observed at all the exposure temperatures. The chloride binding, however, decreased with increasing exposure temperature. The chloride concentration in the chloride-contaminated SRPC, OPC-A and OPC-B mortar specimens exposed to 70 °C was 150, 160, and 270%, of that in the similar specimens exposed 25 °C.

The beneficial role of C_3A in binding chlorides, by forming insoluble calcium chloro-aluminate hydrate, $3CaO.Al_2O_3.CaCl_2.10H_2O$, at lower temperatures of 20 to 25 °C, is well established [15,81,93-97]. Holden et al. [15] investigated the chloride binding capacity of cement paste specimens with C_3A in the range of 1.9 to 14.0%. The proportion of unbound chlorides decreased significantly with increasing C_3A content of cement. More recently, Rasheeduzzafar et al. [96,97] also indicated that the chloride binding increases significantly with C_3A content of cement. In their investigations, the unbound chlorides for 2.04, 7.59, 8.52 and 14 percent C_3A cements were measured to be 41.3, 24.6, 20.6 and 11.6 percent of the total chlorides, respectively.

Another aspect of chloride binding capacity of the cements, in situations where chloride is the only contamination, is the reduction in the quantum of free chloride ions observed even in the low C_3A cements, in the range of 0 to 3.5%. This situation is

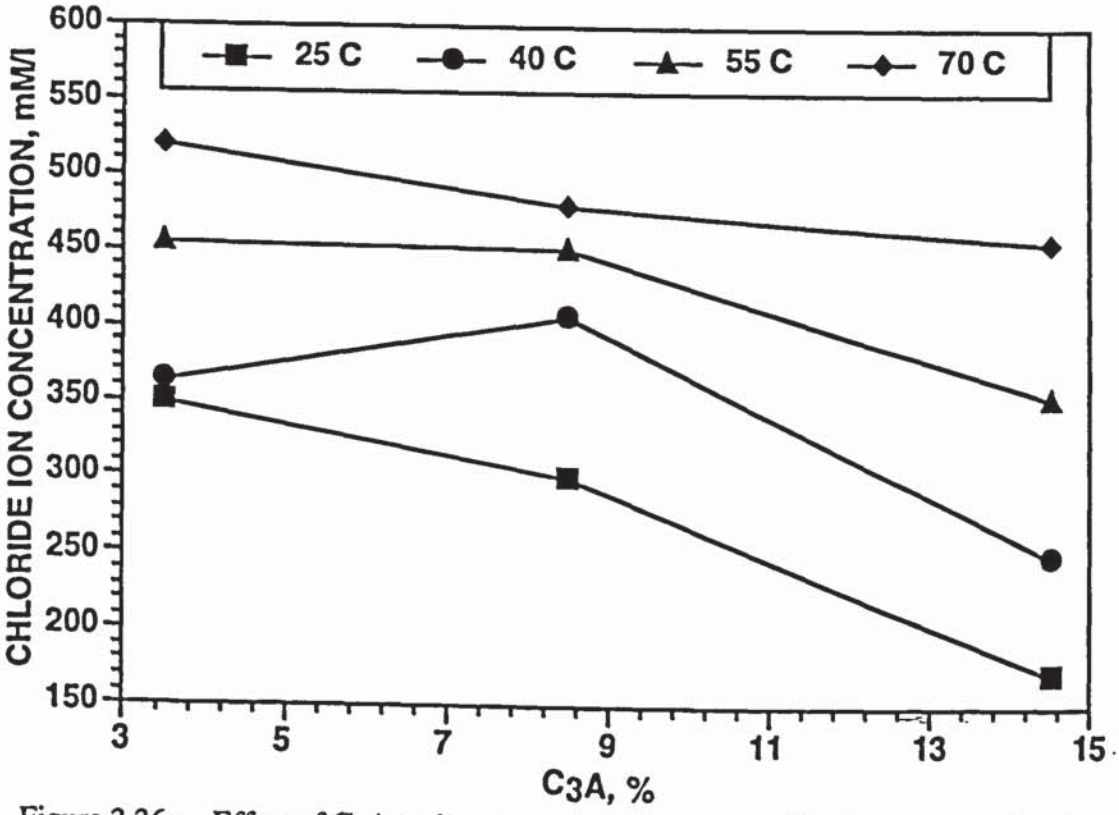

Figure 3.36: Effect of C_3A and exposure temperature on chloride concentration in chloride-contaminated specimens

particularly interesting since gypsum added to unhydrated cement to retard the setting time consumes about 5% C_3A. Further, it is known that during the hydration of portland cement, in the presence of chlorides, ettringite is always formed first, until all the gypsum is consumed, only then calcium monochloro-aluminate hydrate is formed [98]. Thus, in low C_3A sulfate resisting portland cements, the C_3A phase is totally consumed during the formation of ettringite, practically leaving no C_3A for the formation of Friedel's salt. Monfore and Verbeck [99] and Verbeck [100] reported chloride binding in cements that did not contain any C_3A. This indicates that the chloride complexation by C_3A is not the only process involved in the removal of the free chloride ions from the dangerous role of steel depassivation. There is, however, little quantitative information available in the literature concerning the relative influence of cement minerals other than C_3A [101] on the reduction in the quantity of chlorides available in the aqueous phase. In the case of the ferrite phase, C_4AF, the reactions leading to the formation of calcium chloro-aluminate and chloroferrite hydrates have been shown to occur [78], though their practical importance in binding free chloride ions is reported to be small [102]. As regards the chloride binding by calcium silicates, there is a controversy over their role in binding chlorides. Ramachandran [90,103] has suggested that a high proportion of the chloride ions contributed by the admixture are rapidly removed from the solution phase, forming an inter-layer chemisorbed complex within C-S-H gel. Diamond and Lopez-Fores [104], using pore solution expression and analysis technique, indicated that cement pastes made with water/cement ratios of 0.4 to 0.5, retained chloride ions for a fairly long periods of hydration. More recently, Ramachandran [91] suggested that in mature pastes of C_3S, hydrated at a water/solid ratio of 1.0, and contaminated with calcium chloride, a significant proportion of the chloride ions become bound to the hydration products though the extent of this binding was considerably lower than that had previously been indicated [90,103]. Lambert et al. [101] investigated the chloride ion concentration in the substituted tricalcium silicate (Jeffrey's alite, $C_{54}S_{16}AM$) which was contaminated with sodium chloride. The

chloride concentration was almost equivalent to the total chloride content, therefore, it was inferred that the quantity of chloride ions that became incorporated into hydration products of alite was insignificant. Diamond [87] attributed the reduction in the chloride concentration in the pore solution to their removal from the solution to one or more of the cement hydration products, Friedel's salt being the most obvious product.

The effect of C_3A content on the free chloride ion concentration in the cement mortar specimens contaminated with sodium chloride plus sodium sulfate and exposed to temperatures in the range of 25 to 70 °C is plotted in Figure 3.37. These results can be summarized as follows:

1. The chloride concentration decreased with increasing C_3A content for exposure temperatures of 25 and 40 °C. For example, the chloride concentration in the sulfate resisting cement was in the range of 542 to 563 mM/l while in OPC-B it was in the range of 498 to 546 mM/l for these temperatures.

2. The chloride concentration in the specimens exposed to 55 °C did not vary much as the C_3A was increased from 3.5 to 8.5%. However, a significant increase in the chloride concentration was indicated in OPC-B exposed to this temperature. The chloride concentration in SRPC, OPC-A and OPC-B exposed to 55 °C was 574, 552 and 628 mM/l , respectively.

3. The chloride concentration in the specimens exposed to 70 °C increased almost linearly with the C_3A of the cement. The chloride concentration in SRPC, OPC-A and OPC-B was 551, 583 and 642 mM/l , respectively.

The above results indicate that the concomitant presence of sulfate and temperature negates the beneficial role of C_3A in binding the chlorides. Thus, in situations where

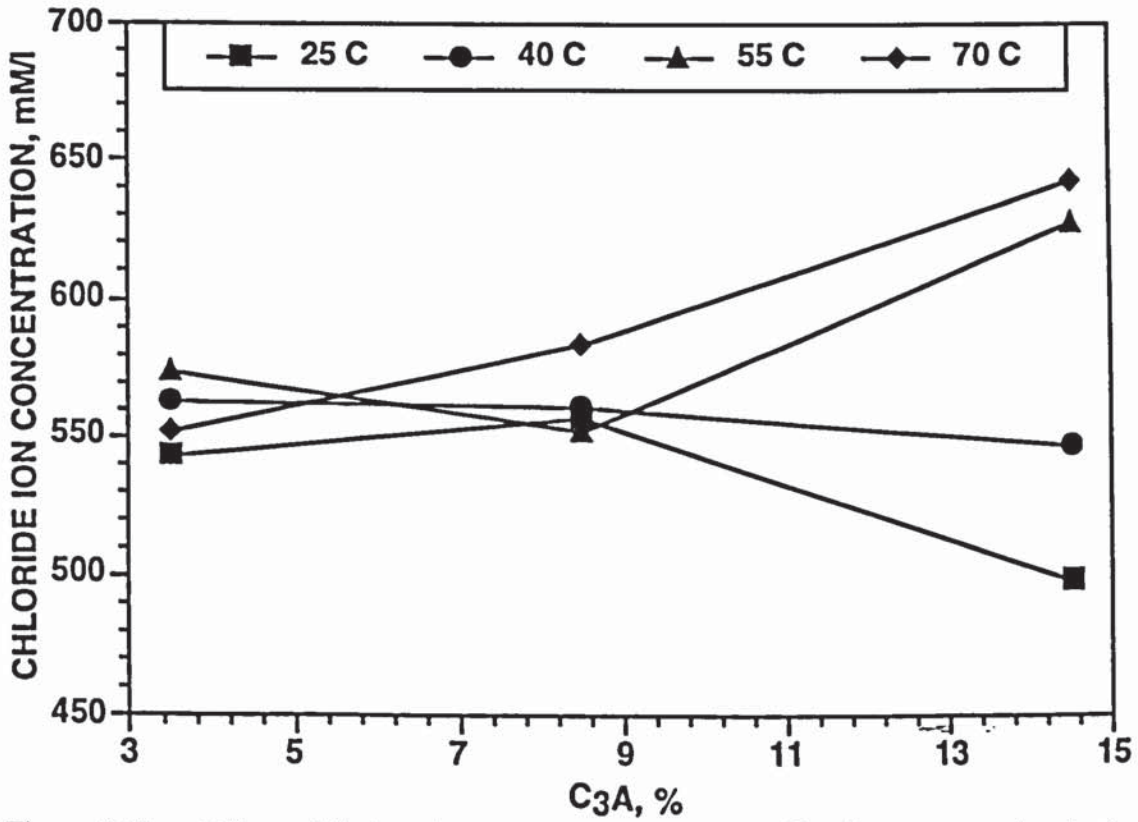

Figure 3.37: Effect of C_3A and exposure temperature on chloride concentration in the specimens with sulfate and chloride

the structural components are contaminated with both chloride and sulfates and exposed to temperatures of 55 °C and above, low to moderate C_3A cement may be more beneficial than high C_3A ordinary portland cement from reinforcement corrosion view point. However, the corrosion risk is not a simple function of the free chloride concentration. Other factors, such Cl^-/OH^-, availability of the reactants, and the resistivity of concrete also govern the reinforcement corrosion process.

The chloride concentrations in the contaminated and uncontaminated blended cement mortar specimens exposed to temperatures in the range of 25 to 70 °C are plotted in Figures 3.38 through 3.41. As in the case of sulfate resisting and ordinary portland cements, the chloride concentration was higher in the specimens contaminated with both sodium chloride plus sodium sulfate compared to those contaminated with only sodium chloride. Further, an increase in the chloride concentration was observed with increasing exposure temperature in the specimens contaminated with only sodium chloride. The increase in the chloride concentration with temperature may be partly due to the decrease in the pore volume resulting from elevated temperature and pozzolanic action in the blended cements. As discussed earlier, the effect of decrease in the pore volume is presumed to be negligible compared to the effect of temperature on chloride binding. In the specimens contaminated with sodium chloride plus sodium sulfate, an increase in the exposure temperature resulted in a decrease in the chloride concentration. This trend was observed in all the blended cements investigated.

The variation in the chloride concentration in the chloride-contaminated ordinary portland and blended cement mortar specimens with temperature is plotted in Figure 3.42 and Table 3.8 shows the chloride concentration as a proportion of the original concentration. The chloride concentration increased with increasing exposure temperature in both the plain and blended cements. The chloride concentration in all the

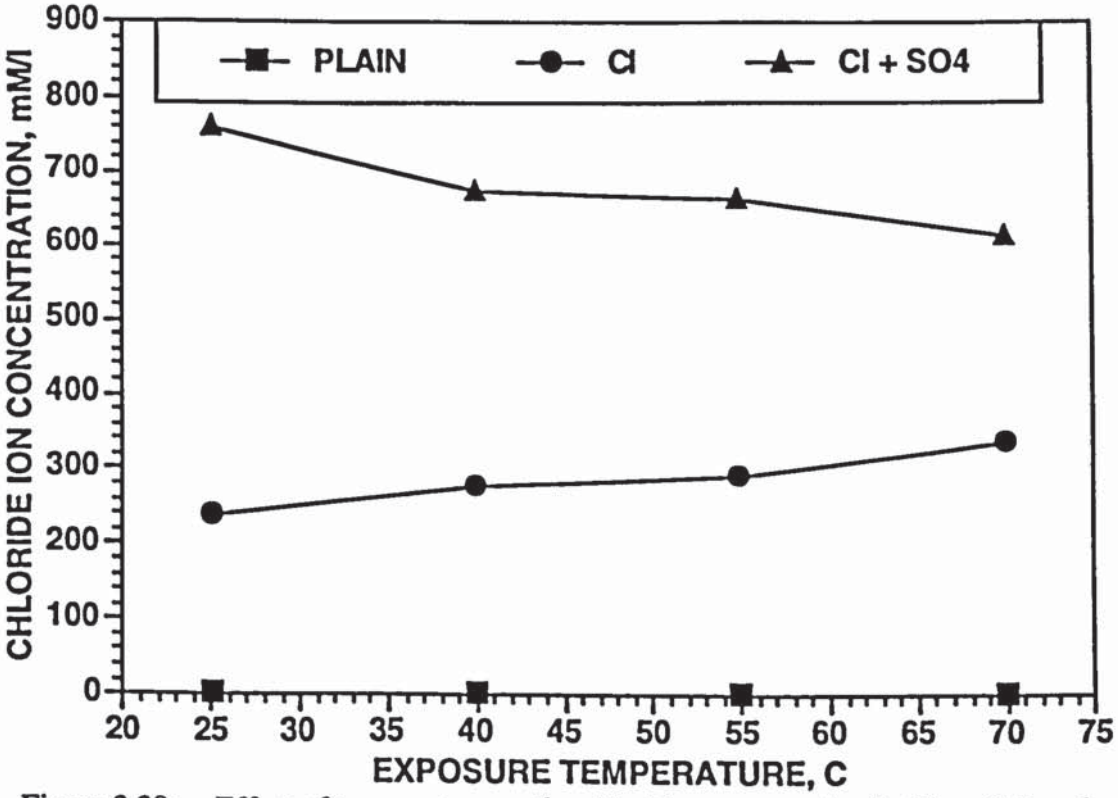

Figure 3.38: Effect of temperature on the chloride concentration in Class C fly ash blended cement mortar specimens

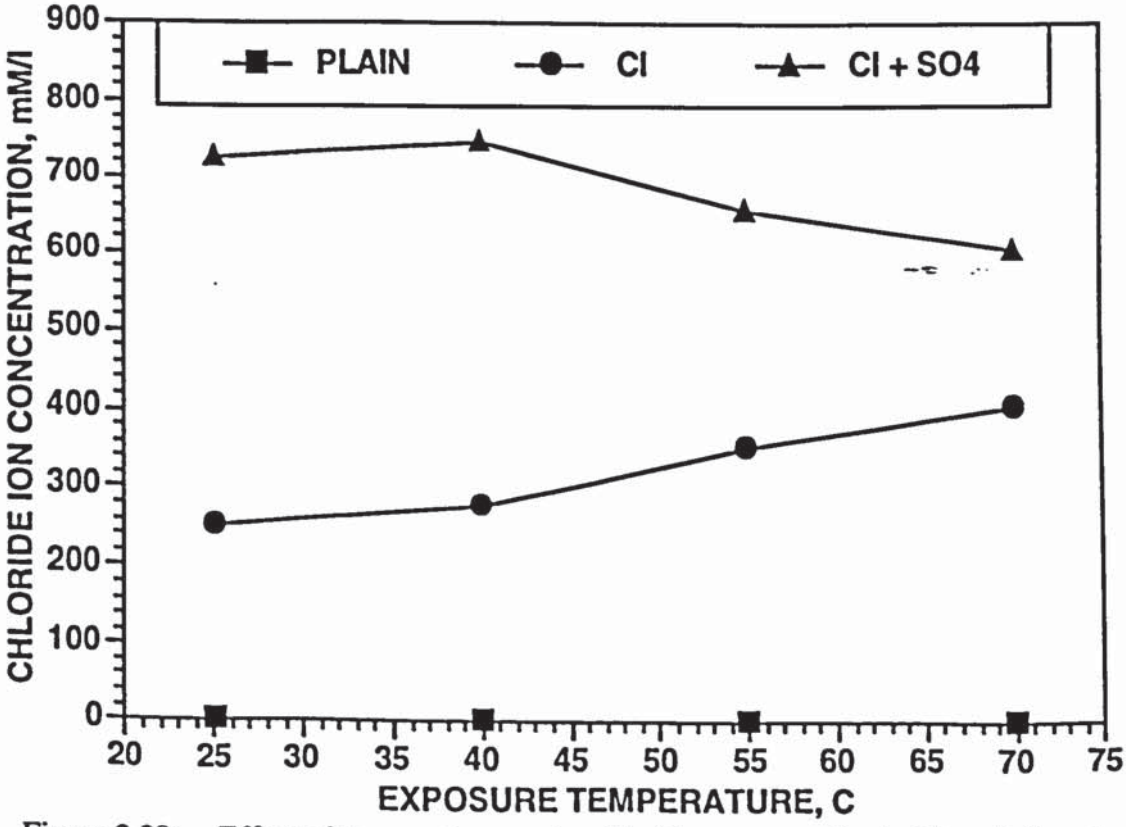

Figure 3.39: Effect of temperature on the chloride concentration in Class F fly ash blended cement mortar specimens

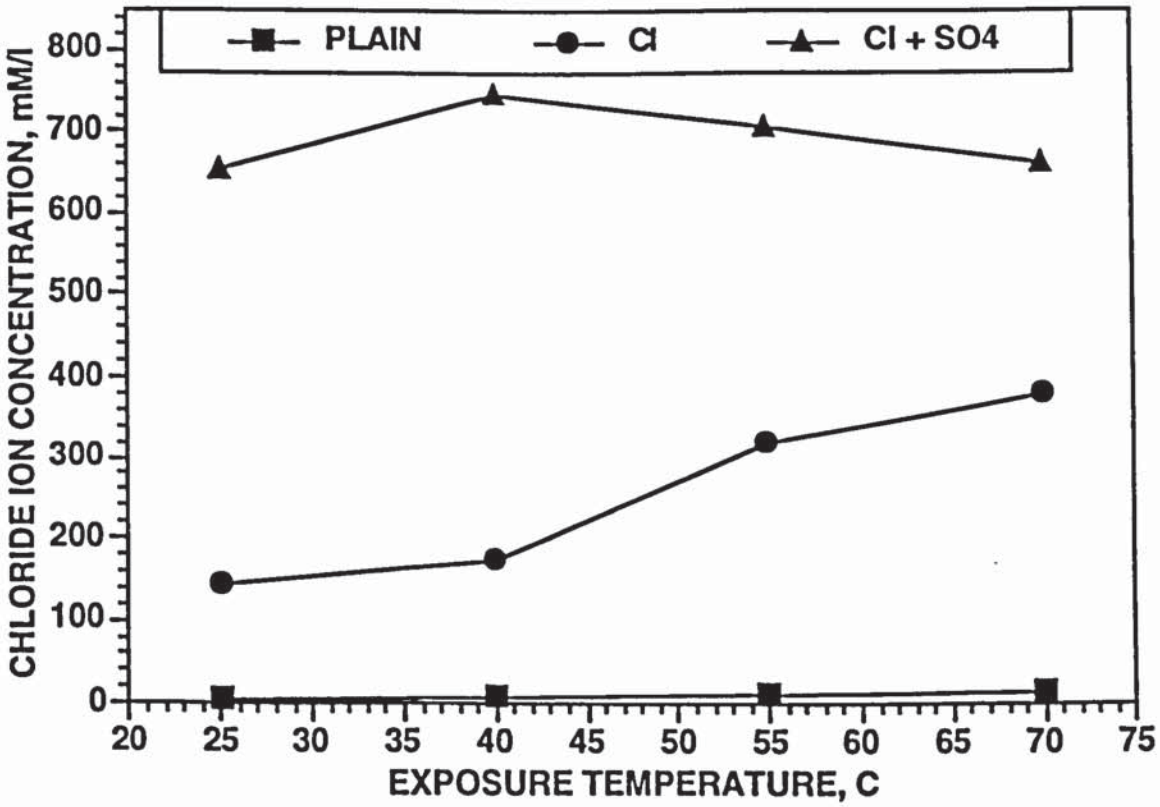

Figure 3.40: Effect of temperature on the chloride concentration in blast furnace slag cement mortar specimens

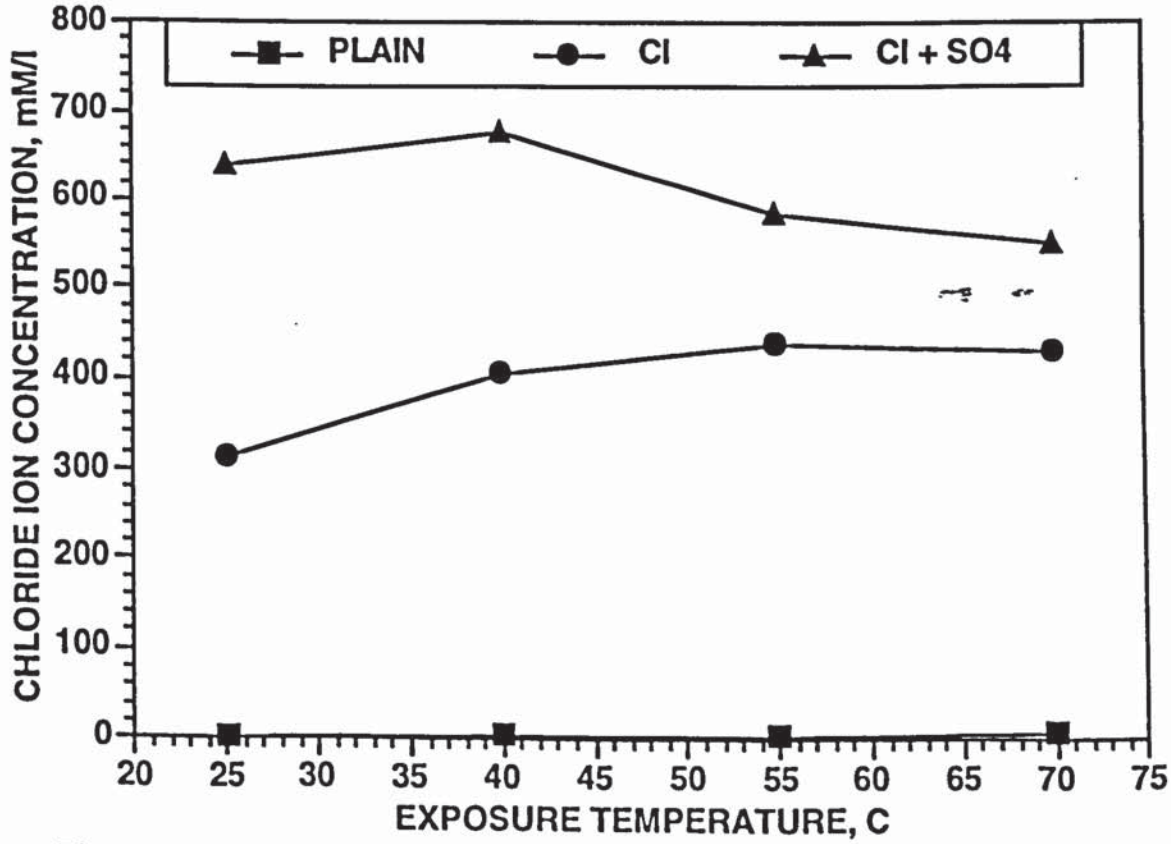

Figure 3.41 : Effect of temperature on the chloride concentration in silica fume blended cement mortar specimens

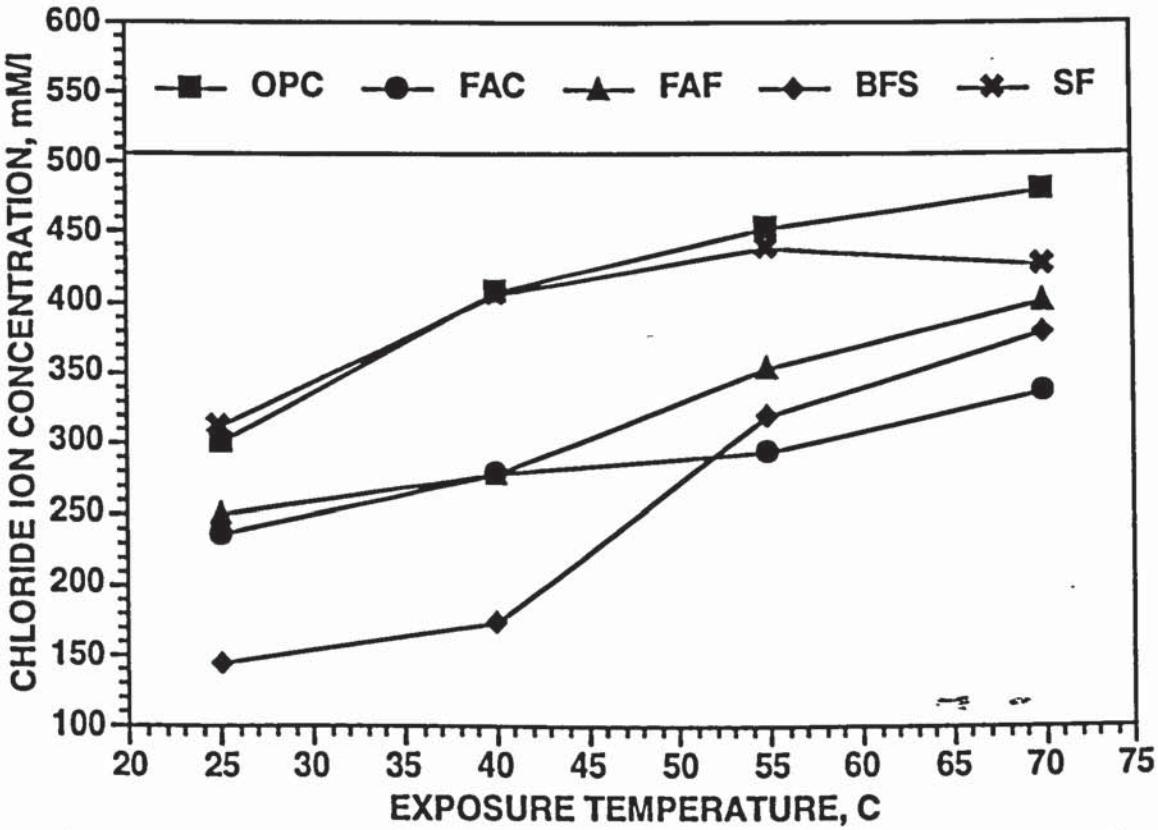

Figure 3.42: Effect of temperature on the chloride concentration in ordinary and blended cement mortar specimens contaminated with sodium chloride

blended cements and at all the exposure temperatures was less than that in the plain cement. An exception to this trend was indicated by the silica fume blended cement. The chloride concentration in this cement was slightly higher than that in the plain cement at exposure temperature of 25 °C.

Table 3.8: Chloride concentration in plain and blended cement mortar specimens contaminated with NaCl

Cement	Chloride concentration, percent in the mix water, for exposure temperatures of			
	25 °C	40 °C	55 °C	70 °C
OPC	40.7	55.3	61.5	65.3
Fly Ash 'C'	32.0	37.8	39.8	45.9
Fly Ash 'F'	34.0	37.8	48.1	54.6
Silica Fume	42.4	55.1	59.7	58.0
BFSC	19.5	23.7	43.4	51.7

The reduced chloride binding capacity of silica fume blended cement compared to other blended cements and OPC at 25 °C, has been reported by several other researchers [64-66,105]. Page and Vennesland [64] investigated the effect of 0, 10, 20 and 30% cement replacement by silica fume on the pore solution alkalinity and chloride binding. Their results indicated that incorporation of increasing percentages of silica fume in portland cement paste would lead to a progressive reduction in the extent to which chloride ions, introduced during mixing, are excluded from the pore solution. Data from differential thermal analyses coupled with differential thermogravimetric analyses indicated that an increase in the silica fume content brought about not only an expected systematic reduction in the quantity of $Ca(OH)_2$, but also a regular diminution in the quantity of calcium chloro-aluminate hydrates [64]. They indicated that this effect of decreased chloride binding may be attributed to the increased solubility of

Friedel's salt due to the reduction in the pH as a result of incorporation of silica fume in the cement.

Diamond [87] referring to the above hypothesis of Page and Vennesland [64], regarding the lowering of the chloride binding due to reduction in the alkalinity, indicated that the reduced chloride binding capacity in the silica fume blended cements, among other phenomena, may be attributed to the reduction in the mix water due to the formation of hydration products. Rasheeduzzafar et al. [65] investigated the pore solution chemistry of silica fume blended cements contaminated with 0.6 and 1.2% chloride ions and indicated that the chloride ion concentration in the 10 to 20% silica fume blended cement was more than double the free chloride ion concentration in the in the ordinary portland cement. Similar results of increased free chloride ion concentration in silica fume blended cements compared to OPC at temperature of 25 °C have been reported by Al-Amoudi et al. [72]. However, results contradicting the above findings have also been reported [67]. Byfors et al. [67] reporting the results of a collaborative research project carried out between The Swedish Cement and Concrete Research Institute, The Danish Corrosion Centre, and The Technical Research Institute for Materials Testing, to evaluate the effect of fly ash, slag and silica fume additions on the degree of chloride binding by the cement, indicated higher chloride binding in silica fume blended cements than in the ordinary portland cement. They [67] attributed this increase in the chloride binding capacity of the silica fume cement over that of the ordinary portland cement to the specific surface area of the gel in the silica fume cement paste.

The superior performance of fly ash and blast furnace slag cements, compared to portland cements, in binding chlorides has been reported by several investigators [15,60,66,68,72,106]. Holden et al. [15] investigated the effect of chloride addition, 0.4% by weight of cement, on the chloride binding capacity of fly ash and blast furnace

slag blended cements. Their results indicated higher chloride binding in fly ash and BFS cements compared to SRPC and OPC. Kayyali et al. [60] studied the effect of fly ash addition on the pore solution concentration in cement mortar specimens contaminated with NaCl and $CaCl_2$. A marginal decrease in the chloride ion concentration was recorded due to incorporation of fly ash in mortar specimens contaminated with NaCl and $CaCl_2$. Kawamura et al. [107] reported the formation of Friedel's salt, detected by DTA, in both plain and fly ash blended cements. Andrade and Page [88] investigated the effect of cation type on the chloride binding capacity of OPC and blast furnace slag cement. The chloride binding in the blast furnace slag cement was higher than that in the ordinary portland cements, when both were contaminated with NaCl and $CaCl_2$. Greater chloride binding in fly ash and slag cements compared to ordinary portland cements has also been reported by Hussain [82]. It is understood that the chloride binding in the slag cements takes place by mechanisms other than the formation of Friedel's salt, possibly the slag itself is capable of removing some of the chlorides. It is also probable that the chloride ions are adsorbed on the C-S-H gel in the slag cements. This chloride being more loosely bound than with C_3A. This was confirmed in a recent study conducted at KFUPM [108], which indicated that the chloride concentration in the blast furnace slag cement (slag constituted 70% of the total cementitious material) was more than that in the ordinary portland cement paste specimens.

The increase in the chloride concentration in all the blended cements with increasing exposure temperature, particularly in excess of 40 °C, indicates the instability of the chloride-complexes formed at lower temperatures.

Another point to be noted from the data in Table 3.8 is the lower chloride concentration in the silica fume cement, compared to OPC at exposure temperature of

40 °C and above. Further, the chloride binding performance of this cement improved with increasing temperature in comparison with OPC.

The chloride concentration in the blended and ordinary portland cement mortar specimens contaminated with sodium chloride plus sodium sulfate is plotted against exposure temperature in Figure 3.43. These data do not show a definite trend with regard to exposure temperature and cement type on chloride binding.

3.2.1.3 Cl^-/OH^- Ratio

The chloride to hydroxyl ion ratios in the contaminated and uncontaminated SRPC mortar specimens are plotted in Figure 3.44. As expected, these values in the uncontaminated specimens and those contaminated with sodium sulfate were very low. Further, the Cl^-/OH^- in all the specimens increased with the exposure temperature. The variation in the Cl^-/OH^- values in the specimens exposed to 25 and 40 °C was insignificant. However, a significant increase in these values was recorded for exposure temperatures of 55 °C and above. The increase in the Cl^-/OH^- ratio due to elevated temperature exposure may be partly attributed to the reduction in the volume of the pore solution. However, as discussed earlier, the effect of temperature on chloride binding and reduction in the OH^- concentration predominates that due to the reduction in the pore volume. The Cl^-/OH^- values in the specimens exposed to 70 °C were 3 to 4 times those in the specimens exposed to 25 °C. This increase may be attributed to the cumulative effect of increase in the chloride concentration and decrease in the hydroxyl ion concentration in the specimens exposed to temperatures of 55 °C and above. The Cl^-/OH^- values in the specimens contaminated with only sodium chloride were more than those in the specimens contaminated with sodium chloride plus sodium sulfate. This trend was observed at all exposure temperatures. The reduction in the Cl^-/OH^- values, in the specimens contaminated with sodium chloride plus sodium sulfate,

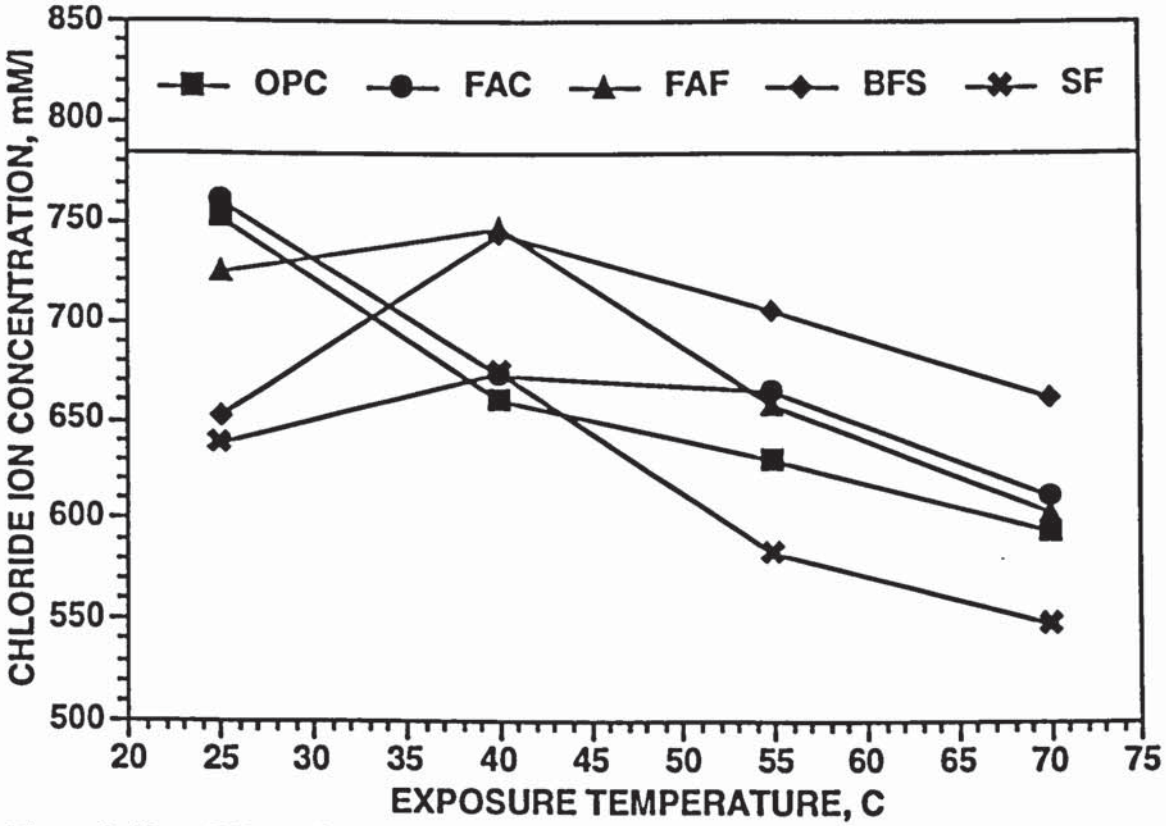

Figure 3.43: Effect of temperature and chloride-sulfate contamination on the chloride concentration in ordinary and blended cements

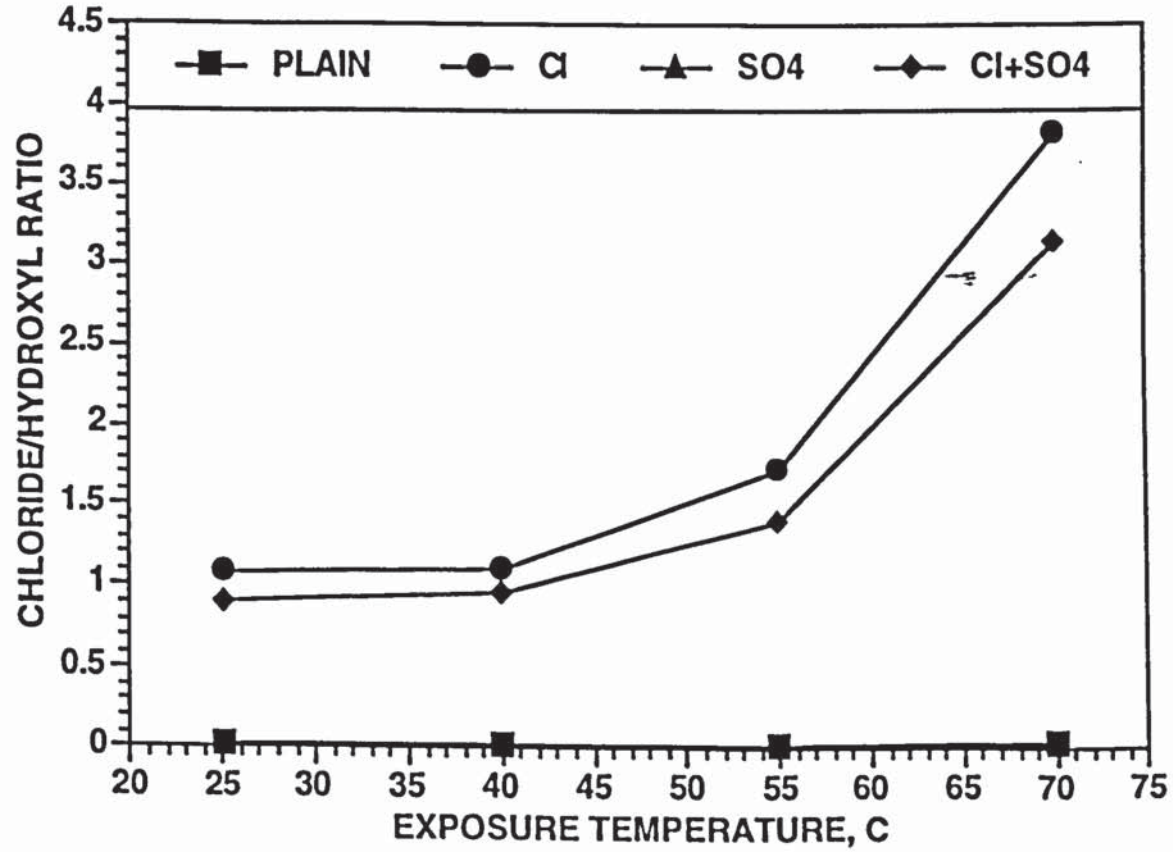

Figure 3.44: Effect of temperature and chloride-sulfate contamination on Cl^-/OH^- in SRPC

inspite of a considerable increase in the chloride ion concentration, may be attributed to the increase in the OH^- concentration due to the incorporation of NaCl and Na_2SO_4. The Cl^-/OH^- ratios in the chloride-contaminated specimens were, however, more than 0.6, the threshold value suggested by Hausmann [73] for steel depassivation, at all the exposure temperatures.

The Cl^-/OH^- in OPC-A cement (C_3A: 8.5%) are plotted against exposure temperature in Figure 3.45. The Cl^-/OH^- values in the specimens contaminated with sodium chloride were more than those in specimens contaminated with sodium chloride plus sodium sulfate. The Cl^-/OH^- in both of these specimens increased with exposure temperature. Again, the increase in the Cl^-/OH^- due to temperature increase from 25 to 40 °C was less significant compared to that from 40 to 70 °C. Further, the Cl^-/OH^- values in the specimens contaminated with sodium chloride and sodium chloride plus sodium sulfate were more than 0.3, the threshold value suggested by Gouda [74].

The Cl^-/OH^- values in OPC-B cement (C_3A: 14.5%) are plotted against exposure temperature in Figure 3.46. These data indicated that the Cl^-/OH^- values in specimens contaminated with sodium chloride plus sodium sulfate were more than those in the specimens contaminated with only sodium chloride. In the chloride-contaminated specimens, the Cl^-/OH^- values were less than 0.60 for exposure temperatures of 25 and 40 °C. However, these values were more than 0.60 for exposure temperatures of 55 °C and above. The Cl^-/OH^- values in the specimens contaminated with sodium chloride plus sodium sulfate were slightly higher than 0.60 for exposure temperature of 25 °C. These values were, however, more than 0.60 for exposure temperatures of 40 °C and above. The high Cl^-/OH^- values measured in the specimens contaminated with sodium chloride plus sodium sulfate, at all the exposure temperatures, indicates that high C_3A cements should not be used in environments characterized by the presence of

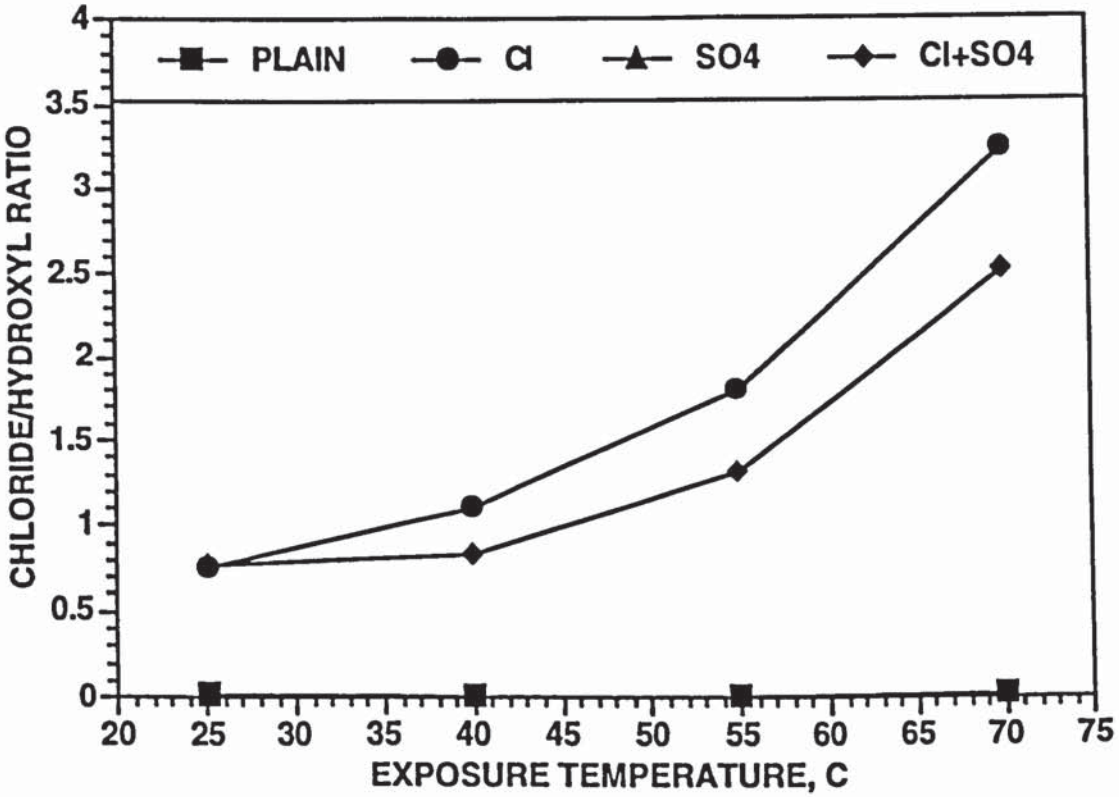

Figure 3.45: Effect of temperature and chloride-sulfate contamination on Cl^-/OH^- in OPC-A

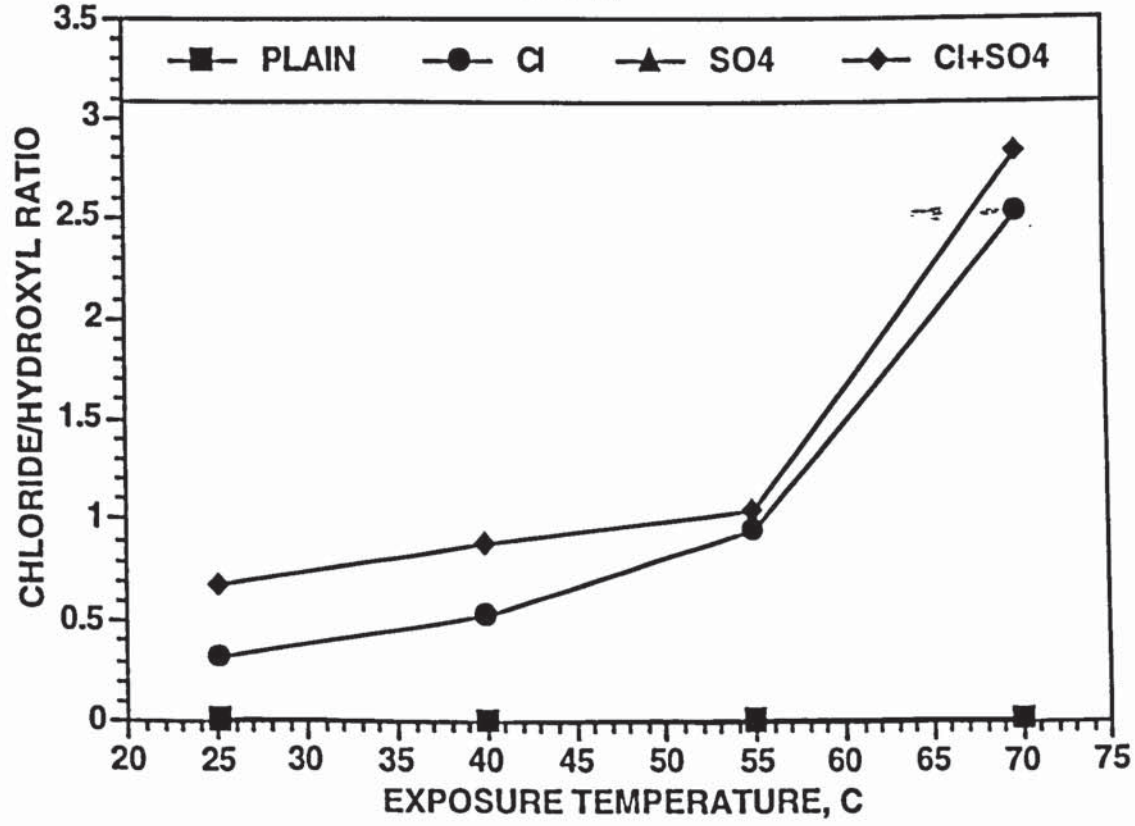

Figure 3.46: Effect of temperature and chloride-sulfate contamination on Cl^-/OH^- in OPC-B

both chloride and sulfate salts. Such a situation is normally representative of substructures in the Arabian Gulf, where the soil and groundwater are normally contaminated with chloride and sulfate salts. In such situations, use of cements with medium to low C_3A is more appropriate. Such cements will also be more resistant to sulfate deterioration compared to high C_3A cements.

The Cl^-/OH^- values in Class C fly ash blended cement are plotted in Figure 3.47. These values in the contaminated specimens were less than 0.6 at all the temperatures. The Cl^-/OH^- values in the specimens contaminated with sodium chloride were more than those contaminated with sodium chloride plus sodium sulfate up to an exposure temperature of about 65 °C. At exposure temperature of 70 °C, this trend was reversed. The Cl^-/OH^- values for Class F fly ash blended cement are plotted in Figure 3.48. The Cl^-/OH^- values in the specimens contaminated with sodium chloride and sodium chloride plus sodium sulfate were more or less similar for exposure temperatures below 45 °C. For temperatures higher than 45 °C, the Cl^-/OH^- values in the chloride-contaminated specimens were more than those contaminated with sodium chloride plus sodium sulfate. Figure 3.49 shows the Cl^-/OH^- values for blast furnace slag cement mortar specimens. These values in the specimens contaminated with sodium chloride were less than those in the specimens contaminated with sodium chloride plus sodium sulfate at all the exposure temperatures. Further, the Cl^-/OH^- values in the chloride-contaminated specimens were 0.43 and 0.58 for temperatures of 25 and 40 °C. In the specimens exposed to 55 and 70 °C, these values were more than 0.6. The Cl^-/OH^- values for silica fume blended cement mortar specimens are plotted against exposure temperature in Figure 3.50. As in other cements, the Cl^-/OH^- values increased with increasing temperature. This trend was more obvious in the specimens contaminated with sodium chloride. The Cl^-/OH^- values in the specimens contaminated with sodium chloride plus sodium sulfate remained more or less similar

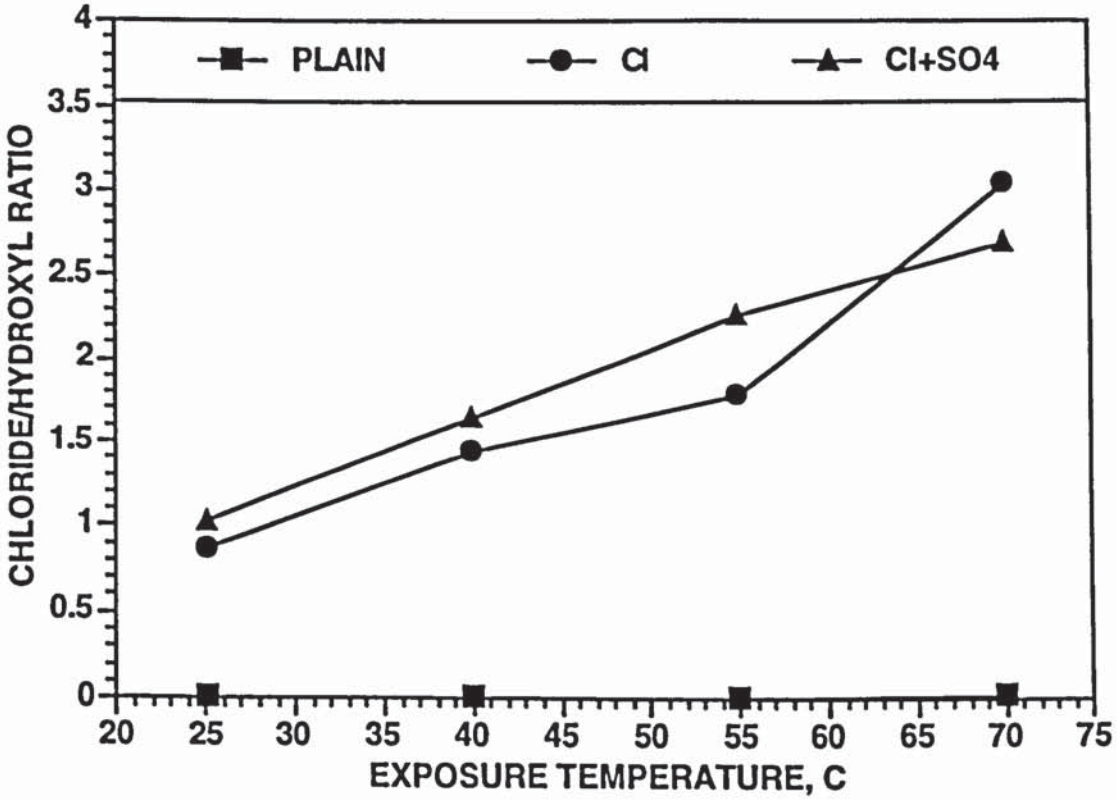

Figure 3.47: Effect of temperature on Cl^-/OH^- in class C fly ash blended cement mortar specimens

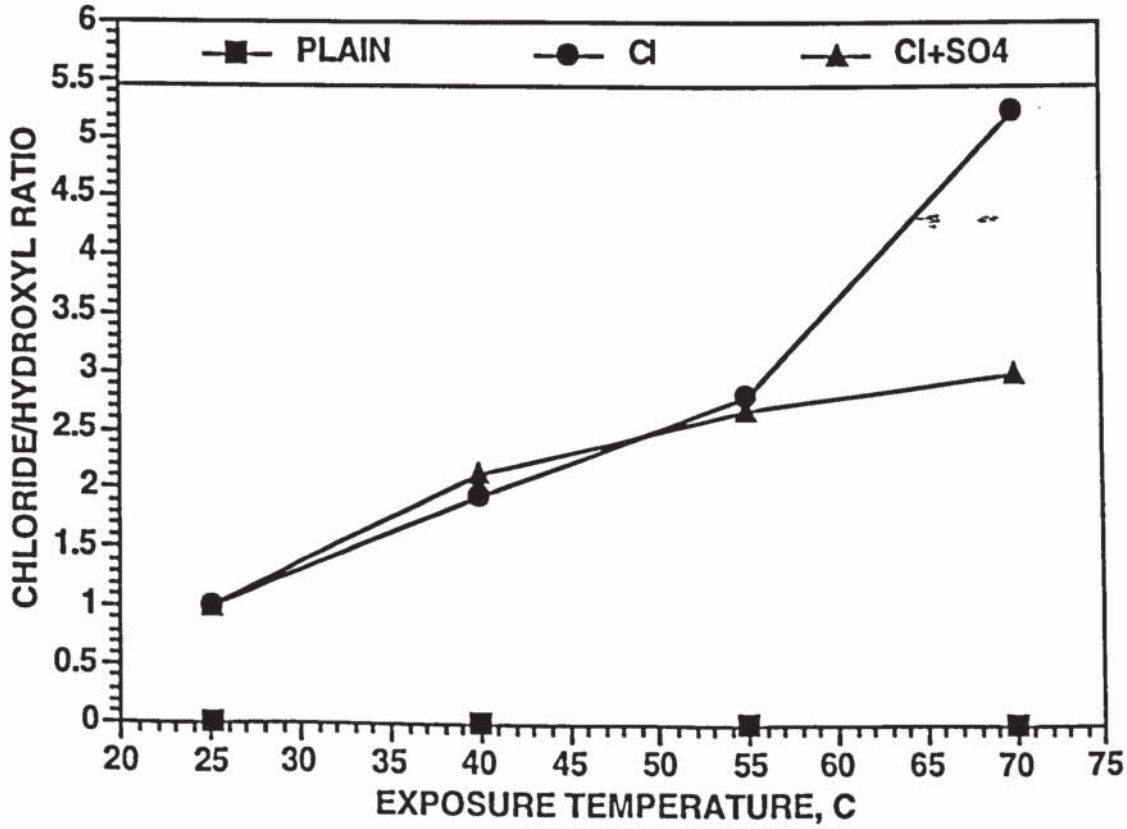

Figure 3.48: Effect of temperature on Cl^-/OH^- in class F fly ash blended cement mortar specimens

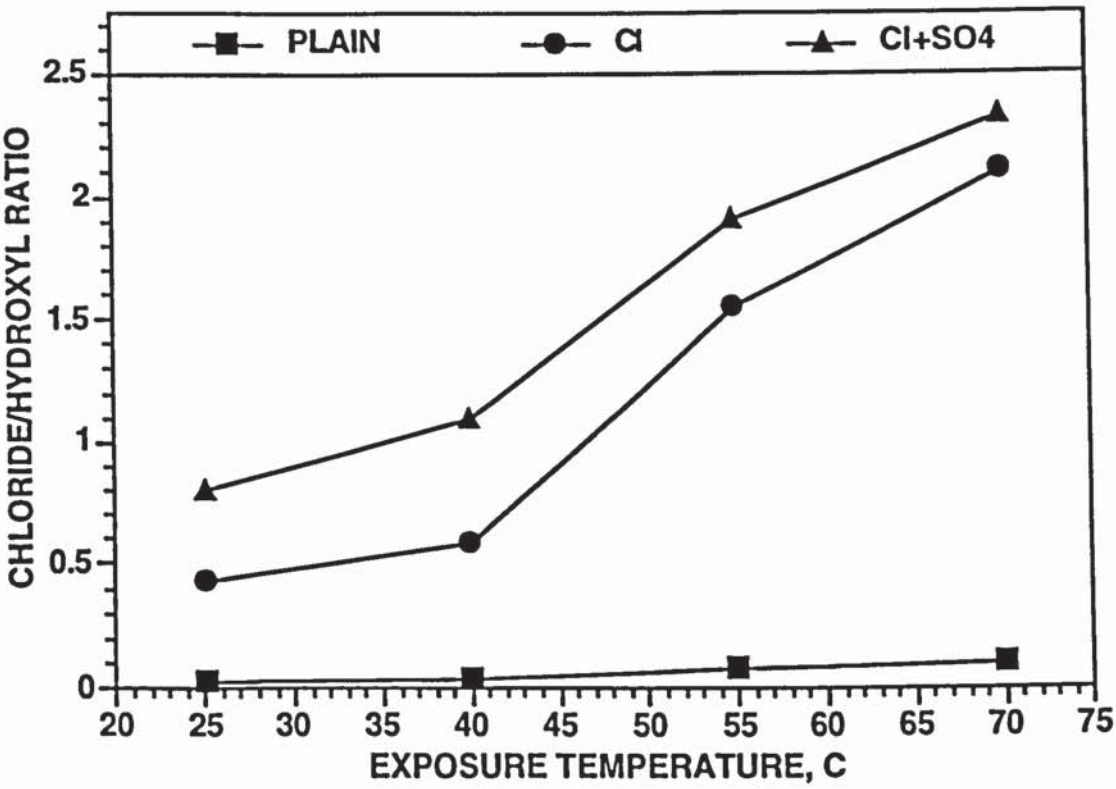

Figure 3.49 : Effect of temperature on Cl^-/OH^- in blast furnace slag cement mortar specimens

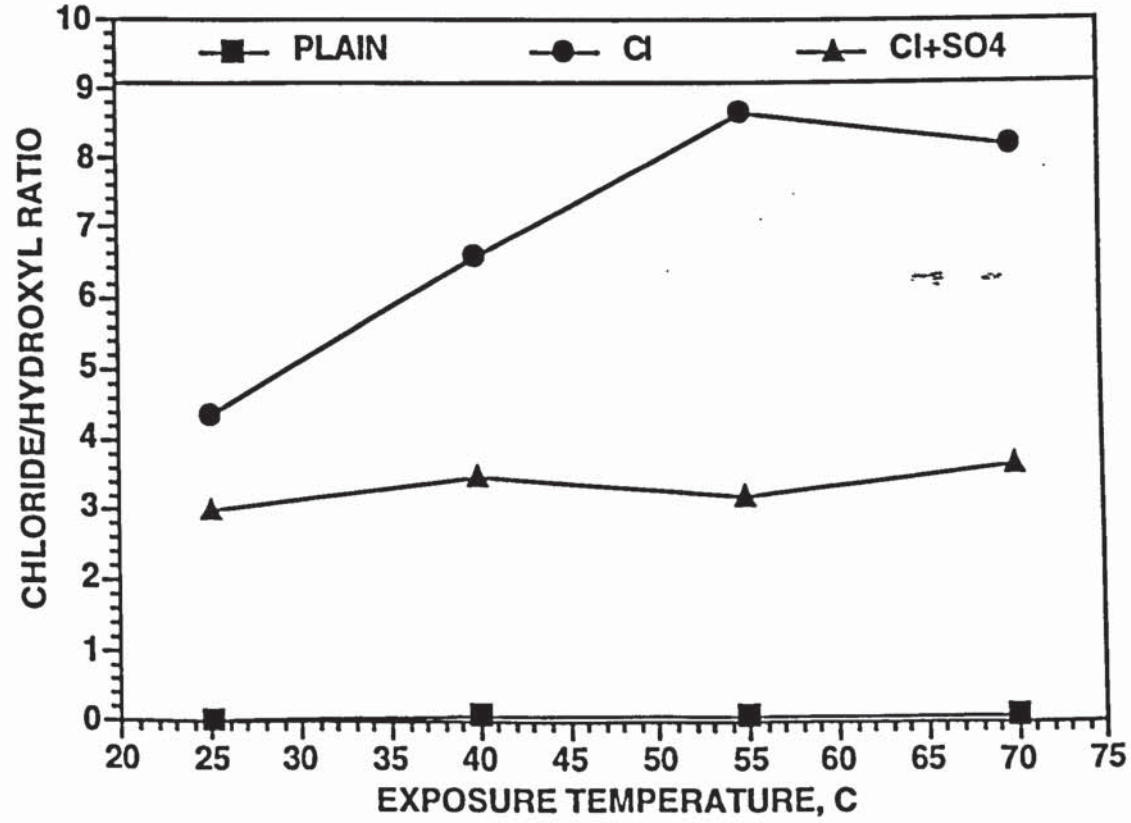

Figure 3.50: Effect of temperature on Cl^-/OH^- in silica fume blended cement mortar specimens

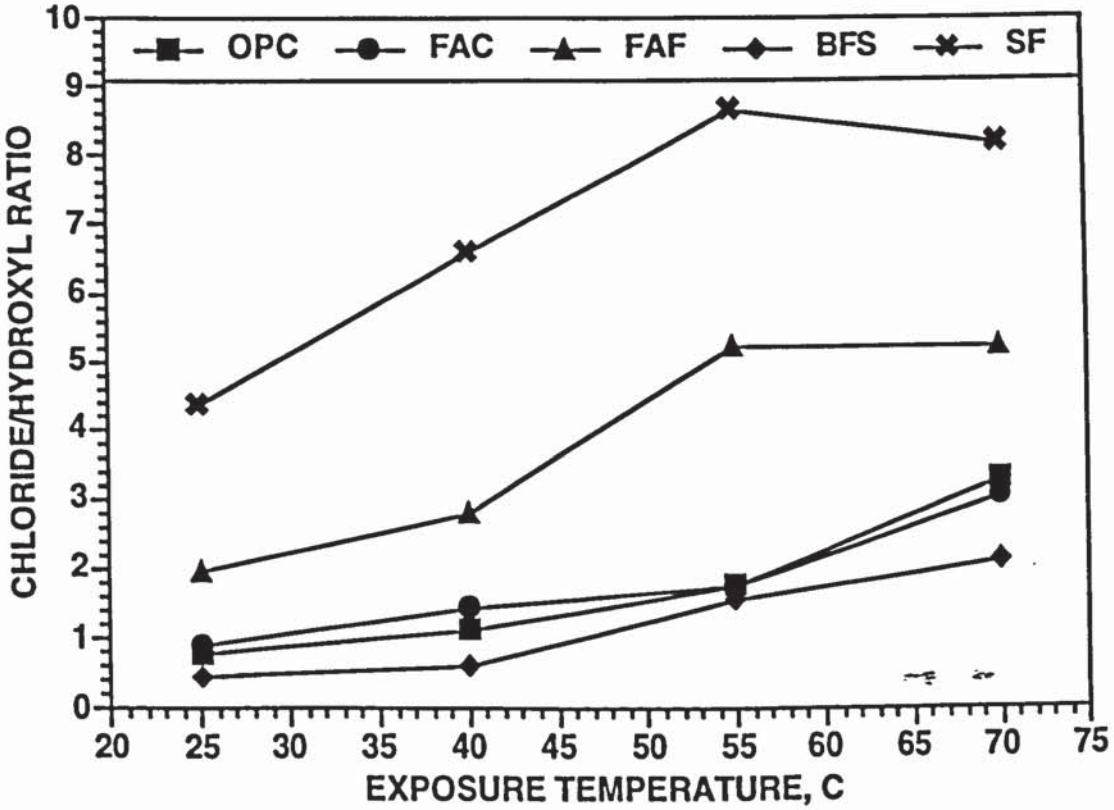

Figure 3.51: Effect of temperature on Cl^-/OH^- in chloride-contaminated ordinary and blended cement mortar specimens

for all exposure temperatures, and were less than those in the specimens contaminated with only sodium chloride.

The variation in the Cl^-/OH^- with the exposure temperature in the chloride-contaminated plain and blended cement mortar specimens is plotted in Figure 3.51. The Cl^-/OH^- values in almost all the blended cements, except blast furnace slag, were more than those in the ordinary Portland cement. The Cl^-/OH^- values in the class C fly ash cement mortar specimens were more or less similar to those in OPC at all the exposure temperatures. The highest Cl^-/OH^- values were recorded in silica fume blended cement mortar specimens. The Cl^-/OH^- values in this cement were 6 and 2.5 times those in the OPC at exposure temperatures of 25 and 70 °C, respectively. These data indicate the usefulness of using blast furnace slag in structures where chloride contamination is inevitable.

The Cl^-/OH^- values in the OPC and blended cements, contaminated with sodium chloride plus sodium sulfate, are plotted against exposure temperature in Figure 3.52. The Cl^-/OH^- values in the OPC were lower than in other blended cements for exposure temperature up to 55 °C. At 70 °C, however, the Cl^-/OH^- values were the least in the blast furnace slag cement mortar specimens. This indicates that while the use of blast furnace slag cement may be beneficial in environments characterized by the presence of chloride ions, its performance in service environments where both chloride and sulfate salts are prevalent may not be very significant compared to OPC particularly at 25 °C. Such a situation is representative of the substructural components in the Arabian Gulf which are exposed to groundwater and the concrete temperature is normally maintained at 25 to 30 °C, even when the ambient temperature is in the range of 40 to 45 °C. At 70 °C, however, the Cl^-/OH^- in blast furnace slag cements was lower than in OPC, indicating the usefulness of this cement in environments characterized by the concomitant presence of chloride-sulfate salts and elevated temperature such as in off-shore structures in warm environments.

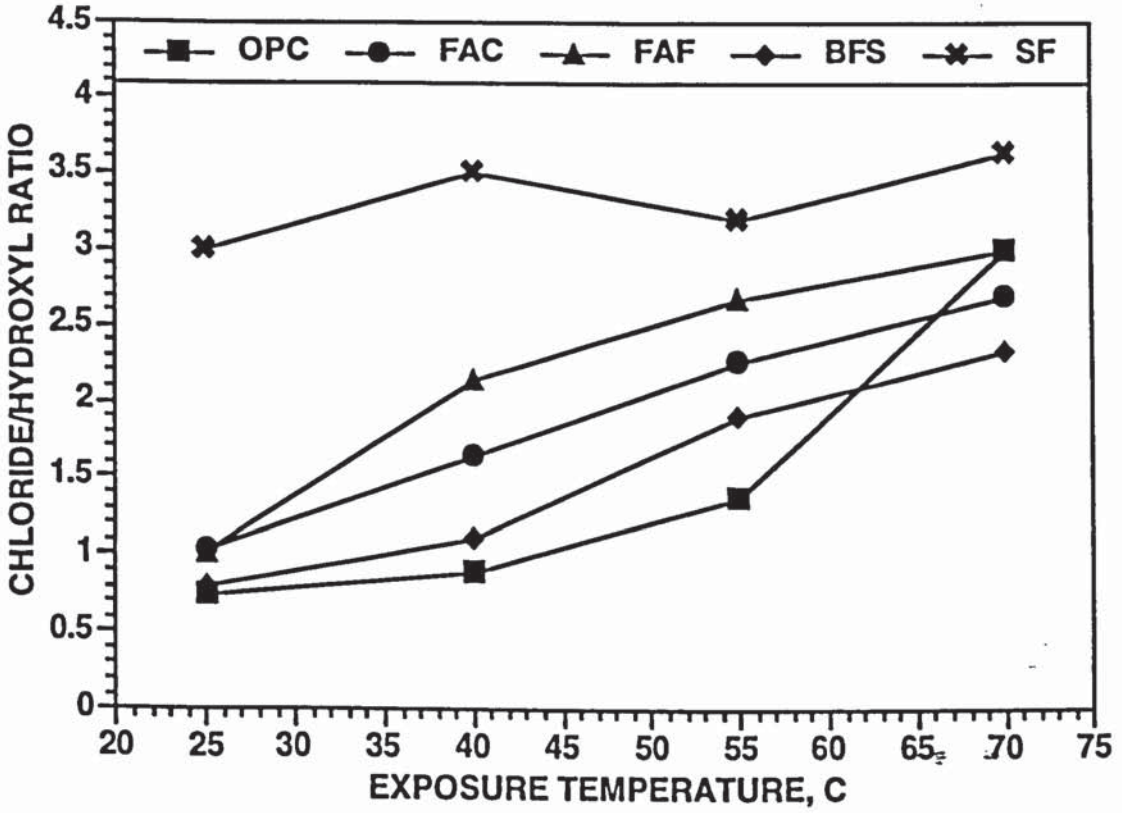

Figure 3.52: Effect of temperature on Cl^-/OH^- in ordinary and blended cement mortar specimens contaminated with chloride-sulfate

Another point of discussion concerns the importance of Cl^-/OH^- with regard to the real danger of reinforcement corrosion. Although a threshold value of 0.30, as suggested by Gouda [74], is now considered to be the threshold value for depassivation of steel, these values may be significantly altered due to temperature and the presence of sulfate ions [64]. Lambert et al. [109] investigated the relationship between Cl^-/OH^- and corrosion current density in various cements. Their investigations indicated that the passive condition on steel in concrete, characterized by corrosion current density (I_{corr}) of less than 100 nA/cm^2, was maintained until a threshold Cl^-/OH^- ratio of approximately 3 was exceeded. There was a considerable scatter in the values of I_{corr} recorded at Cl^-/OH^- ratios in excess of 3 and, even at Cl^-/OH^- ratios as high as 15 to 20 there were instances of bars suffering no significant corrosion. In another study, Mangat and Gurusamy [110] reported that for steel fibers in concrete under conditions of marine exposure, no visible signs of corrosion were present at Cl^-/OH^- ratios as high as 320, suggesting that passive conditions can prevail even under very high values of Cl^-/OH^-. Furthermore, even if the Cl^-/OH^- ratio is high, the kinetics of reinforcement corrosion is dependent on the availability of the reactants and resistivity of concrete. A case in point is silica fume cement concrete. In this cement, the alkalinity of the pore solution is significantly lower than that in other plain and blended cements, and also the chloride-binding capacity of this cement is lower than that of other cements, the net effect being a very high Cl^-/OH^- ratio (Figure 3.51 and 3.52). However, the electrical resistivity of this cement is so great that even if steel is depassivated, due to high Cl^-/OH^- ratio, essentially no corrosion can take place [111]. Al-Amoudi et al. [72] investigated the performance of OPC and blended cements in sulfate-chloride environments. The Cl^-/OH^- ratio in the silica fume cement was 4 to 10 times that in OPC and other blended cements. The reinforcement corrosion in the silica fume cement concrete specimens, exposed to varying concentrations of chloride and sulfate solutions was, however, less than that in other cements. Similar results

projecting the superior performance of silica fume cements over other cements has been indicated in other studies [75,82-83,104,112-115].

3.2.1.4 Sulfate Concentration

The sulfate concentration in the SRP cement (C_3A: 3.5%) mortar specimens exposed to the four temperatures investigated in this study are plotted in Figures 3.53 to 3.56. These data generally indicated an increase in the sulfate concentration with period of exposure. This trend was observed in all the specimens exposed to all the temperatures. The sulfate concentration in the specimens contaminated with sodium chloride plus sodium sulfate was higher than that in the specimens contaminated with only sodium sulfate. The effect of temperature on the sulfate concentration is plotted in Figure 3.57. The sulfate ion concentration was observed to increase almost linearly with the exposure temperature in the specimens contaminated with sodium sulfate and sodium chloride plus sodium sulfate. The difference in the sulfate concentration in these two types of specimens, however, decreased with increasing exposure temperature, in so much so, the sulfate concentration in the specimens exposed to 70 °C was almost similar. The sulfate concentration in the uncontaminated and chloride-contaminated specimens also increased with increasing temperature, particularly for exposure temperatures of 55 °C and above. Further, the sulfate concentration in the chloride contaminated specimens was more than that in the uncontaminated specimens at all the exposure temperatures.

The sulfate concentration in the mortar specimens made with OPC-A (C_3A: 8.5%) is shown in Figures 3.58 through 3.61. These data indicated a trend similar to that exhibited in Figures 3.53 through 3.55. The effect of temperature on sulfate concentration for these specimens is summarized in Figure 3.62. These data indicated that the sulfate concentration in the specimens contaminated with sodium sulfate and

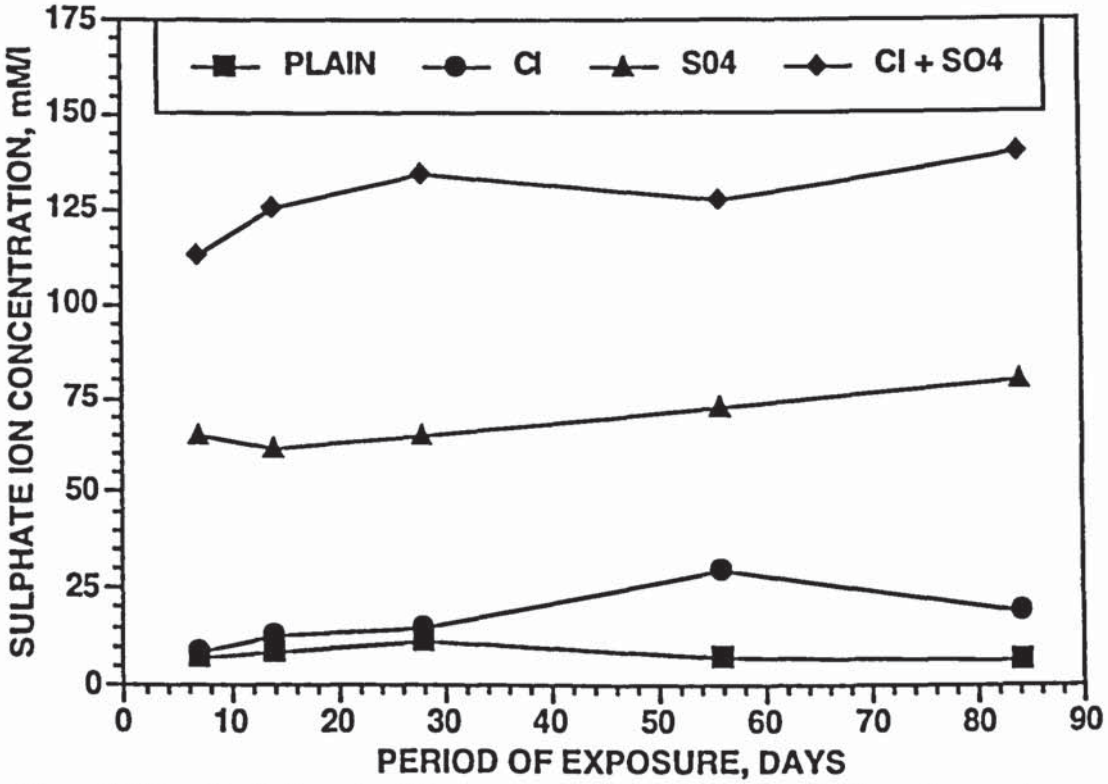

Figure 3.53: Variation of sulfate concentration with age in SRPC mortar specimens exposed to 25 °C

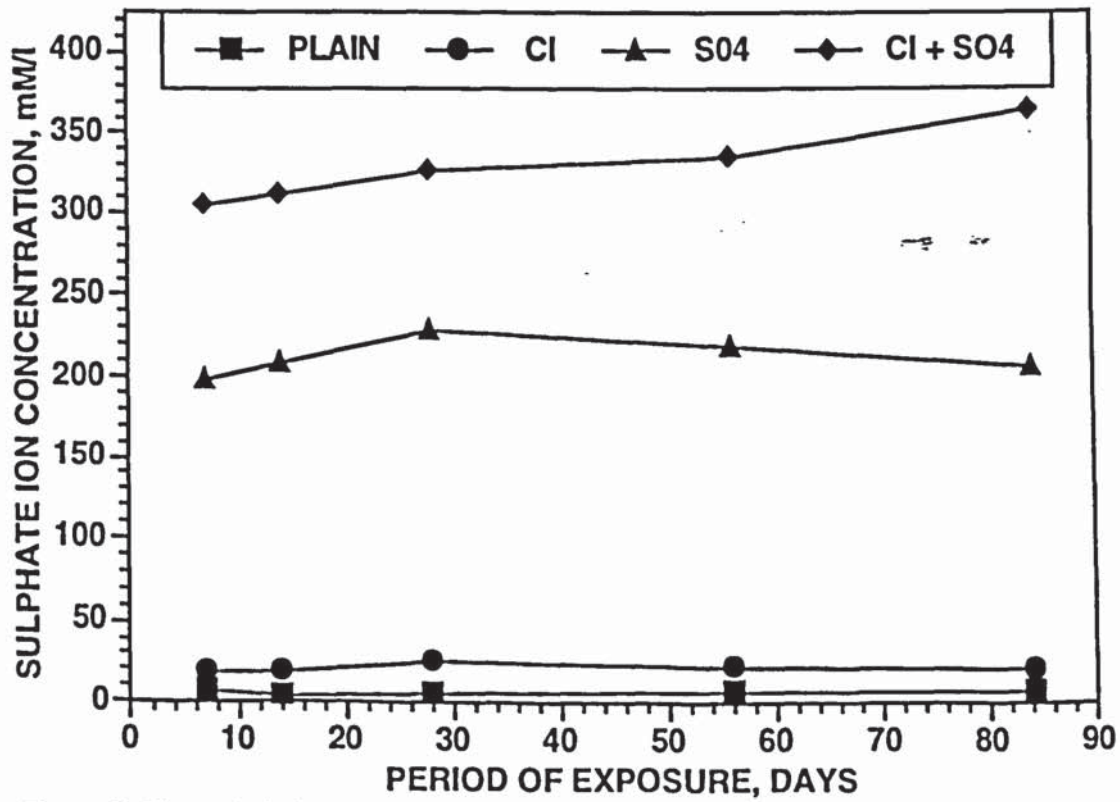

Figure 3.54: Variation of sulfate concentration with age in SRPC mortar specimens exposed to 40 °C

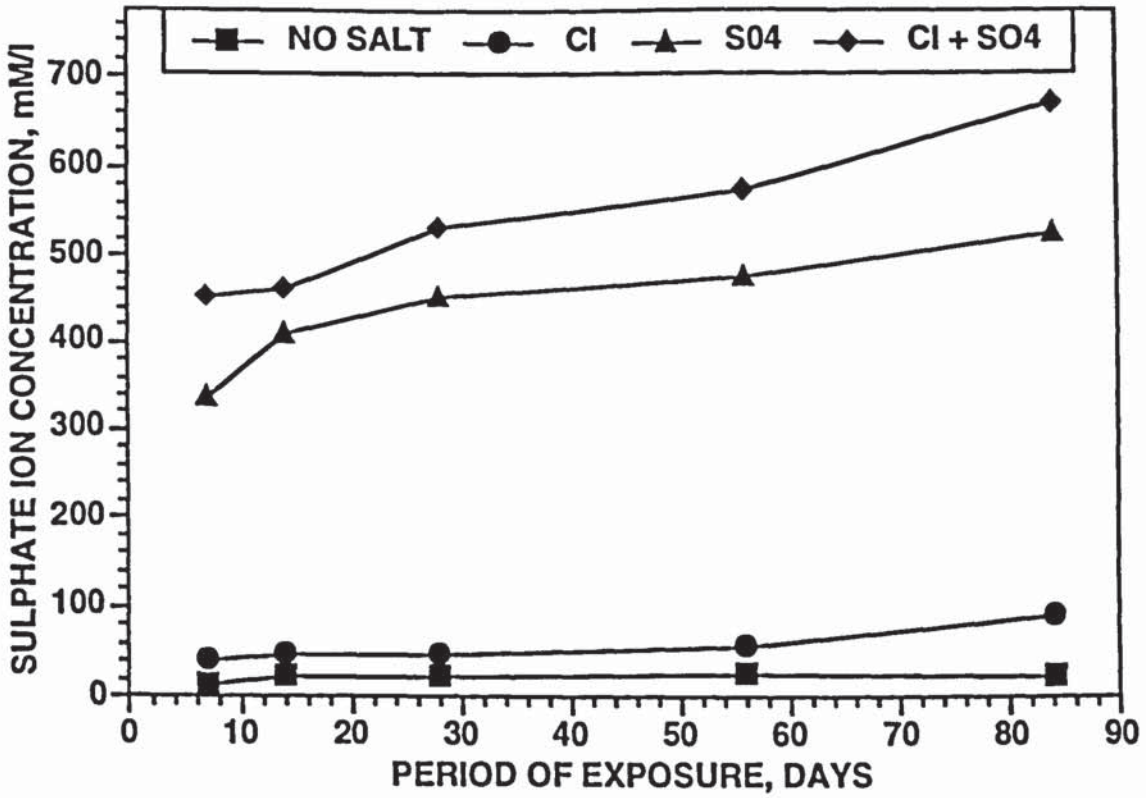

Figure 3.55: Variation of sulfate concentration with age in SRPC mortar specimens exposed to 55 °C

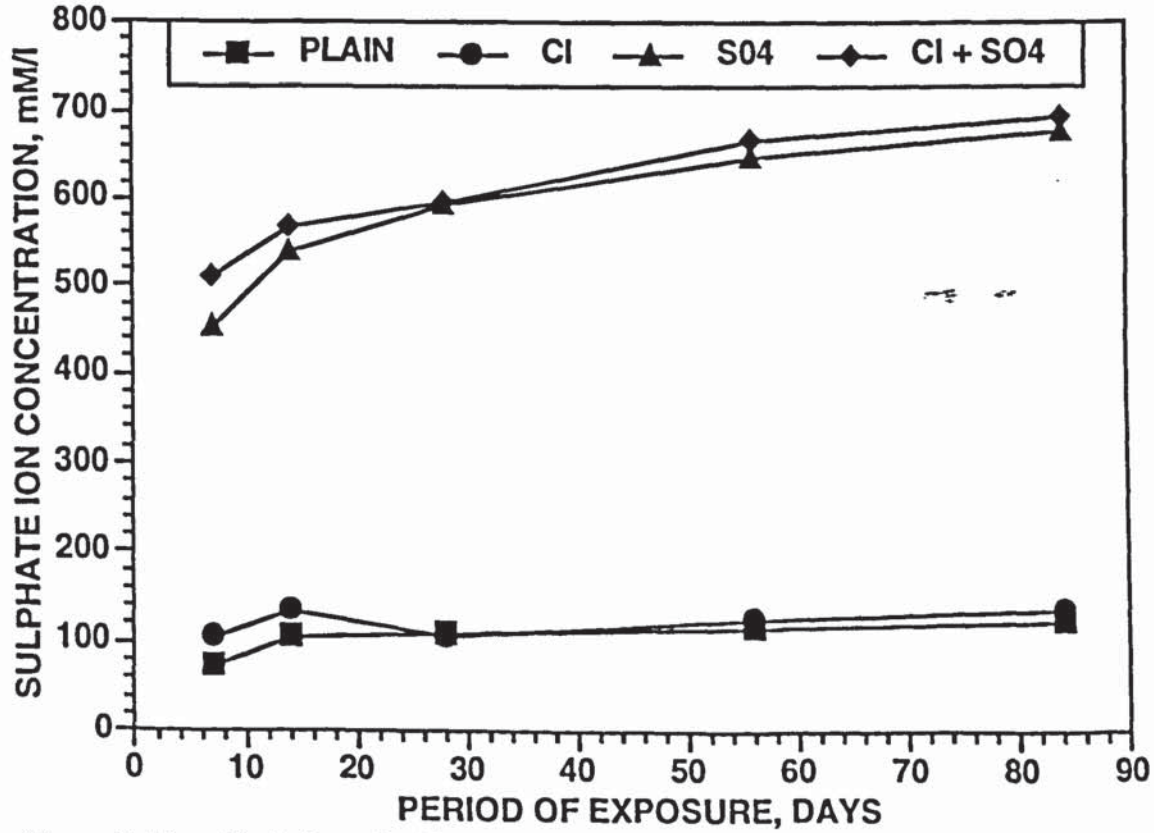

Figure 3.56: Variation of sulfate concentration with age in SRPC mortar specimens exposed to 70 °C

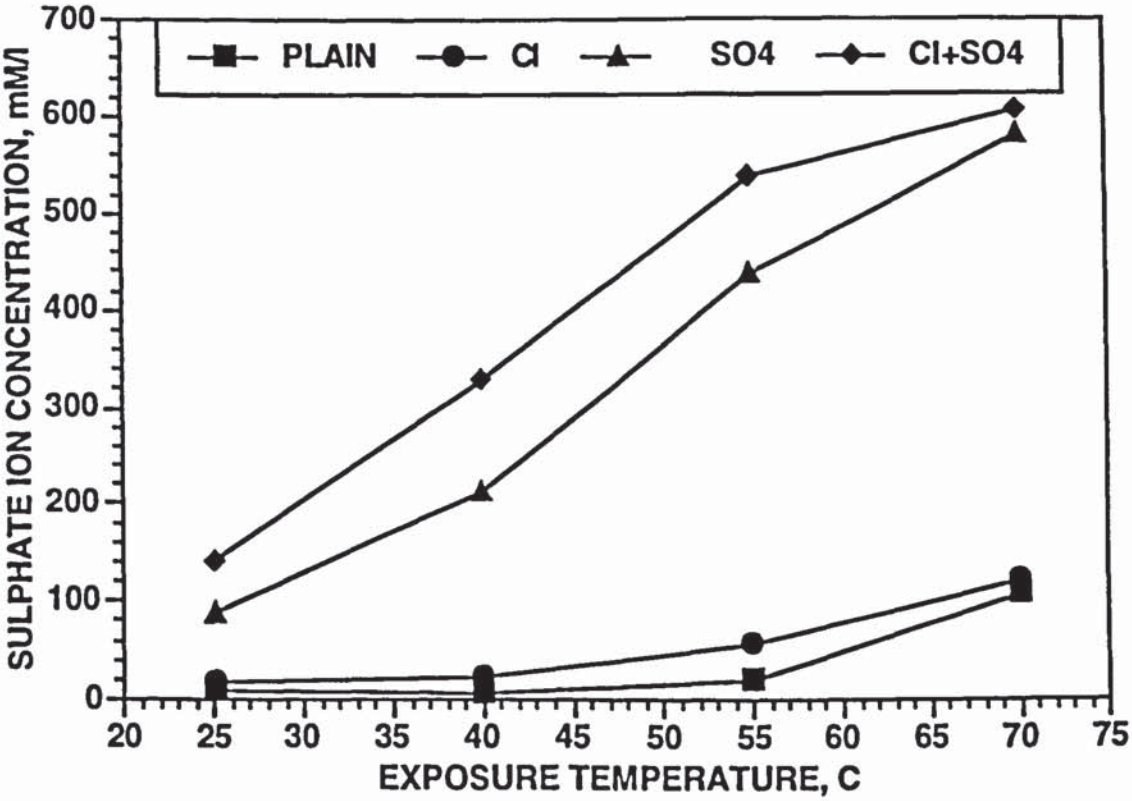

Figure 3.57: Effect of temperature on sulfate concentration in SRPC

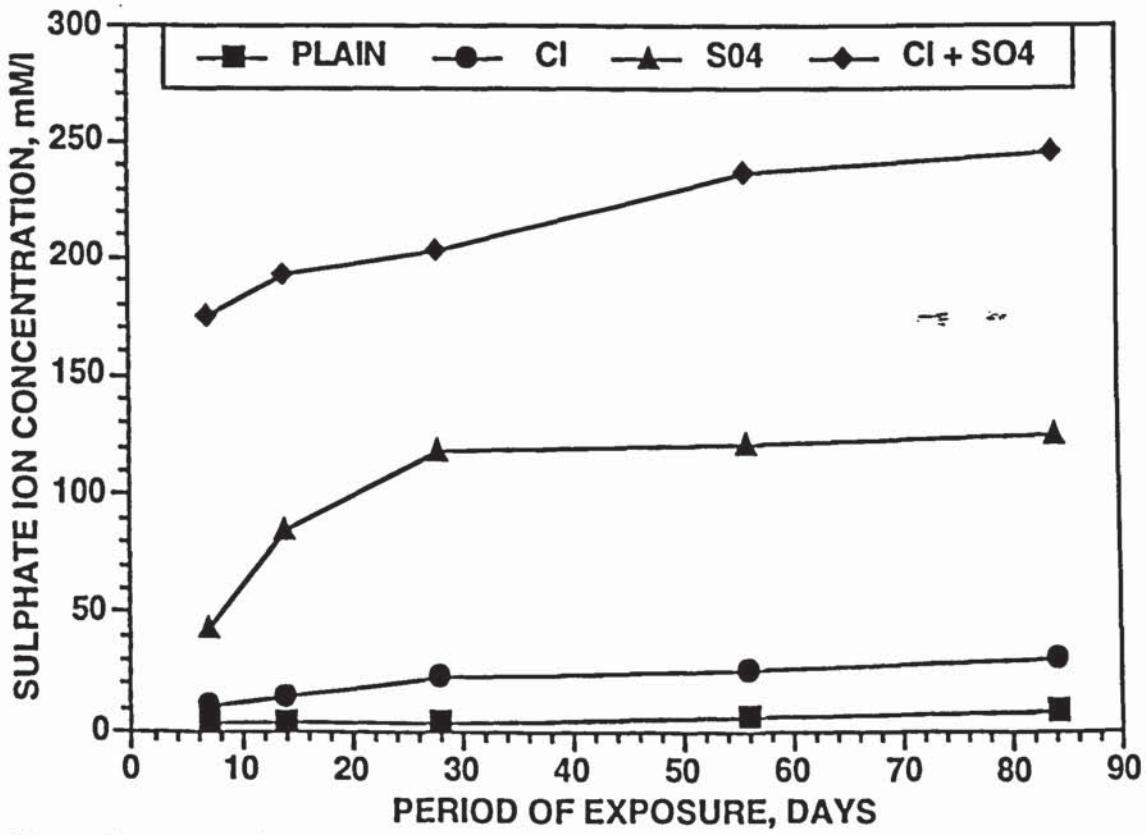

Figure 3.58: Variation of sulfate concentration with age in OPC-A mortar specimens exposed to 25 °C

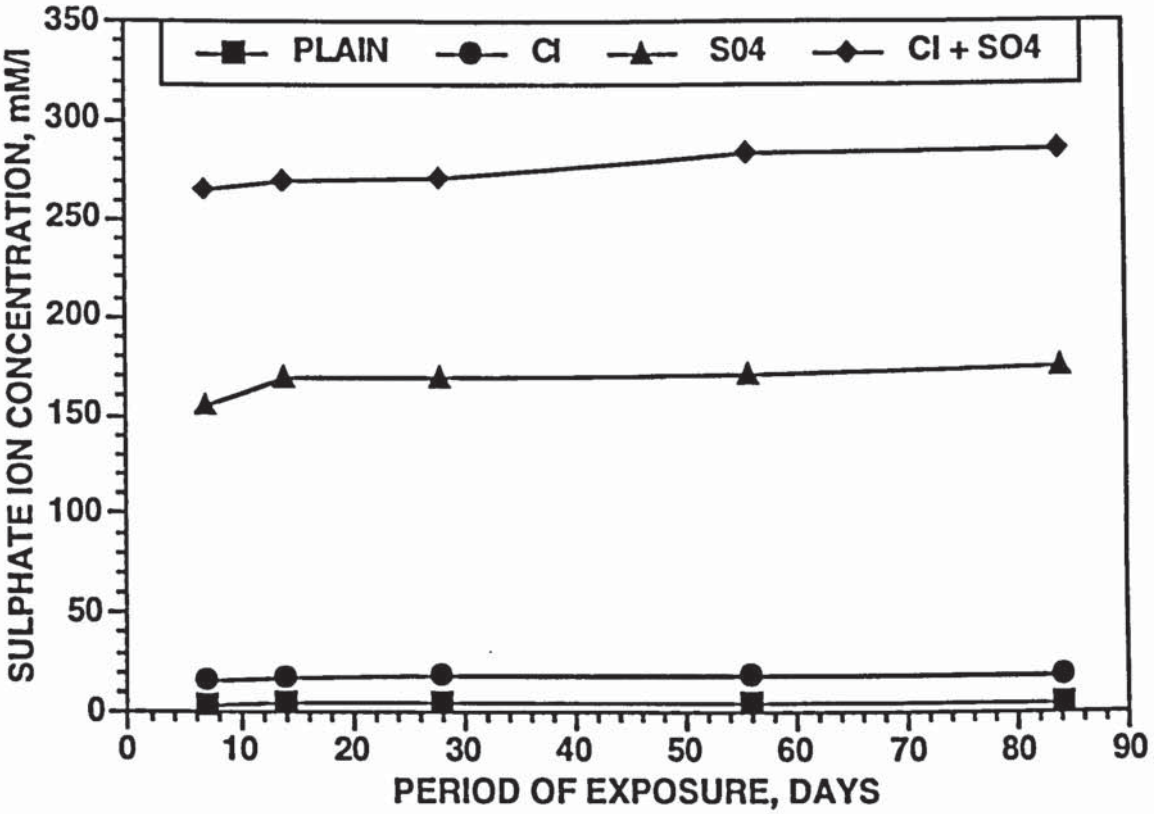

Figure 3.59 : Variation of sulfate concentration with age in OPC-A mortar specimens exposed to 40 °C

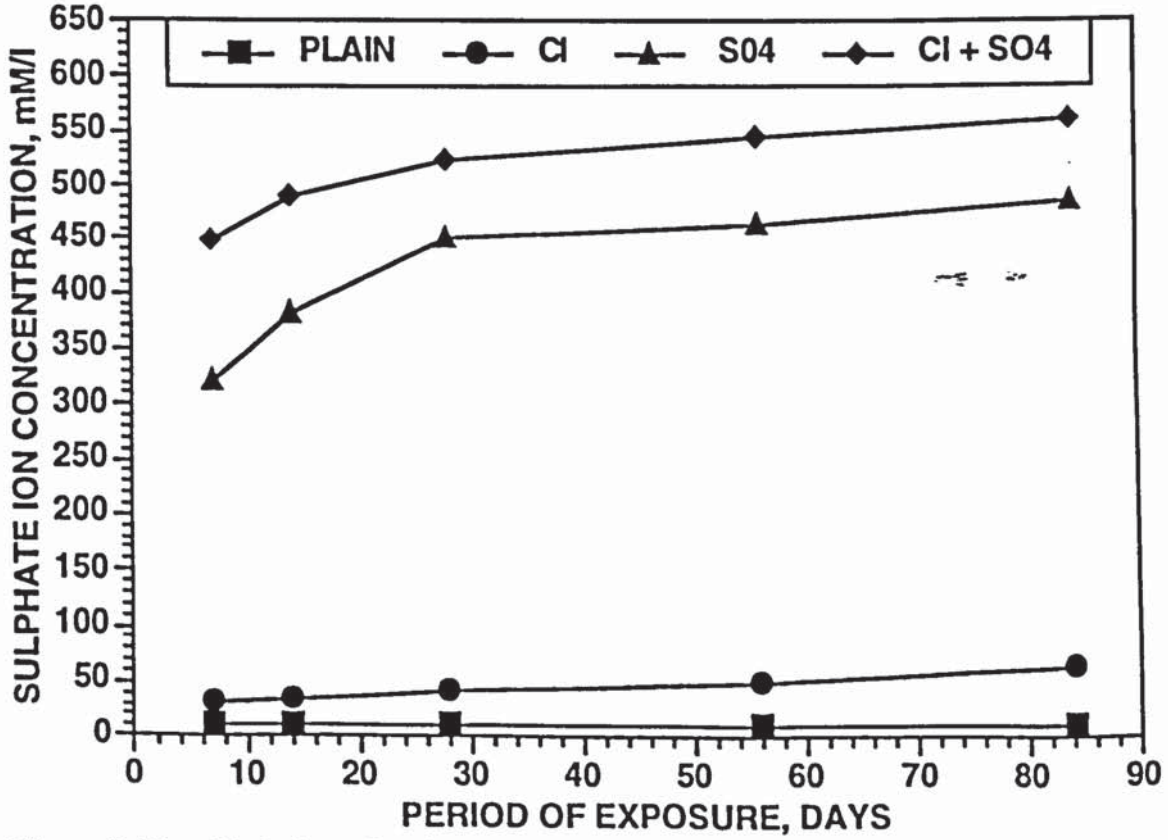

Figure 3.60: Variation of sulfate concentration with age in OPC-A mortar specimens exposed to 55 °C

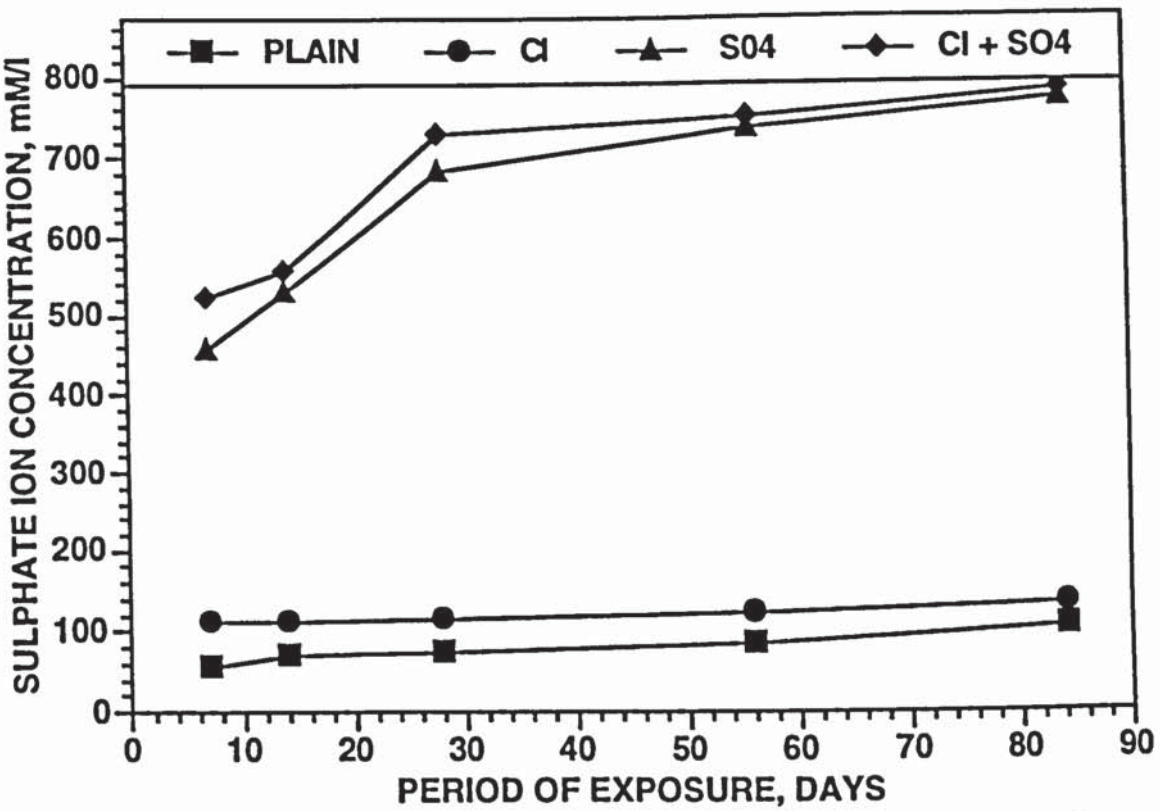

Figure 3.61: Variation of sulfate concentration with age in OPC-A mortar specimens exposed to 70°C

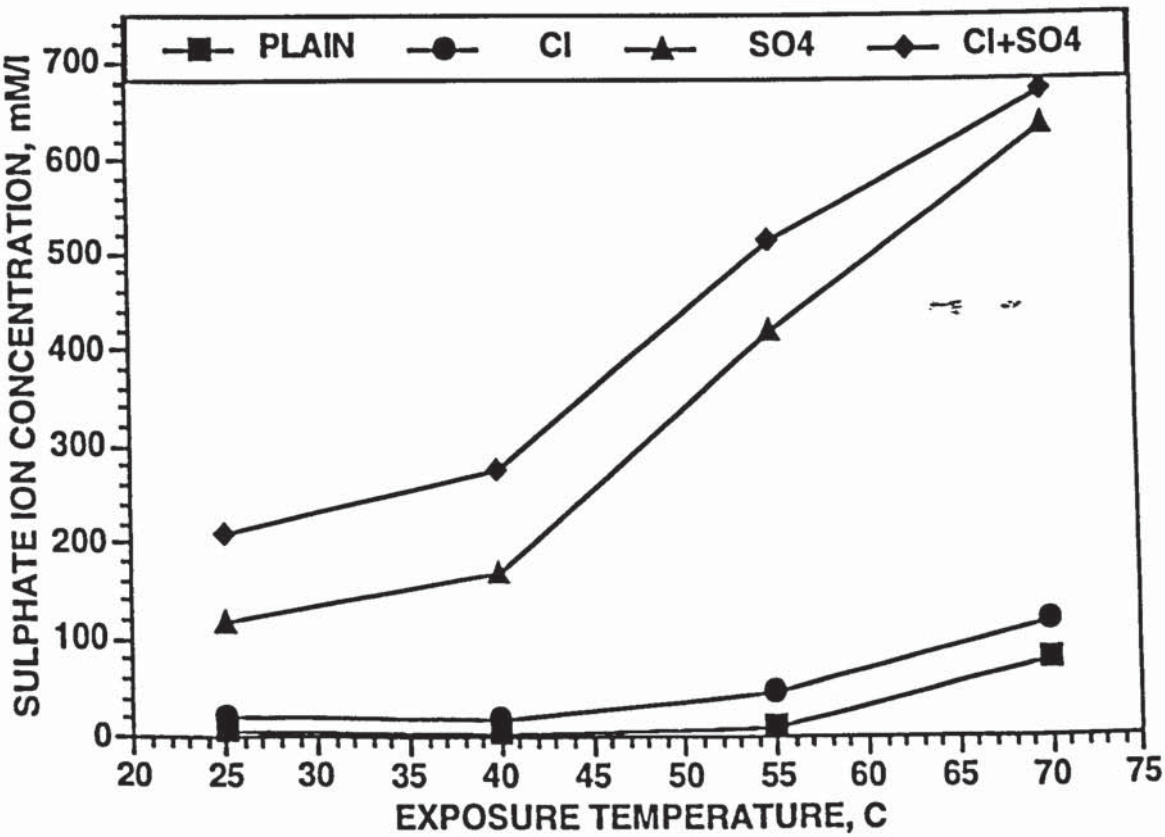

Figure 3.62: Effect of temperature on sulfate concentration in OPC-A

sodium chloride plus sodium sulfate does not vary significantly for exposure temperatures of 25 to 40 °C. However, it increased linearly when the temperature was raised from 55 to 70 °C. The sulfate concentration in the uncontaminated and chloride contaminated specimens also exhibited an increase in the sulfate concentration for exposure temperatures of 55 °C and above. The sulfate concentration in the uncontaminated specimens exposed to 70 °C was 16 times that in the specimens exposed to 25 °C. The sulfate concentration in the chloride-contaminated specimens at 70 °C was 6 times that in the specimens exposed to 25 °C.

The sulfate concentration in OPC-B (C_3A: 14.5%) mortar specimens is plotted in Figures 3.63 through 3.67. These data exhibited a trend similar to that observed in OPC-A mortar specimens (Figure 3.58 through 3.62).

The data in Figures 3.53 through 3.67 indicated that the sulfate concentration is affected by: (i) the presence of chloride contamination, and (ii) exposure temperature. The effect of temperature was evident in all the specimens. This is inferred from the fact that the sulfate concentration in the specimens exposed to 70 °C is 1.5 to 15 times that in the specimens exposed to 25 °C. This increase in the sulfate concentration in the uncontaminated specimens with increasing exposure temperature is attributed to the dissolution of calcium sulfo-aluminate, which is formed due to reaction of C_3A with sulfate ions. Similar findings projecting the instability of the calcium sulfo-aluminate for exposure temperature of more than 60 °C have been reported by Heir and Weiker [62]. They indicated that the reaction between gypsum and C_3A content of cement is reversible for exposure temperatures of more than 40 °C. The following equation expresses that relationship[62]:

$$3CaO.Al_2O_3.6H_2O + 2\ Ca(OH)_2 + CaSO_4.2H_2O + 2(K;Na)_2SO_4 + 24H_2O \leftrightarrow 3CaO.Al_2O_3.3CaSO_4.32H_2O + 4(K;Na)OH \quad (3.5)$$

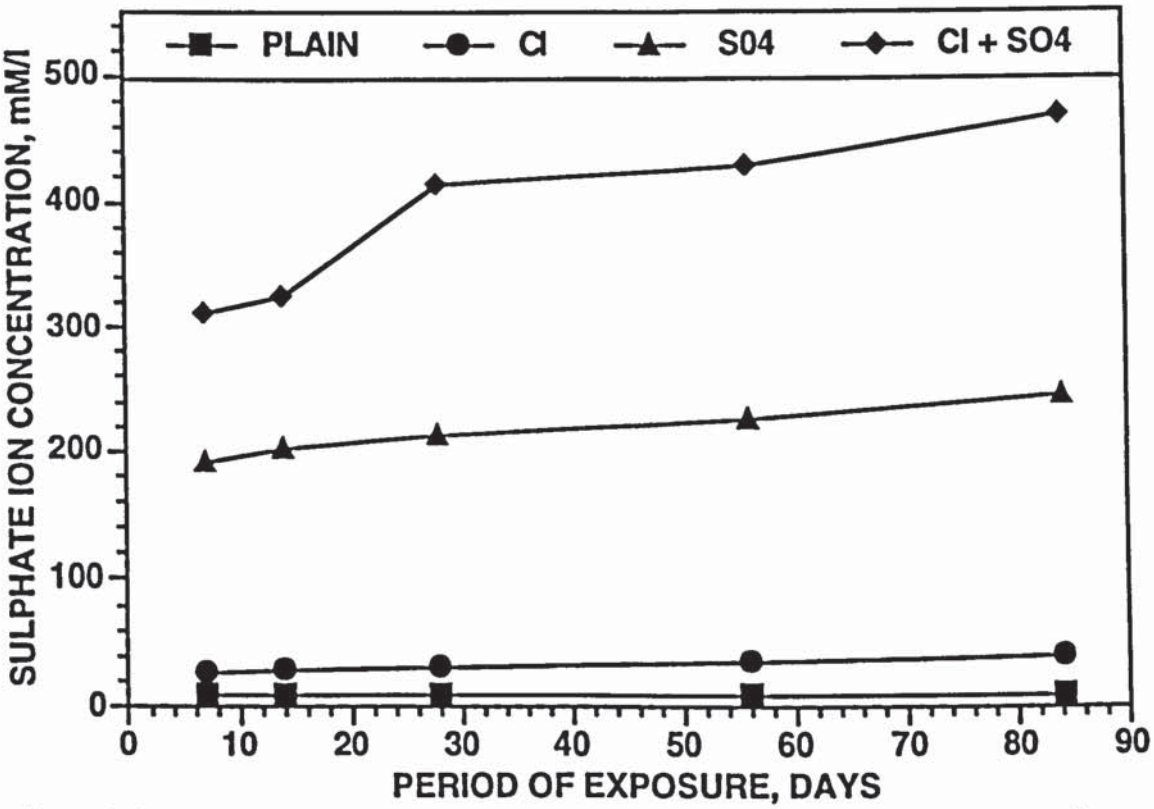

Figure 3.63: Variation of sulfate concentration with age in OPC-B mortar specimens exposed to 25 °C

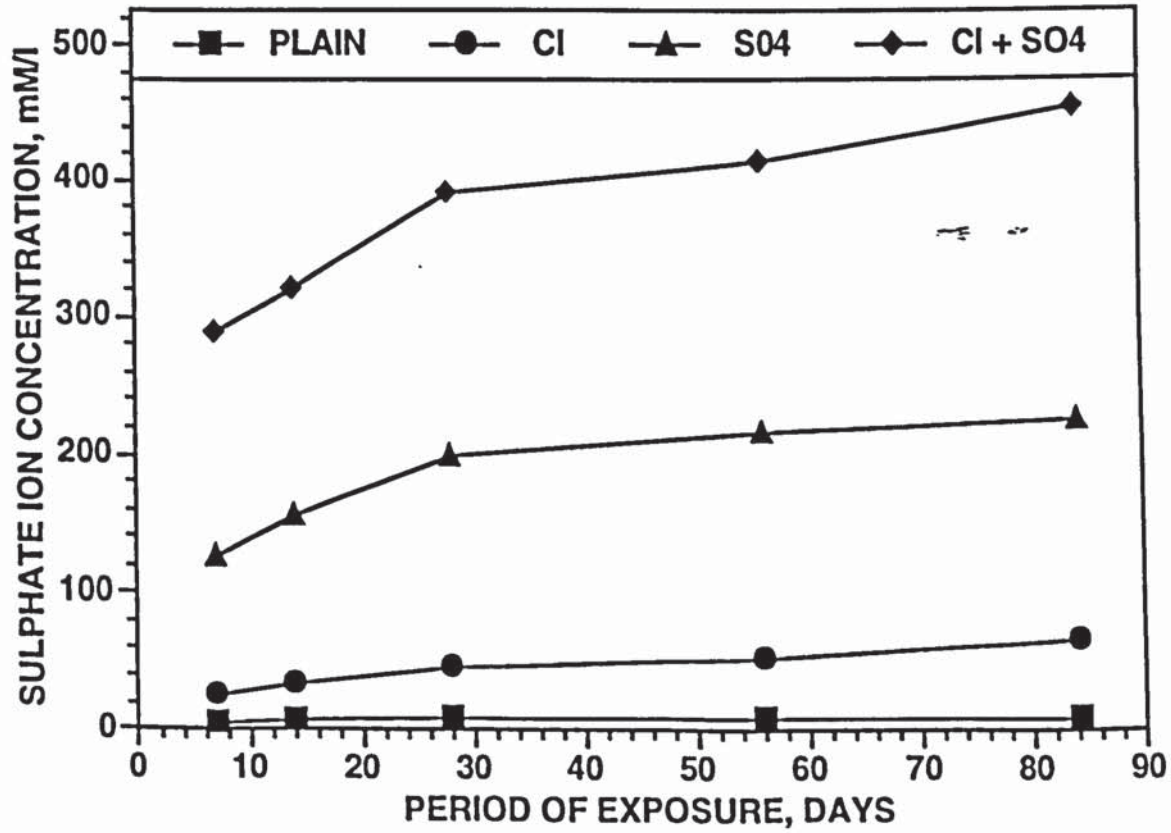

Figure 3.64: Variation of sulfate concentration with age in OPC-B mortar specimens exposed to 40 °C

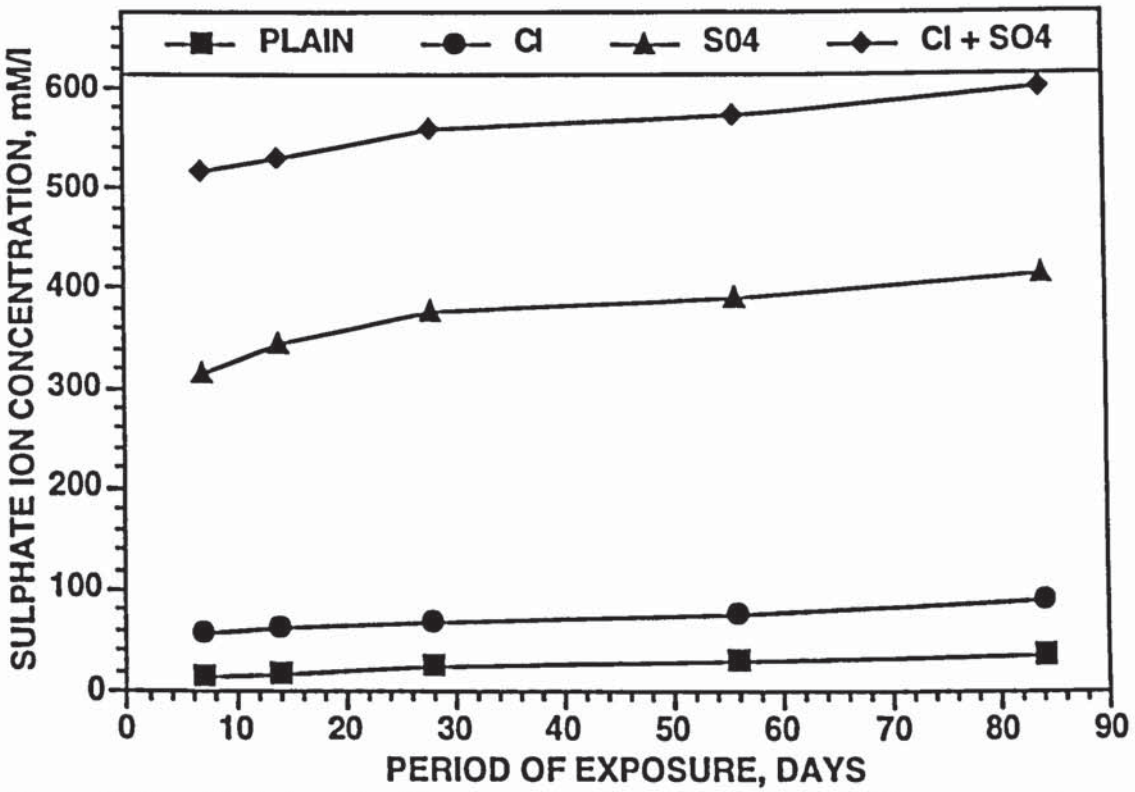

Figure 3.65: Variation of sulfate concentration with age in OPC-B mortar specimens exposed to 55 °C

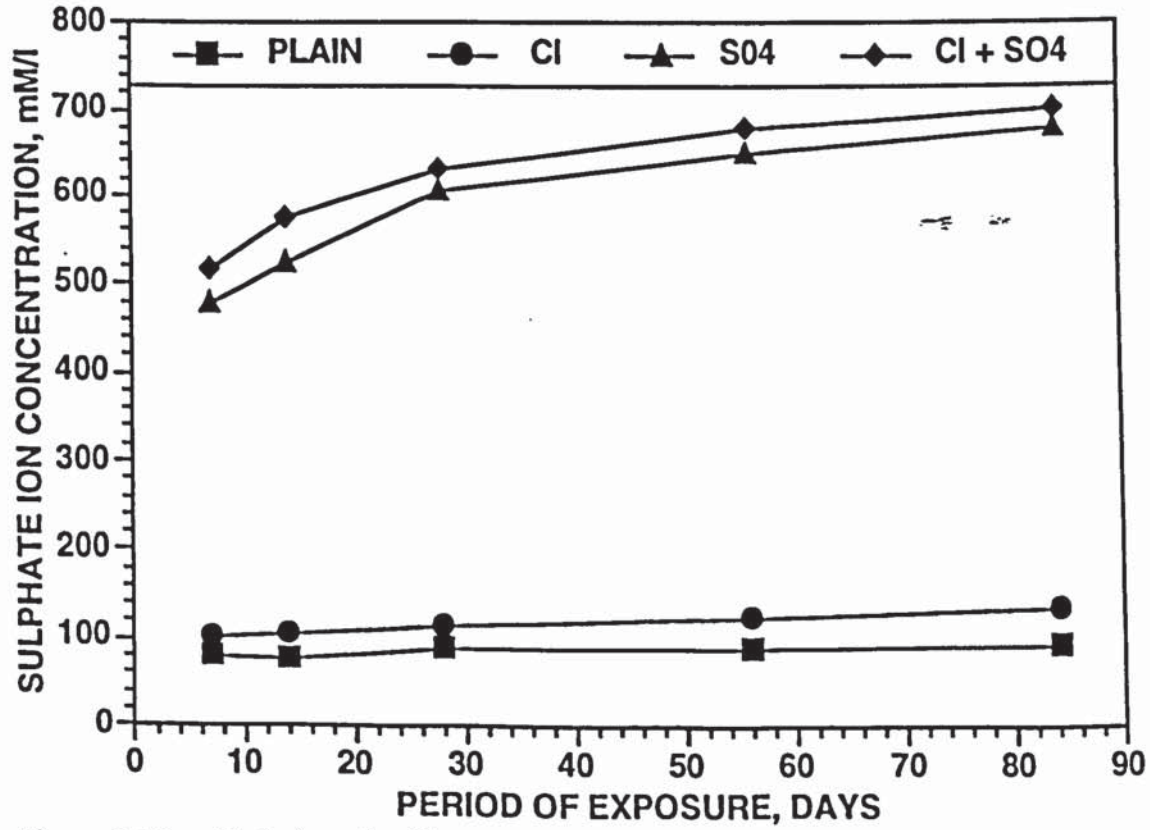

Figure 3.66 : Variation of sulfate concentration with age in OPC-B mortar specimens exposed to 70 °C

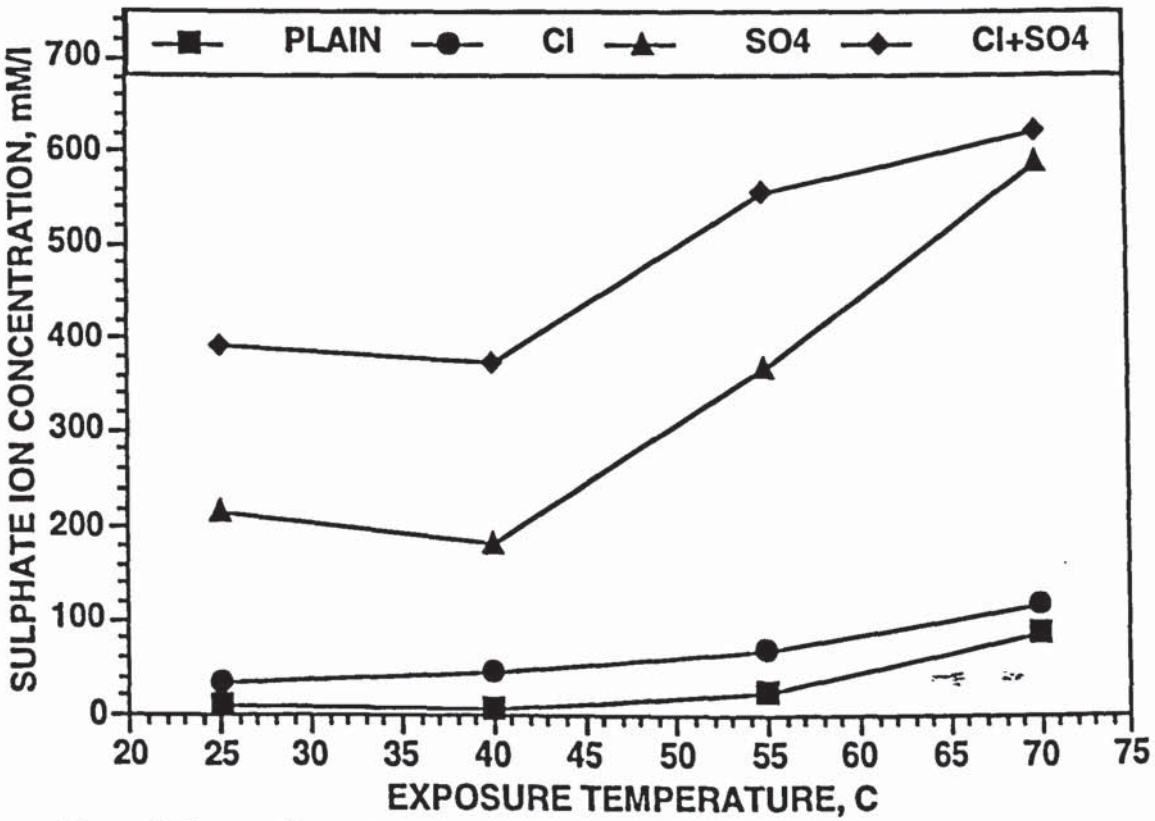

Figure 3.67: Effect of temperature on sulfate concentration in OPC-B mortar specimens

Further, these results also indicated that the chemical and thermal stability of calcium sulpho-aluminate hydrates (Aft and Afm phases) is dependent on the OH^- /SO_4^{--} ratio, which itself is dependent on the alkali content of the cement, the SO_4/Al_2O_3 molar ratio and the temperature. Luke and Glasser [63] also indicated the dissolution of calcium sulpho-aluminate at an exposure temperatures of 55 °C.

The increase in the sulfate concentration, at lower temperatures, in the chloride-contaminated specimens indicates that the reaction between the C_3A phase in cement and gypsum on one hand, and chloride ions on the other takes place concomitantly. This assumption contradicts the findings of Ritchartz [98] who suggested that the C_3A in cement first reacts with the 3 to 5% gypsum, added to cement, during the grinding stage, before the balance C_3A could react with the chlorides to form calcium chloro-aluminate. It has been suggested that the effect of an electrolyte, e.g., $CaCl_2$, on the hydration process is sequential, i.e., it participates in only one reaction at a time [116]. Dekeyser and Tenoutasse [117], in their study of the ferrite phase, concluded that calcium monochloro-aluminate-ferrite $C_3(A,F).\ CaCl_2.10H_2O$, is not formed until all the gypsum is consumed. On the other hand, Rozenberg and Kucheryaeva [118] and Ratinov and Rozenberg [119] concluded that the simultaneous formation of basic salts from a complex hydration system is possible. Using $CaCl_2$, $Ca(NO_3)_2$ and $Ca(NO_2)_2$ with calcium hydroxide alone and with additions of C_3A, they [119] calculated the reaction rates and yields for the various combinations and concluded that, when two or even three electrolytes are added to a system together, the reaction that has the higher rate constant will have the higher yield. The higher sulfate concentration in the pore solution of specimens contaminated with sodium chloride plus sodium sulfate compared to those contaminated with only sodium sulfate can be related to similar mechanisms. In these specimens also the sulfate and chloride ions react concomitantly with the cement hydration products. In the presence of chloride ions, less cement

hydration products are available for the sulfate ions to react, hence a higher quantum of these ions are unreacted.

While no data are reported on the interactive effect of chloride and sulfate salts, introduced at the mixing stage, on the sulfate concentration in the pore solution, several investigations have been devoted to the effect of chloride ions on the sulfate attack in hardened concrete, as these situations are representative of structures serving in the marine and sabkha environments. Chloride ions introduced at the mixing stage through chloride-accelerating admixtures, contaminated aggregates and mix water were reported to enhance the sulfate resistance by Miller [120], Thorvaldson [121] and Yeginobali [122]. Harrison [123] studied the effect of sodium and calcium chloride additions, in the range of 0 to 4.5% in mortar and concrete cubes, on sulfate resistance of OPC and SRPC cements over a period of one year for mortar and over seven years for concrete. Results of the mortar cubes indicated that chloride has either a negligible or generally beneficial influence on the sulfate resistance in both OPC and SRPC mortars. A similar over all trend was observed in the concrete cubes; with the apparent exception of some concretes containing admixed calcium chloride, particularly those containing below 0.5% chloride by weight of cement, and immersed in strong sulfate solutions for which the sulfate resistance was considerably reduced. Kind [124], through his extensive research on chloride-sulfate interaction in water-retaining structures, reported increased sulfate resistance in some cements in sulfate solutions contaminated with high chloride concentrations. He attributed the increased sulfate resistance to:

(1) the increased solubility of calcium aluminate hydrate phase, i.e., ettringite is formed in a non-expansive form,

(2) decrease in lime concentration in the pore solution leading to the conversion of the insoluble highly basic aluminate hydrate phases to soluble low-basic forms, forming ettringite in the liquid phase in the non-expansive form, and

(3) the transformation of aluminate hydrate phases into chloro-aluminates, thereby reducing the quantity of ettringite formed.

Based on microscopic examination, Kind [125] further reported that the calcium sulpho-aluminate occurred in smaller quantities and was formed as weakly-developed crystals in the presence of sodium and magnesium chlorides. This finding formed the basis for specifying higher sulfate limits in the presence of high chloride concentrations in the Russian Standards. Both Biczok [126] and Lea [127] confirmed that the expansion of concrete due to sulfate attack in seawater is retarded due to the concomitant presence of chlorides and sulfates. They attributed this retardation to the increased solubility of sulfate phases in the presence of sodium and calcium chloride solutions. Cornor and Rippstain [128], quoted by Harrison [123], observed that the solubility of ettringite was three times greater in chloride solutions than in water.

The aforementioned studies indicated that sulfate attack is mitigated due to the presence of chloride ions. However, other opinions contradicting this position have also been reported. According to Ikezr, quoted by Al-Samarai and Raouf [129], the addition of calcium chloride of up to 1% to a concrete containing high sulfate content in sand (1 to 2%) increased expansion and drying shrinkage. Smith [130] reported that the addition of 1% calcium chloride at the mixing stage had generally reduced the sulfate resistance of concrete, particularly that made with Type II cement. Moreover, he reported that temperature seems to play a significant role; concretes made with Type II or Type V cement were more sulfate resistant when mixed and cured at 40 °F than similar concretes mixed and cured at normal room temperatures (70 °F). Locher [131]

concluded that sulfate attack is generally increased by the addition of chloride to the sulfate solution. The increased sulfate attack due to the concomitant presence of chlorides was attributed to:

(1) formation of ettringite, which is not hindered by the addition of chlorides,

(2) presence of monochloride by the reaction of chlorides with monosulfate, tetracalcium aluminate hydrate and probably with the nonhydrated C_3A,

(3) monochloride is not stable in the presence of sulfate ions; therefore, it is converted to ettringite when sulfate attack commences with time, and

(4) at higher concentrations of chloride, both monochloride and trichloride hydrates are formed; the former reacts with the penetrating sulfate ions to form ettringite without generation of crystallization pressure and the latter hydrate resists sulfate attack.

The formation of trichloride hydrate ($3CaO.Al_2O_3.3CaCl_2.32H_2O$) was also reported to be favourable at high chloride concentrations by Schwietz, et al., as quoted by Hjorth [132].

Al-Amoudi et al. [133] evaluated the effect of sulfate-chloride solutions on the sulfate deterioration in portland and blended cements. Results of this study indicated the beneficial and ameliorative role of chloride ions on sulfate attack. Through XRD and SEM examination, they indicated the virtual elimination of gypsum formed in the specimens placed in sulfate-chloride solution.

The above discussion is predominantly related to the sulfate attack in hardened concrete and cannot provide an indication on the pore solution chemistry in terms of sulfate concentration due to the concomitant effect of sulfate-chloride and elevated temperature. However, two situations and their repercussion on the concrete deterioration can be visualized. The **first situation**, related to the elevated temperature, is of importance to the superstructures, while the **second situation** is typical of substructures which are subjected to the concomitant presence of chloride and sulfate ions. Due to these two effects, the sulfates are released into the pore solution removing them from the dangerous role of bringing about deterioration of concrete due to softening/disintegration type of attack in low C_3A cements and the expansion/cracking type of degradation in high C_3A cements. The beneficial role of chloride ions in reducing the deterioration of concrete placed in sulfate-chloride environments, as reported by several researchers [120-127,133], supports this hypothesis. The increase in the sulfate concentration in the pore solution due to the presence of chloride ions and/or elevated temperature may, however, lead to depassivation of steel as indicated by Gouda et al. [74].

The variation in the sulfate concentration, in the blended cements, is plotted in Figures 3.68 through 3.71. An increase in the sulfate concentration with increasing temperature was observed in all blended cements. Figure 3.72 compares the sulfate concentration in the uncontaminated OPC and blended cement mortar specimens. The sulfate concentration in the OPC was more than that in the blended cement mortar specimens. Figure 3.73 shows the variation in the sulfate concentration in the chloride-contaminated OPC and blended cement mortar specimens. These data also indicated a trend similar to that exhibited by the uncontaminated OPC and blended cements (Figure 3.72). The sulfate concentration in the OPC and blended cement mortar specimens contaminated with sodium chloride plus sodium sulfate is plotted against exposure temperature in Figure 3.74. These data also indicated higher sulfate concentration in the

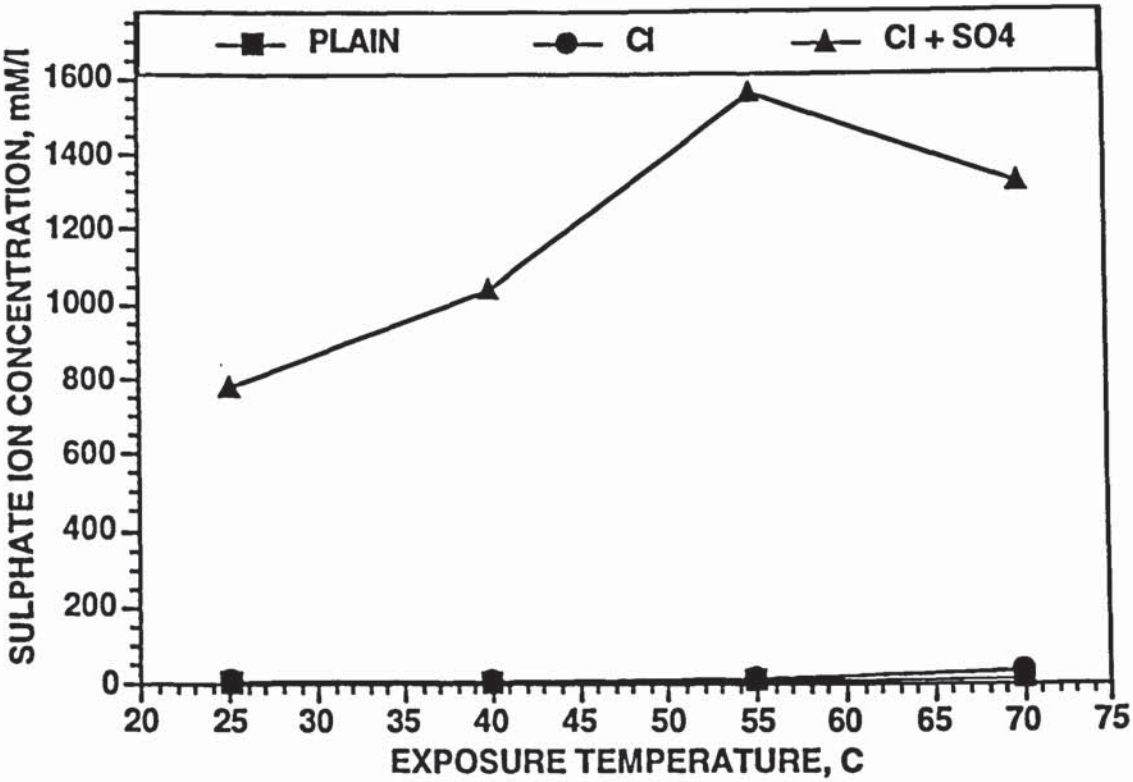

Figure 3.68: Effect of temperature and contamination on sulfate concentration in Class C fly ash

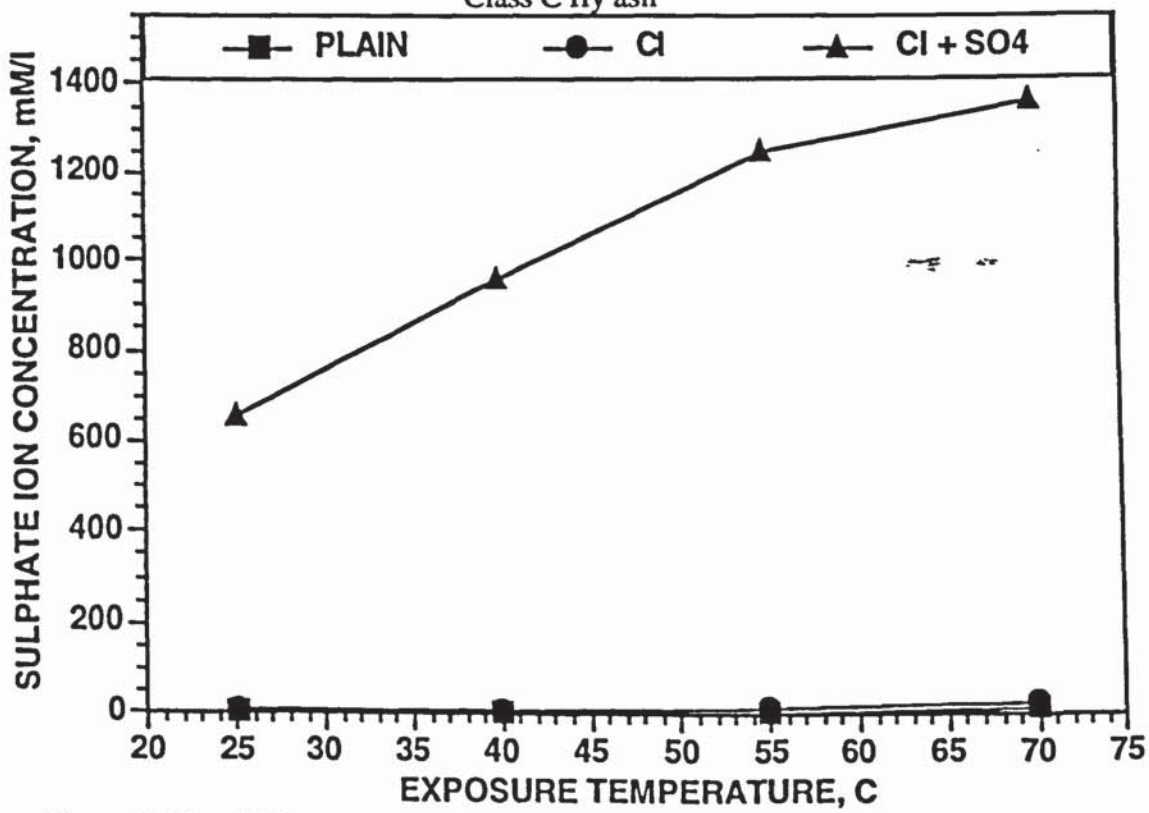

Figure 3.69: Effect of temperature and contamination on sulfate concentration in Class F fly ash

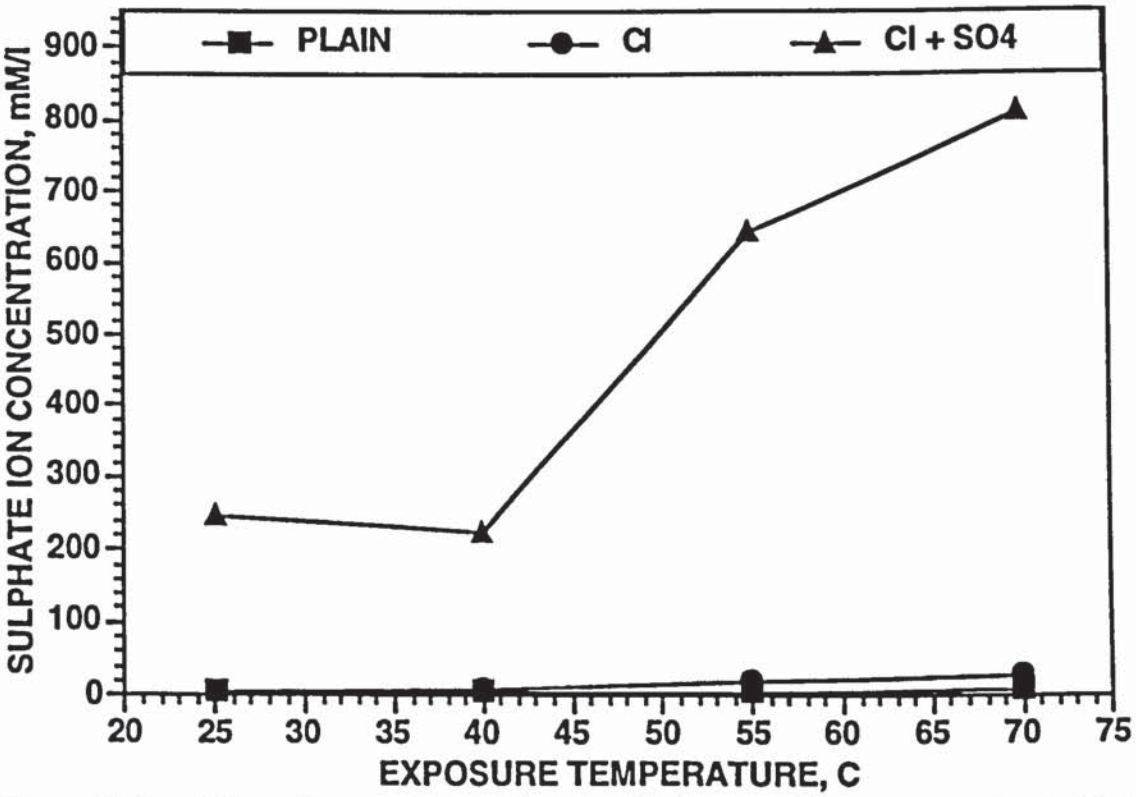

Figure 3.70: Effect of temperature and contamination on sulfate concentration in blast furnace slag cement

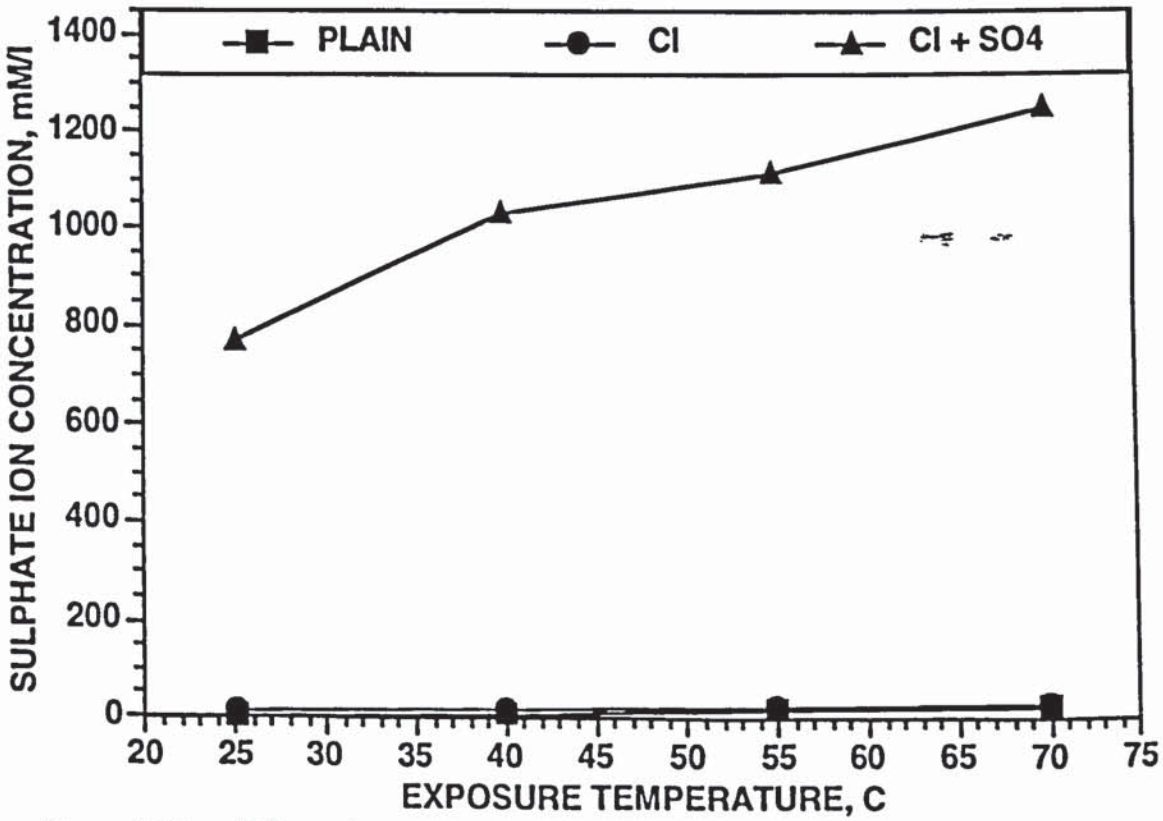

Figure 3.71 : Effect of temperature and contamination on sulfate concentration in silica fume blended cement

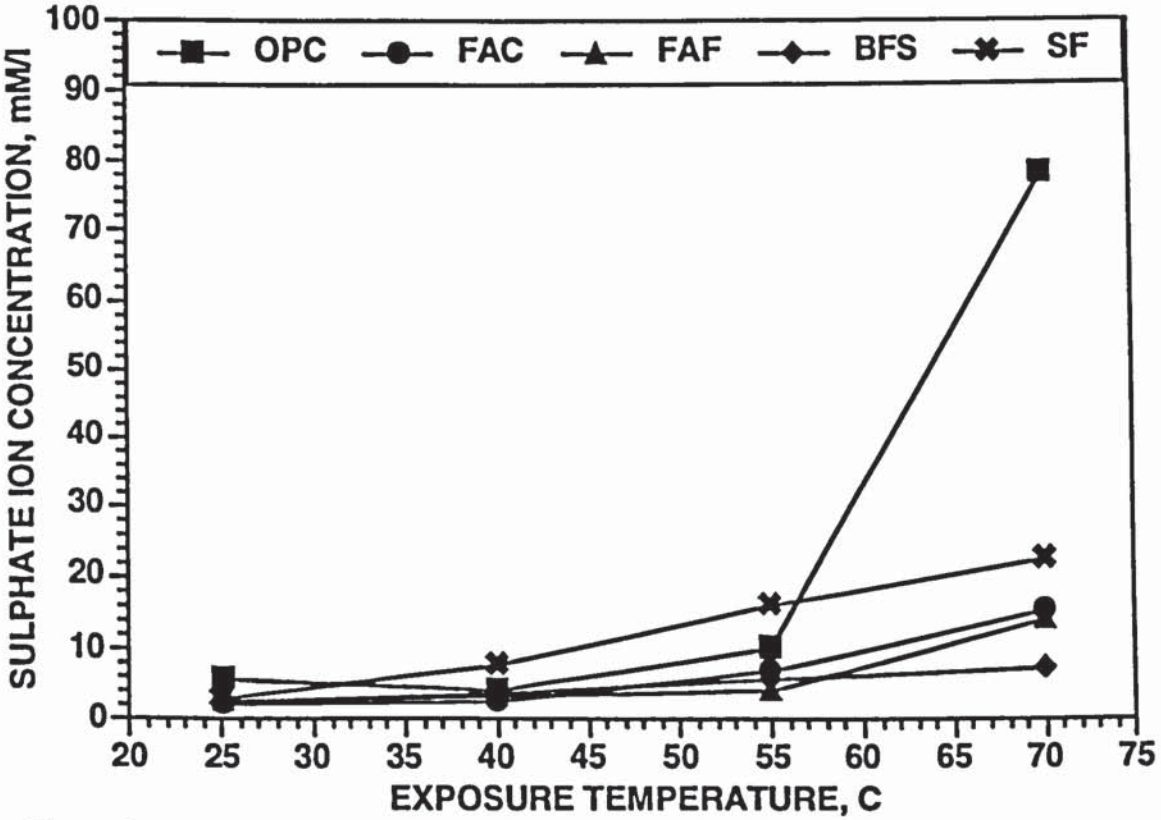

Figure 3.72: Sulfate concentration in uncontaminated ordinary and blended cement mortar specimens

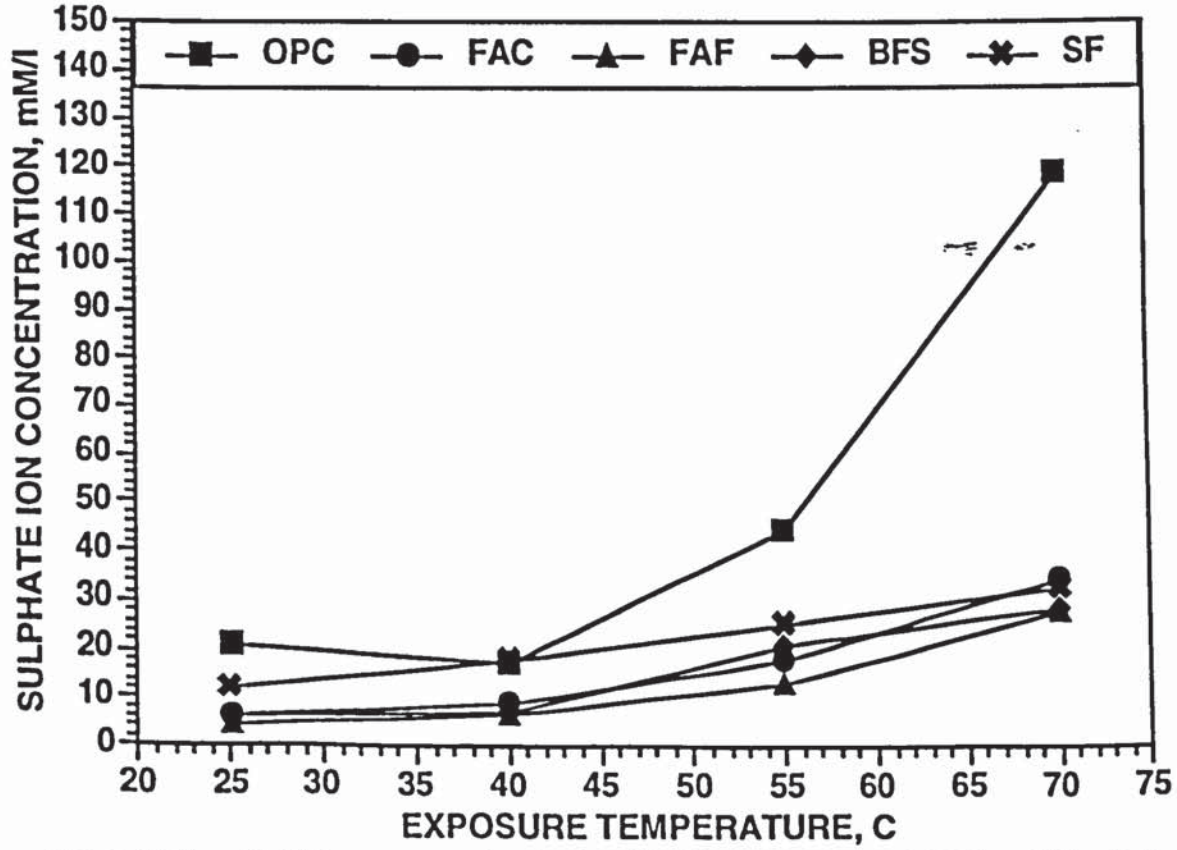

Figure 3.73: Sulfate concentration in the chloride-contaminated OPC and blended cement mortar specimens

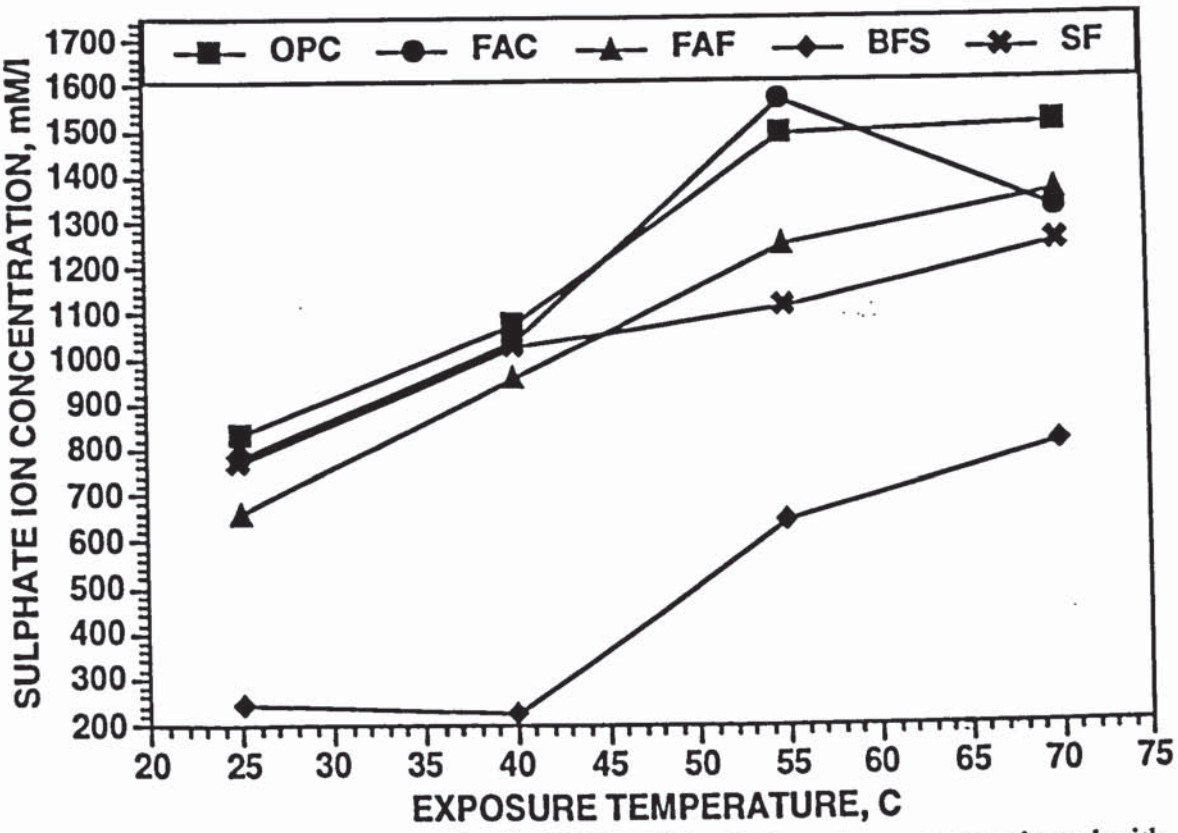

Figure 3.74: Sulfate concentration in OPC and blended specimens contaminated with chloride plus sulfate

OPC mortar specimens than in the blended cement mortar specimens. The lowest sulfate concentrations was measured in the blast furnace slag cement mortar specimens.

3.2.1.5 Sulfate to Hydroxyl Ratio

The sulfate to hydroxyl ion ratio (SO_4^{--}/OH^-) in the uncontaminated and contaminated SRPC (C_3A: 3.5%) mortar specimens are plotted in Figure 3.75. The SO_4^{--}/OH^- values in the uncontaminated specimens exposed to 25 and 40 °C temperatures were in the range of 0.025 to 0.035. However, when the exposure temperature was raised to 55 °C, the SO_4^{--}/OH^- value increased nearly 4 times to 0.1. The SO_4^{--}/OH^- in the specimens exposed to 70 °C was 0.78, this value being 30 times that in the specimens exposed to 25 °C. The SO_4^{--}/OH^- values in the specimens contaminated with sodium chloride indicated a trend similar to that exhibited by the uncontaminated specimens. The SO_4^{--}/OH^- values for specimens contaminated with sodium sulfate also increased with exposure temperature. The SO_4^{--}/OH^- values in the specimens contaminated with sodium chloride plus sodium sulfate also exhibited a trend similar to that indicated by the specimens contaminated with only sodium sulfate. The SO_4^{--}/OH^- values in these specimens were, however, higher than those in the specimens contaminated with sodium sulfate only. This may be attributed to the higher OH^- concentration in the specimens contaminated with sodium sulfate, in comparison to those contaminated with sodium chloride plus sodium sulfate.

The SO_4^{--}/OH^- values in the contaminated and uncontaminated OPC-A mortar specimens are plotted against the exposure temperature in Figure 3.76. These data exhibited a trend similar to that indicated by SRPC. Figure 3.77 shows the variation in the SO_4^{--}/OH^- with exposure temperature for OPC-B mortar specimens. These data also indicated a trend similar to that exhibited in Figures 3.75 and 3.76 for SRPC and OPC-A mortar specimens, respectively.

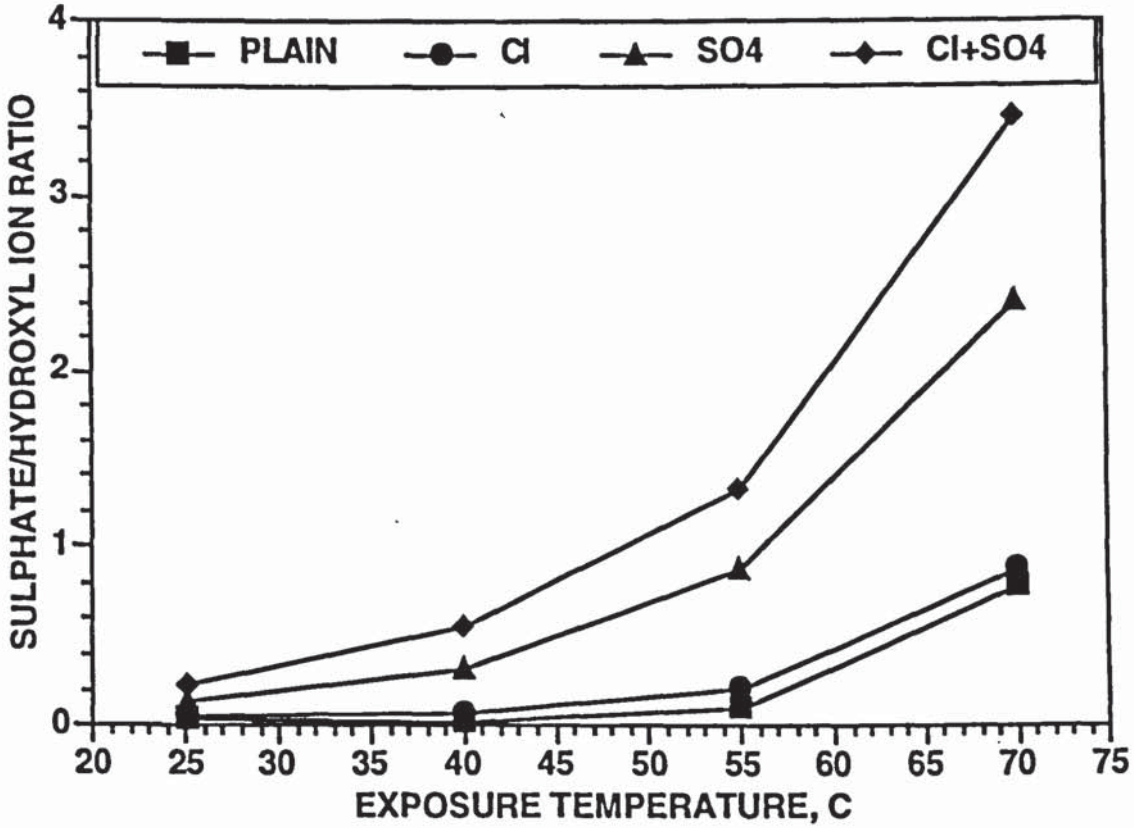

Figure 3.75: Effect of temperature and contamination on SO_4^{--}/OH^- in SRPC

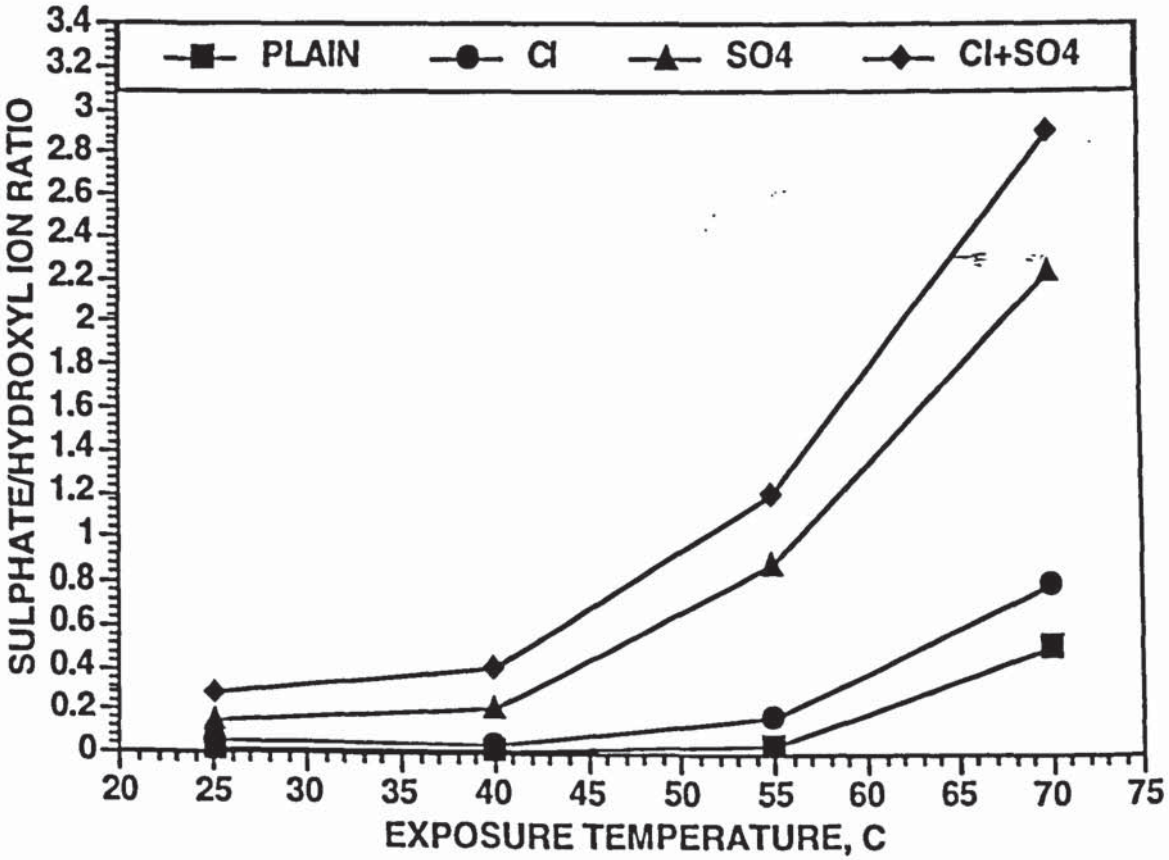

Figure 3.76: Effect of temperature and contamination on SO_4^{--}/OH^- in OPC-A

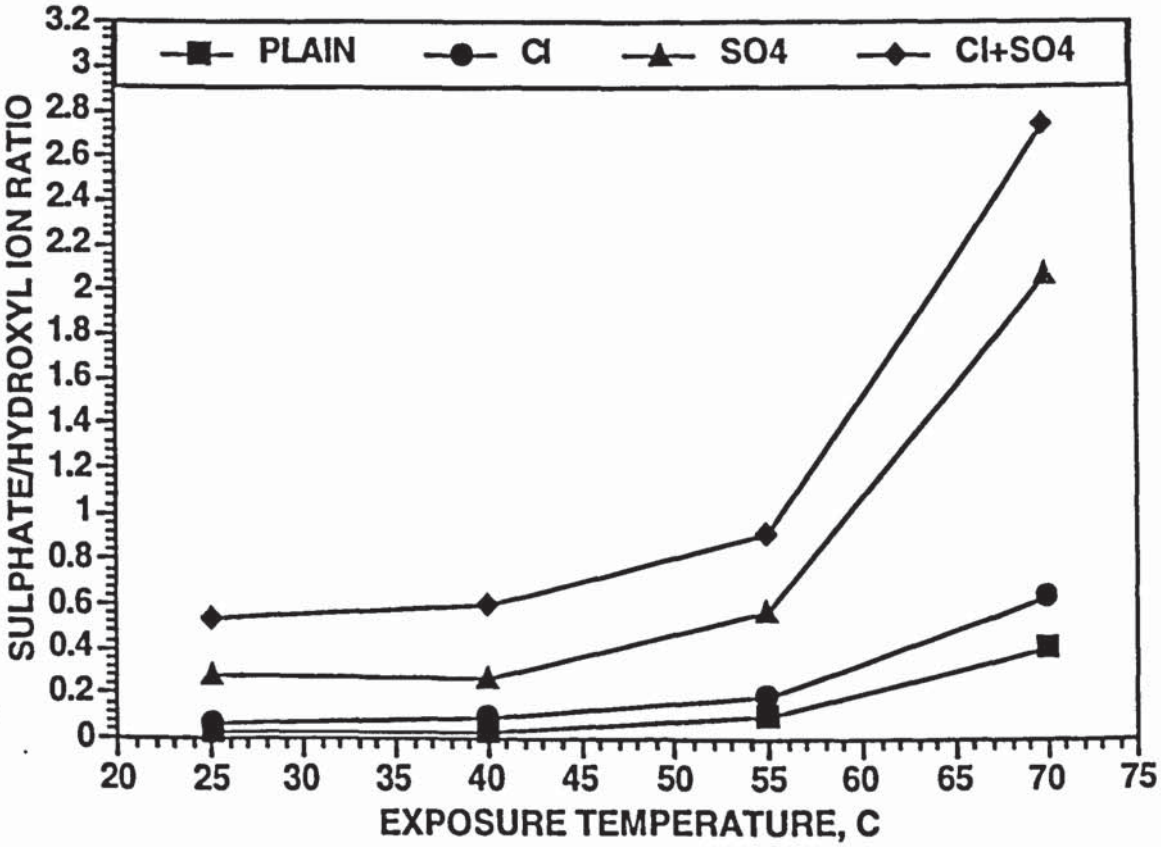

Figure 3.77: Effect of temperature and contamination on SO_4^{--}/OH^- in OPC-B

The SO_4^{--}/OH^- values for the uncontaminated and contaminated Class C fly ash blended cement mortar specimens are plotted against exposure temperature in Figure 3.78. The SO_4^{--}/OH^- values in the uncontaminated and chloride-contaminated specimens increased for exposure temperatures higher than 40 °C, while these values in the specimens contaminated with sodium chloride plus sodium sulfate increased almost linearly with the exposure temperature. Figures 3.79 through 3.81 show the SO_4^{--}/OH^- values for the uncontaminated and contaminated Class F fly ash, blast furnace slag and silica fume cement mortar specimens, respectively. These data exhibited a trend similar to that indicated by class C fly ash blended cement mortar specimens (Figure 3.78).

Figure 3.82 compares the SO_4^{--}/OH^- values in the uncontaminated OPC and blended cement mortar specimens exposed to temperatures in the range of 25 to 70 °C. At lower temperatures, less than 60 °C, the SO_4^{--}/OH^- values in silica fume blended cement were higher than those in other blended cements and OPC. At 70 °C, however, the SO_4^{--}/OH^- values in all the blended cements were lower than those in OPC. The SO_4^{--}/OH^- values in the chloride-contaminated OPC and blended cement mortar specimens are compared in Figure 3.83. These data exhibited a trend similar to that indicated in the uncontaminated specimens (Figure 3.82). The SO_4^{--}/OH^- values for OPC and blended cement mortar specimens contaminated with sodium chloride plus sodium sulfate are plotted in Figure 3.84. An increase in the SO_4^{--}/OH^- value with exposure temperature was observed in all cements. The SO_4^{--}/OH^- values in Class F and Class C fly ash and silica fume blended cement mortar specimens were higher than those in OPC up to an exposure temperature of 60 °C. The SO_4^{--}/OH^- ratios in the blast furnace slag cement mortar specimens were lower than those in other blended cements and OPC at all the temperatures. At 70 °C, the SO_4^{--}/OH^- values in both types of fly ashes were generally lower than in OPC and silica fume blended

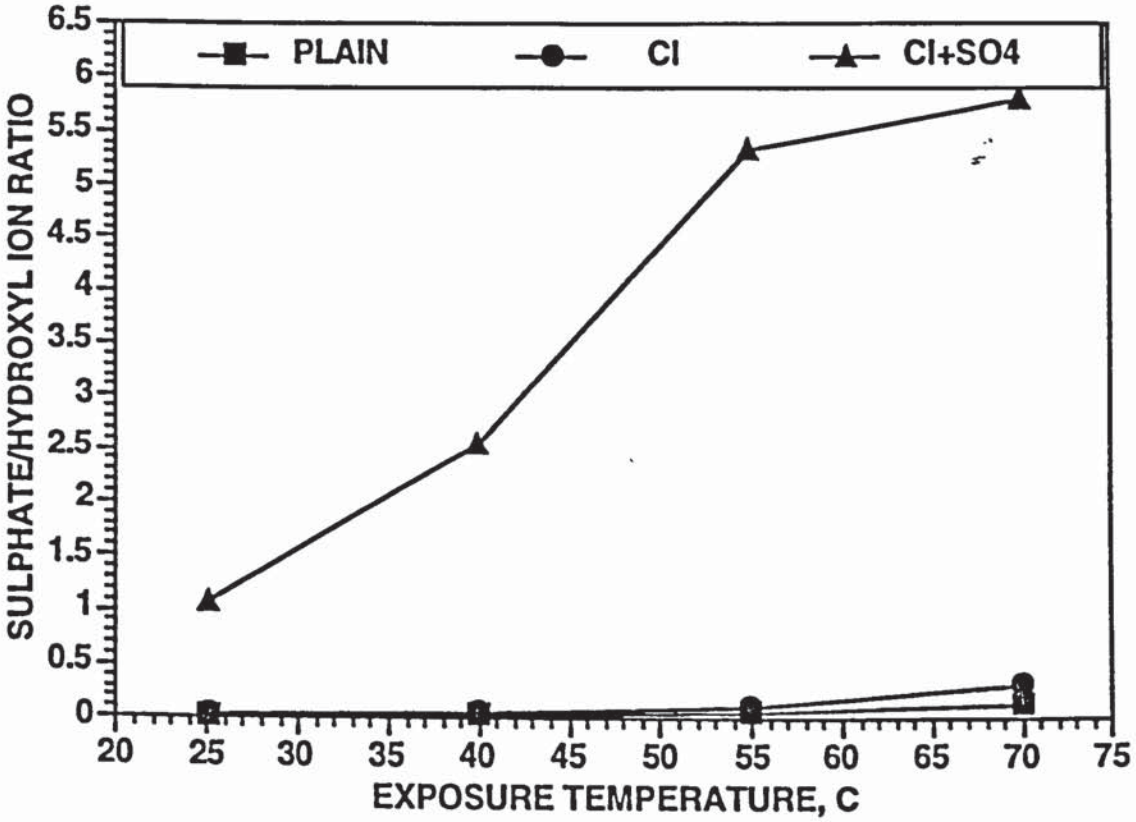

Figure 3.78: Effect of temperature and contamination on SO_4^{-}/OH^{-} in Class C fly ash cement

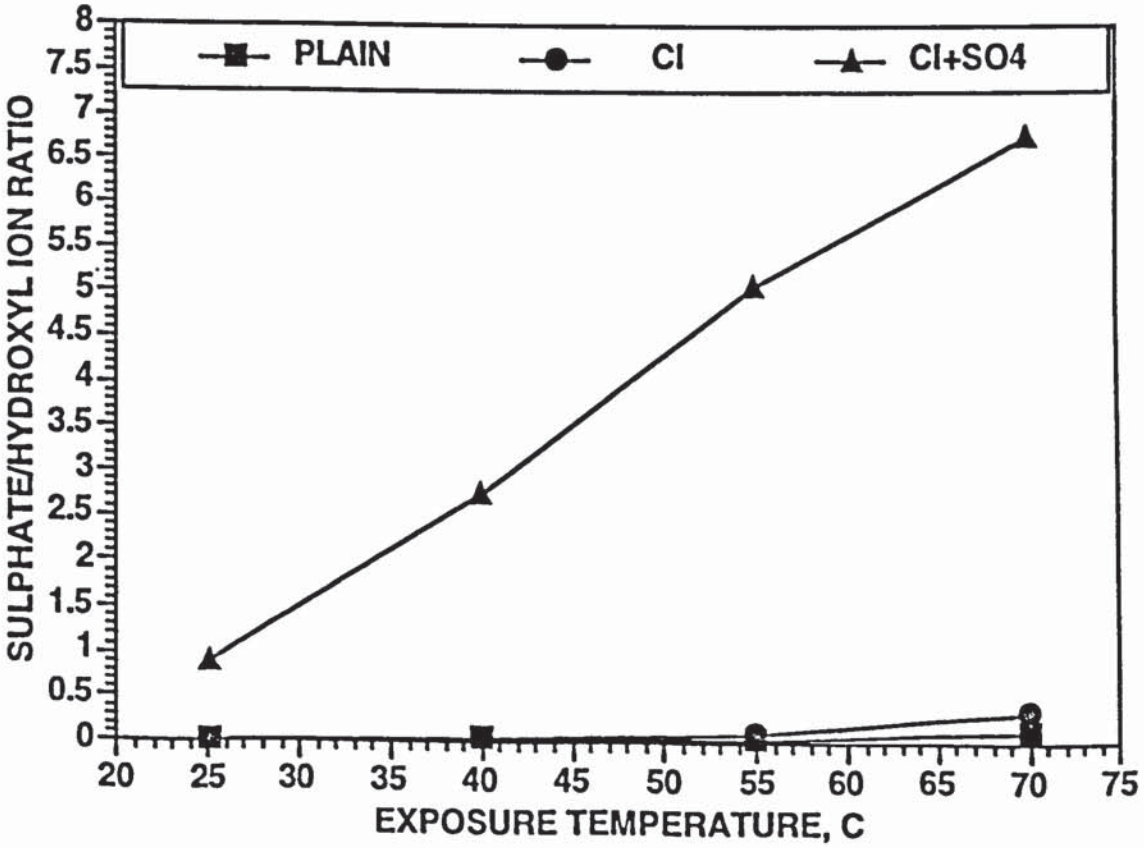

Figure 3.79: Effect of temperature and contamination on SO_4^{-}/OH^{-} in Class F fly ash cement mortar specimens

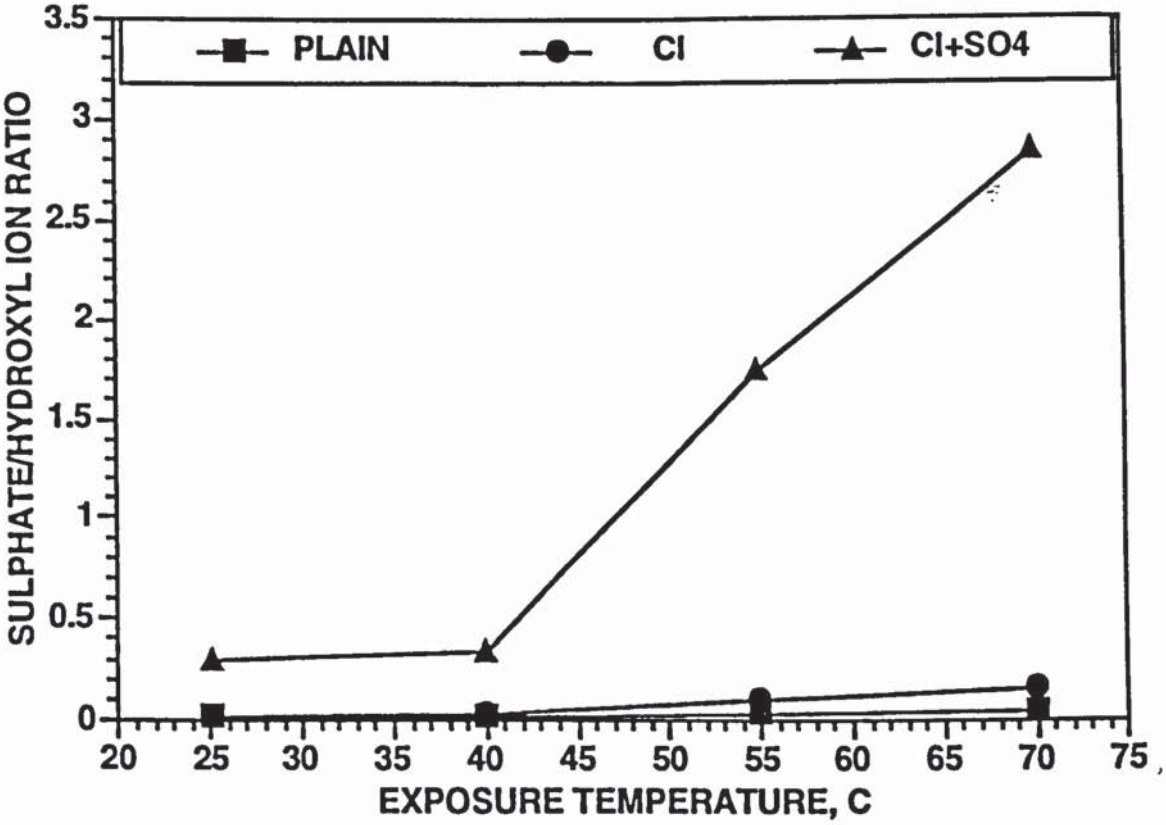

Figure 3.80: Effect of temperature and contamination on SO_4^{--}/OH^- in blast furnace slag cement

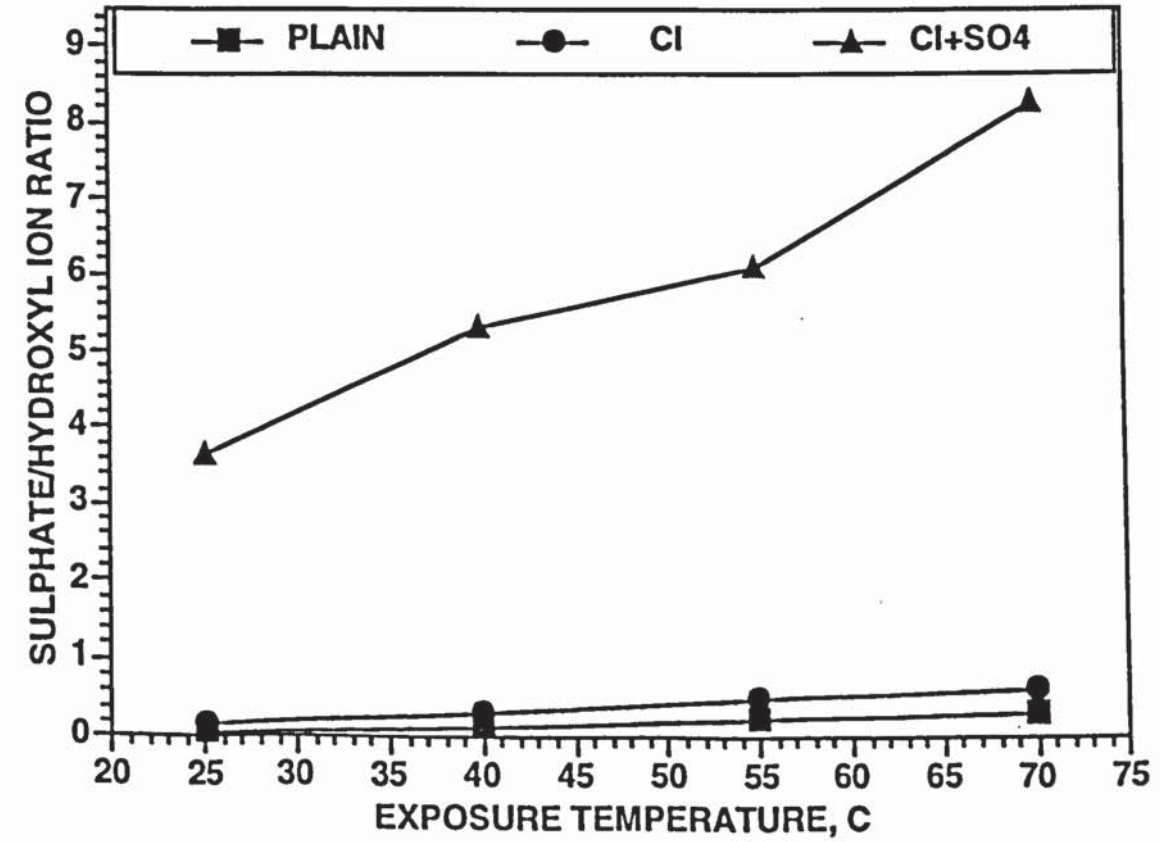

Figure 3.81: Effect of temperature and contamination on SO_4^{--}/OH^- silica fume blended cement mortar specimens

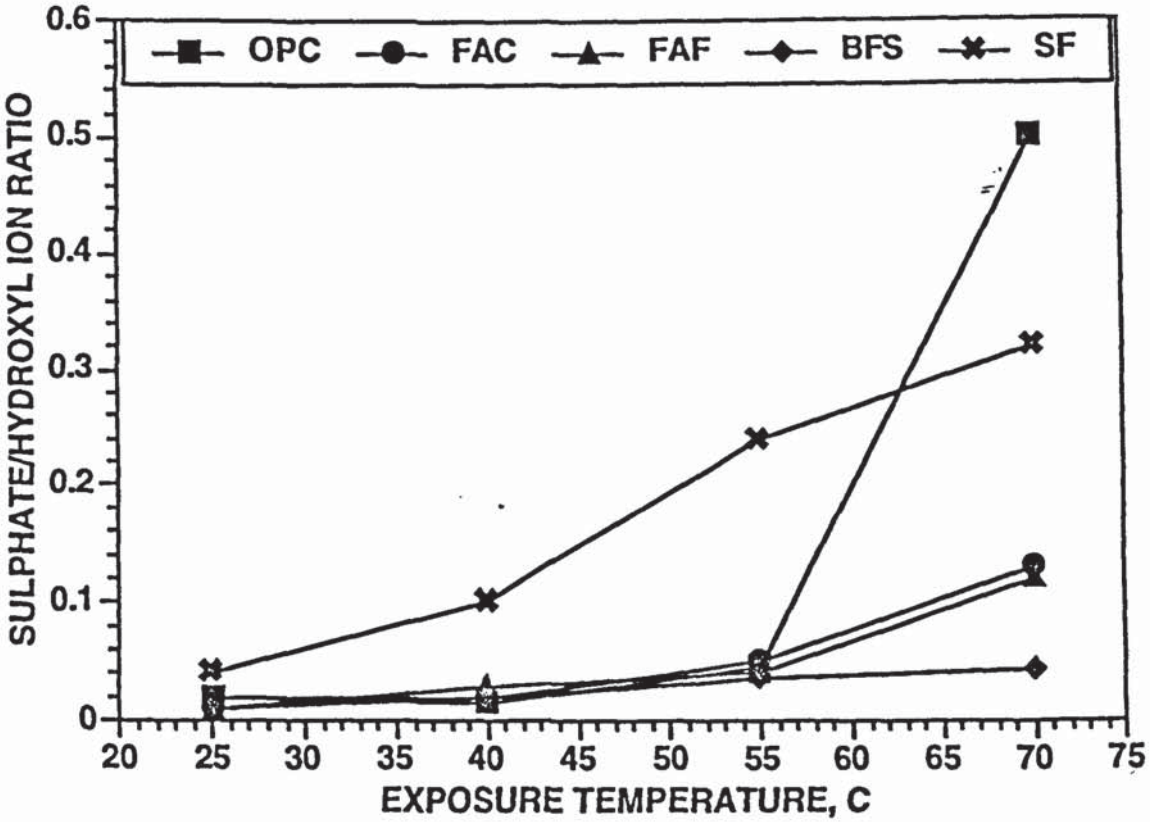

Figure 3.82: SO_4^{--}/OH^- in uncontaminated ordinary Portland and blended cement mortar specimens

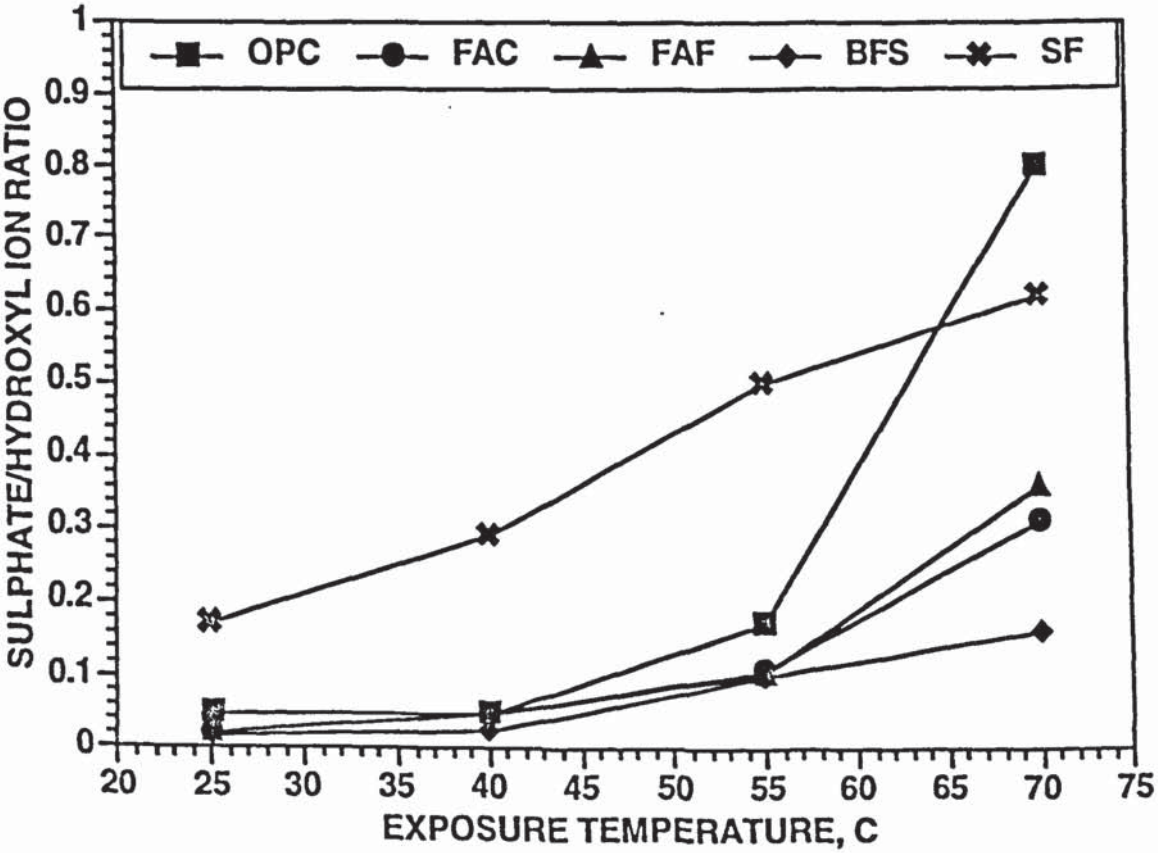

Figure 3.83: SO_4^{--}/OH^- in chloride-contaminated ordinary Portland and blended cement mortar specimens

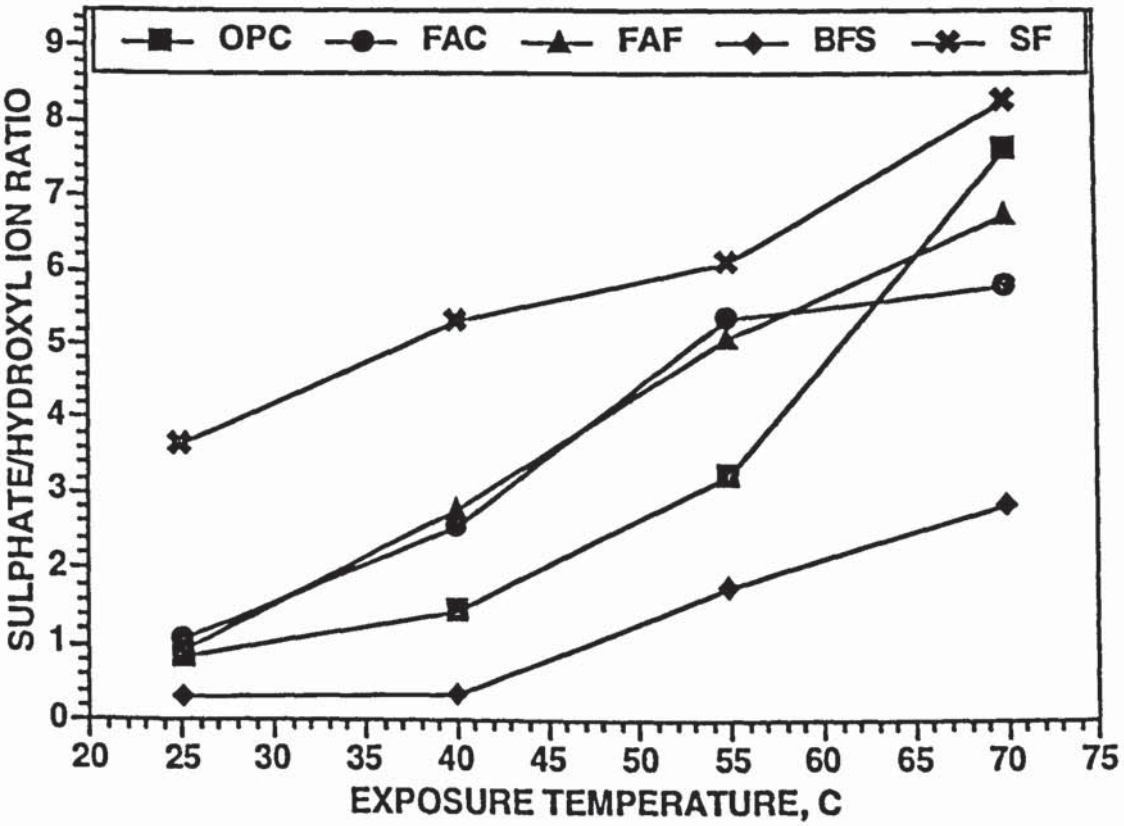

Figure 3.84: SO_4^{--}/OH^- in ordinary Portland and blended cement mortar specimens contaminated with chloride and sulfate

cement. The SO_4^{--}/OH^- values in the silica fume blended cement mortar specimen were higher than OPC and other blended cements at all the exposure temperatures.

The importance of SO_4^{--}/OH^- ratio on concrete durability, viz.-a-viz., sulfate attack and reinforcement corrosion, is not very well understood at this time, and hardly any data are available in the literature on this aspect. However, these values do provide an indication of the aggressivity of the chemical environment with reference to reinforcement corrosion. A higher SO_4^{--}/OH^- value is indicative of greater probability of steel depassivation due to the low alkalinity and/or high sulfate concentration of the pore solution. Presently, no data are available on this aspect, however, studies by Gouda [74] indicated that the concomitant presence of sulfate and chloride ions can significantly influence the kinetics of reinforcement corrosion. Since OH^- is a common factor in both Cl^-/OH^- and SO_4^{--}/OH^-, the ratio of Cl^-/SO_4^{--} may be presumed to influence reinforcement corrosion, particularly after depassivation of steel has occurred. Investigations by Jarrah et al. [134] indicated an increase in the corrosion rate of steel in concrete specimens partially immersed in sulfate-chloride solutions compared with those placed in the pure chloride environment. In another investigation, Al-Amoudi and Maslehuddin [17] observed that the rate of reinforcement corrosion is doubled when the sulfate concentration in 15.7% chloride solution was raised from 0.55 to 2.10%.

3.2.2 X-Ray Diffraction

The X-ray diffractogram for the uncontaminated SRPC (C_3A: 3.5%) mortar specimen exposed to 25 °C is shown in Figure 3.85. The major compounds discerned from these peaks were portlandite ($Ca(OH)_2$), calcite, quartz and ettringite. Figure 3.86 shows the X-ray diffractogram for mortar specimens made with similar cement and

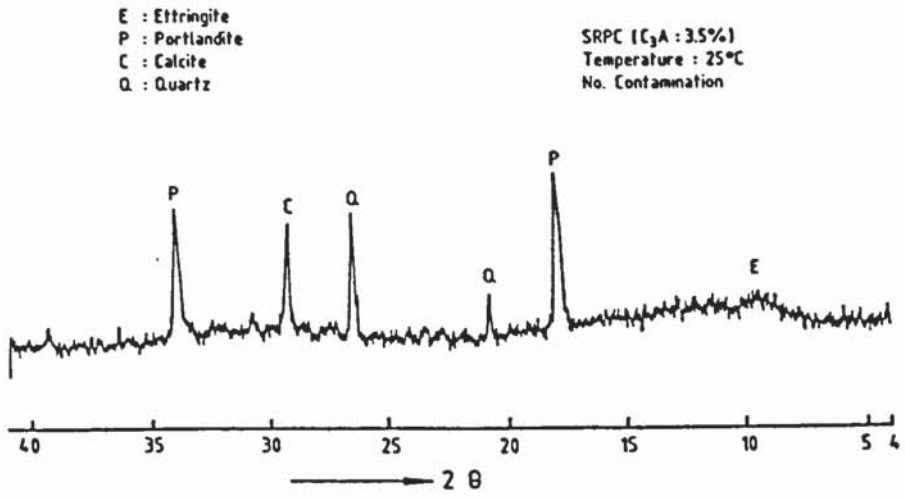

Figure 3.85: X-ray diffractogram for uncontaminated SRPC specimen exposed to 25 °C

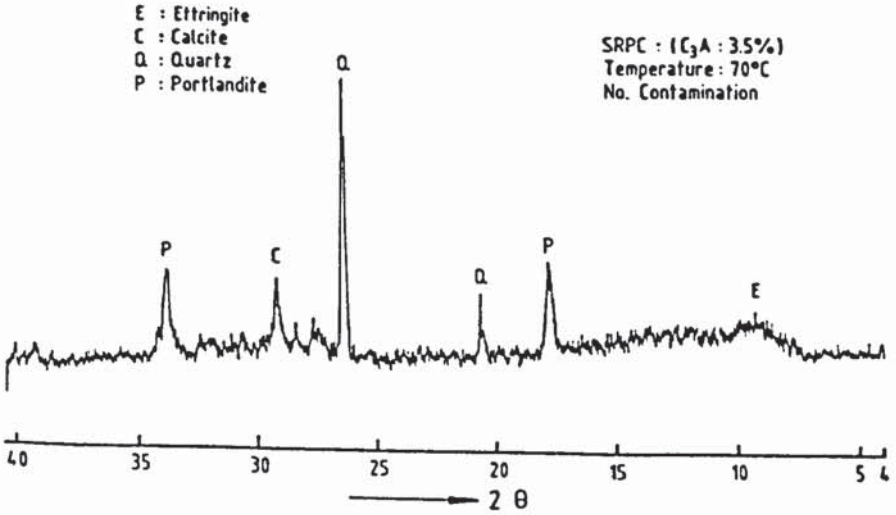

Figure 3.86: X-ray diffractogram for uncontaminated SRPC specimen exposed to 70 °C

exposed to 70 °C. The X-ray peaks for this cement also indicated the same compounds, except that the peak for ettringite, marked by the presence of a defused band between 9 and 10° 2θ, is less distinct in comparison to that observed in the specimens exposed to 25 °C (Figure 3.85). Figure 3.87 shows the X-ray diffractogram for SRPC contaminated with sodium sulfate and exposed to 25 °C. In this specimen the X-ray peaks for ettringite became more distinct. Figure 3.88 shows the X-ray diffractogram for SRPC specimen contaminated with sodium sulfate and exposed to 70 °C. Portlandite, quartz, calcite and ettringite were the main phases discerned. The peaks for ettringite, however, were less distinct than those in the specimen exposed to 25 °C. Figures 3.89 and 3.90 show the X-ray diffractogram for the specimens contaminated with sodium chloride and exposed to 25 and 70 °C, respectively. The major compounds detected were portlandite ($Ca(OH)_2$), quartz, and calcite. The X-ray diffractogram for the specimens contaminated with sodium chloride plus sodium sulfate and exposed to 25 and 70 °C are shown in Figures 3.91 through 3.92, respectively. Formation of portlandite, calcite and quartz was also indicated by these X-ray diffractograms.

The X-ray diffractograms for OPC-A (C_3A: 8.5%) mortar specimens contaminated with sodium sulfate and exposed to 25 and 70 °C are shown in Figures 3.93 and 3.94, respectively. The common compounds detected in these diffractograms were portlandite, quartz, calcite and ettringite. The X-ray peaks for ettringite were less distinct in the specimens exposed to 70 °C compared to those exposed to 25 °C. The X-ray diffractogram for OPC-A specimens contaminated with sodium chloride and exposed to 25 and 70 °C are plotted in Figures 3.95 and 3.96, respectively. In addition to the formation of quartz, portlandite and calcite, crystallization of Friedel's salt with peaks at 11.1, 22.4, 23.0 and 30.8° 2θ was indicated. These peaks were not detected in the specimens exposed to 70 °C. The X-ray diffractograms for OPC-A (C_3A: 8.5%)

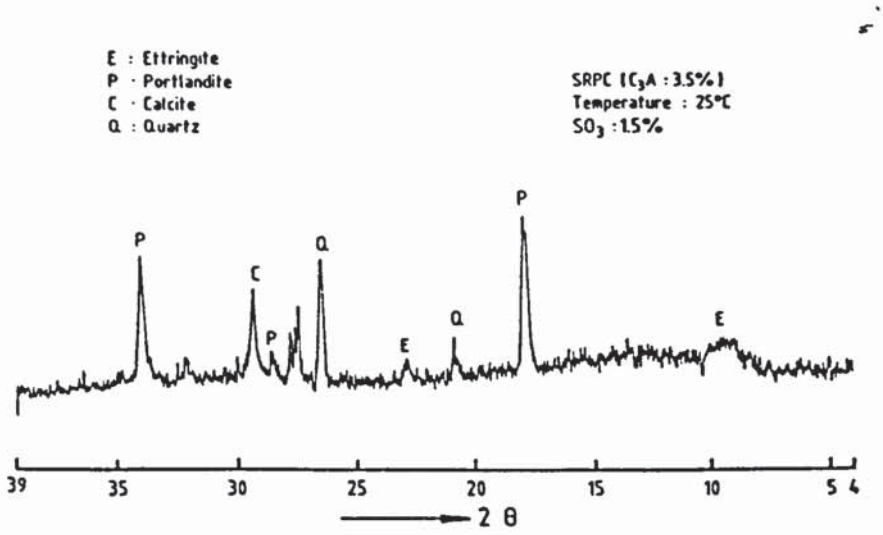

Figure 3.87: X-ray diffractogram for sulfate-contaminated SRPC specimen exposed to 25 °C

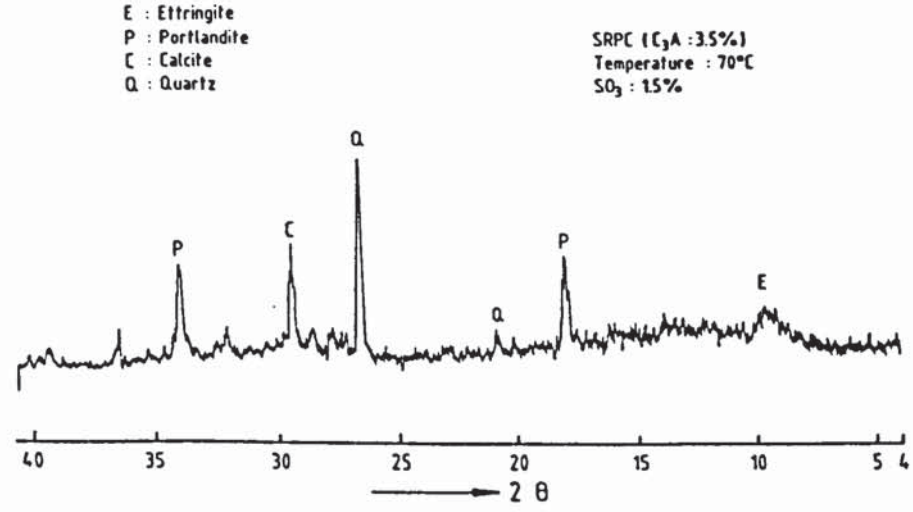

Figure 3.88: X-ray diffractogram for sulfate-contaminated SRPC specimen exposed to 70 °C

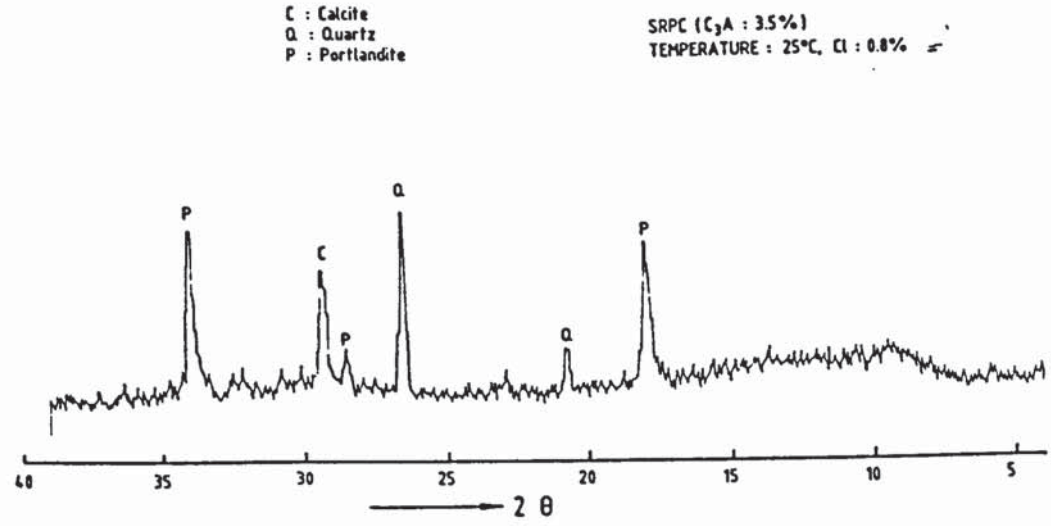

Figure 3.89: X-ray diffractogram for chloride-contaminated SRPC specimen exposed to 25 °C

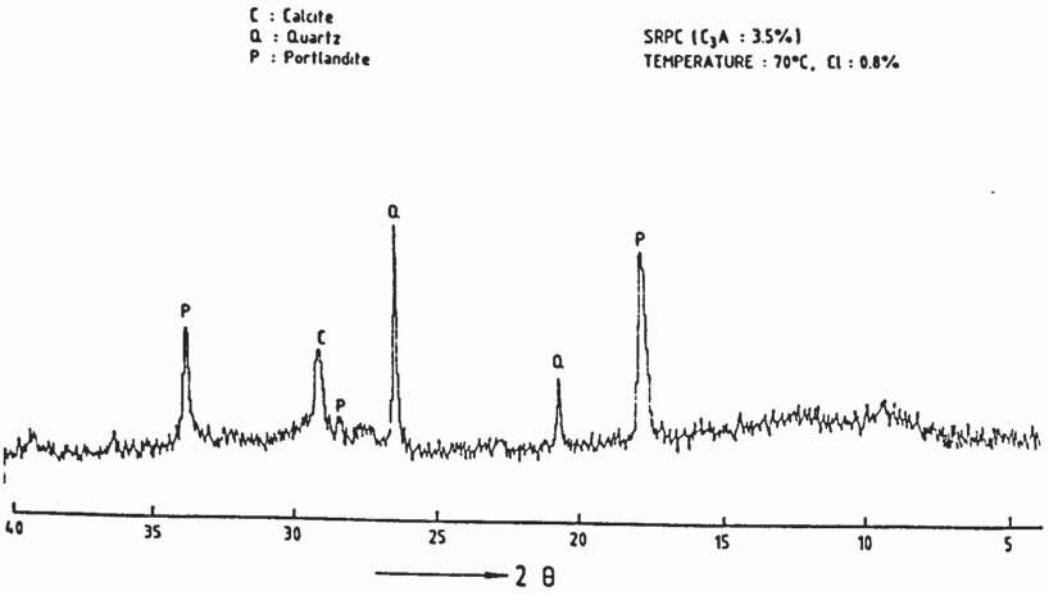

Figure 3.90: X-ray diffractogram for chloride-contaminated SRPC specimen exposed to 70 °C

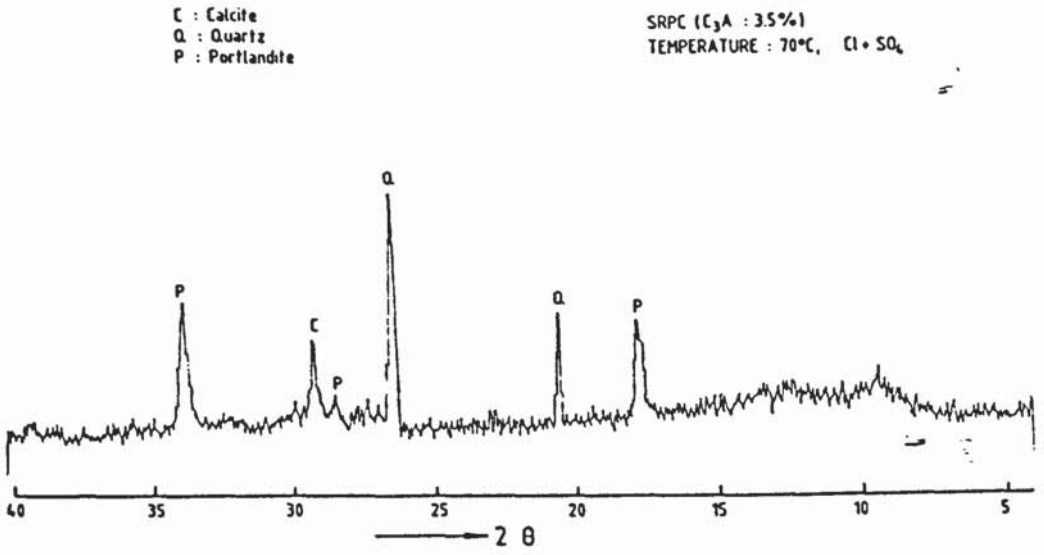

Figure 3.91: X-ray diffractogram for SRPC specimen contaminated with sulfate and chloride and exposed to 25 °C

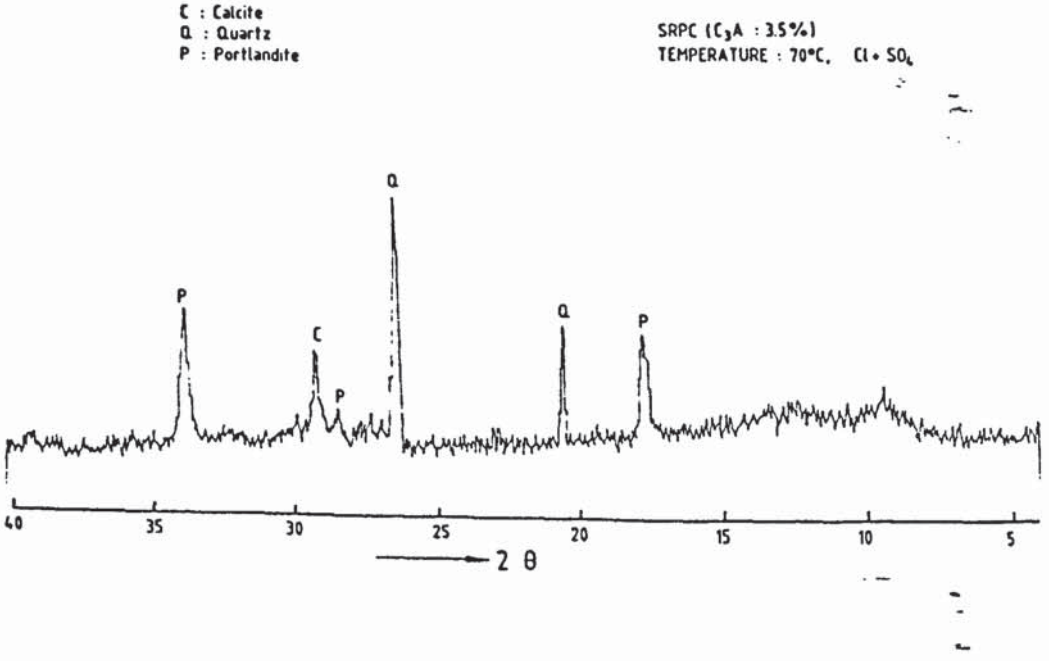

Figure 3.92: X-ray diffractogram for SRPC specimen contaminated with sulfate and chloride and exposed to 70 °C

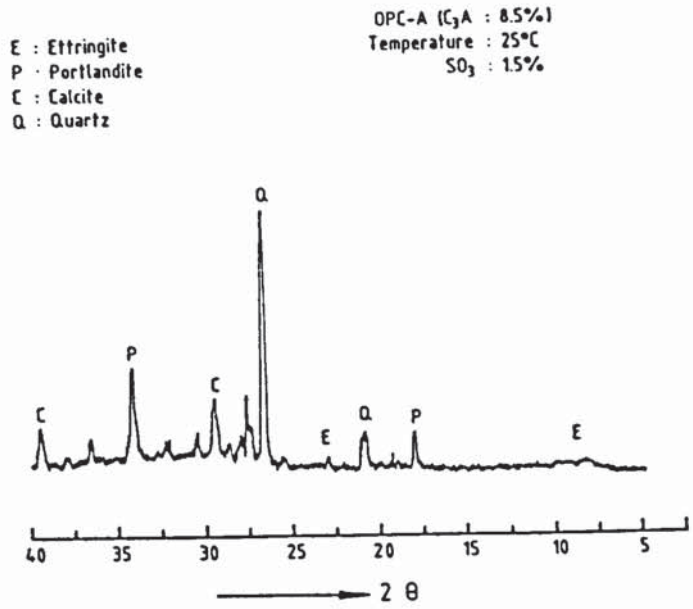

Figure 3.93: X-ray diffractogram for sulfate-contaminated OPC-A and exposed to 25 °C

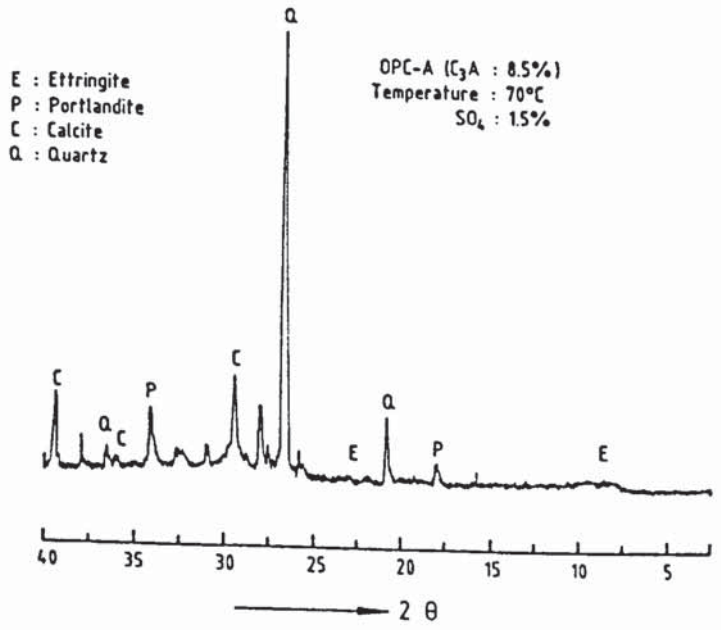

Figure 3.94: X-ray diffractogram for sulfate-contaminated OPC-A and exposed to 70 °C

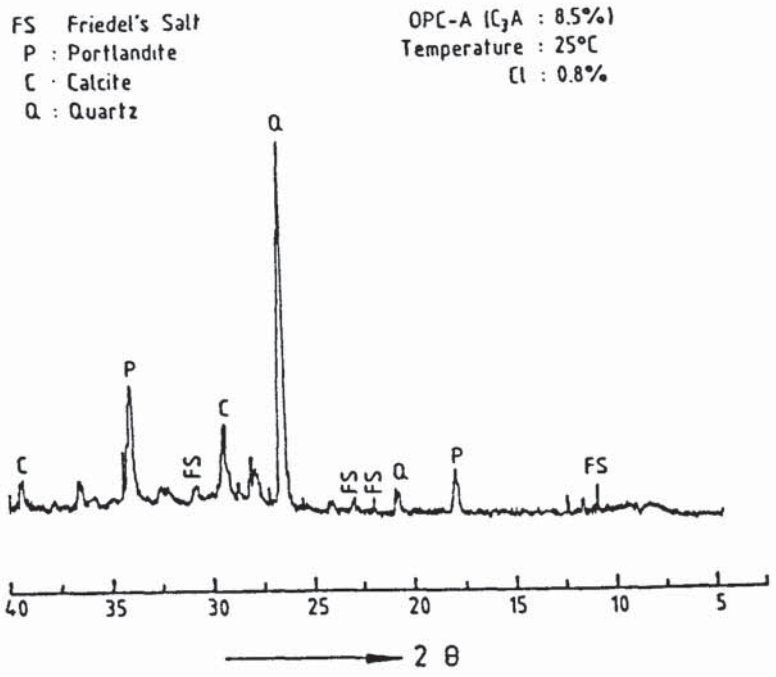

Figure 3.95: X-ray diffractogram for chloride-contaminated OPC-A and exposed to 25 °C

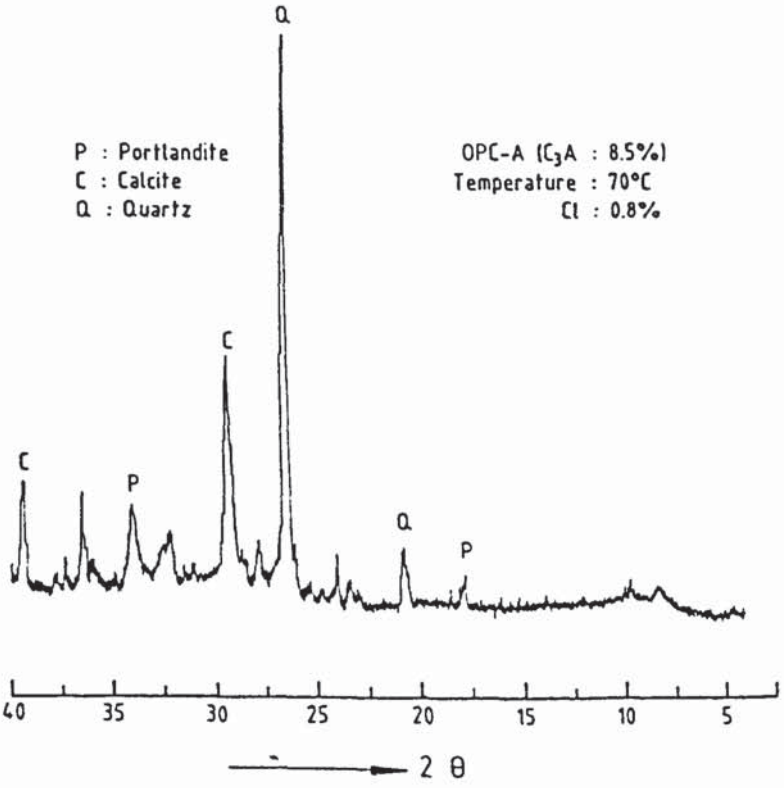

Figure 3.96: X-ray diffractogram for chloride-contaminated OPC-A and exposed to 70 °C

mortar specimens contaminated with sodium chloride plus sodium sulfate and exposed to 25 and 70 °C are shown in Figures 3.97 and 3.98, respectively. Formation of portlandite, quartz and calcite was indicated. The X-ray peaks for ettringite and Friedel's salt were not exhibited by these curves.

In summary, the following trend could be observed from the X-ray diffractograms for SRPC and OPC mortar specimens.

i) Formation of ettringite in uncontaminated specimens and those contaminated with sodium sulfate, at exposure temperature of 25 °C. However, when the exposure temperature was raised, the peaks for this compound became less distinct. In the specimens contaminated with sodium chloride also the X-ray peaks for this compound became less apparent. Further, in the specimens contaminated with sodium chloride plus sodium sulfate, the peaks for ettringite were not discerned. This trend was observed in the specimens exposed to both 25 and 70 °C. The absence of ettringite peaks in the X-ray diffractograms of specimens exposed to 70 °C may be attributed to the destabilization of ettringite at this temperature. The ettringite is reported to be unstable at temperatures of 40 to 100 °C [135]. Barvinok et al. [135] indicated ettringite to be unstable in the range of 50 to 70 °C, while Lalck and Bures [136] observed ettringite up to 90 °C, which is the limiting temperature of stability according to Moldovan and Butucescu [137]. According to Hoglund [138], at temperatures above 50 °C, ettringite is not formed at sulfate concentrations up to 5×10^{-4} mole per liter. At lower temperatures, ettringite is formed at concentrations of 2×10^{-7} moles per liter. Similarly, the ettringite peaks were not discerned in the specimens contaminated with sodium chloride plus sodium sulfate. This indicates that the presence of chloride ions influences the formation of ettringite.

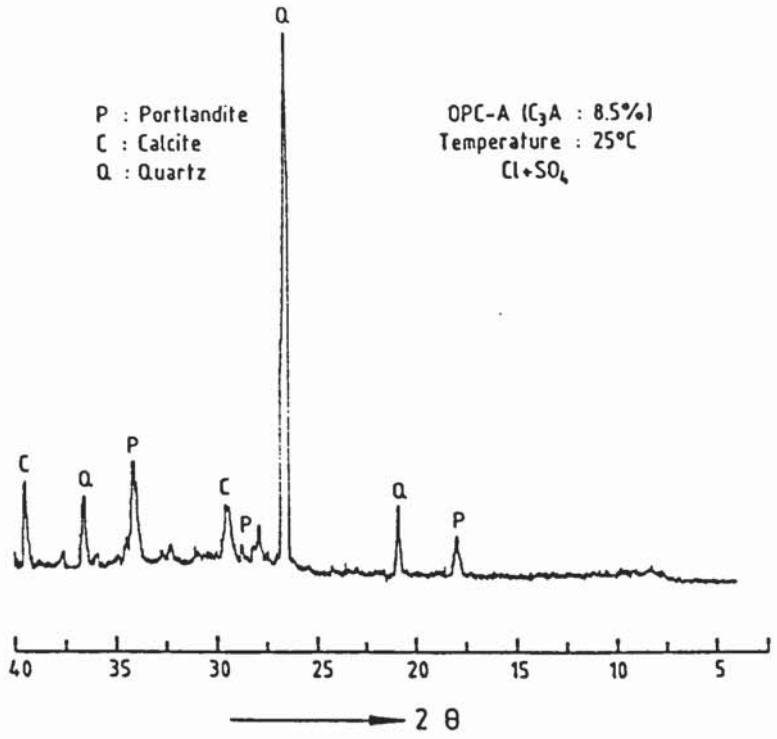

Figure 3.97: X-ray diffractogram for OPC-A contaminated with chloride and sulfate and exposed to 25 °C

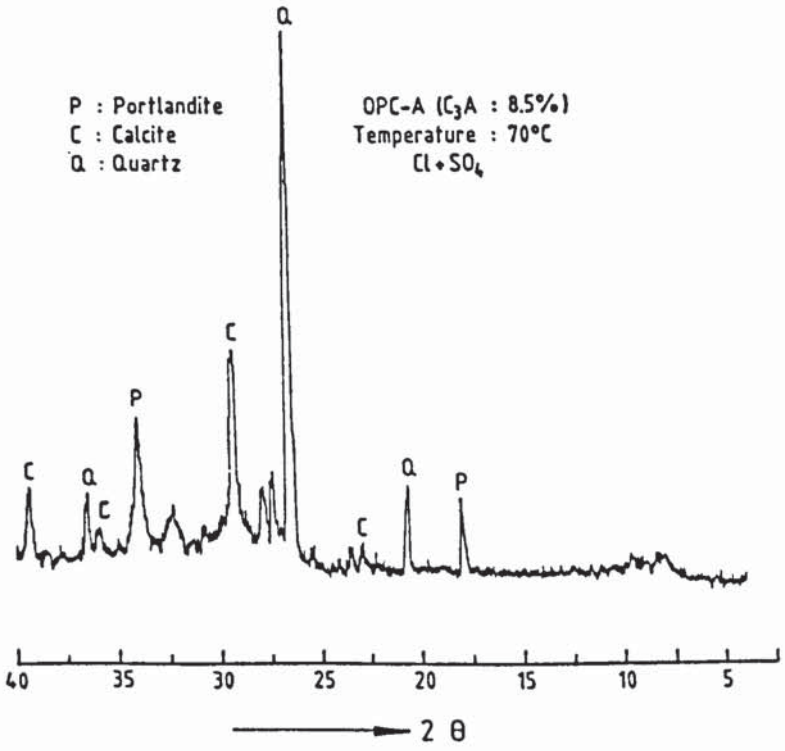

Figure 3.98: X-ray diffractogram for OPC-A contaminated with chloride and sulfate and exposed to 70 °C

ii) The formation of ettringite was observed in both sulfate resisting and ordinary portland cements contaminated with sodium sulfate and exposed to 25 °C, the peaks for the latter cement being more pronounced than in the former. These peaks were not detected in the specimens exposed to 70 °C in both the cements.

iii) The X-ray peaks for Friedel's salt, with the major peak at 11.1° 2θ were observed in OPC-A cement mortar specimens contaminated with sodium chloride and exposed to 25 °C. These peaks were, however, not discerned in the specimens exposed to 70 °C and those contaminated with sodium chloride plus sodium sulfate. These peaks were not observed in SRPC mortar specimens contaminated with sodium chloride, even at 25 °C.

Thus, the X-ray data indicated that both ettringite and calcium chloro-aluminate are destabilized either due to elevated temperature or the presence of chloride/sulfate contamination. Further, it may not be out of place to mention that the intensity of X-ray diffractograms for the two compounds of interest in this study, namely Friedel's salt and ettringite, were not that significant. This trend may be attributed to the relatively low C_3A (3.5 and 8.5%) content of these cements and the marginal quantity of chloride (0.8%) and sulfate (1.5%) used as contamination.

3.2.3 Differential Thermal Analysis

The DTA and TGA curves for SRPC mortar specimens contaminated with sodium chloride and exposed to 25 and 70 °C are shown in Figures 3.99 and 3.100, respectively. The DTA curves indicated the formation of an endothermic peak at about 350 °C in both the specimens exposed to both the temperatures. However, the endothermic peak in the specimens exposed to 70 °C was more shallow than in the specimens exposed to 25 °C. Figures 3.101 and 3.102 show the DTA and TGA

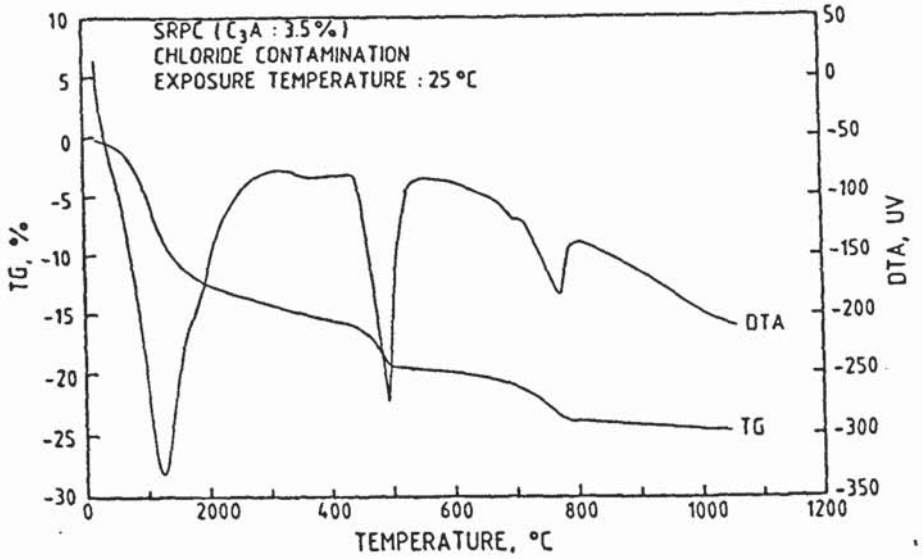

Figure 3.99: DTA and TGA curves for chloride-contaminated SRPC mortar specimens exposed to 25 °C

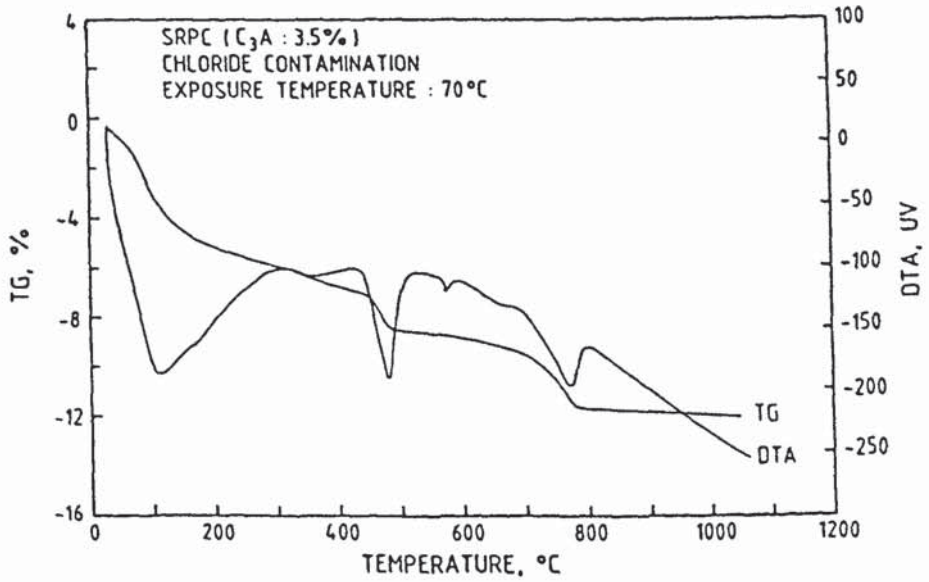

Figure 3.100: DTA and TGA curves for chloride-contaminated SRPC mortar specimens exposed to 70 °C

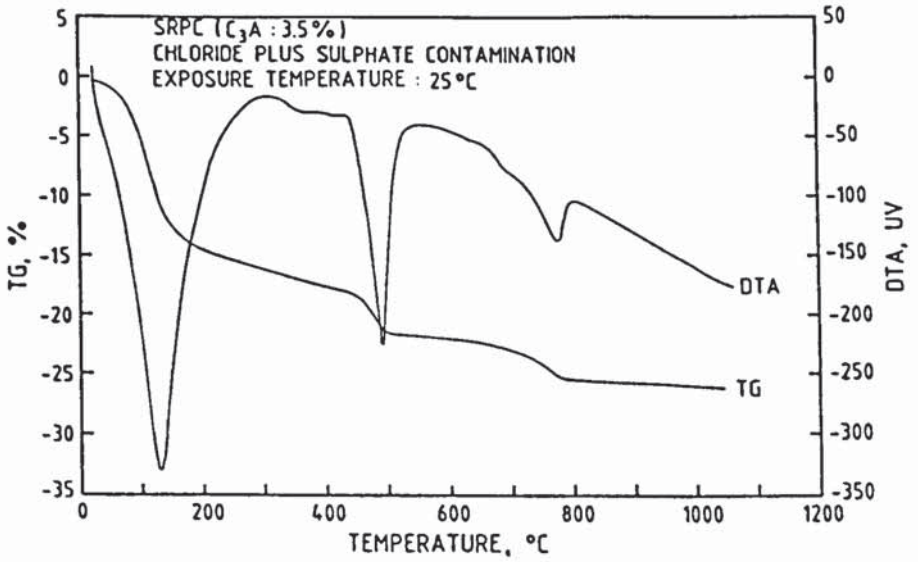

Figure 3.101: DTA and TGA curves for SRPC mortar specimens contaminated with sulfate chloride and exposed to 25 °C

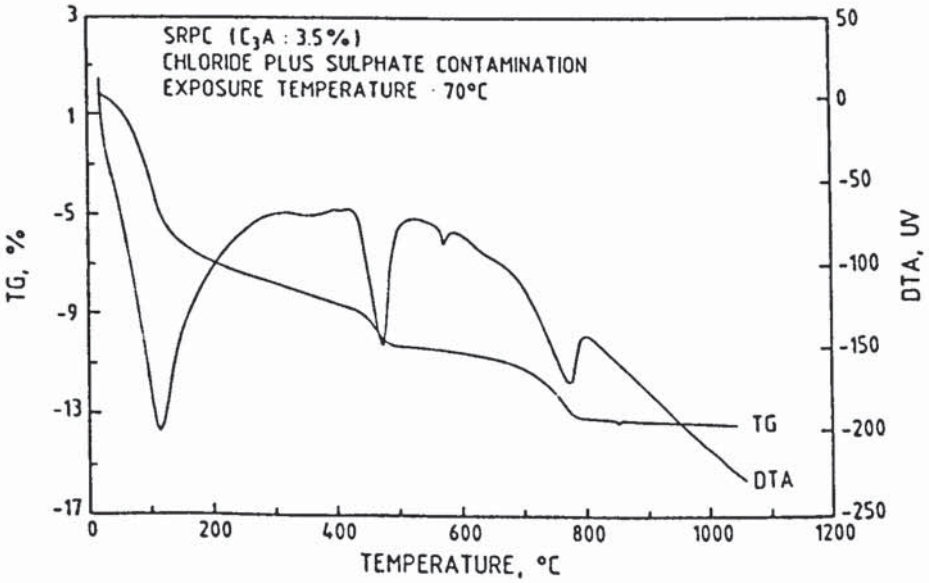

Figure 3.102: DTA and TGA curves for SRPC mortar specimens contaminated with sulfate chloride and exposed to 70 °C

curves for the specimens contaminated with sodium chloride plus sodium sulfate and exposed to 25 and 70 °C, respectively. These curves also indicated the formation of endothermic peaks, attributable to dehydration of calcium chloro-aluminate at 350 °C. However, these peaks were less distinct than those formed in the specimens contaminated with only sodium chloride. Figures 3.103 and 3.104 show the DTA/TGA curves for OPC-A (C_3A: 8.5%) mortar specimens contaminated with sodium chloride and exposed to 25 and 70 °C, respectively. These curves indicated a decrease in the DTA peaks for calcium chloro-aluminate due to increase in the temperature. The DTA/TGA curves for the specimens contaminated with sodium chloride plus sodium sulfate and exposed to these two temperatures are plotted in Figures 3.105 through 3.106, respectively. These curves indicated a behaviour similar to that exhibited by SRPC specimens (Figures 3.99 through 3.100). The DTA/TGA curves for OPC-B (C_3A: 14.5%) mortar specimens contaminated with sodium chloride and exposed to 25 and 70 °C are plotted in Figures 3.107 and 3.108, respectively. The DTA/TGA for these specimens contaminated with sodium chloride plus sodium sulfate and exposed to 25 and 70 °C are plotted in Figures 3.109 and 3.110, respectively. These data indicated a trend similar to that shown by the other two cements.

In summary the DTA peaks indicated the formation of Friedel's salt in all the cements and at all exposure temperatures. However, the endothermic peaks, which provide a qualitative indication of the formation of this compound, were more distinct in the specimens which were contaminated with only sodium chloride and exposed to 25 °C. These peaks were less distinct and shallow in the specimens exposed to 70 °C and contaminated with sodium chloride plus sodium sulfate.

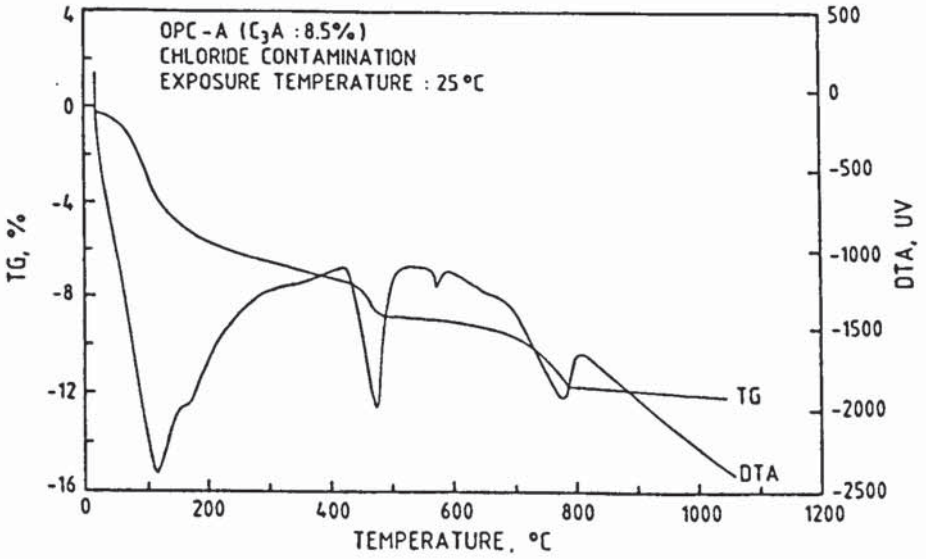

Figure 3.103: DTA and TGA curves for chloride-contaminated OPC-A mortar specimens exposed to 25 °C

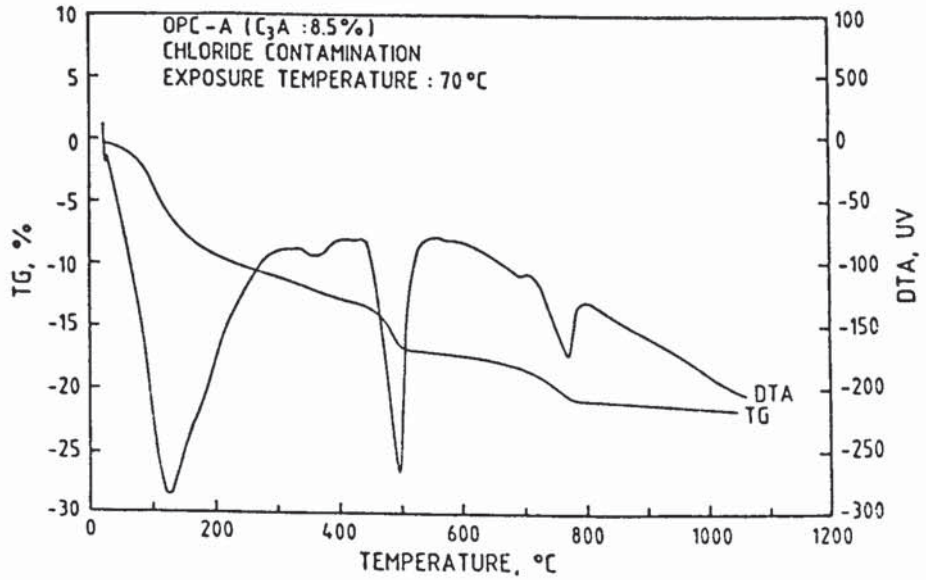

Figure 3.104: DTA and TGA curves for chloride-contaminated OPC-A mortar specimens exposed to 70 °C

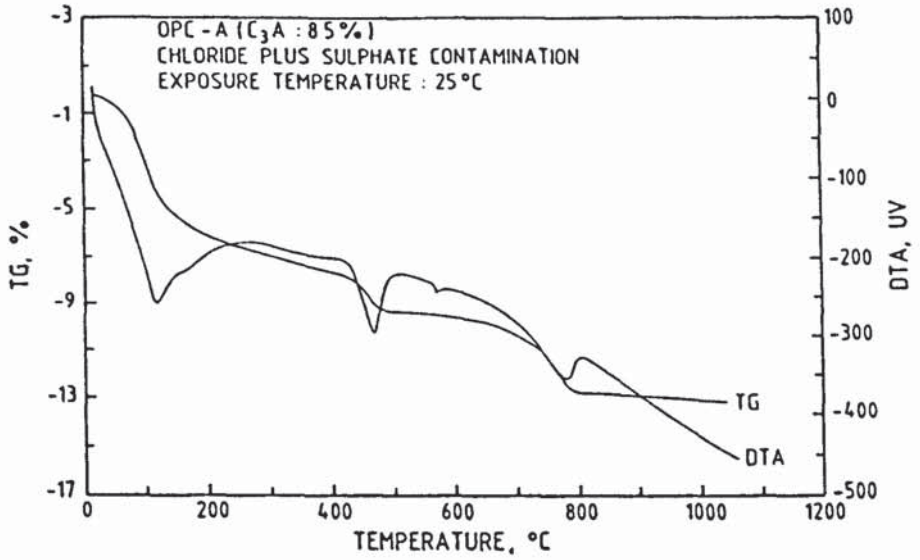

Figure 3.105: DTA and TGA curves for OPC-A mortar specimens contaminated with sulfate chloride and exposed to 25 °C

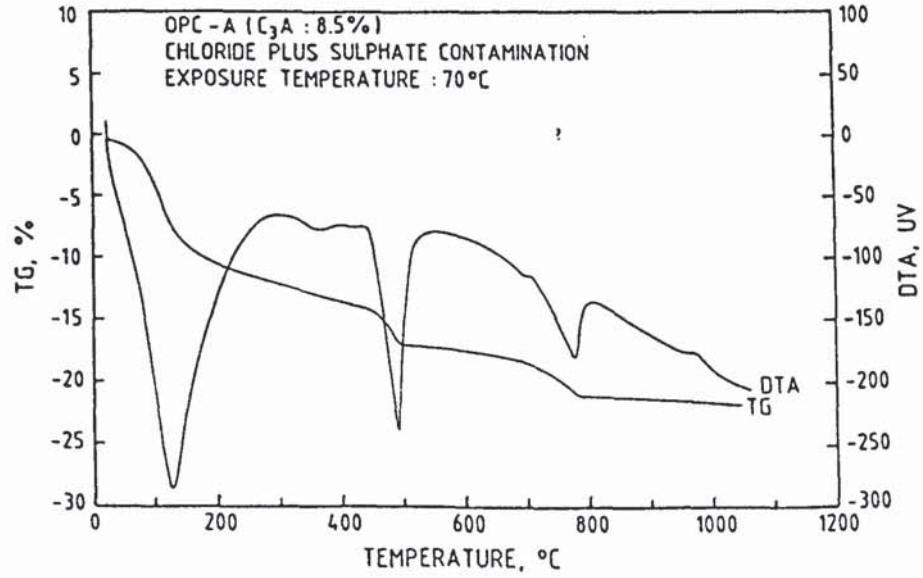

Figure 3.106: DTA and TGA curves for OPC-A mortar specimens contaminated with sulfate chloride and exposed to 70 °C

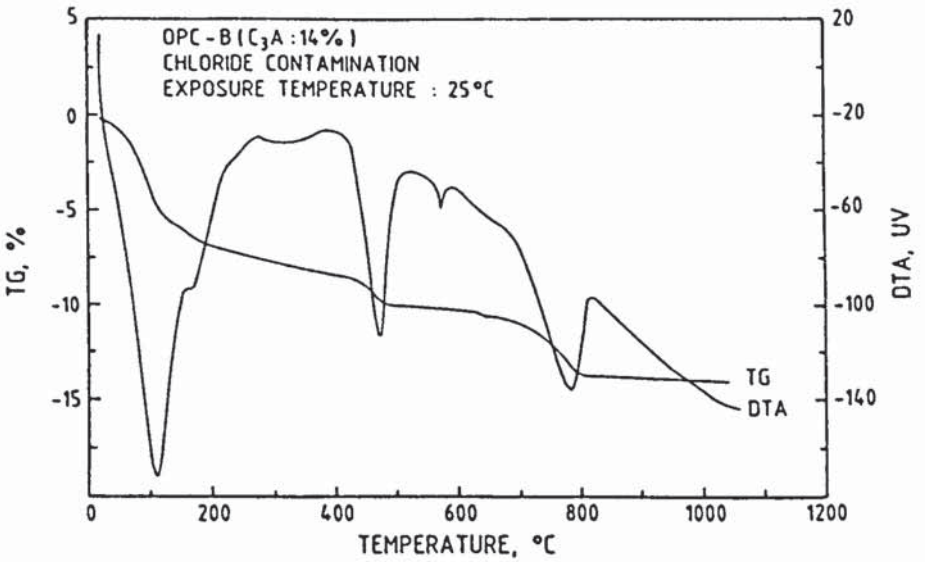

Figure 3.107: DTA and TGA curves for chloride-contaminated OPC-B mortar specimens exposed to 25 °C

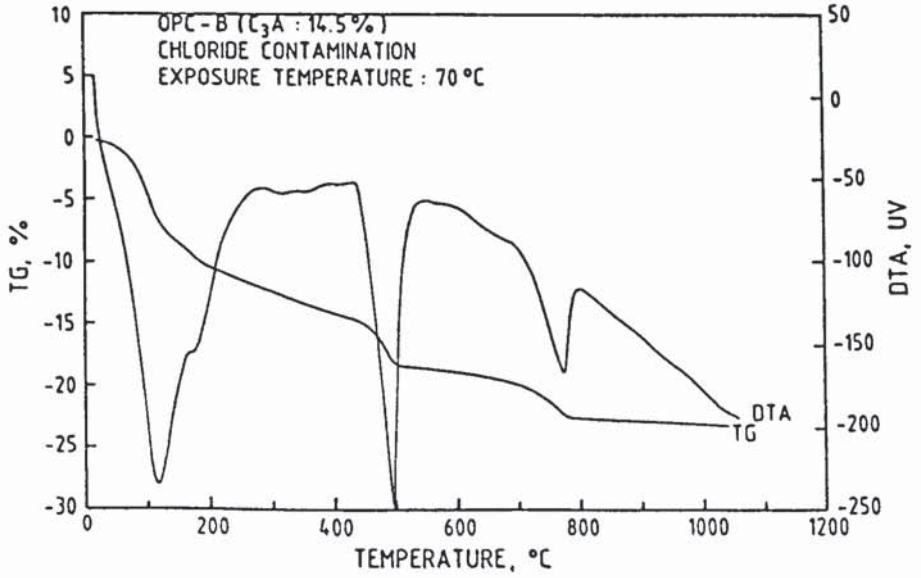

Figure 3.108: DTA and TGA curves for chloride-contaminated OPC-B mortar specimens exposed to 70 °C

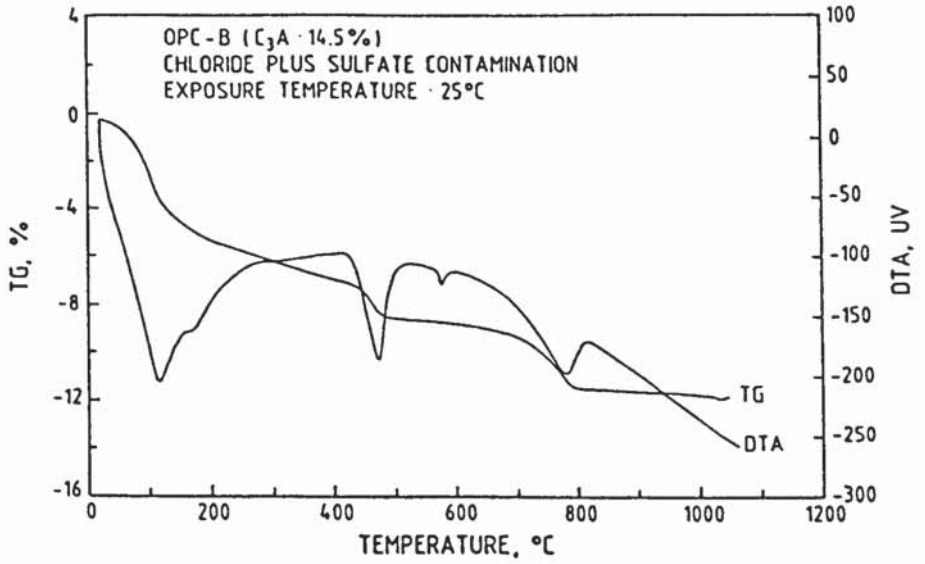

Figure 3.109: DTA and TGA curves for OPC-B mortar specimens contaminated with sulfate chloride and exposed to 25 °C

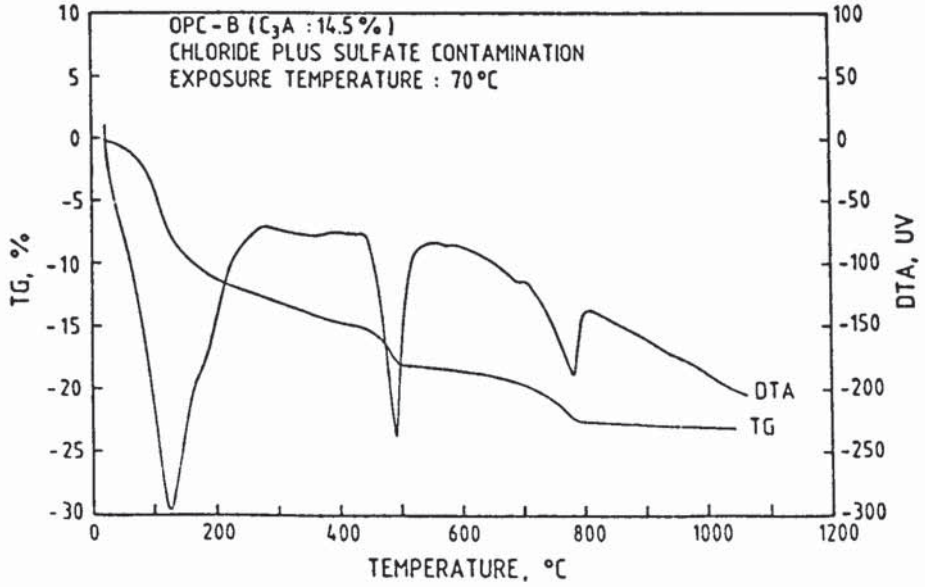

Figure 3.110: DTA and TGA curves for OPC-B mortar specimens contaminated with sulfate chloride and exposed to 70 °C

3.3 SUMMARY OF RESULTS

In this Chapter, the concomitant effect of chloride and sulfate contamination on the pore solution chemistry in ordinary and blended cement mortar specimens exposed to normal and elevated temperatures was investigated. The influence of these parameters on the OH^-, Cl^-, and SO_4^{--} concentration was determined. The relationship between alkalinity, chloride, and sulfate concentrations were evaluated in terms of Cl^-/OH^- and SO_4^{--}/OH^- ratios to understand the influence of the chloride-sulfate contamination and exposure temperature on the aggressivity of the internal chemical environment at the steel-concrete interface.

The results indicated that temperature and sulfate contamination both influence the chloride binding in both ordinary and blended cements. In the chloride-contaminated specimens, the chloride binding was influenced by the exposure temperature. The chloride concentration in the specimens exposed to 25 and 40 °C was not significantly different. However, an appreciable increase in the chloride concentration was noticed for exposure temperature of 55 °C and above. The chloride concentration at 70 °C was 1.5 to 2.7 times that at 25 °C. The increase in the chloride concentration in all the specimens exposed to temperatures of 55 °C and more is attributable to the decomposition of the Friedel's salt.

The chloride binding capacity of cements increased with the C_3A content. It was, however, affected by the exposure temperature. The chloride concentration at 25 °C in SRPC (C_3A: 3.5%) was 2 times that in OPC-B (C_3A: 14.5%). This ratio, however, reduced to 1.12 in the specimens exposed to 70 °C.

The effect of temperature on chloride binding in the blended cements was similar to that in the ordinary portland cements. The chloride concentration in all the blended

cements increased with exposure temperature. However, the chloride concentration in all the blended cements was lower than that in the OPC, at all the exposure temperatures. An exception to this trend was indicated by the silica fume blended cement. The chloride concentration in this cement was marginally different than that in OPC.

The sulfate contamination had a similar effect to that of temperature on chloride binding. In the presence of sulfate ions, the chloride binding capacity of cements was considerably reduced. This trend was observed at all the exposure temperatures. The chloride concentration in the SRPC, OPC-A and OPC-B specimens contaminated with sodium chloride plus sodium sulfate and exposed to 25 °C was 155, 183, and 289%, respectively, of that in the specimens contaminated with only sodium chloride. This ratio in the specimens exposed to 70 °C was 106, 122 and 104%, respectively. The higher chloride concentration in the specimens contaminated with sodium chloride plus sodium sulfate is attributed to the concomitant reaction of these two ions with the C_3A phase in cement forming calcium chloro-aluminate (Friedel's salt) and calcium sulpho-aluminate, respectively. These results have an important bearing on the substructural components which are exposed to soil and groundwater contaminated with both chloride and sulfate salts. The concomitant presence of chloride and sulfate considerably reduces the chloride binding capacity of cements thereby releasing the chloride ions into the pore solution. The free chlorides so liberated cause depassivation of steel even at low temperature of 25 °C.

The chloride concentration in the blended cements contaminated with sodium chloride plus sodium sulfate was also more than that in the specimens contaminated with only sodium chloride.

At temperatures of 25 and 40 °C, the OH^- concentration in the contaminated specimens was more than that in the uncontaminated specimens. The OH^- concentration in the specimens contaminated with sodium sulfate was more than that in the specimens contaminated with sodium chloride and sodium chloride plus sodium sulfate. The increase in the alkalinity of the contaminated specimens, compared to uncontaminated specimens, is attributable to the reaction of the sulfate and/or chloride ions with the C_3A content of cement leading to the formation of sodium hydroxide which considerably increases the alkalinity of the pore solution. At higher temperatures, 55 °C and above, the alkalinity is reduced, in so much so that at 70 °C, the alkalinity of the contaminated specimens is nearly equal to that of the uncontaminated specimens. This reduction in the OH^- also indicates the instability of calcium chloro-aluminate and calcium sulpho-aluminate at higher temperatures. The OH^- concentration in the uncontaminated specimens also decreased with increasing temperature, particularly above 55 °C. This reduction may be attributed to the instability of calcium sulpho-aluminate formed due to the reaction of gypsum with C_3A.

The alkalinity of the blended cements was also affected by the exposure temperature and chloride and sulfate contamination. The OH^- concentration in the blended cements was lower than that in the ordinary portland cements, at all the exposure temperatures. Minimum OH^- was measured in the chloride-contaminated silica fume blended cement exposed to 55 °C. The pH of the pore solution at this temperature was 12.7. This value, however, is higher than the pH of the saturated calcium hydroxide solution (12.5). Further, the OH^- concentration measured in the silica fume blended cement will not cause steel depassivation as the passive conditions are normally observed on mild steel immersed in pure alkali with pH values in excess of 11.5. However, this alkalinity may not be sufficient for steel passivity if high concentrations of chloride and/or sulfates are present.

The sulfate concentration in the pore solution of plain and blended cements was also influenced by the exposure temperature and chloride contamination. The sulfate concentration in the specimens contaminated with sodium chloride plus sodium sulfate was more than that in the specimens contaminated with only sodium sulfate. This indicates that the quantity of calcium sulpho-aluminate formed in the cements contaminated with sodium chloride plus sodium sulfate is less than that formed in the sulfate-contaminated specimens. This may be attributed to the conjoint reaction of C_3A with these two ions. An increase in the sulfate concentration was also indicated in the chloride contaminated and uncontaminated specimens exposed to temperature of more than 55 °C. This increase in the sulfate concentration may be attributed to the de-stabilization of calcium sulpho-aluminate phase formed due to the reaction of gypsum with C_3A of cement. The slightly higher sulfate ion concentration in chloride-contaminated specimens, over uncontaminated specimens, indicates that chloride ions decrease the extent of calcium sulpho-aluminate formation due to reaction of gypsum with C_3A.

The increase in the sulfate concentration in the pore solution, due to higher temperature and/or chloride contamination, is significant from reinforcement corrosion view point, since they not only depassivate steel but also decrease the electrical resistivity of concrete.

The Cl^-/OH^- values increased with temperature in both OPC and blended cements. This increase in the Cl^-/OH^- values with temperature is attributed to the combined effect of increase in the chloride concentration and decrease in the alkalinity. The high Cl^-/OH^- indicates the vulnerability for steel depassivation.

The X-ray diffractograms of the contaminated and uncontaminated specimens exposed to temperatures of 25 to 70 °C support the findings of the pore solution analyses. Formation of ettringite was observed in the cements contaminated with sodium sulfate at 25 °C. In the specimens exposed to 70 °C or contaminated with sodium chloride plus sodium sulfate these peaks were not discerned. Similarly, the formation of Friedel's salt was observed in the specimens contaminated with sodium chloride and exposed to 25 °C. These peaks were not detected in the specimens exposed to 70 °C or contaminated with sodium chloride plus sodium sulfate.

The DTA peaks indicated the formation of Friedel's salt in all the cements and at all exposure temperatures. However, the endothermic peaks, which provide a qualitative indication of the formation of this compound, were more distinct in the specimens which were contaminated with only sodium chloride and exposed to 25 °C temperature. These peaks were less distinct and shallow in the specimens exposed to 70 °C and contaminated with sodium chloride plus sodium sulfate.

The specimen size and exposure conditions used in this part of the study do not necessarily represent the actual field conditions. However, the results do point to the effect of temperature and chloride-sulfate contamination on the pore solution chemistry.

Chapter 4

INFLUENCE OF CHLORIDE-SULFATE CONTAMINATION AND TEMPERATURE ON REINFORCEMENT CORROSION IN CONCRETE

4.1 CORROSION OF REINFORCING STEEL IN CONCRETE

Portland cement concrete provides both chemical and physical protection to the reinforcing steel. The chemical protection is provided by the highly alkaline nature of the pore solution (pH > 13). At this high pH steel is passivated in the presence of oxygen presumably due to the formation of a submicroscopically thin γ-Fe_2O_3 film [139,140]. Hime and Erlin [30] suggested that the passivating layers on steel surface could have a composition other than that of γ-Fe_2O_3. According to Page [141], the lime-rich layer, which is observed at the steel-concrete interface, provides further protection to the steel. This was confirmed by Leek and Poole [142] who reported that the interfacial layer consists of an aggregate-free zone of portlandite ($Ca(OH)_2$) of variable thickness (5 to 15 μm) disrupted by inclusions of calcium silicate hydrate (C-S-H) gel. This layer is thought to screen most of the surface of the steel from direct access of aggressive ions and to act as an alkaline buffer to pH reductions resulting from the hydrolysis of corrosion products [29]. According to Sagoe-Crentsil and Glasser [143], both $Ca(OH)_2$ and C-S-H gel form a buffering pair, and a high pH is as readily maintained by C-S-H as by $Ca(OH)_2$. The physical protection to steel is provided by the dense and impermeable structure of concrete which retards the diffusion of the aggressive species, like chlorides, carbon dioxide, oxygen and moisture, to the steel-concrete interface.

Depassivation of steel occurs by the reduction of the pore solution pH, due to carbonation, or by ingress of chloride ions to the steel-concrete interface. A number of mechanisms by which chlorides break down the passive layer have been proposed, e.g., the chemical dissolution of the film [144], the build up of the metal holes at the film/substrate interface [145], and due to high chloride concentrations at the iron oxide/pore solution interface which leads to local acidification and pitting [146]. Leek and Poole [142], based on SEM-EDS studies of the passive film breakdown on steel in mortar prisms, have shown that chloride ions initiate corrosion by breaking the bond between the film and the metal.

Irrespective of the mechanisms controlling the depassivation of steel due to chloride ions, it is clear that these ions play a dominant role in initiating reinforcement corrosion. From this perspective, the American Building Codes (ACI 318-85) [147] limit the water-soluble chlorides to 0.15% by weight of cement. ACI Committee 224 [148] adopting a more conservative approach has suggested that the acid-soluble chloride concentration should not be more than 0.2% by weight of cement. The British Standard BS 8110 [149] allows a maximum chloride content of 0.4%. The Norwegian Code, NS 3474, allows an acid-soluble chloride content of 0.6%, RILEM permits 0.40% and the revised Australian Standard for Concrete Structures, AS 3600, allows an acid-soluble chloride content of 0.80 kg/m^3 of concrete (0.22 percent by weight of cement for a typical concrete mix). Rasheeduzzafar et al. [96] indicated that the chloride threshold limits for cements with up to 8% C_3A agree very well with the ACI 318 limit of 0.15% water soluble chlorides. Additionally, they reported that ACI, BS and Australian Code limits, however, appear to be conservative for concretes made with high C_3A cements. Lambert et al. [109] suggested that the critical level of chloride below which there was no significant probability of corrosion was around 1.5%. They attributed the increased chloride tolerance in their specimens compared to BS 8110 limit of 0.4% to the protective nature of concrete produced under well-controlled conditions of the laboratory.

Recent research findings, however, have shown that cement alkalinity also significantly influences the chloride binding and hence the free chlorides [64,86,93,150]. Taking into account the concomitant effect of chloride and alkalinity, Hausmann [20] suggested the critical Cl^-/OH^- ratio to be around 0.6. Gouda [74] using pH values of the electrolyte representative of the concrete pore solution indicated that the threshold Cl^-/OH^- ratio was 0.3. Lambert et al. [109] investigated the relationship between Cl^-/OH^- and corrosion current density in various cements. Their investigations indicated that the passive conditions of steel in concrete, characterized by corrosion current density (I_{corr}) substantially lower than 100 nA/cm^2 were maintained until a threshold Cl^-/OH^- ratio of approximately 3 was exceeded. There was a considerable scatter in the values of I_{corr} recorded at Cl^-/OH^- ratios in excess of 3 and even at Cl^-/OH^- ratios as high as 15 to 20, there were instances of bars suffering no significant corrosion. Mangat and Gurusamy [110] reported that for steel fibers in concrete under conditions of marine exposure, no visible signs of corrosion were present at Cl^-/OH^- ratios as high as 320. Mangat and Molloy [151] indicated that a universal threshold Cl^-/OH^- level is not applicable to different cement concretes. In their investigations, reinforcing steel corrosion was observed in the control matrix when the pore fluid Cl^-/OH^- ratio was 13, while at values of 17 and 18, in silica fume cement concrete, reinforcement corrosion was insignificant. Minimal reinforcement corrosion in silica fume and blast furnace slag cement mortar specimens placed in the aggressive environment of sabkha even, at Cl^-/OH^- of 3.3 and 6.5, respectively, was reported by Al-Amoudi et al. [152].

While many studies, partly cited above, were devoted to the effect of chloride, and chloride and sulfate, as in marine environments, data are lacking on the combined effect of temperature, chloride and sulfate contamination on reinforcement corrosion. As discussed in Chapter 3, the concomitant presence of chloride and sulfate ions significantly increases the free chloride concentration in the pore solution. A similar

effect was observed in the specimens exposed to elevated temperatures. The net effect of the temperature and sulfate contamination was to increase the Cl^-/OH^- concentration. These results indicate the need to evaluate the consequence of such an increase in the Cl^-/OH^- ratio on reinforcement corrosion.

This Chapter details the experimental work carried out to investigate the effect of chloride-sulfate contamination and temperature on reinforcement corrosion.

4.2 EXPERIMENTAL WORK

The uncontaminated and contaminated reinforced concrete specimens were exposed to temperatures in the range of 25 to 70 °C. Table 4.1 shows the experimental variables.

Table 4.1: Experimental variables to evaluate the effect of sulfate-chloride contamination and temperature on reinforcement corrosion

Variable	Details
Specimens	Reinforced concrete specimens made with SRPC, OPC-A, and OPC-B (C_3A: 3.5, 8.5 and 14.5%)
Contamination	0% 0.8% Cl^- 0.8% Cl^- + 1.5% SO_3^{--}
Exposure temperature	25, 40, 55 and 70 °C
Tests	Corrosion Potentials monitoring Corrosion current density by linear polarization resistance technique

4.2.1 Reinforced Concrete Specimens

Reinforced concrete specimens were cast using SRPC, OPC-A and OPC-B. The chemical composition of these cements is shown in Table 3.2. The concrete mixes were designed in accordance with the absolute volume method. Proportioning of the materials was carried out on weight basis. The following parameters were kept invariant in all the concrete mixtures.

Coarse to fine aggregate ratio:	1.6
Cement content:	350 kg/m^3 (600 lb/yd^3)
Effective water-cement ratio:	0.50
Workability:	50 to 75 mm slump
Average 28-day compressive strength:	30 MPa (4350 psi)

Crushed limestone, with a specific gravity of 2.48 and absorption 2.3% was used as coarse aggregate. Dune sand, of specific gravity 2.62 and absorption 0.57% and fineness modulus 1.3, was used as fine aggregate. Table 4.2 shows the grading of coarse and fine aggregate used in the concrete mixtures.

Prismatic concrete specimens, 200 x 190 x 75 mm with three 12 mm diameter steel bars, were used for monitoring reinforcement corrosion. An effective cover of 30 mm was provided both at top and bottom. The cover was obtained by using plastic spacers. Two bars were used as working electrode, while the third which was placed in the centre of the specimen was used as a counter electrode in the linear polarization resistance measurements. A small diameter plastic tube was inserted into the concrete specimen for making connection to the reference electrode. The three bars were provided electrical connection for monitoring the corrosion activity. The ends of the

bars and the electrical wire-steel junction were coated with a cement paste overlaid by an epoxy-coating to reduce the risk of crevice corrosion. The cement paste was made by mixing a styrene-butadiene rubber emulsion with cement. Such a system has been found to be effective in preventing crevice corrosion [153]. The steel bars were cleaned mechanically with a silicon carbide paper and degreased with acetone prior to placement in the moulds.

Table 4.2: Aggregate grading

Coarse Aggregate (Crushed Limestone)		Fine Aggregate (Dune Sand)	
Sieve Opening (mm)	Percent Passing	Sieve Opening (mm)	Percent Passing
19.0	90	4.75	100
13.0	55	2.40	100
9.5	20	1.20	100
4.75	0	0.60	96.2
		0.30	61.4
		0.15	21.9
		0.075	1.0

Sulfate and chloride additions were made by dissolving the required quantities of Analar Grade sodium sulfate and sodium chloride, respectively. The concrete ingredients were mixed in a revolving drum mixer for about three minutes, and placed in the moulds and vibrated to consolidate the concrete. After casting, the specimens were covered with plastic sheet and kept at the laboratory conditions for 24 hours at which time they were demoulded. After demoulding, the specimens were covered with wet burlap and kept moist for 13 days.

4.2.2 Exposure Conditions

After 14 days of curing, the concrete specimens were placed in a controlled humidity chamber in which the relative humidity was maintained at 75%. Figure 4.1 shows the specimen geometry and Figure 4.2 is a schematic representation of the test set-up.

4.2.3 Corrosion Monitoring

Reinforcement corrosion was monitored by measuring the corrosion potentials on a weekly basis. The potentials were measured against a saturated calomel reference electrode (SCE). To determine the corrosion current density, the electrical leads from the concrete specimens were connected to a EG&G PAR Model 350 A Potentiostat/Galvanostat. The polarization resistance (Rp) was determined by conducting a linear polarization scan in the range of $\pm$ 10 mV of the corrosion potentials. A scan rate of 0.1 mV/sec. was used. The corrosion current density I_{corr} was determined using Stern Geary formula [154]:

$$I_{corr} = B/Rp$$

Where: I_{corr} = corrosion current density, $\mu A/cm^2$

Rp = Polarization resistance, $\Omega.cm^2$

$B = (\beta a * \beta c)/2.3(\beta a + \beta c)$

βa and βc are the anodic and cathodic Tafel constants, respectively.

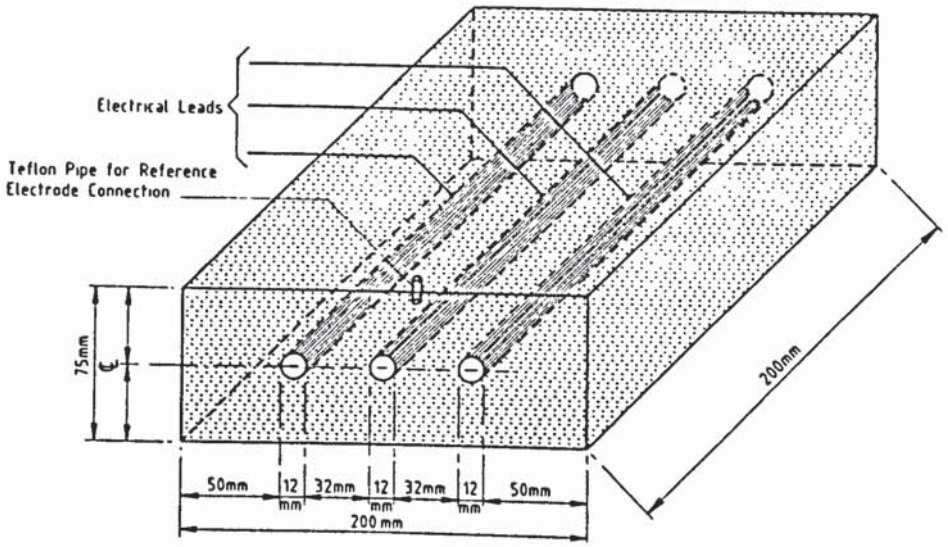

Figure 4.1: Reinforced concrete specimen

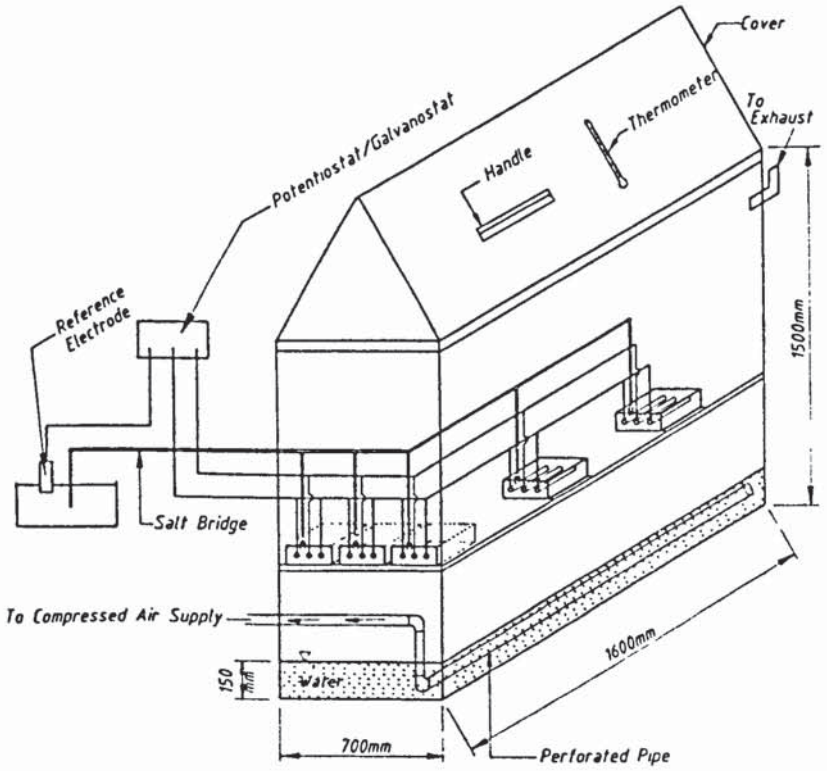

Figure 4.2 : Schematic representation of the exposure chamber with specimens

For steel in an aqueous media, values of ßa and ßc of 100 mV are normally used. However, in the absence of sufficient data on ßa and ßc for steel in concrete, a value of B equal to 52 mV for steel in passive condition and equal to 26 mV for steel in active condition are used. Andrade et al. [155] have indicated a good correlation between the weight loss determined using gravimetric and electrochemical methods using these values. Lambert et al. [109] indicated a good correlation between the corrosion current density determined by linear polarization resistance method (LPRM) and gravimetric weight loss using these values. The anodic and cathodic Tafel constants of 120 mV were used.

For the high resistivity medium, such as concrete, it is necessary to take into account the associated IR drop. Andrade et al. [155] have used a potentiostat with IR compensation for their measurements. Electrochemical impedance spectroscopy (EIS) and other methods have also been used to evaluate the corrosion current density on steel in concrete [156-165]. The EIS technique is free of the Ohmic drop and also provides information on the corrosion kinetics. However, interpretation of the measured impedance presents serious difficulties. Also, the delineation of the data is not easy and many different equivalent circuits can be proposed using the same data. Andrade et al. [155] concluded that this technique is less accurate than the LPRM because of graphical extrapolation and mathematical calculations required to estimate the corrosion rate of steel in this method. Hope et al. [158] are of the opinion that LPRM should only be used to estimate the corrosion rate in simple corroding systems. Transient methods, such as galvanostatic pulse [160] and potentiostatic decay [155], have also been used to determine polarization resistance (Rp) using equivalent circuits. Dawson [164] indicated that naturally occurring fluctuations in the corrosion potential of steel in concrete provide a measure of the electrochemical activity of the surface and their standard deviation is proportional to the corrosion rate. Hardon et al. [165] and

Lambert et al. [109] confirmed the existence of a reproducible relationship between the standard deviation of the noise and corrosion rate for small electrodes suffering microcell corrosion in chloride contaminated concrete. A similar form of relationship was also observed to hold true for larger specimens in which steel was embedded within concrete of variable chloride concentration such that macrocells developed with clearly delineated anodic and cathodic areas. The authors [109,165], however, caution that these effects can be masked by scatter unless precautions are taken to ensure that measurements are made under stable environmental conditions with specimens screened from extraneous sources of noise.

Because of the inherent problems and the time constraints in the determination of corrosion rates using methods other than LPRM this technique was used to monitor reinforcement corrosion in the present investigation.

4.3 RESULTS AND DISCUSSION

4.3.1 Corrosion Potentials

The time-corrosion potential curves for SRPC (C_3A: 3.5%) concrete specimens exposed to 25 °C are plotted in Figure 4.3. The corrosion potentials on steel in the uncontaminated concrete specimens were more noble than in the contaminated specimens. In the contaminated specimens, the corrosion potentials in the specimens contaminated with sodium chloride plus sodium sulfate were less noble than those contaminated with only sodium chloride. The corrosion potentials in all the specimens decreased with exposure period. The corrosion potentials in the specimens contaminated with sodium chloride and sodium chloride plus sodium sulfate were

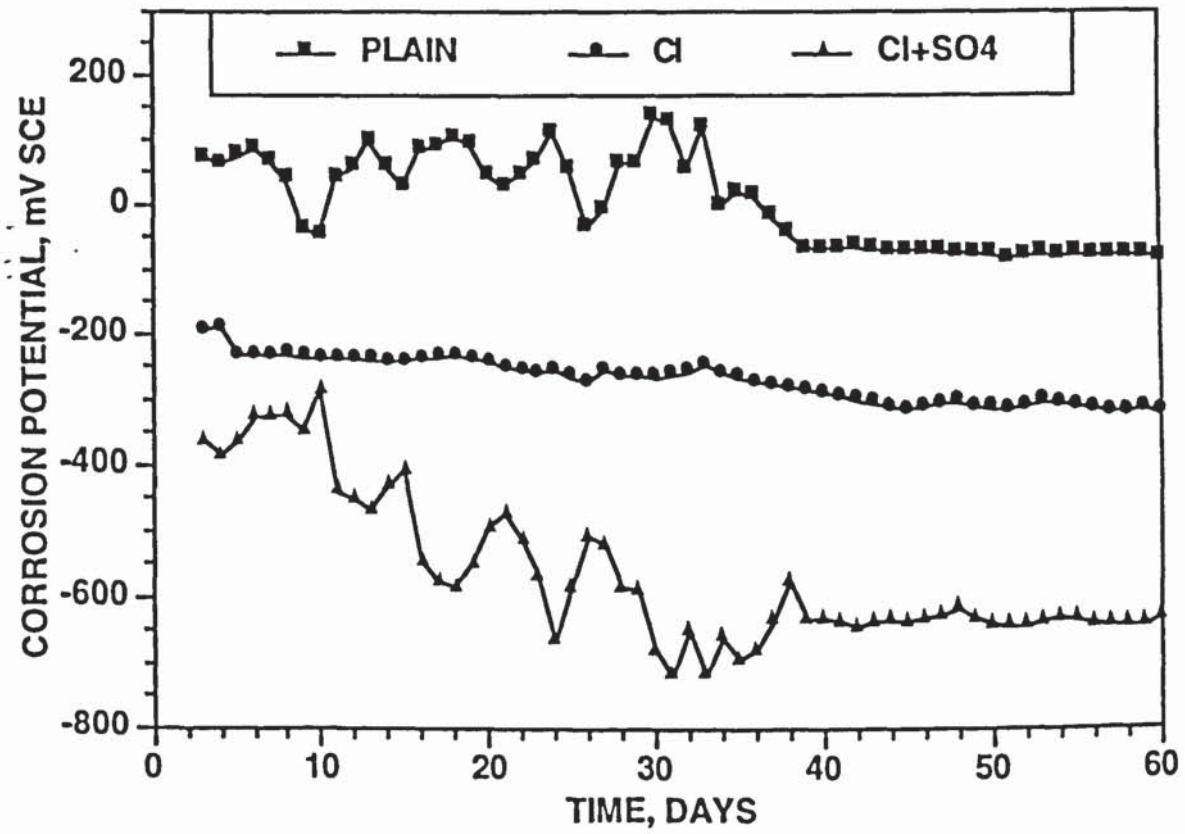

Figure 4.3: Time-potential curves for SRPC concrete specimens exposed to 25 °C

more or less similar up to an exposure period of 10 days, but the differential between the potentials in these specimens increased with the period of exposure. The corrosion potentials in the uncontaminated concrete specimens and those contaminated with sodium chloride and sodium chloride plus sodium sulfate after 60 days of exposure were -84, -322 and -632 mV SCE, respectively.

The corrosion potential-time curves for OPC-A (C_3A: 8.5%) concrete specimens exposed to 25 °C are plotted in Figure 4.4. These curves exhibited a trend similar to that indicated by steel in SRPC concrete specimens exposed to similar temperature. However, the potentials for steel in the contaminated specimens were more or less similar at all the exposure periods. After 60 days of exposure, the corrosion potentials on steel in the uncontaminated concrete specimens and those contaminated with sodium chloride and sodium chloride plus sodium sulfate were -68, -267 and -255 mV SCE, respectively.

Figure 4.5 shows the corrosion potential-time curves for steel in OPC-B (C_3A: 14.5%) concrete specimens exposed to 25 °C. The behaviour of these curves was more or less similar to that indicated by steel in OPC-A concrete specimens (Figure 4.4). The corrosion potentials on steel in the uncontaminated concrete specimens and those contaminated with sodium chloride and sodium chloride plus sodium sulfate, after 60 days of exposure, were -50, -257, -236 mV SCE, respectively.

In general, the data on corrosion potentials, Figures 4.3 through 4.5, indicated that these values in the contaminated specimens were less noble than in the uncontaminated specimens. While the difference in the potentials between the chloride-contaminated and chloride-sulfate-contaminated specimens was significant in the SRPC concrete specimens, it was marginal in the two ordinary portland cement concrete specimens.

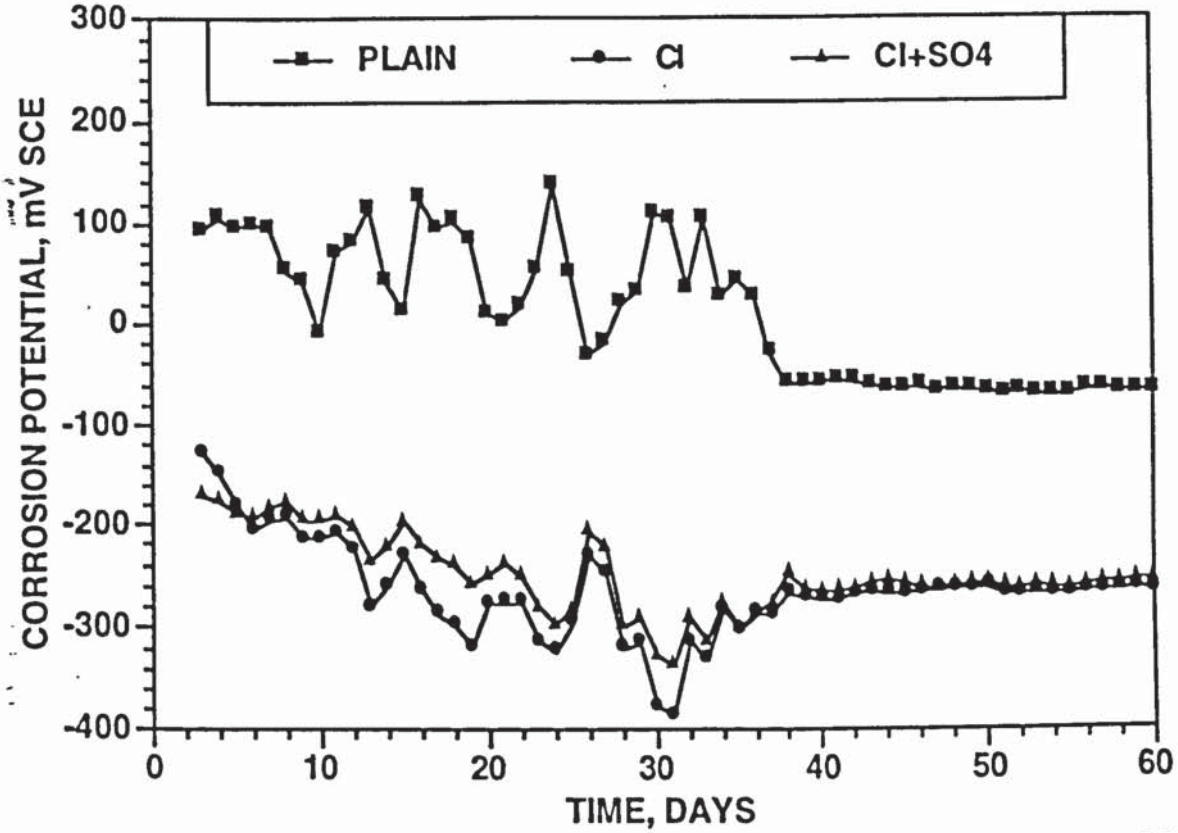

Figure 4.4 : Time-potential curves for OPC-A concrete specimens exposed to 25 °C

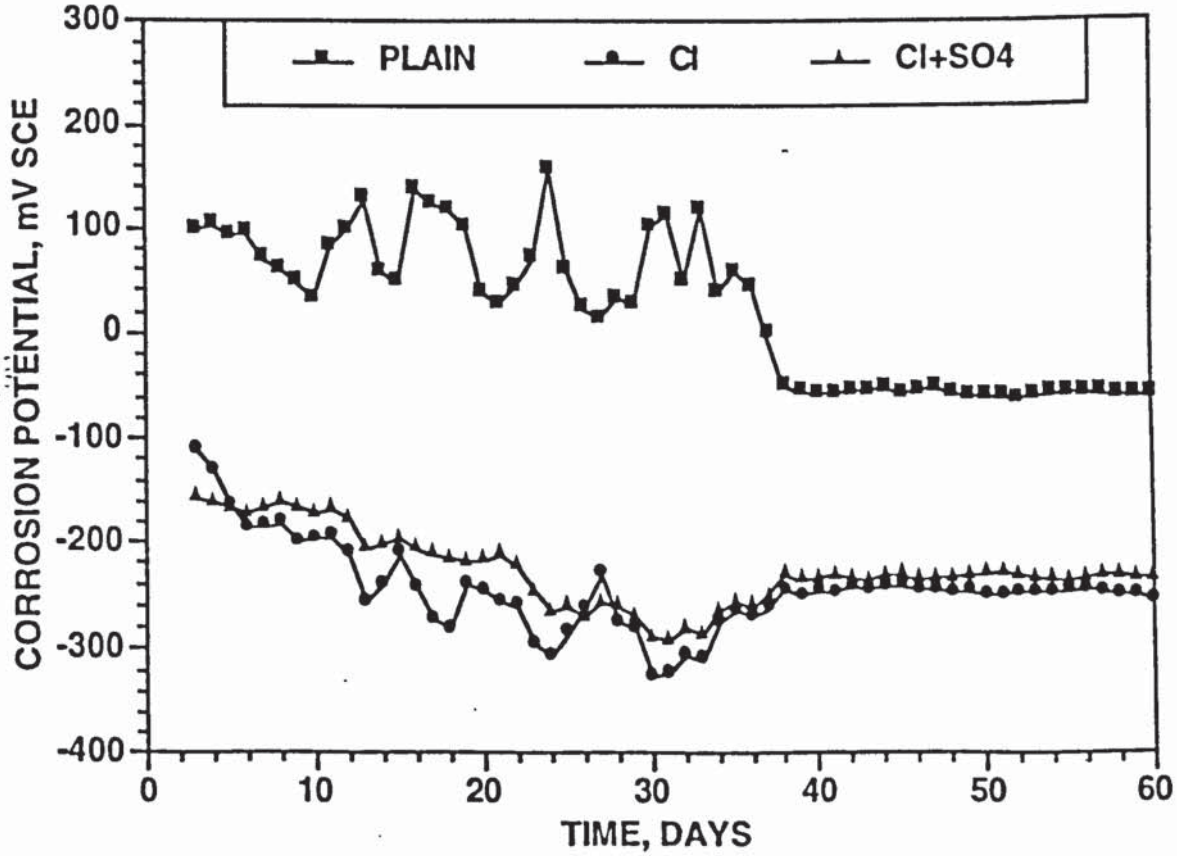

Figure 4.5: Time-potential curves for OPC-B concrete specimens exposed to 25 °C

The corrosion potential-time curves for steel in the uncontaminated and contaminated concrete specimens exposed to 40 °C are shown in Figures 4.6 through 4.8. These data indicated a trend similar to that exhibited by the specimens exposed to 25 °C. The corrosion potentials of steel in the uncontaminated SRPC concrete and those contaminated with sodium chloride and sodium sulfate plus sodium chloride specimens were -94, -480 and -517 mV SCE, respectively, after 60 days of exposure. These values in the OPC-A concrete specimens were -78, -235, and -252 mV SCE, respectively (Figure 4.7). The corrosion potentials of steel in the uncontaminated OPC-B concrete specimens and those contaminated with sodium chloride and sodium chloride plus sodium sulfate, after 60 days of exposure, were -73, -216, and -231 mV SCE, respectively.

Figures 4.9 through 4.11 depict the corrosion potential-time curves for steel in concrete specimens exposed to 55 °C. These data indicated a trend similar to that shown in Figures 4.6 through 4.8. The corrosion potentials on steel in the uncontaminated SRPC, OPC-A and OPC-B concrete specimens, after 60 days of exposure were -43, -50, and -39 mV SCE, respectively. The corrosion potentials of steel in the chloride-contaminated specimens were -404, -222 and -190 mV SCE, respectively. These values in the specimens contaminated with sodium chloride plus sodium sulfate were -367, -303 and -275 mV SCE, respectively.

The corrosion potential-time curves for steel in concrete specimens exposed to 70 °C are plotted in Figures 4.12 through 4.14. These data also indicated a trend similar to that exhibited by the specimens exposed to temperatures in the range of 25 to 55 °C. The corrosion potentials on steel after 76 days of exposure in the uncontaminated

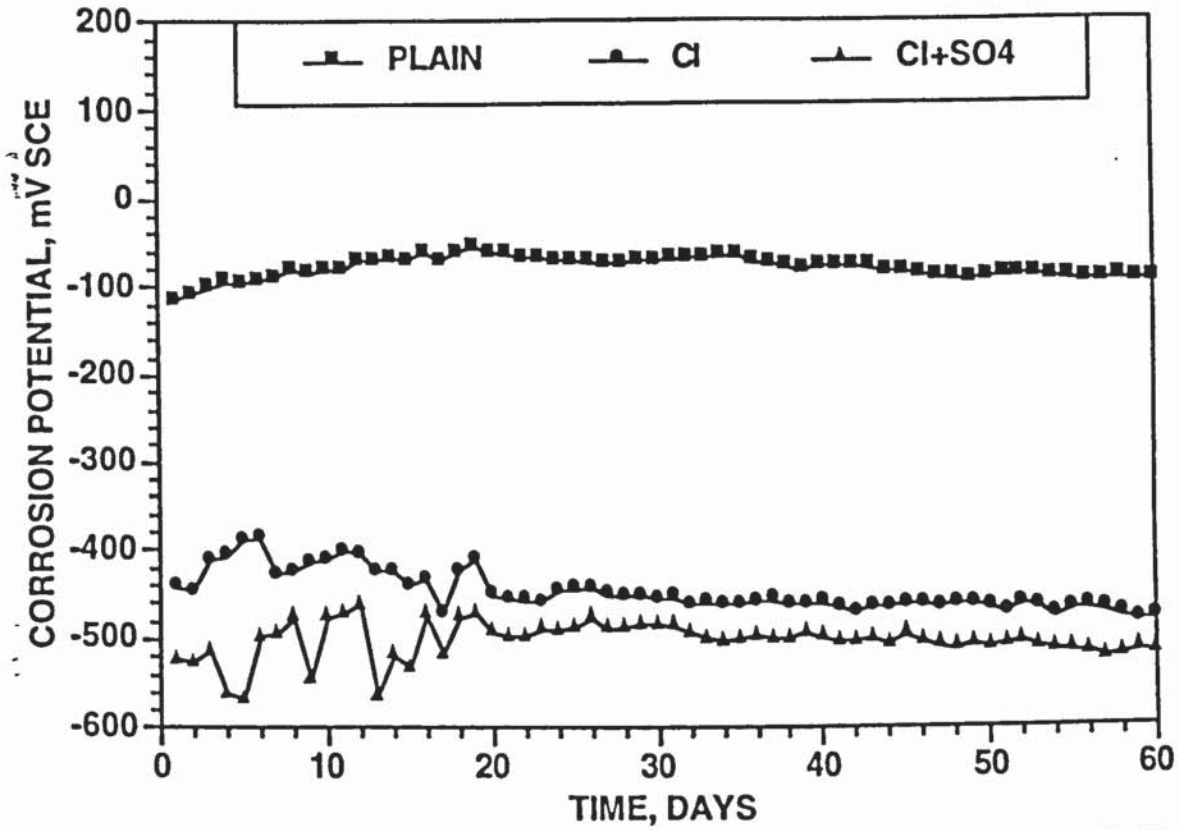

Figure 4.6: Time-potential curves for SRPC concrete specimens exposed to 40 °C

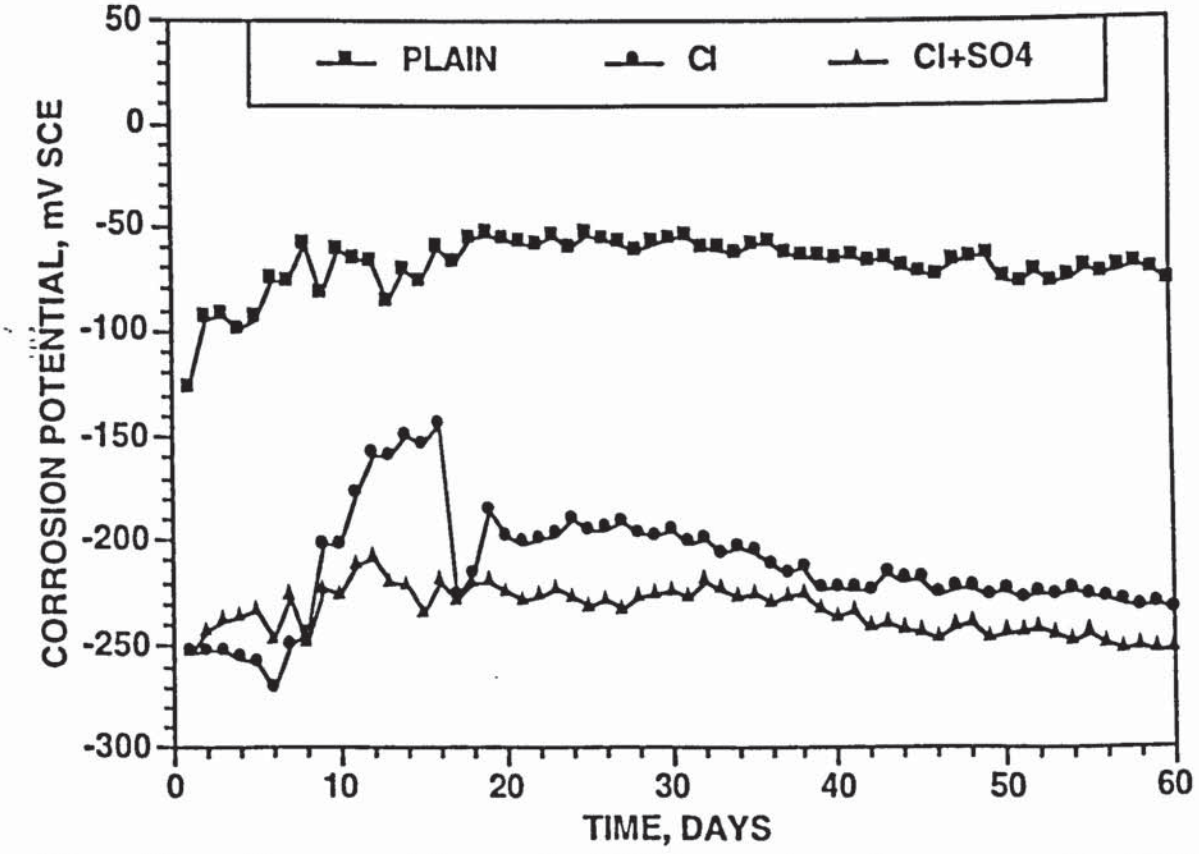

Figure 4.7: Time-potential curves for OPC-A concrete specimens exposed to 40 °C

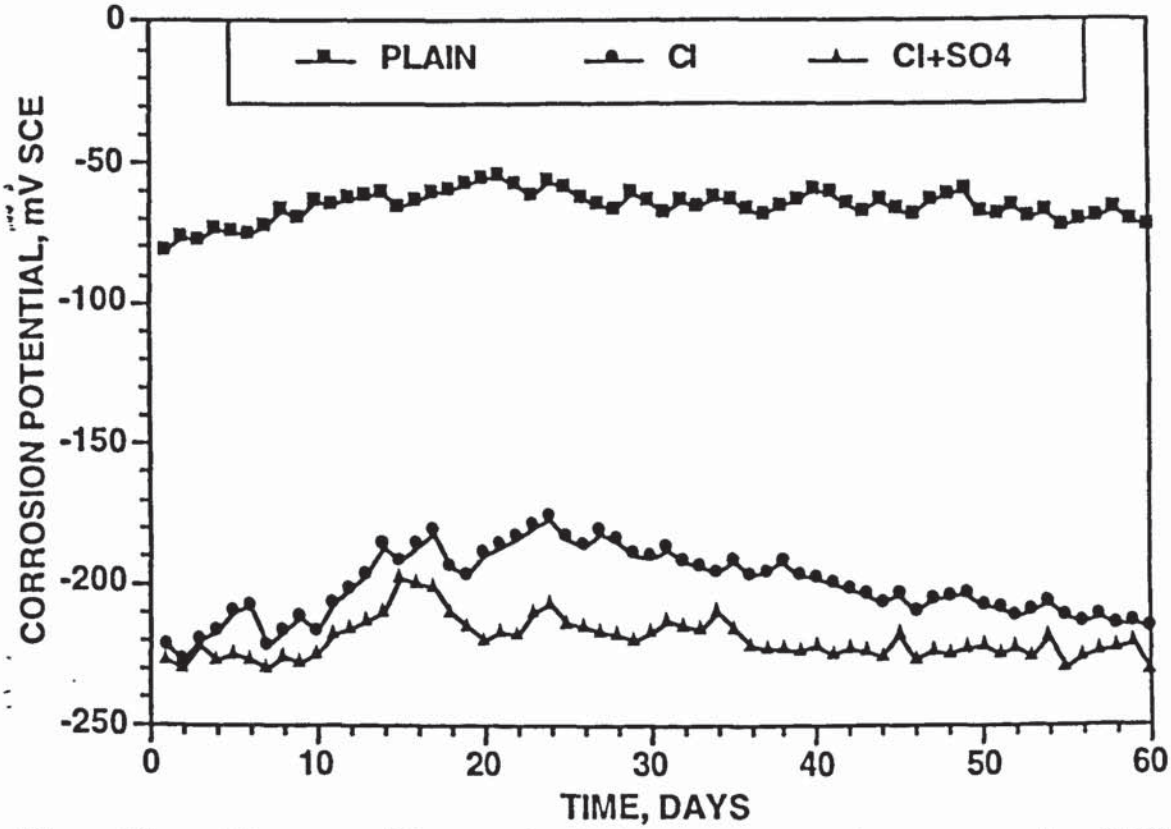

Figure 4.8: Time-potential curves for OPC-B concrete specimens exposed to 40 °C

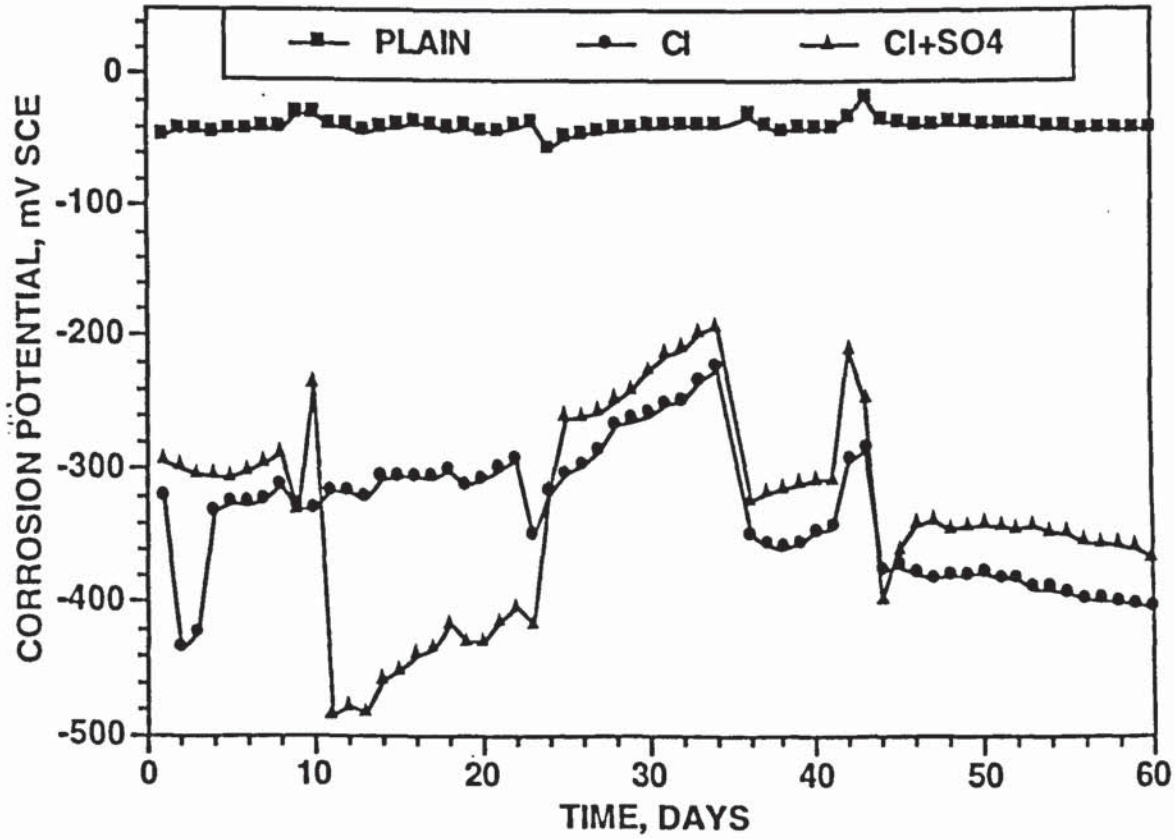

Figure 4.9: Time-potential curves for SRPC concrete specimens exposed to 55 °C

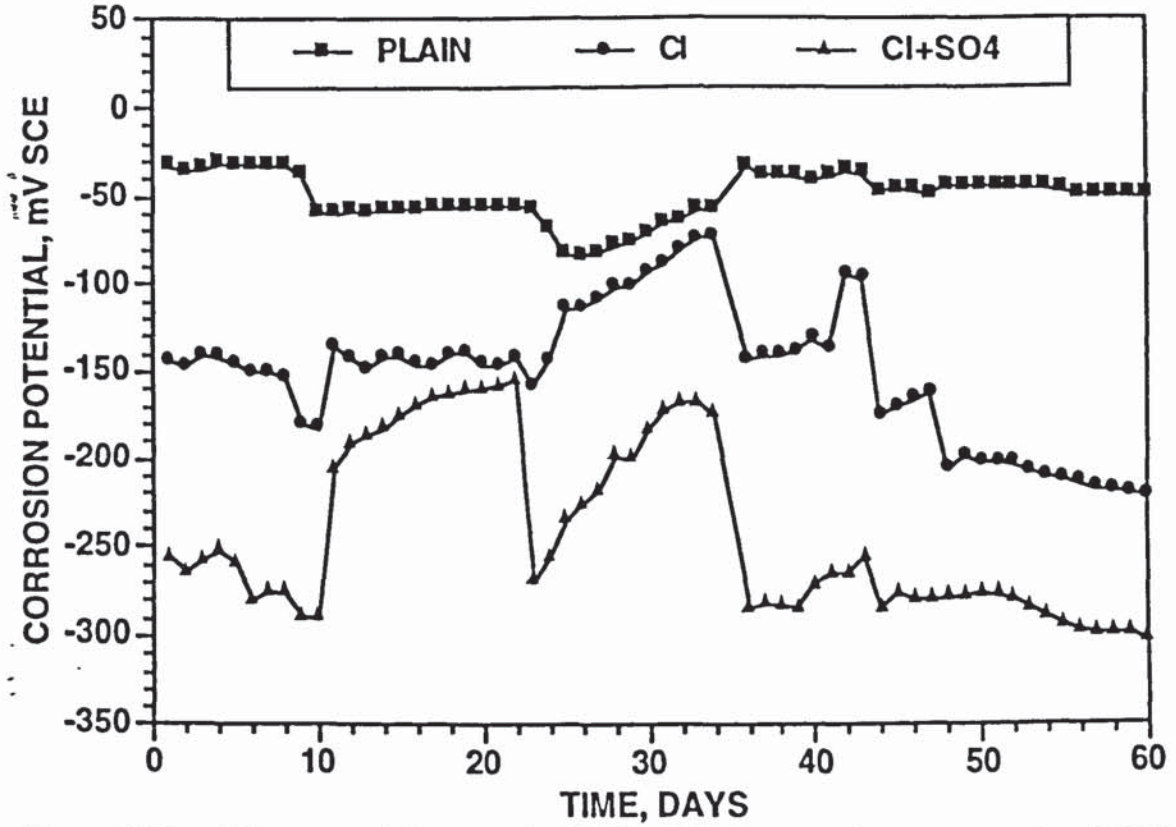

Figure 4.10: Time-potential curves for OPC-A concrete specimens exposed to 55 °C

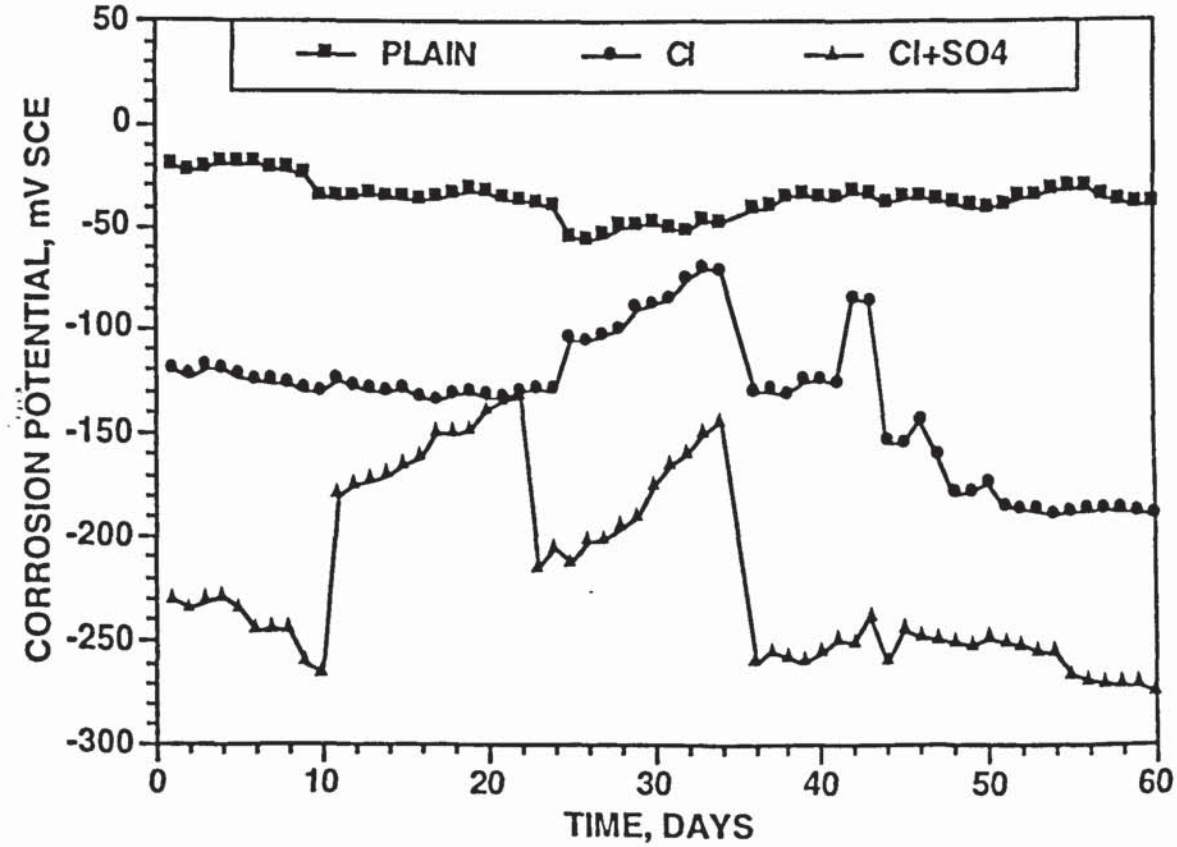

Figure 4.11: Time-potential curves for OPC-B concrete specimens exposed to 55 °C

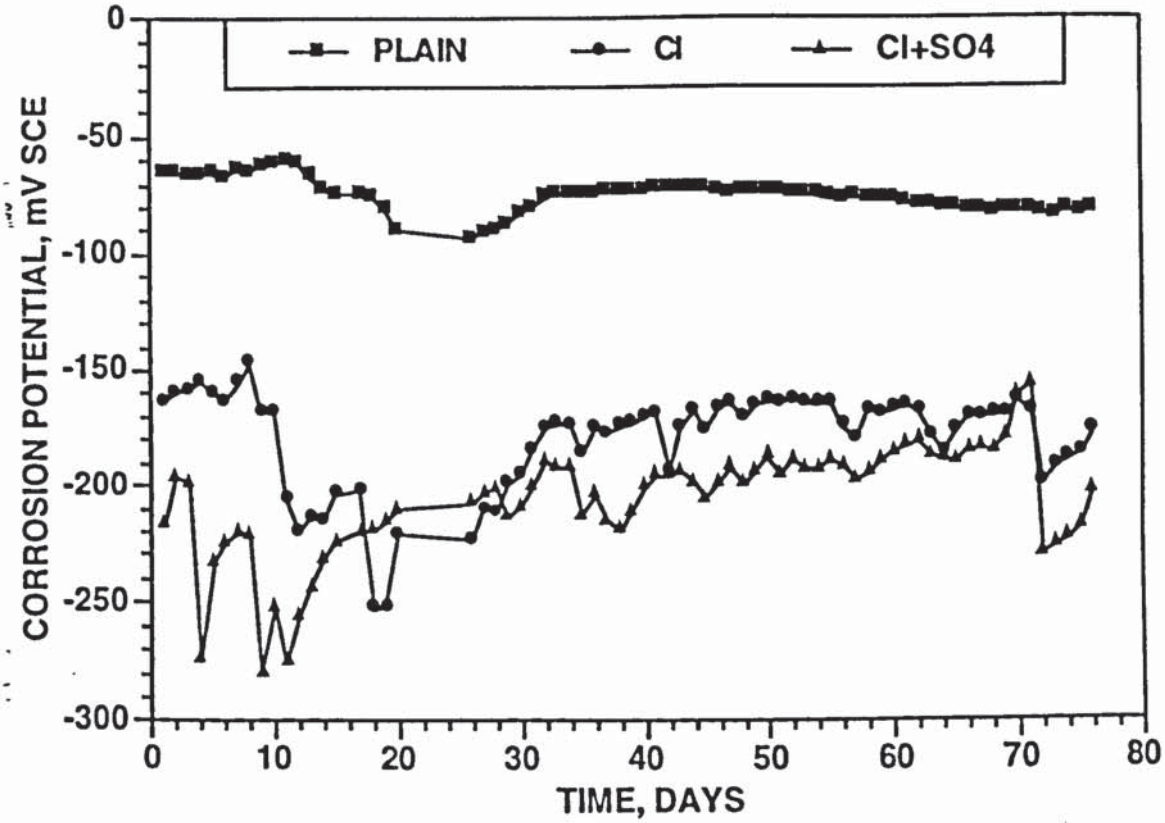

Figure 4.12: Time-potential curves for SRPC concrete specimens exposed to 70 °C

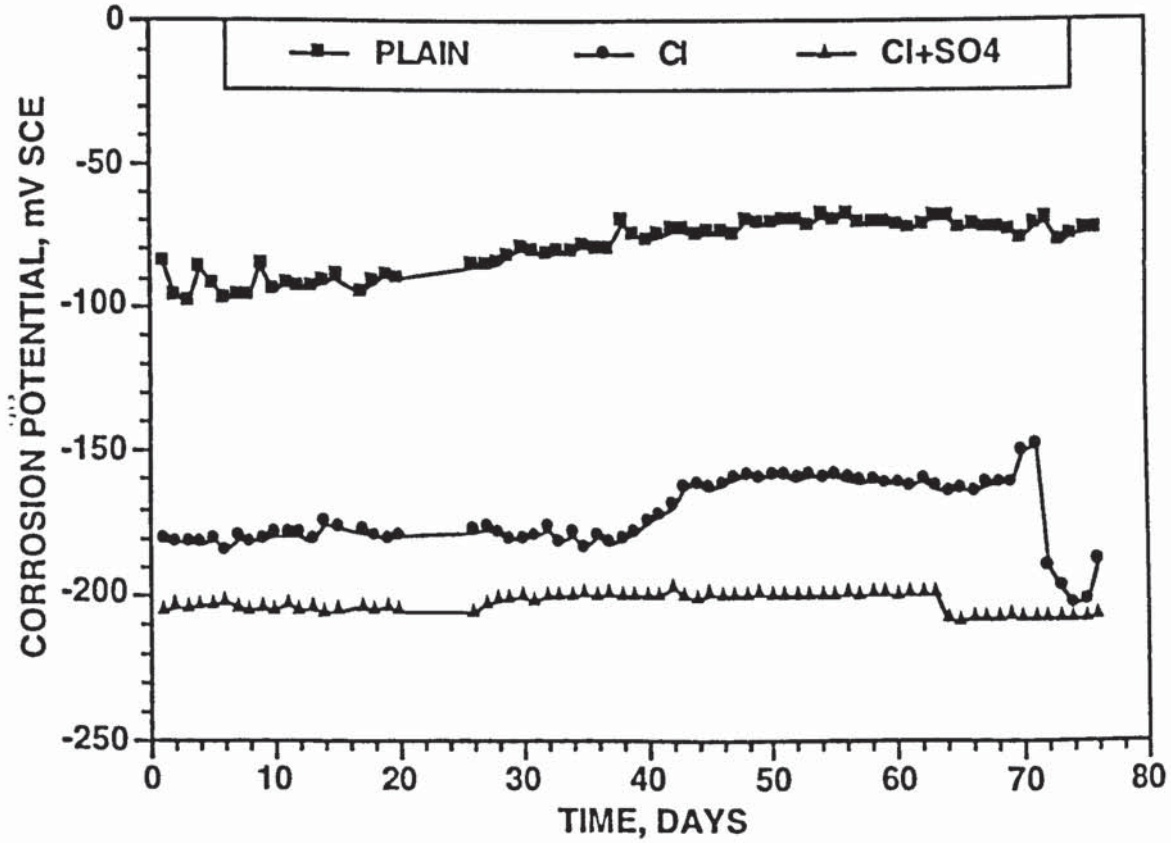

Figure 4.13: Time-potential curves for OPC-A concrete specimens exposed to 70 °C

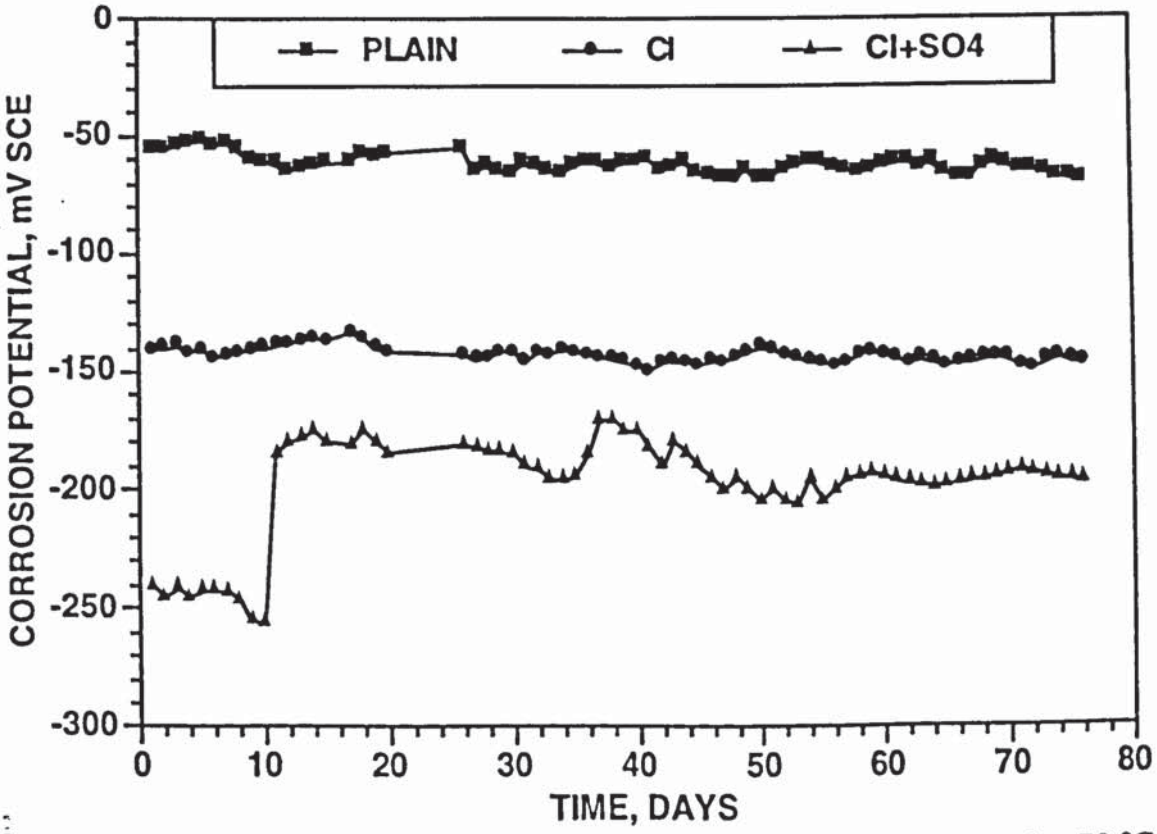

Figure 4.14: Time-potential curves for OPC-B concrete specimens exposed to 70 °C

SRPC, OPC-A and OPC-B concrete specimens were -82, -74 and -70 mV SCE, respectively. The corrosion potentials on steel in the chloride-contaminated specimens were -178, -188 and -147 mV SCE, respectively. These values in the specimens contaminated with sodium chloride plus sodium sulfate were -202, -207 and -197 mV SCE.

It should be noted that the reversible potentials of the saturated calomel electrode may be affected by the exposure temperature. This effect was, however, neglected in this study.

4.3.2 Corrosion Current Density

The corrosion current density (I_{corr}) on steel in the uncontaminated and contaminated SRPC concrete specimens exposed to 25 °C is plotted in Figure 4.15. As expected, the I_{corr} in the uncontaminated specimens was much lower than that in the contaminated specimens. The I_{corr} in the specimens contaminated with sodium chloride plus sodium sulfate was more than that in the specimens contaminated with only sodium chloride. The average I_{corr} in the chloride contaminated specimens was 1.05 $\mu A/cm^2$ compared to 1.18 $\mu A/cm^2$ measured in the concrete specimens contaminated with sodium chloride plus sodium sulfate, where as it was 0.06 $\mu A/cm^2$ on steel in the uncontaminated concrete specimens. Figures 4.16 through 4.18 show the I_{corr} on steel in the uncontaminated and contaminated SRPC concrete specimens exposed to 40, 55 and 70 °C, respectively. These data indicated a trend similar to that exhibited by the specimens exposed to 25 °C.

Figures 4.19 through 4.22 show the I_{corr} on steel in OPC-A (C_3A: 8.5%) concrete specimens exposed to temperatures in the range of 25 to 70 °C. In these specimens also, the I_{corr} on steel in concrete specimens contaminated with sodium chloride plus

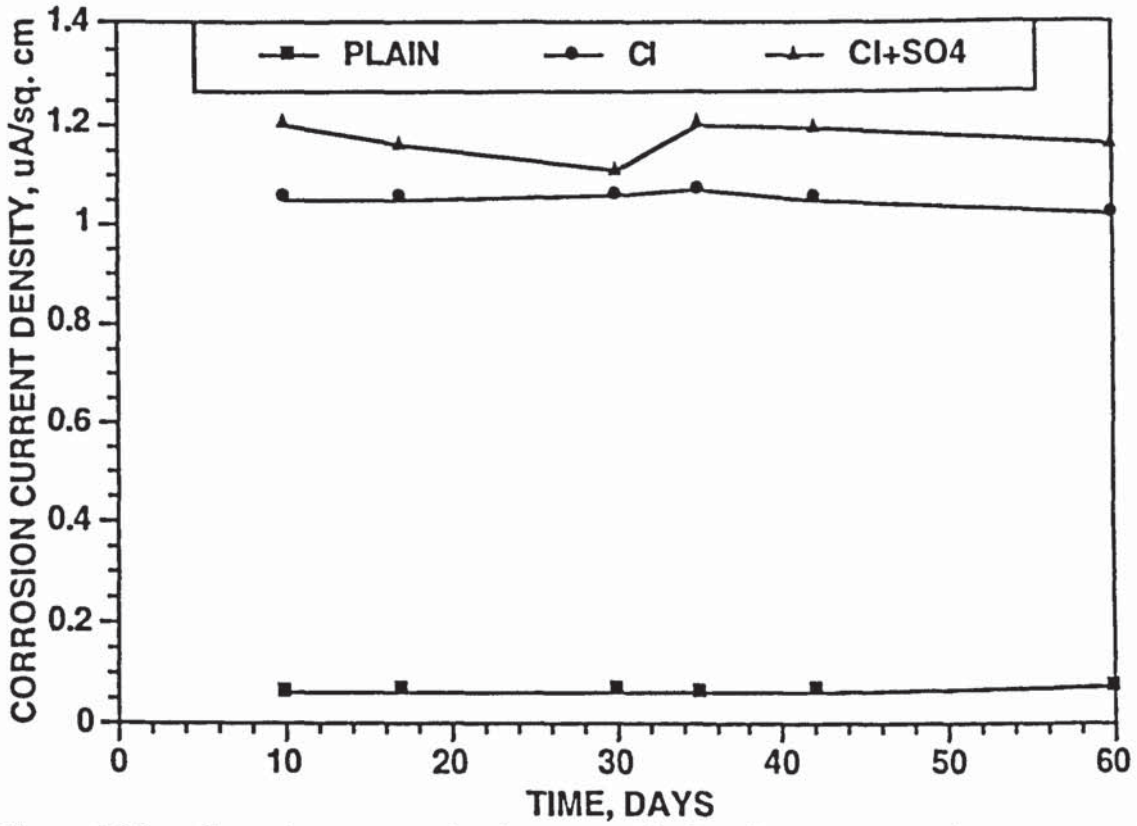

Figure 4.15: Corrosion current density on steel in SRPC concrete specimens exposed to 25 °C

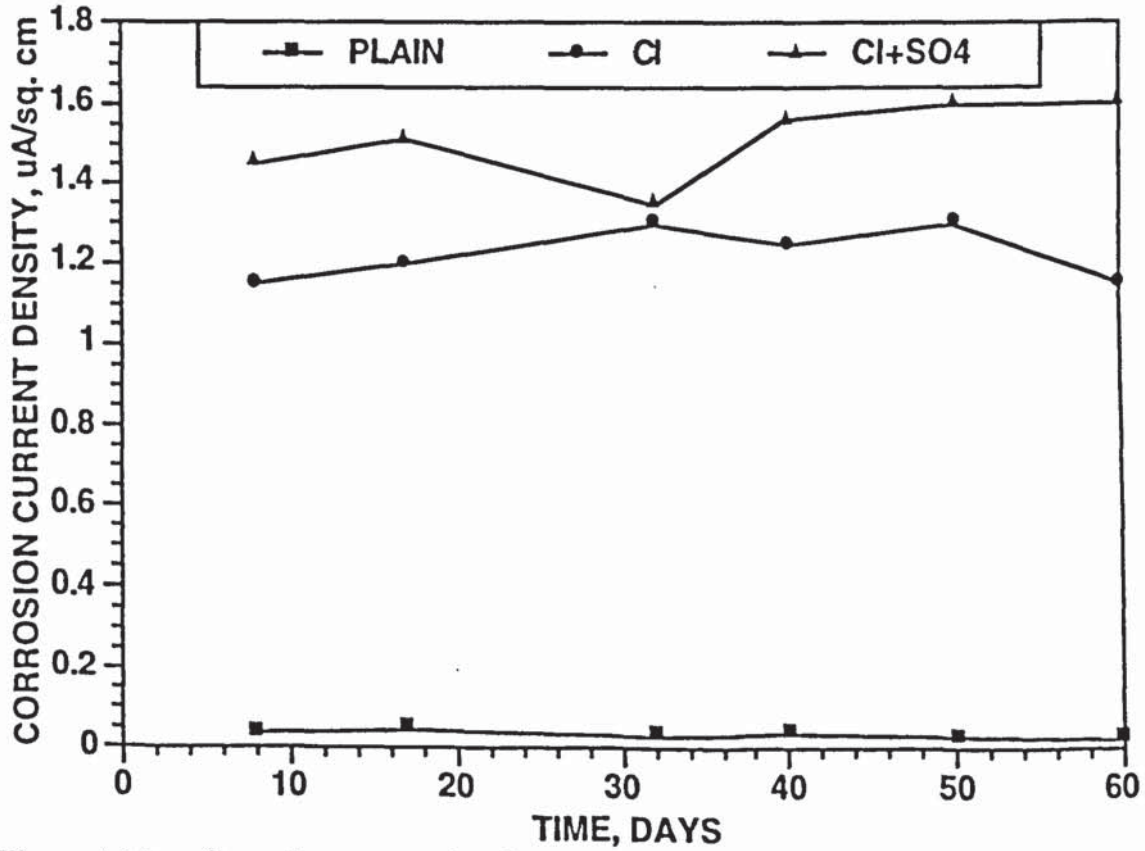

Figure 4.16 : Corrosion current density on steel in SRPC concrete specimens exposed to 40 °C

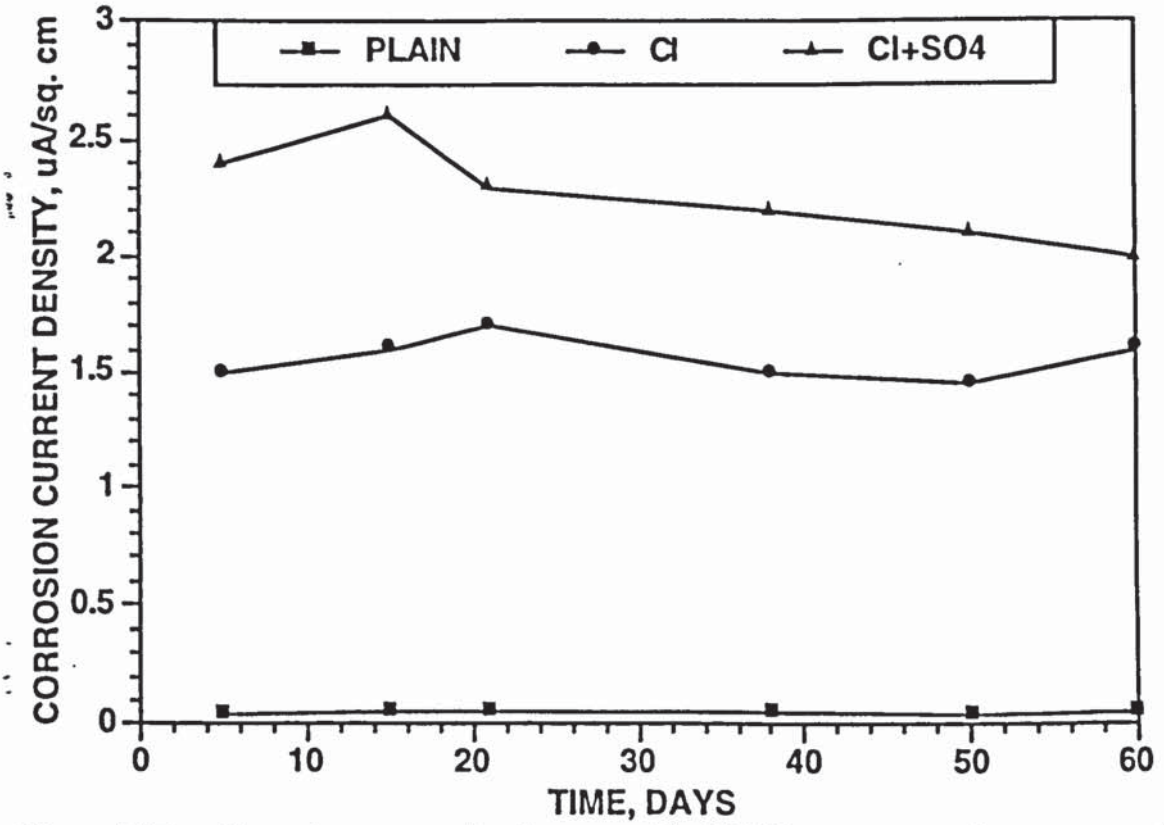

Figure 4.17: Corrosion current density on steel in SRPC concrete specimens exposed to 55 °C

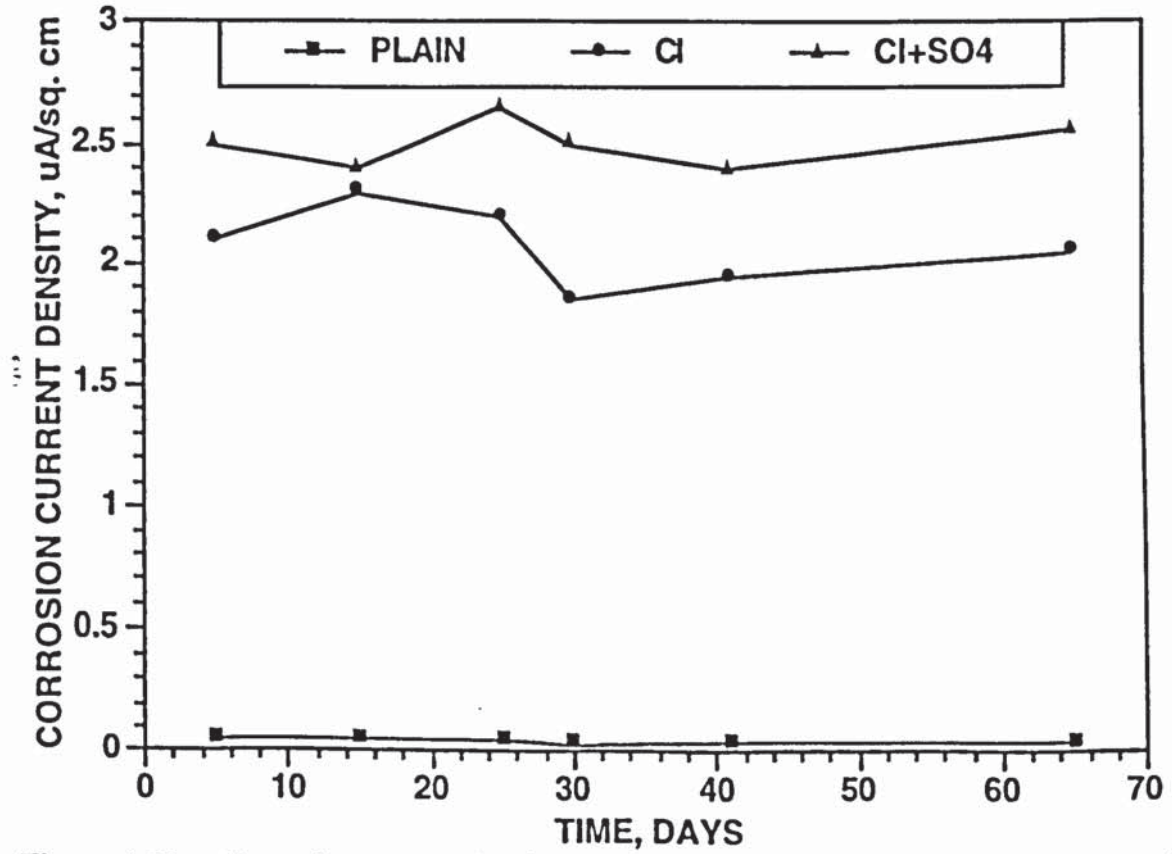

Figure 4.18: Corrosion current density on steel in SRPC concrete specimens exposed to 70 °C

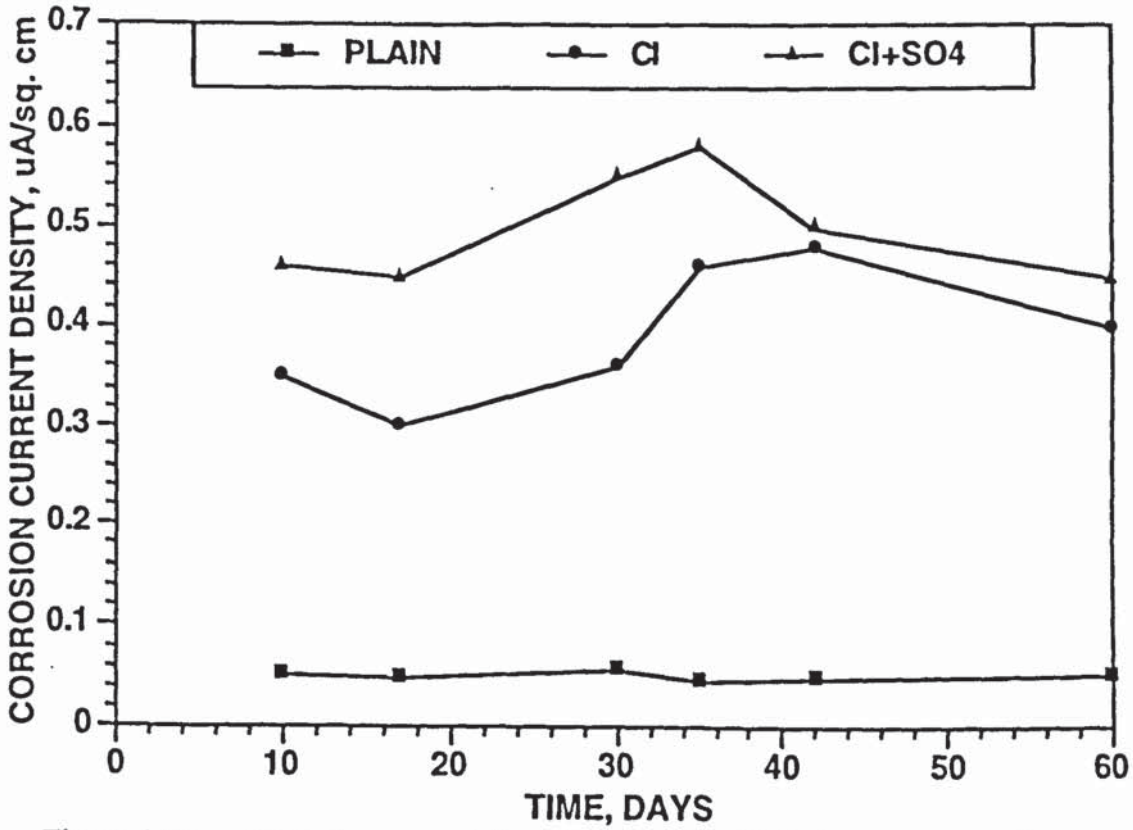

Figure 4.19: Corrosion current density on steel in OPC-A concrete specimens exposed to 25 °C

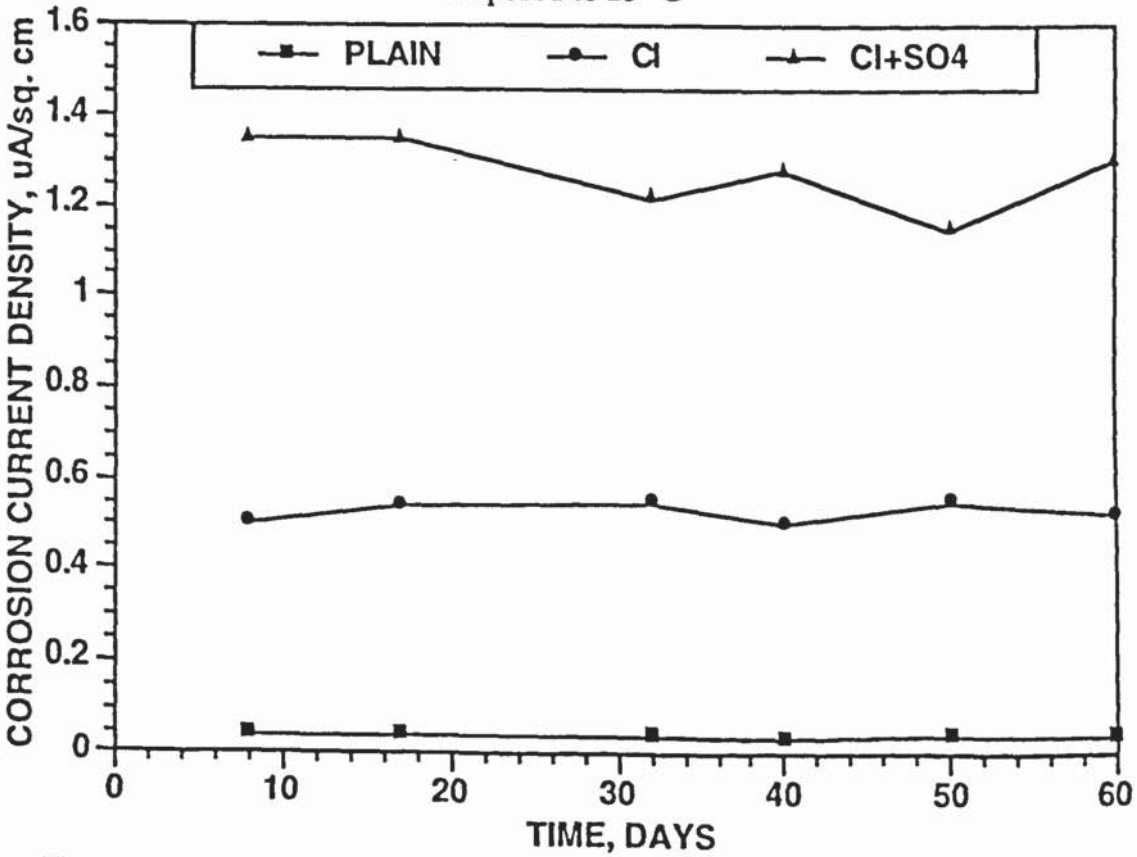

Figure 4.20: Corrosion current density on steel in OPC-A concrete specimens exposed to 40 °C

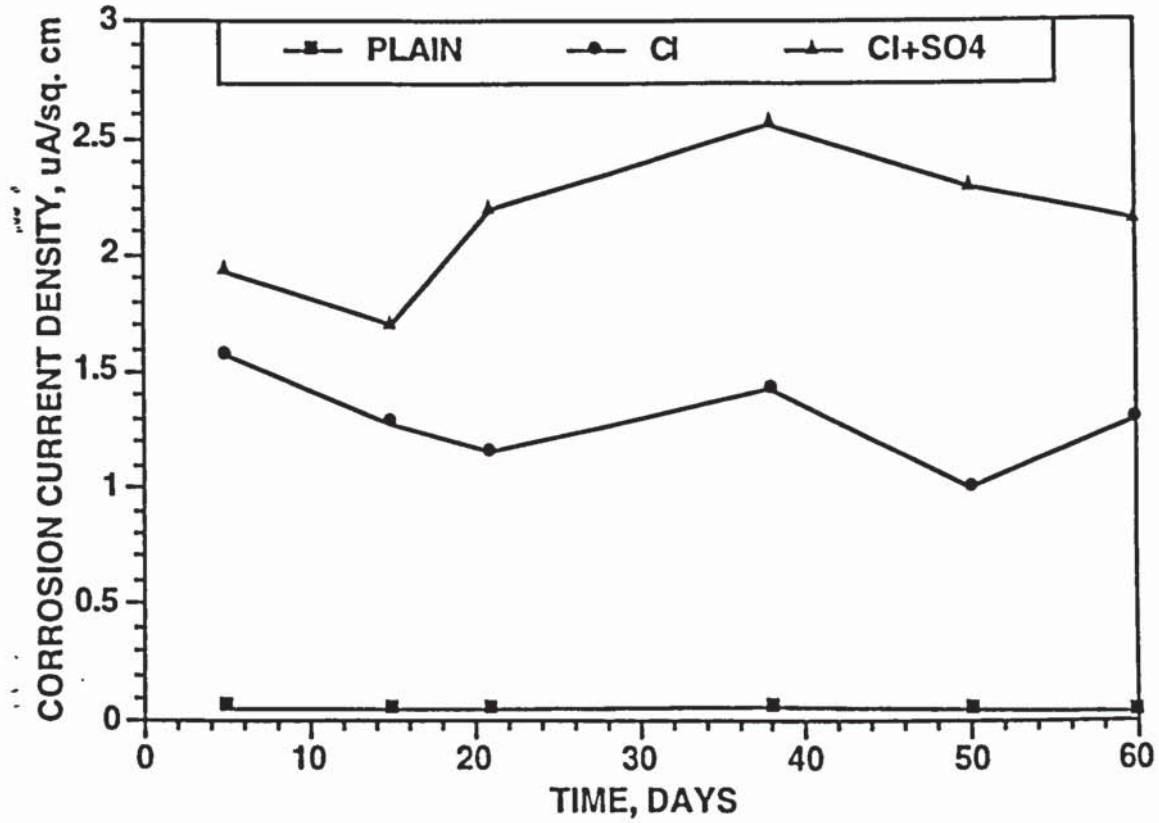

Figure 4.21: Corrosion current density on steel in OPC-A concrete specimens exposed to 55 °C

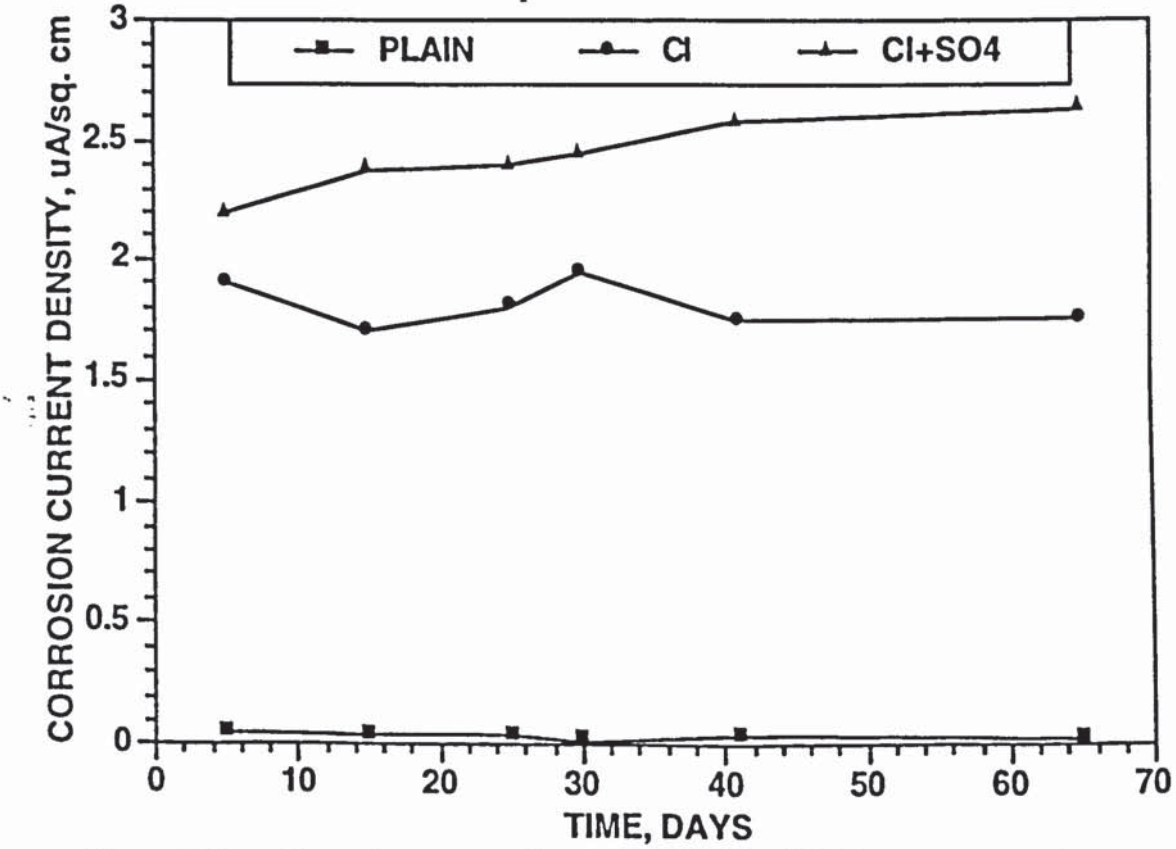

Figure 4.22: Corrosion current density on steel in OPC-A concrete specimens exposed to 70 °C

sodium sulfate was more than that in the uncontaminated specimens and those contaminated with only sodium chloride. The I_{corr} on steel in the uncontaminated and contaminated OPC-B (C_3A: 14.5%) concrete specimens is plotted in Figures 4.23 through 4.26. These data indicated a behaviour similar to that exhibited by steel in concrete specimens made with the other two cements.

The influence of temperature on I_{corr} in the contaminated SRPC concrete specimens is plotted in Figure 4.27. The points in these figures are the mean of those measured at various periods of exposure. The I_{corr} was observed to increase almost linearly with temperature. As discussed earlier, the I_{corr} on steel in concrete contaminated with sodium chloride plus sodium sulfate was more than that in specimens contaminated with only sodium chloride. The I_{corr} in the chloride-contaminated concrete exposed to 25 °C was 1.05 $\mu A/cm^2$, compared to a value of 2.08 $\mu A/cm^2$ measured at 70 °C, indicating a 98% increase in the corrosion activity due to augmentation in the temperature. In the specimens contaminated with sodium chloride plus sodium sulfate, these values were 1.18 $\mu A/cm^2$, 2.5 $\mu A/cm^2$ and 112 %, respectively. Figure 4.28 shows the influence of temperature on the I_{corr} on steel in OPC-A concrete specimens . These data also indicated an increase in I_{corr} with temperature. The I_{corr} on steel in the chloride-contaminated specimens exposed to 25 and 40 °C was more or less similar. However, these values increased almost linearly for exposure temperatures of more than 40 °C. The I_{corr} on steel in the concrete specimens exposed to 25 °C was 0.4 $\mu A/cm^2$, whereas it was 1.8 $\mu A/cm^2$ on steel in the specimens exposed to 70 °C. The I_{corr} on steel in the concrete specimens contaminated with sodium chloride plus sodium sulfate increased almost linearly. The I_{corr} on steel in the specimens exposed to 25 and 70 °C was 0.5 and 2.45 $\mu A/cm^2$, respectively. The effect of temperature on I_{corr} on steel in the OPC-B concrete specimens is plotted in Figure 4.29. These data also

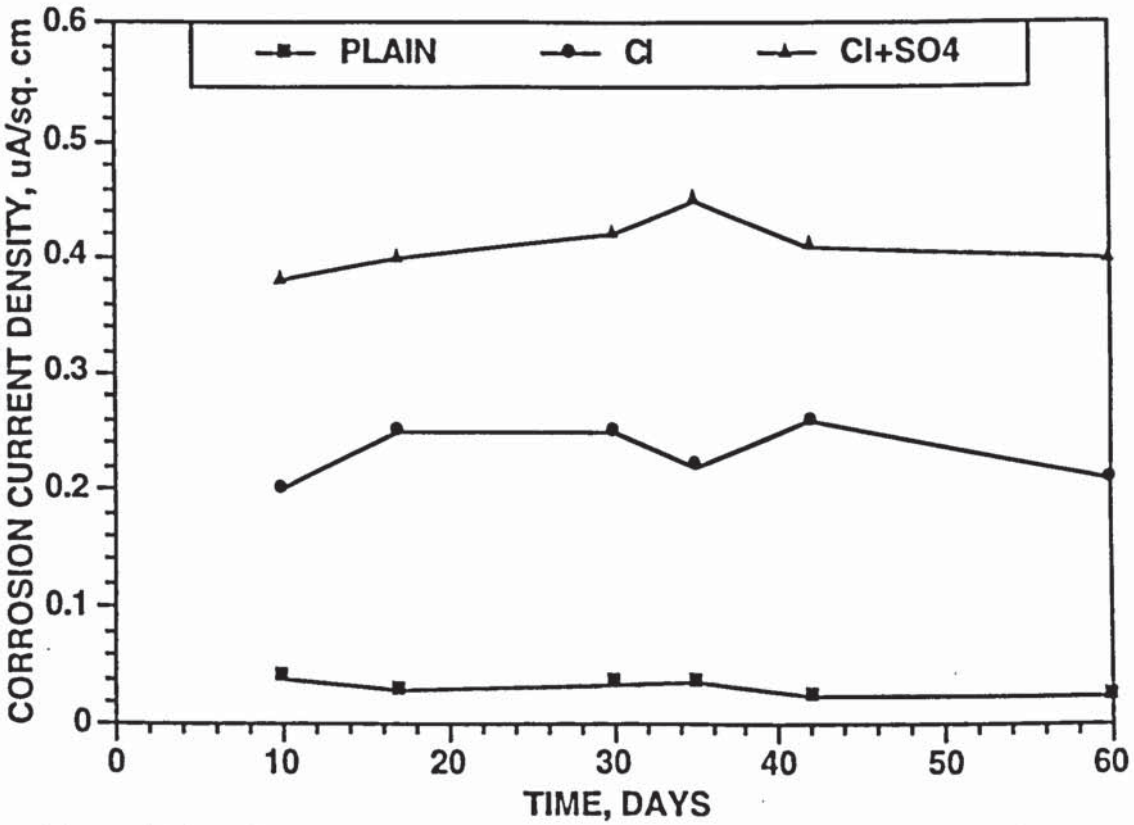

Figure 4.23: Corrosion current density on steel in OPC-B concrete specimens exposed to 25 °C

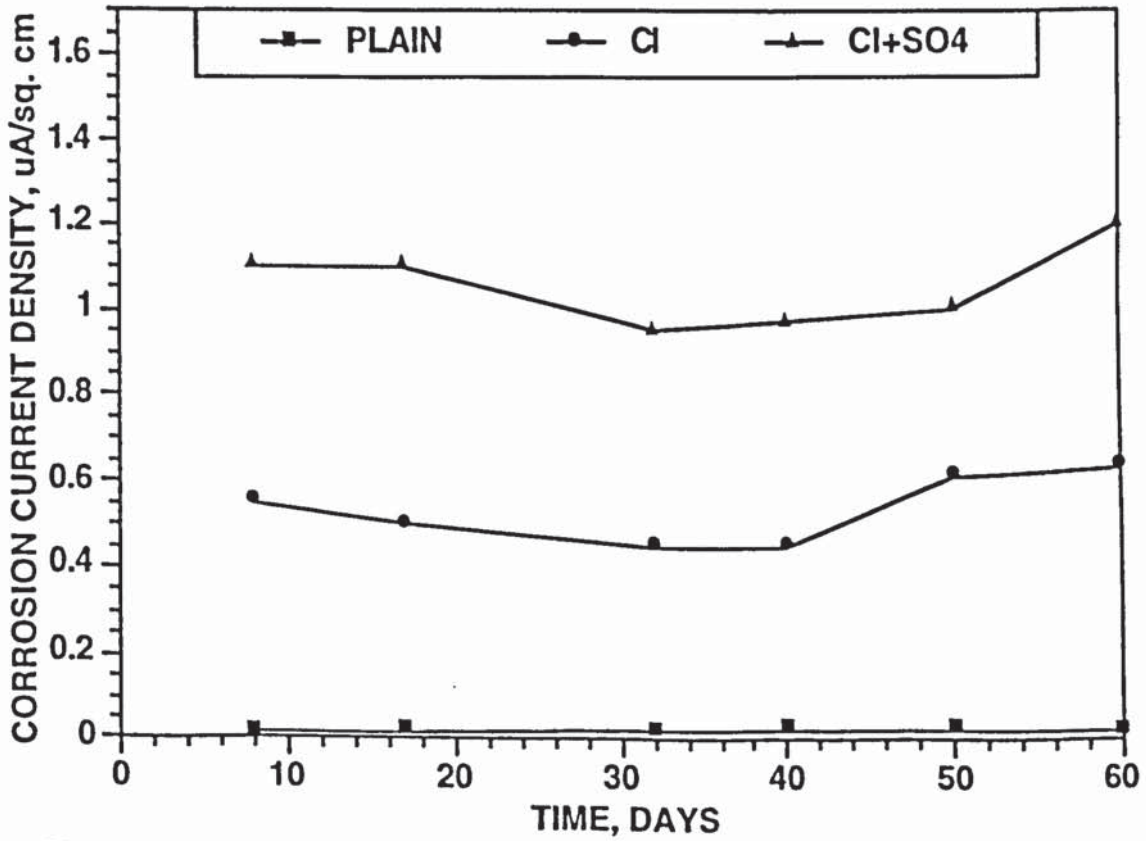

Figure 4.24: Corrosion current density on steel in OPC-B concrete specimens exposed to 40 °C

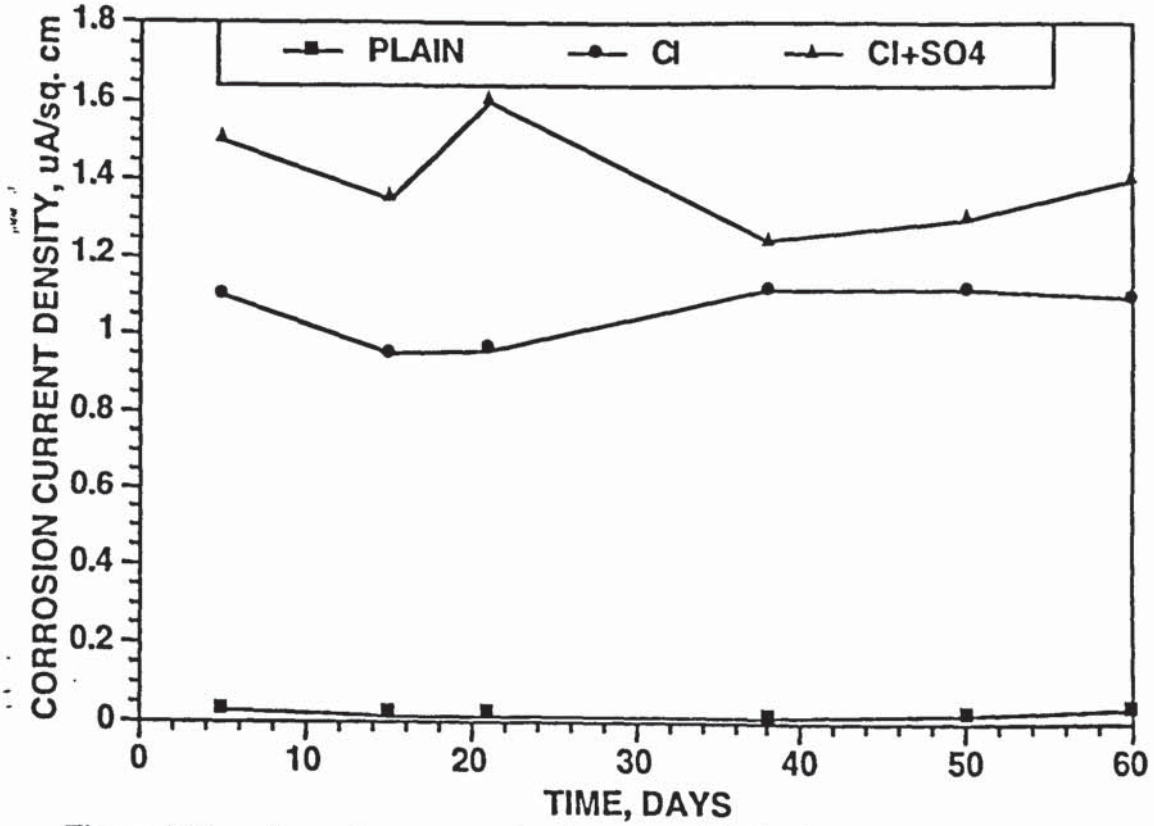

Figure 4.25: Corrosion current density on steel in OPC-B concrete specimens exposed to 55 °C

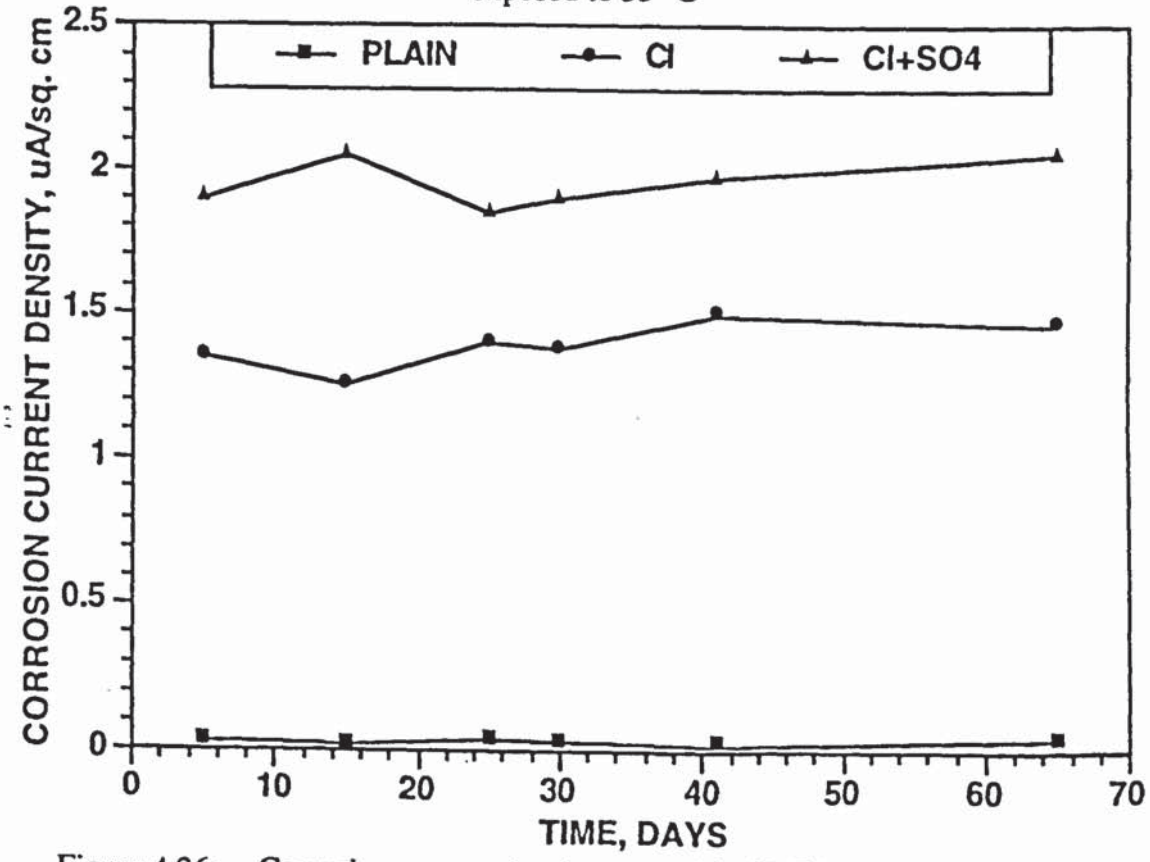

Figure 4.26: Corrosion current density on steel in OPC-B concrete specimens exposed to 70 °C

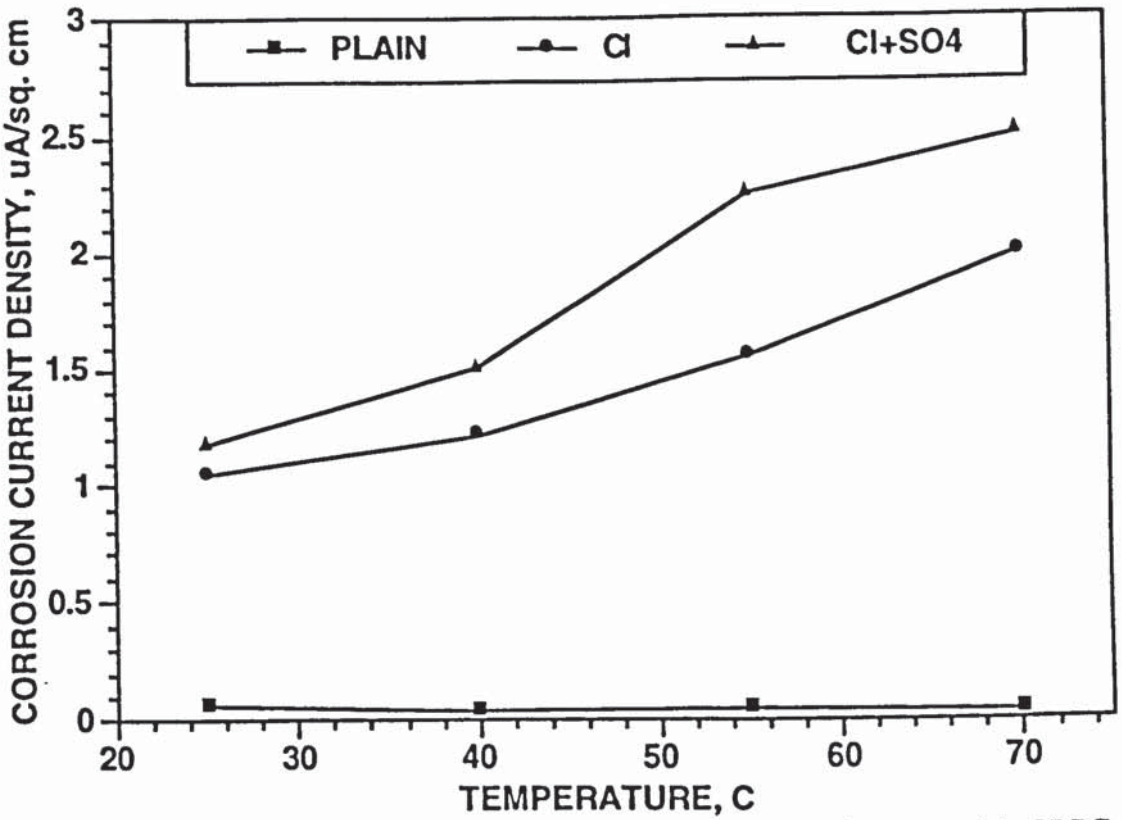

Figure 4.27: Effect of temperature on corrosion current density on steel in SRPC concrete specimens

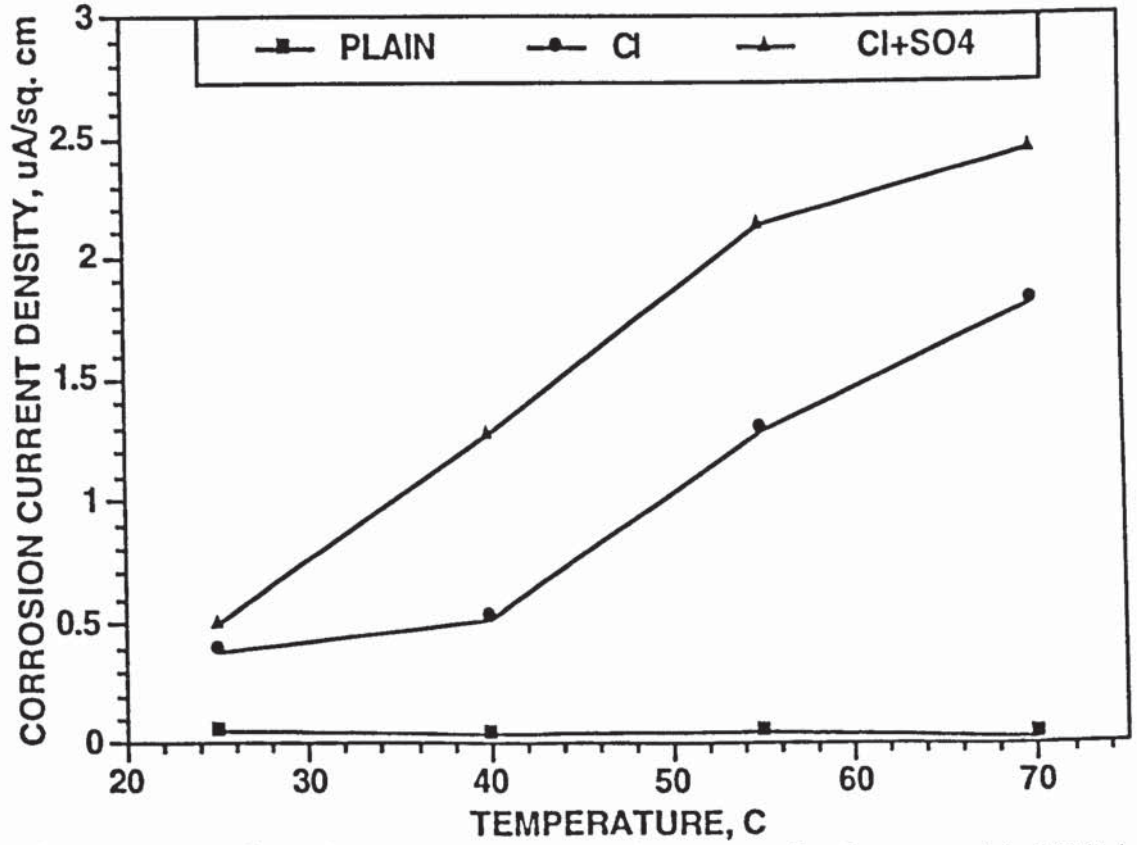

Figure 4.28 : Effect of temperature on corrosion current density on steel in OPC-A concrete specimens

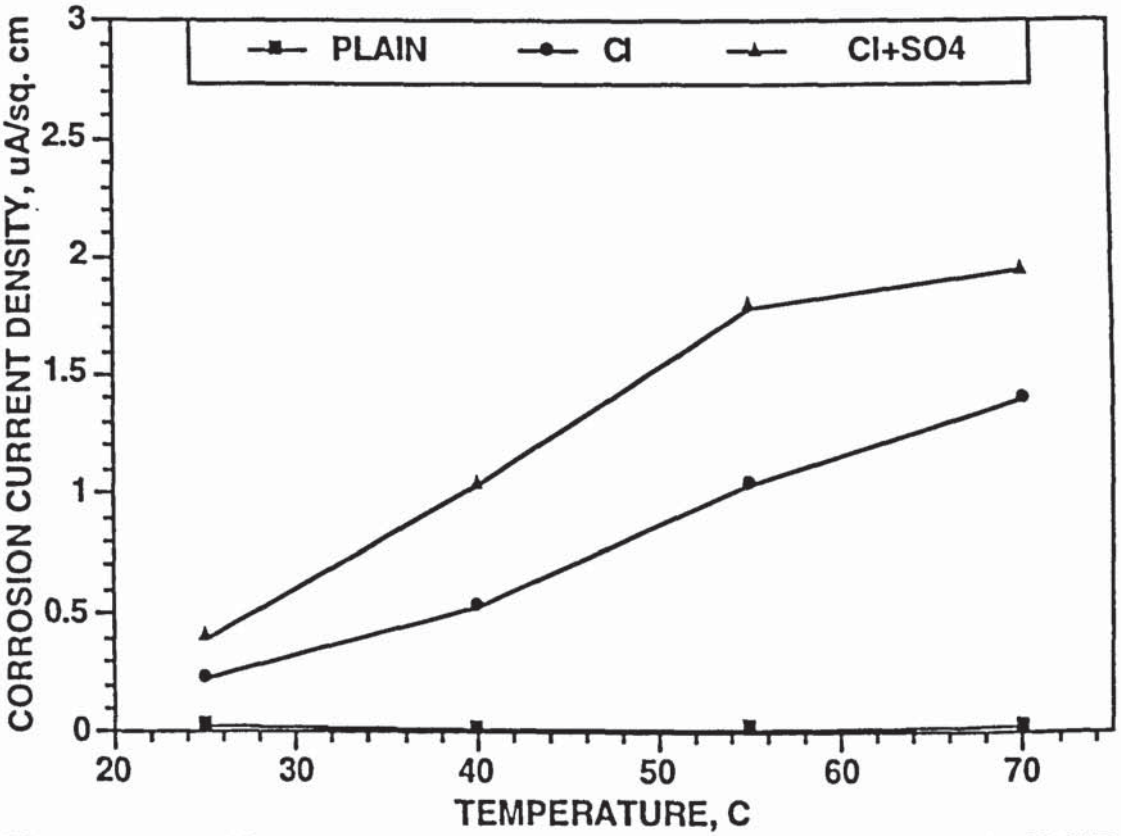

Figure 4.29: Effect of temperature on corrosion current density on steel in OPC-B concrete specimens

indicated an increase in the corrosion activity with exposure temperature. The I_{corr} on steel in the chloride-contaminated concrete was 0.23 and 1.4 $\mu A/cm^2$ for exposure temperatures of 25 and 70 °C, respectively. The I_{corr} on steel in concrete contaminated with sodium chloride plus sodium sulfate increased from 0.4 to 1.95 $\mu A/cm^2$ for a similar rise in temperature.

The data on corrosion current density, discussed in the preceding paragraphs and plotted in Figures 4.15 through 4.29 indicated an increase in the corrosion activity due to: (i) incorporation of sulfate ions in the chloride-contaminated concrete, and (ii) increase in the exposure temperature. Discussing the former aspect first, the role of sulfate ions on the chloride-induced reinforcement corrosion in steel is not very well investigated, particularly the mechanisms involved. However, most of the data developed on this aspect indicated an increase in the corrosion activity due to the concomitant presence of chloride and sulfate salts. The earliest study conducted to study the effect of sulfate ions on reinforcement corrosion was that by Stratfull [166], who investigated the individual effect of sodium sulfate and sodium chloride on reinforcement corrosion. In that study, reinforcement corrosion was observed in the specimens placed in sodium chloride solution while it was not observed in the specimens placed in the sodium sulfate solution within the duration of tests (214 days). According to Gouda and Halaka [76], even high dosages of sulfate ions do not appear to have caused serious corrosion of reinforcing steel embedded in portland cement concrete. Treadaway et al. [167] investigated the concomitant effect of chlorides and sulfates on reinforcement corrosion and reported higher weight loss in the specimens contaminated with sodium chloride plus sodium sulfate compared to the specimens contaminated with only sodium chloride. Macmillan and Treadaway [168] also indicated higher corrosion activity on steel in the specimens contaminated with chloride and sulfate salts than in the specimens contaminated with only sodium chloride. The corrosion rate in the specimens contaminated with 0.4% Cl^- + 1.5% SO_3^{--} was higher

than that in the specimens contaminated with only 0.4% Cl^- and was similar to those contaminated with 1% Cl^- [168]. Al-Amoudi and Maslehuddin [17] investigated reinforcement corrosion in cement paste specimens immersed in the chloride, sulfate and chloride plus sulfate environments. The results of that study indicated that while the sulfate ions are hardly able to induce reinforcement corrosion, it was significant in the specimens immersed in the sodium chloride plus sodium sulfate solutions. Reinforcement corrosion was observed to increase two times when the sulfate concentration in the 15.7% chloride solution was increased from 0.55 to 2.10%. An extension of this study [72] to plain and blended cement concrete specimens indicated a similar trend. The effect of sulfate concentration was observed to be more pronounced on the corrosion rate, while no systematic effect was observed on the time to initiation of reinforcement corrosion.

The influence of sulfate ions on reinforcement corrosion in the system $Ca(OH)_2$-steel-chloride was investigated by Gouda and Halaka [76], Al-Tayyib et al. [16] and Morgan [169]. Gouda and Halaka [76] indicated that small concentrations of Na_2SO_4, as low as 0.2%, could cause steel depassivation. Al-Tayyib et al. [16] indicated that the corrosion activity on steel exposed to sulfate solutions at elevated temperature (50 °C) increases seven times compared to that immersed in the chloride solution. They attributed the increase in corrosion activity to the modification of the protective passive film to a sulfate film, which is less protective than the original iron oxide film. Morgan [169] indicated that addition of 50 ppm of SO_4^{--} brought about pitting at chloride concentrations lower than when sulfate was absent. This corrosion-promoting effect of sulfate ions was also observed in the absence of chloride. Reducing the pH of a saturated lime solution with sulphuric acid encouraged localized corrosion under conditions where the same reduction of pH with acetic acid did not compromise passivity. This was taken as evidence for the depassivating character of sulfate, which was expressed as a critical $[SO_4^{--}]/[OH^-]$ ratio of 0.42 for a pH of 11.5.

Reinforcement corrosion was also observed in 10 mM/l NaOH at threshold sulfate concentrations below 0.3 mM/l by Griffin [77].

The increased reinforcement corrosion in the specimens contaminated with sodium chloride plus sodium sulfate observed in this study and those reported by other researchers may be attributed to the following two causes:

Firstly, the concomitant presence of chloride and sulfate salts increases the concentration of free chloride ions in the pore solution compared to the specimens contaminated with only sodium chloride. This increase in the chloride concentration is attributed to the simultaneous reaction of C_3A with both chloride and sulfate ions.

Secondly, the electrical resistivity of concrete contaminated with sodium chloride plus sodium sulfate is lower than that of the specimens contaminated with only sodium chloride. As shown in Table 4.4 [108], the electrical resistivity of concrete specimens contaminated with sodium chloride was 1.4 to 7.0 times that in the specimens contaminated with sodium chloride plus sodium sulfate. Thus, the presence of sulfate ions in the chloride-contaminated concrete increases the rate of corrosion due to the reduction in the electrical resistivity. Felliu et al. [170] and Lopez and Gonzalez [171] have observed a direct proportionality between the rate of metallic corrosion and the electrical conductivity of concrete. Several other researchers [172-173] have previously related corrosion rate and electrical resistivity of concrete. As a result of an investigation of offshore structures, Browne [172] stated that the concrete resistivity must fall below the range of 5,000 to 10,000 Ω.cm in order to support corrosion. Cavalier and Vassie [173] investigated corrosion damage in a highway bridge and concluded that corrosion is almost certain when resistivity is below 5000 Ω.cm.

Table 4.4: Electrical resistivity of contaminated concrete specimens exposed to varying temperature [108]

Exposure Temperature °C	Electrical Resistivity, k.Ω.cm		
	Uncontaminated	Chloride	Chloride+sulfate
25	18.01	11.41	7.97
40	26.02	25.91	7.79
55	38.99	38.26	5.49
70	311.13	198.43	50.99

The I_{corr} on steel in all the cements investigated increased with the exposure temperature. It increased by 2 to 6 times when the exposure temperature was raised from 25 to 70 °C. The acceleration in the corrosion activity may be attributed to the acceleration of the electrochemical reactions. It is reported that the chemical reactions are doubled when the exposure temperature is increased from 20 to 40 °C [25,39]. In studies conducted by Benjamin and Sykes [37,174] pitting potential was observed to decrease with exposure temperature. This trend was observed in both steel placed in the saturated calcium hydroxide solution and ordinary portland cement mortar specimen. Schiessl and Raupach [38] also reported an increase in the corrosion density when the temperature was increased from 15 to 20 °C. The mean value of acceleration factor was reported to be 1.4. In studies conducted by Tuutti [28], the corrosion rate of steel in the carbonated concrete was observed to increase with temperature. The corrosion rate was reported to have increased two times for each 10 °C rise in temperature. Maslehuddin et al. [175] also investigated the effect of temperature and chloride contamination on the electrochemical behavior of mild steel placed in the electrolyte representing the concrete pore solution. The potentiodynamic curves for the uncontaminated specimens (Figure 4.30) indicated a decrease in the pitting potential with temperature. Pitting was observed in the uncontaminated specimens at potentials

of +700, +226, and +334 mV SCE when exposed to 25, 40, and 70 °C, respectively. The authors attributed the pitting to the small amount of chloride of about 180 to 300 ppm present in the solution. Baumel and Engel [176] indicated that in a saturated calcium hydroxide solution, chloride concentration as small as small 35 ppm has some adverse effect on steel passivity. The polarization resistance (Rp) for specimens exposed to the uncontaminated saturated calcium hydroxide solution at 25 °C was 147 k.Ω.cm^2, while it was 25 and 18 k.Ω.cm^2 for specimens exposed to 40 and 70 °C, respectively [175]. The potentiodynamic curves for mild steel placed in an alkaline solution contaminated with chloride (Figure 4.31) and exposed to temperatures in the range of 25 to 70 °C indicated an increase in the corrosion activity with temperature. While there was a marginal increase in the corrosion current density when the temperature was increased from 25 to 40 °C, the increase in the corrosion current density when the exposure temperature was increased from 40 to 55 °C was substantial. No significant difference in the corrosion current density was observed in the specimens exposed to 55 and 70 °C. Pitting corrosion was indicated in all the specimens exposed to this environment. The pitting potentials were -225, -264, -368 and -386 mV SCE for exposure temperatures of 25, 40, 55 and 70 °C. The Rp was in the range of 28 k.Ω.cm^2 for the specimens exposed to 25 and 40 °C, while it was in the range of 0.6 to 1.1 k.Ω.cm^2 for those exposed to 55 and 70 °C. Investigations conducted by Henriksen [177] on the electrochemical behaviour of steel in $Ca(OH)_2$ solution containing 0.1 N NaCl indicated a linear variation in the pitting potential with a change of 25 mV for every 10 °C. Similarly, the corrosion rate, measured as the current needed to maintain the passive potential on the specimen, increased linearly up to 50 °C, with the rate doubling for every 10 °C. Lopez et al. [178] indicated an increase in the corrosion activity with temperature in saturated concrete, whereas no appreciable effect of temperature was observed in concrete exposed to dry conditions.

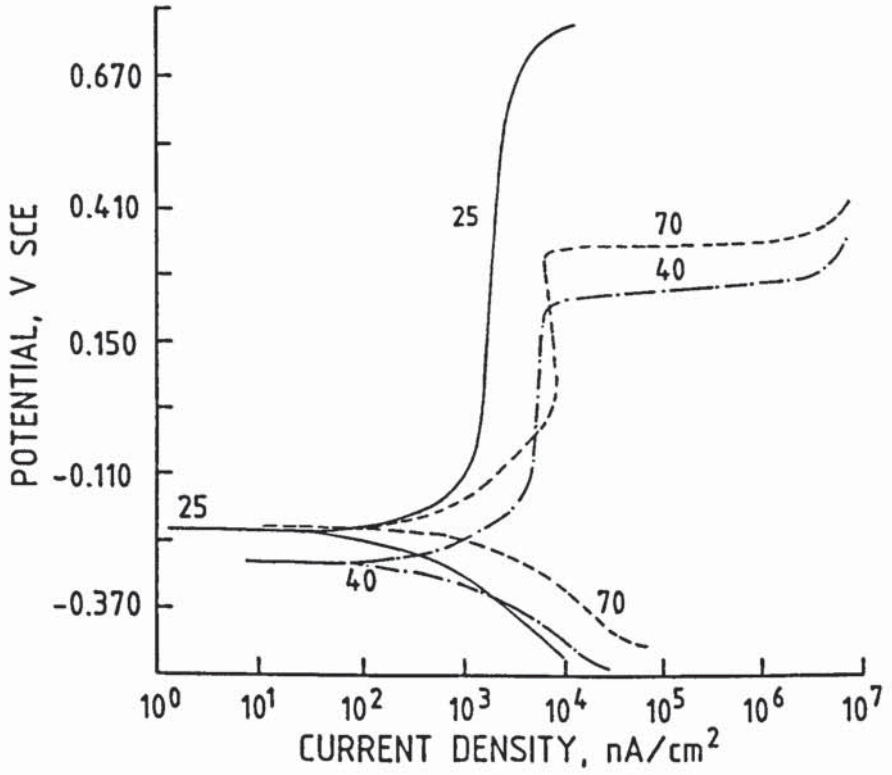

Figure 4.30: Potentiodynamic curves for steel in simulated concrete pore solution

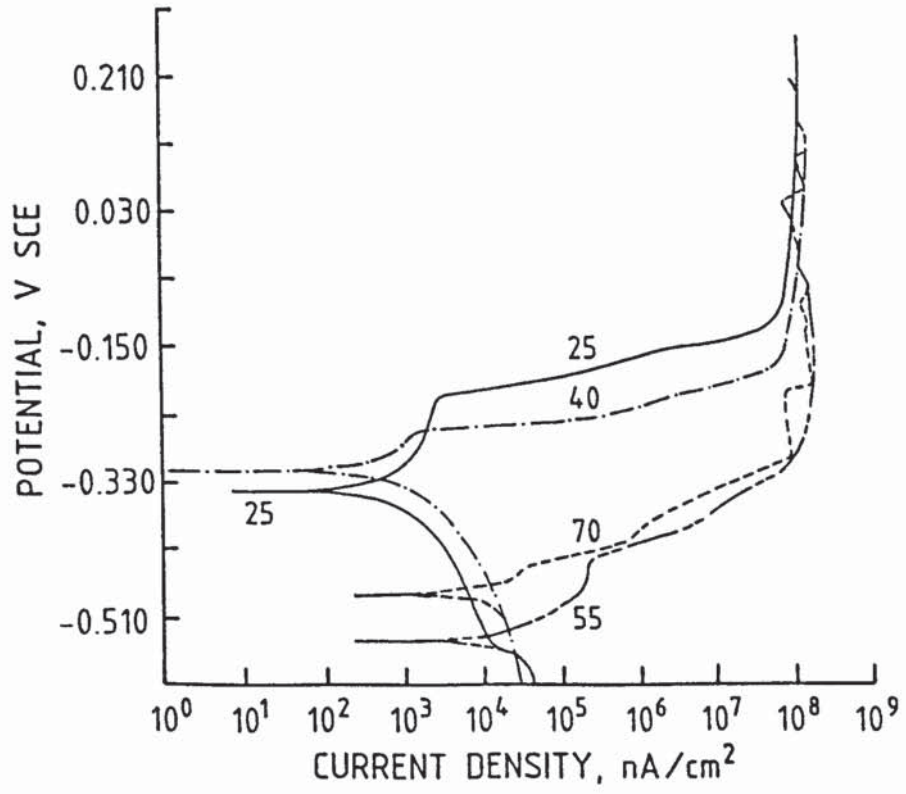

Figure 4.31: Potentiodynamic curves for steel in simulated concrete pore solution contaminated with chloride ions

The effect of C_3A content of cement on the I_{corr} on steel in the concrete specimens exposed to 25 °C is shown in Figure 4.32. The I_{corr} decreased with increasing C_3A content of cement. The I_{corr} decreased significantly when the C_3A increased from 3.5 to 8.5%. However, the reduction in the I_{corr} due to further increase in the C_3A was not that significant. The I_{corr} on steel in the chloride-contaminated specimens decreased from 1.08 to 0.25 $\mu A/cm^2$ as C_3A increased from 3.5 to 14.5%. In concrete specimens contaminated with sodium chloride plus sodium sulfate, the I_{corr} decreased from 1.18 to 0.4 $\mu A/cm^2$ for a similar increase in the C_3A content of cement. Figures 4.33 and 4.34 show the effect of C_3A content of cement on the I_{corr} on steel in the contaminated specimens exposed to 40 and 55 °C, respectively. These data also indicated a trend similar to that exhibited by concrete specimens exposed to 25 °C. The variation in the I_{corr} on steel with the C_3A content of cement in concrete specimens exposed to 70 °C are plotted in Figure 4.35. These data also indicate a decrease in the I_{corr} with increasing C_3A content of cement. The I_{corr} decreased almost linearly with C_3A in the chloride-contaminated concrete specimens. In the concrete specimens contaminated with sodium chloride plus sodium sulfate, the I_{corr} values in SRPC (C_3A: 3.5%) and OPC-A (C_3A: 8.5%) were not that different. The I_{corr} on steel in OPC-B (C_3A:14.5%) was, however, lower than that in OPC-A concrete specimens. The I_{corr} on steel in the chloride-contaminated specimens decreased from 2.0 to 1.4 $\mu A/cm^2$ for the C_3A varying from 3.5 to 14.5%. In the concrete specimens contaminated with sodium chloride plus sodium sulfate this variation was from 2.5 to 1.95 $\mu A/cm^2$.

In general, the data on corrosion current density indicated lower corrosion activity in concrete specimens made with higher C_3A content of cement. This may be attributed to the chloride binding capacity of cements. The beneficial effect of C_3A in reducing the corrosion activity has been reported by several investigators [33,78,99,100,179,180]. Monfore and Verbeck [99] found a five-fold decrease in the free chloride concentration in hardened cement pastes treated with 2% $CaCl_2$ in the mix

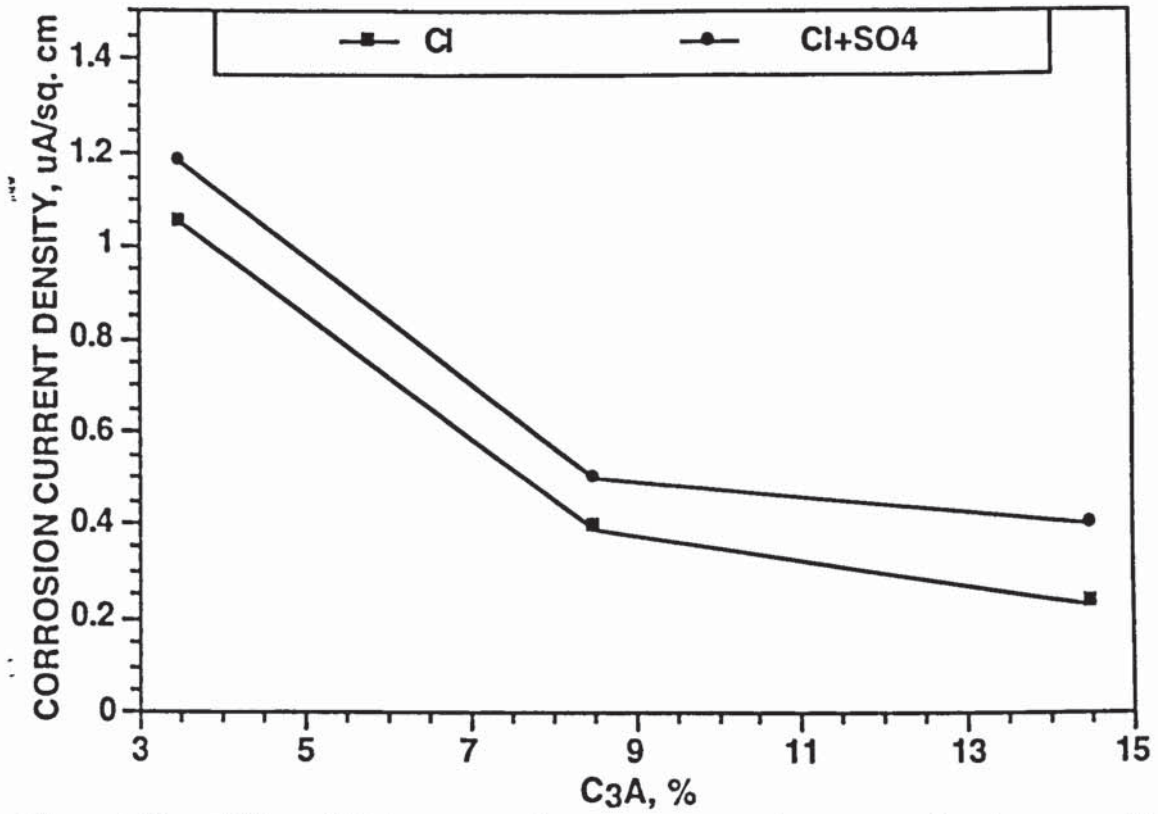

Figure 4.32: Effect of C_3A content of cement on corrosion current density on steel in concrete specimens exposed to 25 °C

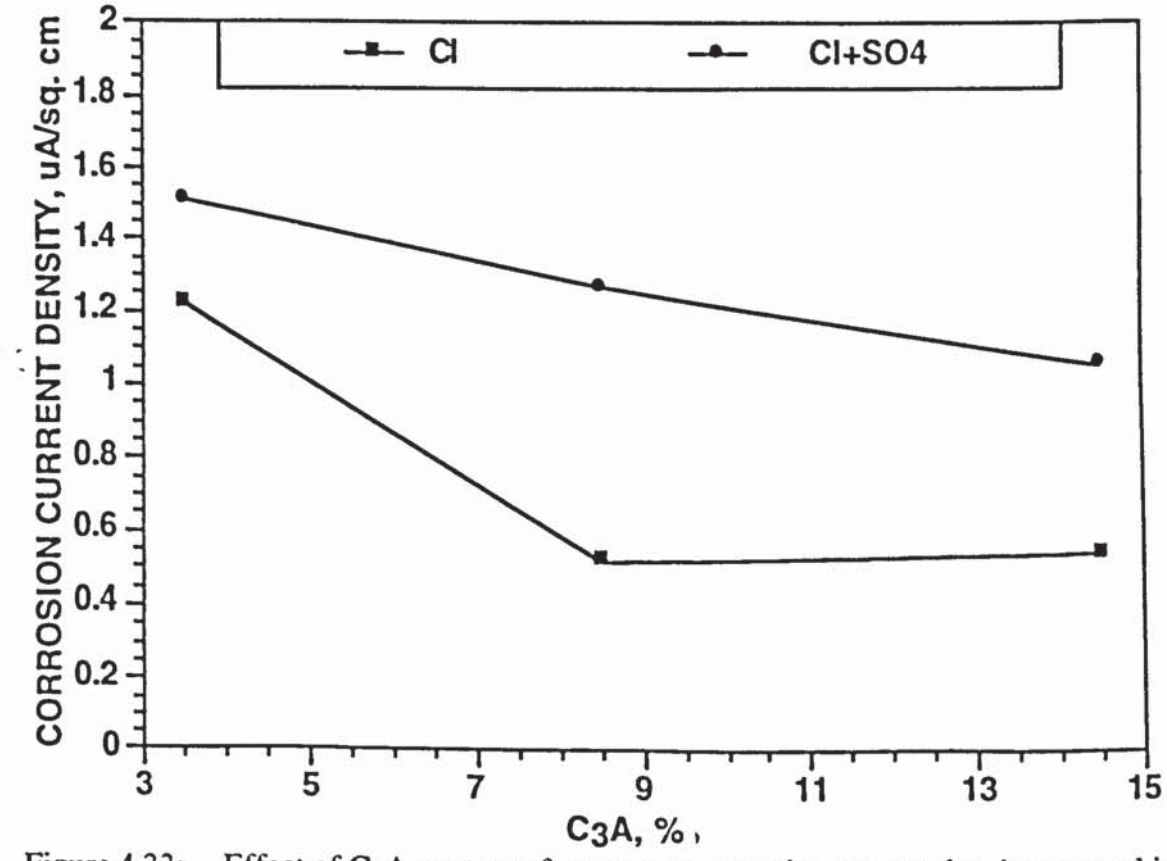

Figure 4.33: Effect of C_3A content of cement on corrosion current density on steel in concrete specimens exposed to 40 °C

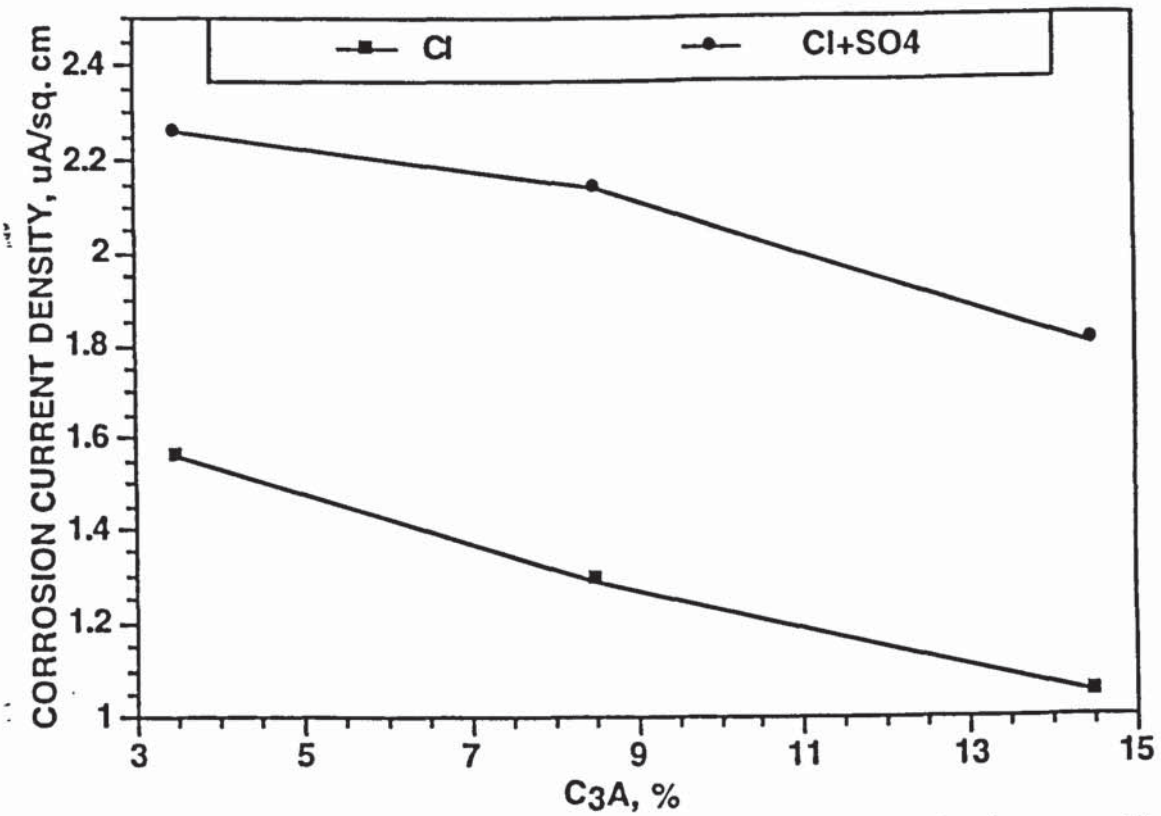

Figure 4.34: Effect of C_3A content of cement on corrosion current density on steel in concrete specimens exposed to 55 °C

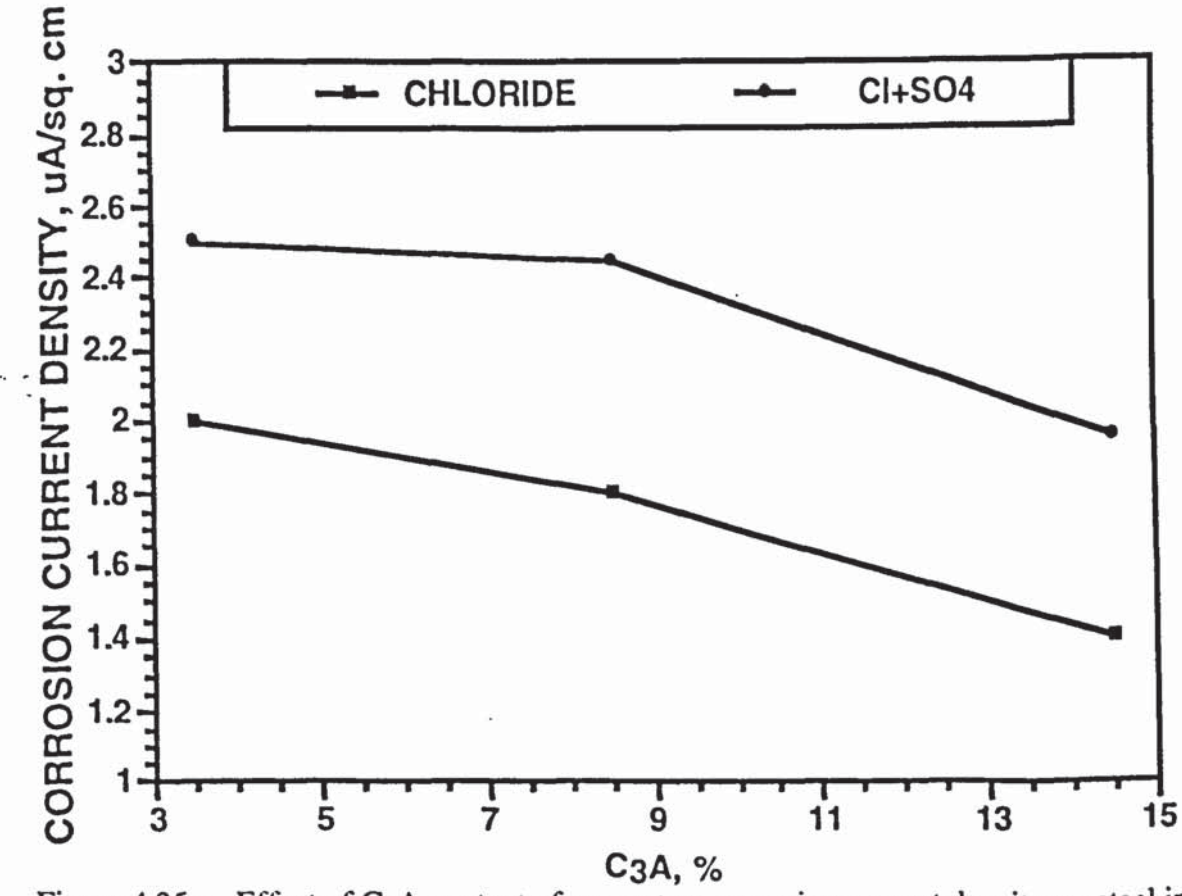

Figure 4.35 : Effect of C_3A content of cement on corrosion current density on steel in concrete specimens exposed to 70 °C

water as C_3A phase of the cement increased from 0 to 12.6%. In another long-term series of tests [100] on reinforced concrete piles exposed to sea water at Florida, concretes made with high C_3A cements showed less cracking and spalling than those made with low C_3A cements. Similar effects have been observed by Baumel and Engel [176] where cements with low C_3A (6.5%) exhibited active corrosion behaviour at lower $CaCl_2$ concentrations than cement containing a C_3A of 14%. Roberts [78] obtained experimental evidence from laboratory tests in which steel wires were embedded in portland cement concretes both with and without calcium chloride added to the mixing water used for making concrete prisms. A very slight corrosion was recorded in OPC (C_3A: 9%) when 1.4% $CaCl_2$, by weight of cement was present, while considerable corrosion occurred in SRPC (C_3A: 1%) containing the same amount of $CaCl_2$. No reinforcement corrosion was reported for either the low C_3A cement concrete or the high C_3A concrete when no calcium chloride was present. The improved performance of OPC over SRPC in reducing reinforcement corrosion was also reported by Page et al. [33]. The beneficial effect of C_3A content of cement on corrosion of reinforcement, measured in terms of time to initiation of reinforcement corrosion, was reported by Rasheeduzzafar et al. [93] based on accelerated corrosion tests carried out on four ordinary portland cements with C_3A contents of 2, 9, 11 and 14%. The time to initiation of reinforcement corrosion was observed to increase linearly with the C_3A content of cement. These results indicated that concretes made with 9, 11, and 14% C_3A performed 1.75, 1.93 and 2.45 times better than the cement concrete specimens made with a 2% C_3A cement. The time to cracking in the concrete specimens containing admixed chlorides was also observed to be lower in OPC concrete specimens compared to SRPC concrete [179]. The OPC cement concrete specimens cracked in a period which varied from 1.87 to 1.60 times than that noted in the SRPC concrete specimens for chloride contamination levels ranging from 1.2 to 2.4 kg/m^3. The data on loss of metal indicated a similar trend [179]. Results projecting the

beneficial effect of C_3A content of cement in reducing reinforcement corrosion have also been reported by Baweja et al. [180].

4.4 SUMMARY OF RESULTS

The data on reinforcement corrosion in chloride-contaminated SRPC and OPC concrete specimens indicated that the corrosion activity is mainly influenced by: (i) exposure temperature and (ii) sulfate contamination. The corrosion activity increased by 2 to 6 times due to increase in the temperature from 25 to 70 °C. The acceleration factor for every 15 °C being in the range of 1.26 to 1.87. The increase in the corrosion activity due to increasing temperature may be attributed to the increase in the rate of chemical reactions.

The increase in the corrosion activity due to the concurrent presence of chloride and sulfate salts was 1.1 to 2.4 times that measured in concrete specimens contaminated with only sodium chloride. The increase in the corrosion activity due to the inclusion of sulfate in the chloride-contaminated concrete specimens may be attributed to the combined effect of decrease in the chloride binding and electrical resistivity of concrete.

The beneficial effect of high C_3A cements in mitigating reinforcement corrosion was evident in the contaminated specimens exposed to all the temperatures. The corrosion current density on steel in the chloride-contaminated SRPC (C_3A: 3.5%) concrete was 2.7 and 4.6 times that in OPC-A (C_3A: 8.5%) and OPC-B (C_3A: 14.5 %), respectively, at 25 °C. The Icorr on steel in the SRPC concrete specimens exposed to 70 °C was 1.2 and 2.5 times that in OPC-A and OPC-B, exposed to similar temperature. The I_{corr} on steel in SRPC concrete specimens contaminated with sodium chloride plus sodium sulfate was 2.4 to 1.02 times that in OPC-A for exposure temperature varying from 25 to 70 °C. The increase in the corrosion current density on

steel in SRPC concrete compared to that in OPC-B concrete was 3 and 1.25 times for exposure temperatures of 25 and 70 °C, respectively.

In summary, the data developed in this Chapter indicated that chloride-sulfate contamination and temperature significantly affect the mechanisms of reinforcement corrosion. This is of particular interest in the hot and arid environments where the concomitant presence of chloride-sulfate contamination and elevated temperatures may drastically reduce the useful-service-life of reinforced concrete structures due to increase in the rate of reinforcement corrosion.

The data developed in this part of the study pertains to situations where the chlorides and sulfates or both, may be inducted into concrete through mixture ingredients, such as unwashed aggregates or usage of brackish water in mixing or curing of concrete. This is a common construction practice in the Arabian Gulf where desalinated or potable water is relatively scarce. Another situation which is commonly observed in the Arabian Gulf region, is that related to permeation of chloride and sulfate ions to the steel-concrete interface through extraneous sources during the service-life of concrete structures. Concrete substructures exposed to sulfate-chloride-bearing sabkha soils and groundwaters in the Arabian Gulf represent a typical situation of this category. On a global scale, concrete structures exposed to a marine environment, which contains both sulfates and chlorides, also fall in this category. An increase in the reinforcement corrosion activity may also be envisaged in such situations. At elevated temperatures, the diffusion of the aggressive species to the steel-concrete interface, is accelerated and as shown in Chapter 3, the chloride binding by cement is significantly decreased due to exposure to elevated temperatures or due to the concomitant presence of chloride and sulfate salts. Further, elevated temperature is detrimental in the uncontaminated concretes as well as the diffusion of aggressive species such as chlorides is known to increase with exposure temperature [80,181-182].

The data developed in this part of the investigation relate to concrete made in the laboratory. The small size of the specimens and controlled laboratory conditions do not truly represent the actual field conditions. Therefore, there is a need to evaluate the effect of temperature and chloride and sulfate concentration on reinforcement corrosion in the in-service structures.

CHAPTER 5

EFFECT OF TEMPERATURE AND SALT CONTAMINATION ON CARBONATION IN OPC AND BLENDED CEMENTS

5.1 CARBONATION IN CONCRETE

Carbonation in concrete normally involves a chemical reaction between atmospheric carbon dioxide and the products of cement hydration. This reaction results in a significant reduction in the pH of the pore solution due to removal of hydroxyl ions. Steinour [183] indicated that virtually all of the cement hydrates in the cement paste matrix react with carbon dioxide. The main cement hydrates, i.e., calcium silicate hydrate, calcium hydroxide and various calcium aluminate or ferro-aluminate hydrates react to produce calcium carbonate, silica gel and hydrated aluminum and iron oxides [183-192]. Factors influencing carbonation of concrete include, concrete mix design, curing, moisture condition, and temperature. Based on DSC and FT-IR analyses, Sakai et al. [193] indicated that C-S-H decomposes to calcite and silica gel or to C-S-H with a low Ca/Si ratio due to carbonation.

5.2 CARBONATION OF CONCRETE IN THE ARABIAN GULF

Though deterioration of concrete structures in the Arabian Gulf is primarily attributed to chloride-induced reinforcement corrosion, carbonation of concrete to an advanced stage, sometimes to the rebar level, is not uncommon. This is particularly true as the environmental conditions in the Arabian Gulf are marked by elevated

ambient temperatures (40 °C and above) and relative humidity (50-60%). These temperature and humidity regimes are particularly suitable to accelerate the carbonation process. There is a general agreement that carbonation is maximum at a relative humidity between 50 and 70% [36, 185, 194-195]. Similarly, the rate of carbonation was observed to increase with temperature [196]. In-situ investigations of buildings in Bahrain were carried out by Treadaway [197] to evaluate the carbonation depth in reinforced concrete structures. Based on these surveys, he concluded that the rate of carbonation in many of the structures was considerably higher than would have been anticipated, to the extent that the depth of cover to the steel in some cases was less than the depth of carbonation, within the design life of the building. Further, based on the experimental work conducted on the exposure site at Bahrain, it was indicated that concrete meeting the requirements of BS 8110 for severe/very severe exposure should be specified for the service conditions of this region to avoid carbonation [197]. Smith and Evans [198] concluded that concrete carbonation depths of 25 to 75 mm after 40 years can be expected in reinforced concrete structures in this region, primarily due to the local environmental conditions, construction materials used and the construction techniques adopted. Weir et al. [199] reported depths of carbonation from 1 to 10 mm after 12 years for a culvert in Oman. The water/cement ratio of the concrete was 0.5 and 28-day compressive strength was 28 MPa. Measurements at a desalination plant in the Arabian Gulf [200] indicated carbonation depths of 8 to 20 mm after 10 years in concrete made with a water/cement ratio of 0.70. The author maintained that use of high quality dense concrete, impermeable finishes and coated or stainless steel was necessary to achieve a life expectancy of 40 to 50 years for reinforced concrete in the environmental conditions of the Arabian Gulf. Studies conducted by Shalon and Raphael [201] on the effect of temperature and humidity on carbonation indicated maximum depth of carbonation at RH between 65 to 75%. At 90% RH, carbonation was considerably less. Shalaby [202] investigated the causes of failure of five deteriorated reinforced concrete structures exposed to marine and non-marine

environments in Kuwait. After about 10 years in service, carbonation depths of 10 to 35 mm were measured in these structures. The author attributed the deterioration of non-marine structures to excessive carbonation. After 3 years of service, the depth of carbonation in the atmospheric zone of the Saudi Arabia-Bahrain causeway was observed to be 13 mm compared to 2 mm observed in the splash zone [203]. No carbonation in the tidal and submerged zone was observed. High quality concrete (cement content of 400 kg/m^3) and portland blast furnace slag cement was used in the construction of this causeway. In-situ investigations conducted by Hussain et al. [204] on a reinforced concrete structure in an industrial area along the Arabian Gulf indicated carbonation to a depth of 15 mm on the exterior components, whereas on the interior components carbonation depths of 3 to 5 mm were recorded after about 6 years in service. Fontenay [22] established the rate of carbonation of different concrete mixes under varying curing and exposure conditions of the Arabian Gulf. He reported that for concrete with low water-cement ratio the rate of carbonation in the Arabian Gulf environment was not significantly higher than that obtained in a temperate climate, provided the concrete had been well cured. In improperly cured concrete, however, the rate of carbonation was two to four times higher than that in a temperate climate. Fattuhi [205] evaluated the long-term effect of Arabian Gulf environment on carbonation in concrete made with varying water-cement ratios. The rate of carbonation was observed to be higher than that reported in Europe for similar concretes.

While the studies cited above have generally indicated accelerated carbonation of concrete in the Arabian Gulf conditions, compared to the temperate climatic conditions, data are lacking on the role of temperature and the chloride-sulfate contamination on the changes in the concrete alkalinity. Limited studies conducted by Rasheeduzzafar [206], Al-Amoudi et al. [207] and Macmillan and Treadaway [168] have indicated that the presence of chloride and/or sulfate contamination within concrete may accelerate carbonation of concrete.

This Chapter discusses the results of the experimental work conducted to evaluate the effect of chloride-sulfate contamination and elevated temperature on carbonation in the ordinary portland cements. Also, the carbonation behaviour of blended cements, incorporating supplementary cementing materials like fly ash, blast furnace slag and silica fume, particularly in the presence of chloride-sulfate contamination was evaluated.

5.3 EXPERIMENTAL WORK

5.3.1 Experimental Variables

The experimental work in this part of the investigation was divided into two series.

In ***Series I***, carbonation of ordinary and sulfate resisting portland cements exposed to elevated temperature and contaminated with sodium chloride and sodium chloride plus sodium sulfate was investigated. In ***Series II***, carbonation of blended cements exposed to elevated temperature and contaminated with sodium chloride plus sodium sulfate was evaluated. For comparison, uncontaminated specimens were also exposed to the carbonation environment. The experimental variables in ***Series I*** and ***Series II*** are detailed in Tables 5.1 and 5.2, respectively. As stated in Chapter 3, the total SO_3 content in all the cements was adjusted to 6% to compensate for the variation in the SO_3 concentrations in the blending materials.

5.3.2 Specimen Preparation

Cement mortar specimens 50 mm Ø and 75 mm height were used to evaluate the effect of chloride-sulfate contamination and temperature on carbonation. The chemical composition of the cements used in ***Series I*** specimens are detailed in Table 3.2, while

Table 3.4 shows the chemical composition of the blending materials used in the blended cement mortar specimens. Dune sand of specific gravity 2.62, absorption 0.57% and fineness modulus 1.3 was used in the cement mortar specimens. A sand to cementitious materials ratio of 2.0 (cement content 1000 kg/m^3 of mortar) and effective water to cementitious materials ratio of 0.50 was used in all the mortar mixes. In the blended cements, the pozzolanic materials were used as a replacement of cement. In the fly ash cement mortar specimens, 20% fly ash was used as a replacement of cement. In the silica fume cement mortar specimens, 10% cement was replaced with silica fume, while blast furnace slag (BFS) cement contained 70% BFS and 30% OPC. Chloride additions were made by dissolving the required quantities of analar grade sodium chloride, while sodium sulfate was used to obtain the required sulfate concentration. The ingredients were mixed in a mortar mixer till a uniform colour was obtained. The mortar was then placed in the plastic containers, which were then lightly tapped to eliminate entrapped air. After about 28 days of curing in the laboratory temperature, in the sealed plastic vials, the specimens were taken out of the molds and placed in an exposure chamber, till the time of testing.

5.3.3 Exposure Conditions

The mortar specimens were exposed to a constant temperature, humidity and CO_2 conditions. The temperature of the exposure chamber was maintained at 55 °C and 75% RH. The exposure temperature, of 55 °C, was selected to represent the concrete surface temperature corresponding to an average ambient temperature of 35 °C normally recorded in the Arabian Gulf. The relative humidity considerably affects the rate of carbonation. It has been shown that the carbonation rate diminishes at low and high moisture contents. The maximum rate is often observed at relative humidities between 50 and 70% [36, 194-195]. Therefore, testing at relative humidities around 60% is a common practice in many laboratories [208]. However, the humidity in the

coastal areas of the Arabian Gulf normally ranges from 70 to 80%, reaching 100% at times. To represent the actual environmental conditions, the relative humidity in the exposure chamber was maintained at 75%.

CO_2 and air were introduced in the exposure chamber such that the resulting CO_2 concentration was 3%. High concentrations of CO_2 have often been used to evaluate the relative durability of the materials in the actual environment. The rate of carbonation is known to increase with the concentration of carbon dioxide [185], but a small increase in the rate of carbonation beyond 1% by volume was noticed. Hamada's extensive results [209] suggest that accelerated test results correlate broadly with depths of carbonation measured at normal carbon dioxide levels. The results of Nischer [210] indicated that the effect of a higher carbon dioxide level is greater with concretes having a strength less than 30 MPa.

Table 5.1: Experimental variables to evaluate the effect of chloride-sulfate contamination on carbonation in ordinary and sulfate resisting portland cements

Variables	Details
Specimens	Cement mortar specimens made with SRPC, OPC-A, and OPC-B (C_3A: 3.5, 8.5, and 14.5%)
Contamination level	0% 0.8% Cl^- 0.8% Cl^- + 1.5% SO_3^{--}
Exposure Temperature	55 °C
Monitoring Period	up to 52 weeks
Tests	Depth of carbonation Weight gain Scanning electron microscopy X-ray diffraction DTA/TG

Table 5.2: Experimental variables to evaluate the effect of chloride-sulfate contamination on carbonation in blended cements

Variables	Details
Specimens	OPC-A (C_3A: 8.5%)
	ASTM C 618 Class F fly ash cement (20% cement replacement)
	Silica fume cement (10% cement replacement)
	Blast furnace slag cement (70% BFS)
Contamination level	0%
	0.8% Cl^- + 6.0% SO_3^{--}
Exposure Temperature	55 °C
Monitoring Period	up to 52 weeks
Tests	Depth of carbonation Weight gain Scanning electron microscopy X-ray diffraction DTA/TG

5.3.4 Test Techniques

5.3.4.1 Carbonation Depth

The carbonation depth was measured by spraying phenolphthalein on a freshly broken specimen. The phenolphthalein indicator gradually changes from colourless to red at broken surfaces with a pH greater than 9.0 to 9.5 [185,211-213], while the carbonated surface remains colourless. This method of monitoring the depth of carbonation is well documented [185,211,213-214], is convenient to use and can give reproducible results [35]. The only draw back with this method is that it indicates the depth at which the pH is about 9.0 and this does not necessarily correspond to either the

boundary between uncarbonated and partially carbonated concrete or the boundary between partially carbonated and fully carbonated concrete. Studies to evaluate alternative methods of measurement of carbonation depth generally concluded that the phenolphthalein indicator provides an approximate and incomplete picture of carbonation, since it cannot show the width of the carbonating zone [212,216-219]. Some investigators recommend the use of additional [220-221], or universal pH indicators [221].

A number of alternative methods are available for monitoring carbonation. X-ray diffraction can be used to measure the reduction in the calcium hydroxide and increase in various forms of calcium carbonate [184,209,216,221]. Similar information can also be obtained using thermal analysis [192,219,221-223]. The amount of bound carbon dioxide can also be determined by chemical extraction method [209,219]. Infra red absorption can be used to monitor the formation of silica gel when calcium silicate hydrate carbonates [184,192]. The presence of calcium carbonate can be observed directly in thin sections of concrete viewed under polarized light in an optical microscope [220]. Curtil et al. [224] indicated that the polarizing microscope picture gives clear indication of the carbonation of concrete and the mineralogical components can be identified. According to them, phenolphthalein test is not accurate for determining the depth of carbonation because it overestimates the depth of carbonation.

Inspite of the inherent drawbacks, the phenolphthalein method is widely used because it is convenient and provides reproducible results.

In this study, the depth of carbonation was measured using phenolphthalein indicator in accordance with the method outlined in RILEM Recommendation CPC-18 [211] for measurement of hardened concrete carbonation depth. At least six readings

spread all over the circumference of three specimens, at each test period, were measured and average values recorded.

5.3.4.2 Weight Gain

The degree of carbonation was also evaluated by measuring the weight change of the specimens. To evaluate the weight change due to carbonation all the specimens were weighed before placement in the chamber. After removing them from the exposure chamber, they were weighed and the weight change was calculated as the percentage of the original weight. This method is a non-destructive means of monitoring the progress of carbonation using small sized specimens, particularly under controlled humidity conditions [185,225]. Parrott [208] has observed a close relationship between weight gain and carbonation and indicates that kinetic aspects of carbonation can be assessed from the weight gain versus time data.

5.3.4.3 X-ray Diffraction

X-ray diffraction has been used to monitor the effect of carbonation on phase composition of the cement [184,209,216,221]. This technique is useful in evaluating the reduction in the calcium hydroxide content and increase in the various forms of calcium carbonate. The X-ray diffraction technique is a semi-quantitative technique primarily used on crystalline materials for determining the weight fractions of crystalline phases down to about 1%. The details of this technique have been discussed in **Chapter 3.**

X-ray diffraction patterns for the carbonated and uncarbonated portions, samples demarcated by the colour change in the phenolphthalein test, were used to identify the compound composition and their weight proportion.

5.3.4.4 Scanning Electron Microscopy

Scanning electron microscopy (SEM) was used to evaluate the morphological changes occurring in the contaminated and uncontaminated cement mortar specimens due to carbonation. These studies were conducted using a JEOL Model JSM-840 scanning electron microscope. The scanning electron microscope used in this investigation is also equipped with energy dispersive X-ray analyzer (EDXA) which provides information on elemental composition of the specimen under consideration.

5.4 RESULTS

5.4.1 Depth of Carbonation

The depth of carbonation in the contaminated and uncontaminated SRPC (C_3A: 3.5%) mortar specimens exposed to the CO_2 atmosphere up to 54 weeks is plotted in Figure 5.1. The depth of carbonation increased with the exposure period. In the mortar specimens contaminated with sodium chloride plus sodium sulfate the carbonation depth was more than that in the uncontaminated specimens and those contaminated with sodium chloride only. These values in the specimens contaminated with sodium chloride plus sodium sulfate were 10 mm compared to about 7 mm observed in the specimens contaminated with only sodium chloride, after 44 weeks of exposure. The depth of carbonation in the uncontaminated mortar specimen was 1 mm. The variation in the carbonation depth with the period of exposure in the uncontaminated and contaminated OPC-A (C_3A: 8.5%) mortar specimens is plotted in Figure 5.2. These curves also indicated a trend similar to that exhibited by the SRPC mortar specimens. The depth of carbonation in the mortar specimens contaminated with sodium chloride and sodium chloride plus sodium sulfate was 7 and 8 mm, respectively, after 54

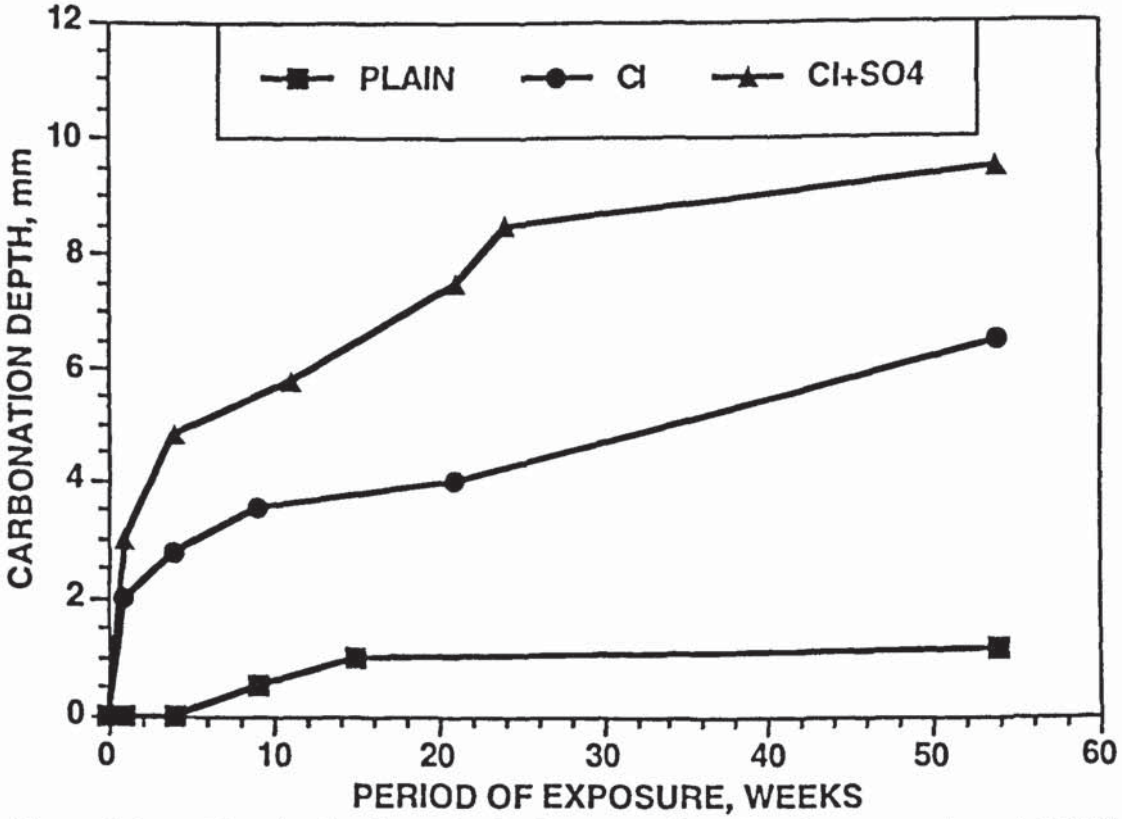

Figure 5.1: Depth of carbonation in the contaminated and uncontaminated SRPC mortar specimens

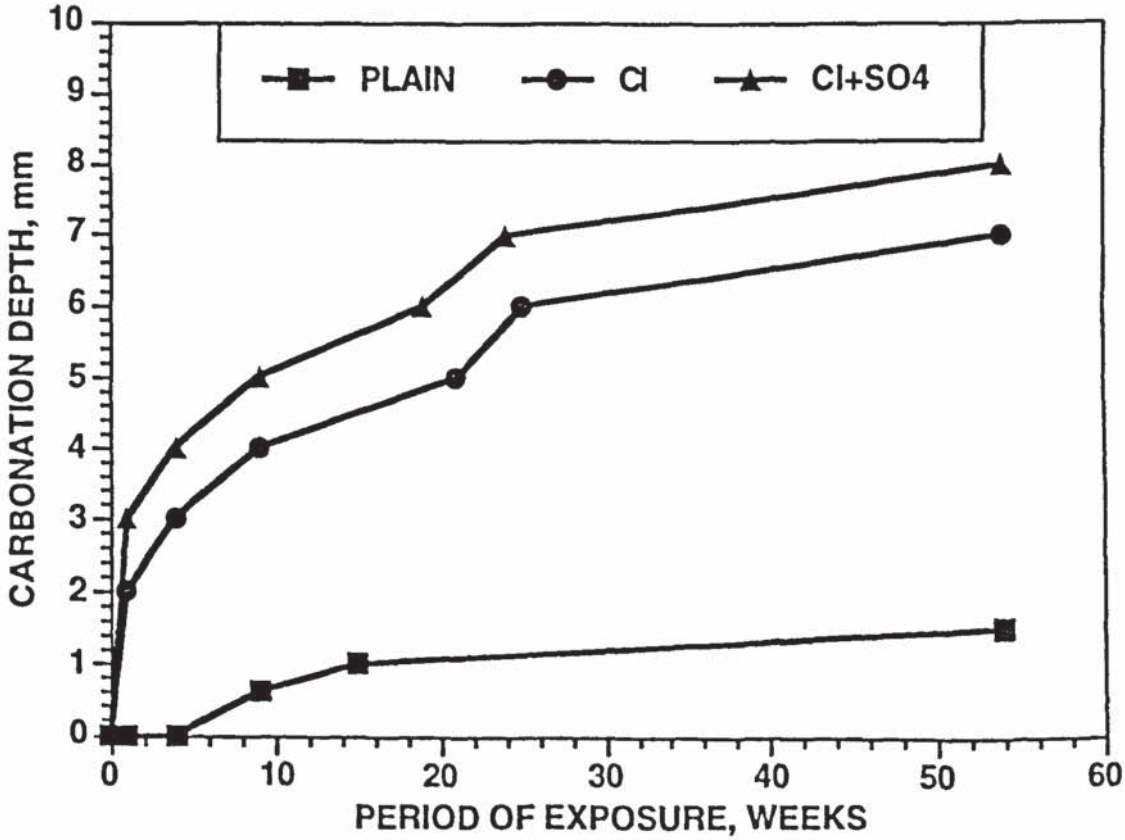

Figure 5.2 Depth of carbonation in the contaminated and uncontaminated OPC-A mortar specimens

weeks of exposure to the CO_2 atmosphere. The depth of carbonation in the uncontaminated specimen was approximately 1.5 mm after this exposure period.

The variation in the depth of carbonation in OPC-B (C_3A: 14.5%) mortar specimens is plotted in Figure 5.3. In this cement also the depth of carbonation in the specimens contaminated with sodium chloride plus sodium sulfate was more than that in the specimens contaminated with only sodium chloride. The depth of carbonation in the specimens contaminated with sodium chloride plus sodium sulfate was about 11 mm after about 33 weeks of exposure to the CO_2 atmosphere. The depth of carbonation in the specimens contaminated with sodium chloride was 7 mm, while it was 0.6 mm in the uncontaminated specimens.

The depth of carbonation in the uncontaminated blended cement mortar specimens are plotted in Figure 5.4. For the sake of comparison, the depth of carbonation in the parent OPC mortar specimens is also plotted in this figure. After about 45 weeks of exposure, the maximum depth of carbonation was indicated in the fly ash cement mortar specimens, being 2 mm. The depth of carbonation in the blast furnace slag and silica fume cement mortar specimens, after this exposure period, was 1.5 and 0.75 mm, respectively. The variation in the carbonation depth in the contaminated OPC and blended cement mortar specimens is plotted in Figure 5.5. The depth of carbonation, after about 51 weeks of exposure, was 11, 9, and 9 mm in the blast furnace slag, silica fume and fly ash cement mortar specimens, compared to 10 mm in the parent OPC mortar specimens.

The data on carbonation depth, plotted in Figures 5.1 through 5.5, indicated a parabolic relationship between the depth of carbonation and the exposure period. Such a relationship has been noted in all the cements. Since carbonation is mainly a diffusion

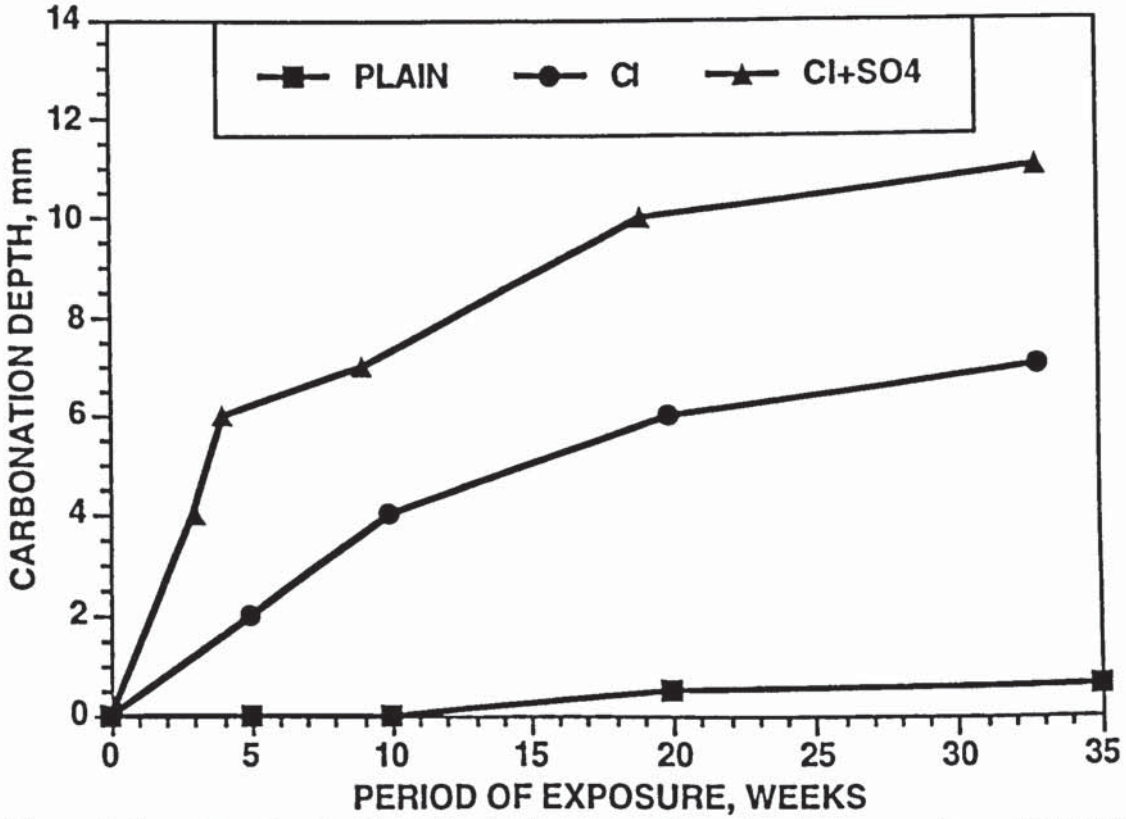

Figure 5.3: Depth of carbonation in the contaminated and uncontaminated OPC-B mortar specimens

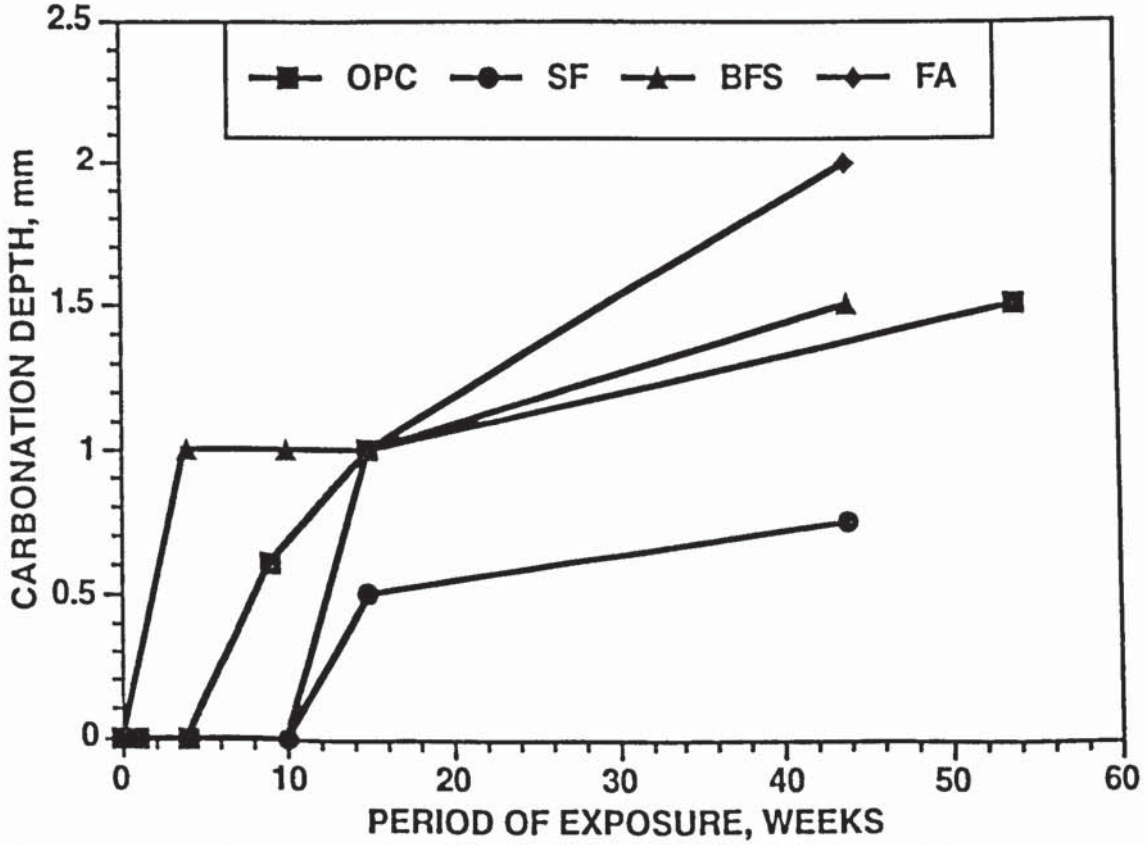

Figure 5.4: Depth of carbonation in the uncontaminated OPC and blended cement mortar specimens

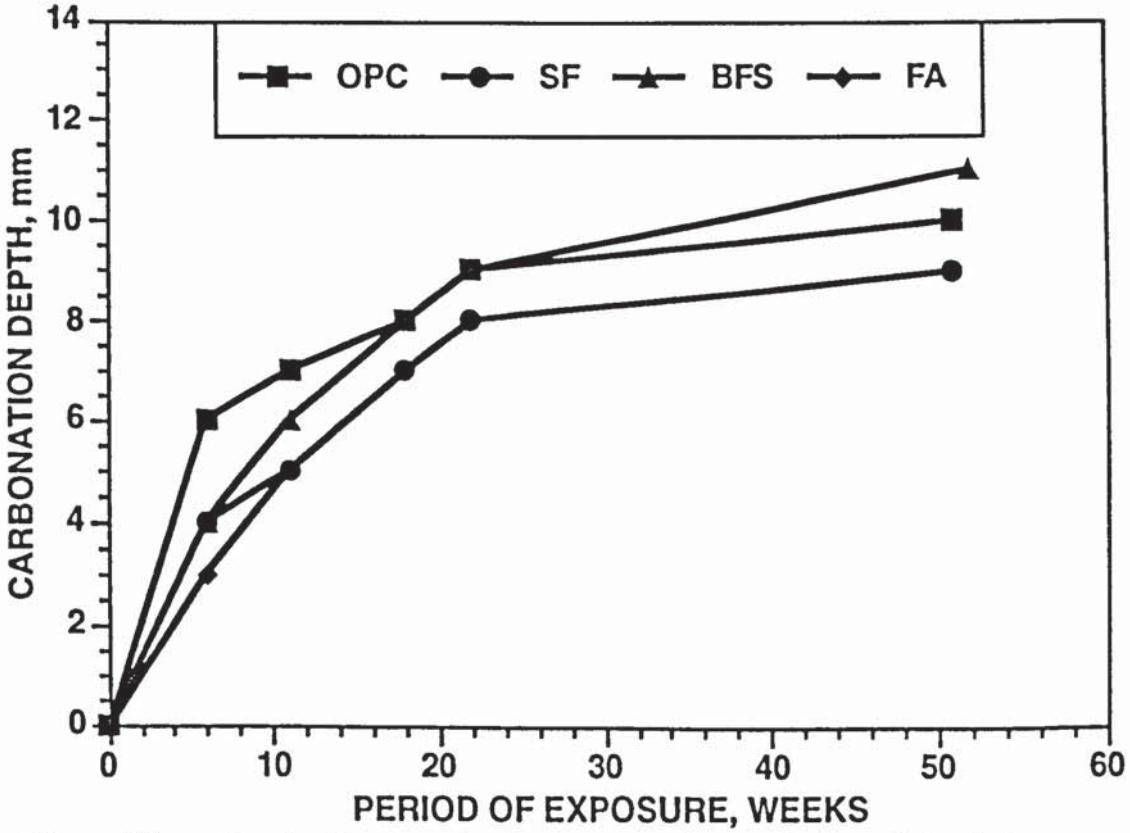

Figure 5.5 Depth of carbonation in the contaminated OPC and blended cement mortar specimens

process its progress is often represented by the relationship:

$$Dc = k\,(t)^{0.5}$$

where: Dc = carbonation depth, mm

k = carbonation rate constant, $mm/(day)^{0.5}$

t = exposure period, days.

The existence of the above relationship between the depth of carbonation and period of exposure has been confirmed by many researchers [226,227]. According to Tuutti [28], the exponent for time depends on the exposure conditions and may be less than 0.5. Smolczyk [228] summarized research carried out in various countries and pointed out that carbonation depended on many factors including the quality of concrete and the conditions of exposure. The important environmental factors which affect carbonation were considered to be carbon dioxide concentration, humidity, and temperature. Ho and Lewis [229] suggested that under similar conditions of exposure, carbonation may be closely related to $1/F^{0.5}$, where F is the compressive strength of concrete at the time of carbonation.

Table 5.3 shows the carbonation rate constant, k, for the contaminated and uncontaminated plain and blended cement mortar specimens investigated in this study. The carbonation rate constant for the uncontaminated plain and blended cements varied from 0.03 to 0.098. The maximum rate of carbonation was observed in the blast furnace slag cement mortar specimens. The increased carbonation in the blast furnace slag cement compared to other cements, exposed to similar environment, has been reported by other researchers [230,231]. The carbonation rate constant in the cement mortar specimens contaminated with only sodium chloride varied from 0.40 to 0.47. The carbonation rate constants for the plain and blended cements contaminated with

sodium chloride plus sodium sulfate were in the range of 0.55 to 0.82, which were on an average 1.5 times those in the chloride-contaminated specimens and 10 times those in the uncontaminated specimens.

Table 5.3: Carbonation rate constant* in the contaminated and uncontaminated OPC and blended cement mortar specimens

Cement Type	Contamination		
	None	Chloride	Chloride + Sulfate
SRPC	0.058	0.40	0.620
OPC-A	0.076	0.410	0.649
OPC-B	0.030	0.468	0.815
Fly Ash	0.088	--	0.540
Silica Fume	0.036	--	0.553
Blast Furnace Slag	0.098	--	0.642

* Carbonation rate constant, k = mm/(days)$^{(0.5)}$

Figures 5.6 through 5.12 demarcate the carbonated (dark) and uncarbonated (white) zones in some of the contaminated and uncontaminated plain and blended cement mortar specimens after about 51 weeks of exposure. These pictures indicate a larger carbonation area in the specimens contaminated with sodium chloride plus sodium sulfate in comparison with the uncontaminated specimens. This behaviour was observed in both the plain and blended cement mortar specimens.

5.4.2 Weight Gain

The change in weight of the mortar specimens, expressed as a percentage of pre-exposure weight, with the duration of exposure to the CO_2 atmosphere is plotted for the contaminated and uncontaminated SRPC mortar specimens in Figure 5.13. Weight gain was indicated in the specimens contaminated with sodium chloride plus sodium sulfate after about 4 weeks of exposure, whereas a reduction in weight was indicated in

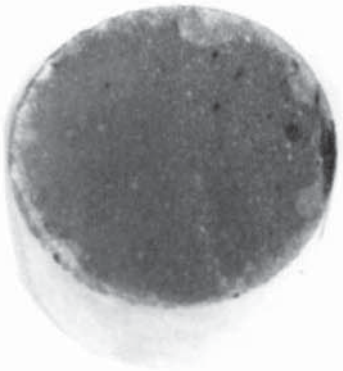

OPC-A (C_3A: 8.5%) MORTAR SPECIMEN
NO CONTAMINATION
EXPOSURE - 54 WEEKS

Figure 5.6: Photograph of uncontaminated OPC-A mortar specimen showing the extent of carbonation

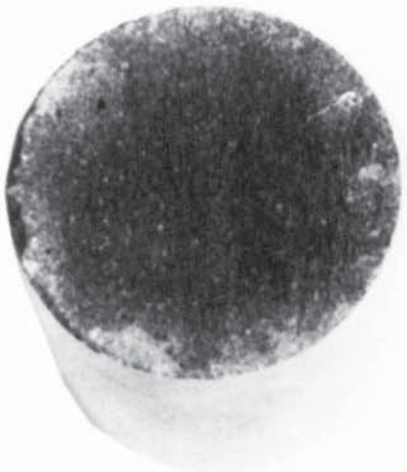

SRPC (C_3A: 3.5%) MORTAR SPECIMEN
NO CONTAMINATION
EXPOSURE - 54 WEEKS

Figure 5.7 Photograph of uncontaminated SRPC mortar specimen showing the extent of carbonation

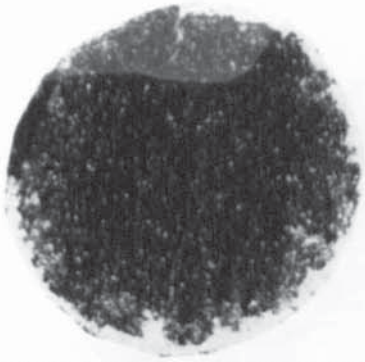

BLAST FURNACE SLAG CEMENT MORTAR SPECIMEN
NO CONTAMINATION
EXPOSURE - 44 WEEKS

Figure 5.8: Photograph of uncontaminated BFSC mortar specimen showing the extent of carbonation

OPC-A (C_3A: 8.5%) MORTAR SPECIMEN
CONTAMINATED WITH $Cl^- + SO_4^{--}$
EXPOSURE - 51 WEEKS

Figure 5.9: Photograph of OPC-A mortar specimen contaminated with $Cl+SO_4$ indicating the extent of carbonation

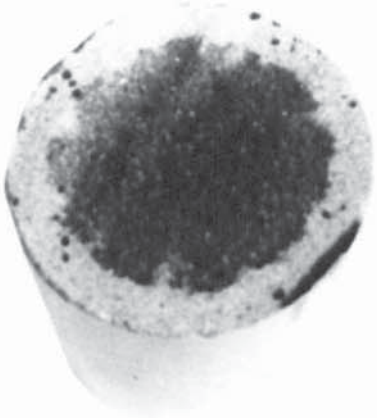

FLY ASH CEMENT MORTAR SPECIMEN
CONTAMINATED WITH $Cl^- + SO_4^{--}$
EXPOSURE - 51 WEEKS

Figure 5.10: Photograph of fly ash cement mortar specimen contaminated with $Cl+SO_4$ indicating the extent of carbonation

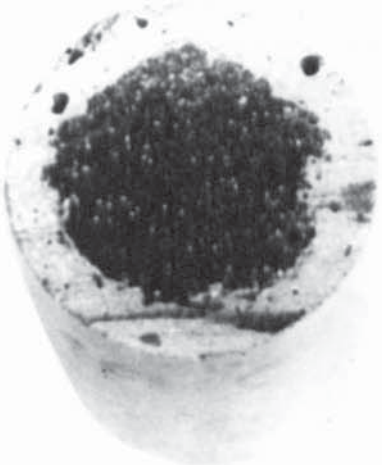

SILICA FUME CEMENT MORTAR SPECIMEN
CONTAMINATED WITH $Cl^- + SO_4^{--}$
EXPOSURE - 51 WEEKS

Figure 5.11: Photograph of silica fume cement mortar specimen contaminated with $Cl+SO_4$ indicating the extent of carbonation

BLAST FURNACE SLAG CEMENT MORTAR SPECIMEN
CONTAMINATED WITH $Cl^- + SO_4^{--}$
EXPOSURE - 51 WEEKS

Figure 5.12: Photograph of blast furnace slag cement mortar specimen contaminated with $Cl+SO_4$ indicating the extent of carbonation

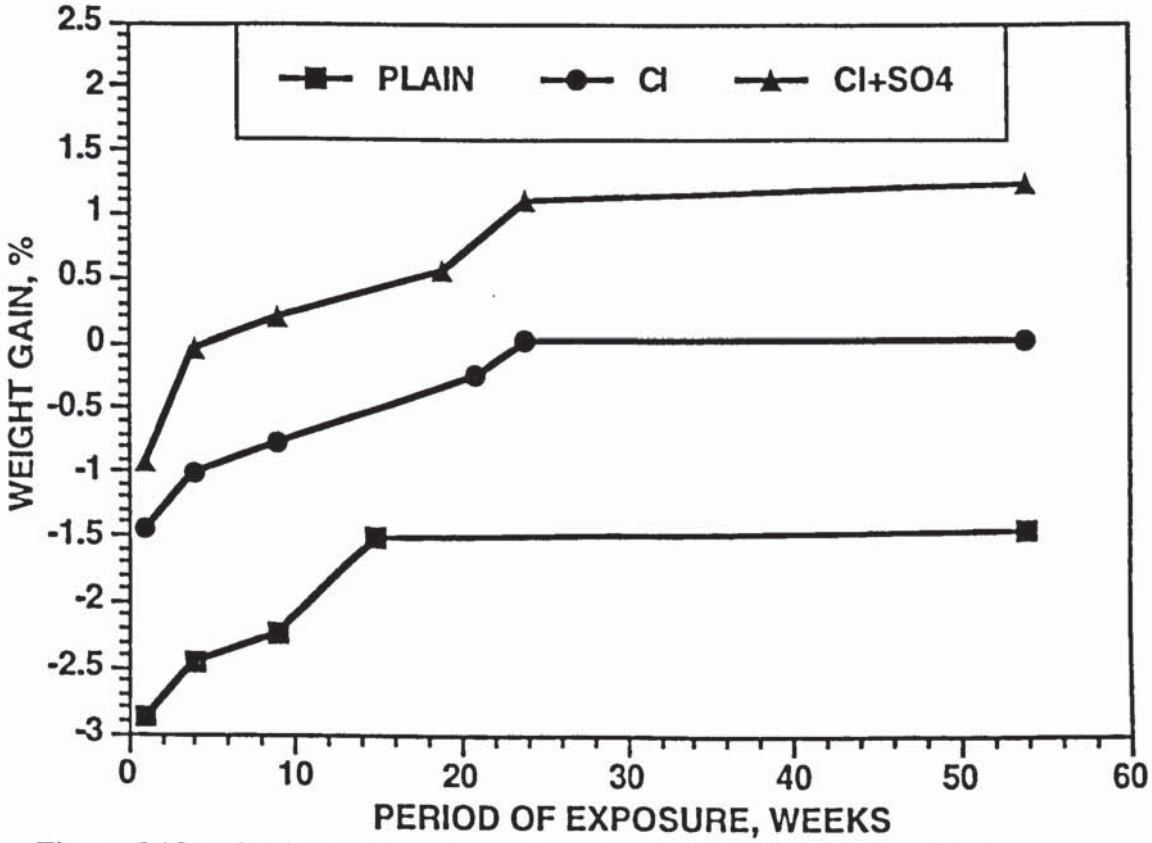

Figure 5.13: Weight gain in the contaminated and uncontaminated SRPC cement mortar specimens

the uncontaminated specimens at all the exposure periods. In the specimens contaminated with sodium chloride the weight was more or less equal to that at the pre-exposure period after 20 weeks of exposure. After 54 weeks of exposure, approximately 1.25% weight gain was indicated in the mortar specimens contaminated with sodium chloride plus sodium sulfate. The weight gain in the uncontaminated specimens and those contaminated with sodium chloride was -1.45 and 0.1%, respectively.

The weight gain in the contaminated and uncontaminated OPC-A (C_3A: 8.5%) mortar specimens is plotted in Figure 5.14. These curves also indicated a trend similar to that observed in SRPC mortar specimens, in that the weight gain was indicated to be higher in the contaminated specimens as compared to the uncontaminated specimens.

The weight gain in the uncontaminated blended cement mortar specimens is plotted in Figure 5.15. No weight gain was indicated in the OPC, fly ash and silica fume cement mortar specimens even after 10 weeks of exposure. After this time, a small gain in weight was indicated in the blast furnace slag cement mortar specimens, while weight gain was indicated in the silica fume cement mortar specimens after about 20 weeks of exposure. The weight gain in the contaminated cement mortar specimens is plotted against the period of exposure in Figure 5.16. The weight gain was indicated in the plain and blended cement mortar specimens, more or less after 5 weeks of exposure. The weight gain in the silica fume, fly ash and blast furnace slag cement mortar specimens, after about 51 weeks of exposure, was approximately 2.95, 1.75 and 1.25%, respectively, compared to a weight gain of 2.0% measured in the contaminated OPC.

In summary, the data on weight gain, discussed in Figures 5.13 through 5.16, indicated higher weight gain in the specimens contaminated with sodium chloride plus

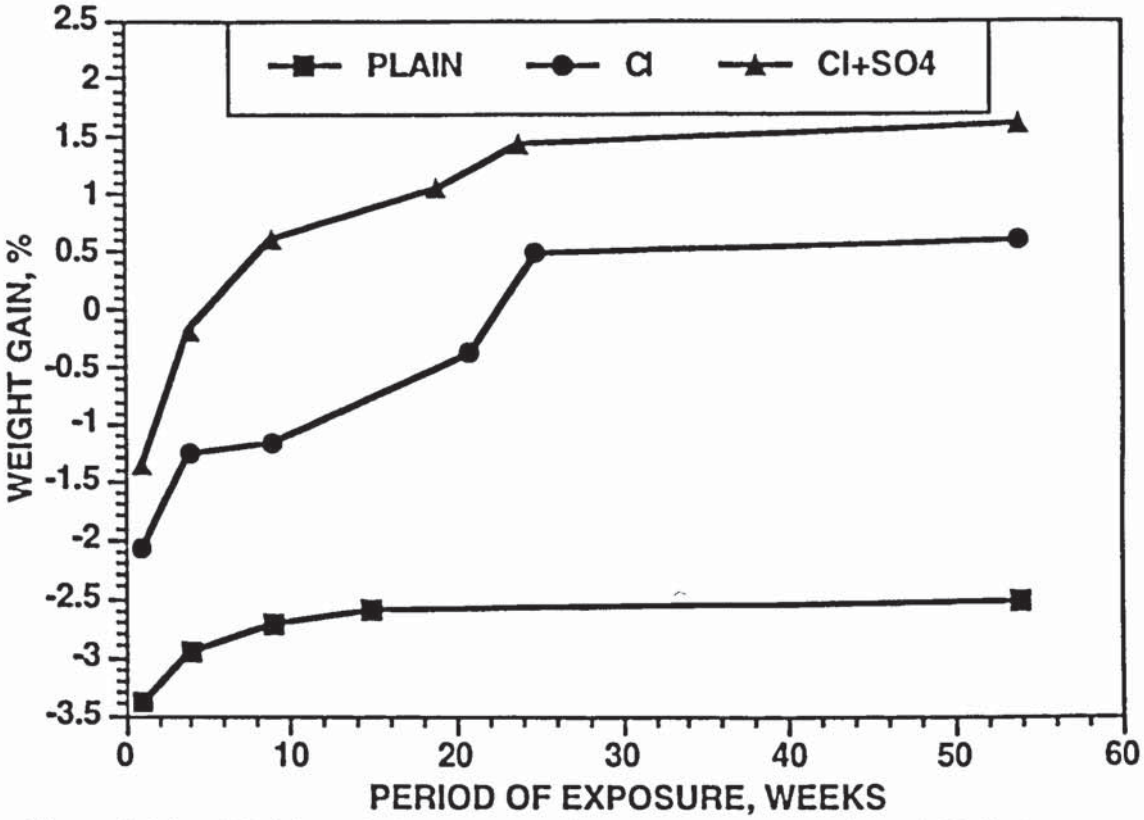

Figure 5.14: Weight gain in the contaminated and uncontaminated OPC-A cement mortar specimens

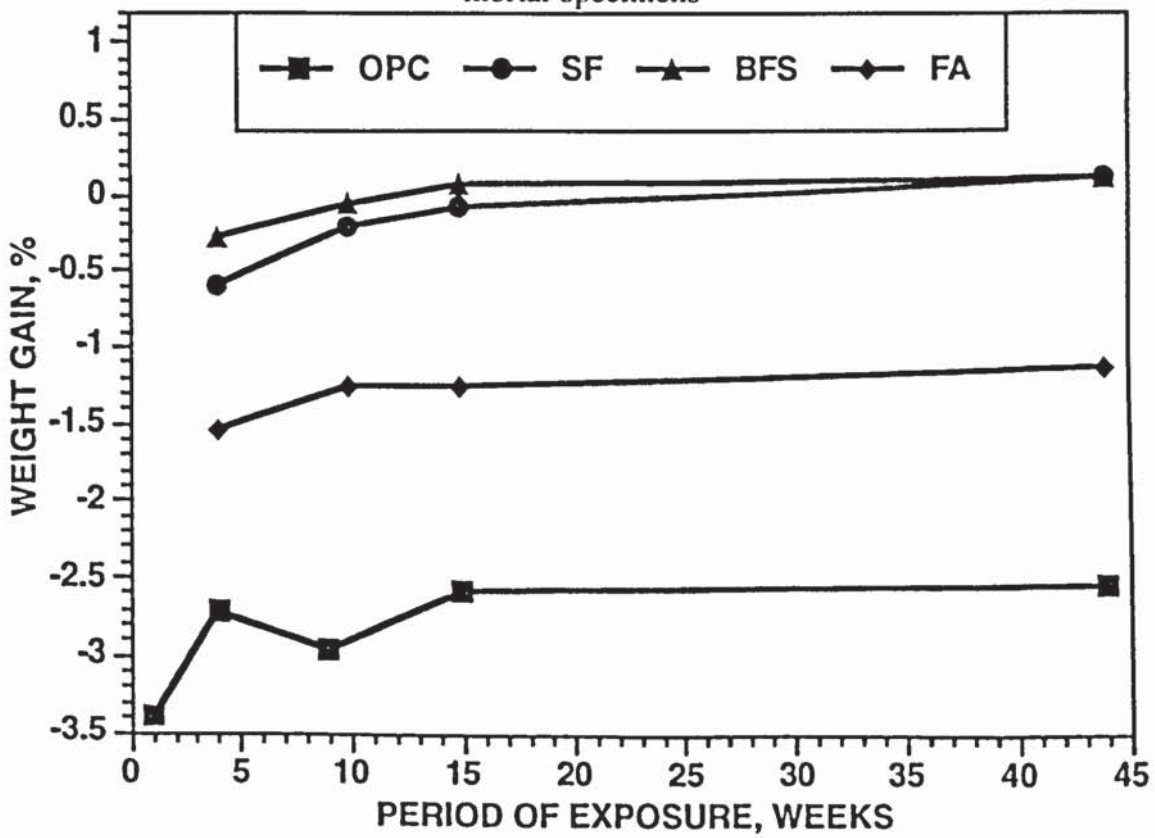

Figure 5.15: Weight gain in the uncontaminated OPC and blended cement mortar specimens

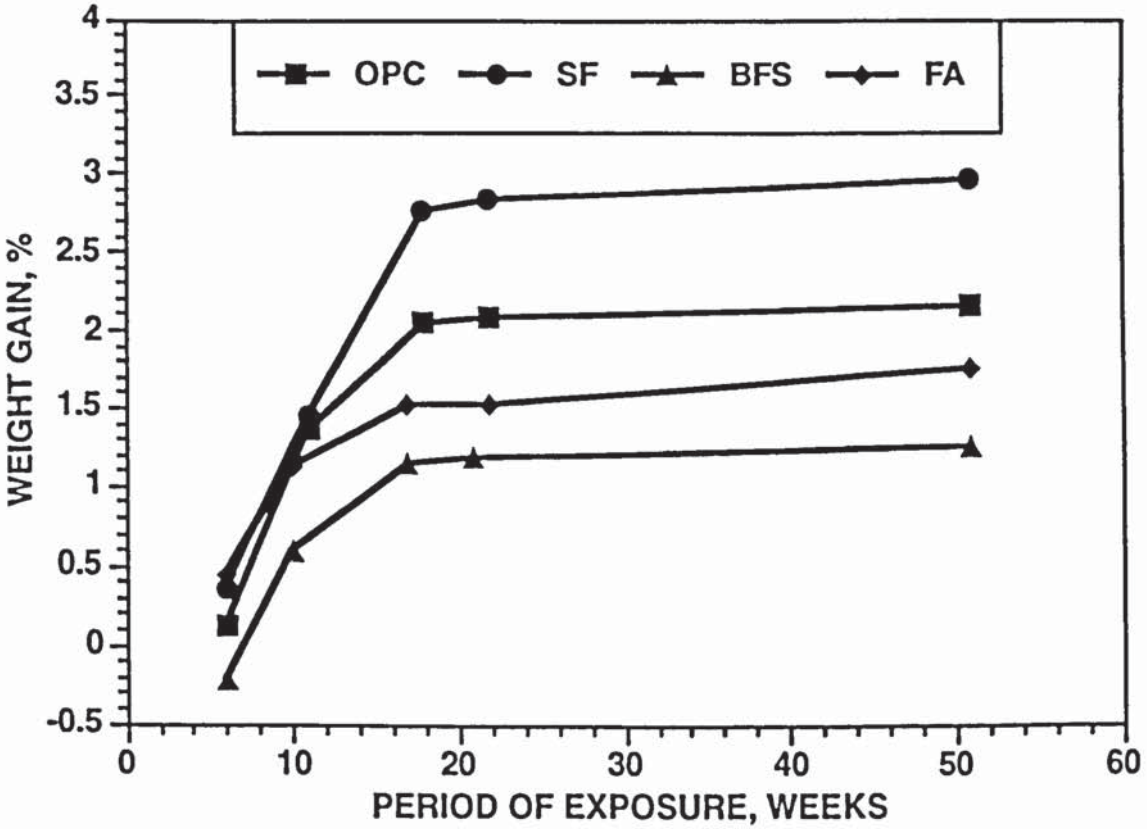

Figure 5.16: Weight gain in the contaminated OPC and blended cement mortar specimens

sodium sulfate compared to the uncontaminated specimens and those contaminated with only sodium chloride. The weight gain in the specimens contaminated with only sodium chloride was more than that in the uncontaminated specimens. In fact, practically no weight gain was observed in the uncontaminated cement mortar specimens. This behaviour was observed in both the plain and blended cements.

5.4.4 SEM Analysis

For SEM analysis the uncarbonated and carbonated portions of the mortar specimens were selected. The specimens were first subjected to EDX analysis and there after coated with gold for examination under the scanning electron microscope. Figure 5.17 shows the scanning electron micrograph for the uncarbonated OPC mortar specimen contaminated with sodium chloride plus sodium sulfate. A fibrous structure of the C-S-H was indicated in this micrograph. The EDX analysis of the area (Figure 5.18) indicated the presence of mainly Ca (74%) and Si (13%). Traces of Al (1.9%), S (3.9%) and Cl (1.8%) were also observed. The SEM micrograph of the carbonated OPC mortar specimen is shown in Figure 5.19. This micrograph indicated a dense micro structure of the C-S-H. The area EDXA (Figure 5.20) indicated the presence of Ca, Si, Al, S and Cl. Si (23.4%) and Ca (69%) were the major components. The presence of white lumped crystalline formations at isolated spots was also indicated in this micrograph. The EDX analysis of one of these crystals (Figure 5.21) indicated it to be mainly Ca (89%) with little Si (5.36%). It is presumed that it is $CaCO_3$, since a higher magnification picture of the uncarbonated specimen did not reveal the presence of such formations. The SEM micrograph of the uncarbonated fly ash cement mortar specimen contaminated with sodium chloride plus sodium sulfate is shown in Figure 5.22. A regular fibrous C-S-H morphology with isolated white crystal formations ($CaCO_3$) is indicated. The area EDX analysis (Figure 5.23) indicated it to be mainly Ca (75.57%), Si (12.7%), in addition to traces of Al, S and Cl. Figure 5.24 is a

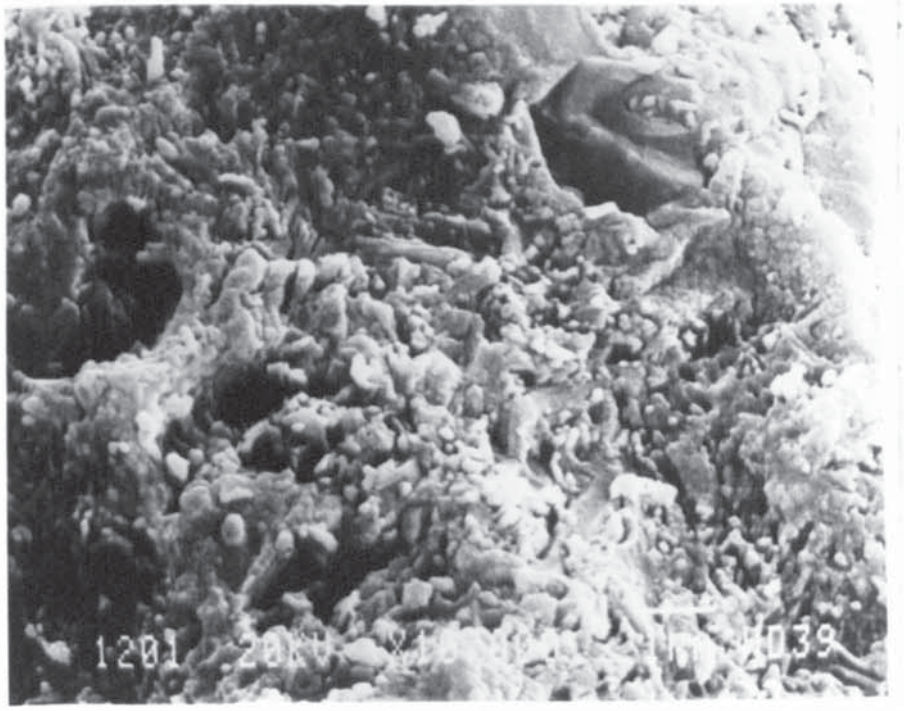

Figure 5.17: Scanning electron micrograph of the uncarbonated portion of OPC mortar specimen contaminated with $Cl+SO_4$

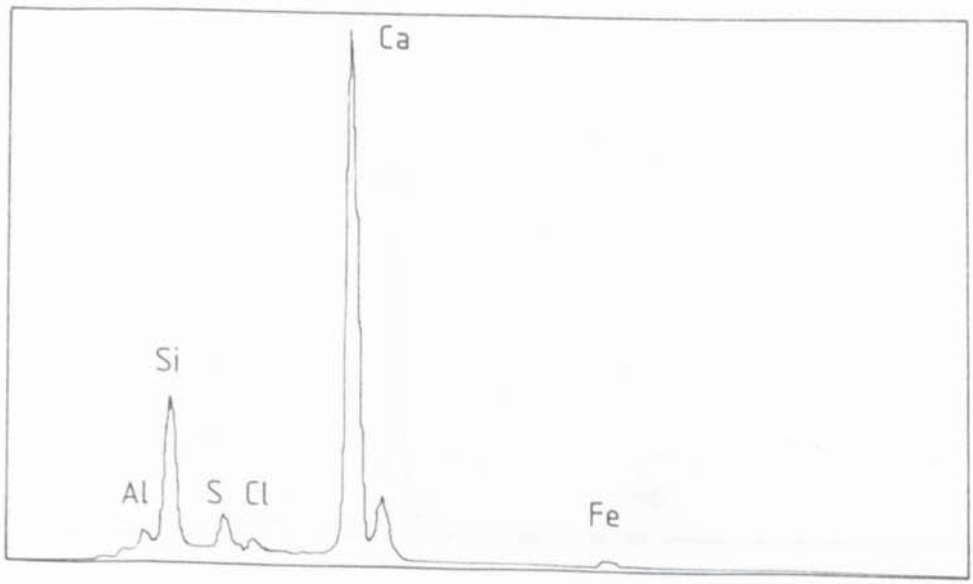

Figure 5.18: Area EDXA of the uncarbonated portion of OPC mortar specimen contaminated with $Cl+SO_4$

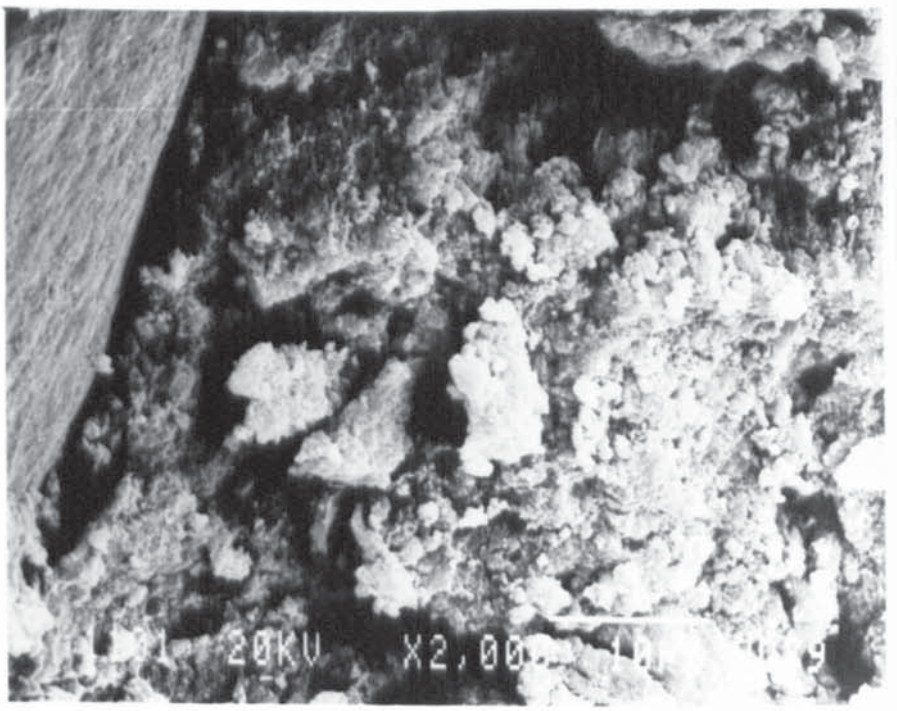

Figure 5.19: Scanning electron micrograph of the carbonated portion of OPC mortar specimen contaminated with $Cl+SO_4$

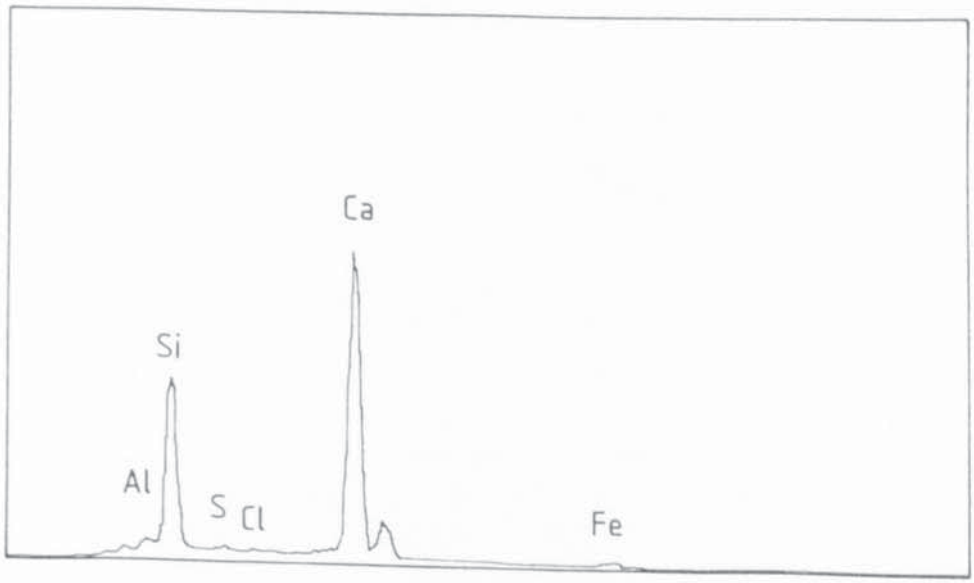

Figure 5.20: Area EDX analysis of the carbonated portion of OPC mortar specimen contaminated with $Cl+SO_4$

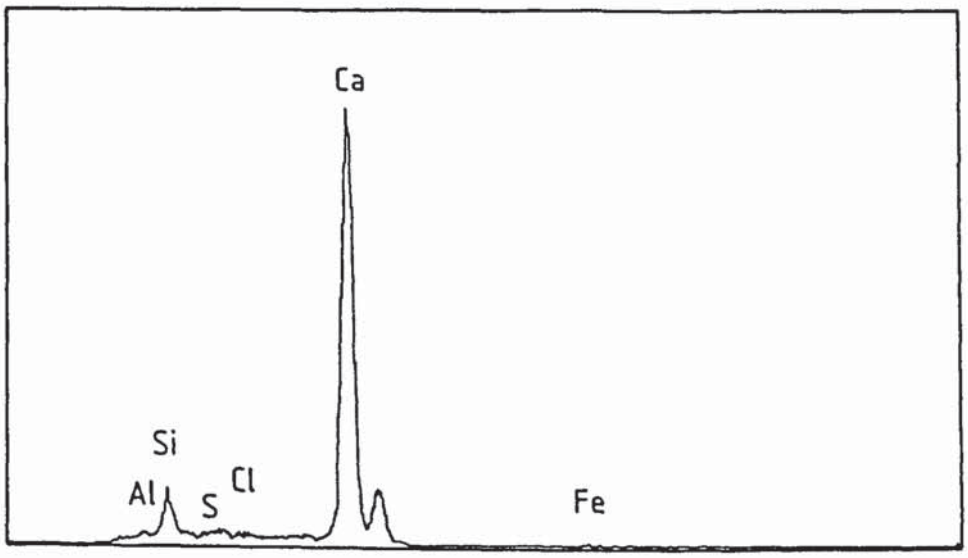

Figure 5.21: EDX analysis of $CaCO_3$

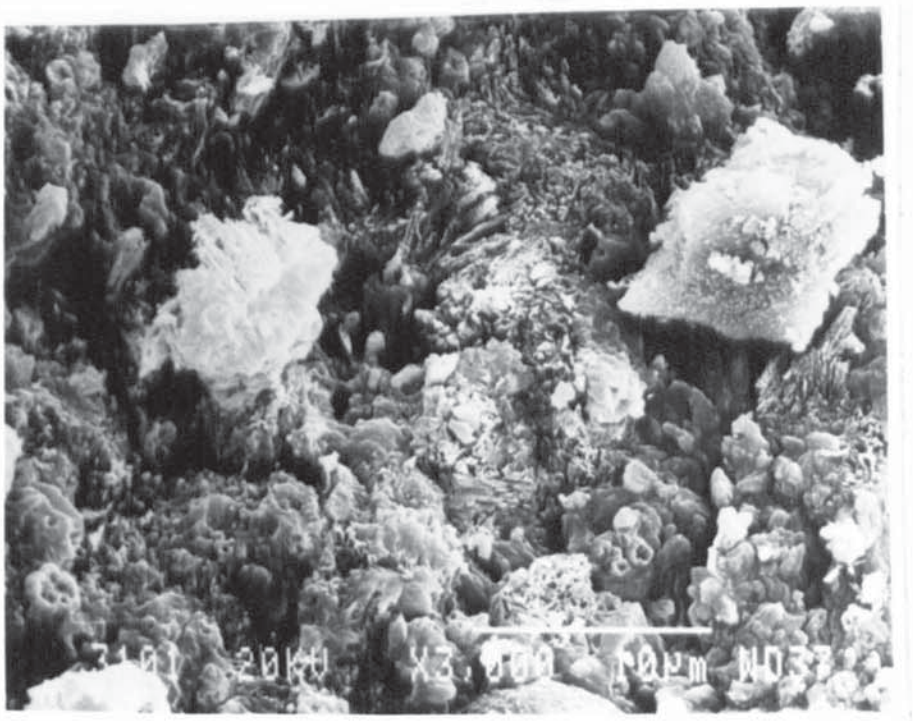

Figure 5.22: Scanning electron micrograph of the uncarbonated portion of fly ash cement mortar specimen contaminated with $Cl+SO_4$

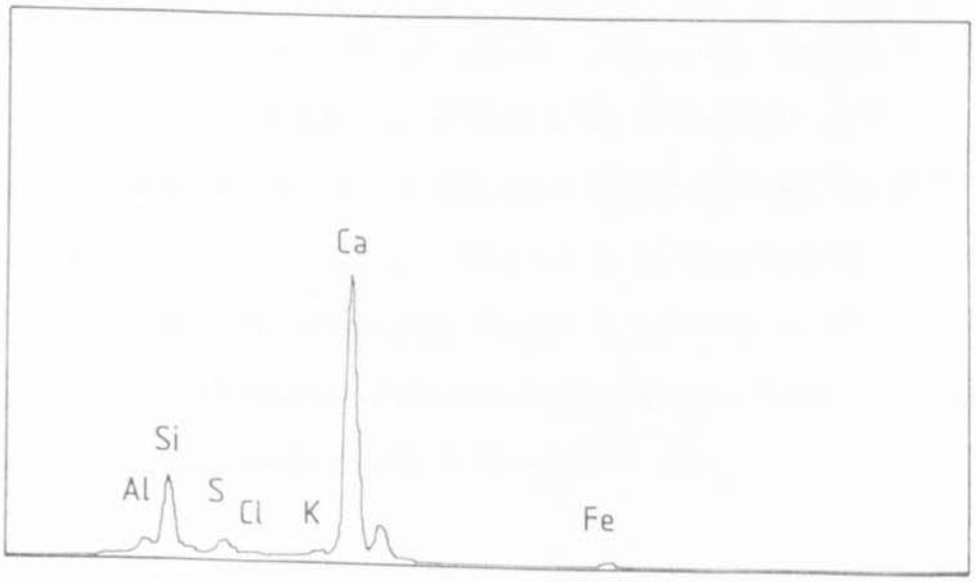

Figure 5.23: Area EDXA of the uncarbonated portion of fly ash cement mortar specimen contaminated with $Cl+SO_4$

scanning electron micrograph of the carbonated portion of the contaminated fly ash cement mortar specimen. This micrograph indicated a dense C-S-H morphology, with white crystalline formation, probably $CaCO_3$, spread all over C-S-H. The general area analysis (Figure 5.25) indicated the presence of Ca (76%), Si (10%) and Al (2%). The scanning electron micrograph for the uncarbonated portion of silica fume cement mortar shown in Figure 5.26, indicated a fibrous structure of the C-S-H gel. The area EDX analysis (Figure 5.27) indicated the presence of Ca (73%), Si (15.7%), Al (1.5%), Cl (1.71%) and S (3.8%). The SEM micrograph for the carbonated silica fume blended cement mortar specimen, shown in Figure 5.28, indicated a dense C-S-H with the presence of concentrated white $CaCO_3$ crystals spread all over it. The EDX analysis, (Figure 5.29), indicated a similar composition as that of the uncarbonated specimen (Figure 5.27). The SEM analysis of the uncarbonated blast furnace slag cement mortar specimen, shown in Figure 5.30, indicated it to be platy C-S-H structure with the presence of white amorphous formations at isolated spots. The area EDX analysis (Figure 5.31) indicated the presence of Ca (58%), Si (28.2%), Al (4%) and S (2.1%). The presence of other elements, such as Na, Mg, K and Fe, in insignificant quantities was also indicated. The scanning electron micrograph of the carbonated portion, (Figure 5.32), at a similar magnification as the uncarbonated portion, indicated a disintegrated C-S-H with the predominant presence of the crystalline formations covering it at isolated spots. These formations lumped together at isolated spots to form crystals bigger than that in the uncarbonated portion. The EDX analysis (Figure 5.33) indicated the presence of Ca (58%), Si (27%), Al (3.7%) and S (4.8%). The EDX analysis of the crystalline formations (Figure 5.34) indicated it to be mainly Ca (72.5%) with little Si (9.8%) and S (11.2%).

In general, the SEM micrographs of the contaminated plain and blended cement mortar specimens indicated the transformation of fibrous to platy C-S-H structure to a more dense structure due to carbonation. While this trend can be generalized for OPC,

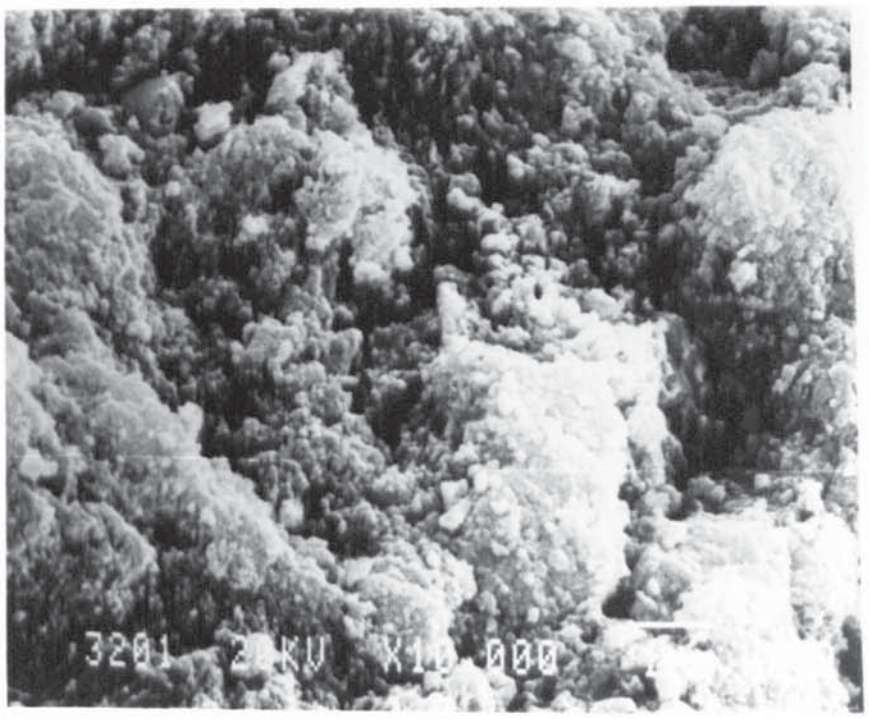

Figure 5.24: Scanning electron micrograph of the carbonated portion of fly ash cement mortar specimen contaminated with $Cl+SO_4$

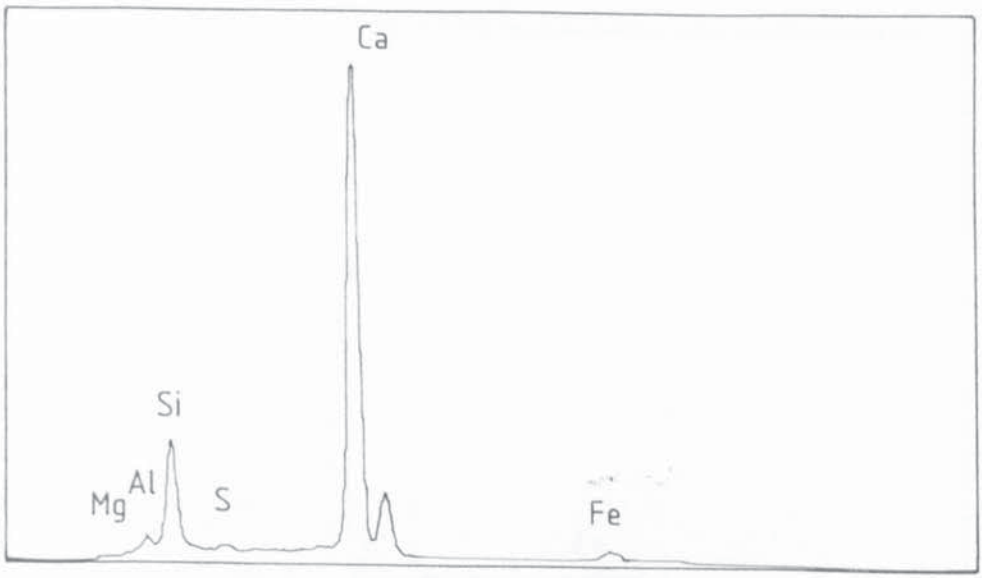

Figure 5.25: Area EDXA of the carbonated portion of fly ash cement mortar specimen contaminated with $Cl+SO_4$

Figure 5.26: Scanning electron micrograph of the uncarbonated portion of silica fume cement mortar specimen contaminated with $Cl+SO_4$

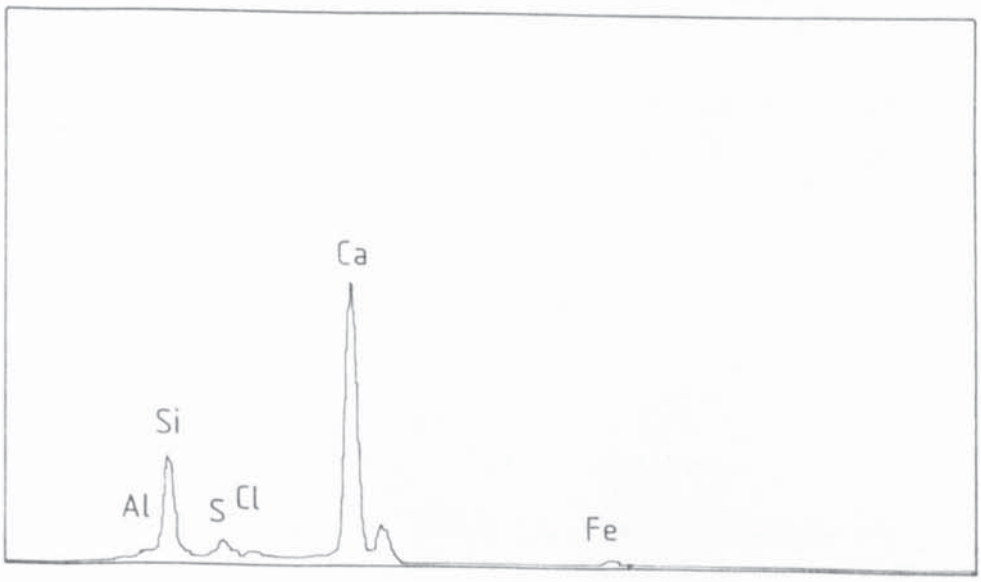

Figure 5.27: Area EDXA of the uncarbonated portion of silica fume cement mortar specimen contaminated with $Cl+SO_4$

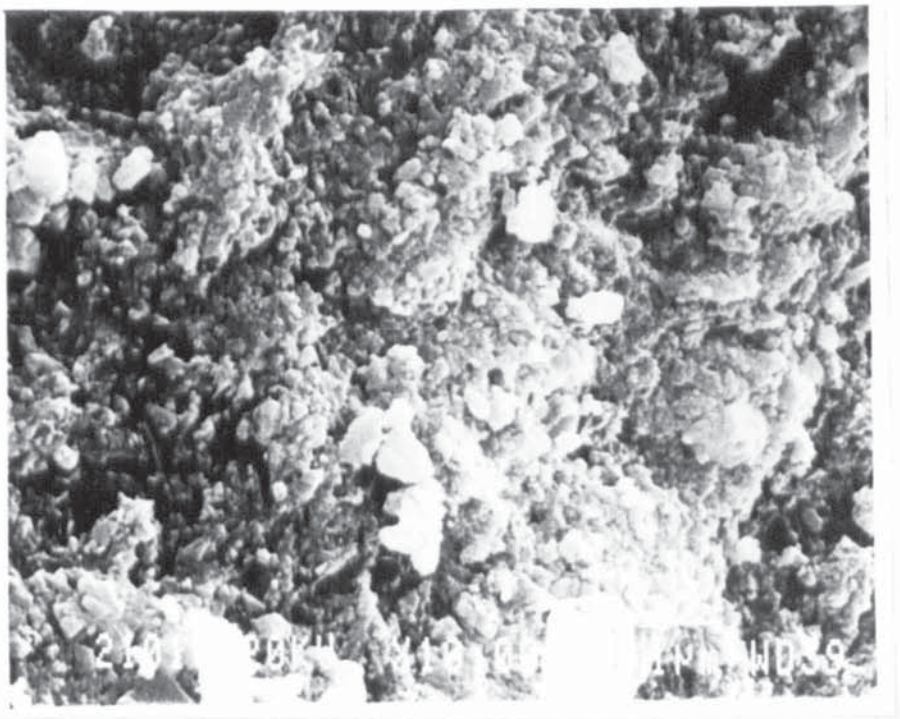

Figure 5.28: Scanning electron micrograph of the carbonated portion of silica fume cement mortar specimen contaminated with $Cl+SO_4$

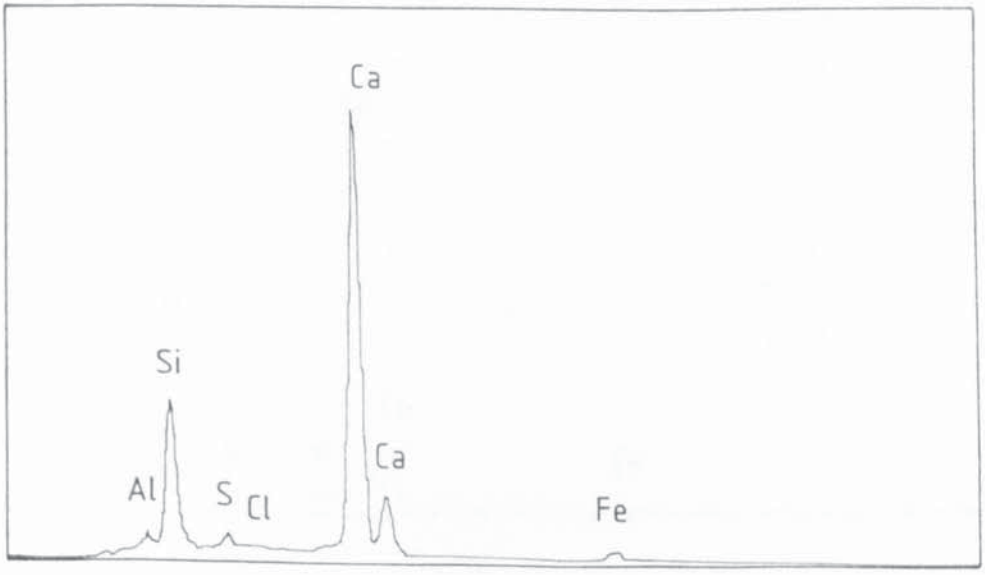

Figure 5.29: Area EDXA of the carbonated portion of silica fume cement mortar specimen contaminated with $Cl+SO_4$

Figure 5.30: Scanning electron micrograph of the uncarbonated portion of BFS cement mortar specimen contaminated with $Cl+SO_4$

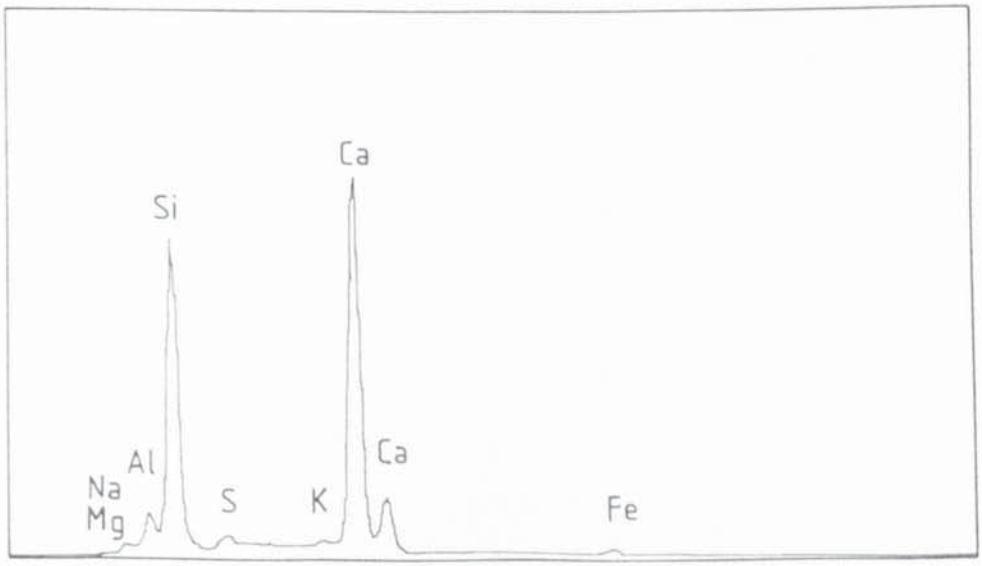

Figure 5.31: Area EDXA of the uncarbonated portion of BFS cement mortar specimen contaminated with $Cl+SO_4$

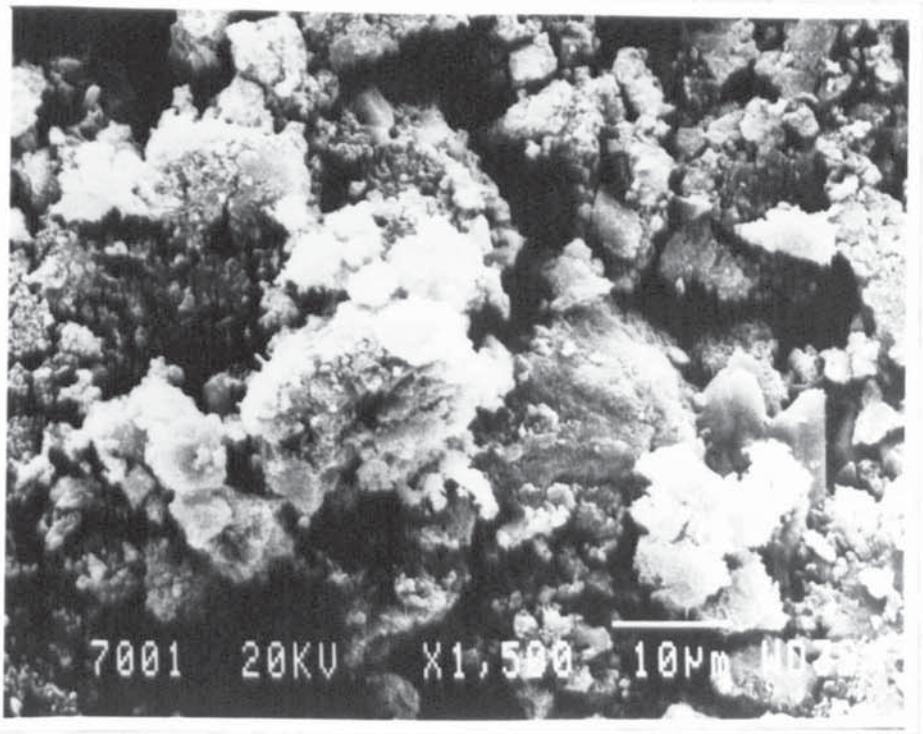

Figure 5.32: Scanning electron micrograph of the carbonated portion of BFS cement mortar specimen contaminated with $Cl+SO_4$

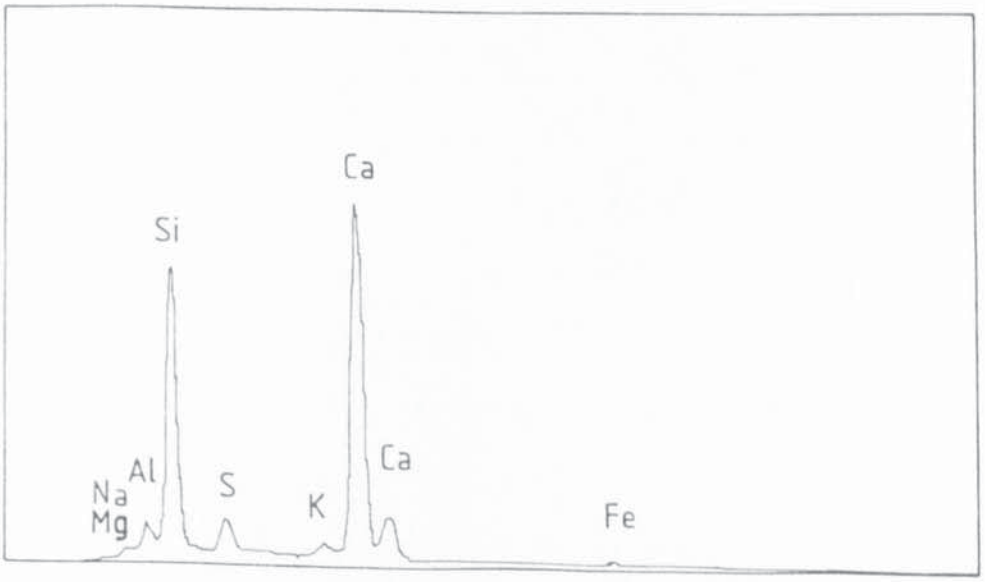

Figure 5.33: Area EDX analysis of the carbonated portion of BFS cement mortar specimen contaminated with $Cl+SO_4$

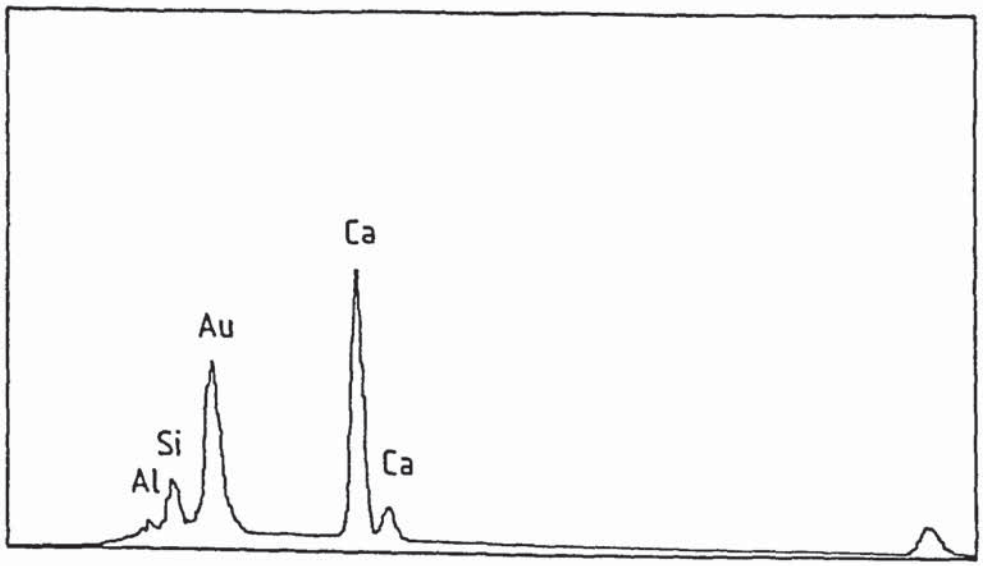

Figure 5.34: EDX analysis of the crystal formations in the carbonated portion of BFS cement mortar specimens contaminated with $Cl+SO_4$

fly ash and silica fume cements, disintegration of the C-S-H due to carbonation was observed in the blast furnace slag cement. However, it may be noted that SEM technique has a severe limitation in that the observation at a location relates to a very small area and one has to be cautious in interpreting the results based on this technique.

5.4.5 XRD Analysis

The X-ray diffractogram for the uncarbonated portion of OPC-A mortar specimen is shown in Figure 5.35. This diffractogram indicated the presence of quartz (SiO_2), portlandite ($Ca(OH)_2$), and calcite. The X-ray diffractogram for the carbonated portion (Figure 5.36) shows the peaks for the same compounds, except that the quantity of portlandite formed in the carbonated sample was slightly lesser than that in the uncarbonated portion. Similarly, the peak for calcite in the carbonated portion becomes slightly more significant than in the uncarbonated portion. The quantitative analysis indicated that the portlandite decreases from 17 to 13% due to carbonation, whereas calcite constituted 12% of the carbonated portion. The insignificant change in the $Ca(OH)_2$ content due to carbonation in the uncontaminated specimens indicates that practically no carbonation has taken place in these specimens. These findings corroborate the results of carbonation depth determined by phenolphthalein solution, which indicated minimum carbonation in the uncontaminated specimens. The X-ray diffractogram for the carbonated portion of the OPC mortar specimens contaminated with sodium chloride plus sodium sulfate is plotted in Figure 5.37. The formation of calcium carbonate and portlandite can be discerned in these specimens. In the carbonated specimen, Figure 5.38, formation of quartz and calcite was only discerned. The X-ray diffractogram for the uncarbonated fly ash cement mortar specimen contaminated with sodium chloride plus sodium sulfate, is plotted in Figure 5.39. This diffractogram indicated the formation of quartz, calcite and portlandite. Quartz constituted about 59% of cement, whereas calcite was 21%. The X-ray peaks for the

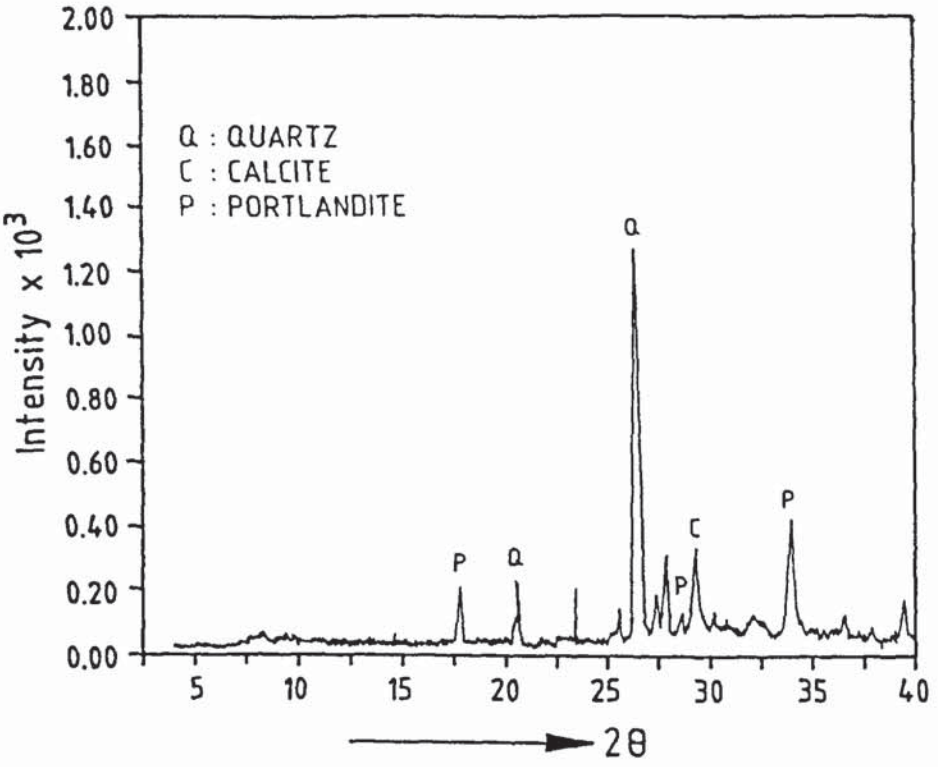

Figure 5.35: X-ray diffractogram for uncarbonated portion of uncontaminated OPC mortar specimen

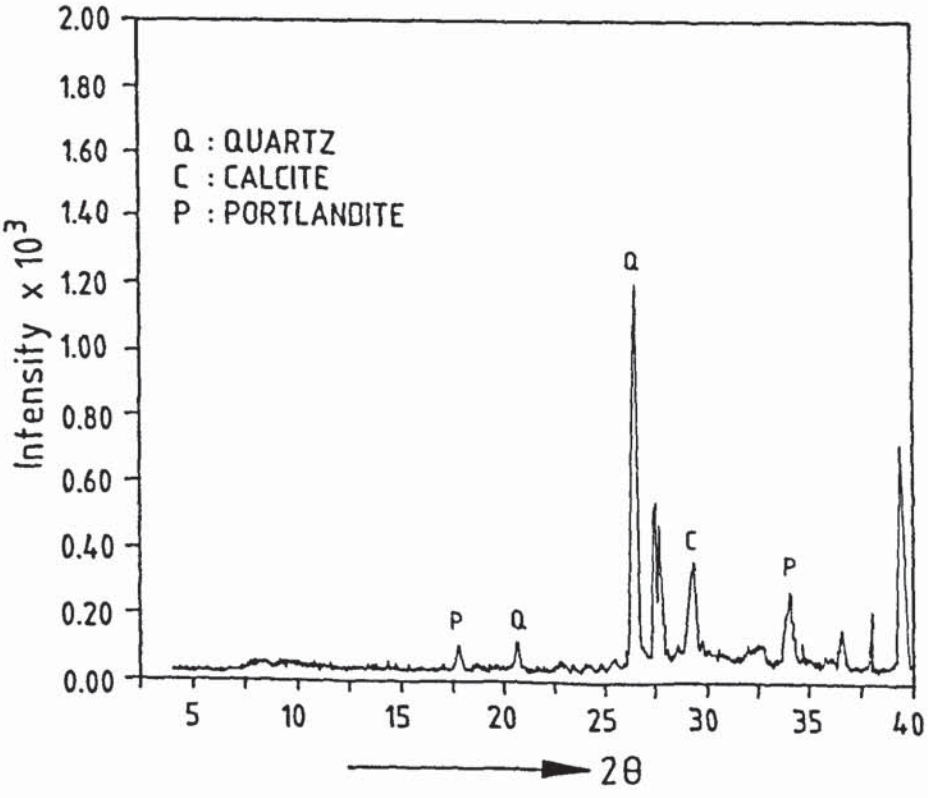

Figure 5.36: X-ray diffractogram for carbonated portion of uncontaminated OPC mortar specimen

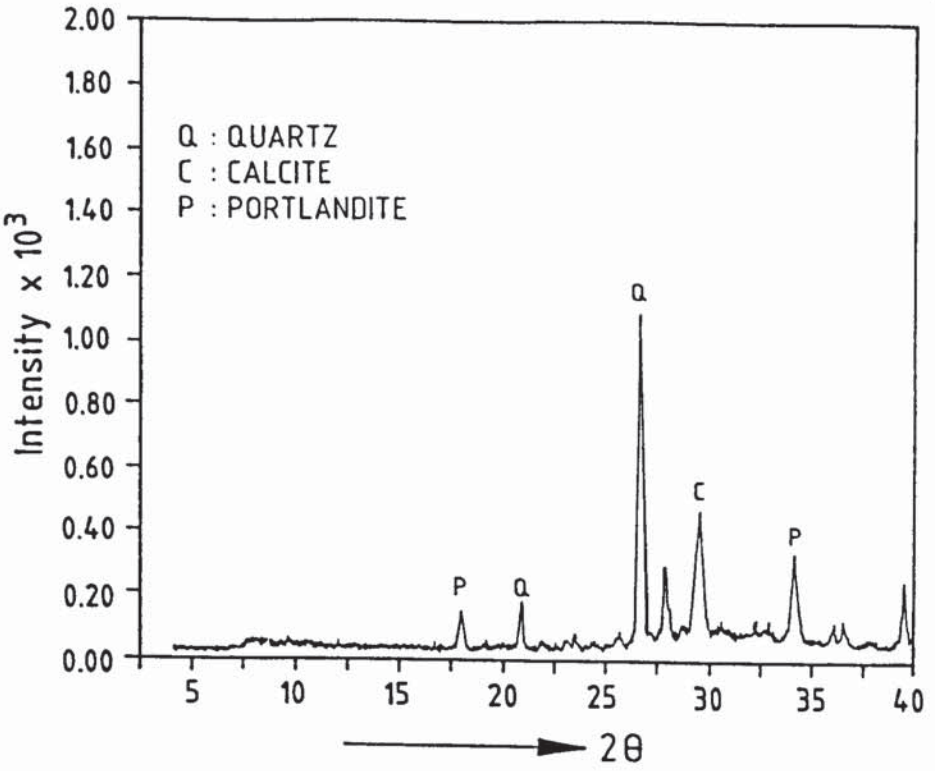

Figure 5.37: X-ray diffractogram for uncarbonated portion of OPC mortar specimen contaminated with Cl+SO_4

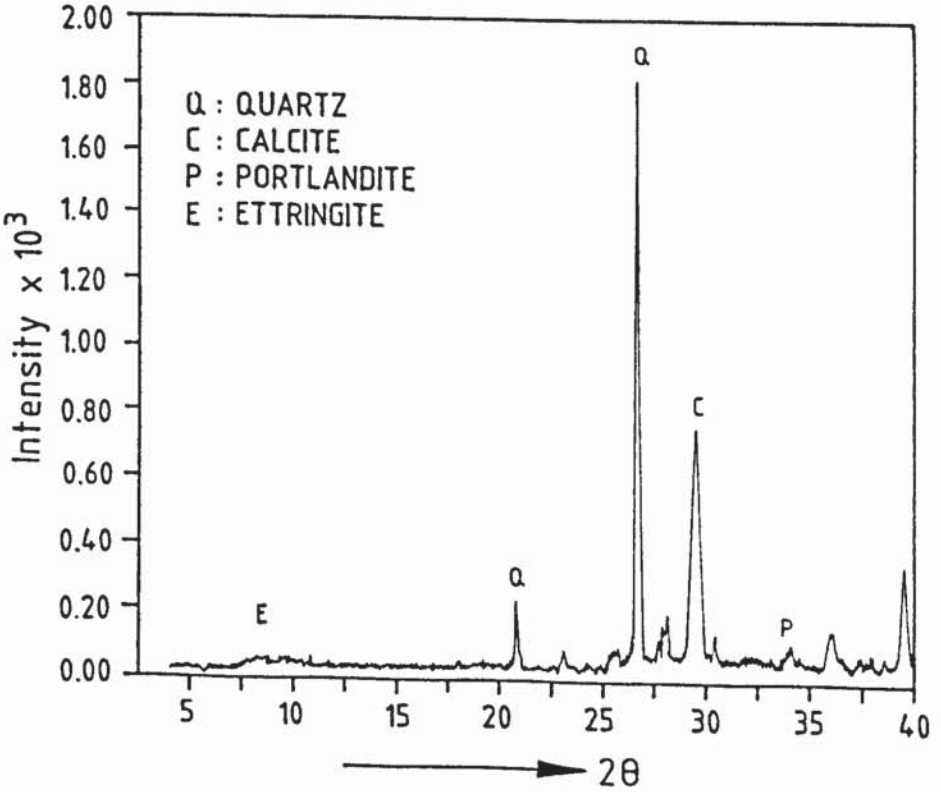

Figure 5.38: X-ray diffractogram for carbonated portion of OPC mortar specimen contaminated with Cl+SO_4

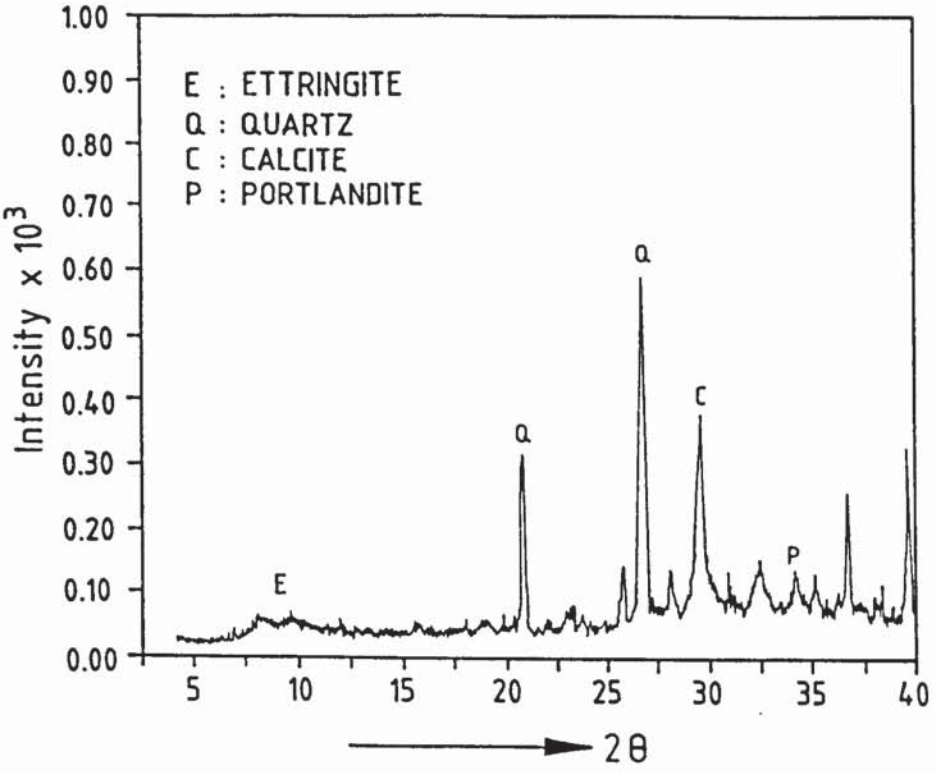

Figure 5.39: X-ray diffractogram for uncarbonated portion of fly ash cement mortar specimen contaminated with $Cl+SO_4$

carbonated portion, Figure 5.40, indicated the formation of quartz, calcite and aragonite. Quartz and calcite constituted about 57 and 23%, respectively, by weight of cement. In addition to calcite, formation of aragonite, 12%, was also discerned. Further, the quantum of portlandite which was observed in the uncarbonated sample was virtually eliminated in the carbonated portion. The X-ray diffractogram for the uncarbonated silica fume blended cement mortar specimen contaminated with sodium chloride plus sodium sulfate is shown in Figure 5.41. The X-ray peaks indicated formation of quartz and calcium carbonate. The peaks for portlandite were not discerned in this diffractogram. The absence of the portlandite peak may be attributed to the pozzolanic action between the silica fume and calcium hydroxide, which virtually consumes all the portlandite due to the highly reactive nature of this pozzolanic material. The X-ray diffractogram for the carbonated silica fume cement mortar, shown in Figure 5.42, indicated the presence of quartz and calcite. However, the intensity of these two peaks is slightly higher than that observed in the uncarbonated portions. The X-ray diffractograms for the uncarbonated and carbonated blast furnace slag cement mortar contaminated with sodium chloride plus sodium sulfate are shown in Figure 5.43 and 5.44, respectively. The peaks for the uncarbonated portion indicated that it consists mainly of quartz. The quantitative analysis indicated the presence of a very small amount (2%) of calcium hydroxide in the uncarbonated specimen, whereas quartz and calcite constituted 70 and 12%, respectively. The X-ray diffractogram for the carbonated portion indicate the presence of quartz, calcite and aragonite (Figure 5.44). The quantitative analysis indicated that quartz constituted about 54%, whereas calcite and aragonite constituted about 15 and 10%, respectively. The 2% $Ca(OH)_2$ observed in the uncarbonated specimen is not discerned in the carbonated portion.

In general, the X-ray diffraction data indicated formation of calcium carbonate in the carbonated and uncarbonated portions of the contaminated specimens. However, the quantity of $CaCO_3$, present either in the form of calcite or aragonite, was more in

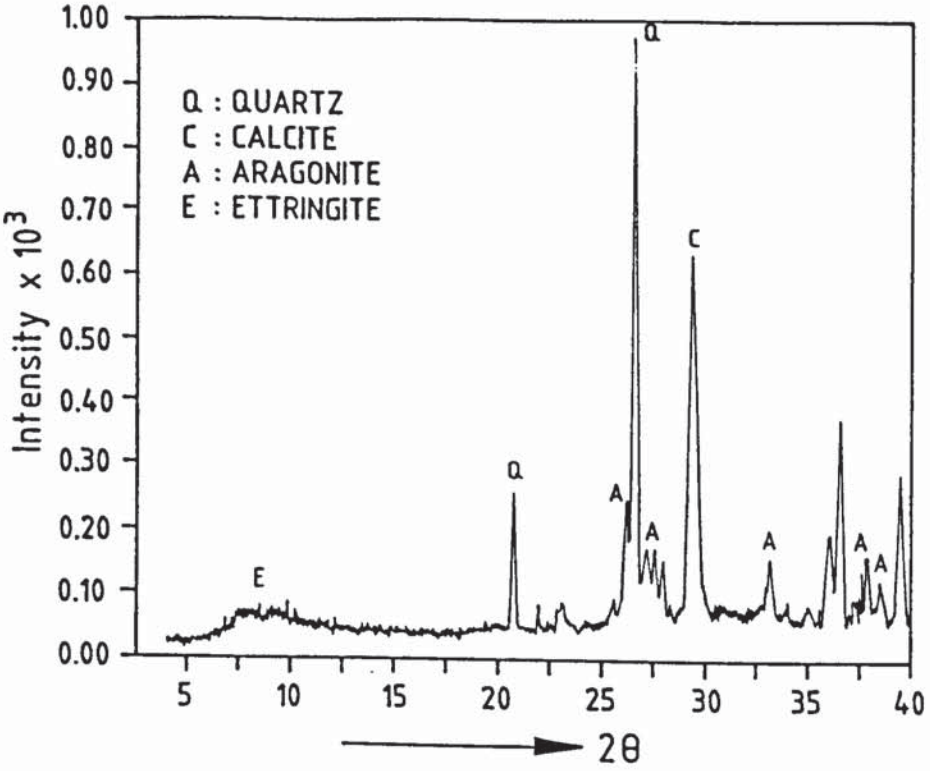

Figure 5.40: X-ray diffractogram for carbonated portion of fly ash cement mortar specimen contaminated with $Cl+SO_4$

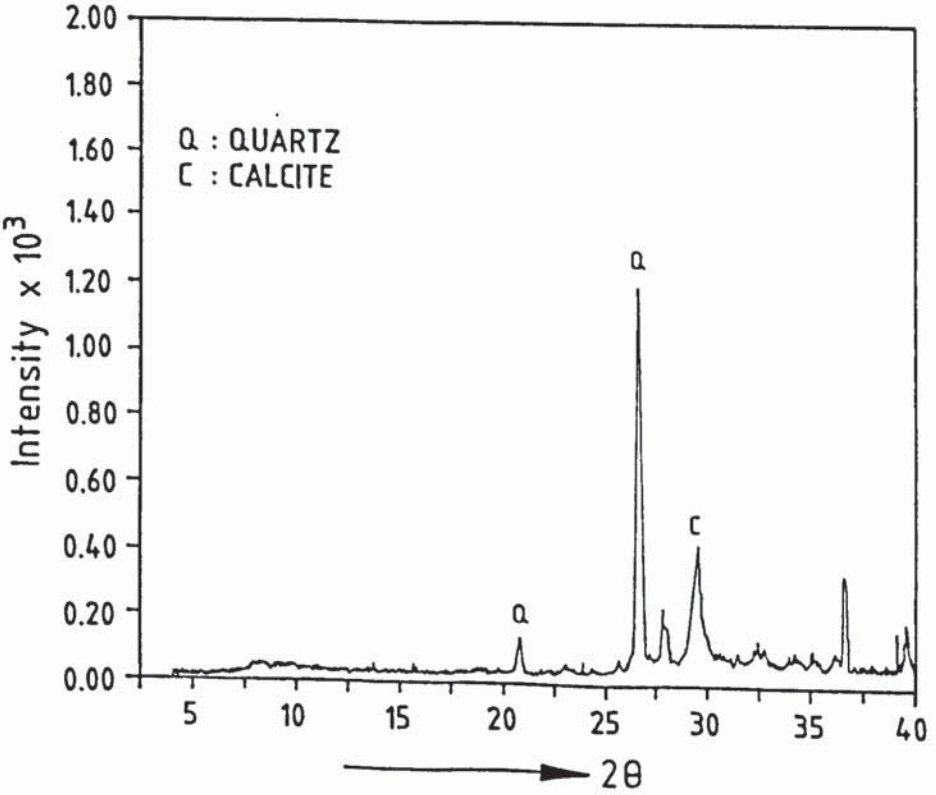

Figure 5.41: X-ray diffractogram for uncarbonated portion of silica fume cement mortar specimen contaminated with $Cl+SO_4$

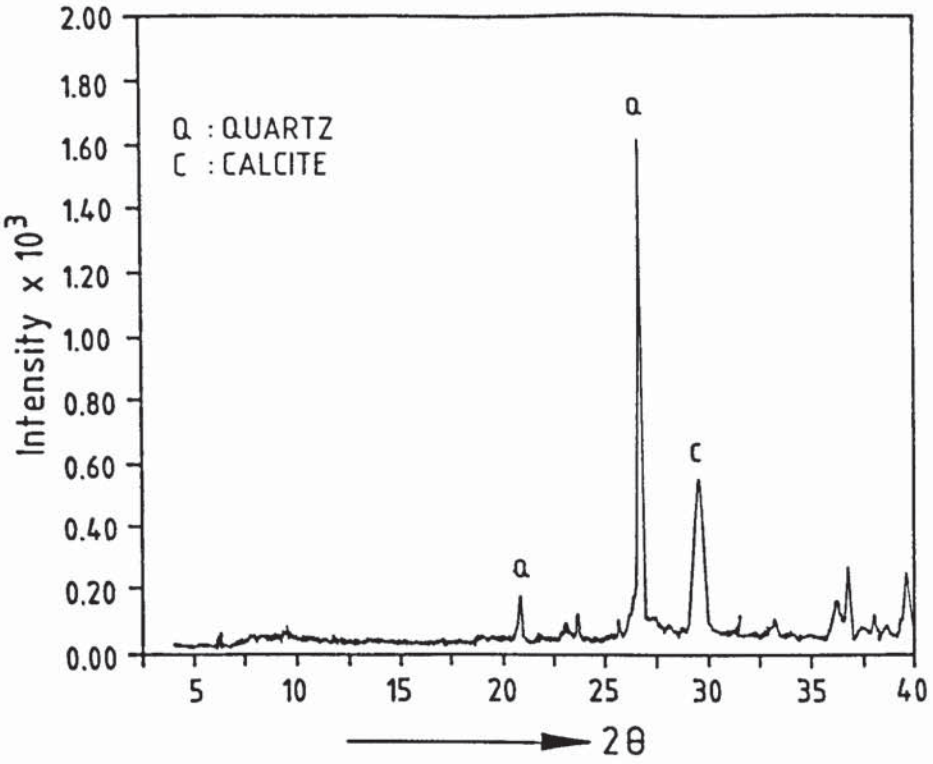

Figure 5.42: X-ray diffractogram for carbonated portion of silica fume cement mortar specimen contaminated with $Cl+SO_4$

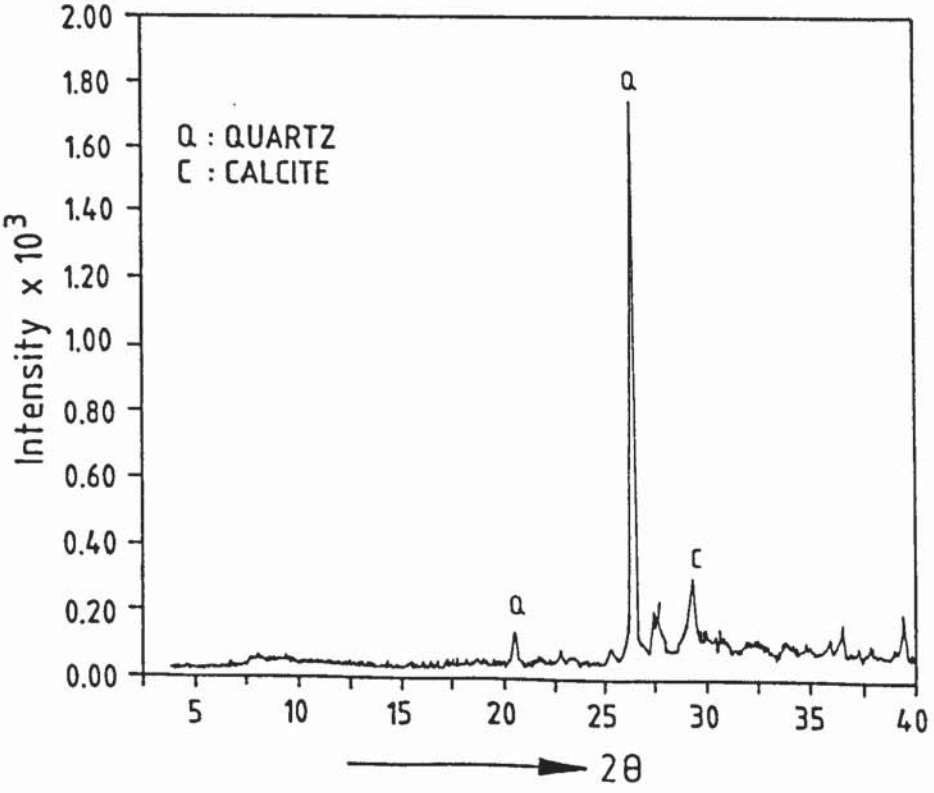

Figure 5.43: X-ray diffractogram for uncarbonated portion of BFS cement mortar specimen contaminated with $Cl+SO_4$

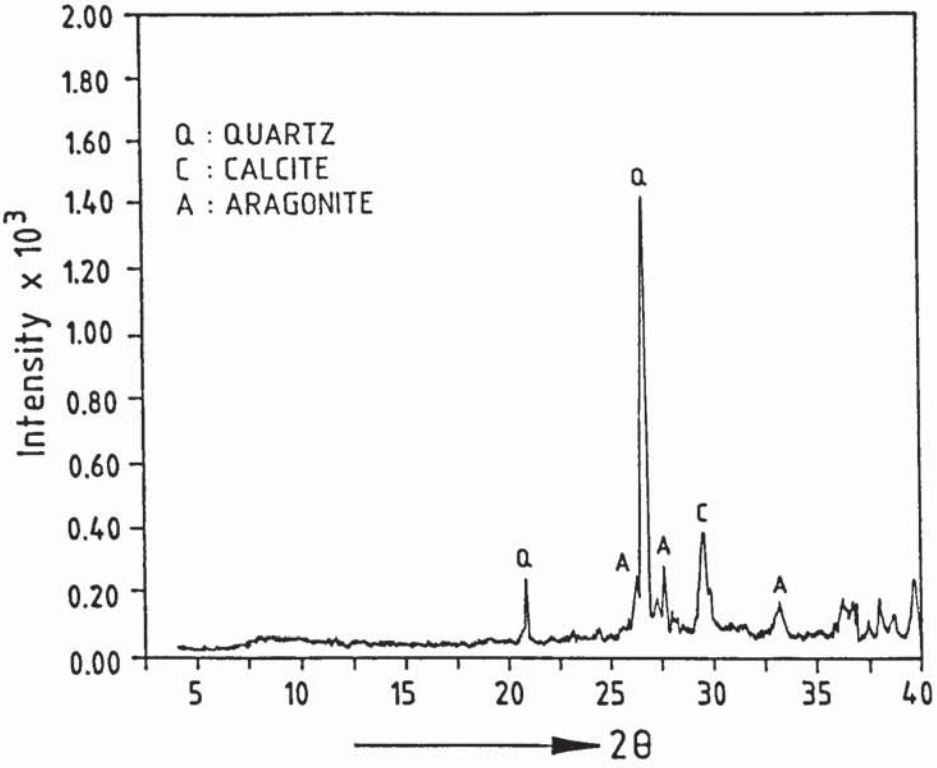

Figure 5.44: X-ray diffractogram for carbonated portion of BFS cement mortar specimens contaminated with $Cl+SO_4$

the carbonated specimens than that in the uncarbonated specimens. This trend was observed in both the OPC and blended cement mortar specimens. In the carbonated blended cements, silica fume and blast furnace slag in particular, formation of $CaCO_3$ may be attributed to the decomposition of C-S-H and other cement hydration products.

5.4.6 Differential Thermal Analysis

The differential thermal analysis (DTA) and thermogravimetry (TG) curves for the uncarbonated portion of the uncontaminated OPC mortar are plotted in Figure 5.45. The DTA curve indicated the formation of endothermic peaks at 450 and 850 °C for $Ca(OH)_2$ and $CaCO_3$, respectively. The $Ca(OH)_2$ and $CaCO_3$ content of this specimen calculated from the TG curves was 5.48 and 2.05%, respectively. The DTA and TG curves for the carbonated portion of the same specimen are shown in Figure 5.46. The DTA curve again indicated the formation of endothermic peaks corresponding to $Ca(OH)_2$ and $CaCO_3$. The endothermic peak for $Ca(OH)_2$ for this specimen, was however, more shallow than that in the uncarbonated portion and the peak for $CaCO_3$ tended to become deep. The $Ca(OH)_2$ and $CaCO_3$ content in this portion was calculated to be 2.3 and 7.7%, respectively, by weight of cement. Figures 5.47 and 5.48 depict the DTA and TG curves for the uncarbonated and carbonated portions of the uncontaminated fly ash cement mortar specimens, respectively. The DTA curves for these two specimens also indicated the presence of $Ca(OH)_2$ and $CaCO_3$. The $Ca(OH)_2$ content in the uncarbonated and carbonated portion was 3.13 and 2.3%, respectively. The $CaCO_3$ content in these specimens was 3.11 and 4.45% by weight of cement, respectively.

The DTA and TG curves for the uncarbonated OPC mortar, contaminated with only sodium chloride, are plotted in Figure 5.49. The formation of endothermic peaks

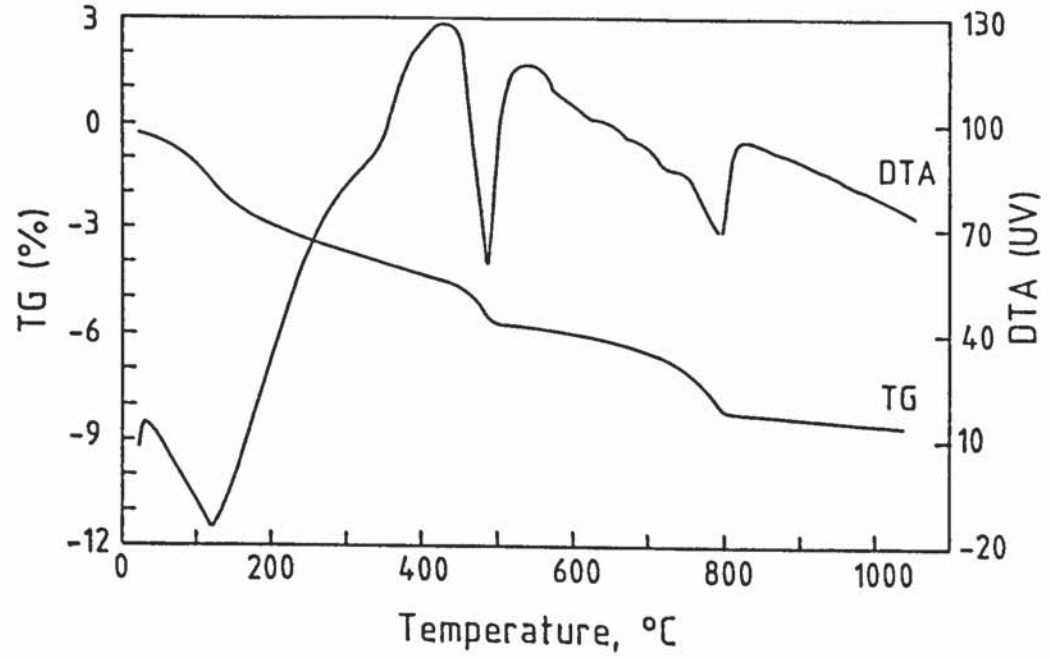

Figure 5.45: DTA/TG curves for uncarbonated portion of uncontaminated OPC mortar specimen

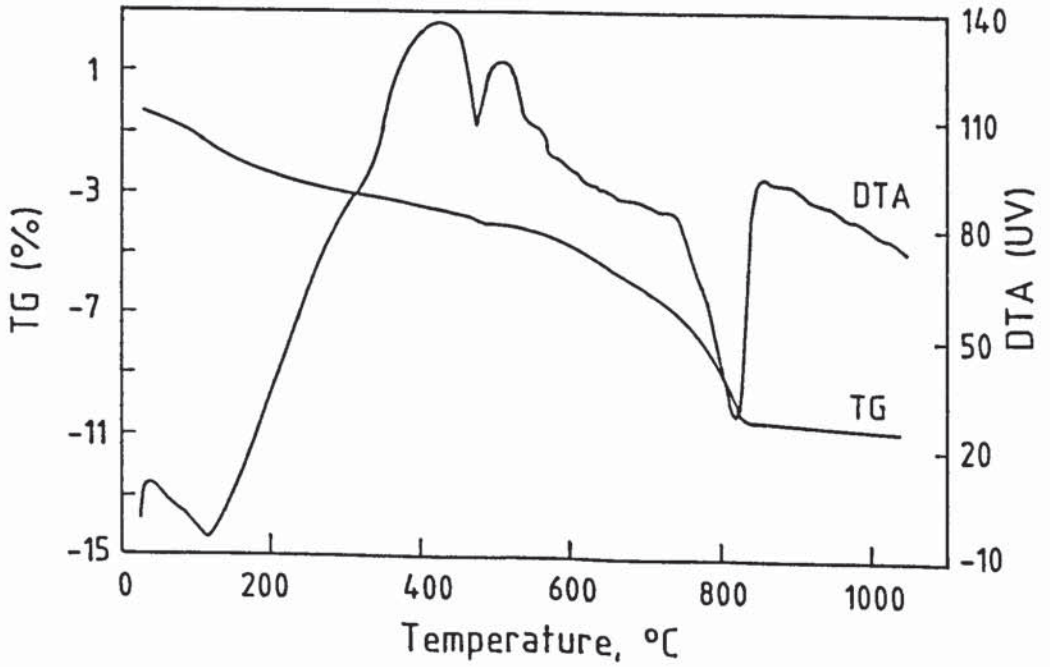

Figure 5.46: DTA/TG curves for carbonated portion of uncontaminated OPC mortar specimen

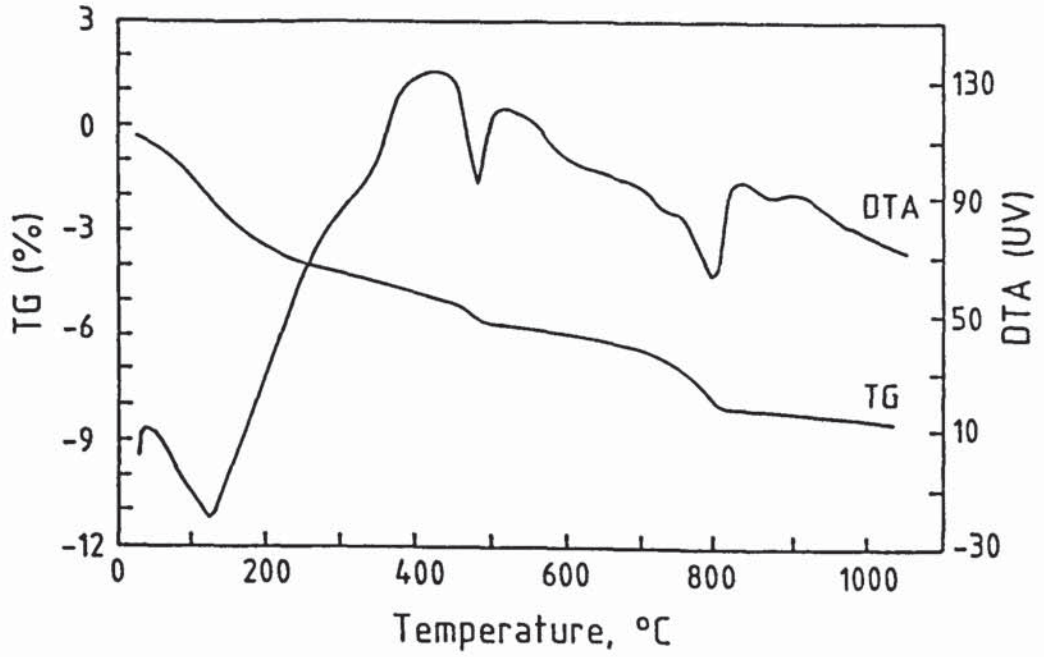

Figure 5.47: DTA/TG curves for uncarbonated portion of uncontaminated fly ash cement mortar specimen

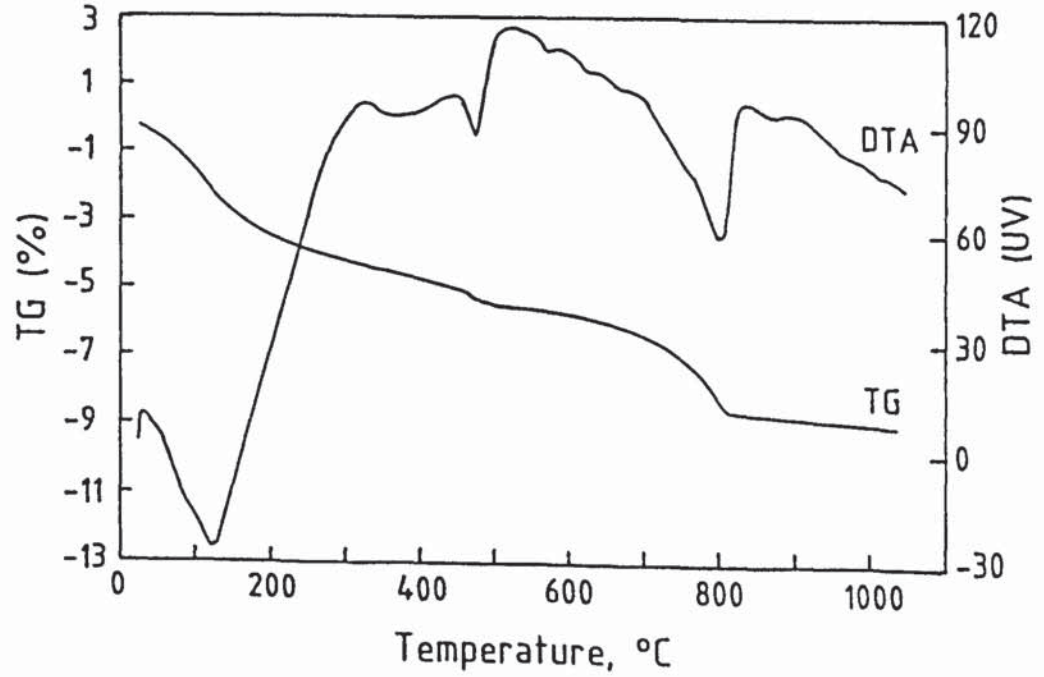

Figure 5.48: DTA/TG curves for carbonated portion of uncontaminated fly ash cement mortar specimen

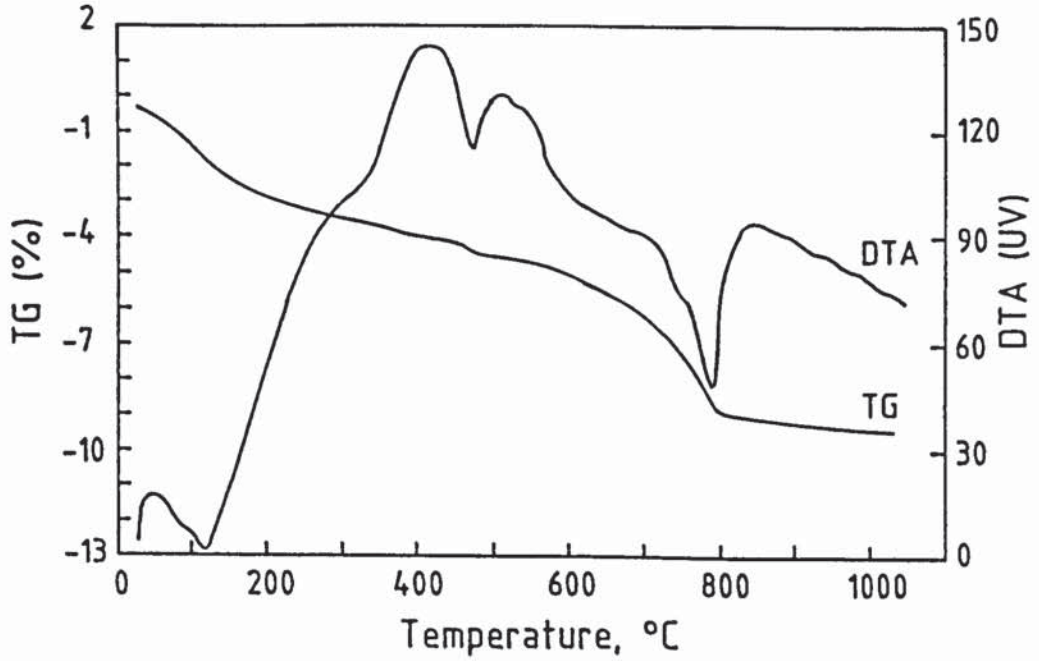

Figure 5.49: DTA/TG curves for the uncarbonated portion of chloride-contaminated OPC mortar specimens

for $Ca(OH)_2$ and $CaCO_3$ are indicated in this specimen, whereas in the carbonated portion, the endothermic peak for $Ca(OH)_2$ was not detected (Figure 5.50). The $Ca(OH)_2$ and $CaCO_3$ content in the uncarbonated portion was 3.03 and 4.93%, respectively. In the carbonated portion the $CaCO_3$ content was 5.78%. The DTA and TG curves for the uncarbonated OPC mortar specimen contaminated with sodium chloride plus sodium sulfate are plotted in Figure 5.51. These curves indicated the presence of both $Ca(OH)_2$ and $CaCO_3$. The quantity of these compounds was 2.06 and 4.80%, respectively. Figure 5.52 shows the DTA and TG curves for the carbonated OPC mortar contaminated with sodium chloride plus sodium sulfate. The DTA curve indicated the formation of an endothermic peak for $CaCO_3$ only. The weight of $CaCO_3$ in this specimen was 7.06%. The DTA and TG curves for the uncarbonated fly ash cement mortar contaminated with sodium chloride plus sodium sulfate are plotted in Figure 5.53. Formation of $Ca(OH)_2$ and $CaCO_3$ was indicated by the DTA curve. The weights of $Ca(OH)_2$ and $CaCO_3$ were 1.98 and 2.23%. Figure 5.54 shows the DTA and TG curves for the carbonated portion of the same specimen. The weights of $Ca(OH)_2$ and $CaCO_3$ were 1.52 and 2.46%, respectively. The DTA and TG curves for the uncarbonated silica fume cement mortar contaminated with sodium chloride plus sodium sulfate are shown in Figure 5.55. Formation of only $CaCO_3$ was indicated, the quantum of this compound being 2.87% by weight of cement. The weight of this compound in the carbonated portion (Figure 5.56) was 2.95%. The endothermic peak for $Ca(OH)_2$ was not detected in either the carbonated or the uncarbonated portion. Figures 5.57 and 5.58 show the DTA and TG curves for the uncarbonated and carbonated portions of blast furnace slag cement mortar specimen. In these specimens also formation of endothermic peaks conforming to $Ca(OH)_2$ were not detected. The weight of $CaCO_3$ was 2.66 and 4.48%, respectively.

In general, the data on $Ca(OH)_2$ and $CaCO_3$, developed using DTA and TG techniques also indicated greater carbonation in the contaminated cements than in the

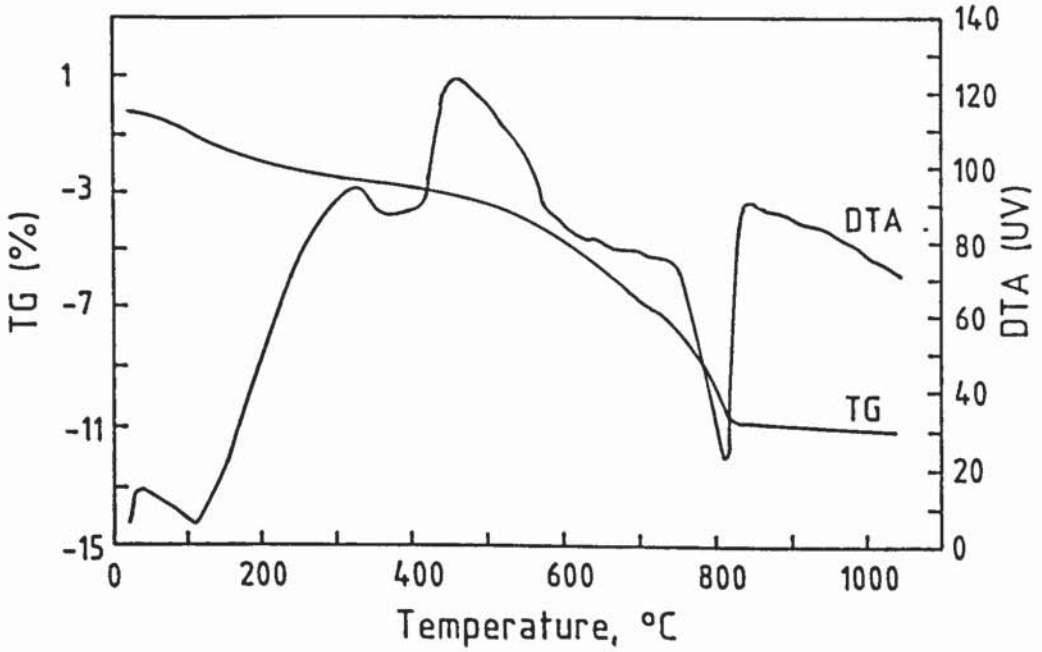

Figure 5.50: DTA/TG curves for the carbonated portion of chloride-contaminated OPC mortar specimens

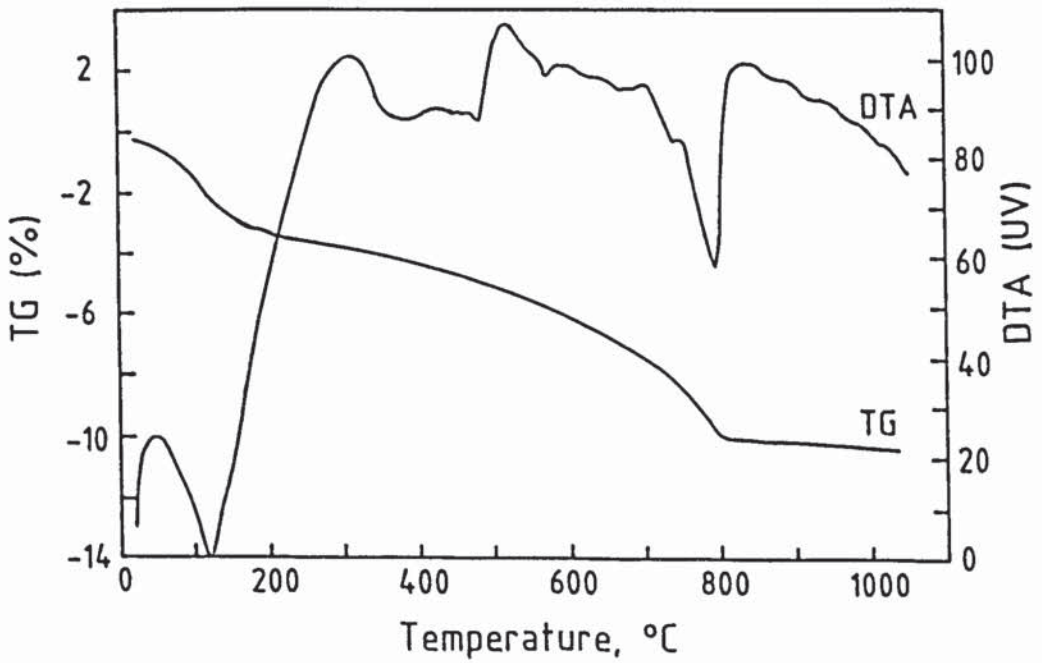

Figure 5.51: DTA/TG curves for the uncarbonated portion of OPC mortar specimen contaminated with $Cl+SO_4$

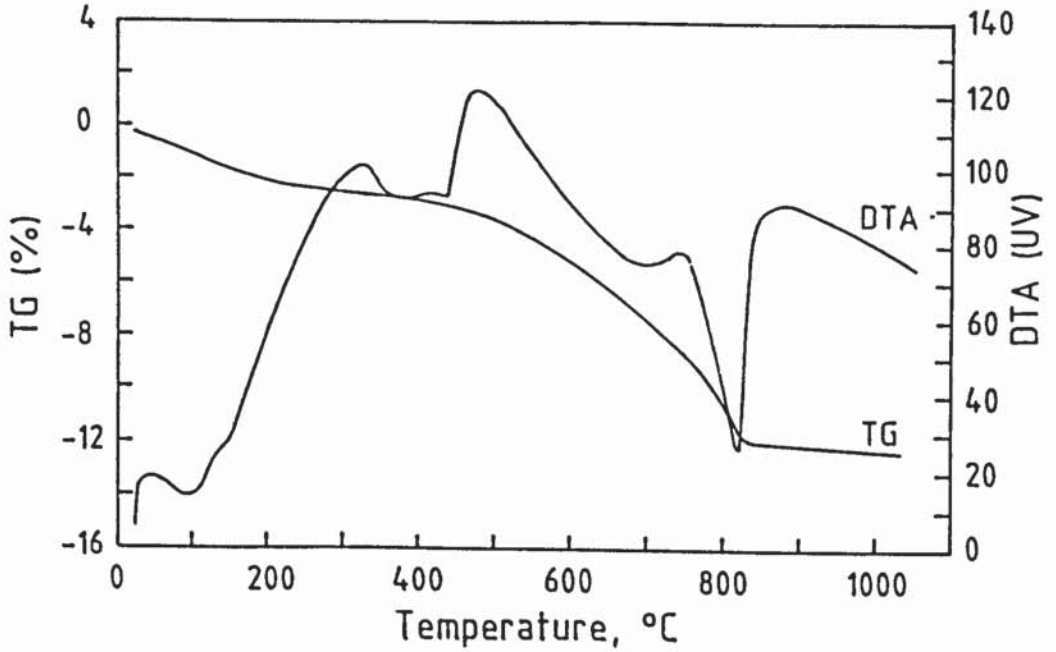

Figure 5.52: DTA/TG curves for the carbonated portion of OPC mortar specimen contaminated with $Cl+SO_4$

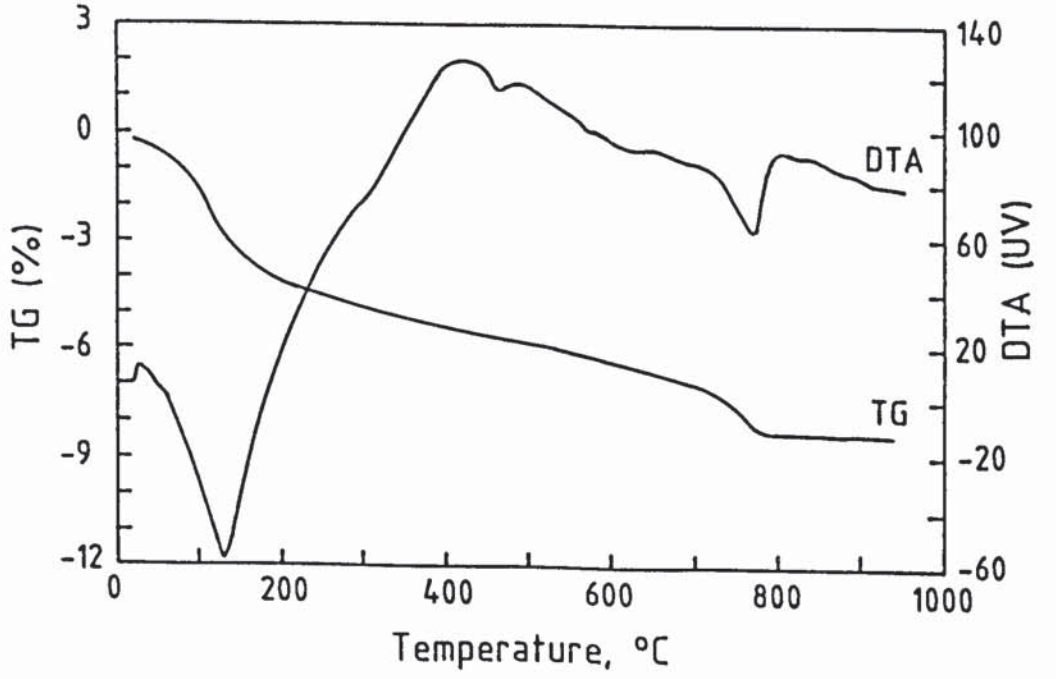

Figure 5.53: DTA/TG curves for the uncarbonated portion of fly ash cement mortar specimen contaminated with $Cl+SO_4$

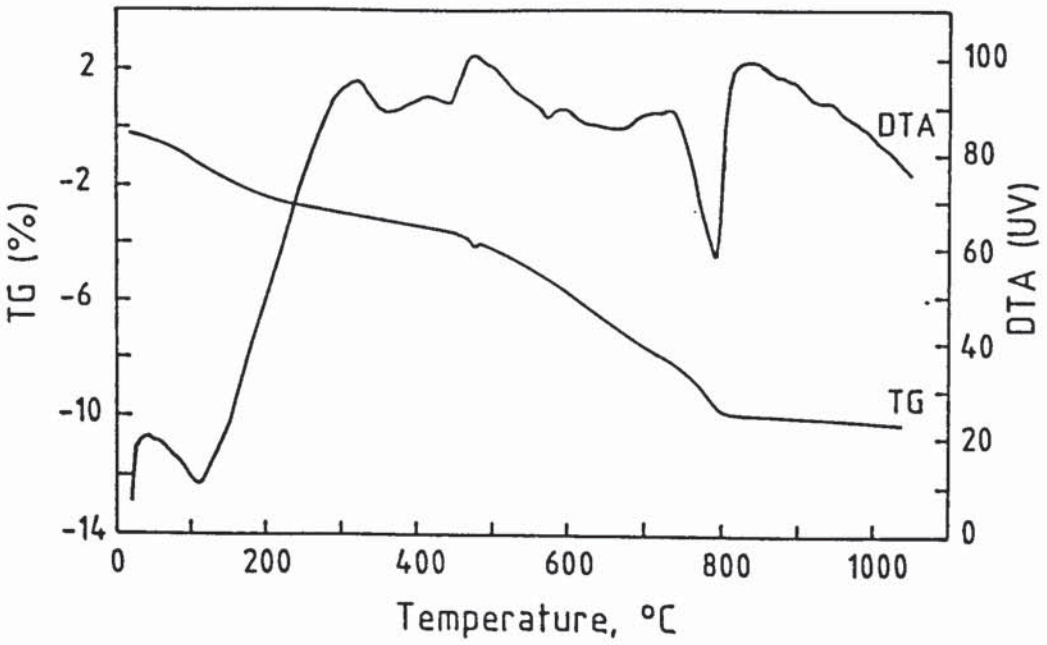

Figure 5.54: DTA/TG curves for the carbonated portion of fly ash cement mortar specimen contaminated with $Cl+SO_4$

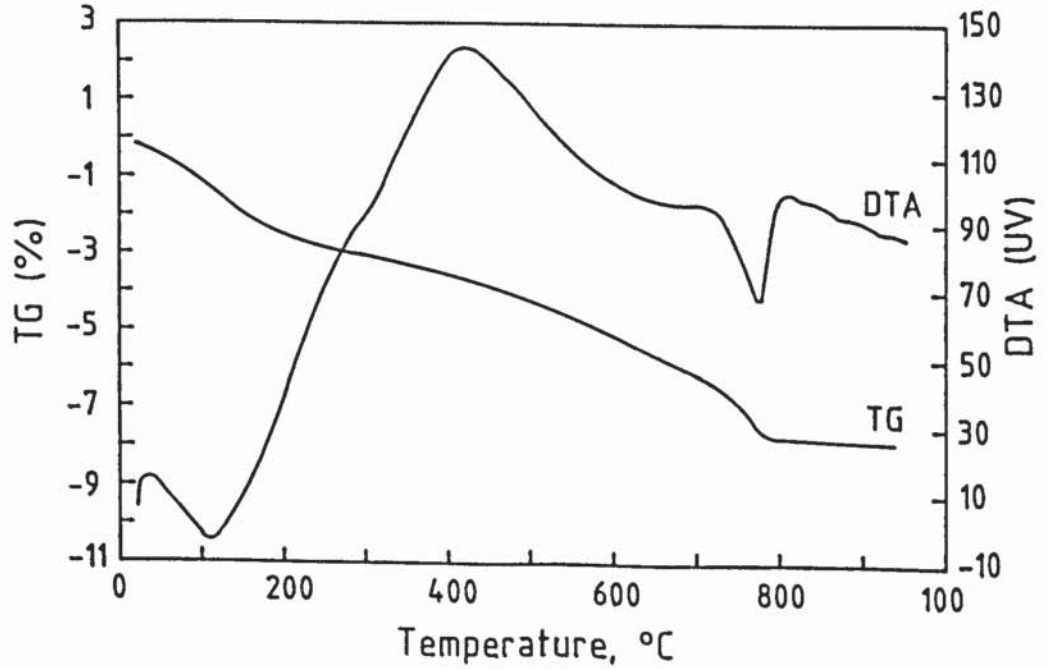

Figure 5.55: DTA/TG curves for the uncarbonated portion of silica fume cement mortar specimen contaminated with $Cl+SO_4$

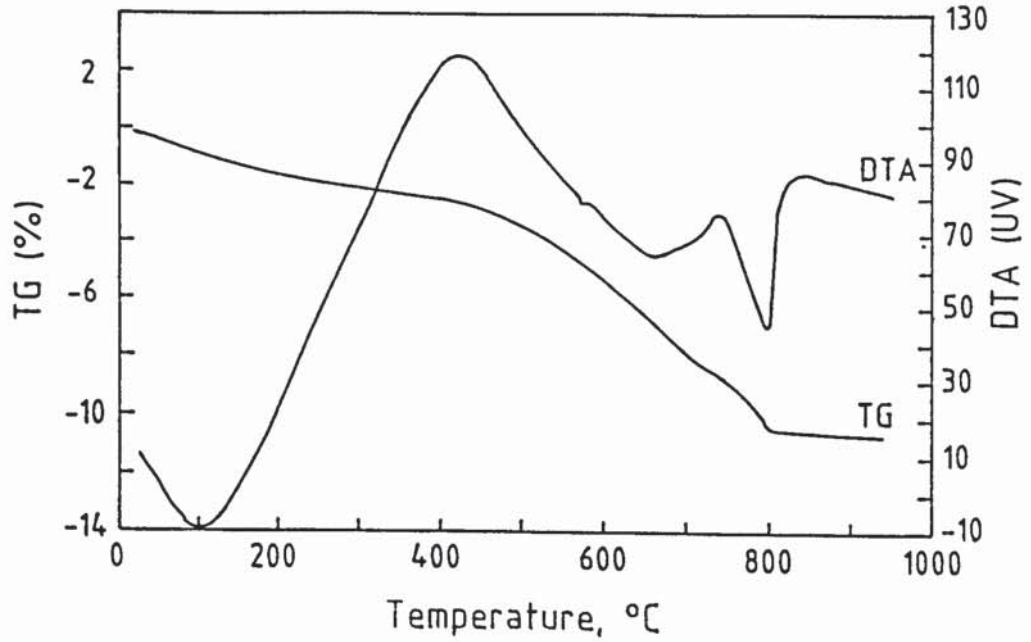

Figure 5.56: DTA/TG curves for the carbonated portion of silica fume cement mortar specimen contaminated with $Cl+SO_4$

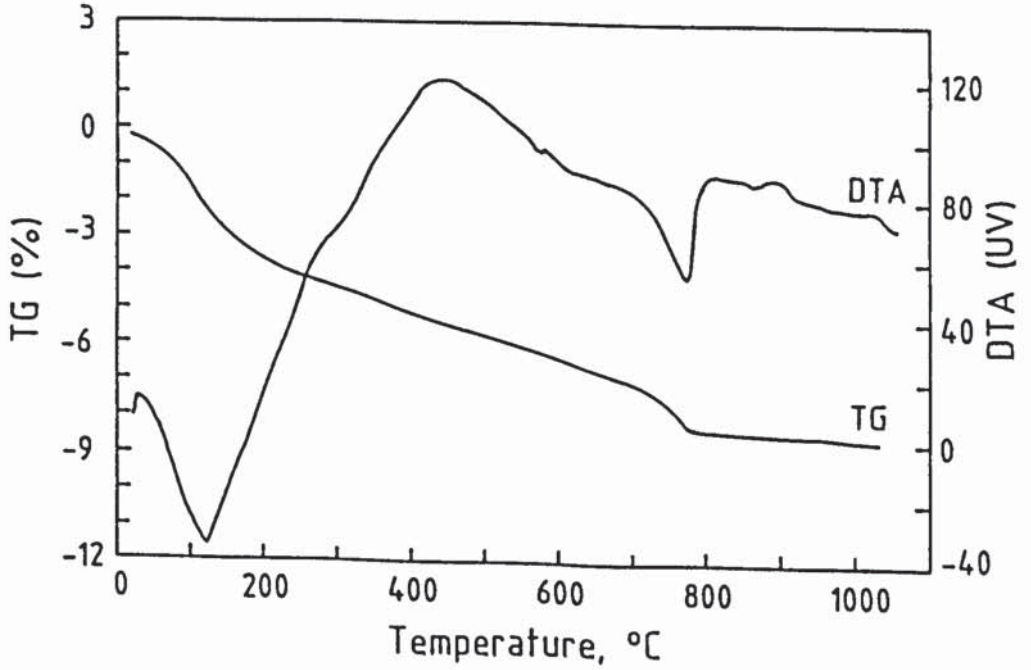

Figure 5.57: DTA/TG curves for the uncarbonated portion of BFS cement mortar specimen contaminated with $Cl+SO_4$

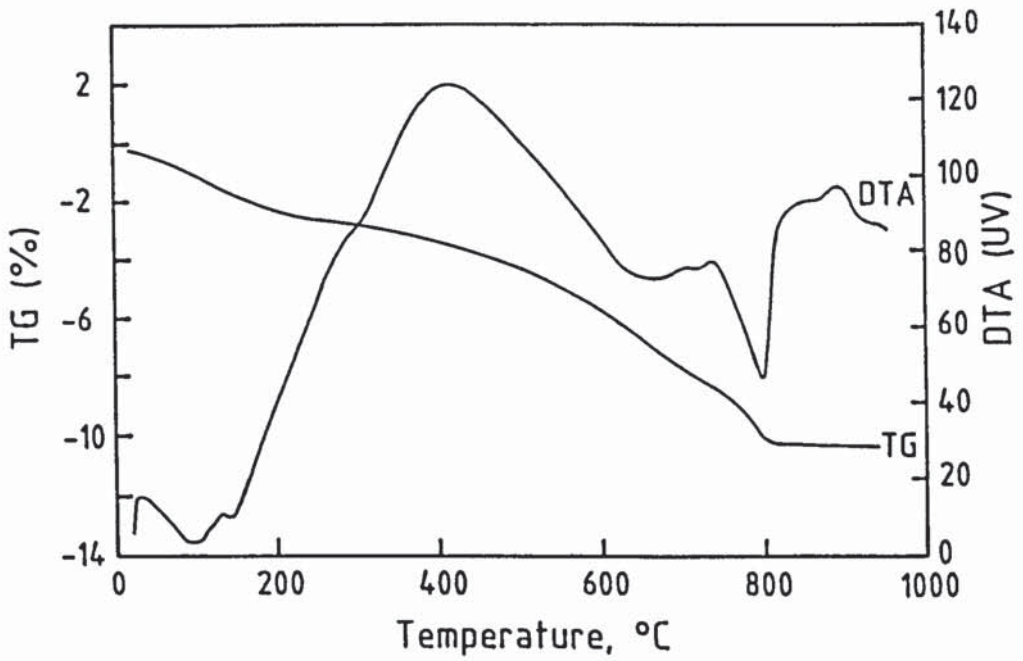

Figure 5.58: DTA/TG curves for the carbonated portion of BFS cement mortar specimen contaminated with $Cl+SO_4$

uncontaminated specimens. This trend was observed both in the plain and blended cement mortar specimens. This is indicated by the greater amount of $CaCO_3$ formed in these specimens partially due to the consumption of $Ca(OH)_2$. The absence of $Ca(OH)_2$ in the uncarbonated silica fume blended cement may be attributed to the pozzolanic reaction which reduces the quantity of portlandite to very insignificant levels. In the blast furnace slag cement the quantum of $Ca(OH)_2$ formed was also very low. The significant quantity of $CaCO_3$ formed in the carbonated portions of these cements, even in the absence of $Ca(OH)_2$, indicates that other cement hydration products may be reacting with CO_2 to produce $CaCO_3$, the main constituent being C-S-H, which is abundantly available for the CO_2 to react.

5.5 DISCUSSION

The data developed through carbonation depth measurements, weight gain, XRD, DTA/TG and SEM analyses indicated greater carbonation in the contaminated specimens than in the uncontaminated specimens. This trend was observed in both plain and blended cements. The increased depth of carbonation observed in the contaminated cement mortar specimens, corroborates the exposure site data developed by Rasheeduzzafar [206]. After 6 years of exposure, the depth of carbonation in the uncontaminated specimens was in the range of 2 to 5 mm, while in the contaminated concrete specimens the depth of carbonation was in the range of 8 to 23 mm, depending on the cement type, being the highest in the 20% silica fume cement and the lowest in the fly ash blended cement. Macmillan and Treadaway [168] indicated that the inclusion of sodium chloride and sodium sulfate increased the depth of carbonation in both the plain and blended cement concrete specimens, though this difference was not consistent in all the specimens investigated. Al-Amoudi et al. [207] evaluated the effect of salt inclusion in OPC/PFA concretes on the alkalinity, carbonation depth and rebar corrosion in specimens exposed to the Arabian Gulf environment for one year.

An insignificant change in the depth of carbonation was observed both in the OPC and fly ash cement concrete specimens due to the salt inclusion. The depth of carbonation was in the range of 3.9 to 5.1 mm in the OPC and in the range of 5.4 to 6.0 mm in the 20% fly ash concrete specimens. The depth of carbonation in the 40% fly ash cement concrete containing 0, 0.17 and 0.34% Cl^- was about 6.8 mm. It, however, increased to about 10 mm when the chloride inclusion was raised to 0.68% by weight of cement. No further increase in the depth of carbonation was observed when the chloride level was raised up to 2.72%. Kayyali and Haque [23] investigated the effect of 1% Cl^-, added as $CaCl_2$, to the mortar specimens made with and without fly ash, on the carbonation depth and pore solution chemistry. The mortar specimens were exposed to accelerated carbonation tests, 5% CO_2, 30 °C and 50% RH. Their results indicated a higher depth of carbonation in the uncontaminated specimens than that in the contaminated specimens, both in the plain and fly ash cement mortar specimens. They attributed this reduced depth of carbonation in the contaminated specimens to the chemical changes brought about by the formation of calcium monochloro-aluminate hydrate and the complex formed between $Ca(OH)_2$ and $CaCl_2$ [232]. According to them [23], these formations hinder the reaction between CO_2 and cement hydration products. Kobayashi and Uno [233], investigating the effect of cement alkalinity on carbonation reported that the rate of carbonation increases with the alkali content of cement. Two cements of Na_2O equivalent of 0.57% and 0.31% were used and NaOH was added to the former to obtain Na_2O equivalent of 0.9, 1.2 and 1.5%. The specimens were exposed to 10% CO_2 atmosphere and the depth of carbonation was measured up to 16 weeks of exposure. The depth of carbonation, which the authors represented as carbonation ratio, was observed to be strongly influenced by the Na_2O equivalent of the cement. In a later work, the same authors [234] investigated the effect of cement alkalinity on carbonation in concrete specimens. The results of this study indicated that the depth of carbonation was dependent on the water-cement ratio and

alkalinity of the cement. For mixes with similar water-cement ratio, the depth of carbonation was observed to be higher in concrete made with higher Na_2O equivalent.

Bensted [235] indicated that the enhanced carbonation in the cements with a higher alkalinity can be related to the coarser pore structure formed in the presence of alkalies. He observed that the alkalies in concrete accelerate the hydration of portland cement. This results in greater quantities of hydrates, such as C-S-H and ettringite, being formed at earlier stages of the hydration process than under non-accelerated conditions. This results in relatively greater heterogeneities in the microstructure developed during hydration. Mori et al. [236], as quoted by Jawed and Skalny [237], indicated that the specific surface area of the hydrated C_3S decreased at all ages in the presence of alkalies, and the morphology and microstructure also changed. The microstructure of C-S-H became coarse; particles grew from the grain surface into the NaOH solution. In the presence of Na_2SO_4, fine acicular C-S-H particles (probably containing SO_4^{--} ions) densely covered the C_3S grain surface, but did not grow extensively outward from the surface. Alkalies have also been found to affect the optimum SO_3 content of cement. Lerch [238] showed that the optimum gypsum requirement for a properly retarded cement increased with an increase in both the C_3A and alkali contents. Thus cement pastes contaminated with chloride and sulfate, particularly NaCl and Na_2SO_4, produce a more heterogeneous structure. In a recent study conducted at KFUPM [239] the total pore volume in the contaminated OPC and blended cement paste specimens was found to be more than that in the uncontaminated specimens. The pore volume in the contaminated specimens, contaminated with sodium chloride plus sodium sulfate, was 1.1 to 3.7 times that in the uncontaminated specimens (Table 5.4) [239].

Table 5.4: Total pore volume in the contaminated and uncontaminated OPC and blended cements [239]

Cement	Pore Volume (mm^3/g)	
	Uncontaminated	Contaminated*
OPC	61.63	79.81
Silica Fume	88.00	110.00
Blast Furnace Slag	43.30	161.54
Fly Ash	79.36	90.00

* Chloride + Sulfate

It can thus be hypothesized that the inclusion of contaminants, namely NaCl and Na_2SO_4, results in a heterogeneous pore structure and increased pore volume which aids in the ingress of CO_2 in the cement matrix. Dhir et al. [240] examined the relationship between the intrinsic permeability and carbonation of concrete. Their results indicated that the Figg air permeation index, which is a measure of the porosity of cover concrete, relates directly to the rate of carbonation. This result has an important practical implication, in that the chloride-sulfate contamination not only aids in the depassivation of steel but also helps in accelerating carbonation of cement. The overwhelming cases of concrete deterioration due to reinforcement corrosion in the Arabian Gulf may thus be related to these two phenomena primarily resulting from the inadvertent inclusion of chloride-sulfate due to the use of contaminated aggregate and/or mix water. Further, the increased carbonation depth observed in the blended cements is of particular concern, in this region, as these materials have to be imported for their technical merit and cost two to three times that of ordinary portland cement. To accrue the technical benefits of the supplementary cementing materials, it is necessary to restrict the quantum of contamination contributed by the concrete mixture ingredients.

Further, the presence of sodium chloride plus sodium sulfate within the cement matrix may be advantageous in maintaining a relatively higher humidity compared to uncontaminated concrete, particularly in situations where the concrete components are exposed to elevated temperature similar to that used in this study. The weight gain observed in the contaminated specimens (Figure 5.13 through 5.16) indicates towards such a possibility. The moisture retained within the pores may be beneficial for the carbonation process. Glass et al. [241] suggested that low levels of chlorides increase the ionic conductivity of the pore solution, while higher levels favour moisture retention and slow down the effects of drying.

Another consequence of chloride-sulfate contamination, which might influence the carbonation behaviour of these cements, is the reduction in compressive strength. It is known that inclusion of contaminants, such as chlorides and sulfates, the latter salt in particular, reduces the compressive strength. An average strength reduction of 15% was observed in sulfate-chloride bearing concrete over uncontaminated concrete [108]. The decrease in strength of OPC, fly ash and silica fume concrete specimens with the addition of chloride and chloride-sulfate has also been reported by Hughes [242]. He observed a decrease in the strength in OPC mortars, which were immersed in sodium sulfate and magnesium chloride solutions. This reduction in strength was correlated to the expansion due to sulfate attack.

The sensitivity of the carbonation process to the compressive strength has been reported by several investigators. A large number of publications clearly show a pronounced reduction in the depth of carbonation of ordinary portland cement concrete with an increase in the 28-day compressive strength [22,242-245]. Presumably this is because strength and carbonation have a common dependence upon the porosity of the cement paste matrix [13]. However, it should be recognized that the relationship is not unique and can be affected by the level of compaction, bleeding [228], total calcium

oxide in the reacted binder [247-248], permeable aggregate [214,248], curing [249], carbon dioxide level [247] and moisture conditions [185].

The other experimental variable that needs to be discussed is the exposure temperature (55 °C) used in this study. The detrimental effect of temperature on the durability performance of concrete is now well recognized. It is well appreciated that the diffusion of the aggressive species, like chloride, oxygen and carbon dioxide, into the concrete is increased with temperature. According to Richartz [250], at low temperatures, long and fibrous calcium silicate crystals form and interlock with each other. However, when the cements hydrate at elevated temperature more distinct but very short-fibrous calcium silicate hydrates are formed. Chapman [251] studied portland cement hydration products at different temperatures (17, 40 and 60 °C), and indicated that at elevated temperatures coarse and long calcium silicate hydrates are formed. Ludwig and Pence [252], quoted by Berhane [253], measured the specific surface area of portland cement hydration products hydrated at different temperatures (27 and 66 °C). The specific surface areas at these two temperatures was 103.4 m^2/g and 122.6 m^2/g, respectively. The measurements were made after 7 days of hydration at different temperatures. According to Idorn [254], temperatures above 50 °C affect the strength and rigidity of cement mortar and concrete.

The effect of w/c ratio and curing temperature on the permeability of hardened cement paste was studied by Goto and Roy [255]. Their results indicated that the porosity of the cement paste cured at 60 °C, measured by mercury intrusion porosimetry, was more than those cured at 27 °C. Marsh et al. [70] studied the permeability of plain and fly ash blended cement specimens cured over a temperature range of 20 to 65 °C for periods from seven days to one year. Their results indicated that the porosity of the ordinary portland cements was affected by the curing temperature, the specimens cured at elevated temperature being more porous than those

cured at normal temperatures. The effect of temperature on the pore structure, measured using mercury intrusion porosimetry and helium intrusion pycnometry, was insignificant. The effect of set and curing temperature on the microstructure of cementitious pastes was investigated by Justnes and Havdahl [256] using ^{29}Si NMR, DTA/TG and MIP. Pastes based on portland cement with 0 to 20% replacements of cement by microsilica and w/(c+s) ratios ranging from 0.20 to 0.40 were set or partly cured at 20, 50, 70 or 90 °C followed by a sealed cure at 20 °C until 7, 28 or 90 days. The results of this study indicated that the micro structure of the cement paste is strongly influenced by the initial curing temperature. This effect was particularly distinct for the lowest w/(c+s) ratio specimens with the highest microsilica dosage. Several other researchers have dealt with the effect of elevated temperature curing on the microstructure of calcium silicate [257] and portland cement [258]. All these publications agree that the C-S-H becomes coarser and that the paste becomes more permeable with increasing curing temperature. Verbeck and Helmuth [259] state that, because of their low solubility and diffusibility, cement hydration products cannot diffuse to a significant distance from the cement grain in the time allowed by rapid hydration. This results in a non-uniform distribution of the hydration products and a corresponding reduction in strength. Skalny and Odler [260] found that elevated curing temperatures cause a coarsening of the hydration products. Radjy and Richards [258] using data obtained from desorption isotherms, concluded that steam curing of cement pastes results in large pores. Using mercury intrusion porosimetry, Sellevold [261] also found that curing cement pastes at elevated temperatures results in a coarser pore structure. In a recent study [108] conducted at KFUPM, the effect of exposure temperature on the pore size distribution in OPC and blended cements was evaluated. An increase in the pore volume was observed in all the cements with increasing exposure temperature. The total pore volume in the specimens cured at 25, 40, 55 and 70 °C in the uncontaminated OPC paste specimens, was 61.63, 123.83, 184.12 and 179.61 mm^3/g. These results also indicated that temperature has a significant effect on

the finer pores, in that the effect of temperature seems to be negligible on pore sizes greater than 10^3 Å. Luke and Glasser [63] also indicated a coarsening of the pore size distribution with increasing exposure temperature. According to them the total intruded volume does not change significantly between 25 and 55 °C curing temperature being 21.6 and 21.2%, respectively. However, the pore size distribution does change. The porosity in the specimens cured at 55 °C was observed to be concentrated in the larger pore size range. Kjellsen et al. [262] studied the pore structure of OPC pastes hydrated at 5, 20, and 50 °C, using mercury intrusion porosimetry and back scattered electron microscopy. They observed that an increase in the curing temperature results in increased porosity, particularly for the pore radii in the range of 200 - 1000 Å. They compared these results with back scattered electron images and found that an increase in temperature resulted in an increased porosity particularly for pore radii in the range of 2500 - 12,500 Å. They attributed this difference to the ink bottle effect inherent in the mercury intrusion porosimetry technique.

The above review indicates that the elevated temperature of 55 °C used in this part of the investigation might have lead to a coarsening of the pore structure leading to a higher carbonation. However, the specimens were initially cured at a laboratory temperature of 25 °C for 28 days before being exposed to the carbonation environment. Therefore, it is expected that temperature might not have affected the pore structure development in these specimens. However, elevated temperature accelerates the rate of diffusion of CO_2. Thus, the concomitant effect of elevated temperature exposure and chloride-sulfate contamination may accelerate carbonation of cements compared to situations where one of the factors does not exist.

5.6 SUMMARY OF RESULTS

In this Chapter the effect of chloride-sulfate contamination and elevated temperature on the carbonation behaviour of plain (OPC and SRPC) and blended cements was evaluated. The cement mortar specimens were exposed to an accelerated carbonation atmosphere, 3% CO_2, and the progress of carbonation was assessed mainly by measuring the depth of carbonation. The weight gain in the specimens with period of exposure was also evaluated. Selected specimens were analyzed using XRD and DTA and TG techniques. The changes in the morphology of the plain and blended cements, due to carbonation, were also evaluated using scanning electron microscopy. Based on the results the following conclusions can be drawn :

The depth of carbonation in the contaminated cement mortar specimens was more than that in the corresponding uncontaminated specimens. In the contaminated specimens, a higher depth of carbonation was measured in the specimens admixed with sodium chloride plus sodium sulfate than those contaminated with only sodium chloride. This trend of increased carbonation in the contaminated specimens was also observed in the blended cements. The depth of carbonation in the uncontaminated plain and blended cements was in the range of 0.75 to 2 mm, while in the contaminated specimens it varied from 9 to 11 mm after about 52 weeks of exposure to the CO_2 environment.

Higher weight gain was indicated in the specimens contaminated with sodium chloride plus sodium sulfate compared to the uncontaminated specimens and those contaminated with only sodium chloride. In the uncontaminated specimens practically no weight gain was recorded.

The scanning electron micrographs for the carbonated OPC, fly ash and silica fume indicated a relatively compact C-S-H compared to the uncarbonated portions, while the C-S-H in the carbonated blast furnace slag cement was disintegrated. Formation of $CaCO_3$, was indicated both in the carbonated and uncarbonated portions of these cements. Formations in the carbonated portions were more distinct, isolated and bigger in size than those observed in the uncarbonated portions. The formation of $CaCO_3$ in the blended cements despite the limited quantum of $Ca(OH)_2$, indicates the decomposition of C-S-H.

The X-ray diffractograms for the carbonated and uncarbonated portions of OPC and blended cements indicated the presence of quartz (SiO_2), portlandite ($Ca(OH)_2$), and calcite and aragonite. The intensity of the quartz peaks was more or less similar in both the carbonated and uncarbonated portions. The quantity of $CaCO_3$, present either in the form of calcite or aragonite, was more in the carbonated specimens than in the uncarbonated portions.

The DTA and TG curves also indicated greater carbonation in the contaminated cements than in the uncontaminated specimens. This trend was observed both in the OPC and blended cement mortar specimens. In the OPC specimens, the $Ca(OH)_2$ peaks tended to become more shallow with carbonation. In the blended cements, the depth of $Ca(OH)_2$ peaks was very insignificant, indicating the consumption of this cement hydration product due to pozzolanic reaction. An increase in the $CaCO_3$ peak in the blended cements indicates that other cement hydration products may be reacting with CO_2.

The increased depth of carbonation in the contaminated specimens may be attributed to the changes brought about in the microstructure of the hardened cement paste due to inclusion of NaCl and Na_2SO_4. The inclusion of alkalies accelerates

hydration of cement which results in relatively greater heterogeneities in the microstructure. These heterogeneities in the microstructure provide channels for gas transport thereby increasing the rate of carbonation. The other causes may be the increase in the total pore volume and moisture retention due to the incorporation of the chloride-sulfate contamination.

The results obtained in this part of the study have an important practical implication in that the chloride-sulfate contamination of concrete not only aids in steel depassivation, but also accelerates carbonation. Also, the increased carbonation depth observed in the blended cements, is of particular concern in this region as these materials have to be imported for their technical merit and are two to three times costlier than the ordinary portland cement. Thus to utilize the technical benefits that accrue with the use of blended cements, guidelines for limiting the chloride and sulfate contamination should be established. Further, the size of the specimens used in this study might have accelerated the carbonation process. Therefore, there is a need to evaluate the effect of chloride-sulfate contamination on carbonation in concrete.

CHAPTER 6

INFLUENCE OF CHLORIDE-SULFATE CONTAMINATION AND CARBONATION ON REINFORCEMENT CORROSION

6.1 EFFECT OF CARBONATION ON REINFORCEMENT CORROSION

The role of carbonation on reinforcement corrosion is primarily attributed to the breakdown of the passive layer by reduction in the alkalinity of the pore solution. In non-carbonated concrete and without chlorides, steel is protected by the formation of a passive layer on its substrate. However, due to carbonation, the pH of the pore solution is decreased leading to steel depassivation and subsequently corrosion is initiated. Hamada [209], using polished steel samples immersed in calcium hydroxide solution, indicated that the corrosion rate increases with a reduction in the pH. Similar results have been reported by Shalon and Raphael [12] and Uhlig and Revic [263]. Saeki et al. [218] observed rust formation on steel specimens embedded in carbonated mortar at a pH level of about 11.4. The degree of rust formation was reported to increase rapidly with further pH reductions [218]. Another aspect of carbonation which may be of importance in the chloride-contaminated concretes is that the hydrates that chemically bind chlorides can decompose on carbonation, releasing chlorides into the pore solution [264]. Further, chloride contamination and carbonation of concrete increase the Cl^-/OH^- ratio leading to depassivation of steel earlier than when one of these factors is not present. Furthermore, the risk of corrosion at low chloride concentrations, which may be negligible in the uncarbonated concrete, will increase significantly upon carbonation [265]. Studies conducted by Roper and Baweja [266] indicated that both carbonation

and chlorides increase the corrosion rates. The compounding action of chloride and carbonation has also been reported by Sagoe-Crentsil et al. [267] and Alonso and Andrade [268]. Nagataki and Ohga [269] reported higher corrosion activity under CO_2 environment in specimens cured with chloride-contaminated water. This effect was observed to be more pronounced in fly ash cement mortar specimens compared to OPC.

Deterioration of concrete structures in the Arabian Gulf has been mainly attributed to the chloride ions, but there is also a concern with regard to carbonation [22,197-198], particularly as the environmental conditions of this region are conducive for rapid carbonation of concrete. Smith and Evans [198] reviewed published data and concluded that carbonation rates in the Arabian Gulf were particularly rapid because the exposure conditions were warm and dry. However, the atmosphere was not dry enough to prevent reinforcement corrosion. Their [198] views are generally consistent with those expressed by Treadaway [197]. Raphel and Shalon [201] indicated that the degree of reinforcement corrosion correlated very well with the level of carbonation.

While the studies cited above have evaluated the effect of chlorides and carbonation on reinforcement corrosion, the conjoint effect of temperature, chloride-sulfate contamination and carbonation is not yet elucidated. Such a study is essential to verify whether the presence of chloride-sulfate contamination will accelerate reinforcement corrosion in carbonated concrete.

This Chapter details the experimental work conducted to fulfill the above objectives.

6.2 SPECIMENS AND EXPERIMENTAL METHODS

The contaminated and uncontaminated reinforced concrete specimens were exposed to elevated temperature and humidity conditions in a carbonation chamber, similar to that described in Chapter 5. Table 6.1 details the experimental variables.

Table 6.1: Experimental variables to evaluate the effect of chloride-sulfate contamination and carbonation on reinforcement corrosion.

Variable	Details
Specimens	Reinforced concrete specimens made with SRPC, and OPC-A (C_3A: 3.5 and 8.5%)
Contamination	0% 0.8% Cl^- 0.8% Cl^- + 1.5% SO_3^{--}
Exposure temperature	55 °C
Relative humidity	75%
CO_2	3%
Corrosion Monitoring	Corrosion Potentials
	Corrosion current density using linear polarization resistance technique
	AC impedance spectroscopy

The concrete specimens were similar to those used in Chapter 4. These specimens were cured for 28 days in the laboratory at a controlled temperature of 25 °C, and there after placed in the exposure chamber. Reinforcement corrosion was monitored by measuring the corrosion potentials and corrosion current density as described in Section 4.2.3. In addition to DC measurements, reinforcement corrosion was also evaluated using AC impedance spectroscopy.

In the AC impedance measurements, a series of AC perturbations in the form of sine waves with an amplitude of 10 to 15 mV about the free corrosion potential is applied and the resulting impedance is plotted as a complex plain plot typically known as Nyquist plot (Figure 6.1) [270]. In the Nyquist plot, the high frequency intercept gives the resistance of the concrete, RΩ, while the diameter of the semi-circle gives the charge transfer resistance, Rct, (equivalent to the polarization resistance of the Stern-Geary equation) [160]. An uncompensated DC measurement of Rp includes RΩ as well as Rct which results in an error in measuring the corrosion rate if the Ohmic drop associated with the concrete electrolyte is not compensated. John et al. [156, 271], using AC impedance, demonstrated the need for a more complex equivalent circuit. An additional high frequency time constant was included and associated with the steel/concrete interface and a Warburg impedance is added to account for the effect of diffusion on the electrode kinetics at low frequencies [160]. Several researchers [271-274] have used AC impedance spectroscopy to examine steel corrosion in concrete and mortar.

Further, by dividing the potential wave form by the current wave form, a plot of the logarithm of impedance versus logarithm of frequency can be created. Such a plot is called a Bode plot and a typical curve is shown in Figure 6.2 [275]. The high frequency resistance represents RΩ and the low frequency resistance represents RΩ+Rct. By subtracting the high frequency resistance from the low frequency resistance, the value of Rct is deduced. The corrosion current density can then be calculated using the following relationship:

$$I_{corr} = B/Rct$$

Where: I_{corr} = corrosion current density, $\mu A/cm^2$

B = ßa.ßc/2.3(ßa+ßc)

Rct = charge transfer resistance, $k\Omega.cm^2$

ßa and ßc are the anodic and cathodic Tafel constants, respectively.

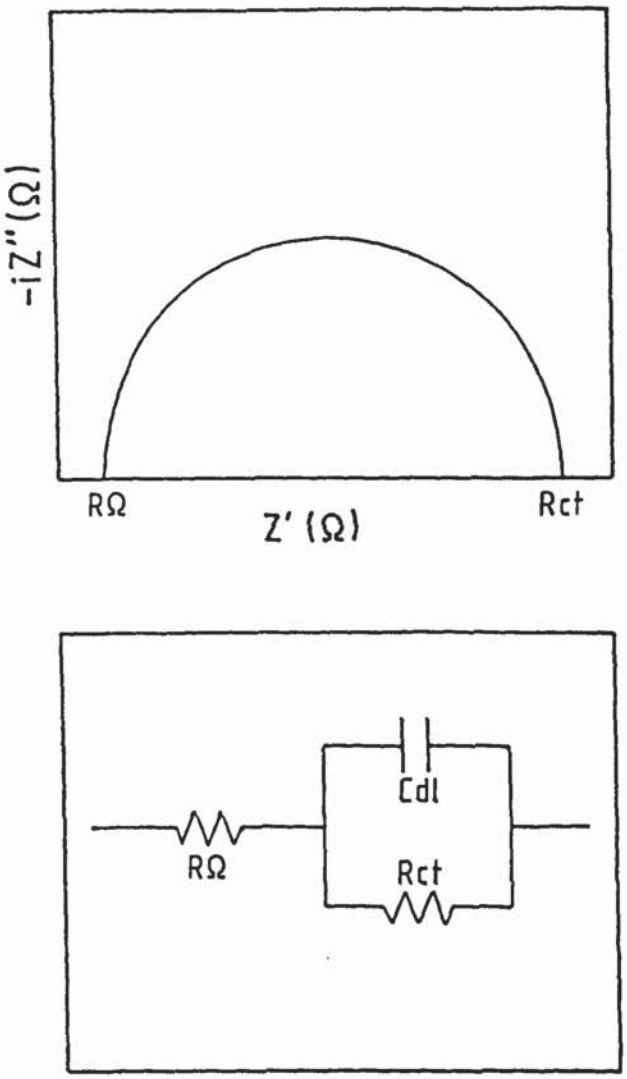

Figure 6.1: Typical Nyquist plot and its equivalent circuit

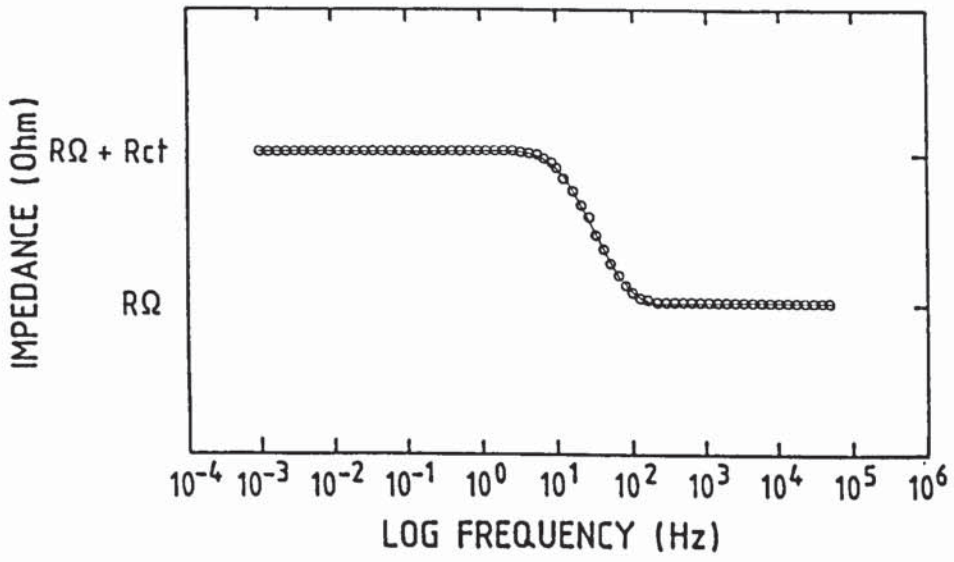

Figure 6.2: Typical Bode plot for steel in concrete

The AC impedance measurements were carried out on a frequency response analyzer (FRA) interfaced to a HP85 computer for data logging and analysis. The instrument used for the frequency measurements was a Solartron 1250/1286 FRA/Electrochemical interface. The following test conditions were used:

(a) Amplitude 10 mV

(b) Sweep from 50 kHz to 1 mHz

(c) DC potential E_{corr}

(d) 4 steps per decade on the log scale sweep

(e) A delay of 3 seconds between frequencies

The AC impedance data were generated in the form of Nyquist and Bode plots. Anodic and cathodic Tafel constants of 120 mV, i.e., B=26 mV have been used to calculate the corrosion current density.

6.3 RESULTS AND DISCUSSION

6.3.1 Corrosion Potentials

The corrosion potentials of steel in the uncontaminated SRPC (C_3A: 3.5%) concrete specimens are plotted against period of exposure in Figure 6.3. The corrosion potentials during the initial stages of exposure were in the range of -150 to -200 mV SCE. However, after about 50 days of exposure, a sharp decrease in the potential readings was recorded. After 300 days of exposure to the CO_2 atmosphere, the corrosion potentials were -360 mV SCE. The corrosion potentials on steel in the chloride-contaminated SRPC concrete specimens are plotted in Figure 6.4. The potentials in the initial stages of exposure to CO_2 were in the range of -200 to -270 mV SCE. After about 20 days of exposure, they decreased to -350 mV SCE and remained more or less similar at all times. Figure 6.5 shows the variation in the corrosion

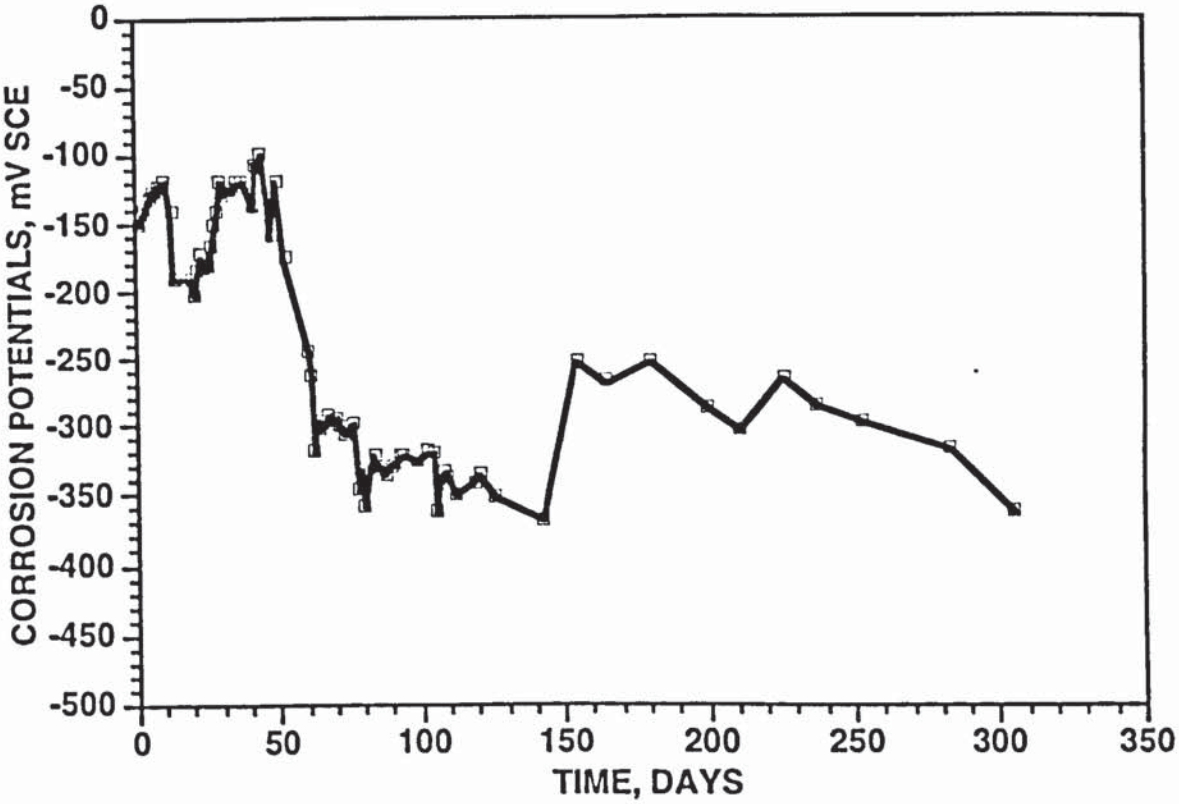

Figure 6.3: Corrosion potentials for steel in the uncontaminated SRPC concrete

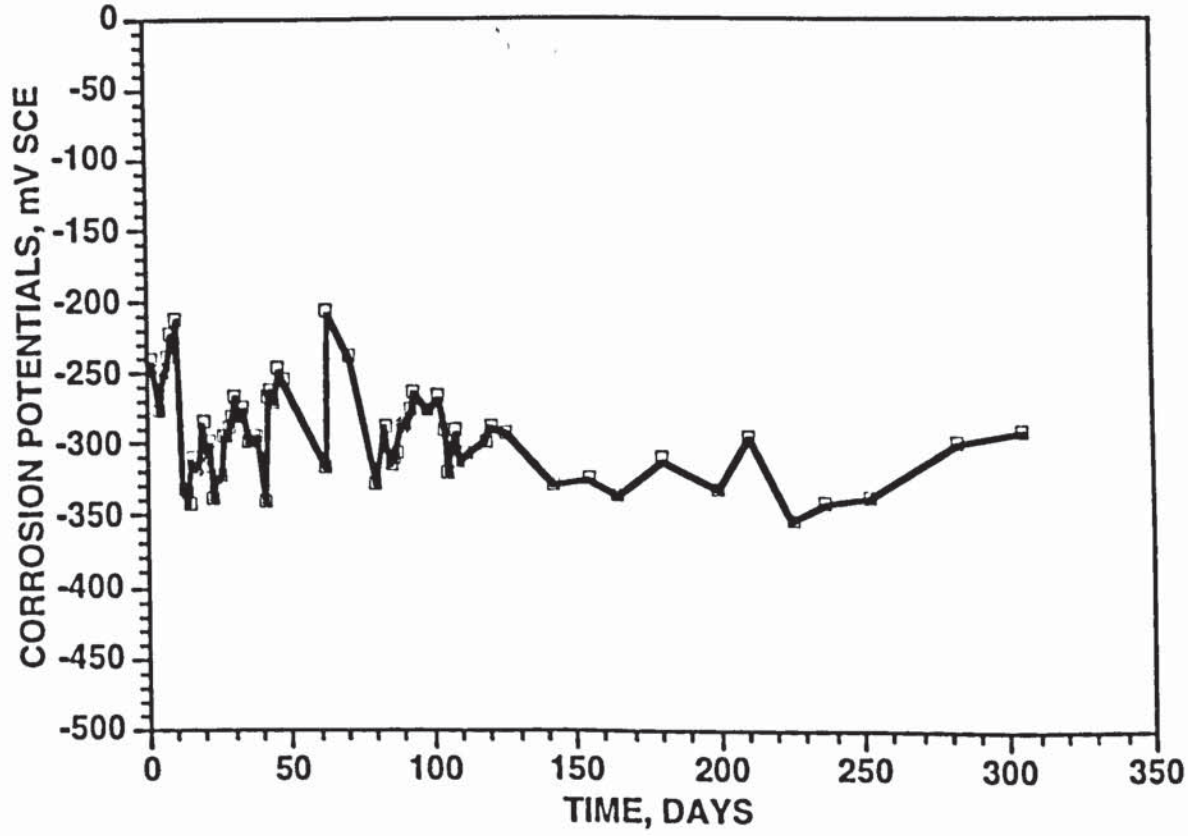

Figure 6.4 : Corrosion potentials for steel in the chloride-contaminated SRPC concrete

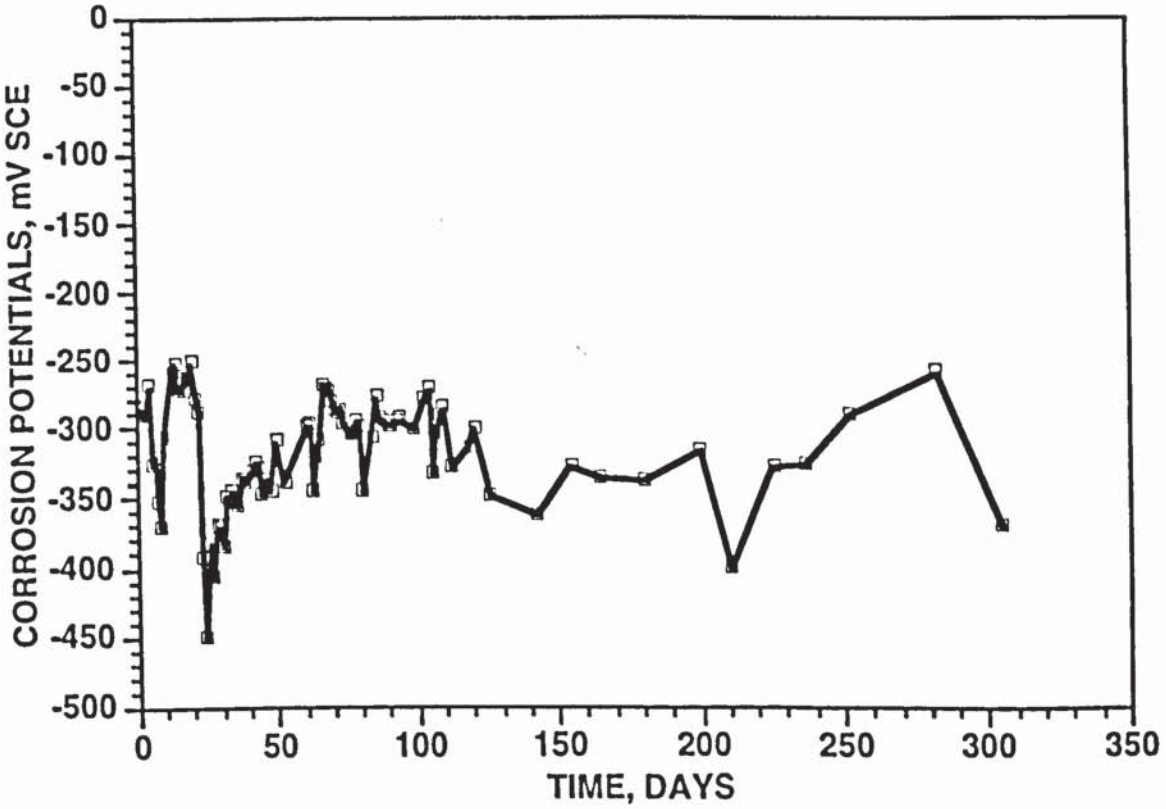

Figure 6.5: Corrosion potentials for steel in SRPC concrete contaminated with sodium chloride plus sodium sulfate

potentials on steel in SRPC concrete specimens contaminated with sodium chloride plus sodium sulfate. The corrosion potentials before exposure were -290 mV SCE. A sharp decrease in the potential values to -450 mV SCE was recorded after about 20 days of exposure. However, the potentials at all the other times were in the range of -300 to -400 mV SCE.

The corrosion potentials on steel in the uncontaminated OPC-A (C_3A: 8.5%) concrete specimens are plotted in Figure 6.6. The corrosion potentials in the initial stages (10 to 20 days) of exposure were -140 mV SCE and thereafter decreased to -200 mV SCE after about 60 days of exposure. After about 300 days of exposure, the potentials were -250 SCE. Figure 6.7 shows the corrosion potentials for steel in the chloride-contaminated OPC-A concrete specimens. The potentials in these specimens decreased from -220 mV SCE to -330 mV SCE after 250 days of exposure to the CO_2 environment. The corrosion potentials for steel in the OPC-A concrete specimens contaminated with sodium chloride plus sodium sulfate are plotted in Figure 6.8. The corrosion potentials before exposure to CO_2 were -320 mV SCE. A slight increase in the potential values was recorded up to an exposure period of 40 days, beyond which the potentials tended to be in the range of -300 to -350 mV SCE. The potentials after 300 days of exposure were -325 mV SCE.

In general, the corrosion potentials for steel in the SRPC and OPC concrete specimens, plotted in Figures 6.3 through 6.8, were generally less noble in the contaminated specimens than that in the uncontaminated specimens. The corrosion potentials in the specimens contaminated with sodium chloride plus sodium sulfate were less than in the specimens contaminated with only sodium chloride. The potentials tended to decrease with time. While the change in the potentials with the period of exposure was insignificant in the contaminated specimens, a considerable decrease in the potentials, particularly in SRPC, was measured in the uncontaminated

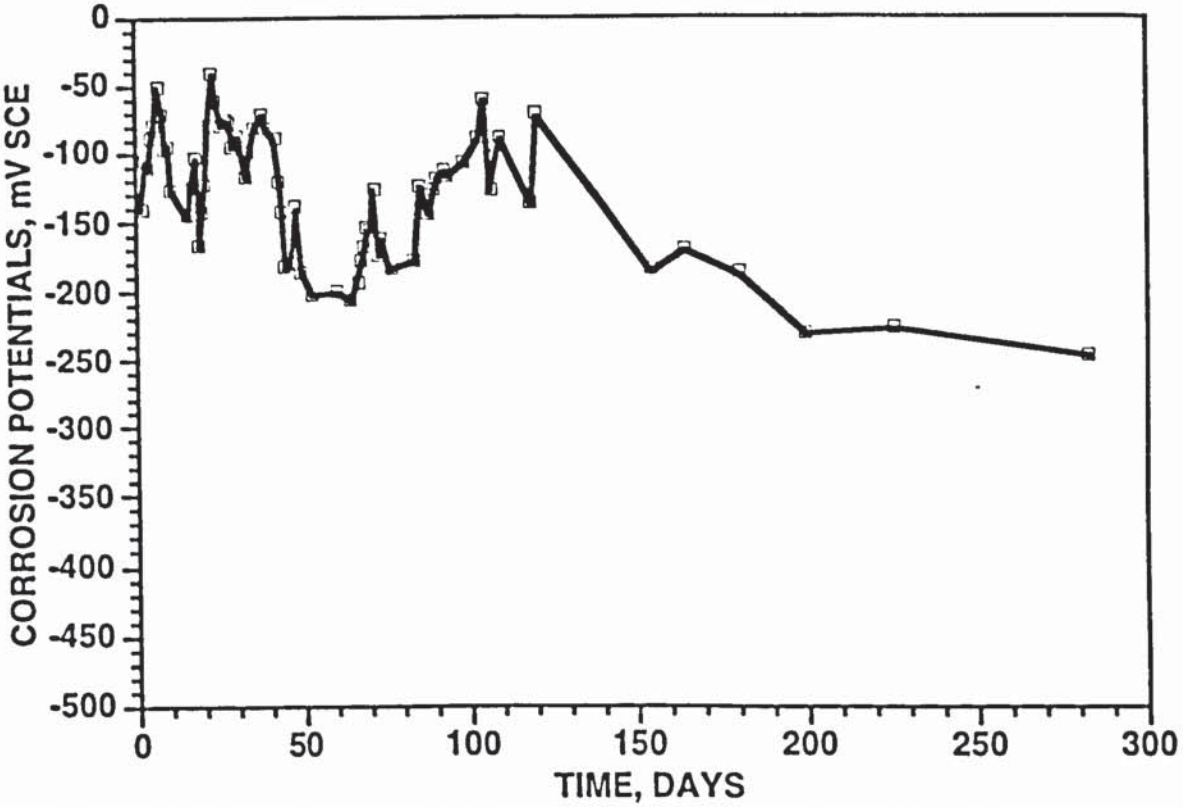

Figure 6.6: Corrosion potentials for steel in the uncontaminated OPC-A concrete

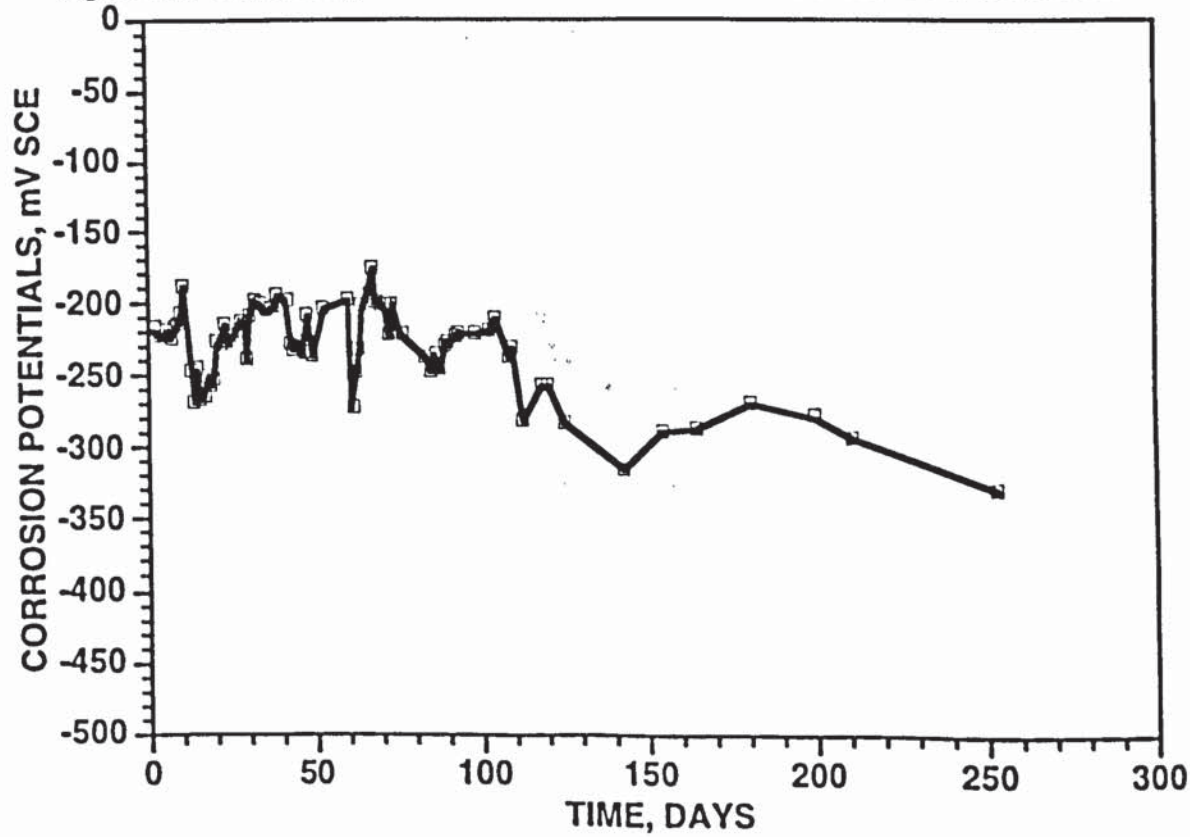

Figure 6.7: Corrosion potentials for steel in the chloride-contaminated OPC-A concrete

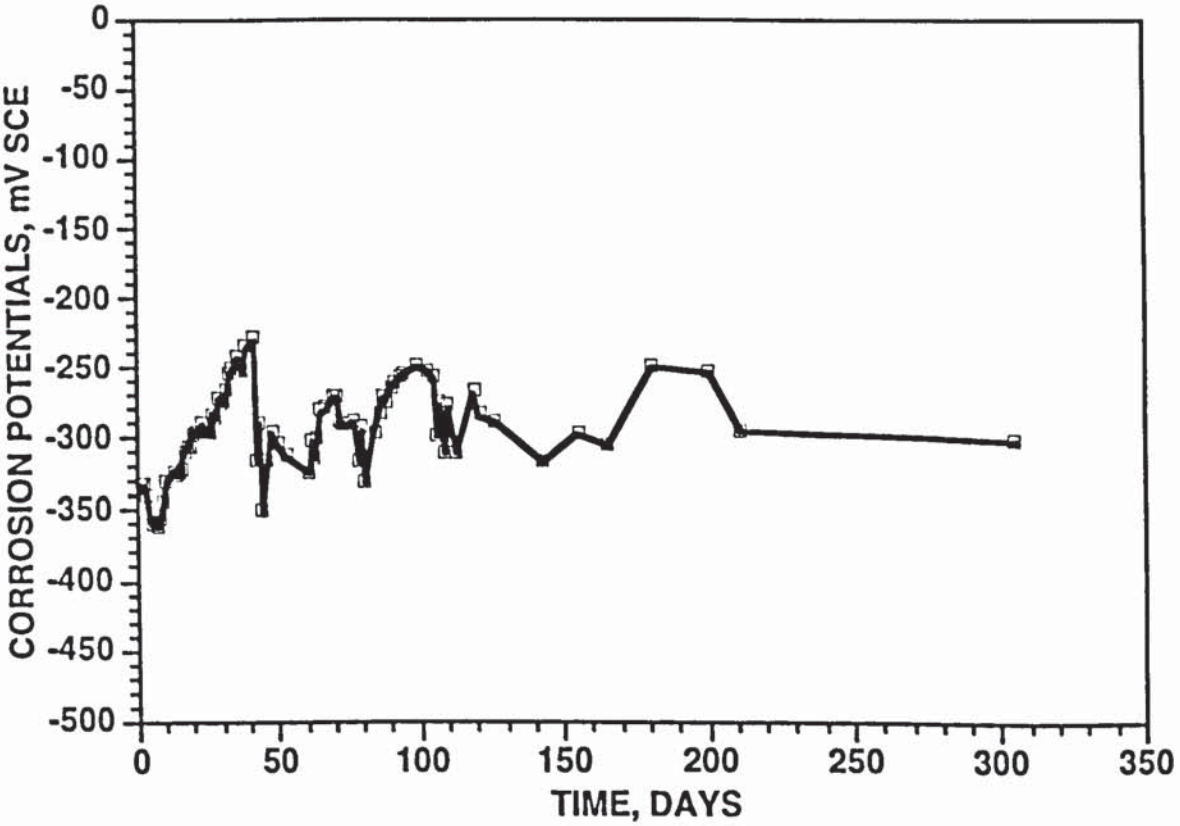

Figure 6.8: Corrosion potentials for steel in OPC-A concrete contaminated with sodium chloride plus sodium sulfate

concrete specimens. This difference in behaviour, viz.-a-viz. a drop in the corrosion potentials, may be explained by the fact that in the contaminated specimens the passive layer is not formed due to the presence of chloride and sulfate contamination as such the effect of carbonation is not consequential. The decrease in the corrosion potentials in the uncontaminated specimens may be attributed to the penetration of CO_2 to the steel-concrete interface. A considerable decrease in the potential value after about 60 days in SRPC concrete indicates towards such a phenomenon.

6.3.2 Corrosion Current Density

The variation in the corrosion current density on steel in the uncontaminated SRPC concrete specimens is plotted in Figure 6.9. The corrosion current density (I_{corr}) was in the range of 0.06 to 0.16 $\mu A/cm^2$. The I_{corr} on steel in the SRPC concrete specimens contaminated with sodium chloride is plotted in Figure 6.10. These values were in the range of 0.7 to 1.4 $\mu A/cm^2$. The I_{corr} on steel in the SRPC concrete specimens contaminated with sodium chloride plus sodium sulfate varied from 0.8 to 1.9 $\mu A/cm^2$ (Figure 6.11).

The I_{corr} on steel in the uncontaminated and contaminated OPC-A concrete specimens is plotted in Figures 6.12 through 6.14. In the uncontaminated specimens, the I_{corr} varied from 0.06 to 0.18 $\mu A/cm^2$ (Figure 6.12). The I_{corr} on steel in the concrete specimens contaminated with only sodium chloride (Figure 6.13) was in the range of 0.3 to 0.80 $\mu A/cm^2$, while it was in the range of 0.41 to 1.10 $\mu A/cm^2$ in the concrete specimens contaminated with sodium chloride plus sodium sulfate (Figure 6.14).

The data on corrosion current density, discussed in Figures 6.9 through 6.14, are summarized in Table 6.2. In agreement with the corrosion potentials data, the I_{corr} on

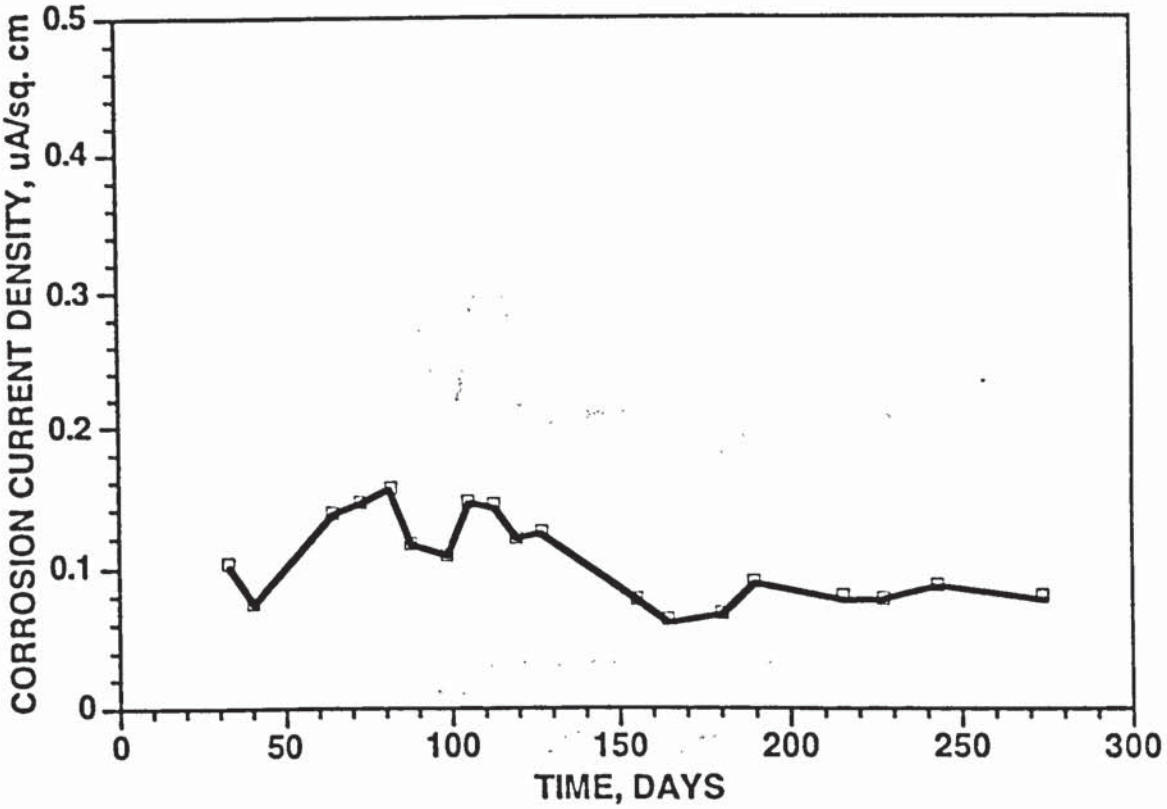

Figure 6.9: Corrosion current density on steel in the uncontaminated SRPC concrete

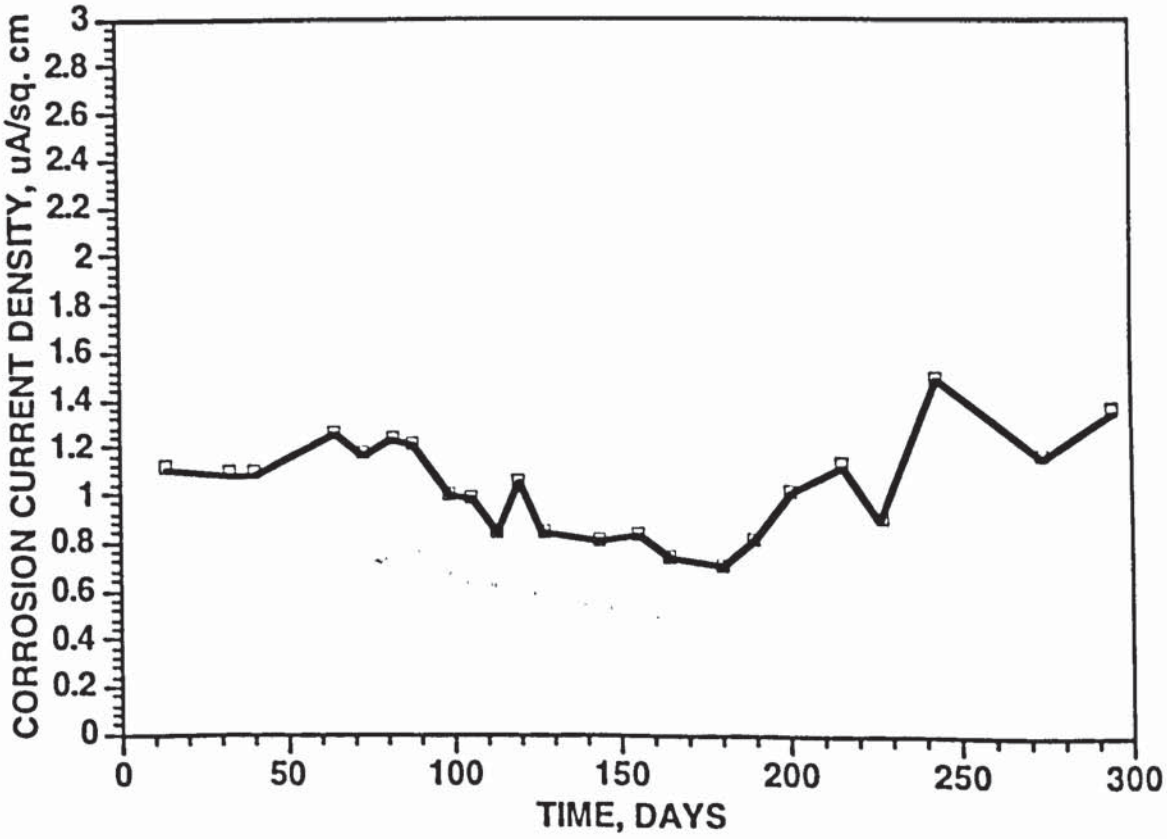

Figure 6.10: Corrosion current density on steel in the chloride-contaminated SRPC concrete

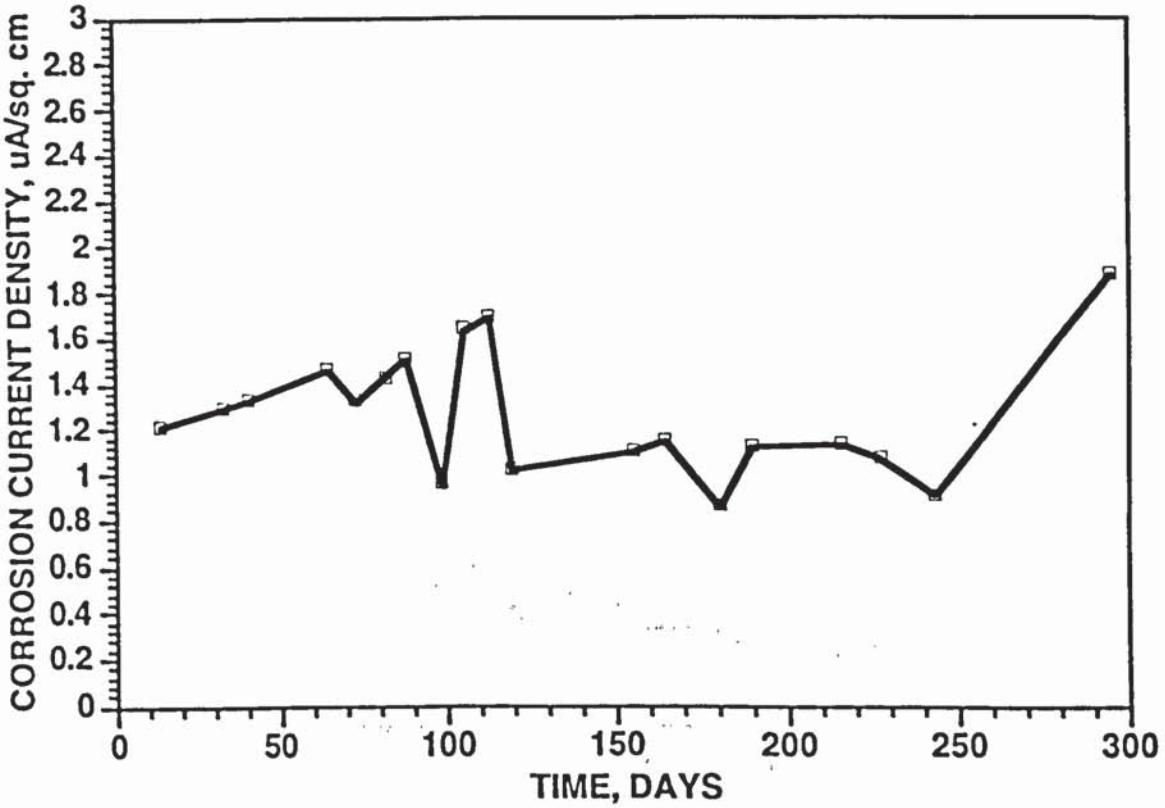

Figure 6.11: Corrosion current density on steel in SRPC concrete contaminated with sodium chloride plus sodium sulfate

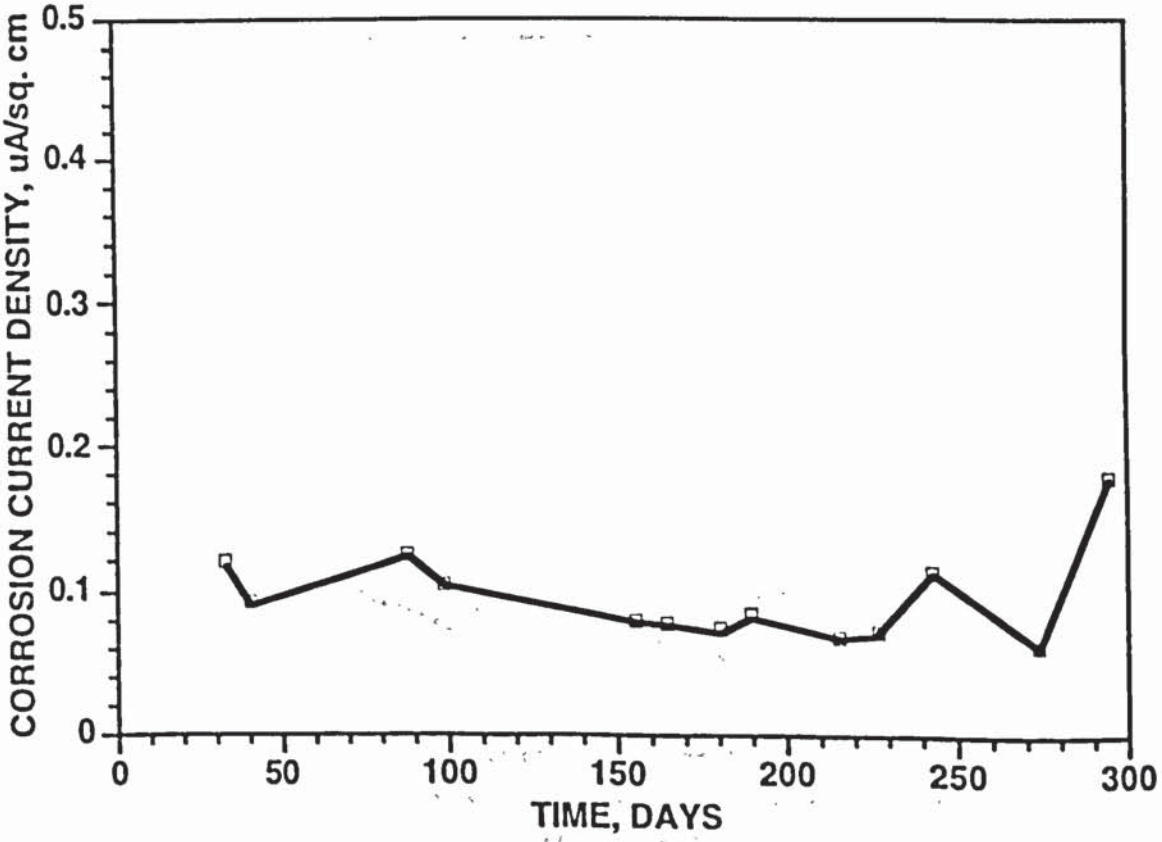

Figure 6.12: Corrosion current density on steel in the uncontaminated OPC-A concrete

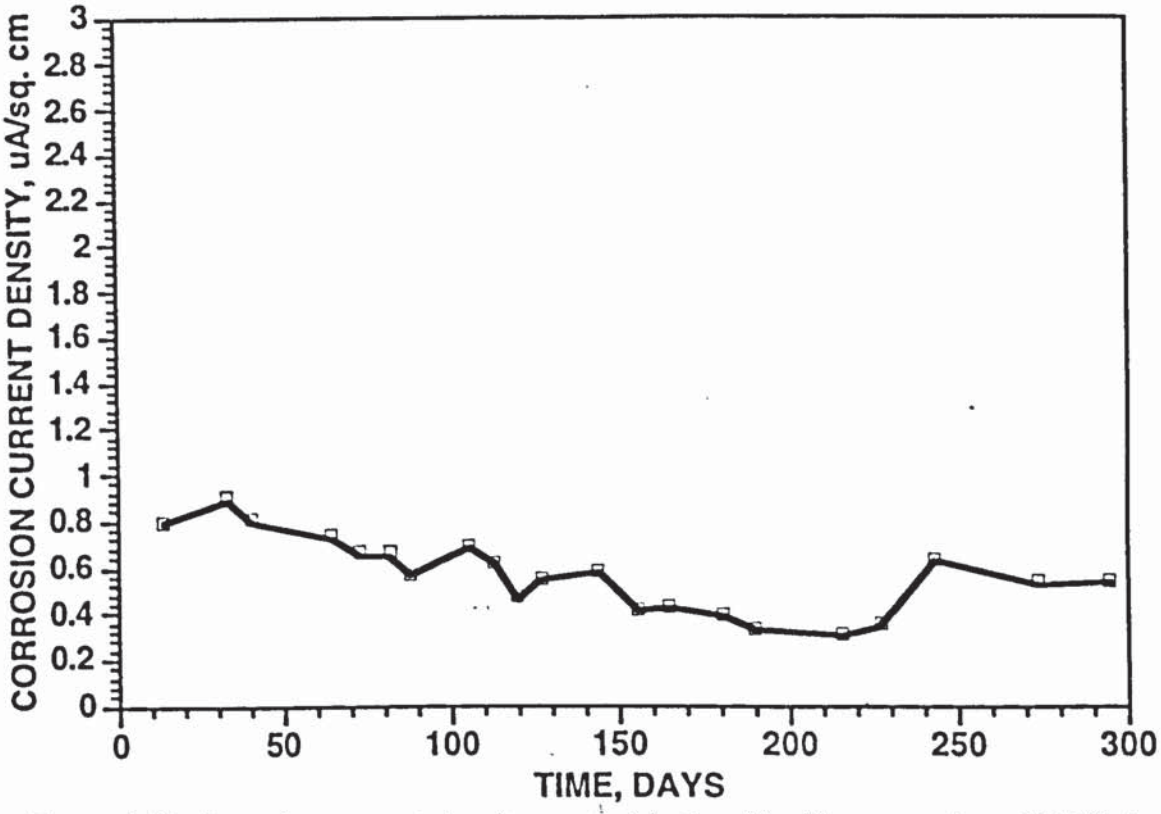

Figure 6.13: Corrosion current density on steel in the chloride-contaminated OPC-A concrete

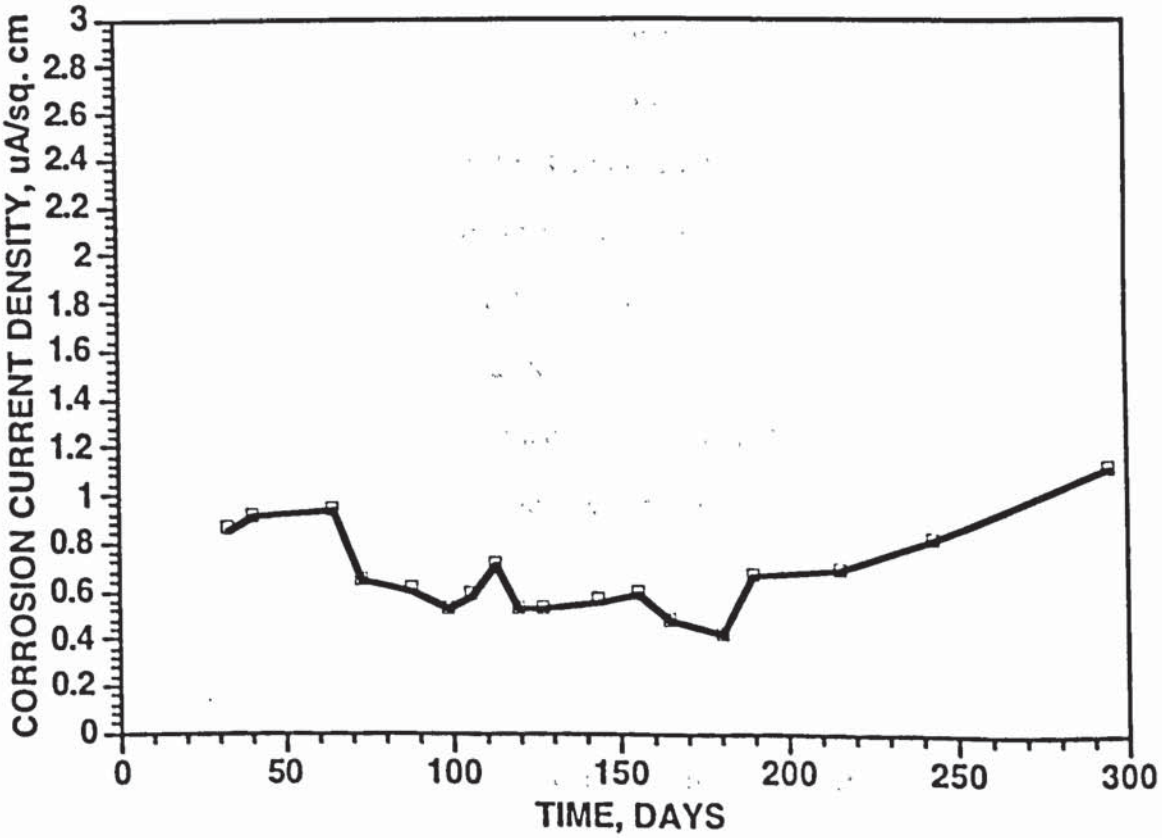

Figure 6.14: Corrosion current density on steel in the OPC-A concrete contaminated with sodium chloride plus sodium sulfate

Table 6.2: Corrosion current density on steel in the contaminated and uncontaminated concrete specimens exposed to CO_2

Cement	Contamination	Corrosion current density ($\mu A/cm^2$)
SRPC	None	0.16
	0.8% Cl^-	1.34
	$Cl^-+SO_4^{--}$	1.87
OPC	None	0.18
	0.8% Cl^-	0.52
	$Cl^-+SO_4^{--}$	1.10

steel in the contaminated specimens was more than that in the uncontaminated specimens. However, the variation in the I_{corr} with the period of exposure was not very significant in the uncontaminated specimens. This anomaly may be attributed to the large Ohmic drop associated with the carbonated concrete. As the uncompensated resistance is a function of the concrete resistivity [241,276], the corrosion rates measured without compensation for the Ohmic drop are bound to be in error. In the DC linear polarization method, this resistance is normally compensated for by using either positive feed back or current interrupt method. Several researchers [241,268,277-279] have indicated a good correlation between the corrosion rates estimated by the polarization resistance method with IR compensation, and those evaluated using gravimetric metal loss measurements.

6.3.3 A.C. Impedance

AC impedance spectra were developed both for the contaminated and uncontaminated concrete specimens. The results are presented in the form of Nyquist

plots which represent the real and imaginary components of the impedance. The kinetic information on the corrosion processes was developed using Bode plots.

Figure 6.15 shows the Nyquist plot for the uncontaminated OPC-A concrete specimens. The Nyquist plot after 14 days of exposure (inset in Figure 6.15) indicated a greater resistance compared to other exposure periods. The AC impedance spectra after 67, 120 and 255 days of exposure indicated more or less similar behaviour. The AC spectra for chloride-contaminated OPC-A concrete specimens are plotted in Figure 6.16. The AC spectra after 14 days of exposure (inset in Figure 6.16) again indicated very high resistance compared to those determined after 67 and 120 days of exposure. Figure 6.17 shows the AC spectra for OPC-A concrete specimens contaminated with sodium chloride plus sodium sulfate. These data also qualitatively indicated a trend similar to that exhibited by the specimens contaminated with only sodium chloride.

The kinetic information on the concomitant effect of chloride and sulfate contamination and carbonation was evaluated by calculating Rct from Bode plots. Figures 6.18 through 6.20 show some typical Bode plots for the contaminated and uncontaminated concrete specimens. The Rct for steel in the uncontaminated and contaminated specimens measured after 14, 67, 120 and 255 days of exposure are plotted in Figures 6.21 through 6.23. The corrosion current density (I_{corr}) evaluated using a value of 'B' of 26 mV is also plotted in these figures. Figure 6.21 shows the variation in the Rct and I_{corr} values with period of exposure to the CO_2 environment for the uncontaminated SRPC concrete specimens. The Rct in the uncontaminated specimens decreased from about 240 k.Ω.cm^2 to 135 k.Ω.cm^2 for the exposure period varying from 14 to 67 days. The variation in this value after 67 days of exposure, however, was not significant. The Rct and I_{corr} values for the chloride-contaminated SRPC concrete specimens are plotted against the period of exposure to CO_2 environment in Figure 6.22. Again, the decrease in the Rct was more prominent from

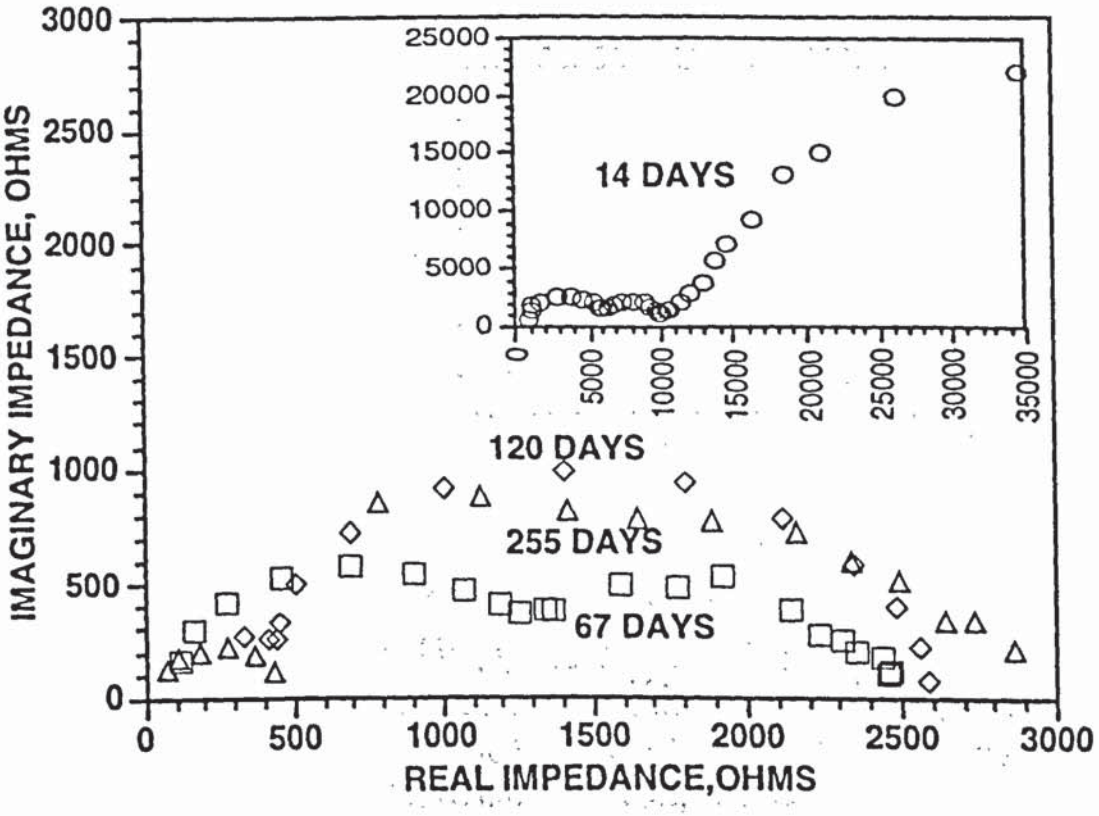

Figure 6.15: Nyquist plot for steel in the uncontaminated OPC-A concrete

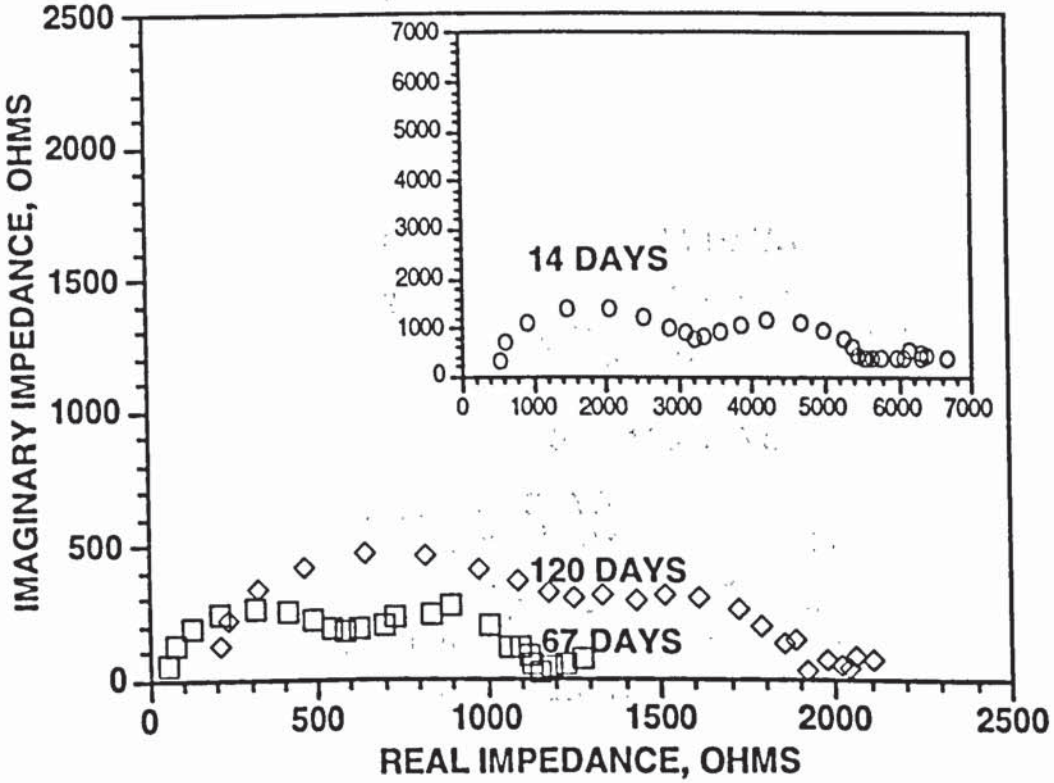

Figure 6.16: Nyquist plot for steel in the chloride-contaminated OPC-A concrete

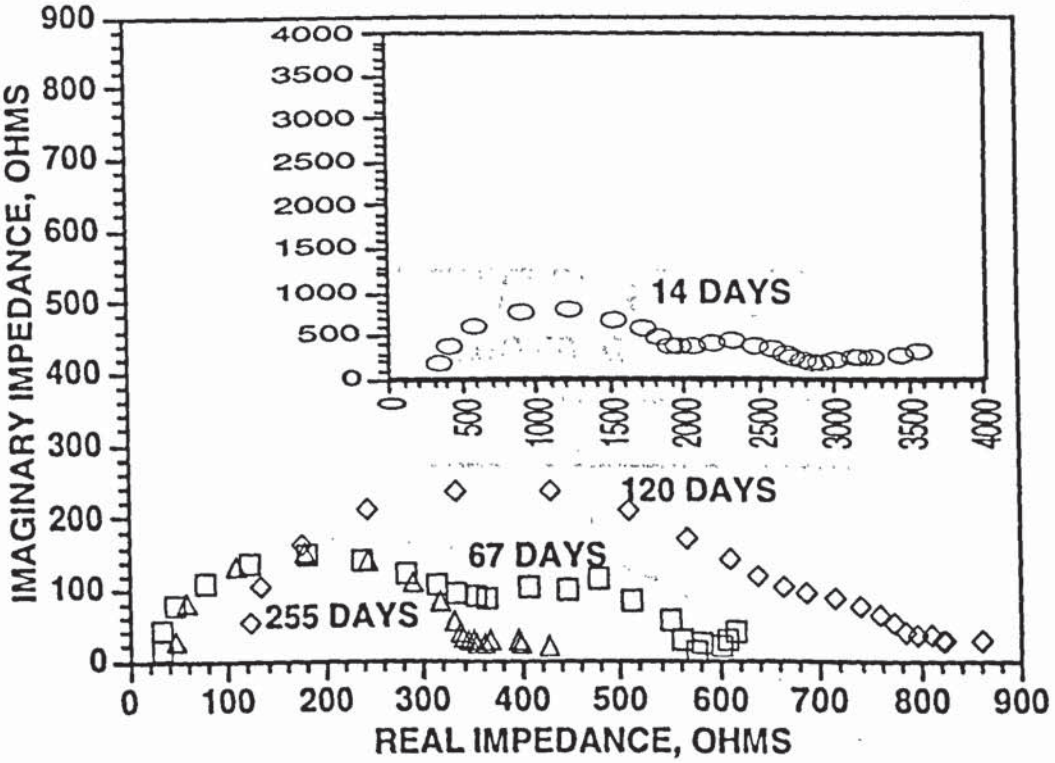

Figure 6.17: Nyquist plot for steel in OPC-A concrete contaminated with sodium chloride plus sodium sulfate

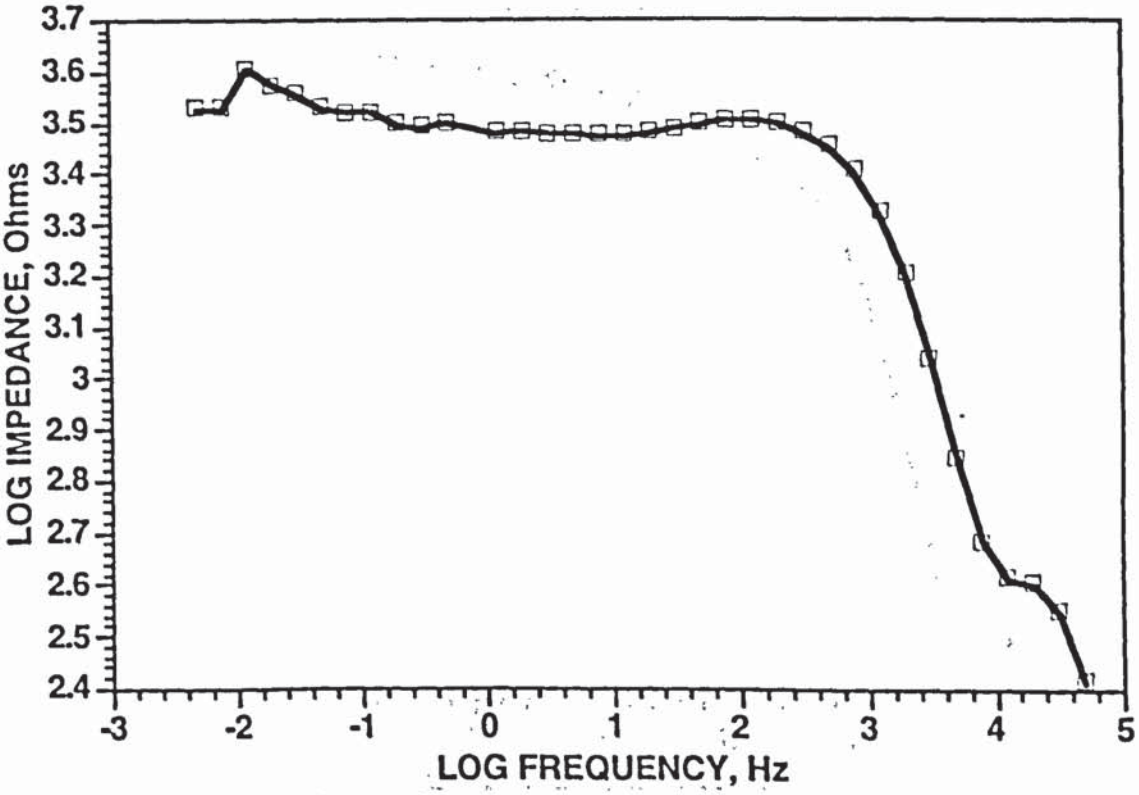

Figure 6.18: Bode plot for steel in the uncontaminated SRPC concrete

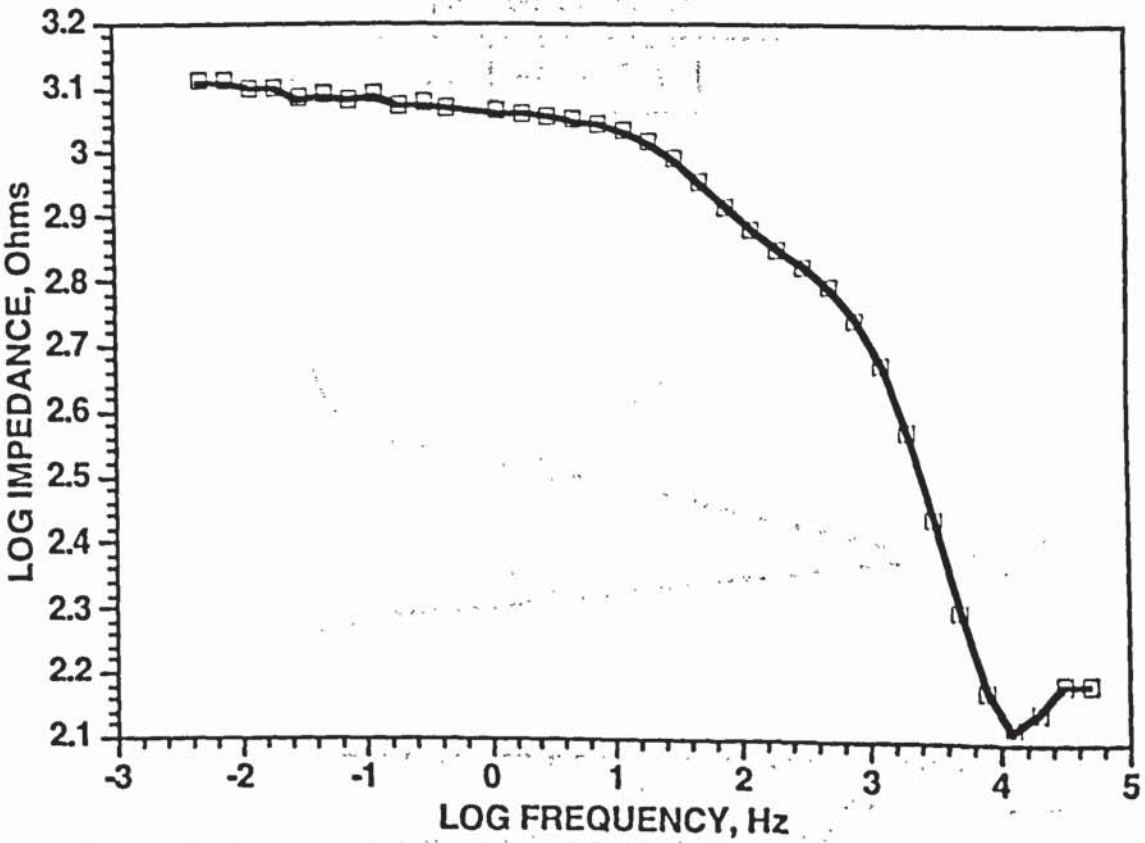

Figure 6.19: Bode plot for steel in the chloride-contaminated SRPC concrete

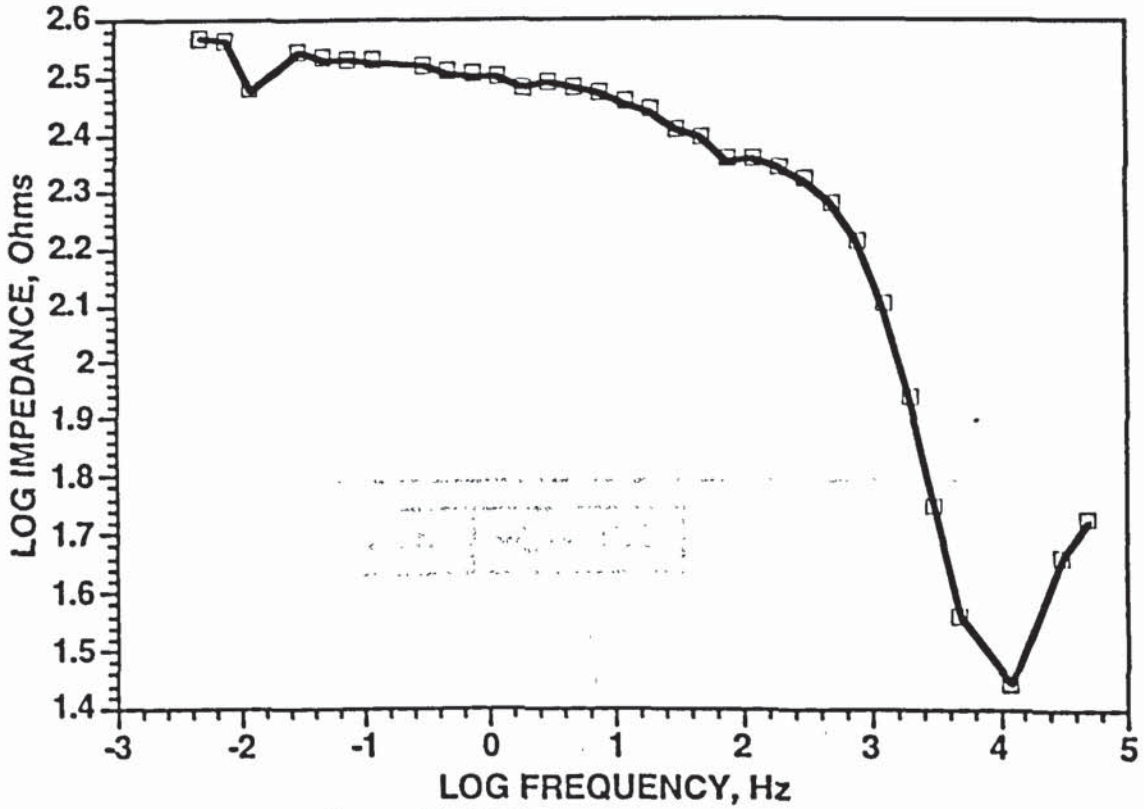

Figure 6.20: Bode plot for steel in SRPC concrete contaminated with sodium chloride plus sodium sulfate

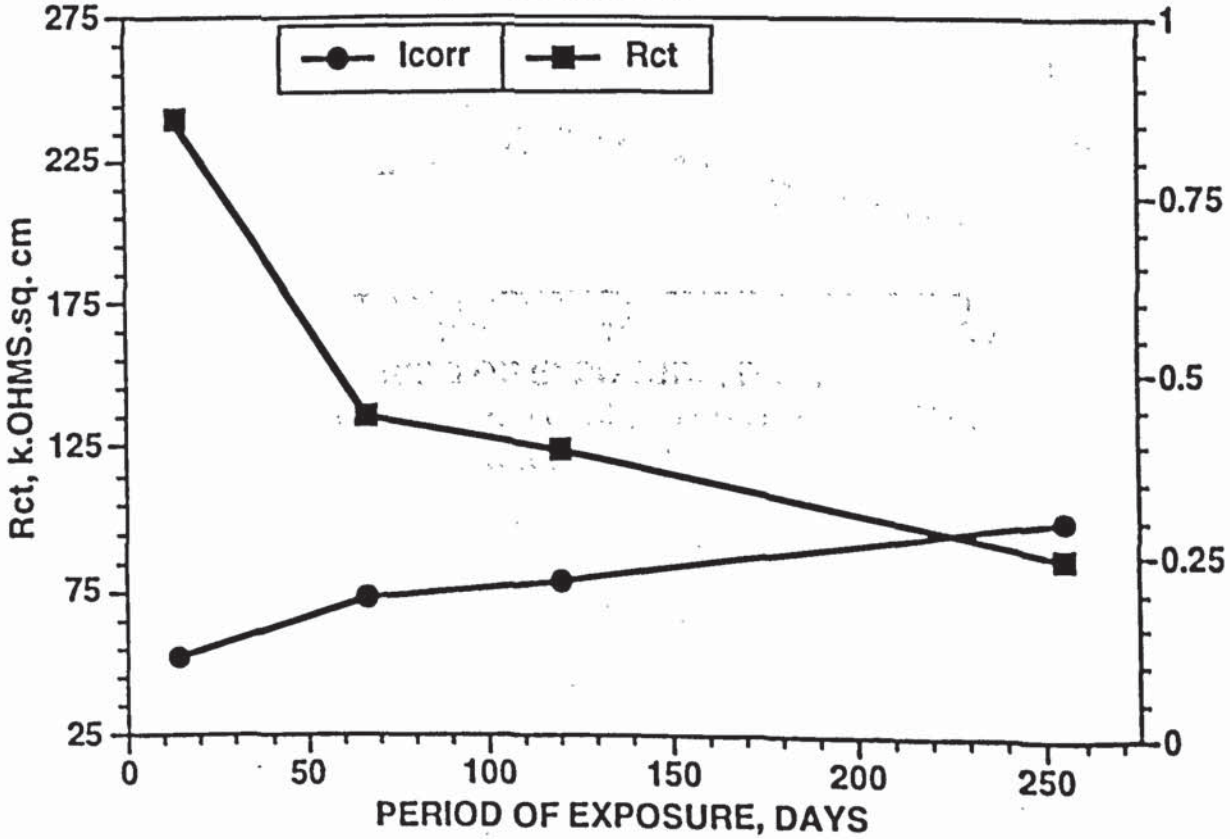

Figure 6.21: Rct and corrosion current density on steel in the uncontaminated SRPC concrete

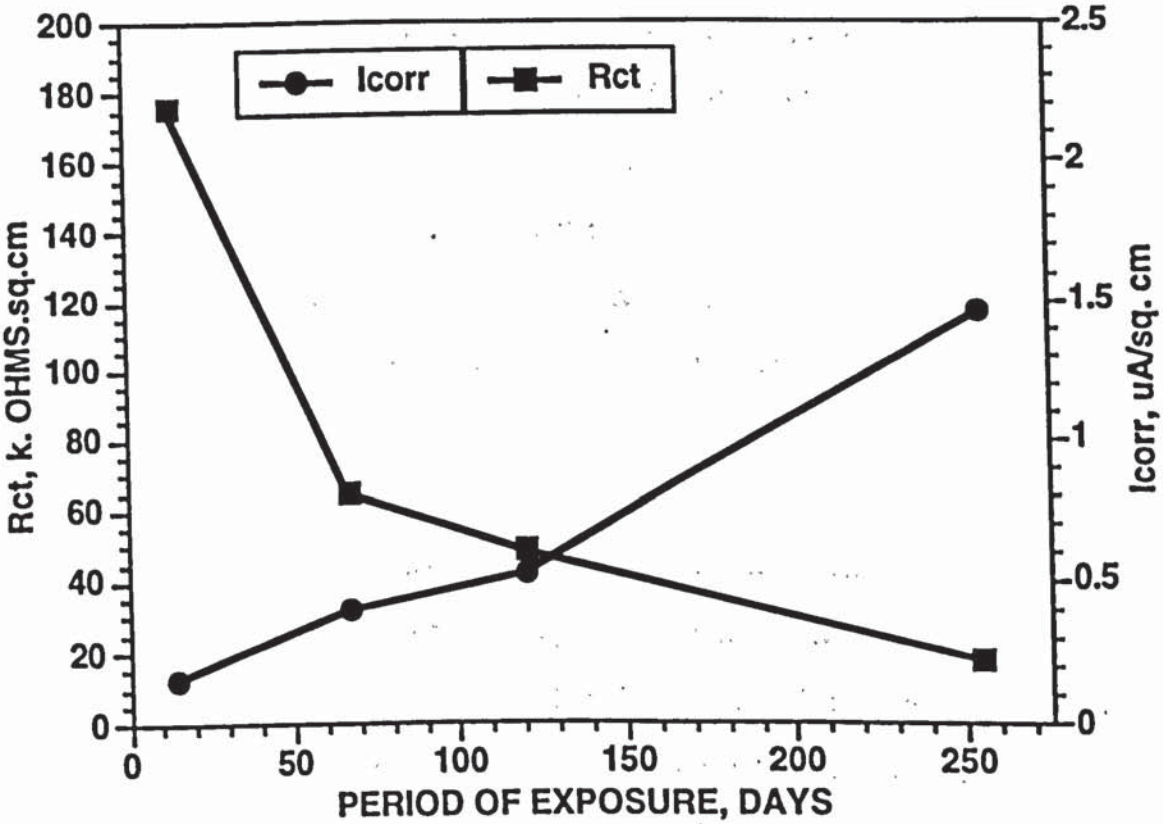

Figure 6.22: Rct and corrosion current density on steel in the chloride-contaminated SRPC concrete

14 to 67 days, becoming insignificant later. The Rct decreased from 175 to 18 $k\Omega.cm^2$ for the exposure period varying from 14 to 255 days. Figure 6.23 shows the variation in the Rct and I_{corr} values due to CO_2 exposure in the SRPC concrete specimens contaminated with sodium chloride plus sodium sulfate. These data also indicated a trend similar to that exhibited by the chloride-contaminated SRPC concrete specimens. The Rct values decreased from 80 to 7 $k.\Omega.cm^2$ for an exposure period of 240 days. A comparison of these data and that pertaining to chloride contaminated specimens (Figure 6.22) reveals that the Rct values tended to decrease, indicating higher corrosion activity, with the incorporation of sodium sulfate in the chloride-contaminated concrete.

The variation in the Rct values for the contaminated and uncontaminated OPC concrete specimens due to CO_2 exposure are plotted in Figures 6.24 through 6.26. These data also indicated a trend similar to that observed in the SRPC concrete specimens.

The corrosion current density on steel in the contaminated and uncontaminated concrete specimens after 255 days of exposure, calculated from the Rct data obtained from the Bode diagrams, are summarized in Table 6.3. This table also summarizes the corrosion current density on steel in the uncarbonated specimens exposed to similar temperature and humidity regimes. These data indicated higher corrosion activity on steel in the contaminated specimens compared to the uncontaminated specimens, both in the carbonated and uncarbonated specimens. The corrosion current density on steel in the contaminated carbonated concrete specimens was 70 to 200% of that in similar uncarbonated specimens. On the other hand, the corrosion activity in the uncontaminated specimens increased several fold due to exposure to the CO_2 atmosphere. For example, the corrosion current density in the carbonated uncontaminated concrete specimens was 6 to 10 times that in the uncarbonated specimens exposed to similar temperature and humidity environments.

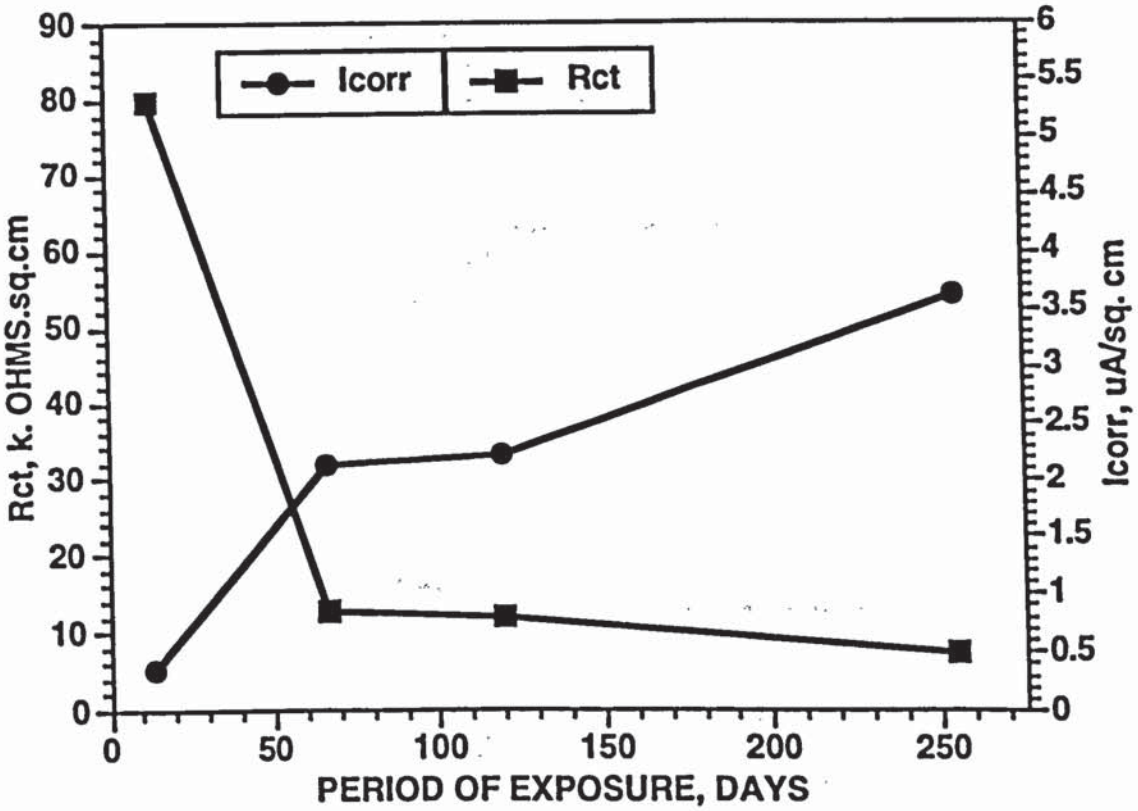

Figure 6.23: Rct and corrosion current density on steel in SRPC concrete contaminated with sodium chloride plus sodium sulfate

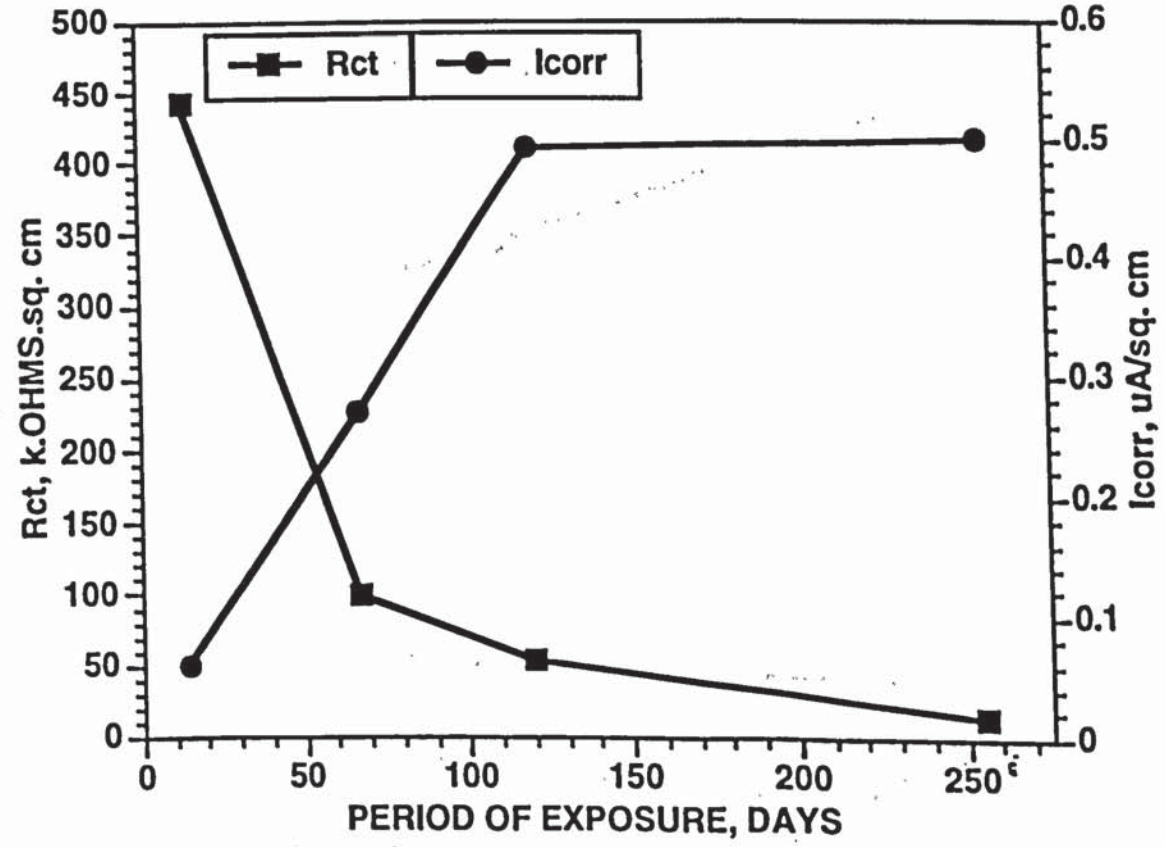

Figure 6.24: Rct and corrosion current density on steel in the uncontaminated OPC-A concrete

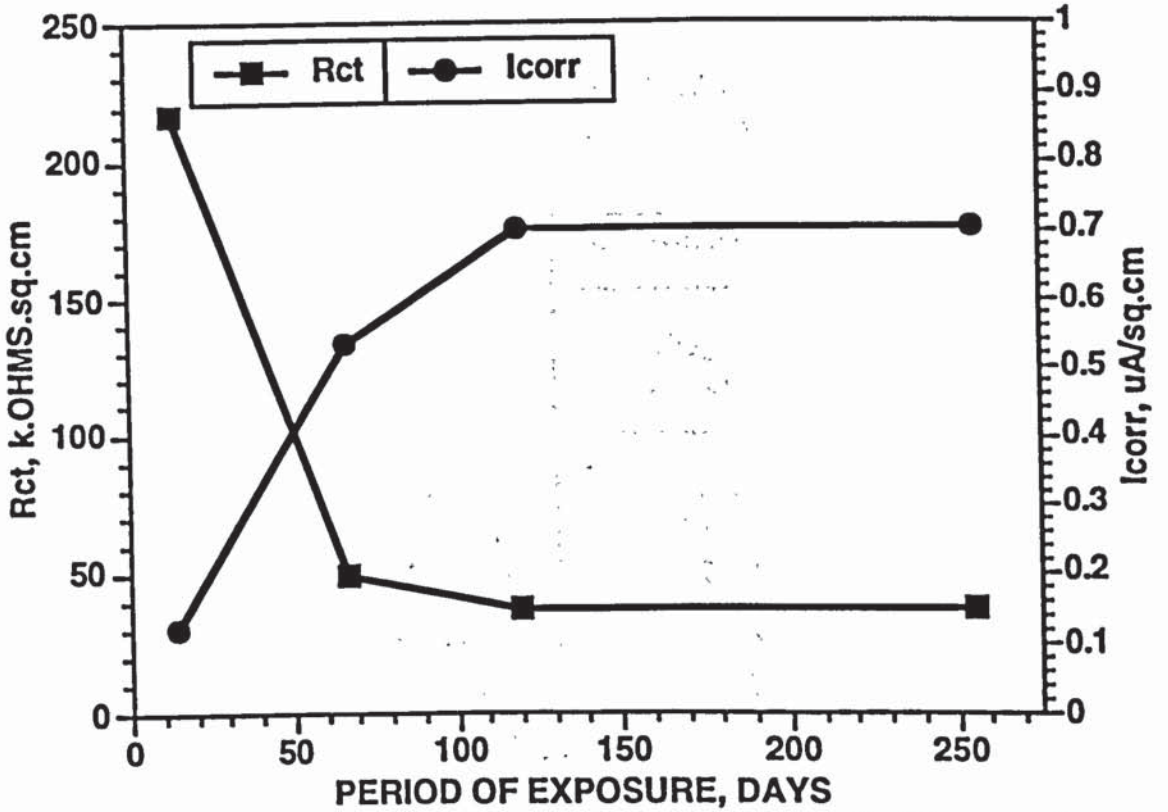

Figure 6.25: Rct and corrosion current density on steel in the chloride-contaminated OPC-A concrete

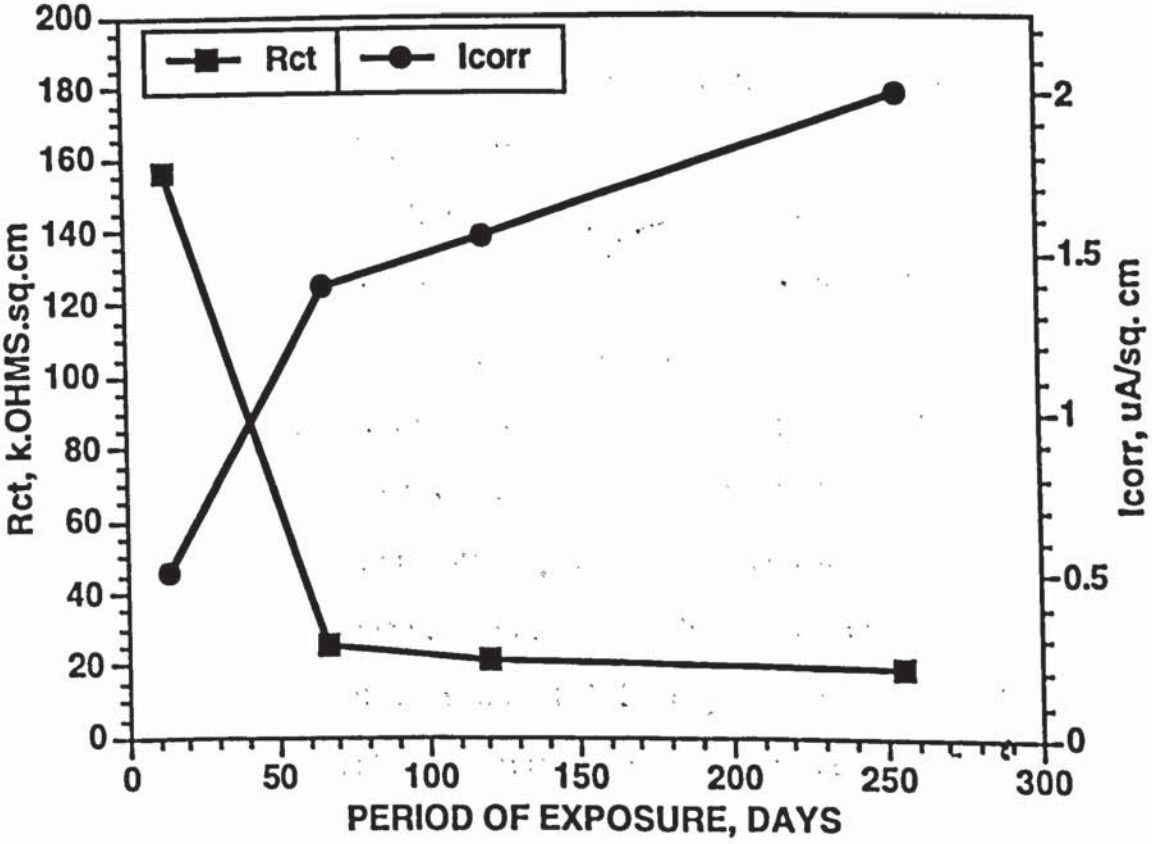

Figure 6.26: Rct and corrosion current density on steel in OPC-A concrete contaminated with sodium chloride plus sodium sulfate

Table 6.3: Comparison of corrosion current density on steel in the carbonated and uncarbonated concrete specimens measured by DC LPR and AC Impedance techniques

Cement	Contamination	Corrosion Current Density ($\mu A/cm^2$)	
		CO_2 Exposure*	Normal Exposure**
SRPC	None	0.30	0.05
	0.8% Cl^-	1.46	1.56
	$Cl^-+SO_4^{--}$	2.40	2.26
OPC	None	0.50	0.05
	0.8% Cl^-	0.90	1.29
	$Cl^-+SO_4^{--}$	1.39	2.14

* Measured using AC Impedance spectroscopy
** Measured using DC LPR technique

Another point which needs discussion is the use of technique for the measurement of reinforcement corrosion in carbonated concrete. A comparison of data in Tables 6.2 and 6.3 indicates that the I_{corr} in the uncontaminated specimens measured using AC impedance spectroscopy was 2 to 3 times that measured using linear polarization resistance method. This ratio was 1 to 1.4 in the contaminated specimens. This discrepancy in the results may be attributed to the uncompensated IR drop which will be significant in the carbonated concrete. In the contaminated concrete, the presence of sodium chloride and sodium sulfate partly offsets this increase in the concrete resistivity by improving the ionic conductivity and by moisture retention [241]. Several researchers [241,276-279] have indicated the importance of IR compensation in reinforcement corrosion studies, particularly in the carbonated concrete.

6.4 SUMMARY OF RESULTS

In this part of the study, the effect of chloride and sulfate contamination and CO_2 on reinforcement corrosion was evaluated. The corrosion potentials and corrosion current density measurements indicated a higher corrosion activity in the contaminated specimens compared to the uncontaminated specimens. Reinforcement corrosion in the specimens contaminated with sodium chloride plus sodium sulfate was more than that in the specimens contaminated with only sodium chloride.

The corrosion current density in the uncontaminated concrete specimens exposed to CO_2 was 6 to 10 times that in the uncarbonated specimens exposed to similar temperature and humidity conditions. This increase in I_{corr} due to CO_2 exposure in the contaminated specimens was 1 to 2 times in the uncarbonated specimens.

These results indicated that while reinforcement corrosion is imminent in the contaminated concrete, the corrosion initiation, due to CO_2 ingress to the steel interface, is of a finite duration in the uncontaminated concrete. Therefore, to extend the useful-service life of reinforced concrete structures, elimination of chloride and sulfate contamination and protecting the structural components through anti-carbonation coating is necessary.

As mentioned earlier, the size of the specimen and the exposure conditions used in this study do not represent the actual field conditions. Therefore, there is a need to evaluate the effect of carbonation, and chloride and sulfate contamination on reinforcement corrosion in the in-service structures.

CHAPTER 7

CONCLUSIONS AND RECOMMENDATIONS

The environmental conditions in the coastal areas of the Arabian Gulf constitute a very aggressive service environment for concrete construction in this part of the world. The deterioration of concrete, in this region, is mainly attributed to reinforcement corrosion. While this phenomenon is primarily related to the chloride ions, presence of sulfate salts may accelerate the deterioration process. Another factor which might influence reinforcement corrosion is the elevated temperature often recorded in this area. While few studies [15,20,72] have been conducted to evaluate the concomitant effect of chloride-sulfate contamination on the chloride binding of cements at normal temperature, others [78-81] have been devoted to investigate the effect of elevated temperature on this parameter. However, no data are available on the concomitant effect of elevated temperature and chloride-sulfate contamination on chloride binding capacity of cements. The concrete structures, in this region, are exposed to elevated temperatures and measurable quantity of chloride and sulfate contamination is inadvertently admixed in concrete through the use of brackish water for mixing and curing concrete, and contaminated aggregates. Further, the conjoint effect of chloride-sulfate contamination and elevated temperature on reinforcement corrosion has not been systematically investigated. Meager data reported on this subject have been mainly concerned with steel immersed in the $Ca(OH)_2$ solution [16,134,169] or concrete exposed to the natural environment [167-168].

Furthermore, the environmental conditions of the Arabian Gulf, characterized by elevated temperature and humidity, are conducive for accelerated carbonation [23]. However, the concomitant effect of chloride-sulfate contamination and elevated

temperature on the carbonation behaviour of plain and blended cements has not been studied. Investigations to evaluate the effect of aforementioned factors on carbonation in the blended cements is of particular interest, in this region, as these materials have to be imported and work out to be costlier than the ordinary portland cements.

This investigation was, therefore, conducted to evaluate the conjoint effect of chloride-sulfate contamination and temperature on the pore solution chemistry and reinforcement corrosion. Also, the effect of chloride-sulfate contamination and elevated temperature on carbonation in plain and blended cements was investigated.

7.1 CONCLUSIONS

The results of this study indicated that the concomitant presence of chloride and sulfate contamination at elevated temperature significantly influences concrete durability. The chloride-binding capacity of all the cements investigated was observed to be influenced by the sulfate ions. This behaviour was observed at all exposure temperatures. The chloride binding capacity of cements in chloride-contaminated specimens was, however, affected by the exposure temperature. While the free-chloride concentration in the specimens exposed to 25 and 40 °C was not significantly different, an appreciable increase in the free chloride concentration was noticed for exposure temperatures of 55 °C and above.

The Cl^-/OH^- values also increased with the exposure temperature in both plain and blended cements. This increase in the Cl^-/OH^- due to rise in temperature may lead to steel depassivation much earlier than at lower temperatures.

The sulfate concentration in the plain and blended cements was also affected by the exposure temperature and chloride contamination. The sulfate concentration in the specimens contaminated with sodium chloride plus sodium sulfate was more than that

in specimens contaminated with only sodium sulfate. This may be attributed to the concomitant reaction of chloride and sulfate ions with C_3A leading to an increase in their concentration in the pore solution compared to situations where only one of these salts is present. An increase in the sulfate concentration was also indicated in the chloride contaminated and uncontaminated specimens exposed to temperatures of more than 55 °C. The rise in the sulfate concentration due to higher temperature and/or chloride contamination, is significant from reinforcement corrosion view point, since sulfate ions not only depassivate steel but also decrease the electrical resistivity of concrete increasing the corrosion rate.

Corrosion of reinforcing steel in chloride-contaminated SRPC and OPC concretes was mainly influenced by: (i) exposure temperature, and (ii) sulfate contamination. The corrosion activity increased two to six times due to an increase in the temperature from 25 to 70 °C. The increase in the corrosion activity due to the concurrent presence of chloride and sulfate salts was 1.1 to 2.4 times that measured in concrete specimens contaminated with only sodium chloride. This increase may be attributed to the compounded effect of decrease in chloride binding and electrical resistivity of concrete.

Another important finding of this research is the accelerated carbonation noted in the contaminated specimens. The depth of carbonation in the contaminated specimens was more than that in the corresponding uncontaminated specimens. In the contaminated specimens, a higher depth of carbonation was measured in the specimens admixed with sodium chloride plus sodium sulfate than those contaminated with only sodium chloride. This trend of increased carbonation in the contaminated specimens was also observed in blended cements.

The accelerated carbonation in the contaminated specimens may be attributed to the changes brought about in the microstructure of the hardened cement paste due to inclusion of NaCl and Na_2SO_4. The inclusion of alkalies the accelerates hydration of

cement which results in relatively greater heterogeneities in the microstructure. These heterogeneities provide channels for gas transport thereby increasing the rate of carbonation. The other causes may be the increase in the total pore volume and moisture retention due to the incorporation of the chloride-sulfate contamination.

The results pertaining to accelerated carbonation indicated that chloride-sulfate contamination in concrete is not only conducive for steel depassivation, but also accelerates carbonation. Also, the increased carbonation depth observed in the blended cements is of particular concern, in this region, as these materials have to be imported for their technical merit and are two to three times costlier than the ordinary portland cement. Thus to utilize the technical benefits that accrue with the use of blended cements, guidelines for limiting the chloride and sulfate contamination should be established.

Corrosion of reinforcing steel in the concrete contaminated with sodium chloride and sodium chloride plus sodium sulfate and exposed to 3% CO_2 , 55 °C and 75% RH environment was more than that in the uncontaminated concrete. The reinforcement corrosion activity in the concrete contaminated with sodium chloride plus sodium sulfate was more than that in the specimens contaminated with only sodium chloride.

The corrosion current density on steel in the uncontaminated concrete specimens exposed to CO_2 was 6 to 10 times that in the uncarbonated specimens exposed to similar temperature and humidity conditions. This increase in the corrosion current density due to CO_2 exposure in the contaminated specimens was 1 to 2 times that in the uncarbonated specimens.

These results indicated that while reinforcement corrosion is imminent in the contaminated concrete, the corrosion initiation, due to CO_2 ingress to the steel, is of a finite duration in the uncontaminated concrete.

7.2 RECOMMENDATIONS

The data developed in this study indicated that the concomitant presence of chloride and sulfate contamination and temperature significantly influences the durability performance of concrete by: (i) decreasing the chloride binding, (ii) increasing reinforcement corrosion, and (iii) accelerating the carbonation process. Therefore, the level of contamination contributed by the concrete mixture ingredients should be controlled and minimized to extend the useful-service life of reinforced concrete structures. Minimizing the level of contamination contributed to concrete becomes all the more important as the coarse and fine aggregate available in this region are highly contaminated with chloride and sulfate salts. As such, concrete specifications should emphasize the need for washing the aggregates.

To avoid premature deterioration of concrete, threshold chloride and sulfate concentrations, for situations where both of these salts are present, should be established. In order to mandate such limits, further data should be generated on the effect of a combination of chloride and sulfate concentrations on concrete durability.

In the present study, sodium chloride and sodium sulfate were used as a source of chloride and sulfate contamination. The effect of other cations, namely magnesium and calcium, associated with sulfate ions on the chloride binding capacity, reinforcement corrosion and carbonation is not very well elucidated in the literature. Further studies towards this direction should also be conducted.

Furthermore, the data developed in this part of the study pertains to situations where the chlorides and sulfates or both, may be inducted into concrete through mixture ingredients, such as unwashed aggregates or usage of brackish water in mixing or curing of concrete. This is a common construction practice in the Arabian Gulf where

desalinated or potable water is relatively scarce. Another situation which is commonly observed in the Arabian Gulf region, is that related to permeation of chloride and sulfate ions to the steel-concrete interface through extraneous sources during the service-life of concrete structures. Concrete substructures exposed to sulfate-chloride-bearing sabkha soils and groundwaters in the Arabian Gulf represent a typical situation of this category. On a global scale, concrete structures exposed to a marine environment, which contains both sulfates and chlorides, also fall in this category. The effect of sulfates permeating from external sources under elevated temperature conditions on chloride binding and reinforcement corrosion need also to be evaluated. Such studies should also evaluate the performance of concrete surface coatings, coated steels and non-ferrous reinforcing bars in the environmental conditions of the Arabian Gulf.

REFERENCES

1. Strategic Highway Research Program, *Concrete and Structures : Progress and Product Update,* National Research Council, Washington, DC, 1989.

2. Wallbank, E. J., *The Performance of Concrete in Bridges,* HMSO, London, 1989.

3. Rasheeduzzafar, Dakhil, F. H., and Al-Gahtani, A. S., "Corrosion of Reinforcement in Concrete Structures in the Middle East," *Concrete International: Design and Construction,* Vol. 7, No. 9, 1985, pp. 48-55.

4. Maslehuddin, M., *Optimization of Concrete Mix Design for Durability in the Eastern Province of Saudi Arabia,* M.S. Thesis, King Fahd University of Petroleum and Minerals, Dhahran, Saudi Arabia, 1981.

5. Al-Saadoun, S. S., Rasheeduzzafar and Al-Gahtani, A. S., "Mix Design Considerations for Durable Concrete in the Gulf Environment," *The Arabian Journal for Science and Engineering,* Vol. 17, No. 1, January 1992, pp. 17-33.

6. Rasheeduzzafar, Dakhil, F. H., and Al-Gahtani, A. S., "The Deterioration of Concrete Structures in the Environment of Eastern Saudi Arabia," *The Arabian Journal for Science and Engineering,* Vol. 7, No. 3, 1983, pp. 21-27.

7. Emery, K. O., "Sediments and Water of Persian Gulf," *Bull. American Association of Petroleum Geologists,* Vol. 40, 1956, p. 2354.

8. Rasheeduzzafar, Dakhil, F. H. and Al-Gahtani, A. S., "Deterioration of Concrete Structures in the Environment of the Middle East," *ACI Journal Proceedings,* January-February 1984, Vol. 81, No. 1, pp. 13-20.

9. Hsu, T. T. C., "Mathematical Analysis of Shrinkage Stresses in a Model of Hardened Concrete," *ACI Journal Proceedings,* Vol. 60, No. 3, March 1963, pp. 371-390.

10. Slate, F. O. and Matheus, R. E., "Volume Changes upon Setting and Curing of Cement Paste and Concrete from Time Zero to Seven Days," *ACI Journal Proceedings,* Vol. 64, No. 1, January 1967, pp. 34-39.

11. Jaegermann, C. H., Ravina, D. and Pundak, B., "Accelerated Curing of Concrete by Solar Radiation," *Concrete and Reinforced Concrete in Hot Countries, Proceedings, International RILEM Symposium,* Haifa, August 1971, Vol. II, pp. 339-362.

12. Shalon, R. and Raphel, M., "Corrosion of Reinforcing Steel in Hot Countries," *RILEM Bulletin, No. 24,* Sept. 1964, pp. 29-45.

13. Parrott, L. J., *A Review of Carbonation in Reinforced Concrete,* British Cement Association Report C/1-0987, 1987.

14. Mehta, P. K. and Gjorv, O. E., "A New Test for Sulfate Resistance of Cements," *ASTM Journal of Testing and Evaluation,* Vol. 2, No. 6, 1974, pp.

510 - 515.

15. Holden, W. R., Page, C. L. and Short N. R., "The Influence of Chlorides and Sulfates on Concrete Durability," *Corrosion of Reinforcement in Concrete Construction*, Alan P. Crane (Ed.), Society of Chemical Industry, London, 1983, pp. 143-149.

16. Al-Tayyib, A. J., Somuah, S. K., Boah, J. K., Leblanc, P. and Al-Mana, A. I., "Laboratory Study on the Effect of Sulfate Ions on Reinforcement Corrosion," *Cement and Concrete Research*, Vol. 18, No. 5, 1988, pp. 774-782.

17. Al-Amoudi, O. S. B. and Maslehuddin, M., "The Effect of Chloride and Sulfate Ions on Reinforcement Corrosion," *Cement and Concrete Research*, Vol. 23, No. 1, 1993, pp. 139-146.

18. Al-Amoudi, O. S. B., Abduljauwad, S. N., Rasheeduzzafar and Maslehuddin, M., "Effect of Chloride and Sulfate Contamination in Soils on Corrosion of Steel and Concrete," *Transportation Research Record No. 1345*, 1992, pp. 67-73.

19. Al-Amoudi, O. S. B., Rasheeduzzafar, Maslehuddin M. and Abduljauwad, S. N., "Durability Evaluation of Plain and Blended Cements in Aggressive Media," *Proceedings Ninth International Congress on the Chemistry of Cement*, 1992, Vol. V, pp. 438-444.

20. Al-Amoudi, O. S. B., *Studies on Soil-Foundation Interaction in the Sabkha Environment of Eastern Province of Saudi Arabia*, Ph.D. Thesis, King Fahd University of Petroleum and Minerals, Dhahran, Saudi Arabia, 1992.

21. Treadaway, K. W. J., MacMillan, G., Hawkins, P. and de Fontenay, C., "The Influence of Concrete Quality on Carbonation in Middle Eastern Conditions - A Preliminary Study," *Corrosion of Reinforcement in Concrete Construction*, Crane A.P. (Ed.), Ellis Horwood, 1983, pp. 101-118.

22. de Fontenay, C., "A Study of the Effect of Concrete Admixtures, Concrete Composition and Exposure Conditions on Carbonation in Bahrain," *Proceedings, First International Conference on Deterioration and Repair of Reinforced Concrete in the Arabian Gulf*, Bahrain, 1985, pp. 467-483.

23. Kayyali, O. A. and Haque, M. N., "Effect of Carbonation on the Chloride Concentration in Pore Solution of Mortars with and without Fly Ash," *Cement and Concrete Research*, Vol. 18, No. 4, 1988, pp. 636 - 648.

24. Fookes, P. G., "A Simple Guide to Risk Assessment for Concrete in Hot Dry Salty Environments," *Proceedings, Fourth International Conference on Deterioration and Repair of Reinforced Concrete in the Arabian Gulf*, Bahrain, 1993, pp. 161-213.

25. Holmes, C. W. and Brundle, S. G., "The Deterioration of Reinforced Concrete through Chloride Attack," *Proceedings, Second International Conference on Deterioration and Repair of Reinforced Concrete in the Arabian Gulf*, Bahrain, 1987, pp. 469-487.

26. Hanson, C. M., "Comments on Electrochemical Measurements of the Rate of Corrosion of Steel in Concrete," *Cement and Concrete Research*, Vol. 14, No. 4, pp. 574-584, 1984.

27. Mehta, P. K., "Effect of Cement Composition on Corrosion of Reinforcing Steel in Concrete," *Chloride Corrosion of Steel in Concrete*, ASTM STP 629, American Society for Testing and Materials, Philadelphia, 1977, pp. 12-19.

28. Tuutti, K., *Corrosion of Steel in Concrete*, Research Report 4/82, Swedish Cement and Concrete Research Institute, Stockholm, 1982.

29. Page, C. L. and Treadaway, K. W. J., "Aspects of Electrochemistry of Steel in Concrete," *Nature*, V. 279, No. 5862, 1982, pp. 109-115.

30. Hime, W. and Erlin, B., "Some Chemical and Physical Aspects of Phenomena Associated with Chloride-induced Corrosion," *Corrosion, Concrete and Chlorides*, ACI SP-102, American Concrete Institute, Detroit, 1987, pp. 1-12.

31. Erlin, B., and Hime, W., "Chloride Induced Corrosion," *Ibid*, pp. 155-160.

32. Rasheeduzzafar, Dakhil, F. H. and Mukarram, K., "Influence of Cement Composition and Content on the Corrosion Behavior of Reinforcing Steel in Concrete," ACI Special Publication SP-100, American Concrete Institute, Detroit, 1987, pp. 1477-1502.

33. Page, C. L., Short, N. R. and Holden, W. R., "The Influence of Different Cements on Chloride-Induced Corrosion of Reinforcing Steel," *Cement and Concrete Research*, Vol. 16, No. 1, 1986, pp. 79-86.

34. Cook, H. K. and McCoy, W. J., "Influence of Chlorides in Reinforced Concrete," *Chloride Corrosion of Steel in Concrete*, ASTM STP 629, American Society for Testing and Materials, Philadelphia, 1977, pp. 20-29.

35. Hobbs, D. W., "Carbonation of Concrete containing PFA," *Magazine of Concrete Research*, Vol. 40, No. 143, June 1988, pp. 69-78.

36. Kawamura, K., Sereda, P. J. and Swenson, E. G., "Changes in Weight and Dimensions in the Drying and Carbonation of OPC Mortars," *Magazine of Concrete Research*, Vol. 17, No. 50, 1965.

37. Benjamin, S. E. and Sykes, J. M., "The Effect of Temperature on the Pitting Corrosion of Iron in OPC Mortars," *Proc. 3rd International Conference on Deterioration and Repair of Reinforced Concrete in the Arabian Gulf*, Bahrain, 1989, pp. 573-580.

38. Schiessl, R. and Raupach, M., "Influence of Concrete Composition and Microclimate on the Critical Chloride Content in Concrete," *Corrosion of Reinforcement in Concrete*, Page, Treadaway and Bamforth, Eds., Elsevier Applied Science, London, 1990, pp. 59-64.

39. Uhlig, H. H. *Corrosion and Corrosion Control*, John Wiley and Sons, New York, 1983.

40. Fookes, P. G., Pollock, G. J., and Kay, E. A., "Middle East Concrete: Rates of Deterioration," *Concrete*, September 1981, pp. 12-19.

41. Rasheeduzzafar, Dakhil, F. H. and Bader, M. A., "Toward Solving Concrete Deterioration Problem in the Arabian Gulf Region," *Arabian Journal for Science and Engineering*, Vol. 11, No. 2, 1986, pp. 129-146.

42. Fookes, P. G. and Collis, L., "Problems in the Middle East," *Concrete*, 1975, Vol. 9, No. 7, 1975, pp. 12-17.

43. Fookes, P. G. and Collis, L., "Cracking and the Middle East", *Concrete*, 1975, Vol. 10, No. 2, 1975, pp. 14-19.

44. Rasheeduzzafar and Dakhil, F. H., "Field Studies on the Durability of Concrete Construction in High Chloride-Sulphate Environment," *International Journal of Housing Science*, Vol. 4, No. 3, 1980, pp. 203-232.

45. Al-Gahtani, A. S., *An Investigation of Corrosion of Steel Reinforcement in Concrete in the Eastern Province of Saudi Arabia*, M.S. Thesis, King Fahd University of Petroleum and Minerals, Dhahran, Saudi Arabia, 1981.

46. Al-Tayyib, A. J., Rasheeduzzafar and Al-Mana, A. I., "Deterioration of Concrete Structures in the Gulf States," *Proceedings, First International Conference on Deterioration and Repair of Reinforced Concrete in the Arabian Gulf*, Bahrain, 1985, pp. 27-28.

47. Pollock, D. J., Kay, E. A. and Fookes, P. G., "Crack Mapping for Investigation of Middle East Concrete," *Concrete*, May 1981, pp. 12-18.

48. Kay, E. A., Fookes, P. G. and Pollock, D. J., "Deterioration related to Chloride Ingress," *Concrete*, November 1981, pp. 22-28.

49. Maslehuddin, M., Saricimen, H., Al-Mana, A. I. and Shameem, M., "Performance of Concrete in a High Chloride-Sulfate Environment," ACI Special Publication, SP-122, 1990, American Concrete Institute, Detroit, pp. 469-494.

50. Browne, R. D., Geoghegan, M. P. and Bakker, A. F., "Analysis of Structural Condition from Durability Tests," *Corrosion of Reinforcement in Concrete Construction*, Crane, A. P., Ed., Society of Chemical Industry, London, 1985, pp. 193-222.

51. Bashenini, M. S., Bhandari, B. M. and Davies, K. G., "Corrosion Control Procedures for Reinforced Concrete Power Manholes," *Materials Protection*, October 1989, pp. 17-24.

52. Saricimen, H., Al-Tayyib, A. J., Maslehuddin, M. and Shamim, M., "Concrete Deterioration in High Chloride-Sulphate Environment and Repair Strategies", ACI Special Publication, SP-128, American Concrete Institute, Detroit, USA, 1991, pp. 19-34

53. Bashenini, M. S., Eid, O. A., and Paul, I. S., "Corrosion Damage and Rehabilitation of Foundations of a Reinforced Concrete Office Building,"

Proceedings, Fourth International Conference on Deterioration and Repair of Reinforced Concrete in the Arabian Gulf, Bahrain, October 1993, pp. 303-312.

54. Hejji, J. A., John, D. G. and Sullivan, R. K., "Protection of Reinforced Concrete Seawater Cooling System," Paper No. 388, NACE Corrosion 89, New Orleans, March 1989.

55. Barneyback, R. S. and Diamond, S., "Expression and Analysis of Pore Fluids from Hardened Cement Pastes and Mortars," *Cement and Concrete Research*, Vol. 11, No. 2, 1981, pp. 279-285.

56. Vogel, I. A. *A Textbook of Quantitative Inorganic Analysis*, 5th Edition, Revised by J. Basset, Longman, London, 1985, p. 754.

57. *Standard Methods for the Examination of Water and Waste Water*, 16th Edition, American Public Health Association, Washington, 1985.

58. Yonezawa, T., Ashworth, V. and Procter, R. P. M., "The Mechanism of fixing Cl^- by Cement Hydrates resulting in the transformation of NaCl to NaOH," *Proceedings, 8th International Conference on Alkali-Aggregate Reaction*, Kyoto, 1989, pp. 153-160.

59. Kakihana, H. and Mori, Y., *Introduction to Ion-exchange Reaction*, Hirokawa Shoten, 1971.

60. Kayyali, O. A., Kawamura, M. and Haque, M. N., "Fly Ash and Cation Effects on Free Cl^- and OH^- Concentrations in Mortar," ASCE *Journal of Materials in Civil Engineering*, Vol. 3, No. 2, May 1991, pp. 113-125.

61. Glasstone, S., *Textbook of Physical Chemistry*, Macmillan and Co., London, 1986, p. 959.

62. Herr, R. and Weiker, W., "The Hydroxide-Sulphate ion Equilibrium in Cement Paste Pore Solutions and its Significance to the Theory of AAR in Concrete," *Proc. 9th International Conference on Alkali-Aggregate Reaction in Concrete*, London, 1992, pp. 440-450.

63. Luke, K. and Glasser, F. P., "Effect of Temperature on the Hydration Chemistry and Durability of Cement Concrete," *Proc. Fourth International Conference on Durability of Building Materials and Components*, Singapore, 1987, pp. 188-195.

64. Page, C. L. and Vennesland, O., "Pore Solution Composition and Chloride Binding Capacity of Silica-Fume Cement Pastes," *Materials and Structures*, Vol. 16, No. 91, 1983, pp. 19-25.

65. Rasheeduzzafar, Hussain, S. E. and Al-Gahtani, A. S., "Pore Solution Composition and Reinforcement Corrosion Characteristics of Microsilica Blended Cement Concrete," *Cement and Concrete Research*, Vol. 21, No. 6, 1991, pp. 1035-1048.

66. Byfors, K., "Influence of Silica Fume and Fly Ash on Chloride Diffusion and pH Values in Cement Paste," *Cement and Concrete Research*, Vol. 17, No. 1,

1987, pp. 115-130.

67. Byfors, K., Hansson, C. M. and Tritthart, J., "Pore Solution Expression as a Method to Determine the Influence of Mineral Additives on Chloride Binding," *Cement and Concrete Research*, Vol. 16, No. 5, 1986, pp. 760-770.

68. Diamond, S., "Effects of Two Danish Fly Ashes on Alkali Contents of Pore Solutions of Cement Fly Ash Pastes," *Cement and Concrete Research*, Vol. 11, No. 3, 1981, pp. 383-394.

69. Nixon, P. J., Page, C. L., Canham, I. and Bollinghaus, R., "Influence of Sodium Chloride on Alkali-Silica Reaction," *Advances in Cement Research*, Vol. 1, No. 2, 1988, pp. 99-106.

70. Marsh, B. K., Day, R. L. and Bonner, D. G., "Strength Gain and Calcium Hydroxide Depletion in Hardened Cement Pastes Containing Fly Ash," *Magazine of Concrete Research*, Vol. 38, No. 134, 1986, pp. 23-29.

71. Sellevold, E. J. "Silica Fume Cement Pastes: Hydration and Pore Structure," *Condensed Silica Fume in Concrete*, Gjorve, O. E. Ed., The Norwegian Institute of Technology, Division of Building Materials, 82.610, Trondheim, 1982.

72. Al-Amoudi, O. S. B., Rasheeduzzafar, Maslehuddin, M. and Abduljauwad, S.N. "Influence of Sulfate Ions on Chloride-Induced Reinforcement Corrosion in Portland and Blended Cement Concretes," *Cement, Concrete and Aggregates*, Vol. 16, No. 1, June 1994, pp. 3-11.

73. Hausmann, D. A., "Steel Corrosion in Concrete, How Does it Occur?," *Materials Protection*, Vol. 6, November 1967, pp. 19-23.

74. Gouda, V. K., "Corrosion and Corrosion Inhibition of Reinforcing Steel: I. Immersed in Alkaline Solution," *British Corrosion Journal*, Vol. 5, 1970, pp. 198-203.

75. Page, C. L. and Havdahl, J., "Electrochemical Monitoring of Corrosion of Steel in Microsilica Cement Pastes," *Materials and Structures*, Vol. 18, No. 103, 1988, pp. 41-48.

76. Gouda, V. K., Halaka, W. Y., "Corrosion and Corrosion Inhibition of Reinforcing Steel: II. Embedded in Concrete," Vol. 5, 1970, pp. 204-208.

77. Griffin, D. F., "Corrosion Inhibitors for Reinforced Concrete," *American Concrete Institute Special Publication SP-49*, 1975, pp. 95-102.

78. Roberts, M. H., "Effects of Calcium Chloride on the Durability of Pre-Tensioned Wire in Prestressed Concrete," *Magazine of Concrete Research*, Vol. 14, No. 42, November 1962, pp. 143-152.

79. Arya, C., Buenfeld, N. R. and Newman, J. B., "Factors Influencing Chloride-Binding in Concrete," *Cement and Concrete Research*, Vol. 20, No. 2, 1990, pp. 291-300.

80. Hussain, S. E. and Rasheeduzzafar, "Effect of Temperature on Pore Solution Composition in Plain Cements," *Cement and Concrete Research*, Vol. 23, No. 6, 1993, pp. 1357-1368.

81. Arya, C., Buenfeld, N. R. and Newman, J. B., "Assessment of Simple Methods of Determining the Free Chloride Ion Content of Cement Paste," *Cement and Concrete Research*, Vol. 17, 1987, pp. 907-918.

82. Hussain, S. E., *Mechanisms of High Durability Performance of Plain and Blended Cements*, Ph.D. Dissertation, King Fahd University of Petroleum and Minerals, Dhahran, Saudi Arabia, August 1991.

83. Al-Amoudi, O. S. B., Maslehuddin, M., Rasheeduzzafar and Abduljauwad, S. N., "Durability Considerations for Construction of Substructures in Sabkha Environments," *Proc. 4th International Conference on Structural Failure, Durability and Retrofitting*, Singapore, 1993, pp. 819-834.

84. Calleja, J., "Durability," *7th International Congress on the Chemistry of Cement*, Paris, 1980, Vol. 1, Paris, France, 1980, pp. 2/1-2/48.

85. Gunkel, P., "Chloridgehalte Ausgeprebter Porenlosungen", *International Mitteilungen, FEhs* 1983.

86. Tritthart, J., "Chloride Binding in Cement, II: The Influence of the Hydroxide Concentration in the Pore Solution of Hardened Cement Paste on Chloride Binding," *Cement and Concrete Research*, Vol. 19, No. 5, 1989, pp. 683-691.

87. Diamond, S., "Chloride Concentrations in Concrete Pore Solutions Resulting from Calcium and Sodium Chloride Admixtures," *Cement, Concrete, and Aggregates*, Vol. 8, No. 2, Winter 1986, pp. 97-102.

88. Andrade, C. and Page, C. L., "Pore Solution Chemistry and Corrosion in Hydrated Cement Systems Containing Chloride Salts: A Study of Cation Specific Effects," *British Corrosion Journal*, Vol. 21, No. 1, 1986, pp. 49-53.

89. Theissing, E. M., Hest-Wardenier, P. V. and Wind, G., "Combining of Sodium Chloride and Calcium Chloride by a Number of Hardened Cement Pastes," *Cement and Concrete Research*, Vol. 8, No. 6, 1978, pp. 683-691.

90. Ramachandran, V. S., "Possible States of Chloride in the Hydration of Tricalcium Silicate in the Presence of Calcium Chloride," *Materiaux et Constructions (RILEM)*, Vol. 4, No. 19, 1971, pp. 3-12.

91. Ramachandran, V. S., Seeley, R. C., and Polomark, G. M., "Free and Combined Chloride in Hydrating Cement and Cement Components," *Materiaux et Constructions (RILEM)*, Vol. 17, No. 100, 1984, pp. 285-289.

92. Ben-Yair, M., "The Effect of Chlorides on Concrete in Hot and Arid Regions," *Cement and Concrete Research*, V. 4, No. 3, 1974, pp. 405-416.

93. Rasheeduzzafar, Hussain, S. E. and Al-Saadoun, S. S., "Effect of Cement Composition on Chloride Binding and Corrosion of Reinforcing Steel in Concrete," *Cement and Concrete Research*, Vol. 21, No. 5, 1991, pp. 777-794.

94. Maslehuddin, M., Rasheeduzzafar, Page, C. L., Al-Mana, A. I. and Al-Tayyib, A. J., "Effect of Temperature and Sulfate Contamination on the Chloride Binding Capacity of Cements," *Proc., 4th International Conference on Deterioration and Repair of Reinforced Concrete in the Arabian Gulf*, Macmillan, G. L., Ed., 1993, pp. 735-750.

95. Page, C. L., Lambert, P. and Vassie, P. R. W., "Investigations of Reinforcement Corrosion: 1. The Pore Electrolyte Phase in Chloride-Contaminated Concrete," *Materials and Structures*, 24(142), 1991, pp. 243-252.

96. Rasheeduzzafar, Hussain, S. E. and Al-Saadoun, S. S., "Effect of Tricalcium Aluminate Content of Cement on Chloride Binding and Corrosion of Reinforcing Steel in Concrete," *ACI Materials Journal*, January-February, 1992, pp. 3-12.

97. Rasheeduzzafar, "Influence of Cement Composition on Concrete Durability," *ACI Materials Journal*, November-December 1992, pp. 574-586.

98. Richartz, W., "Die Bindung Von Chlorid bei der Zement hartung," *Zement-Kalk-Gips* Vol. 22, No. 10, 1969, pp. 447-456.

99. Monfore, G. M., and Verbeck, G. J., " Corrosion of Pre-stressed Wire in Concrete," *ACI Journal, Proceedings*, Vol. 57, No. 5, 1960, pp. 491-516.

100. Verbeck, G. J., *Corrosion of Metals in Concrete*, ACI Special Publication SP-49, American Concrete Institute, Detroit, 1975, pp. 21-38.

101. Lambert, P., Page, C. L. and Short, N. R., "Pore Solution Chemistry of the Hydrated System Tricalcium Silicate/Sodium Chloride/Water," *Cement and Concrete Research*, Vol. 15, No. 4, 1985, pp. 675-680.

102. Mehta, P. K., "Effect of Cement Composition on Corrosion of Reinforcing Steel in Concrete," *Chloride Corrosion of Steel in Concrete*, Special Technical Publication STP 629, American Society for Testing and Materials, Philadelphia, USA, 1977, pp. 12-17.

103. Ramachandran, V. S., *Calcium Chloride in Concrete*, Applied Science Publishers, London, 1976, pp. 57-59.

104. Diamond, S. and Lopez-Fores, F., *Journal of the American Ceramic Society*, 64, 1981, pp. C162-C164.

105. Rasheeduzzafar, Al-Saadoun, S. S. and Al-Gahtani, A. S., "Reinforcement Corrosion Resisting Characteristics of Silica Fume Blended Cement Concrete," *ACI Materials Journal*, Vol. 89, No. 4, July-August 1992, pp. 337-344.

106. Glasser, F. P. and Marr, J., "The Effect of Mineral Additives on the Composition of Cement Pore Fluids," *The Chemistry and Chemically-Related Properties of Cement*, Glasser, F. P. Ed., British Ceramic Society, No. 35, 1984, pp. 419-429.

107. Kawamura, M., Kayyali, O. A. and Haque, M. N., "Effects of Fly Ash on Pore Solution Composition in Calcium and Sodium Chloride Bearing Mortars," *Cement and Concrete Research,* Vol. 18, No. 5, September 1988, pp. 763-773.

108. Khan, C. N. S. A., *The Effect of Temperature and Salt contamination on Corrosion of Reinforcing Steel in OPC and Blended Cement Concretes*, M.S. Thesis, King Fahd University of Petroleum and Minerals, Dhahran, Saudi Arabia, August 1993.

109. Lambert, P., Page, C. L. and Vassie, P. R. W., "Investigations of Reinforcement Corrosion. 2. Electrochemical Monitoring of Steel in Chloride-Contaminated Concrete," *Materials and Structures*, 24, 1991, pp. 351-358.

110. Mangat, P. S. and Gurusamy, K., "Corrosion Resistance of Steel Fibers in Concrete Under Marine Exposure," *Cement and Concrete Research*, V. 18, No. 1, Jan. 1989, pp. 44-54.

111. Hanson, I. L. H. and Hansson, C., "Ion-Conduction in Cement-Based Materials," *Cement and Concrete Research,* Vol. 15, No. 2, 1985, pp. 201-212.

112. Gjorve, O. E., "Durability of Concrete containing Condensed Silica Fume," *American Concrete Institute Special Publication, SP-79,* ACI, Detroit, 1983, pp. 695-708.

113. Vennesland, O. E. and Gjorve, O. E., "Silica Fume Concrete-Protection Against Corrosion of Embedded Steel", American Concrete Institute, Special Publication, SP-79, ACI, Detroit, pp. 721-729.

114. Cao, H. T. and Sirivivatnanon, V., "Corrosion of Steel in Concrete with and without Silica Fume," *Cement and Concrete Research,* Vol. 21, Nos. 2/3, 1991, pp. 316-324.

115. Preece, C. M., Arup, H. and Frolund, T., "Electrochemical Behavior of Steel in Dense Silica-Cement Mortar," American Concrete Institute, Special Publication, SP-79, ACI, Detroit, pp. 785-796.

116. Skalny, J. and Young, J. F., "Mechanisms of Portland Cement Hydration," *Proc. 7th International Congress on the Chemistry of Cements*, Paris, France, 1980, pp. II-1/3-II-1/45.

117. Dekeyser, W. L. and Tenoutasse, N. "The Hydration of Ferrite Phase of Cements," *Proc. 5th International Symposium on Chemistry of Cement,* Tokyo, Vol. II, 1968.

118. Rozenberg, T. I. and Kucheryaeva, G. D., "Concurrent Reactions of C_3S and C_3A with the Additions of Electrolytes," *Proc., 6th International Congress on the Chemistry of Cements,* Moscow, 1974.

119. Ratinov, V. B., and Rozenberg, T. I., *Concrete Additives*, Strojizdat, Moscow, 1973.

120. Miller, D. G., "Laboratory Investigation of the Influence of Curing Conditions

and Various Admixtures on the Life of Concrete Stored in Sulphate Solutions as Indicated by Physical Changes," *Proceedings, ASTM*, Vol. 2, Part 2, 1924, pp. 847-863.

121. Thorvaldson, T., "Chemical Aspects of the Durability of Cement Products," *Proceedings, 3rd International Symposium on the Chemistry of Cement*, London, 1952, pp. 436-466.

122. Yeginobali, A., "Sulphate Resistance of Mortars Mixed with Sea Waters," *Proceedings, 3rd International Conference on Durability of Building Materials and Components*, Espoo, Finland, Vol. 3, 1984, pp. 55-65.

123. Harrison, W. H., "Effect of Chloride in Mix Ingredients on Sulphate Resistance of Concrete," *Magazine of Concrete Research*, Vol. 42, 152, 1990, pp. 113-126.

124. Kind, V. V., "Some Questions and Problems in the Field of Corrosion of Concrete Used in Hydrotechnical Structures," *Proceedings, Conference on Corrosion of Concrete*, Moscow, 1953, English Translation: I.P.S.T., Jerusalem, 1962, pp. 31-38.

125. Kind, V. V., "Effect of Chlorides on the Speed of Sulfate Corrosion of Portland Cement, *Tsement*, BRE Digest No. 346, Vol. 22, Part 1, 1956, pp. 3-6.

126. Biczok, I., *Concrete Corrosion, Concrete Protection*, 8th Edition, Akademiai Kiado, Budapest, 1980.

127. Lea, F. M., *The Chemistry of Cement and Concrete*, 3rd Edition, Edward Arnold Ltd., London, 1970.

128. Corner, H. and Rippstain, D., "Effect of Aqueous Sodium Chloride Solution on Ettringite," *Touindustrie-Zeitung (TIZ), Fachberichte*, 109, No. 9, 1985, pp. 680-683.

129. Al-Samarai, M. A. and Raouf, Z. A., "Deterioration of Concrete Due to Sulphate Attack in Iraq," *Proceedings, 2nd International Conference on Deterioration and Repair of Reinforced Concrete in the Arabian Gulf*, Bahrain, Vol. 1, 1987, pp. 555-566.

130. Smith, F. L., "Effect of Calcium Chloride Additions on Sulfate Resistance of Concrete Placed and Initially Cured at 40 and 70 °F Temperatures," *Concrete Laboratory Report No. C-900*, Division of Engineering Laboratories, Bureau of Reclamation, Washington D. C., July 7, 1959.

131. Locher, F. W., "Influence of Chloride and Hydrocarbonate on Sulphate Attack," *Proceedings, 5th International Symposium on the Chemistry of Cement*, Tokyo, Supplementary Paper III-124, Vol. 3, 1968, pp. 328-335.

132. Hjorth, L., "Cement Specifications for Concrete Exposed to Chlorides and Sulfates," *Proceedings, CEB-RILEM International Workshop on Durability of Concrete Structures*, Copenhagen, May 1983, pp. 229-235.

133. Al-Amoudi, O. S. B., Rasheeduzzafar, Maslehuddin, M. and Abduljauwad,

S.N., "Influence of Chloride Ions on Sulfate Deterioration in Plain and Blended Cements," *Magazine of Concrete Research*, Vol. 46, No. 167, June 1994, pp. 113-123.

134. Jarrah, N. R., Al-Amoudi, O. S. B., Maslehuddin, M., Ashiru, O. A., and Al-Mana, A. I., "Electrochemical Behavior of Steel in Plain and Blended Cement Concretes in Sulfate and/or Chloride Environments," *Construction and Building Materials Journal*, to be published.

135. Barvinok, M. S., Komokhov, P. G. and Bondoreva, N. F., "Effect of Temperature on Additives in the Early Stages of Hardening," *Proc., 6th International Congress on Chemistry of Cement*, Moscow, 1974.

136. Lalck, V., and Bures, I., "The Phase Composition and Microstructure of Cement Pastes Hydrated at Elevated Temperatures," *Ibid.*

137. Maldovan, V. and Butucescu, N., "Essential Aspects Concerning the Effects of Temperature (20-90 °C) on the Hydration of the Main Mineralogical Components of Portland Cement," *Mater. Const.*, 6 (65), 1976.

138. Hoglund, L. O., "Some Notes on Ettringite Formation in Cementitious Materials: Influence of Hydration and Thermodynamic Constraints for Durability," *Cement and Concrete Research*, Vol. 22, Nos. 2/3, 1992, pp. 217-228.

139. Pourbaix, M., "Applications of Electrochemistry in Corrosion Science and Practice," *Corrosion Science*, 14, 1974, pp. 25-28.

140. Pourbaix, M., *Atlas of Electrochemical Equilibria in Aqueous Solutions*, translated by J. A. Franklin, New York, Pergamon Press, 1966, pp. 312.

141. Page, C. L., "The Mechanisms of Corrosion Protection in Reinforced Concrete Marine Structures," *Nature*, 1975, 258, 1975, pp. 514-515.

142. Leek, D. S., and Poole, A. B., "The Breakdown of the Passive Film on High Yield Mild Steel by Chloride Ions," *Corrosion of Reinforcement in Concrete*, Page, Treadaway and Bamforth, Editors, Elsevier Applied Science, London, 1990, pp. 65-73.

143. Sagoe-Crenstil, K. K. and Glasser, F. P., "Analysis of the Steel Concrete Interface," *Corrosion of Reinforcement in Concrete*, Page, Treadaway and Bamforth, Editors, Elsevier Applied Science, London, 1990, pp. 74-86.

144. Hoar, T. P., "The Anodic Behaviour of Metals," *Corrosion Science*, 7, 1967, pp. 341-355.

145. Chao, C. Y., Lin, L. F., and MacDonald, D. D., "A Point Defect Model for Anodic Passive Films. Part I: Film Growth Kinetics. Part II: Chemical Breakdown and Pit Initiation," *Journal of Electrochemical Society*, 128, 1981, pp. 1187-1194.

146. Alvarez, M. G., and Galvele, J. R., "The Mechanisms of Pitting of High Purity Iron in NaCl Solutions," *Corrosion Science*, 24, 1984, pp. 27-48.

147. American Concrete Institute, ACI 318-85 *Building Code Requirements for Reinforced Concrete*, 1985.

148. ACI 224, Causes, Evaluation and Repair of Cracks in Concrete," American Concrete Institute, Detroit.

149. British Standards Institution, *The Structural Use of Concrete* BS 8110: Part 1: 1985.

150. Al-Amoudi, O. S. B., Maslehuddin, M. and Rasheeduzzafar, "Effect of Sulphate on the Chloride Binding of Cements: Sulfate Cation Effect," to be published.

151. Mangat, P. S. and Molloy, B. T., "Influence of PFA, Slag and Microsilica on Chloride Induced Corrosion of Reinforcement in Concrete," *Cement and Concrete Research*, Vol. 21, No. 5, 1991, pp. 819-834.

152. Al-Amoudi, O. S. B., , Rasheeduzzafar Abduljauwad, S. N. and Maslehuddin, M., "Corrosion of Reinforcing Steel in Sabkha Environment," *King Saud University Journal for Science and Engineering*, in press.

153. Lambert, P., *Corrosion and Passivation of Steel in Concrete*, Ph.D. Thesis, Aston University, 1983.

154. Stern, M. and Geary, A. L., "A Theoretical Analysis of the Slope of the Polarization Curves," *Journal of Electrochemical Society*, Vol. 104, 1957, pp. 56.

155. Andrade, C., Castelo, V., Alonso, C. and Gonzalez, J. A., "Determination of the Corrosion Rate of Steel Embedded in Concrete," *ASTM STP 906*, Philadelphia, 1986, p. 43.

156. John, D. G., Searson, P. C. and Dawson, J. L., *British Corrosion Journal* 16, 1981, p. 102.

157. Andrade, C., Castelo, V., "Practical Measurement of the AC Impedance of Steel Bars Embedded in Concrete by Means of a Spectrum Analyzer," *British Corrosion Journal*, Vol. 19, No. 2, 1984, pp. 98 -100.

158. Hope, B. B., Page, J. A. and Ip, A. K. C., "Corrosion Rates of Steel in Concrete," *Cement and Concrete Research*, Vol. 16, No. 5, 1986, pp. 771.

159. Macdonald, D. D., McKubre, M. C. J., and Urquidi-Macdonald, M., "Theoretical Assessment of AC Impedance Spectroscopy for Detecting Corrosion of Rebar in Reinforced Concrete," *Corrosion*, Vol. 44, No. 1, January 1988, pp. 2-6.

160. Newton, C. J. and Sykes, J. M., "A Galvanostatic Pulse Technique for Investigation of Steel Corrosion in Concrete," *Corrosion Science*, Vol. 28, No. 11, 1988, p. 1051-1074.

161. Felieu, S., Gonzalez, J. A., Andrade, C. and Felieu, V., "On-Site Determination

of the Polarization Resistance in a Reinforced Concrete Beam," *Corrosion*, Vol. 44, No. 10, October 1988, pp. 761-765.

162. Gonzalez, J. A., Molina, A., Escudero, M. L. and Andrade, C., "Errors in the Electrochemical Evaluation of Very Small Corrosion Rates - I. Polarization Resistance Method Applied to Corrosion of Steel in Concrete," *Corrosion Science*, Vol. 25, No. 10, 1985, pp. 917-930.

163. Gonzalez, J. A., Molina, A., Escudero, M. L. and Andrade, C., "Errors in the Electrochemical Evaluation of Very Small Corrosion Rates - II. Other Electrochemical Techniques Applied to Corrosion of Steel in Concrete," *Corrosion Science*, Vol. 25, No. 10, 1985, pp. 917-930

164. Dawson, J. L. "Corrosion Monitoring of Steel in Concrete," *Corrosion of Reinforcement in Concrete Construction*, Crane, A. P. Ed. Ellis Horwood, Chichester, 1983, pp. 175-192.

165. Hardon, R. G., Lambert, P. and Page, C. L., "Relationship between Electrochemical Noise and Corrosion Rate of Steel in Salt Contaminated Concrete," *British Corrosion Journal*, Vol. 23, No. 4, 1988, pp. 225-228.

166. Stratful, R. F., "Effect on Reinforced Concrete in Sodium Chloride and Sodium Sulfate Environments," *Materials Protection*, Vol. 3, No. 12, December 1964, pp. 74-80.

167. Treadaway, K. W. J., Page, C. L. and Macmillan, G. L., "The Prediction of Reinforcement Corrosion: From Laboratory Study to Exposure Trials," *Durability of Construction Materials*, J. C. Maso, Editor, Vol. 3, Chapman and Hall, London, 1987, pp. 1323-1329.

168. Macmillan, G. L. and Treadaway, K. W. J., "An Exposure Trial of Concrete Durability in Arabian Gulf Conditions," *Corrosion of Reinforcement in Concrete*, Page, Treadaway and Bamforth, Editors, Elsevier Applied Science, London, 1990, pp. 109-118.

169. Morgan, T. D. B., "Some Comments on Reinforcement Corrosion in Stagnating Saline Environments," *Corrosion of Reinforcement in Concrete*, Page, Treadaway and Bamforth, Editors, Elsevier Applied Science, London, 1990, pp. 29-38.

170. Feliu, S., Gonzalez, J. A., Feliu Jr., S. and Andrade, C., "Relationship between Conductivity of Concrete and Corrosion of Reinforcing Bars," *British Corrosion Journal*, Vol. 24, No. 3, 1989, pp. 195-198.

171. Lopez, W. and Gonzalez, J. A., "Influence of the Degree of Pore Saturation on the Resistivity of Concrete and the Corrosion Rate of Steel Reinforcement," *Cement and Concrete Research*, Vol. 23, No. 2, 1993, pp. 368-376.

172. Browne, R. D., "Design Prediction of the Life for Reinforced Concrete in Marine and Other Chloride Environments," *Durability of Building Materials*, Vol. 1, 1982, pp. 113-125.

173. Cavalier, P. G., and Vassie, P. R., "Investigation and Repair of Reinforcement

Corrosion in a Bridge Deck," *Proc. Inst. of Civil Engineers*, Vol. 70, Part 1, August 1981, pp. 461-480.

174. Benjamin, S. E. and Sykes, J. M., "Chloride-Induced Pitting Corrosion of Swedish Iron in Ordinary Portland Cement Mortars and Alkaline Solutions: The Effect of Temperature", *Corrosion of Reinforcement in Concrete*, Page, Treadaway and Bamforth, Editors, Elsevier Applied Science, London, 1990, pp. 59-64.

175. Maslehuddin, M., Jarrah, N. R., Ashiru, O. A. and Al-Mana, A. I., "Corrosion of Steel in Alkaline Media," *Proc. Sixth Middle East Corrosion Conference*, Bahrain, 1994, pp.

176. Baumel, A. and Engel, H. J., "Korrosion von stohl in Beton", *Archieu fun dus Eisenhuttenwenesen*, Vol. 30, 1959, pp. 417-428.

177. Henrikesen, J. F., "The Corrosion and Protection of Steel in Saturated $Ca(OH)_2$ Contaminated with NaCl," *Corrosion Science*, Vol. 20, 1980, pp. 1241-1249.

178. Lopez, W., Gonzalez, J. A. and Andrade, C., "Influence of Temperature on the Service Life of Rebars," *Cement and Concrete Research*, Vol. 23, No. 5, 1993, pp. 1130-1140.

179. Rasheeduzzafar, Al-Saadoun, S. S., Dakhil, F. H. and Al-Gahtani, A. S., "Effect of Cement Composition on Corrosion of Reinforcing Steel in Concrete," *Corrosion of Reinforcement in Concrete*, Page, Treadaway and Bamforth, Editors, Elsevier Applied Science, London, 1990, pp. 213-226.

180. Baweja, D., Roper, H., Guirguis, S. and Sirivivatnonon, V., "Measurement of Corrosion of Steel Reinforcement under High Chloride Conditions," *ACI Special Publication SP-132*, American Concrete Institute, Detroit, 1993, pp. 1543-1563.

181. Dhir, R. K., Jones, M. R. and Elghaly, A. E., "PFA Concrete: Exposure Temperature Effects on Chloride Diffusion," *Cement and Concrete Research*, Vol. 23, No. 5, 1993, pp. 1105-1114.

182. Page, C. L., Short, N. R. and El-Tarras, A., "Diffusion of Chloride Ions in Hardened Cement Pastes," *Cement and Concrete Research*, Vol. 11, 1981, pp. 395-406.

183. Steinour, H., "Some Effects of Carbon dioxide on Mortars and Concrete - Discussion," *Journal of the American Concrete Institute*, Feb. 1959, pp. 394 - 401.

184. Baird, T., Cairn-Smith, G. and Snell, D., "Morphology and Carbon dioxide uptake in Tobermorite Gel," *Journal of Colloidal and Interface Science*, Vol. 50, No. 2, Feb. 1975, pp. 387-391.

185. Verbeck, G. J., "Carbonation of Hydrated Portland Cement," *ASTM Special Publication No. 205*, ASTM, Philadelphia, U.S.A., 1958, pp. 17-36.

186. Suzuki, K., Nisihkawa, T., and Ito, S., "Formation and Carbonation of CSH in

Water," *Cement and Concrete Research,* Vol. 15, No. 2, 1985, pp. 213-224.

187. Cole, W. and Kroone, B., "Carbon Dioxide in Hydrated Portland Cement," *Proc. Journal of the American Concrete Institute*, June 1960, pp. 1275-1295.

188. Sauman, Z., "Carbonization of Porous Concrete and its Main Binding Components," *Cement and Concrete Research*, Vol. 1, No. 6, 1971, pp. 645-662.

189. Slegers, P. and Rouxhet, P., "Carbonation of the Hydration Products of Tricalcium Silicate," *Cement and Concrete Research*, Vol. 6, No. 3, pp. 381-388.

190. Grounds, T., Midgley, H. and Nowell, D., "Use of Thermal Methods to Estimate the State of Hydration of Ettringite," *Thermochemica Acta*," Vol. 85, 1985, pp. 215-218.

191. Forrester, J., "Measurement of Carbonation," *RILEM Symposium on Carbonation of Concrete*, Paper 2.4, 1976, 6 pp.

192. Bier, T., "Influence of Type of Cement and Curing on Carbonation and Pore Structure of HCP," *Proc. MRS Symposium,* Boston, 1986, 18 pp.

193. Sakai, E., Kosuge, K., Teramura, S. and Nakagawa, K., "Carbonation of Expansive Concrete and Change of Hydration Products," *ACI Special Publication SP 126*, ACI, Detroit, U.S.A., 1993, pp. 989-999.

194. Wierig, H., "Longtime Studies on the Carbonation of Concrete under Normal Outdoor Exposure," *Proc., RILEM Seminar*, Hannover, 1984, pp. 239-249.

195. Kroone, B., Blakey, F., "Reaction between Carbon Dioxide Gas and Mortar," *Proc., Journal, of the American Concrete Institute,* December 1959, pp. 497-510.

196. Daimon, M., Akiba, T. and Kondo, R., "Through Pore Size Distribution and Kinetics of Carbonation Reaction of OPC Mortars," *Journal, American Ceramic Society,* Vol. 54, No. 9, 1971, pp. 423-428.

197. Treadaway, K. W. J., "Review of Comparative Performance of Reinforced Concrete in UK and Arabian Gulf Conditions," *Proc., 1st International Conference on Deterioration and Repair of Reinforced Concrete in the Arabian Gulf*, Bahrain, October 1985, pp. 301 - 308.

198. Smith, D. and Evans, A., "Purple Concrete in a Middle East Town," *Concrete*, February 1986, pp. 36 - 41.

199. Weir, K., Holmes, C. and Brundle, S., "Assessment and Replacement of Muttrah Corniche Culverts in Oman," *Proc., 1st International Conference on Deterioration and Repair of Reinforced Concrete in the Arabian Gulf*, Bahrain, 1985, pp. 375 - 392.

200. Walter, R., "Concrete Deterioration at Desalination Plant in the Arabian Gulf," *Proc. 1st International Conference on Deterioration and Repair of Reinforced*

Concrete in the Arabian Gulf, Bahrain, October 1985, pp. 351 - 363.

201. Shalon, R. and Raphael, M., "A Study of the Influence of Climate on Corrosion of Reinforcement," *Proc., RILEM Symposium on Concrete in Hot Countries*, 1971, pp. 77-96.

202. Shalaby, H. M., "Case Studies of Corrosion and Deterioration of Reinforced Concrete Structures in the State of Kuwait," *Proc., 1st International Conference on Deterioration and Repair of Reinforced Concrete in the Arabian Gulf*, October 1985, pp. 309 - 320.

203. Al-Rabiah, A. A., *Concrete Durability in the Arabian Gulf Marine Environment*, Ph.D. Thesis, University of Salford, England, 1990.

204. Hussain S. E., Paul, I. S. and Ruthaiyea, H. M., "Evaluation and Repair Strategies for Shallow Foundations," *Proc., Sixth Middle East Corrosion Conference*, 1994, Bahrain, pp. 613 - 628.

205. Fattuhi, N. I., "Changes in Alkalinity of Concrete Exposed to Kuwaiti Atmospheric Conditions," *Durability of Building Materials*, 4, 1987, pp. 309 - 321.

206. Rasheeduzzafar, "Carbonation in Plain and Blended Cement Concrete in the Arabian Gulf Environment," to be published.

207. Al-Amoudi, O. S. B., Rasheeduzzafar and Maslehuddin, M., "Carbonation and Corrosion of Rebars in Salt Contaminated OPC/PFA Concretes," *Cement and Concrete Research*, Vol. 21, No. 1, 1991, pp. 38 - 50.

208. Parrott, L. J., "Carbonation, Moisture and Empty Pores," *Advances in Cement Research*, Vol. 4, No. 15, 1991/92, pp. 111-118.

209. Hamada, M., "Neutralisation of Concrete and Corrosion of Reinforcing Steel," *Proceedings, Fifth International Symposium on the Chemistry of Cement*, Tokyo, 1968, pp. 343-368.

210. Nischer, P., "Influence of Concrete Quality and Environment on Carbonation," *Proc. RILEM Seminar*, Hannover, 1984, pp. 231-238.

211. RILEM Committee CPC-18, "Measurement of Hardened Concrete Carbonation Depth," *Materials and Structures*, Vol. 17, No. 102, 1984, pp. 435 - 440.

212. Kashino, N., "Investigation into limit of initial Corrosion in Existing RC Structures," *Durability of Building Materials and Components*, Vol. 3, 1984, pp. 176 - 186.

213. Theophilus, J., "Uncertainties in Assessing the Durability of Concrete," *Civil Engineering*, August 10 - 13, 1986.

214. Roberts, M. H., *Carbonation of Concrete made with Dense Natural Aggregates*, BRE Information Digest, IP 6/81, 1981.

215. Theophilus, J. and Bailey, M., "Significance of Carbonation and Chloride Tests for Assessing Durability of RC," *Durability of Materials and Components*, Vol. 3, 1984, 209 - 238.

216. Ohgishi, S. and Ono, H., "Study to estimate Depth of Neutralisation on Concrete Members," *Cement Association of Japan, Review*, 1983, pp. 168 - 170.

217. Peterson, C. G. and Poulsen, E., "In-situ NDT Methods for Concrete with Particular Reference to Strength, Permeability, Chloride content and disintegration," *Proc., 1st International Conference on Deterioration and Repair of Reinforced Concrete in the Arabian Gulf*, Bahrain, 1985, pp. 497 - 507.

218. Saeki, N., Takada, N. and Fujita, Y., "Influence of Carbonation and Sea Water on Corrosion of Steel in Concrete," *Trans., Japan Concrete Institute*, Vol. 6, No. 1, 1984, pp. 71 - 78.

219. Litvan, G. and Meyer, A., "Carbonation of GBFS Concrete during 20 Years of Field Exposure," *ACI Special Publication, SP - 91*, Vol. 2, 1986, pp. 1445 - 1462.

220. Meyer, A., "Investigations on the Carbonation of Concrete," *Proceedings, International Symposium on Chemistry of Cements*, Tokyo, 1968, Vol. 3, pp. 394 - 401.

221. Kokubu, M. and Nagataki, S., "Carbonation and Corrosion of Reinforcement in Fly Ash Concrete," *RILEM Symposium on Concrete Durability*, Pt. 2, 1969, pp. 71 -79.

222. Patel, R., Parrott, L. J. and Killoh, D. C., "Gradients of Microstructure and Diffusion Properties in HCP Caused by Drying," *Cement and Concrete Research*, Vol. 15, No. 2, 1985, pp. 343 - 356.

223. Butler, F., Decter, H. M., and Smith, G., "Studies on Dessiccation and Carbonation of Systems containing OPC & PFA," *ACI Special Publication, SP - 79*, 1983, pp. 367 - 381.

224. Curtil, L., Gielly, J. and Murat, M., "The Polarizing Microscope: a Tool of Interest for Investigation on Concrete; Application to Carbonation," *Cement and Concrete Research*, Vol. 23, No. 2, 1993, pp. 329 - 334.

225. Parrott, L. J., "Increase in Creep of Hardened Cement Paste due to Carbonation under Load," *Magazine of Concrete Research*, Vol. 27, No. 92, 1975, pp. 179 - 181.

226. Halstead, P. E., *Materials and Structures*, Vol. 9, No. 51, 1976, p. 187.

227. Schubert, P., and von Berg, W., *RILEM International Symposium on Carbonation of Concrete*, 1976.

228. Smolczyk, H. G., *RILEM International Symposium on Carbonation of Concrete*, paper 1.1, 1976, 10 pp.

229. Ho, D. W. S. and Lewis, R. K., "Carbonation of Concrete and its Prediction," *Cement and Concrete Research*, Vol. 17, No. 3, 1987, pp. 489 - 504.

230. Schroder, F. and Smolczyk, H. G., "Carbonation and Protection against Steel Corrosion," Principal Paper: *Proceedings, Fifth International Symposium on the Chemistry of Cement*, Tokyo, Vol. 5, 1968, p. 188.

231. Litvan, G. G. and Meyer, A., "Carbonation of Granulated Blast Furnace Slag Cement Concrete During Twenty Years of Field Exposure," *ACI Special Publication, SP- 91*, 1985, pp. 1445 - 1462.

232. Ramachandran, V. S., Feldman, R. F. and Beaudoin, J. J., *Concrete Science - Treatise on Current Research*, Heyden, London, 1981.

233. Kobayashi, K. and Uno, Y., "Influence of Alkali on Carbonation of Concrete, Part 1, Preliminary Tests with Mortar Specimens," *Cement and Concrete Research*, Vol. 19, No. 5, 1989, pp. 821 - 826.

234. Kobayashi, K., and Uno, Y., "Influence of Alkalies on Carbonation of Concrete, Part 2 - Influence of Alkali in Cement on Rate of Carbonation of Concrete," *Cement and Concrete Research*, Vol. 20, No. 4, 1990, pp. 619 - 622.

235. Bensted, J., "A Discussion of the Paper Influence of Alkali on Carbonation of Concrete, Part 2: Influence of Alkali in Cement on Rate of Carbonation of Concrete," *Cement and Concrete Research*, Vol. 21, 1991, p. 675.

236. Mori, H., et al. *Review, 15th General Meeting*, Cement Association, Japan, 1961, p. 43.

237. Jawed, I. and Skalny, J., "Alkalies in Cement: A review - II. Effects of Alkalies on Hydration and Performance of Portland Cement," *Cement and Concrete Research*, Vol. 8, No. 1, 1978, pp. 37 - 52.

238. Lerch, W., *PCA Bulletin, No. 12*, 1946.

239. Basunbul, I. A., Khan, C. N. S. A. and Maslehuddin, M., "Temperature and Contamination Effect on Strength and Porosity of Plain and Blended Cement Concretes," to be published.

240. Dhir, R. K., Hewlett, P. C. and Chan, Y. N., "Near-Surface Characteristics of Concrete: Prediction of Carbonation Resistance," *Magazine of Concrete Research*, 41, No. 148, September 1989, pp. 137 - 143.

241. Glass, G. K., Page, C. L. and Short, N. R., "Factors affecting the Corrosion Rate of Steel in Carbonated Mortars, *Corrosion Science*, Vol. 32, No. 12, 1991, pp. 1283-1294.

242. Hughes, D. C., "Sulfate Resistance of Fly Ash/OPC Grouts," *Blended Cements in Construction*, Swamy, R. N., Ed., 1992, Elsevier Applied Science, London, pp. 336 - 350.

243. Ho, D. W. S. and Lewis, R., "Carbonation of Concrete incorporating PFA or Chemical Admixture, " *ACI Special Publication, SP- 79*, 1983, pp. 333 - 346.

244. Haque, M. N. and Kayalli, O. A., Discussion of a paper "Carbonation and Corrosion of Rebars in Salt Contaminated Concrete," *Cement and Concrete Research*, Vol. 21, No. 5, 1991, pp. 954-955.

245. Hobbs, D. W., "Carbonation of Concrete containing PFA," *Magazine of Concrete Research*, Vol. 40, No. 14, June 1988, pp. 69 - 78.

246. Scholz, E. and Wierig, H., "Carbonation of Fly Ash Concrete," *Proc. RILEM Seminar, Hannover*, 1984, pp. 258 - 265.

247. Smolczyk, H., "Discussion of Principal paper on Carbonation of Concrete by Hamada," *Proc. Fifth International Symposium on Chemistry of Cement*, Tokyo, Vol. 3, 1969, pp. 369 - 384.

248. Collins, R., *Porous Aggregates in Concrete: Jurassic Limestones*, BRE Information Paper, IP 2/86, 1986, 4 pp.

249. Grube, H., "Influence of Concrete Materials, Mix and Construction Techniques on Permeability," *Proc. Concrete Society Conference*, December 1985, pp. 77 - 88.

250. Richartz, W., "Electron Microscope Investigation of Hardened Cement Paste," *Proc. of International Symposium on the Chemistry of Cement*, Tokyo, October 1968, Part III, pp. 119 - 128.

251. Chapman, D. A., *A Study of the Movement of Moisture in and from Concrete at Elevated and non-uniform Temperatures*, Ph.D. Thesis, University of London, 1976, pp. 479 - 483.

252. Ludwig, N. C. and Pence, S. A., "Properties of Portland Cement Pastes Cured at Elevated Temperature - Pressure," *ACI Journal*, Vol. 52, No. 6, 1956, pp. 673 - 764.

253. Berhane, Z., "The Behaviour of Concrete in Hot Climates," *Materials and Structures*, 25, 1992, pp. 157 - 162.

254. Idorn, G. M., "Hydration of Portland Cement Paste at High Temperature under Atmospheric Pressure", *Proceedings, Fifth International Symposium on Chemistry of Cement*, Tokyo, October 1968, Part III, pp. 411 - 428.

255. Goto, S. and Roy, D. M., "The Effect of w/c ratio and Curing Temperature on the Permeability of Hardened Cement Paste," *Cement and Concrete Research*, Vol. 11, No. 4, 1981, pp. 575 - 579.

256. Justnes, H. and Havdahl, J., "The Effect of Curing Temperature on the Microstructure of Cementitious Paste for LWA Concrete," *Blended Cements in Construction*, Swamy, R. N., Editor, 1992, pp. 138-151.

257. Bentur, A., Berger, R. L., Kung, J. H., Milestone, N. B. and Young, J. F., "Structural Properties of Calcium Silicate Pastes: II. Effect of Curing

Temperature," *Journal, American Ceramic Society*, Vol. 62, 1979, pp. 362 - 365.

258. Radjy, F., Richards, C. W., "Effect of Curing and Heat Treatment History on the Dynamic Mechanical Response and the Pore Structure of Hardened Cement Paste," *Cement and Concrete Research*, Vol. 3, 1973, pp. 7 - 21.

259. Verbeck, G. J. and Helmuth, R. H., "Structure and Physical Properties of Cement Paste," *Proceedings, 5th International Symposium on the Chemistry of Cement*, Tokyo, Vol. III, 1968, pp. 1 - 32.

260. Skalny, J. and Odler, I., "Pore Structure of Calcium Silicates," *Cement and Concrete Research*, Vol. 2, No. 4, 1972, pp. 387 - 400.

261. Sellevold, E. J., "Mercury Porosimetry of Hardened Cement Cured or Stored at 97 °C," *Cement and Concrete Research*, Vol. 4, No. 3, 1974, pp. 399 - 404.

262. Kjellsen, K. O., Detwiler, R. J. and Gjorv, O. E., "Development of Microstructures in Plain Cement Pastes Hydrated at Different Temperatures," *Cement and Concrete Research*, Vol. 21, No. 1, 1991, pp. 179 - 189.

263. Uhlig, H. H., and Revie, R., *Corrosion and Corrosion Control*, Third Edition, John Wiley and Sons, New York, 1985.

264. Treadaway, K. W. J., "Research into Durability of Reinforcement in Concrete Structures," *Proc. RILEM Seminar*, Hannover, 1984, pp. 182-196.

265. Muller, K., Proc. RILEM International Symposium, Budapest, 1984, pp. 36-41.

266. Roper, H. and Baweja, D., "Carbonation-Chloride Interactions and their Influence on corrosion Rates of Steel in Concrete," *American Concrete Institute, Special Publication, SP-126*, American Concrete Institute, Detroit, U.S.A., 1992, pp. 295-315.

267. Sagoe-Crentsil, K. K., Glasser, F. P. and Irvine, J. T. S., "Electrochemical Characteristics of Reinforced Concrete Corrosion as Determined by Impedance Spectroscopy," *British Corrosion Journal*, Vol. 27, No. 2, 1992, pp. 113-118.

268. Alonso, C. and Andrade, C., *Advances in Cement Research*, 1, 1988, p. 155.

269. Nagataki, S. and Ohga, H., "Combined Effect of Carbonation and Chloride on Corrosion of Reinforcement in Fly Ash Concrete," *American Concrete Institute Special Publication, SP 132*, ACI, Detroit, U.S.A., 1993, pp. 227-245.

270. Hladky, K., Callow, L. M. and Dawson, J. L., *British Corrosion Journal*, Vol. 15, No. 1, 1980, pp. 20-25.

271. John, D. G. and Treadaway, K. W. J., "The Repair of Concrete - a Laboratory and Exposure Site Investigation," *Corrosion of Reinforcement in Concrete Construction*, Crane, A.P. Ed., Ellis Horwood Limited, Chichester, 1983, pp. 263-286.

272. Hope, B. B., Ip, A. K. C. and Manning, D. G., "Corrosion and Electrical Impedance in Concrete," *Cement and Concrete Research,* Vol. 15, No. 3, 1985, pp. 525-534

273. Hachani, L., Carpio, J., Fiaud, C., Raharinaivo, A. and Triki, E., "Steel Corrosion in Concretes Deteriorated by Chlorides and Sulphates: Electrochemical Study using Impedance Spectrometry and Stepping Down the Current Method," *Cement and Concrete Research,* Vol. 22, No. 1, 1992, pp. 56-66.

274. Kranc, S. C. and Sagues, A. A., "Computation of Corrosion Macrocell Current Distribution and Electrochemical Impedance of Reinforcing Steel in Concrete," *ASTM STP 1154,* ASTM, Philadelphia, 1992.

275. Lawson, K. M., Thompson, N. G. and Islam, M., "Interpretation of Corrosion Rate Measurements of Reinforcing Steel in Concrete," *Proc., Sixth Middle East Corrosion Conference,* Bahrain, 1993, pp. 581-596.

276. Alonso, C., Andrade, C. and Gonzalez, J. A., "Relation between Resistivity and Corrosion Rate of Reinforcement in Carbonated Mortar made with Several Cement Types," *Cement and Concrete Research,* Vol. 8, No. 5, 1988, pp. 687-698.

277. Gonzalez, J. A. and Andrade, C., "Study of the Bahavior of Galvanized Concrete Reinforcements in Carbonated and Noncarbonated Concrete," *British Corrosion Journal,* Vol. 17, No. 1, 1982.

278. Gonzalez, J. A., Algaba, S. and Andrade, C., "Corrosion of Reinforcing Steel in Carbonated Concrete," *British Corrosion Journal,* Vol. 15, No. 3, 1980, pp. 135 -139.

279. Millard, S. G., Gowers, K. R. and Gill, J. S., "Reinforcement Corrosion Assessment using Linear Polarization Techniques," *American Concrete Institute Special Publication SP-128,* ACI, Detroit, U.S.A., 1991, pp. 373-394.